

REVERSING CANCER CELL FATE: DRIVING THERAPEUTIC
DIFFERENTIATION OF HEPATOBLASTOMA TO FUNCTIONAL
HEPATOCYTE-LIKE CELLS

A Dissertation Presented

By

Jordan L. Smith

Submitted to the Faculty of the
University of Massachusetts Graduate School of Biomedical Sciences, Worcester
In partial fulfillment of the requirement for the degree of

DOCTOR OF PHILOSOPHY

MARCH 20, 2020

MD/PhD Program, Cancer Biology

REVERSING CANCER CELL FATE: DRIVING THERAPEUTIC
DIFFERENTIATION OF HEPATOBLASTOMA TO FUNCTIONAL
HEPATOCYTE-LIKE CELLS

A Dissertation Presented
By

Jordan L. Smith

This work was undertaken in the Graduate School of Biomedical Sciences, RNA
Therapeutics Institute

MD/PhD Medical Scientist Training Program, Cancer Biology

Under the mentorship of

Wen Xue, Ph.D., Thesis Advisor

Silvia Corvera, MD, Member of Committee

Craig Mello, Ph.D., Member of Committee

Art Mercurio, Ph.D., Member of Committee

David Barbie, M.D., External Member of Committee

Leslie Shaw, Ph.D., Chair of Committee

Mary Ellen Lane, Ph.D.,
Dean of the Graduate School of Biomedical Sciences

MARCH 20, 2020

DEDICATION

Mom, this one's for you.

ACKNOWLEDGEMENTS

This work is only possible through, “standing on the shoulders of giants.” I would be remiss not to acknowledge all of the bold, creative scientists before me who paved the way. I’m grateful for all the support, guidance, and efforts of the many people that made this project happen. Specifically, I want to start with thanking Wen, my PI, who taught me to strive for, “no wasted efforts.” Effectively, take the time to design experiments that are well controlled, and interpretable- positive or negative. Wen instilled the values of thoughtfulness, diligence, and perseverance. Thank you, Wen, for always taking the time to look at histology slides with me, and to hear out all of my concerns- no matter how small.

I would next like to thank the Xue lab members for their technical support, encouragement, and constructive comments. In particular, I would like to thank former postdoc Haiwei Mou for teaching me the art of mouse work, hydrodynamic injections, and immunohistochemistry. Haiwei taught me to see the beauty in science, and to maintain a sense of wonder.

I would also like to thank Dr. Suet-yan Kwan for her extensive mentorship, assistance with tissue culture, monitoring mice throughout the project, and perhaps most importantly, all the humor and friendship along the way. Finally, I would like to acknowledge and thank all current and former Xue lab members including Dr. Tingting Jiang, Dr. Chun-qing Song, Dr. Shun-qing Liang, Dr. Zachary Kennedy, Dr. Ankur Sheel, Dr. Max Hazeltine, and Yueying Cao. I could not have asked for better lab mates during my graduate training.

I would next like to thank my TRAC, Drs. Leslie Shaw (chair), Art Mercurio, Craig Mello, and Silvia Corvera, for their time, guidance, and critical feedback that brought this project to fruition. I want to thank them for challenging me and supporting my physician scientist training.

I want to also acknowledge the immense institutional and administrative support from the RNA Therapeutics Institute, Graduate School of Biomedical Sciences, Medical School, and the MD/PhD Program Leadership. Specifically, to Emily Mohn, Ann Powers, Darryl Conte, Dean Lane, Dean Knight, Anne Michelson, and Dr. Corvera- thank you. To my MD/PhD cohort, I wouldn’t have made it here without you- thank you Alysia Bryll, Grace Masters, Tomas Rodriguez, Henry Pratt, Eric Ding, Nick Peterson, and Chantal Ferguson.

Finally, to my parents, my sister, and my husband who have been unfailingly supportive of my dreams and aspirations, often at great personal cost. Thank you for always prioritizing my education, and giving me the confidence to think big, take risks, and always, always try again.

ABSTRACT

Background & Aims: Despite advances in surgical care and chemotherapeutic regimens, the five-year survival rate for Stage IV Hepatoblastoma (HB), the predominant pediatric liver tumor, remains at 27%. YAP1 and β -Catenin co-activation occurs in 80% of children's HB; however, a lack of conditional genetic models precludes exploration of tumor maintenance and therapeutic targets. Thus, the clinical need for a targeted therapy remains unmet. Given the predominance of YAP1 and β -catenin activation in children's tumors, I sought to evaluate YAP1 as a therapeutic target in HB.

Approach & Results: Herein, I engineered the first conditional murine model of HB using hydrodynamic injection to deliver transposon plasmids encoding inducible YAP1^{S127A}, constitutive β -Catenin^{DeIN90}, and a luciferase reporter to murine liver. Tumor regression was evaluated using *in vivo* bioluminescent imaging, and tumor landscape characterized using RNA sequencing, ATAC sequencing and DNA foot-printing. Here I show that YAP1 withdrawal in mice mediates >90% tumor regression with survival for 230+ days. Mechanistically, YAP1 withdrawal promotes apoptosis in a subset of tumor cells and in remaining cells induces a cell fate switch driving therapeutic differentiation of HB tumors into Ki-67 negative "hbHep cells." hbHep cells have hepatocyte-like morphology and partially restored mature hepatocyte gene expression. YAP1 withdrawal drives formation of hbHeps by modulating liver differentiation transcription factor (TF) occupancy. Indeed, tumor-derived hbHeps, consistent with their reprogrammed transcriptional landscape, regain partial hepatocyte function and can rescue liver damage in mice.

Conclusions: YAP1 withdrawal, without modulation of oncogenic β -Catenin, significantly regresses hepatoblastoma, providing the first *in vivo* data to support YAP1 as a therapeutic target for HB. Modulating YAP1 expression alone is sufficient to drive long-term regression in hepatoblastoma because it promotes cell death in a subset of tumor cells and modulates transcription factor occupancy to reverse the fate of residual tumor cells to mimic functional hepatocytes.

TABLE OF CONTENTS

DEDICATION	III
ACKNOWLEDGEMENTS	IV
ABSTRACT	V
TABLE OF CONTENTS	VI
LIST OF FIGURES	XII
LIST OF TABLES	XVII
LIST OF COPYRIGHTED MATERIALS PRODUCED BY AUTHOR	XX
LIST OF THIRD PARTY COPYRIGHTED MATERIAL	XXI
ACKNOWLEDGMENT OF FUNDING SOURCES	XXII
DATA SET ACCESSION	XXIII
LIST OF SYMBOLS, ABBREVIATIONS, OR NOMENCLATURE	XXIV
PREFACE	XXXIII
CHAPTER I INTRODUCTION	1
Chapter 1.1 Liver Cancer Primer	3
Subtypes of Pediatric Liver Cancer	8
Chapter 1.2 Epidemiology of Hepatoblastoma	11
Incidence and Associations	11
Risk Factors	15
<i>Birth Weight and NICU Exposures</i>	16
<i>Maternal Obesity</i>	17
<i>Young Maternal Age</i>	18

<i>Maternal/Paternal Smoking</i>	18
<i>Infertility Treatment</i>	19
Chapter 1.3 Clinical Management of Hepatoblastoma	20
Clinical Presentation	20
<i>History and Physical</i>	20
<i>Laboratory Findings and Imaging</i>	21
Histologic Subtypes of Hepatoblastoma	23
Clinical Treatment and Prognosis	29
<i>Clinical Staging</i>	29
<i>Treatment by Stage</i>	34
<i>Surgical Resection</i>	36
<i>Chemotherapy</i>	37
<i>Liver Transplantation</i>	39
<i>Clinical Trials</i>	41
Chapter 1.4 Molecular Profiling of Hepatoblastoma	42
Genetic Alterations.....	42
Epigenetic Alterations	43
Cytogenetics	46
Gene Expression Profiles	47
<i>Cairo Classes, C1/C2</i>	48
<i>Sumazin HB1, HB2, HB3</i>	50
<i>Hooks Four Gene Signature</i>	51
microRNA Regulation	52
Chapter 1.5 Laboratory Models	55
In Vitro	55
In Vivo	57
Chapter 1.6 Liver Development	60
From Hepatoblast to Hepatocyte	62
Wnt Signaling in Liver Development	63
Hippo Signaling in Liver Development	65
Chapter 1.7 Liver Differentiation	66
Transcriptional Control	68
Liver Cell Plasticity	70
Chapter 1.8 Liver Tumorigenesis	73
Wnt/ β -catenin Signaling in Liver Tumorigenesis	76
Hippo/YAP1 Signaling in Liver Tumorigenesis.....	79
Wnt and Hippo Crosstalk in Tumorigenesis	83

Chapter 1.9 Hallmarks of Hepatoblastoma.....	86
Rationale	86
CHAPTER II TUMOR MAINTENANCE REQUIRES YAP1.....	89
Chapter 2.1 Introduction	89
Hepatoblastoma Primer	89
Tumor Initiation, Tumor Maintenance, and Oncogene Addiction	90
Chapter 2.2 Results	93
Generation of conditional mouse model of hepatoblastoma	93
YAP1 withdrawal reprograms hepatoblastoma gene expression	97
Conditional mouse model mimics aggressive human subtype.....	98
Genetic YAP1 inhibition results in >90% tumor regression	101
YAP1 withdrawal promotes long-term survival.....	104
Chapter 2.3 Discussion	106
Chapter 2.4 Tables.....	110
Chapter 2.5 Materials and Methods	112
CHAPTER III YAP1 WITHDRAWAL INDUCES GENERATION OF “HB-HEPS”	118
Chapter 3.1 Introduction	118
Chapter 3.2 Results	121
YAP1 Inhibited livers harbor tumor lineage cells.....	122
YAP1 inactivation promotes liver differentiation signaling	124
Modulation of chromatin contributes to generation of hbHeps	124
YAP1 Inhibition modulates liver transcription factor occupancy	131
Chapter 3.3 Discussion	134
Chapter 3.4 Tables.....	137
Chapter 3.5 Materials and Methods	145
CHAPTER IV HB-HEPS PARTIALLY RESCUE LIVER FUNCTION.....	150
Chapter 4.1 Introduction	150

Chapter 4.2 Results	155
Generation of liver damage model system.....	155
hbHeps behave like functional hepatocytes in liver damage context	156
YAP1 withdrawal partially restores normal hepatocyte function in hbHeps...	160
Chapter 4.3 Discussion	164
Chapter 4.4 Tables.....	167
Chapter 4.5 Materials and Methods	172
CHAPTER V DISCUSSION	175
Chapter 5.1 Mouse Models of Hepatoblastoma	177
In Vivo Modeling Primer	177
Hydrodynamic Models	181
Inducible Models	185
Sleeping Beauty Transposon Systems	186
Caveats of the Conditional Model of Mouse Hepatoblastoma.....	191
Future directions for mouse modeling of pediatric hepatoblastoma	193
Chapter 5.2 Role of Hippo/YAP Signaling in Liver Cancer.....	195
YAP1 Signaling Primer	196
Canonical/Non-Canonical YAP1 Signaling in Liver Tumorigenesis.....	197
YAP1-TEAD	197
YAP1 and Epigenetic Regulation	199
TEAD Independent Transcription	200
YAP1 Activation in Hepatoblastoma	201
YAP1 and Hepatoblastoma Tumor Maintenance	203
Defining Tumor Initiation and Tumor Maintenance.....	204
YAP1 promotes proliferation, survival and stemness in hepatoblastoma ..	204
YAP1 and Differentiation.....	207
Chapter 5.3 Wnt signaling in Liver Cancer.....	211
Wnt/ β -Catenin Signaling in Liver Tumorigenesis	211
Wnt Pathway Activation in Hepatoblastoma.....	212
Differential Wnt Signaling in Hepatoblastoma	213
Chapter 5.4 Crosstalk between Wnt and Hippo Signaling	215
YAP1 Regulation of Wnt/ β -Catenin.....	215
Wnt Regulation of YAP1 in Liver Cancer	217
Chapter 5.5 Cell Fate Switch: Apoptosis or hbHeps?	219

Cancer and Development	220
Differentiation or Apoptosis?	221
Cell Fate and p53.....	223
Hippo/YAP1 and p53	225
Chapter 5.6 Therapeutic Differentiation of Cancer Cells	226
Differentiation Therapy Primer	226
Stemness and Differentiation in Hepatoblastoma	228
Caveats to Differentiation Therapy.....	229
Challenges to Permanent Therapeutic Differentiation.....	231
Chapter 5.7 YAP1 Targeted Therapies for Hepatoblastoma	233
YAP1 Therapeutics, Primer.....	233
YAP1 Small Molecules.....	235
<i>YAP1-TEAD Disruptors</i>	235
<i>Monoclonal Antibodies</i>	235
<i>Therapeutic Peptides</i>	236
<i>Small RNAs</i>	237
Clinical Applications	240
CONCLUDING REMARKS AND FUTURE DIRECTIONS	242
Summary of Findings and Model	242
Future Directions	244
APPENDIX I CRISPR-CAS9 INDUCES EXON SKIPPING.....	247
Introduction.....	247
Methods.....	248
Significant Results and Discussion.....	251
APPENDIX II CRISPR-SONIC CANCER MODELING.....	263
Introduction.....	263
Methods.....	265
Significant Results and Discussion.....	271
APPENDIX III REVIEW OF CANONICAL WNT SIGNALING.....	286

Wnt Signaling ON/ β -catenin ON	286
Wnt Signaling OFF/ β -catenin OFF	287
APPENDIX IV REVIEW OF CANONICAL HIPPO SIGNALING	289
Hippo Signaling ON/ YAP1 OFF	289
Hippo Signaling OFF/ YAP1 ON	291
APPENDIX V MURINE HEPATOBLASTOMA GENE EXPRESSION	293
APPENDIX VI HBHEP CELL GENE EXPRESSION.....	330
REFERENCES	356

LIST OF FIGURES

CHAPTER ONE

- Figure 1.1** Hallmarks of cancer
- Figure 1.2** Common mutations in adult hepatocellular carcinoma
- Figure 1.3** Incidence of hepatoblastoma by age
- Figure 1.4** Radiologic imaging of hepatoblastoma
- Figure 1.5** Histologic subtypes of pediatric hepatoblastoma
- Figure 1.6** PRETEXT, POSTEXT clinical staging
- Figure 1.7** PRETEXT Designation survival curves
- Figure 1.8** Cairo C1/C2 hepatoblastoma classes
- Figure 1.9** Clinical characteristics of Cairo hepatoblastoma classes
- Figure 1.10** Hooks hepatoblastoma signature
- Figure 1.11** Hepatoblastoma histology and prenatal stage
- Figure 1.12** Liver zonation
- Figure 1.13** Expression of HNF family members by tissue
- Figure 1.14** Immunohistochemical staining in patient liver tumor samples
- Figure 1.15** *In vivo* generation of constitutive hepatoblastoma
- Figure 1.16** Hallmarks of hepatoblastoma

CHAPTER TWO

- Figure 2.1** Conditional YAP1^{S127A} and constitutive β -Catenin^{DeIN90} drive hepatoblastoma *in vivo*
- Figure 2.2** YAP1 withdrawal reprograms gene expression in murine hepatoblastoma
- Figure 2.3** Conditional murine hepatoblastoma mimics the poor prognosis human subtype
- Figure 2.4** Genetic YAP1 inhibition results in >90% tumor regression in a conditional mouse model of hepatoblastoma
- Figure 2.5** Genetic YAP1 inhibition promotes reduced proliferation and a mild increase in cleaved caspase-3 (CC3) *in vivo*
- Figure 2.6** YAP1 withdrawal promotes long term survival in mice

CHAPTER THREE

- Figure 3.1** Outcomes of oncogene withdrawal
- Figure 3.2** Sustained YAP1 withdrawal generates non-proliferative tumor lineage cells with hepatocyte morphology
- Figure 3.3** Reactivation of YAP1 promotes tumor proliferation
- Figure 3.4** YAP1 withdrawal induces mature hepatocyte gene expression in hepatoblastoma tumors
- Figure 3.5** YAP1 target gene *CTGF* and *HNF4 α /FOXA2* are inversely correlated in human hepatoblastoma and hepatocellular carcinoma

- Figure 3.6** *In vitro* YAP1 knockdown in human hepatoblastoma cells upregulates markers of differentiation
- Figure 3.7** YAP1 withdrawal promotes upregulation of mature hepatocyte marker, Mup
- Figure 3.8** Generation of lineage tracing system to track “hbHep” cells
- Figure 3.9** YAP1 withdrawal reprograms hepatoblastoma chromatin accessibility
- Figure 3.10** Decreased Tead and Fos-Jun occupancy in hbHeps D33 compared to YAP1 ON tumors
- Figure 3.11** Increased occupancy at liver differentiation transcription factors in hbHeps D33 compared to YAP1 ON tumors

CHAPTER FOUR

- Figure 4.1** Schematic of experimental design
- Figure 4.2** Hepatoblastoma-derived hepatocyte-like cells (hbHep cells) rescue liver damage in *Fah*^{-/-} mutant mice.
- Figure 4.3** hbHeps repopulate the *Fah*^{-/-} liver and partially rescue long-term weight loss
- Figure 4.4** hbHeps show partially restored hepatocyte gene expression

CHAPTER FIVE

Figure 5.1 Experimental Model

APPENDIX I

Figure A1.1 sgRNA targeting *Kras* induces exon skipping in single cell clones

Figure A1.2 *Ctnnb1* sgRNAs targeting exon 3 induces exon skipping

Figure A1.3 Cas9 nuclease activity required for skipping of one or more exons

Figure A1.4 An sgRNA targeting exon 23 of *Dmd* can partially restore in-frame *dystrophin* mRNA

APPENDIX II

Figure A2.1 CRISPR-SONIC enables homology-independent IRES-GFP integration in mouse cells

Figure A2.2 CRISPR-SONIC enables efficient IRES-GFP integration *in vivo*

Figure A2.3 CRISPR-SONIC enables IRES-HRAS^{G12V} integration *in vivo* for tumor modeling

Figure A2.4 CRISPR-SONIC enables combinatorial *Kras* knockin and p53 knockout in B6 wildtype mice

Figure A2.5 CRISPR/Cas9 enables generation of bioluminescent liver tumors

APPENDIX III

Figure A3.1 Canonical Wnt Signaling

APPENDIX IV**Figure A.4.1** Canonical Hippo Signaling

LIST OF TABLES

CHAPTER ONE

- Table 1.1** Classification of pediatric liver tumors
- Table 1.2** Genetic syndromes with increased hepatoblastoma risk
- Table 1.3** Hepatoblastoma risk factors
- Table 1.4** Histologic subtypes of pediatric hepatoblastoma
- Table 1.5** PRETEXT designations and overall survival
- Table 1.6** Evans surgical staging and hepatoblastoma prognosis
- Table 1.7** Chemotherapeutic agents used in hepatoblastoma
- Table 1.8** Interventional Trials for Hepatoblastoma
- Table 1.9** Genetic mutations observed in hepatoblastoma
- Table 1.10** Cell culture models of hepatoblastoma
- Table 1.11** Mouse models of hepatoblastoma

CHAPTER TWO

- Table 2.1** Primer sequences
- Table 2.2** Immunohistochemistry antibodies

CHAPTER THREE

- Table 3.1** Top 20 upregulated genes in YAP1 OFF regressing tumors

Table 3.2 DNA Footprinting reveals increased occupancy of Tead and Fos-Jun in YAP1 ON tumors compared to D33 hbHeps

Table 3.3 DNA Footprinting reveals increased occupancy in D33 hbHeps of canonical liver differentiation factors compared to YAP1 ON tumors

CHAPTER FOUR

Table 4.1 Top 50 IPA Analysis *Upstream Regulator* Signatures in hbHeps, YAP1 OFF D6, and YAP1 ON tumors

Table 4.2 Top 50 IPA Analysis *Disease and Function* Signatures in hbHeps, YAP1 OFF D6, and YAP1 ON tumors

Table 4.3 Top 50 IPA Analysis *Canonical Pathways* Signatures in hbHeps, YAP1 OFF D6, and YAP1 ON tumors

Appendix V

A5.1 RNA-Sequencing Fold Change YAP1 D6. Tumors vs YAP1 ON

Appendix VI

A6.1 Top genes downregulated in hbHep cells compared to WT Fah mice

A6.2 Top genes upregulated in hbHep cells compared to WT Fah mice

LIST OF COPYRIGHTED MATERIALS PRODUCED BY AUTHOR

The following materials (listed below) and associated text appearing throughout *Chapters 2,3, and 4* are adapted in whole or in part from, “*YAP1 withdrawal in hepatoblastoma drives therapeutic differentiation of tumor cells to functional hepatocyte-like cells*” accepted for publication in *Hepatology*, April 2020. The *Hepatology* figures herein are reformatted with modifications with permission from *Wiley* and the accepted paper license agreement.

Modified from Smith et al, Hepatology, 2020

Figures 2.1-2.6, 3.2-3.11, 4.2-4.4

Tables 3.1-3.3, 4.1-4.3

Appendix A5.1, A6.1-2

Figure Number	Publisher	License Number
Figure A1.1	Springer Nature	CC.BY.4.0
Figure A1.2	Springer Nature	CC.BY.4.0
Figure A1.3	Springer Nature	CC.BY.4.0
Figure A1.4	Springer Nature	CC.BY.4.0
Figure A2.1	Springer Nature	CC.BY.4.0
Figure A2.2	Springer Nature	CC.BY.4.0
Figure A2.3	Springer Nature	CC.BY.4.0
Figure A2.4	Springer Nature	CC.BY.4.0

LIST OF THIRD PARTY COPYRIGHTED MATERIAL

Figure	Publisher	License Number	Reference
Figure 1.1	Elsevier	4750301332015	Hanahan et al, 2011.
Figure 1.2	Elsevier	4750390663555	Schulze et al, 2016.
Figure 1.3	Wiley and Sons	4750900108310	Spector et al, 2012.
Figure 1.4	Springer Nature	4752530889817	Robertson et al, 2016
Figure 1.5	Springer Nature	4744871479795	Lopez-Terrada et al, 2013
Figure 1.6	Springer Nature	4744871479795	Lopez-Terrada et al, 2013
Figure 1.7	Elsevier	4754230433612	Czauderna et al, 2016
Figure 1.8	Elsevier	4745461078520	Cairo et al, 2008.
Figure 1.9	Elsevier	4745461078520	Cairo et al, 2008.
Figure 1.10	Wiley and Sons	4775480419553	Hooks et al, 2019
Figure 1.11	Cognizant	1017810-1	Bell et al, 2017
Figure 1.12	Annual Reviews	1015090-1	Russell et al, 2018.
Figure 1.13	Elsevier	4755400169994	Lau et al, 2018.
Figure 1.14	Elsevier	4746010774608	Tao et al, 2014
Figure 1.15	Elsevier	4746010774608	Tao et al, 2014
Figure A3.1	Springer Nature	CC BY-NC-ND 4.0	Zhan et al, 2017
Figure A4.1	AACR	4757861213875	Ehmer et al, 2016

Table	Publisher	License Number	Reference
Table 1.1	Springer Nature	4744871479795	Lopez-Terrada et al, 2013
Table 1.4	Springer Nature	4744871479795	Lopez-Terrada et al, 2013

ACKNOWLEDGMENT OF FUNDING SOURCES

During my graduate career I was supported by the National Cancer Institute F30CA239483, the University of Massachusetts Medical School Cancer Biology, National institutes of Health T32CA130807, and the University of Massachusetts Medical School MSTP National Institutes of Health T32GM107000.

DATA SET ACCESSION

RNA-sequencing, and ATAC-sequencing datasets are available at reasonable request, and available at NCBI GEO GSE146548.

LIST OF SYMBOLS, ABBREVIATIONS, OR NOMENCLATURE

α -fetoprotein (Afp)

β - Transducin Repeat containing E3 ubiquitin ligase (β -TrCP)

β -catenin 1 (CTNNB1)

β -Transducin repeat containing protein (β -TRCP)

3' untranslated region (3'-UTR)

Activator-protein-1 (AP-1)

Acute promyelocytic leukemia (APL)

Adenomatous Polyposis Coli (APC)

v-AKT murine thymoma viral oncogene homolog 1 (AKT)

Amphiregulin (AREG)

Angiomotin Like 2 (Amotl2)

Apolipoprotein A2 (ApoA2)

Asialoglycoprotein receptor (ASGR)

Assay for Transposase Accessible Chromatin Sequencing (ATAC-seq)

B-cell Lymphoma 2 (BCL-2)

B-cell Lymphoma extra-large (BCL-XL)

Baculoviral inhibitor of apoptosis repeat-containing (Birc5/Survivin)

Beckwith Wiedemann Syndrome (BWS)

Body Mass Index (BMI)

Bone Morphogenic Protein (BMP)

BRAC2 and CDKN1A Interacting Protein (BCCIP)

Breast Cancer Gene (BRCA)

Complementary DNA (cDNA)

Cairo Hepatoblastoma Class 1 (C1)

Cairo Hepatoblastoma Class 2 (C2)

Cancer stem cells (CSCs)

Carboxylesterase 3 (CES3)

Casein kinase 1 α (CK1 α)

Caspase 8 (CASP8)

Caudate Lobe involvement (C)

CCAAT-enhancer binding protein-alpha (C/EBP α)

Cell cycle checkpoint protein RAD17 (RAD17)

Cell Cycle Division Cycle Protein 20 Homolog B (CDC20B)

Children's Oncology Group (COG)

Colorectal Cancer (CRC)

Computed Tomography (CT)

Connective tissue growth factor (CTGF)

Cyclin D1 (CCND1)

Cysteine rich angiogenic receptor-1 (CYR61)

Cytokeratin-19 (CK19, KRT19)

Cytoplasmic Activation/Proliferation Associated Protein 2 (CAPRIN2)

Delta Like Non-Canonical Notch Ligand-1 (DLK1)

Disheveled (Dvl)

Distant Metastases (M)

di-(2-ethylhexyl) phthalate (DEHP)

E-Cadherin (CDH1)

Embryonic stem cell (ES)

Epidermal growth factor receptor (EGFR)

Epithelial cell adhesion molecule (EPCAM)

Extrahepatic abdominal disease (E)

Familial Adenomatous Polyposis (FAP)

Fanconi Anemia (FA)

Fibroblast Growth Factor (FGF)

Forkhead box A1 (FOXA1)

Forkhead box A2 (FOXA2)

Forkhead box protein M1 (FoxM1)

Frizzled (FZD)

Fumarylacetoacetate (FAH)

Gastrointestinal (GI)

GATA Binding Factor (GATA)

Gene set enrichment analysis (GSEA)

Glioma-associated oncogene homolog 1 (Gli1)

Glycogen synthase kinase 3 β (GSK3 β)

Glypican 3 (GPC3)

G-protein coupled receptor (GCPR)

G-protein coupled receptor 180 (GPR180)

G-protein Coupled Receptor HPR177 (Wntless)

Green fluorescent protein (GFP)

H19 Imprinted Maternally Expressed Transcript (H19)

Hedgehog interacting protein (HHIP)

Hepatic Veins (V)

Hepatoblastoma (HB)

Hepatocellular Carcinoma (HCC)

Hepatocyte nuclear factor 1 alpha (HNF1 α)

Hepatocyte nuclear factor 1 beta (HNF1 β)

Hepatocyte nuclear factor 4 alpha (HNF4 α)

Hepatocyte nuclear factor 4 gamma (HNF4 γ)

Hepatocyte-Like Hepatoblastoma Cells (hbHeps)

Homeobox Nanog (Nanog)

HRAS Proto-Oncogene, GTPase/HRAS

Hydrodynamic Injection (HDI)

Hydroxysteroid 17-beta dehydrogenase 6 (HSD17B6)

Inferior Vena Cava (IVC)

Ingenuity pathway analysis (IPA)

Insulin-Like Growth Receptor-II (IGF2)

Integrin Alpha 6 (ITGA6)

Interleukin 6 (IL-6)

Internal ribosomal entry site (IRES)

International Childhood Liver Tumor Strategy Group (SIOPEL)

Intrahepatic cholangiocarcinoma (ICC/CCA)

Involvement of the Inferior Vena Cava (IVC)

Jagged-1 (JAG1)

KRAS Pro-Oncogene, GTPase (KRAS)

Large Tumor Suppressor Kinase 1/2 (LATS 1/2)

Low density lipoprotein receptor-related protein 5/6 (LRP5/6)

Lysophosphatidic acid (LPA)

Lymph Node Metastases (N)

Macrophage stimulating 1 (MST1/2)

Macrophage stimulating 1 receptor (MST1R)

Magnetic Resonance Imaging (MRI)

Major urinary protein (MUP)

MCL Apoptosis Regulator, BCL2 Family Member (MCL-1)

MDM2 proto-oncogene (MDM2)

Messenger RNA (mRNA)

MET Proto-oncogene Receptor Tyrosine Kinase (MET)

microRNA (miRNA)

Mitogen Activated Protein Kinase (MAPK)

Mps one binder 1a (MOB1A)

MYC Proto-Oncogene, BHLH Transcription Factor (MYC)

N-acetylgalactosamine (GalNAc)

Neonatal Intensive Care Unit (NICU)

Nitisione (NTBC)

Notch Receptor 1 (Notch1)

Nuclear Factor Erythroid 2 Like 2 (NFE2L2)

Nuclear Receptor Binding SET Domain Protein 1 (NSD1)

OCIA domain containing 2 (OCIAD2)

Olfactory Receptor Family 5 Subfamily 1 Member 1 (ORF11)

One cut homeobox 1(Onecut1)

One cut homeobox 3 (Onecut3)

Ornithine aminotransferase (OAT)

Overall Survival (OS)

Paired box 3 (PAX3)

Paternally Expressed Protein Gene 3 (PEG3)

Phosphatidylinositol 3-kinase/protein kinase B (PI3K/AKT)

Poly (ADP-ribose) polymerase family, member 6 (PARP6)

Porcupine (PORCN)

Portal Vein Involvement (P)

Positron Emission Tomography (PET)

POSTreatment Extent of Disease (POSTEXT)

PREtreatment Extent of Disease (PRETEXT)

Promyelocytic Leukemia Protein-Retinoic Acid Receptor α (PML-RAR α)

RAD17 Checkpoint Clamp Loader Component (RAD17)

Ras association domain family I isoform A (RASSF1A)

Retinoid X receptor alpha (Rxra)

Reverse tetracycline transactivator (rtTA)

RNA induced silencing complex (RISC)

RUNX Family Transcription Factor (RUNX)

Salvador-Hippo-Warts Pathway (Hippo)

Secreted frizzled related protein 1 (SFRP1)

Secreted frizzled related protein 5 (SFRP5)

Short-hairpin RNA (shRNA)

Signal transducer and activator of transcription 3 (STAT3)

Single guide RNA (sgRNA)

Sleeping Beauty (SB)

Sleeping Beauty Transposase rtTA (SB-rtTA)

SMAD Family member4 (SMAD4)

Small interfering RNA (siRNA)

Speckle Type POZ Protein (SPOP)

Sphingosine 1-phosphophate (S1P)

Suppressor of cytokine signaling (SOSC1)

T-box 3 (TBX3)

T-box 5 (TBX5)

T-cell factor/lymphoid enhancer factor (TCF)

Telomerase Reverse Transcriptase (TERT)

Tetracycline inducible-ON (TET-ON)

Topoisomerase 2-alpha (TOP2A)

Transcription factor CP2 (TFCP2)

Transcriptional co-activator with PDZ-binding motif (TAZ)

Transcriptional enhancer factor TEF-1/TEA domain family member (TEAD/TEFs)

Transforming Growth Factor β (TGF β)

Transgenic-rtTA (Tg-rtTA)

Tribbles Pseudokinase 2 (TRIB2)

Tumor focality (F)

Tumor protein p73 (p73)

Tumor necrosis factor (TNF)

Tumor Rupture (H)

Tumor suppressor p53 (TP53)

Tyrosine kinase inhibitor (TKI)

Ultrasound sonography (US)

Very high birth weight (VHBW)

Very low birth weight (VLBW)

Vestigial Like Family Member 4 (VGLL4)

Vimentin (VIM)

Wild-type (WT)

Wingless-type MMTV integration site family (WNT)

Yes-Associated Protein 1 (YAP1)

PREFACE

All pediatric cancers are “orphan diseases.” By definition, in the United States an orphan disease affects less than 200,000 people per year. The relative rarity of orphan diseases challenges researchers and patients alike. Rare disease exploration and subsequent management is difficult due to a lack of biomedical models, understanding of disease pathogenesis, and consequently a shortage of evidence-based treatments. For orphan disease patients and their family members, “rare” is their everyday.

Experience truly is the best teacher. In my clinical training, I have witnessed the frustration and confusion of rare disease management. In my second year of graduate school, “witnessing” transitioned to “experiencing”. My family has now personally experienced life with a rare cancer. My combined experiences now as a medical student, caregiver, and family advocate have enriched my science, provided critical motivation, and clarified my understanding of rare disease research.

Rapid improvements in genetic profiling, *in vivo* modeling, and rational drug design have put new treatments within reach for the nearly 30 million people with rare diseases. In this dissertation, I set out to utilize rapid *in vivo* modeling to identify a new tractable therapeutic strategy for the rare pediatric liver cancer, hepatoblastoma. Typically, children under the age of five are diagnosed with

hepatoblastoma. Optimization of chemotherapeutic regimens has drastically improved survival; however, the five year overall survival rate for Stage IV tumors remains at 27%. Further, the use of chemotherapeutics in children has life-long toxicities like hearing loss, heart damage, and risk of future cancers. Thus, my goal was to identify new anti-cancer targets in hepatoblastoma to reduce reliance on chemotherapeutics, and improve survival in children with aggressive disease.

Herein, I develop a new conditional genetic mouse model of hepatoblastoma that mimics the poor prognosis subtype most in need of new therapeutics. I find that hepatoblastoma tumors are remarkably sensitive to loss of one oncogenic protein, YAP1. Specifically, YAP1 loss provides greater than >90% tumor regression, and long-term survival. I propose that targeting YAP1 may satisfy the unmet clinical need for hepatoblastoma therapy.

CHAPTER I INTRODUCTION

Successful treatment of neoplastic lesions requires an intimate understanding of what defines, drives, and maintains a cancer cell. Over the last forty years, clinicians and researchers alike have made substantial progress towards understanding the vast complexity existing between the greater than 100 types of human cancer (3).

Despite the many tissue-specific differences, most adult cancers do share unifying features. Hanahan and Weinberg famously proposed several characteristics that collectively define and drive malignancy, termed the “*Hallmarks of Cancer*.” Described by Hanahan and Weinberg in 2000, the six defining *Hallmarks of Cancer* include (**Figure 1.1**): “self-sufficiency in growth signals, insensitivity to growth-inhibitory (antigrowth) signals, evasion of programmed cell death (apoptosis), limitless replicative potential, sustained angiogenesis, and

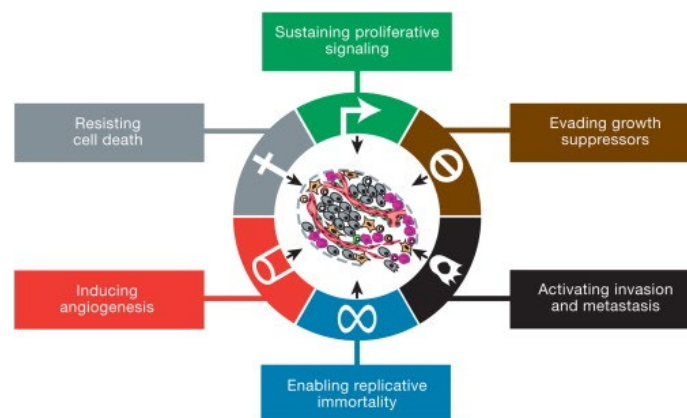


Figure 1.1 Hallmarks of cancer. The “Hallmarks of Cancer” are unifying characteristics found in most neoplasms, regardless of tissue origin. *Re-used with permission from Hanahan, Weinberg (2011).*

tissue invasion and metastasis” (3). Particularly for rare cancers, including pediatric cancers, the “Hallmarks” remain under-investigated. In this dissertation, I focus on the predominant pediatric liver cancer, hepatoblastoma.

In *Chapter I Introduction*, I propose the “Hallmarks of Hepatoblastoma”, the defining molecular and clinical characteristics, of the most common pediatric liver tumor. *Chapter I* provides critical context to understand the need for hepatoblastoma targeted therapeutics. Specifically, I discuss hepatoblastoma incidence, clinical presentation, management and disease pathogenesis. Further, I detail what is understood about the regulation of hepatoblastoma tumor initiation, and maintenance. Finally, I discuss emerging liver cancer biology that may underlie strategies for future treatment of hepatoblastoma.

Chapter 1.1 Liver Cancer Primer

Adult and pediatric liver cancer share some features including genetic perturbations in the Wnt/ β -catenin pathway and significant mortality (4); however, adult and pediatric liver tumors are distinct entities. Despite arising from the same organ, adult and pediatric liver cancer differ on several key points including disease etiology, tumorigenesis, mutational burden, and clinical management. Consequently, clinicians and researchers should treat, and study liver tumors treated in context. To provide the necessary framework for investigation of pediatric liver cancer, herein, I will briefly introduce the epidemiology, molecular pathogenesis, and treatment of adult liver cancer.

Hepatocellular carcinoma (HCC) is the predominant primary adult liver cancer, the sixth most common cancer, and third leading cause of cancer-related death (5). Unlike pediatric liver cancer, adult liver cancer tumorigenesis is more heavily linked to behavioral, environmental, and infectious exposures. In contrast to pediatric cases, most cases of HCC develop from a fibrotic, fatty, and/or cirrhotic disease state. Cirrhosis can result from hepatitis infection, alcohol, obesity and diabetes mellitus (6-8).

Tumorigenesis in adult HCC remains a poorly understood complex process; further, most patients exhibit multiple genetic perturbations (9). The most common activating mutations occur in the proto-oncogenes Telomerase Reverse Transcriptase *TERT* (70%), *CTNNB1* (30%) and loss of function mutations in the

tumor suppressor p53 *TP53* (30%) (**Figure 1.2**) (9-13). Compared to pediatric hepatoblastoma where most cases have 2.9-3.9 mutations per tumor (14, 15), HCC has a significantly higher mutational burden. Most HCC patients present with >40 non-synonymous mutations per tumor (16). Thus, pediatric liver tumors are

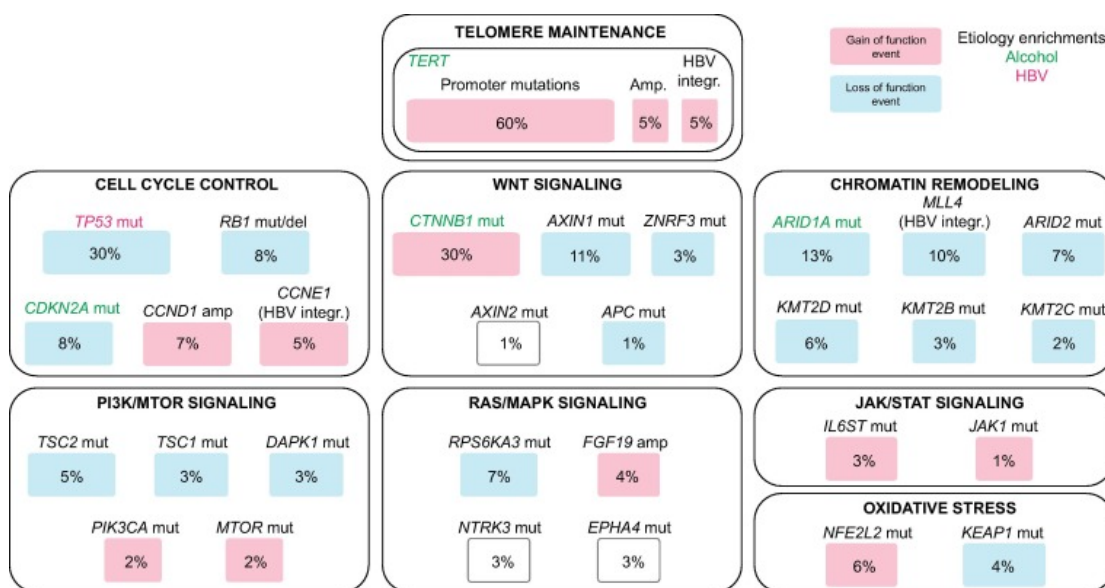


Figure 1.2 Common mutations in adult hepatocellular carcinoma.

Most common mutations in adult HCC: *TERT* (70%), *CTNNB1* (30%), and *TP53* (30%).

Adapted with permission from Schulze et al, (2016).

genetically “simpler” than adult tumors. The relative simplicity of pediatric lesions is advantageous for *in vivo* modeling; this is further discussed in *Chapter 1.5 Laboratory Models and 5.1 Mouse Models of Hepatoblastoma*.

Strikingly, in adult HCC co-occurrence of *TP53* and *CTNNB1* mutations is rare, suggesting distinct molecular lineages of HCC (9, 10). Similarly, in pediatric hepatoblastoma, co-occurrence of *TP53* and *CTNNB1* mutations is uncommon

(15). The mutational profile of hepatoblastoma is discussed further in *Chapter 1.4 Molecular Profiling of Hepatoblastoma*.

Adult and pediatric liver cancer frequently contain activating mutations in *CTNNB1*, and in other members of the Wingless-type MMTV integration site family (Wnt) pathway. *CTNNB1* codes for the protein β -catenin, a major mediator of the Wnt pathway. Wnt pathway activation occurs following binding of Wnt growth factor to membrane receptors, Frizzled (FZD) and Low-density lipoprotein receptor-related protein 5/6 (LRP5/6). Following activation, the receptor complex inactivates the β -catenin destruction complex via binding of Axin and Disheveled (DVL). Binding of DVL and Axin allows β -catenin to translocate to the nucleus and act as a transcriptional co-activator (17). β -catenin does not contain a DNA binding domain; therefore, it partners with other transcription factors to promote gene expression. For a more thorough review of Wnt signaling, please reference *Appendix III Review of Canonical Wnt Signaling*.

In both adult and pediatric liver cancer, constitutively active β -catenin supports tumorigenesis through expression of target genes like Proto-Oncogene C-Myc (*MYC*) and Cyclin D1 (*CCND1*). *MYC* and Cyclin D1 promote proliferation and cell cycle progression. *Chapter 1.8 Liver Tumorigenesis* further discusses the role of Wnt signaling in liver tumorigenesis.

Yes-Associated Protein-1, or YAP1 also contributes to disease pathogenesis of both adult and pediatric liver cancer (18-28). YAP1 is a key

signaling component of the Salvador-Hippo-Warts (Hippo) pathway. The Hippo pathway plays an essential role in controlling organ size, stemness, and proliferation (19-22, 25, 29, 30). When Hippo is ON, the Large Tumor Suppressor Kinase 1/2 (LATS 1/2) phosphorylates YAP1. Phosphorylation retains YAP1 in the cytoplasm; consequently, YAP1 is rendered inactive and targeted for proteasomal degradation. When Hippo is OFF, YAP1 translocates to the nucleus and acts as a transcriptional co-factor (19). Similarly, to β -catenin, YAP1 also does not have a DNA-binding domain. For a detailed review of Hippo signaling, reference *Appendix IV Review of Canonical Hippo Signaling*.

Up to 50% of adult HCC cases have nuclear YAP1. Further, YAP1 activation in HCC has been associated with poor prognosis (26, 28). Unlike hepatoblastoma, where YAP1 and β -catenin activation cooperate to promote tumorigenesis (31), adult HCC is more responsive to YAP1 inhibition in the absence of *CTNNB1* mutations (23). *Chapter V* discusses possible hypotheses for the observed contextual differences in YAP1 tumor dependency between adult and pediatric liver cancer. Nevertheless, understanding YAP1's differential role in adult and pediatric liver cancer requires further investigation.

For adult and pediatric liver cancer patients with limited disease, surgical resection is standard of care and affords the greatest odds of survival (32-34). For adult HCC patients that fit surgical criteria, resection offers a five-year overall survival (OS) rate of nearly 60%; however, surgical resection is not considered

curative. A majority of surgical patients with HCC relapse within five years (35).

Conversely, surgical resection can be curative in children with a low risk histologic subtype hepatoblastoma. The five-year OS rate for completely resectable lesions with pure fetal histology approaches 100% (See *Chapter 1.3, Histologic Subtypes of Hepatoblastoma*) (36-38). Liver transplantation has similar rates of five-year OS in candidate adults and children with non-metastatic disease, but donor supply limits this therapeutic option for many patients (See *Chapter 1.3 Liver Transplantation*) (35, 39-42).

Systemic therapy for liver cancer varies substantially between pediatric and adult cohorts. Systemic chemotherapy with cytotoxic agents, i.e. doxorubicin, cisplatin, gemcitabine, has shown limited efficacy in adult populations, and is no longer administered as first line therapy (43-45). Currently, the tyrosine kinase inhibitor (TKI) Sorafenib is first line for systemic therapy in adult HCC; however, its' survival benefit is modest. Sorafenib extends the overall survival from approximately 8 months to 12 months in adult patients (46). Unlike adult medical management, systemic chemotherapy remains first line for the treatment of pediatric liver cancer, a point that will be further explored in *Chapter 1.3 Clinical Prognosis and Treatment* (47-49).

Subtypes of Pediatric Liver Cancer

Childhood cancers account for 1% of all malignancies (4, 50-52). In the United States, there are an estimated 12,000 new cases of pediatric cancer annually. Pediatric liver cancer remains rare, comprising less than 2% of the 12,000 cases of childhood cancer. Accordingly, all pediatric cancers, including pediatric liver cancer, earn orphan disease classification. Orphan diseases are rare health conditions that collectively affect less than 200,000 individuals per condition in the United States (53, 54). Even the most common pediatric liver cancer, hepatoblastoma, presents with approximately 100 cases per year (55). For more information on the epidemiology of hepatoblastoma, please reference *Chapter 1.2 Epidemiology of Hepatoblastoma*.

Perhaps unsurprisingly, clinicians and researchers face considerable challenges trying to define, study, and successfully treat pediatric liver tumors due to the relatively few children presenting yearly with liver masses. In 2011, the Children's Oncology Group (COG) sponsorship of an "*International Pediatric Liver Tumor Consensus Classification*" provided the critical opportunity to establish diagnostic classification and consensus of pediatric liver tumors (56). An important conclusion from this effort was that even seasoned pediatric pathologists encountered difficulty in securing diagnostic consensus. Difficult diagnostic consensus highlights the plasticity and diversity of liver neoplasms, a point that will

be echoed in upcoming chapters (See *Chapter 1.7 Liver Differentiation, Chapter 1.8 Liver Tumorigenesis*).

Pathologists divide liver masses by cell of origin, or malignant potential. The majority of pediatric liver masses, whether primary or secondary, are malignant (57, 58). On histopathologic examination, approximately 30% of masses are

Classification of Pediatric Liver Masses

<i>Cell of Origin</i>	<i>Benign</i>	<i>Malignant</i>
<i>Epithelial</i>		
Hepatocyte	Adenomatosis Focal Nodular Hyperplasia Macro-regenerative Nodule	Hepatocellular Hepatoblastoma
Bile Duct Cell	Adenoma Hamartoma	Cholangiocarcinoma Mixed, Hepatocellular Cholangiocarcinoma
<i>Mesenchymal</i>		
Vascular	Hemangioma	Epithelioid Hemangioendothelioma Angiosarcoma
Other	Mesenchymal Hamartoma Pecoma	Embryonal Sarcoma Rhabdomyosarcoma
<i>Germ Cell</i>		Teratoma Yolk Sac Tumor

Table 1.1. Classification of pediatric liver masses. Pediatric liver tumors are classified by cell of origin: epithelial, mesenchymal, or germ cell. *Classification shown adapted with permission from the Children's Oncology Group (COG) liver tumor consensus (Lopez-Terrada et al, 2013).*

reported as benign. Benign diagnoses include adenoma, focal nodular hyperplasia, vascular tumors and mesenchymal hamartomas (**Table 1.1**) (57).

Of the nearly 2/3 of pediatric liver tumor cases that are malignant, approximately 70% are classified as tumors arising from hepatocytes or hepatocyte precursors including hepatoblastoma, and hepatocellular cancer (57). Other malignant liver neoplasms include tumors arising from bile duct cells, mesenchymal cells, germ cells and secondary neoplasms metastasized to the liver (**Table 1.1**).

Hepatoblastoma is the most common malignant pediatric primary liver tumor, typically occurring in children under 3-5 years of age (40-42). While considered an epithelial tumor, the cell of origin in hepatoblastoma remains contested. To this point, most children with hepatoblastoma present with mixed histology in their tumors including mesenchymal, and undifferentiated features (see *Chapter 1.3 Histologic Subtypes of Hepatoblastoma*) (56). The remaining chapters will focus exclusively on hepatoblastoma.

Chapter 1.2 Epidemiology of Hepatoblastoma

Incidence and Associations

Careful analysis of affected populations, associated genetic syndromes, and risk factors can provide needed insight into the molecular pathogenesis of hepatoblastoma. Nearly 80% of malignant liver masses in children, under 16 years of age, are hepatoblastoma (59). For children under the age of five, the percentage of liver masses identified as hepatoblastoma increases to 91% (60).

Approximately 100 cases of hepatoblastoma occur per year in the United States, and the incidence increased 4.3% yearly from 1992-2004 (59-61). The 4.3% increase in incidence outpaced any other childhood cancer for this same time period (52, 61). Clues as to the cause of increased incidence from 1992- 2004 are lacking, but some have speculated increasing incidence may be linked to more

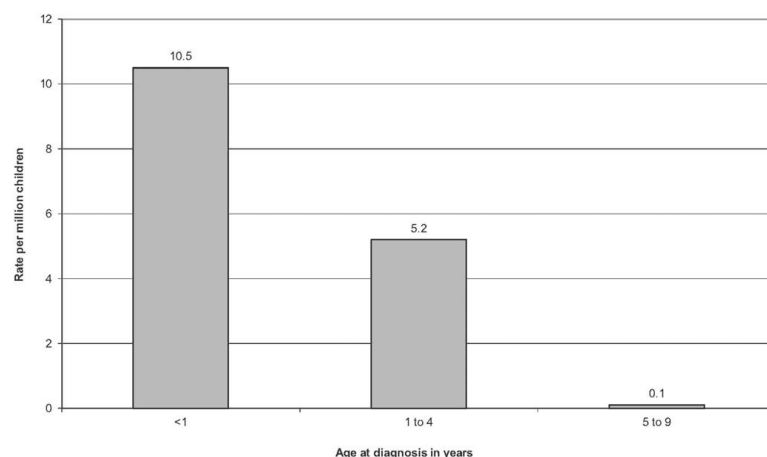


Figure 1.3 Incidence of hepatoblastoma by age. United States SEER Program 2004–2008 data for hepatoblastoma incidence. *Re-used with permission from Spector et al, 2012.*

frequent premature births (*see Chapter 1.2 Risk Factors*) (62-66).

Currently, the age-standardized rate internationally is 2.5 cases of hepatoblastoma per million children under 18 years of age. This is an increase from the 1.5 cases per million children in 2004 (67). While the incidence of hepatoblastoma is still increasing, the *rate* of increase has slowed. Between 2000 and 2015, hepatoblastoma incidence increased at a rate of approximately 2.2% per year (33, 34). A rate of 2.2% is down from the 4.3% increase in incidence observed between 1992-2004. From 2000-2015, Feng et al observed the increased incidence of hepatoblastoma more frequently in males, children ages 2-4 years old, and in African American children (33). Understanding the factors driving fluctuation of incidence requires further investigation.

If the cohort of children diagnosed between 2000 and 2015 is narrowed to include just children under the age of 1, the incidence increases to 10.5 cases per one million children (**Figure 1.3**) (61). The increased incidence of hepatoblastoma in very young children (>1-year-old) suggests that tumor initiation may begin *in utero*. Indeed, the literature contains multiple case reports of hepatoblastoma detected *in utero* (68-72) (*See Chapter 1.6 Liver Development*).

Genetic Syndromes

Genetic syndromes account for an estimated 15% of all hepatoblastoma cases (73). In a small subset of genetic disorders, hepatoblastoma risk increases

compared to the general population. These disorders include: Familial Adenomatous Polyposis (FAP), Beckwith-Wiedemann Syndrome (BWS), Simpson-Goblai-Behmel, and Sotos Syndrome (**Table 1.2**) (61, 73-76). Trisomy 18 also increases the risk of hepatoblastoma (61, 73-76).

Familial Adenomatous Polyposis (FAP) Syndrome is an inherited autosomal dominant syndrome, where affected patients have a mutation in the Adenomatous Polyposis Coli (*APC*) tumor suppressor gene. *APC* functions in the Wnt Pathway with Axin as a scaffold protein to target β -catenin for proteasomal degradation (See *Appendix III*) (77-82). Individuals with FAP develop numerous colorectal polyps by adolescence, and colorectal cancer (CRC) by adulthood.

<i>Risk Factors</i>	<i>Syndrome</i>	<i>Mutation</i>
Genetic Syndromes (assx with 15% of cases)	<i>Familial Adenomatous Polyposis</i>	Adenomatous Polyposis coli (<i>APC</i>)
	<i>Beckwith-Wiedemann</i>	Imprinting on chromosome band 11p15.5 at loci H19 and IGF2
	<i>Simpson-Goblai-Behmel</i>	Glypican 3 (<i>GPC3</i> mutation)
	<i>Sotos Syndrome</i>	Nuclear Receptor Binding SET Domain Protein 1 (<i>NSD1</i>) mutation
	<i>Constitutional Trisomy 18</i>	Three copies of chromosome 18

Table 1.2 Genetic syndromes with increased hepatoblastoma risk. Genetic Syndromes and associated mutations.

Individuals with FAP also experience increased risk of developing hepatoblastoma in childhood. Specifically, children with FAP are at 750-7500x greater risk than the general population for hepatoblastoma. As many as 8% of children with hepatoblastoma have a family history of FAP (83-87). Notably, children without a history of FAP, but with germline mutations in *APC*, also experience increased risk of developing hepatoblastoma in early childhood (88). This may be unsurprising given the predominance of β -catenin mutations in Hepatoblastoma patients' tumors (>80%) (see *Chapter 1.4 Genetic Alterations, Appendix III*).

Beckwith-Wiedemann Syndrome (BWS), caused by defective imprinting on chromosome 11, is another congenital disorder that confers approximately a 2000x fold increase in hepatoblastoma (73, 89). Children with overgrowth syndromes, like BWS, experience high birth weights, umbilical hernias and increased risk of other malignancies. Specifically, in BWS, children have altered imprinting at locus 11p15.5 which encodes for Insulin-like Growth Factor-II (*IGF2*) and *H19* Imprinted Maternally Expressed Transcript (*H19*). Paternal alleles normally express *IGF2*, whereas maternal alleles express *H19* (89).

Early reports suggested that imprinting was maintained in hepatoblastoma and therefore did not likely play a role in tumorigenesis (90, 91). More recent work has challenged this view showing loss of imprinting and epigenetic alternations at multiple loci in hepatoblastoma, including the 11p15.5 loci for *H19* and *IGF2*.

Interestingly loss of imprinting at *IGF2* and *H19* in hepatoblastoma occurs in children with and without BWS (89, 92-96).

Similarly, to BWS, other overgrowth syndromes, i.e. Sotos Syndrome, and Simpson Goblai Behmel Syndrome, increase hepatoblastoma risk. Children with overgrowth syndromes should be screened every three months after birth for malignancy (97). Of note, hepatoblastoma overexpresses the mutated gene in Simpson Goblai Behmel syndrome, Glypican-3 (*GPC3*). Indeed, *GPC3* staining in hepatoblastoma samples signals stemness and disease aggressiveness (See *Chapter 1.4 MicroRNA Regulation, Chapter 1.8 Liver Tumorigenesis*) (98). Understanding how the underlying genetic aberrations and pathology of overgrowth syndromes contribute to hepatoblastoma tumorigenesis requires future investigation.

Risk Factors

Genetic syndromes only account for 15% of hepatoblastoma cases, suggesting unknown genetic, environmental, or iatrogenic causes contributing to tumorigenesis. The etiology of hepatoblastoma remains unclear, but some work has suggested very low (VLBW) or very high birthweight (VHBW), maternal body mass index (BMI), young maternal age, parental smoking, infertility treatments, and neonatal intensive care unit (NICU) iatrogenic exposures increases hepatoblastoma risk (**Table 1.3**).

RISK FACTORS

*Birth weight**Maternal obesity***Young maternal age***Maternal/ Paternal smoking***Infertility treatment***Neonatal intensive care exposures*

Table 1.3 Hepatoblastoma risk factors. Risk factors demonstrated to increase risk of hepatoblastoma *Conflicting reports

Birth Weight and NICU Exposures

Since the 1990s, multiple investigators across multiple populations reported that low (>2500g) or very low (>1000g) birth weight (VLBW) increases risk of hepatoblastoma; to that end, the association between low birth weight and hepatoblastoma is the only uncontested risk factor (62-64, 66, 99-103). As discussed in the previous section on genetic risks, congenital high birth weight from overgrowth syndromes (i.e. BWS, Sotos Syndrome, Simpson-Goblai) also predisposes children to hepatoblastoma (**Table 1.2, Table 1.3**) (97).

Many have speculated that the increasing incidence of hepatoblastoma observed since the 1970s may be related to the increasing survival of preterm, low birth weight babies, and associated iatrogenic exposures in neonatal intensive care units (NICUs) (52, 55, 100-104). The predominant theory is that preterm birth

contributes to hepatoblastoma tumorigenesis by delaying normal liver maturation, potentially increasing the number of liver progenitor cells. The cell of origin in hepatoblastoma is contested, but the prevailing theory claims that hepatoblastoma tumors arise from early liver progenitor cells, hepatoblasts, present in the embryonic liver (See *Chapter 1.6 Liver Development*).

To date, the causation between iatrogenic NICU exposures and hepatoblastoma has yet to be fully established (105, 106); however, some have suggested that increased exposure to di-(2-ethylhexyl)phthalate (DEHP), a common plasticizer in NICU medical equipment, promotes hepatoblastoma tumorigenesis (107). In animal models, DEHP exposure drives hepatocarcinogenesis (107, 108). Finally, there is some evidence that maternal pre-eclampsia further increases the risk of low birth weight, often resulting in further NICU exposures, and increased hepatoblastoma risk (106, 109). Nevertheless, if and how birth weight and NICU exposures accelerate hepatoblastoma tumorigenesis remains under investigated.

Maternal Obesity

Adiposity increases cancer incidence (110-112). At present, it appears that excess adipose tissue promotes tumorigenesis through a number of mechanisms including: increased growth factor signaling, increased availability of insulin, altered sex hormone regulation, and/or increased inflammation (111). McLaughlin

et al. found in a case control study in New York mothers that women clinically classified as overweight prior to pregnancy (BMI 25-29) were at 3X greater risk of having children with hepatoblastoma. Interestingly, weight gain during pregnancy did not increase the risk of hepatoblastoma (102). A more recent population study by Contreras et al. in California mothers did not recapitulate an increasing risk of hepatoblastoma with maternal obesity (113). Taken together these studies suggest, at best, a weak association of maternal obesity with hepatoblastoma

Young Maternal Age

McLaughlin's New York cohort study noted slightly increased risk of hepatoblastoma for both young (<20) and older mothers (>40) (102). In this population, the father's age did not increase nor decrease risk of hepatoblastoma (102). Conversely, two similar population-based studies, including the California Contreras study, did not find an increased risk of hepatoblastoma with maternal age (103, 113). To appreciate if maternal age increases risk of hepatoblastoma, population studies need larger sample sizes. Further, understanding if and how young maternal age promotes tumorigenesis requires additional investigation.

Maternal/Paternal Smoking

Similar to other contested risk factors with conflicting evidence (**Table 1.3**), the impact of parental smoking on hepatoblastoma risk remains controversial. Two reports have suggested that only *paternal* smoking is associated with increased

risk, and not *maternal* smoking (114, 115). To the contrary, others have suggested that any *parental* smoking increases hepatoblastoma risk (116). Recent reports suggest that parental smoking may increase the risk of hepatoblastoma by 1) oxidative DNA damage to sperm and/or 2) carcinogenic damage to the fetal liver *in utero* (102, 114, 116, 117).

Infertility Treatment

Infertility treatment, including assistive reproductive technologies like *in vitro* fertilization, may increase the overall risk of cancer in offspring; however, it remains unknown if infertility treatment itself promotes carcinogenesis, or if there is underlying pathology of infertility that predisposes offspring to cancer (118). For hepatoblastoma specifically, infertility treatment may not confer additional risk. Two studies find an increased risk of hepatoblastoma with infertility treatment (102, 118), while a majority of studies show no association (119-124).

The relative rarity of hepatoblastoma limits the power of most studies; consequently, researchers struggle to accurately detect reproducible associations and determine risk. To this point, nearly every hepatoblastoma risk factor reported remains contested including maternal age and weight, parental smoking, and iatrogenic causes. Clarity around the etiology of hepatoblastoma and its associated risk factors requires larger sample sizes through multi-center studies.

Chapter 1.3 Clinical Management of Hepatoblastoma

Clinical Presentation

History and Physical

As with other liver tumors, clinical presentation of hepatoblastoma varies substantially between patients. Hepatoblastoma tumors often remain asymptomatic until disease advances significantly, extending into multiple lobes of the liver, or metastasizing. Hepatoblastoma frequently metastasizes to the lungs. In as many as 50-70% of patients, surgeons cannot safely resect hepatoblastoma at time of diagnosis (47, 49). In advanced cases, children most often present to clinic with abdominal distension and constitutional signs and symptoms including: fatigue, abdominal pain, early satiety and anorexia (125, 126). Constitutional signs like anorexia and early satiety often reflect a mass effect of a large tumor compressing neighboring gastrointestinal organs. Rarely, children may also present with anemia, and osteopenia (127).

The causes of osteopenia are unknown in hepatoblastoma, but Towbin et al. proposed that osteopenia results from altered metabolism in tumorigenesis or an unknown paraneoplastic syndrome (127). Children rarely have bone metastases with hepatoblastoma; however, numerous reports detail children presenting for diagnosis of hepatoblastoma with abnormal bone scans and increased rate of fractures. In one retrospective study, approximately 18% of

children diagnosed with hepatoblastoma had fractures in the 50 days preceding diagnosis (127). In a subset of patients, bone abnormalities typically resolve with regression of disease. The resolution of osteopenia with tumor regression suggests that the tumor may directly alter bone metabolism (128).

Children rarely present with paraneoplastic syndromes at time of diagnosis. Symptoms including early puberty, hypertension, altered mental status or abnormal lab findings including hyper/hypocalcemia, and hypoglycemia warrant further evaluation (125, 127, 129-131).

Laboratory Findings and Imaging

Children with suspected malignant liver masses typically undergo a number of imaging exams and laboratory screenings. Magnetic Resonance Imaging (MRI) is preferred for visualization of liver masses, but often Computed Tomography (CT), Positron Emission Tomography (PET) or ultrasound sonography (US) are used alternatively or in conjunction with MRI (132). Using both CT and MRI, hepatoblastoma generally appears heterogenous (133).

Children typically present with 1-2 large masses, and tumors are radiologically staged by the Preoperative Evaluation of the Tumor Extent (PRETEXT) staging system (47, 48). The PRETEXT system will be discussed in greater detail in *Chapter 1.3 Clinical Treatment and Prognosis*. **Figure 1.4.** shows representative radiologic imaging of a child with hepatoblastoma. Because there

are multiple subtypes of liver masses in children (**Table 1.1**), accurate diagnosis and treatment planning requires histologic confirmation by biopsy (134).

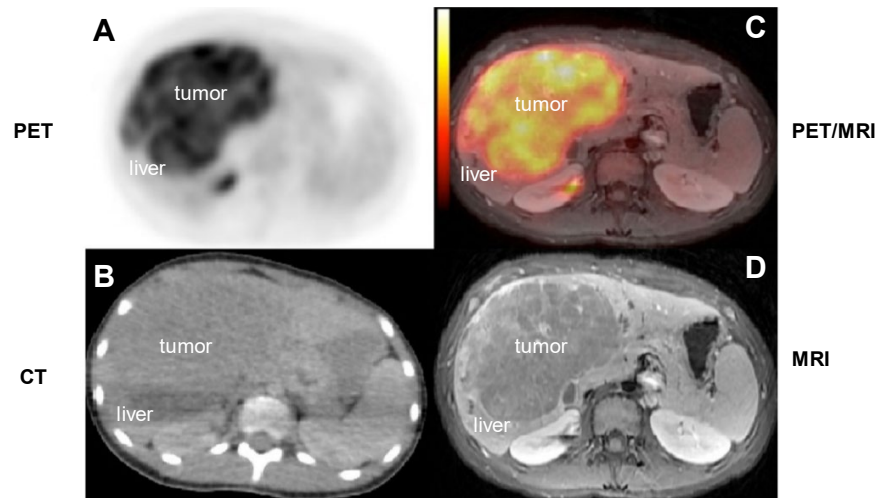


Figure 1.4 Radiologic imaging of hepatoblastoma. (A) PET, (B) CT (C) PET/MRI (D) Composite software generated images PET/MRI. Adapted with permission from Robertson et al, 2016.

If a diagnosis of hepatoblastoma is suspected in a child based on history and presentation, standard of care next requires a serum α -Feto-protein (AFP) level. The embryonic yolk sac, fetal liver and fetal gastrointestinal structures preferentially express AFP. Accordingly, AFP expression marks stem-like liver populations (47, 135-139).

At time of diagnosis, 90% of patients with hepatoblastoma have grossly elevated levels of AFP. A normal AFP level is <10 ng/ml (136). An AFP serum level $>263,000$ ng/mL is associated with reduced disease-free survival and poor prognosis (135). For the majority of patients with hepatoblastoma, serum AFP levels can help stratify patients into prognostic groups, and AFP levels generally

track with disease burden (See *Chapter 1.4 Molecular Profiling of Hepatoblastoma*) (47, 135-139). To this point, AFP levels that remain elevated following resection or systemic therapy may indicate residual disease or relapse (47, 136, 139).

Clinicians should carefully interpret serum AFP levels in an age-dependent manner. Because fetal and embryonic structures express AFP, neonates and premature infants may have elevated AFP in the absence of malignancy (135). Further elevated AFP may be observed in other conditions including hepatitis, cirrhosis, colitis, and immunodeficiency syndromes; thus, AFP elevation alone is insufficient for diagnosis of a malignancy (137).

Finally, an estimated 5-10% of children with hepatoblastoma have unexpectedly *minimally elevated* AFP serum levels (>100 ng/ml) or normal levels (<10 ng/ml). Minimally elevated levels of serum AFP often correlate with aggressive small cell undifferentiated histology (See *Chapter 1.3 Histologic Subtypes of Hepatoblastoma*) (140-143). Similar to children with grossly elevated levels of AFP (>263,000 ng/ml), these children typically have aggressive disease, and poor response to treatment (139, 141, 143, 144).

Histologic Subtypes of Hepatoblastoma

This section will review the Children's Oncology Group (COG) International Pathology Symposium Classification of hepatoblastoma tumors, introduced in

Chapter 1.1 Subtypes of Pediatric Liver Cancer (56). Pathologists classify hepatoblastoma broadly into epithelial histology or mixed histology containing epithelial and mesenchymal elements (osteoid, skeletal muscle, spindle cells, and cartilage). Frequently, children's tumors contain multiple histologic subtypes of hepatoblastoma; thus, correctly typing children's tumors requires adequate clinical sampling (56).

Fetal

On histologic analysis, well-differentiated, small, uniform cells with a low nucleus to cytoplasmic ratio comprise fetal hepatoblastoma (56, 57, 145) (**Table 1.4, Figure 1.5A**). In pure fetal histology, mitotic cells infrequently appear. Conversely, cytoplasmic glycogen, and lipid are frequently noted (56, 57, 145). For children with pure fetal histology, complete surgical resection is typically curative without adjuvant chemotherapy (See *Chapter 1.1 Liver Primer, Chapter 1.3 Clinical Treatment and Prognosis*) (36, 68).

Fetal, Mitotic

The fetal mitotic subtype is similar to the pure fetal subtype of hepatoblastoma but features mitotic or rapidly dividing cells (**Table 1.4, Figure 1.5B**). It is critical to differentiate between *Fetal* and *Fetal, Mitotic* histology. Per the COG hepatoblastoma treatment protocols, the *Fetal, Mitotic* subtype requires chemotherapy, and is not responsive to surgical resection alone (36, 48, 49, 56).

Histology	Subtype	Description	Clinical Features
Epithelial	Fetal	Well-differentiated, round nuclei, limited mitotic foci, more uniform in appearance, inconspicuous nuclei, clear nuclear membranes Figure 1.5A	Favorable Prognosis, responds to surgical resection alone
	Fetal, Mitotic	Clear nucleoli, mitotic foci, uniform, crowded, higher nuclear/cytoplasmic ratios, fine granular positivity for GPC3, Figure 1.5B	Requires surgical resection and chemotherapy
	Pleomorphic	Poorly differentiated, eosinophilic cytoplasm, high nuclear to cytoplasmic ratio, large nuclei, pronounced nucleoli, hyperchromatic Figure 1.5D	Associated with metastases and post-chemotherapy lesions
	Embryonal	Round, grow in sheets or form acinar/tubular structures, high nuclear to cytoplasmic ratio, scant cytoplasm, resemble 6w old gestational liver, Figure 1.5C	Most common subtype of hepatoblastoma
	Small Cell Undifferentiated	>50% of the size of normal hepatocytes, minimal pale cytoplasm, frequently found with other subtypes	Poor prognosis, Assx w/ paradoxically low serum AFP, often missed due to insufficient sampling
	Cholangioblastic	Presence of bile ducts, express CK19, can resemble the embryonal component, express nuclear β -catenin, Figure 1.5E	Common in post-chemotherapy tumors, prognosis unknown
	Macrotrabecular	Fetal or embryonal pattern where cells grow >5 thick trabeculae	Seen in less than 5% of cases, prognosis unknown
Mesenchymal Mixed	With Teratoid Features	Endoderm elements including neural components, melanin, squamous, glandular	Prognostic significance unknown
	Without Teratoid Features	Spindle cells, blastema, osteoid, skeletal muscle, cartilage,	20-30% of HB samples contain mixed mesenchymal elements

Table 1.4 Histologic subtypes of pediatric hepatoblastoma. Subtype and clinical features for the most common subtypes of hepatoblastoma. *Adapted with permission from Lopez-Terrada et al, 2013*

Pleomorphic

Children's tumors following chemotherapy and metastatic hepatoblastoma tumors frequently feature the pleomorphic subtype (**Table 1.4, Figure 1.5D**) (56, 145). Pleomorphic subtypes display regions of eosinophilic cytoplasm, large nuclei/nucleoli, and abnormal mitoses. Pleomorphic hepatoblastoma can resemble or co-occur with hepatocellular carcinoma. Whether pleomorphic histology portends poor prognosis is unknown and requires further investigation (56).

Embryonal

Most children's tumors contain the epithelial embryonal pattern of histology (56). Embryonal hepatoblastoma forms acinar or tubular structures. Further, embryonal hepatoblastoma resembles the early fetal (6 week to 8 week) liver (See *Chapter 1.6 Liver Development*). When compared to primary fetal histology, embryonal tumors display a higher nuclear to cytoplasmic ratio, more frequent mitotic regions, larger nuclei, and confer poorer prognosis. Treatment of embryonic histology always requires chemotherapy(1, 56, 57, 145).

Small Cell Undifferentiated

Small cell undifferentiated histology is an aggressive hepatoblastoma subtype paradoxically associated with low serum AFP and poor overall prognosis (47, 141, 143) (see *Chapter 1.3 Laboratory Findings and Imaging*). Small Cell

histology presents in nests of round cells typically smaller than lymphocytes. Small cell tumors have pale cytoplasm, and perhaps paradoxically, limited mitoses. The small cell histology sometimes presents in conjunction with other histologic components (47, 141, 143). The presence of any small cell regions warrants more aggressive systemic chemotherapy (See *Chapter 1.3 Clinical Treatment and Prognosis*) (**Table 1.4**) (56).

Cholangioblastic

Similar to the pleomorphic subtype, hepatoblastoma tumors post-chemotherapy also frequently present with the cholangioblastic subtype (**Figure 1.5E, Table 1.4**). Hepatoblasts, the presumed cell of origin for hepatoblastoma, retain the ability to differentiate into bile-duct cells (See *Chapter 1.6 Liver Development, Chapter 1.8 Liver Tumorigenesis*). Accordingly, in cholangioblastic hepatoblastoma, some of the tumor cells may de-differentiate into pseudo-cholangiocytes (bile duct cells). Cholangioblastic regions stain positive for classic bile duct markers like cytokeratin-19, CK19. The prognostic significance of cholangioblastic regions is unknown; however, elevated expression of CK19 associates with poor clinical outcomes (See *Chapter 1.4 Molecular Profiling of Hepatoblastoma*) (1, 56).

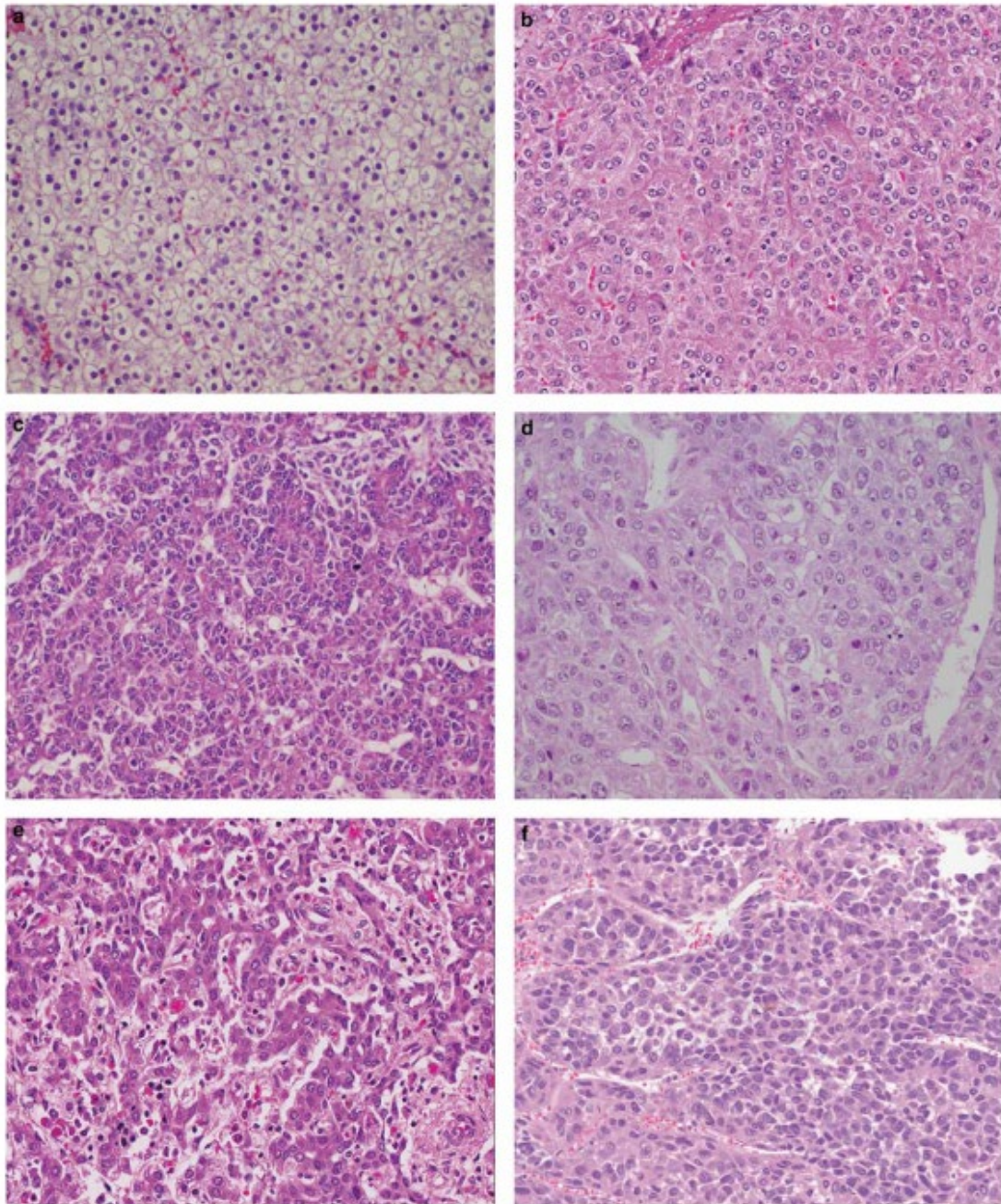


Figure 1.5 Subtypes of pediatric hepatoblastoma. **A)** Well-differentiated fetal hepatoblastoma, **B)** Crowded Mitotically Active Fetal Pattern **C)** Embryonal, **D)** Pleomorphic, **E)** Cholangioblastic, **F)** Macrotrabecular. *Adapted with permission from Lopez-Terrada et al, Modern Pathology, 2014.*

Epithelial Macrotrabecular

Less than <5% of documented hepatoblastoma cases present with the macrotrabecular subtype. Macrotrabecular histology indicates a redundant structure of either fetal or embryonal like cells formed in trabeculae of 10-20+ cells (**Figure 1.5F, Table 1.4**) (145). Often the histology appears to mimic HCC. Clinical information documenting the course of children with predominant macrotrabecular histology is limited; however, some reports suggests the prognosis is unfavorable (1, 56).

Mixed Epithelial

Up to 30% of hepatoblastoma cases present with mesenchymal/stromal features including spindle cells, skeletal muscle, cartilage, and osteoid. Occasionally, hepatoblastoma tumors also feature endodermal/teratoid components, like melanin. Thus, a “mixed” designation refers to a hepatoblastoma case with epithelial and stromal elements. How and if the presence of stromal elements impacts the patient’s disease course warrants consideration (56, 57).

Clinical Treatment and Prognosis

Clinical Staging

As with other tumor types, the goal of clinical staging for hepatoblastoma is to 1) *evaluate the extent of disease*, 2) *to assess disease aggressiveness and risk*,

and 3) to determine the appropriate course of treatment. Discussed briefly in *Chapter 1.1 Liver Cancer Primer*, surgical resection provides the greatest chance of survival for children with hepatoblastoma, and adults with other forms of liver cancer (32-34, 49). With the goal of resection at the forefront, the International Childhood Liver Tumor Strategy Group (SIOPEL) developed staging guidelines, termed PRETEXT (**Figure 1.6**) (146-148). Following surgical resection and/or chemotherapeutics, clinicians reevaluate children's tumors using POSTtreatment Extent of Disease, POSTTEXT (**Figure 1.6**).

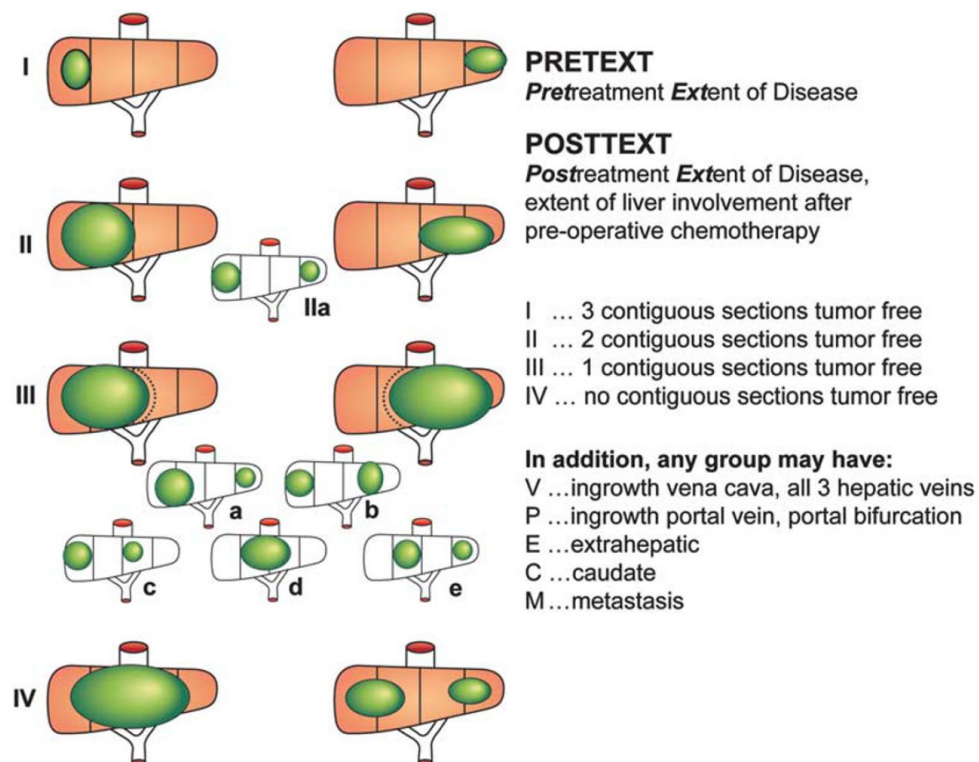


Figure 1.6 PRETEXT, POSTTEXT clinical staging. PRETEXT and POSTTEXT staging systems used to classify patients' hepatoblastoma. Adapted with permission from Lopez-Terrada et al, *Modern Pathology*, 2014.

PRETEXT describes the burden and localization of liver disease before treatment using Couinand's segmentation of the liver as a scaffold (**Figure 1.6**) (48, 139, 146, 149). PRETEXT staging and risk stratification relies on quality clinical imaging of the liver, described in *Chapter 1.3 Laboratory Findings and*

PRETEXT Designation	5y OS	Definition	Clinical Associations
Stage I	90%	One section involved, three free	Favorable prognosis, small proportion of patients, unifocal tumors, traditional surgical candidates
Stage II	83%	Two sections involved, two free	Favorable prognosis at time of diagnosis
Stage III	73%	Three sections involved, one free	Most children present as PRETEXT III
Stage IV	52%	Four sections involved	Unifocal tumors uncommon, Marker of poor prognosis
Criteria V	51%	Involvement of all three hepatic veins or the IVC	Marker of poor prognosis at time of diagnosis
Criteria P	49%	Right and Left portal vein involvement	Marker of poor prognosis at time of diagnosis
Criteria E	53%	Extrahepatic Tumor	Marker of poor prognosis at time of diagnosis
Criteria F	52%	Multifocal Tumors	Marker of poor prognosis at time of diagnosis
Criteria H	51%	Tumor Rupture	Marker of poor prognosis at time of diagnosis
Criteria M	41%	Distant Metastases	Marker of poor prognosis at time of diagnosis

Table 1.5 PRETEXT designations and overall survival. PRETEXT Staging with five-year overall survival rates, and clinical associations

Imaging (132, 133, 150) (**Figure 1.4**). PRETEXT staging stratifies children into four major groups: PRETEXT I, PRETEXT II, PRETEXT III, and PRETEXT IV.

Each child's case is further annotated to describe invasion into the vasculature, and extrahepatic/metastatic lesions (**Figure 1.6**) (48, 139, 146, 149). The extent of vascular invasion significantly impacts a tumors probability of resection. Imaging does have limitations, and determining the extent of vascular involvement relies heavily on radiologic acumen (132, 150).

PRETEXT I staging signifies favorable prognosis, with a five-year OS of 90% (**Figure 1.7, Table 1.5**) (151, 152). PRETEXT I defines only a small group of children at time of diagnosis. PRETEXT I tumors localize to one section of the liver and are unifocal (**Table 1.5**). Similarly, to PRETEXT I tumors, PRETEXT II tumors are limited to either the right side or left side of the liver. Further the majority of PRETEXT II tumors are also unifocal; however, unlike PRETEXT I, PRETEXT II tumors only leave *two* contiguous sections of the liver free (**Figure 1.6, Table 1.5**). Children with PRETEXT II tumors have a five year OS rate of 83%, slightly less than children with PRETEXT I tumors (**Figure 1.7, Table 1.5**) (151, 152).

Children most frequently present with PRETEXT III tumors. When unifocal, PRETEXT III tumors spare only one section of the liver (147). The PRETEXT III 5-year OS rate is 73% (**Figure 1.7, Table 1.5**) (151, 152). Unlike PRETEXT I-III, PRETEXT IV tumors are more frequently multifocal, and the five-year OS reflects

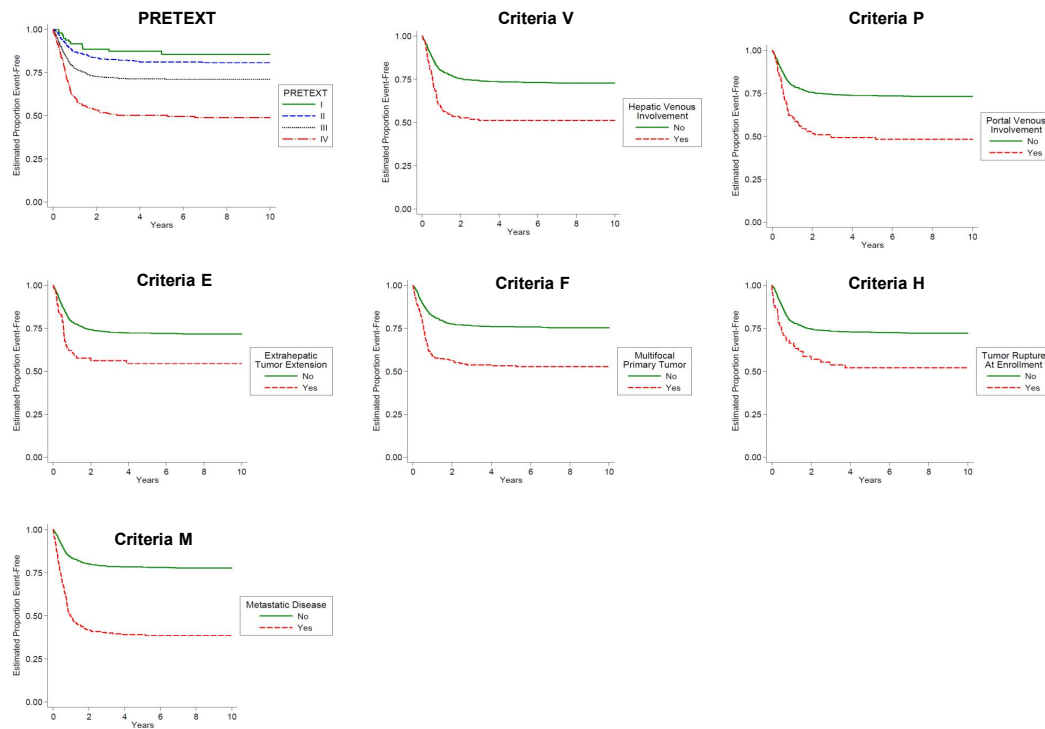


Figure 1.7 PRETEXT designation survival curves. Overall survival in children with specific PRETEXT additional designations. *Adapted with Permission from Czauderna et al, 2016.*

this increase in tumor burden at 52% (**Figure 1.7, Table 1.5**) (151, 152). Rarely, a singular tumor impacts all four contiguous sections of the liver (**Figure 1.6**) (151, 152).

PRETEXT III-IV tumors represent the most challenging surgical cases. Successful resection depends heavily on surgical expertise; to this point, many PRETEXT III-IV patients following evaluation are not surgical candidates (133, 147, 148, 153).

In addition to broad staging (I-IV), the PRETEXT system allows for careful annotation of other prognostic factors that impact the feasibility of surgical

resection, and subsequently the overall survival of the patient. PRETEXT additional criteria includes evaluation and annotation of: *Caudate Lobe involvement (C)*, *Extrahepatic abdominal disease (E)*, *Tumor focality (F)*, *Tumor Rupture (H)*, *Distant Metastases (M)*, *Lymph Node Metastases (N)*, *Involvement of the Inferior Vena Cava (IVC)*, *Hepatic Veins (V)*, and *Portal Vein Involvement (P)* (**Table 1.5**). PRETEXT IV, and PRETEXT E, H, M, N, P, and V designation signifies high risk status for children with hepatoblastoma (**Table 1.5, Figure 1.6**) (147). Technical imaging concerns, including discernment of complex anatomical relationships, limits the scope of PRETEXT staging.

Alternatively, clinicians may also stratify patients by risk using Evans Surgical Staging (**Table 1.6**) (49, 154). By Evan's Surgical Staging approximately 50-70% of children present with unresectable disease at time of diagnosis, *Stage III-IV* (**Table 1.6**) (49, 154). Reports of five-year OS varies substantially for children with unresectable tumors at time of diagnosis, from >20% to 70% (**Table 1.6**) (154). Histologic subtype of tumor impacts variability in survival rates. For example, children with unresectable small cell undifferentiated hepatoblastoma have the worst prognosis (See *Chapter 1.3 Histologic Subtypes of Hepatoblastoma*).

Treatment by Stage

Clinical management of hepatoblastoma is informed by three major considerations: 1) *resectability of the primary tumor* 2) *presence of metastases*

and 3) *tumor histology*. The mainstays of clinical management include primary surgical resection, neoadjuvant and adjuvant DNA-Damaging chemotherapy, and orthotopic liver transplantation (37, 42, 153). For the small percentage of children with low grade, well-differentiated fetal histology, surgical resection offers a potential cure (See *Chapter 1.1 Liver Cancer Primer, Chapter 1.3 Histologic Subtypes of Hepatoblastoma*). All other children with hepatoblastoma require a combination of chemotherapeutic and surgical interventions (37, 42, 153). To date,

Evans Surgical Stage	% Children	Definition	5-year OS	PRETEXT Equivalent
Stage 1	20-30%	Complete resection	Fetal subtype (100%) Well-Differentiated Non-differentiated w/o small cell histology (90-100%) Small cell component (40% to 70%)	PRETEXT I w/o V,P,E,F,R,M
Stage 2	20-30%	Microscopic residual disease	Same as stage I	Varies
Stage 3	50-70%	No distant mets, but tumor is unresectable, OR tumor is resected with gross residual, OR positive extrahepatic lymph nodes	Less than 70%	Varies
Stage IV	10-20%	Distant Mets	20-60%	PRETEXT I-IV w/ GROUP M

Table 1.6 Evans surgical staging and hepatoblastoma prognosis. Alternative staging method used in hepatoblastoma to determine if a tumor is surgically resectable. Five year overall survival and PRETEXT equivalent shown.

there are no approved targeted therapies for use in hepatoblastoma. Below I discuss treatment indications, successes and pitfalls of each modality.

Surgical Resection

As echoed multiple times in previous sections, surgical resection offers the highest chance of survival, and is the primary goal of clinical management for liver malignancy (49, 155, 156). Most guidelines advise surgical resection for children with primary tumors staged PRETEXT I/II with tumor clearance >1cm from major vessels (51, 146, 154-157). Most guidelines also advise surgical resection of pulmonary metastases. In some cases, metastatic pulmonary tumor resection prolongs life (158-160). By Evans Surgical Staging, only 20-30% of children's tumors are resectable at time of diagnosis (**Table 1.6**) (49); thus, the majority of children require treatment with neoadjuvant chemotherapy first to regress tumors sufficiently for resection (further discussed in *Chapter 1.3 Chemotherapy*).

For the <5% of children with well-differentiated pure fetal histology (**Table 1.4, Figure 1.5A, See Chapter 1.3 Histologic Subtypes of Hepatoblastoma**), surgical resection sufficiently eradicates disease. The five-year OS rate for pure fetal histology patients approaches 100% (36, 47, 49). All other histologic subtypes, including mitotic fetal histology (**Table 1.4**), have enough increased risk to warrant adjuvant chemotherapy to clear any micro-metastatic or residual disease (36, 47, 49). For patients with very aggressive disease where surgical

resection is challenging and will likely result in positive disease margins (Evans Stage III-IV, **Table 1.6**), current guidelines do not recommend resection (161). Post-operative complications from challenging cases associate with worse survival outcomes, likely due to the associated delay in adjuvant chemotherapy (161). Thus, surgical resection to “debulk” liver tumors is not clinically advised in children with hepatoblastoma.

Chemotherapy

Chemotherapy falls into two major categories for hepatoblastoma treatment regimens: *Presurgical/ Neoadjuvant* or *Postsurgical/Adjuvant*. Less than 30% of children present with resectable tumors at time of diagnosis; therefore, the majority of children receive presurgical chemotherapy (**Table 1.6**) (49, 154). The goal of presurgical chemotherapy is to promote sufficient tumor regression to allow for safe, “clean margin” surgical resection.

The standard *Presurgical* chemotherapeutic regimen employs up to four cycles of either cisplatin/vincristine/fluorouracil or cisplatin/doxorubicin (**Table 1.7**) (36, 49, 162-164). Following standard chemotherapeutic regimens, an estimated 80% of children can safely undergo surgical resection. Of those children with newly resectable tumors following chemotherapy, the five-year OS rate is estimated to be 60-75% (48, 164, 165). Children presenting with metastatic disease at diagnosis are first medically managed with cisplatin and carboplatin/doxorubicin

on alternating cycles. Results are mixed with OS ranging from 20% to 79%(48, 164, 165). Most children are treated with systemic therapy to promote surgical resection, but in some cases trans-arterial chemoembolization (TACE) has been used with success in rendering children's tumors resectable (166-169).

<i>Chemotherapeutic Agent</i>	<i>Class</i>	<i>Mechanism of Action</i>
<i>Cisplatin</i>	Alkylating agent	Forms platinum complexes that bind to GC rich DNA areas, cross linking DNA
<i>Doxorubicin</i>	Anthracycline	Intercalates between base pairs, preventing DNA replication
<i>Vincristine</i>	Vinca Alkaloid	Binds to microtubules and inhibits S phase of the cell cycle
<i>Fluorouracil</i>	Antimetabolite	Inhibits RNA processing, inhibits thymidylate synthase, depleting dNTPs

Table 1.7 Chemotherapeutic agents used in hepatoblastoma. Standard of care chemotherapeutic for hepatoblastoma and their expected mechanism of action.

<30% of children present with surgically resectable lesions (49, 154). For this small population of children, guidelines advise postsurgical chemotherapy for all children who present with any histology other than pure fetal (36, 47, 68, 145). Children with non-fetal histology receive postsurgical chemotherapy *regardless* of clear surgical margins. Children typically receive one of the following adjuvant regimens: 2-4 cycles of cisplatin/vincristine/fluorouracil, cisplatin/doxorubicin or cisplatin alone (48, 49, 163, 164). Histology of the tumor, specifically whether any small cell component is present, largely determines success of chemotherapy and

recurrence of disease (**Table 1.4**). In one study, Haas et al, found that 10/16 children with small cell histologic components present at diagnostic biopsy experienced tumor recurrence despite sufficient post-operative chemotherapy (142).

The use of DNA damaging agents in the pediatric population has significant acute and long-term toxicities associated with treatment (159, 160, 162, 170, 171). Children frequently experience acute episodes of vomiting, anorexia, mucositis, neutropenia, anemia and myelosuppression. Infection, sepsis, and rarely death have also been documented following chemotherapy in hepatoblastoma (41, 171, 172). The most common permanent side effect is hearing loss/ototoxicity (172). Other frequent chronic toxicities include cardiotoxicity, nephrotoxicity, and secondary cancers (41). Limiting unnecessary and prolonged exposure to chemotherapeutics by using the minimum number of necessary cycles for tumor regression is of paramount importance in pediatric populations.

Liver Transplantation

Clinicians should consider liver transplantation for children who present with any of the following features 1) *multifocal disease* 2) *disease with low probability of resection* 3) *AFP >100 ng/ml* 4) *Age >5 years old* and 5) *Refractory local disease following chemotherapy* (155, 173-177). Interestingly, presence of small cell undifferentiated histology does not promote recurrence following transplant

(140). This finding suggests that locally aggressive subtypes of hepatoblastoma may not seed extra-hepatic metastases early in disease prorecession.

Liver transplantation should *not* be considered for children who have evidence of metastases not previously cleared by chemotherapy or surgical resection (42). Presence of metastatic disease strongly predicts recurrence following transplant; however, the success of transplants in patients with resected metastatic disease remains debated, and further investigation is warranted (41, 42, 140, 143, 170, 178).

Recent guidelines suggest referring poor prognosis PRETEXT patients with a low probability of resection early to transplant centers (154). Survival reported following liver transplantation varies widely, from 50% to 100% (151, 155, 174, 178, 179). It remains difficult to assess liver transplantation survival due to a number of confounding variables including small sample size, and missing clinical variables (i.e. comorbidities, age, chemotherapy, disease recurrence)(41).

For children with unresectable or chemo-resistant disease, liver transplantation represents a chance at curative disease control; however, donor availability severely restricts liver transplantation. Further, transplantation requires lifelong immunosuppression and substantial risk of complications including thrombosis, infection, rejection, bile leak, lymphoproliferative disease, and secondary malignancies.

Clinical Trials

There are a number of interventional clinical trials currently underway investigating the use of new chemotherapeutic regimens, tyrosine kinase inhibitors, mTOR inhibitors, hedgehog inhibitors, cell cycle inhibitors, and Chimeric Antigen Receptor T-Cell (CAR-T) therapy in hepatoblastoma (**Table 1.8**). To date, there have been no approved targeted therapeutics; thus, continued dissection of the underlying molecular pathogenesis of hepatoblastoma is warranted.

<i>Drug</i>	<i>Mechanism</i>	<i>Trial Number</i>	<i>Phase</i>
Irinotecan	Topoisomerase I Inhibitor	NCT00287976	2
GPC3-CART	CAR-T Immunotherapy	NCT04093648	1
LDE225	Hedgehog Inhibitor	NCT01125800	2
Cabozantinib	Tyrosine Kinase Inhibitor, C-Met	NCT02867592	2
Ivosidenib	IDH1 Inhibitor	NCT04195555	2
Palbociclib	CDK4/6 Inhibitor	NCT03526250	2
Larotrectinib	TrKA,B,C Inhibitor	NCT03213704	2
Olaparib	BRCA1 Inhibitor	NCT03233204	2
EGFR806 CAR-T	CAR-T Immunotherapy	NCT03618381	1
Erdafitinib	Tyrosine Kinase Inhibitor, FGFR	NCT03210714	2
Vemurafenib	BRAF Inhibitor	NCT03220035	2
LY3023414	Pi3K/mTOR Inhibitor	NCT03213678	2
Tazemetostat	EZH2 Inhibitor	NCT03213665	2

Table 1.8 Interventional targeted agents under clinical investigation for hepatoblastoma. *Compiled from clinicaltrials.gov.*

Chapter 1.4 Molecular Profiling of Hepatoblastoma

Genetic Alterations

For low grade tumors, a combination of surgery and chemotherapy can boost five-year OS >80% (48, 49, 145, 146, 163, 172). For children with high-grade tumors, overall survival remains poor with five-year OS >20% See *Chapter 1.3 Clinical Management of Hepatoblastoma* (142, 143). Designing new targeted therapies and repurposing existing compounds for therapeutic use requires understanding the molecular underpinning of hepatoblastoma, its genetic drivers and vulnerabilities.

Several groups have characterized the genomic landscape of hepatoblastoma using exome sequencing, and gene expression analyses (1, 14, 15, 180, 181). Exome sequencing suggests that hepatoblastoma is a very simple cancer with 2.9-3.9 mutations per tumor (See *Chapter 1.1 Liver Primer*) (14-16). The relatively small number of genetic mutations suggests that epigenetic alterations may contribute to hepatoblastoma tumorigenesis (see *Chapter 1.4 Epigenetic Alterations*).

50% to ~90% of children with hepatoblastoma have sporadic β -catenin mutations. Further, upwards >95% of children have Wnt pathway activation (1, 14, 15, 87, 88, 182). Importantly, frequency of Wnt pathway mutations does not discriminate between favorable and poor prognosis subtypes of hepatoblastoma (See *Chapter 1.4 Gene Expression Profiles*) (81, 183-185). Uncommon, but

Gene	Function	Frequency	Reference
CTNNB1	Oncogene	72.5%	Eichenmuller, 2014
RAD17	Tumor Suppressor	Infrequent	Eichenmuller, 2014
TP53	Tumor Suppressor	Infrequent	Eichenmuller, 2014
TERT	Oncogene	5.9%	Eichenmuller, 2014
NFE2L2	Oncogene	9.8%	Eichenmuller, 2014
SPOP	Tumor Suppressor	Infrequent	Jia, 2014
CAPRIN2	Oncogene	Infrequent	Jia, 2014
OR51L	Tumor Suppressor	Infrequent	Jia, 2014
CDC20B	Tumor Suppressor	Infrequent	Jia, 2014

Table 1.9 Genetic mutations observed in hepatoblastoma. Most common genetic mutations observed in children's hepatoblastoma tumors. Suspected function, and frequency shown

observed, mutations also occur in RAD17 Checkpoint Clamp Loader Component (*RAD17*), *TP53*, *TERT*, Nuclear Factor Erythroid 2 Like 2 (*NFE2L2*), Speckle Type BTB/Poz Protein (*SPOP*), Cytoplasmic Activation/Proliferation Associated Protein 2 (*CAPRIN2*), Olfactory Receptor Family 5 subfamily I member I (*OR51I*), and Cell Cycle Division 20 B (*CDC20B*) (**Table 1.9**) (14, 181). Sumazin et al. found that NFE2L2/NRF2 was a recurrent hot spot mutation in high risk, aggressive hepatoblastoma cases (15). Indeed, knockdown of NRF2 in mouse hepatoblastoma mediates reduced proliferation (186). *Chapter 1.8 Liver Tumorigenesis* further reviews mechanistic insights into known hepatoblastoma oncogenes and tumor suppressors.

Epigenetic Alterations

As discussed above and in *Chapter 1.1 Liver Cancer Primer*, pediatric solid tumors including hepatoblastoma typically have low mutational burdens compared

to adult cancers (14-16). As such, cancer cells frequently inactivate tumor suppressors via epigenetic silencing by hypermethylation of promoter regions (73, 187). Hypermethylation of tumor suppressor promoters typically occurs on the 5-carbon cytosine residue (5mC) in CpG dinucleotides. CpG dinucleotides are regions where a cytosine nucleotide is followed by a guanine nucleotide (188, 189). Notably, CpG hypermethylation can also cause aberrant regulation of non-coding RNAs (see *Chapter 1.4 microRNA Regulation*) (190).

Without the use of genome wide mapping, multiple reports demonstrated hypermethylation/epigenetic silencing in the promoter regions of several pro-apoptotic, antiproliferation, and known tumor suppressor genes including: Cyclin dependent kinase inhibitor 2A (*CDKN2A*)(191), Caspase 8 (*CASP8*) (192), *APC* (193), the Wnt inhibitor *SFRP1* (194), Ras association domain family I isoform A (*RASSF1A*) (192, 193), hedgehog interacting protein (*HHIP*) (14, 195, 196), and Suppressor of cytokine signaling (*SOSC1*) (197). Hypermethylation of *RASSF1A* and *CASP8* were independently associated with poor prognosis (192).

A recent report by Papaspyropoulos et al, demonstrated that in embryonic stem (ES) cells, *RASSF1A* functions to block stem cell renewal by uncoupling β -catenin and YAP1 transcriptional signaling (198). When *RASSF1A* is active, YAP1 cannot complex with β -catenin/TCF and promotes differentiation of ES cells via p73. Notably, hepatoblastoma is a stem-like cancer driven by oncogenic crosstalk between β -catenin and YAP1; thus, loss of *RASSF1A* expression may promote

hepatoblastoma by allowing for uncontrolled transcriptional cooperativity between Wnt and Hippo/Yap1. Indeed, 80% of children's tumors have nuclear co-staining of YAP1 and β -catenin (See *Chapter 1.8 Liver Tumorigenesis*)(31).

Three independent groups have now mapped the DNA methylome of hepatoblastoma (199-201). Consistent with previous reports in other cancer types, Cui et al, and Maschietto et al. found *global hypomethylation* with site specific hypermethylation in tumor samples compared to control livers (190, 199, 200). Specifically, Cui et al. demonstrated hypomethylation/activation of AFP, a known prognostic marker for hepatoblastoma, in the majority of patient samples (see *Chapter 1.3 Laboratory Findings and Imaging*) (199).

In Honda et al, nine genes were found to be hypermethylated and thus inactivated. Of those nine genes, four were suspected tumor suppressor genes: G coupled protein receptor 180 (*GPR180*), Macrophage stimulating 1 receptor (*MST1R*), OCIA domain containing 2 (*OCIAD2*), and Poly-(ADP-ribose) polymerase family member 6 (*PARP-6*). All four genes confer poor prognosis in children with hepatoblastoma (201). Intriguingly, G-coupled proteins activate or repress Hippo/YAP1 in a context dependent manner (See *Appendix IV*) (202). Thus, loss of GPR180 may contribute to YAP1 activation in hepatoblastoma.

Finally, using whole genome sequencing of methylation marks, Maschietto et al, characterized >1000 CpG sites (corresponding to ~ 750 genes) exhibiting abnormal methylation in hepatoblastoma tumor samples. Strikingly,

hepatoblastoma methylation patterns closely mimicked fetal liver methylation during development (200). These results support the hypothesis that hepatoblastoma tumorigenesis is promoted by an abnormal developmental arrest during liver differentiation. Further, these findings are consistent with the early observations that hepatoblastoma histology mimics the embryonic and fetal liver (see *Chapter 1.3 Histologic Subtypes of Hepatoblastoma*, *Chapter 1.6 Liver Development*).

As reviewed in *Chapter 1.4 Genetic Alterations*, most children have *CTNNB1* mutations. Infrequently, children's tumors also have hypermethylation of Wnt inactivators (194). Despite the co-nuclear localization of YAP1 and *CTNNB1* in >90% of children's tumors, YAP1 mutations have not been detected in children's tumors (See *Chapter 1.8 Liver Tumorigenesis*). Interestingly, to date no reports directly resolve epigenetic causes of YAP1 activation in hepatoblastoma either (See *Appendix IV for Review of Hippo Signaling*). Further investigation is required to understand the source of YAP1 activation in children's tumors (See *Chapter 5.2*).

Cytogenetics

A large cytogenetic survey of 111 hepatoblastomas revealed that nearly 50% of children's tumor karyotypes were abnormal. The most common alteration was complete gain of chromosome 2, 8, or 20 (203). Translocations were observed

in 39% of cases, with breakpoints at 1q being frequent (18%)(73, 203). Cytogenetic changes affect hepatoblastoma disease course. Specifically, aggressive proliferative subtypes of hepatoblastoma often have gains of 8q and 2p (See *Chapter 1.4 Gene Expression Profiling*) (1).

Gene Expression Profiles

Gene expression analyses have allowed more thorough characterization of children's hepatoblastoma. Further, several groups have used gene expression analyses to generate prognostic gene signatures that aid in identification of patients at high risk for metastases and recurrence (1, 15, 180). The earliest profiles of hepatoblastoma gene expression noted increased expression of imprinted genes frequently observed in genetic syndromes like BWS (See *Chapter 1.2 Incidence and Associations*) (89, 90, 92-94, 96, 204, 205). Imprinted overexpressed genes in hepatoblastoma and other solid pediatric tumors include but are not limited to: *IGF2*, Delta Like Non-Canonical Notch Ligand-1 (*DLK1*), and Paternally Expressed Protein Gene 3 (*PEG3*) (90, 93, 183, 204, 205). Dysregulated imprinted genes may be symptomatic of larger epigenetic irregularities in the tumorigenesis process, and not specific to hepatoblastoma tumor initiation (73).

Upregulation of Hedgehog signaling at the transcript and protein level has also been noted in hepatoblastoma cases. Multiple groups have shown expression

of hedgehog pathway member Glioma-associated oncogene homolog 1 (*GLI1*) associates with poor prognosis (195, 206-208). Similarly, children's tumors often have hypermethylation of regulatory Hedgehog members (See *Chapter 1.4 Epigenetic Alterations*). Currently, one hedgehog inhibitor, LDE225, is being evaluated in a Phase 2 clinical trial for hepatoblastoma (See *Chapter 1.3 Clinical Trials*) (**Table 1.8**).

Cairo Classes, C1/C2

In 2008, a landmark paper used microarray gene expression analysis in 25 children's hepatoblastoma samples. Cairo et al. found that a 16-gene signature could distinguish between well-differentiated favorable prognosis Cairo Hepatoblastoma C1 tumors, or poor prognosis proliferative C2 tumors (**Figure 1.8**) (1). Despite considerable differences in tumor biology, prognosis, and histology, C1 and C2 tumors were found to have comparable rates of β -catenin mutations, 85% and 77% respectively. Similar rates of Wnt pathway mutations suggests other genetic or environmental factors contribute to disease aggressiveness (**Figure 1.9**).

C1 tumors correspond clinically to fetal well-differentiated cases that typically respond to surgical resection alone, or surgical resection with limited chemotherapy (**Figure 1.5A-B, Figure 1.8, Figure 1.9, Table 1.4**). These tumors typically display fetal histology (See *Chapter 1.3 Histologic Subtypes of*

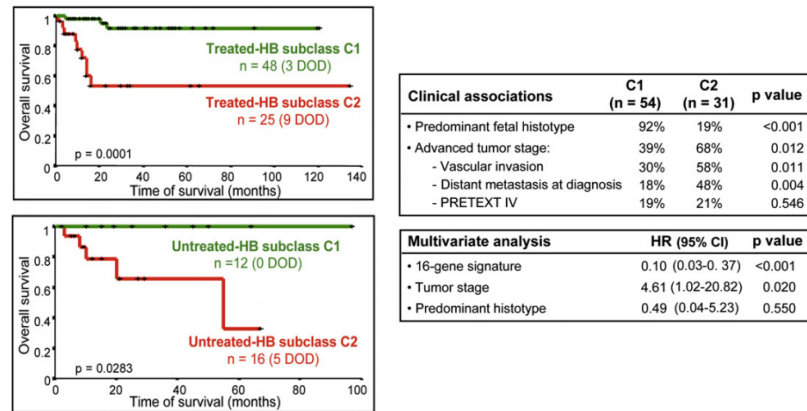


Figure 1.8 Cairo hepatoblastoma classes. Cairo et al. identified two sub-groups of hepatoblastoma tumors using a 16-gene signature: C1 favorable and C2 poor prognosis. Survival curves and class associations for C1 and C2 tumors shown. Adapted with permission Cairo et al. 2008.

Hepatoblastoma, Chapter 1.6 Liver Development). C1 tumors are enriched for gene signatures associated with well differentiated hepatocytes (i.e. hepatic perivenous metabolism), have low proliferation rates, and minimal chromosomal instability (**Figure 1.9**).

In contrast, C2 tumors are associated with embryonal, macrotrabecular, and crowded fetal histologic subtypes. Children with C2 tumors have advanced disease stage at presentation, PRETEXT 4 w/ M, V (**Figure 1.8, Figure 1.9, Table 1.5, Table 1.6**). Further, C2 tumors exhibit upregulation of proliferation and antiapoptotic genes, are strongly positive for hepatic progenitor markers including AFP, Epithelial Cell Adhesion Molecule (EPCAM), and KRT19/CRT19, and are enriched for Gene Set Enrichment Analyses (GSEA) signatures *Cell cycle*, *Mitotic checkpoints*, and *Myc signaling* (**Figure 1.9**). The Cairo class signature highlights

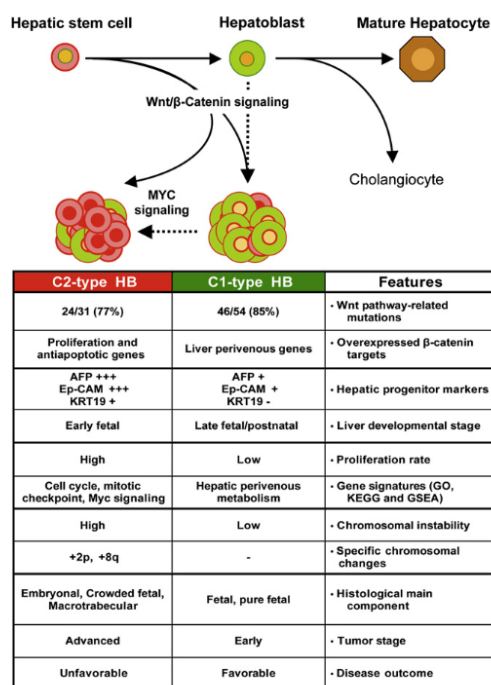


Figure 1.9 Clinical Characteristics of Cairo Hepatoblastoma Classes. Cairo C1 and C2 tumors have distinct β -Catenin transcriptional programs. Tumor stage, prognosis and molecular characteristics of C1, C2 tumors shown. *Adapted with permission from Cairo et al, 2008.*

a feature of hepatoblastoma first noted through histopathologic correlations: *differentiation status impacts clinical course.*

Sumazin HB1, HB2, HB3

Following the Cairo signature, multiple other groups further expanded the effort to molecularly subtype and stratify children's hepatoblastomas into risk-informed treatment groups. Sumazin et al. profiled the mRNA expression of 88 hepatoblastoma samples, and hierarchically clustered the tumors into three subgroups: Low-Risk HB1 (100% 5yr overall survival), High-Risk HB-2, and Intermediate Risk HB-3 (15). Similar to the Cairo Analysis, the Sumazin signature

shows a high rate of β -catenin mutations, and Wnt pathway activation regardless of risk-group. The Sumazin HB subgroups are stratified largely by differential expression of hepatic/stem cell marker expression (*LIN28B*, *AFP*, *SALL4*), hepatocyte markers (HNF family), the metabolic gene *NFE2L2/NRF2*, and DNA Replication/Cell Cycle pathway genes (15).

Consistent with the Cairo signatures and previous histopathologic reports, Sumazin et al, found HB1 low risk tumors were more frequently well-differentiated fetal histology and expressed high levels of HNF1A and low levels of stem-markers AFP, EPCAM, and LIN28B. HB2 and HB3 higher risk subgroups displayed embryonal and small cell undifferentiated histology, as seen in the poor prognosis Cairo C2 classes (1, 15).

Hooks Four Gene Signature

More recently, Hooks et al. sought to further refine and narrow the Cairo Hepatoblastoma Subclasses for greater ease of clinical diagnostic use (1, 180) . Hooks et al. profiled the gene expression of 25 additional hepatoblastomas with matched normal liver. Similarly, to Sumazin et al, they identified three prognostic subgroups related to the Cairo C1/C2 classes termed: C1 (Low-Risk), C2A (High-Risk), and C2B (Intermediate Risk) (**Figure 1.10**). Hooks' groups largely align with Sumazin's HB1/C1, HB2/C2A, and HB3/C2B (15, 180) . With use of a four gene signature containing Hydroxysteroid 17-beta dehydrogenase 6 (*HSD17B6*),

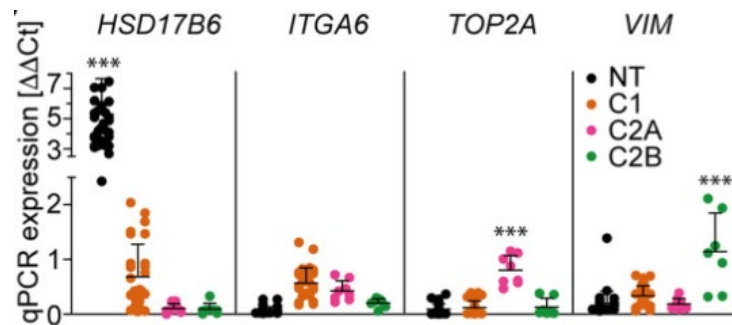


Figure 1.10 Hooks hepatoblastoma signature. Relative expression of four-gene signature for hepatoblastoma subtypes. Aggressive C2A tumors express high levels of Top2A, and low levels of VIM, and HSD17B6. *Reused with permission Hooks et al, 2019.*

Integrin Alpha 6 (*ITGA6*), Topoisomerase 2-alpha (*TOP2A*), and Vimentin (*VIM*), Hooks et al. shows discrimination between the three prognostic groups. Top2A expression is specific to the highly proliferative, aggressive C2A subtype (**Figure 1.10**). Further, they found that frequently chemo-resistant C2A tumors likely evade lethal levels of DNA damage following alkylating chemotherapy through upregulation of the Fanconi Anemia-Breast Cancer Gene Pathway, (FA-BRCA)(180).

microRNA Regulation

Cancer cell gene expression can also be modulated post-transcriptionally by small noncoding microRNAs (miRNAs) (209, 210). In fact, altered miRNA production is a feature of most cancer types, regardless of tissue context (211-215). Together with the RNA induced silencing complex (RISC), miRNAs typically bind the 3' untranslated region (3'-UTR) of a messenger RNA (mRNA), leading to

translational repression of the mRNA (216). As such, miRNAs can function as either oncogenes or tumor suppressors (210).

In the context of hepatoblastoma, miRNAs related to Wnt, Hippo, and Myc tumorigenic signaling are frequently dysregulated. Specifically, Cairo et al, using miRNA expression profiling, found that C1 favorable prognosis tumors and C2 class tumors differentially express Myc regulated miRNAs (217) (see *Cairo Classes C1/C2*). Consistent with the stem-like phenotype driven by Myc signaling in aggressive hepatoblastoma, C2 tumors down-regulate the Myc-target miR-100/let-7a-2/miR-125b-1 cluster and upregulate the mir-371-3-cluster, reminiscent of embryonic stem cell (ES) miRNA expression (217). The mir-371-3 cluster upregulated in C2 tumors and ES cells, is downregulated in differentiated liver tissue. Cairo et al's observations further characterize hepatoblastoma as a developmentally "arrested" cancer (217) (See *Chapter 1.3 Histologic Subtypes of Hepatoblastoma, Chapter 1.6 Liver Development*). They propose that Myc-signaling, downstream of oncogenic β -catenin, contributes to the aggressive phenotype through miRNA dysregulation (217).

Von Frowein et al. recently found overexpression of miRNA-492, expressed from KRT19 in hepatoblastoma tumors (218). Discussed in *Chapter 1.3*, the poor prognosis cholangioblastic subtype of hepatoblastoma overexpresses KRT19. Further, KRT19 expression is a key feature of C2 tumors (1) (See *Chapter*

1.3 Histologic Subtypes of Hepatoblastoma). Future work will determine the exact role of miRNA-492 in hepatoblastoma tumorigenesis.

Hepatoblastoma tumor initiation relies on oncogenic cooperation between Wnt/ β -catenin and Hippo/YAP1 signaling (31). Recently, Indersie et al, reported that hepatoblastoma patient samples downregulate four Wnt inhibitory miRNAs: Let-7i-3p, miR-449b-3p, miR-624-5p, and miR-885-5p (219). When the authors overexpressed miR-624-5p *in vitro*, they found hepatoblastoma cell proliferation could be inhibited, and β -catenin inactivated (219). Similarly, miRNAs that downregulate expression of GPC3, a WNT activator, were reduced in hepatoblastoma samples (220). *GPC3* is the mutated gene in Simpson Goblai Behmel syndrome, an overgrowth syndrome that increases the risk of hepatoblastoma (see *Chapter 1.2 Incidence and Associations*) (98).

In hepatoblastoma, the crosstalk between miRNAs and Hippo/YAP1 signaling remains under investigated. To date, there are no reports that detail miRNA regulation of YAP1, or other Hippo pathway members, in hepatoblastoma. However, hepatoblastoma-like HepG2 cells express miRNA-206, a miRNA target of YAP1 in cardiomyocytes (see *Chapter 1.5 Laboratory Models, Table 1.10*) (221, 222). There are several reports detailing interactions between YAP1 and miRNAs in adult HCC, but whether the regulatory relationships are maintained in hepatoblastoma remains unknown (223-226).

Chapter 1.5 Laboratory Models

The relative rarity of hepatoblastoma has limited the availability and characterization of cell lines, patient derived xenografts, and *in vivo* models. Recently there have been renewed efforts to establish tissue banks, and cell lines for hepatoblastoma (227). Therapeutic discovery requires well characterized *in vitro* and *in vivo* models.

In Vitro

To date, approximately 15 cell lines thought to be hepatoblastoma have been described in the literature. **Table 1.10** summarizes the most common hepatoblastoma cell lines (31, 227-229). Characterizing hepatoblastoma cell lines has proved challenging because of the mixed subtype most patients have, and the stem like nature of the tumor that complicates *in vitro* culture. Further, multiple groups have debated the origin of several available lines, including HepG2 (**Table 1.10**). HepG2 was first identified as hepatocellular carcinoma from a 15 year old child, and later re-characterized by another group as an unusual hepatoblastoma in an older child (**Table 1.10**) (227, 230).

Current hepatoblastoma cell lines are primarily characterized as either unspecified epithelial histology or a mixed epithelial (**Table 10**). There are no cell lines classified as small cell undifferentiated, the poorest prognosis subtype of

hepatoblastoma. Increasing the histologic spectrum of available cells is crucial to improving the likelihood of identifying a tractable therapeutic strategy.

Approximately ~80% of children's tumors, regardless of histologic subtype, have co-expression of nuclear YAP1 and β -catenin (31). Several groups have

Human Cell Line	Origin	Histologic Subtype	YAP1 Status	CTNNB1 Mutation
Huh6	1y Male, Hepatoblastoma	Epithelial	Nuclear (Matsumoto et al, 2019)	T41A
HepG2	15 y Male, controversial, identified as Hepatocellular carcinoma and Hepatoblastoma*	Embryonal, mixed	Cytoplasmic, Weakly nuclear sporadically (Matsumoto et al, 2019, Tao et al, 2014)	Δ 116 Amino Acids Exon 3
HepT1	2y 10m Female, hepatoblastoma	Embryonal, poor differentiation	YAP1 expression, localization unknown (Tao et al, 2014).	Δ 76 Amino Acids, Exon 3
Hep293TT	5y Female, hepatoblastoma	Mixed, embryonal	Nuclear YAP1 (Liu et al, 2017)	Δ 117 Amino Acids Exon 3
HC-AFW1	4y 6m Male, controversial, identified as Hepatocellular carcinoma and Hepatoblastoma*	Unknown	YAP1 expression, localization unknown (Tao et al, 2014).	Δ 49 Amino Acids, Exon 3
HepT3	4m Female, Hepatoblastoma	Fetal, Embryonal	YAP1 status unknown	T41A
HepT5	Sex and age not disclosed	Epithelial	YAP1 status unknown	Δ 76 Amino Acids, Exon 3

Table 1.10 Cell culture models of hepatoblastoma. Selected hepatoblastoma-like cell lines shown with origin, histologic subtype, and mutational status.

characterized the YAP1 and β -catenin status of available hepatoblastoma cell lines, and I have summarized their findings in **Table 1.10** (31, 227-229). Interestingly, the controversial HepG2 cell line expresses YAP1, but does *not* have strong nuclear co-localization of YAP1 and β -catenin (31, 228). Currently, Huh6 may be the most representative cell line; however, its histologic subtype remains unknown (**Table 1.10**).

In Vivo

There are limited *in vivo* models to study tumor maintenance in childhood cancers, and no inducible conditional mouse models for hepatoblastoma. Transgenic mouse models are ideal for probing tumor dependencies because they more closely mimic the human tumor microenvironment lost by most *in vitro* model systems; however, the transgenic models for hepatoblastoma generate mixed liver malignancies producing both hepatocellular carcinoma and hepatoblastoma *in vivo* (**Table 1.11**) (231, 232). Currently, none of the transgenic models generate hepatoblastoma alone (186, 228, 233, 234).

Alternatively, multiple labs have established hepatoblastoma *in vivo* using subcutaneous or intrasplenic injection of hepatoblastoma cell lines or patient derived xenografts (**Table 1.11**) (228, 235-238). Xenograft models typically require immunocompromised murine backgrounds and may not fully recapitulate the tumor microenvironment.

More recently, several groups established liver-specific genetic models of hepatoblastoma-like tumors with hydrodynamic injection (31, 228, 229). Hydrodynamic injection is a high-speed, high-volume tail-vein injection that allows

Model	Type of Model	YAP1 STATUS	CTNNB1 MUTATION
Hepatoblastoma Cell Xenograft	Subcutaneous (<i>Berger et al, 2014</i>), (<i>Eicher et al, 2013</i>), (<i>Matsumoto et al, 2019</i>)	Cell line dependent (see table 1.X)	Cell line dependent (see table 1.X)
Huh6 Orthotopic	Intrasplenic Injection to form liver tumors (<i>Woodfield et al, 2017</i>)	Nuclear	T41A
BY Model β-catenin^{DeIN90}, YAP1^{S127A}	Hydrodynamic Injection (<i>Tao et al, 2014</i>) (<i>Liu et al, 2017</i>)	Nuclear	Δ 1-90 Exon 3
Conditional BY Model β-catenin^{DeIN90}, TET-ON YAP1^{S127A}	Hydrodynamic Injection (<i>Smith et al, in review</i>)	Doxycycline inducible Nuclear expression	Δ 1-90 Exon 3
BYM Model β-catenin^{DeIN90}, YAP1^{S127A}, C-Met	Hydrodynamic (<i>Matusmoto et al, 2019</i>)	Nuclear	Δ 1-90 Exon 3
MYC Model	*Transgenic (<i>Shachaf et al, 2004</i>).	Unknown	Unknown
Lin28B Model	*Transgenic (<i>Nguyen et al, 2014</i>).	Unknown	Unknown
β-catΔEx3:Myc mice	*Transgenic (<i>Comerford et al, 2016</i>)	Unknown	Δ Exon 3
Patient Derived Xenografts	Subcutaneous, Orthotopic (<i>Bissig-Choisat et al, 2016</i>).	Patient Dependent	Patient Dependent

Table 1.11 Mouse models of hepatoblastoma . Available mouse models of hepatoblastoma. Mutation status shown. *Generates mixed Hepatocellular and hepatoblastoma

for targeted in vivo transfection of the pericentral (zone 3) liver by plasmid DNA (See *Chapter 1.8 Liver Tumorigenesis, Chapter 5.1 Mouse Models of Hepatoblastoma*) (**Figure 1.11**) (239-241). The *BY Model* integrates oncogenic YAP1 and β -catenin by sleeping beauty transposase into adult hepatocytes recapitulating the nuclear co-localization of β -catenin and YAP1 seen in 80% of children's tumors. Similarly, the *BYM Model* introduces oncogenic β -catenin, YAP1 and MET Proto-oncogene Receptor Tyrosine Kinase (MET) for generation of hepatoblastoma-like tumors (**Table 1.11**).

Following hydrodynamic injection, hepatoblastoma tumors are established within 4-8 weeks, and lethal by >11 weeks (31). Hydrodynamic models force gene expression and subsequent transformation from mature hepatocytes, and not from hepatoblasts, the presumed cell of origin in hepatoblastoma. Caveats of hydrodynamic, transposases and inducible modes are discussed in *Chapter 5.1*.

Chapter 1.6 Liver Development

In the last decade, extensive similarities between gene expression signatures of developing pluripotent tissues, and tumors emerged (242-244); in fact, more stem-like, early expression patterns frequently associate with aggressive lesions, and poorer prognosis hepatoblastoma (See *Chapter 1.4 Molecular Profiling of Hepatoblastoma*) (1, 14, 15). Many reports have detailed the

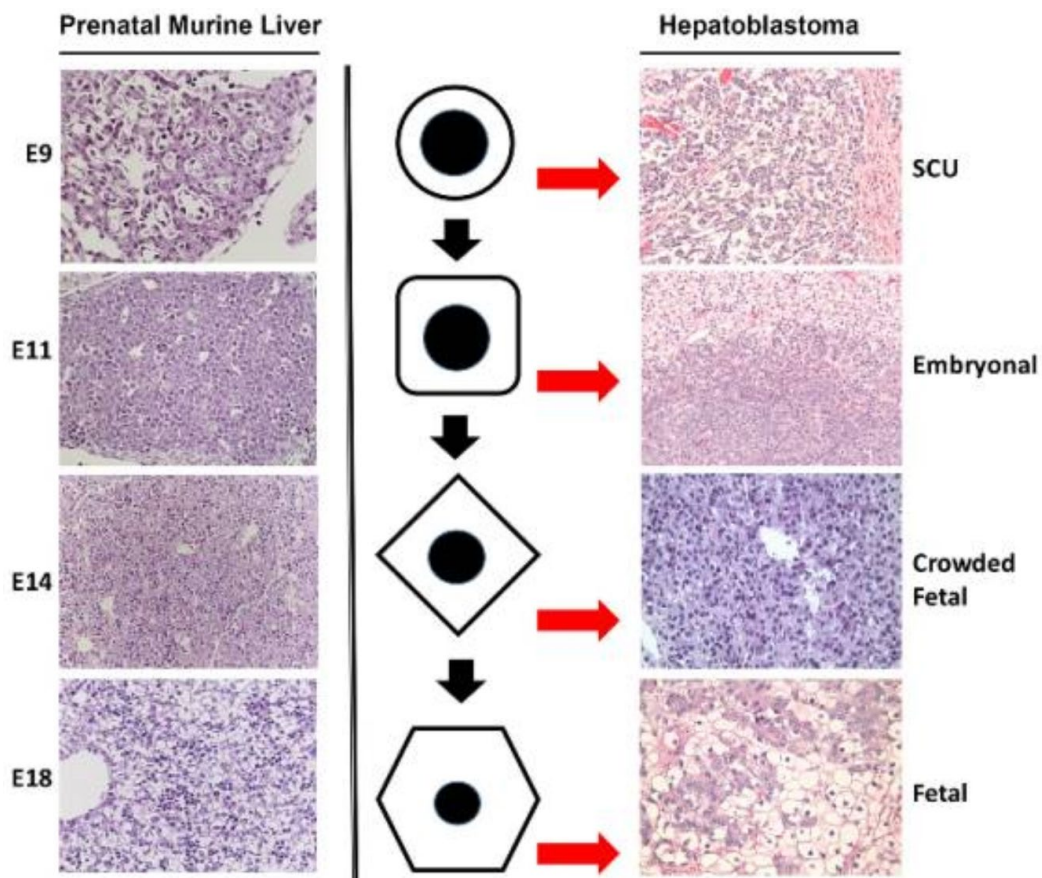


Figure 1.11 Hepatoblastoma histology and prenatal stage. Hepatoblastoma histologic subtypes correspond to early developmental stages of mouse liver. More aggressive histology mimic earlier embryonic timepoints. *Reused with permission from Bell et al, 2017.*

intimate relationship between development and tumorigenesis present at a histologic and molecular level (1, 14, 15, 17). For example, small cell undifferentiated hepatoblastoma has the poorest prognosis, and its histology matches the earliest prenatal timepoint relative to other subtypes, embryonic day E9 (245). On the contrary, favorable prognosis fetal histology corresponds to the latest prenatal, most-differentiated time point, embryonic day E18 (**Figure 1.11**) (245). Further, the multiple cases of hepatoblastoma noted *in utero* suggests aberrant developmental signaling may play a role in hepatoblastoma tumorigenesis (See *Chapter 1.2 Incidence and Associations*) (68-71, 104). Finally, most cases of hepatoblastoma occur under the age of 5. Incidentally, the human liver matures around age 5 (246).

As previously discussed, the majority of children's tumors display dysregulated Hippo/YAP1 and Wnt/ β -catenin signaling. Perhaps unsurprisingly, YAP1 and β -catenin are tightly controlled and well-regulated spatially and temporally during liver development (18, 21, 22, 25, 29, 30, 247-252). Understanding the genetic regulators of liver development may provide critical insight into hepatoblastoma tumorigenesis. This section first reviews how Wnt and Hippo signaling regulate liver development. Finally, I discuss how bipotential hepatoblast progenitor cells, the presumed cell of origin in hepatoblastoma, differentiate into hepatocytes.

From Hepatoblast to Hepatocyte

Hepatocytes and cholangiocytes (bile duct cells) are the major epithelial cells of the liver. Epithelial liver cells originate from a common progenitor cell, the hepatoblast. Hepatoblasts are bipotential progenitor cells derived from foregut endoderm. Hepatoblasts play a crucial role in liver development; specifically, hepatoblasts form the liver bud at approximately embryonic day E8 (253). Early events in hepatogenesis are largely conserved along most vertebrates including humans and mice; thus, the mouse serves as an acceptable model to study liver development (246).

In the mouse, hepatoblast cell fate and lineage commitment occur in a stepwise fashion. A number of transcriptional and growth signaling pathways exact precise control of lineage specification (254). Specifically, both formation of the hepatic bud at embryonic day E8, and eventual generation of hepatoblasts at day E9+ require Fibroblast Growth Factor (FGF) and Bone morphogenic protein (BMP) signaling (253, 255-257). Of note, the most aggressive subtypes of hepatoblastoma resemble E8-9 histologically (See *Chapter 1.3 Histologic Subtypes of Hepatoblastoma*) (**Figure 1.11**).

Recent reports suggest that nascent hepatoblasts default towards hepatocyte differentiation at the direction of several transcription factors including T-box 3 (Tbx3), and hepatocyte nuclear factor 4 (HNF4 α) (See *Chapter 1.7 Wnt/Hippo Signaling in Liver Development*)(258-262). Cholangiocyte

differentiation from hepatoblasts appears to require temporal coordination between embryonic day E10.5 and E14.5 of mitogen activated protein kinase (MAPK), FGF, NOTCH and Wnt signaling (258).

The controversial role of and presence of hepatoblasts in adult liver persists, with groups debating if hepatoblasts or hepatoblast-like progenitor cells remain active in adult liver following injury (263-268). More recently, Lin et al, suggested that stem-like zonally dispersed hepatocytes expressing high levels of telomerase drive repopulation of both hepatocytes and cholangiocytes following damage in the adult liver (319). To date, the consensus states that following acute injury, new hepatocytes can be supplied by a pool of healthy hepatocytes. If healthy hepatocytes are in short supply, hepatoblasts, or other non-hepatocyte populations provide hepatocyte-like cells for repopulation (263, 265, 266, 269-272).

Wnt Signaling in Liver Development

Wnt/ β -catenin signaling plays an intricate, and sometimes contradictory role, during liver development (245, 248, 249, 252, 253, 273, 274). β -catenin knockout mice are embryonic lethal, demonstrating the essential role of β -Catenin in development (247). Proper liver development necessitates carefully timed activation of Wnt signaling. In line with this, proper foregut endoderm generation, and subsequent liver bud development requires *Wnt inactivation*. In *Xenopus*

model systems, Wnt inactivation in the foregut results from secreted frizzled related protein 5, (Sfrp5), a secreted Wnt inhibitor (275, 276). To this point, hepatoblastoma tumors frequently epigenetically silence secreted Wnt inhibitors (See *Chapter 1.4 Epigenetic Alterations*). At embryonic day 8.5, reactivation of Wnt signaling follows increased expression of several transcription factors including: GATA Binding factor (GATA), Hepatocyte Nuclear Factor 1 β (HNF-1 β), Forkhead Box A1 (FOXA1), and Forkhead Box A2 (FOXA2). Wnt reactivation is essential for hepatoblasts to form and proliferate from the liver bud (See *Chapter 1.7 From Hepatoblast to Hepatocyte*) (250, 269, 277, 278).

Following generation of hepatoblasts, the role of Wnt in lineage specification of hepatoblast fate remains unclear. Depletion of β -catenin in hepatoblasts leads to increased apoptosis of early hepatocytes starting around embryonic day E12, decreased levels of HNF4 α and CCAAT-enhancer binding protein-alpha (CEBP α) (250). Paradoxically, disrupting β -catenin's destruction complex in hepatoblasts, leading to increased levels of β -catenin, promotes the cholangiocyte lineage over hepatocyte formation (251). These two seemingly contradictory results suggest that there may be a dose dependent effect of β -catenin in liver development, and that its expression must be carefully titrated for hepatoblast maintenance, proliferation and differentiation.

Hippo Signaling in Liver Development

Hippo/YAP1 signaling is a well-known regulator of liver proliferation, organ size, and regeneration after acute damage in the adult liver (18-22, 25, 29, 279-282). More recently, Alder et al. implicated Hippo signaling in critical control of differentiation gene expression in liver development (283). Alder et al. found that Hippo signaling contributes to control of liver development by promoting use of specific temporal enhancers of liver differentiation factors, HNF4 α and FOXA2, in embryos compared to adult liver. Their findings place Hippo/YAP1 signaling as a temporal regulator of developmental gene expression. Specifically, they propose that nuclear YAP1 influences HNF4 α and FOXA2 binding site choice further implementing YAP1 in control of liver differentiation (20, 283). While the role of YAP1 in adult liver regeneration is well characterized, the role of Hippo signaling in development requires further exploration.

Chapter 1.7 Liver Differentiation

The adult liver performs critical and fundamental metabolic processes including but not limited to fatty acid and cholesterol synthesis, xenobiotic metabolism, and gluconeogenesis. Successful execution of these processes relies on proper liver zonation, i.e. cells performing prescribed functions in spatial relation to one another (**Figure 1.12**). The liver is made up of repeating lobules- separated into three contiguous zones, organized around the portal vein, hepatic artery and central vein. Blood flows from the gastrointestinal tract back to the portal vein and central vein. Bile flows from the hepatocytes into the bile canaliculi and then into the bile duct. The liver is organized into three zones: Zone 1 (periportal), Zone 2 (midzonal), and Zone 3 (pericentral). Blood flows from the gastrointestinal tract back to the portal vein and central vein. Bile flows from the hepatocytes into the bile canaliculi and then into the bile duct. The liver is organized into three zones: Zone 1 (periportal), Zone 2 (midzonal), and Zone 3 (pericentral).

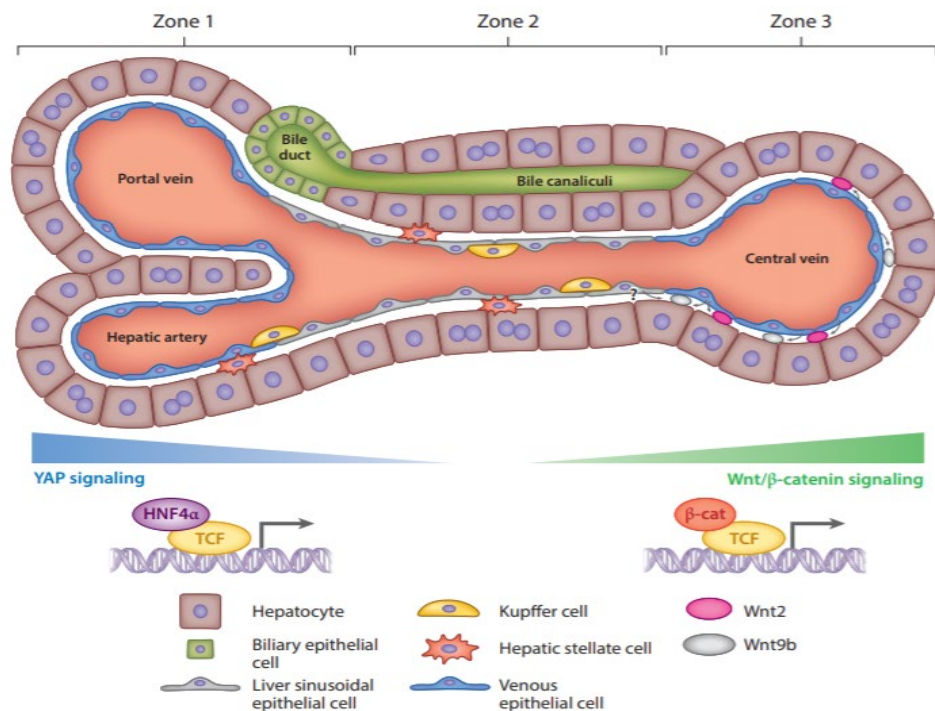


Figure 1.12 Liver zonation. The liver is comprised of repeating units called lobules. Each lobule breaks down into three spatially and metabolically distinct zones. Blood flows from Zone 1 to Zone 3, and bile vice versa. Liver zonation is maintained by Hippo and Wnt Signaling. *Reused with permission from Russell et al, 2018.*

(Zone 1) and is drained by the central vein (Zone 3). In contrast, bile flows from the central vein to the bile duct. Accordingly, the cross flow of blood and bile establishes a chemical gradient across each liver lobule.

Periportal Zone 1 of the liver primarily carries out cholesterol synthesis, β -oxidation of fats, and gluconeogenesis. Zone 2 of the liver is a transitional zone performing multiple functions, and pericentral Zone 3 is primarily responsible for lipogenesis, triglyceride synthesis, xenobiotic metabolism and glycolysis (**Figure 1.12**) (284, 285). Recent single cell sequencing of the spatial genome and epigenome of the liver zones confirmed distinct chromatin and expression profiles in each zone (285-287). The zonation gradient may influence liver cell fate, and gene expression epigenetically. Indeed, one group reported necroptotic signaling altering liver cell fate by methylation of the Tbx3 promoter (see *Chapter 1.7 Liver Plasticity*) (288).

Specific transcriptional profiles orchestrated by YAP1 and Wnt/ β -catenin signaling dictate liver zonation profiles (19, 20, 22, 285, 289-291). In the normal adult liver lobule, Yap1 and Wnt/ β -catenin signaling appear to work in opposition, running spatially distinct transcriptional programs. Nuclear expression of YAP1 is found primarily in Zone 1 periportal hepatocytes; whereas, β -catenin expression localizes to Zone 3 pericentral hepatocytes (**Figure 1.12**).

Depletion of β -catenin, or conversely overexpression of YAP1, leads to a Zone 1 Periportal phenotype throughout the liver (20, 292). Hepatocyte nuclear

factor 4 α (HNF4 α), well known for its role in promoting hepatocyte differentiation (290), and β -Catenin compete with binding to T-cell factor/lymphoid enhancer factor (TCF) to further dictate liver zonation (292). Specifically, Gougelet et al. finds that TCF-4 binds Wnt-responsive elements in the presence of β -catenin; however, contrary to suspected function, TCF-4 can also bind HNF4 α -responsive elements independent of β -catenin and promote Wnt repressive genes (292).

Interestingly, HNF4 α also plays a critical role in Zone 1 maintenance. Several groups have reported that Zone 1 identity and liver differentiation necessitates a careful balance between HNF4 α and YAP1 (20, 23, 283). YAP1 is necessary for proper liver zone 1 metabolism; however, YAP1 overexpression is not without consequence. YAP1 overexpression in the adult liver promotes downregulation of HNF4 α , and progression of a stem like phenotype (23, 293). The next section, *Transcriptional Control*, further discusses the role of HNF family members in the liver.

Transcriptional Control

The supergroup family of hepatocyte nuclear transcription (HNF) factors initiates and maintains first liver development and subsequent differentiation through timely and spatially regulated expression in the liver. The HNF supergroup of transcription factors is made up of four subgroups: *Pou homeodomain family* (HNF1 α , HNF1 β), *FOXA family* (FOXA1, FOXA2, FOXA3), *Orphan Nuclear*

Receptors (*HNF4 α* , *HNF4 γ*), and the *ONECUT Homeodomain family* (*HNF6*, *OC2*, *OC1*) (294, 295). The HNF supergroup members all have DNA binding sites and transactivation complexes; additionally, each subgroup also contains unique domains leading to greater mechanistic capacity (294, 295).

Interestingly, the liver does not exclusively express any HNF family member. Further, overexpression of any *singular* HNF transcription factor cannot rewire non-hepatocyte cells to produce a functional hepatocyte (**Figure 1.13**) (296-299). For example, transformation of human fibroblasts to hepatocyte like cells required lentiviral expression of HNF1 α , HNF4 α , and FOXA3. To this point, multiple studies suggest that HNF1 α , HNF4 α , and FOXA2/FOXA3 are essential for hepatocyte differentiation (259, 290, 295, 300-302). Indeed, germline homozygous loss of *HNF4 α ^{-/-}* or *FOXA2^{-/-}* is embryonic lethal. Homozygous loss of *HNF1 α ^{-/-}* and *FOXA3^{-/-}* promotes diabetes, and sterility respectively (290, 300, 303-307). The lack of liver phenotype in both *HNF1 α ^{-/-}* and *FOXA3^{-/-}* homozygous mice points to the potential redundancy and compensation of other HNF family members in the murine liver.

The presence of HNF binding motifs in other tissues (**Figure 1.13**), suggests that maintenance of liver metabolic function requires cross-talk and cross-regulation by multiple HNFs (293, 295, 308-312). Indeed, mechanisms of cross talk in the murine liver reported include: auto-regulation via binding to self-promoter (313), binding to other factors promoters and enhancers for repressive

or synergistic activity (295, 311, 314), and acting as a scaffolds to recruit other factors to open chromatin (294, 295, 298).

		Brain	Endocrine tissues*	Bone marrow & immune system	Muscle tissues	Lung	Liver and gall bladder	Pancreas	Gastrointestinal tract	Kidney & urinary bladder	Male reproductive tissues	Female reproductive tissues	Adipose & soft tissue	Skin
Human embryo	HNF1 α													
	HNF1 β													
	FOXA1													
	FOXA2													
	FOXA3													
	HNF4 α													
	HNF4 γ													
Adult human	HNF1 α													
	HNF1 β													
	FOXA1													
	FOXA2													
	FOXA3													
	HNF4 α													
	HNF4 γ													
	OC1													
	OC2													

Figure 1.13 Expression of HNF family members by tissue. HNF family members are expressed primarily in gastrointestinal tissues, and responsible for maintaining tissue maturation. Expression of HNF Family members in embryonic and adult tissues shown. *Reused with Permission from Lau et al, 2018.*

Finally, given the role of HNF family members in promoting hepatocyte differentiation, several groups have proposed that HNF4 α functions as both a master transcriptional regulator and a tumor suppressor in the adult liver (301, 315-318). Specifically, overexpression of HNF4 α *in vivo* delays, and in some cases blocks, progression of HCC by inhibiting hepatocyte proliferation (315). Similarly, loss of HNF4 α in a chemical induced model of HCC promotes accelerated tumorigenesis (316).

Liver Cell Plasticity

Liver cell fate is incredibly plastic and strongly influenced by genetic, epigenetic, and microenvironmental factors; thus, cell of origin for most neoplastic

liver lesions is a “headache”; because many factors may shift the differentiation status of a presumed epithelial malignancy. Specifically, Seehawer et al, recently demonstrated in a landmark paper that a necroptotic microenvironment promoted epithelial HCC to differentiate into a bile-duct origin intrahepatic ICC. If Seehawer et al. inhibited the necroptotic environment, ICC could be reverted to HCC (288). Using Assay for Transposase Accessible Chromatin Sequencing (ATAC-Seq), Seehawer et al. found that the transcription start-site of *Tbx3* was accessible in HCC, and inaccessible in ICC. Concordantly, they found increased mRNA expression of *Tbx3* in HCC, and decreased levels in necroptosis-induced ICC (288).

Interestingly, differentiation of hepatoblasts towards hepatocytes requires *Tbx3* expression (see *Chapter 1.6 From Hepatoblast to Hepatocyte*) (258-262). Further Renard et al, demonstrated that hepatoblastoma-like HepG2 cells require *Tbx3* expression, downstream of Wnt/ β -catenin, for proliferation and survival (See *Chapter 1.5 Laboratory Models*) (319). Taken together, these results highlight the role of Wnt/ β -Catenin via *Tbx3* in modulating liver cell fate. Finally, Seehawer et al’s recent finding provides potential clues as to the cause of mixed tumorigenic lesions in transgenic models, and in patients with the same genetic background (**See Table 1.11**) (288).

Understanding hepatoblastoma tumorigenesis and more broadly liver cell fate requires continued investigation of epigenetic and microenvironment cues

during development, and liver maturation. The substantial diversity in hepatoblastoma histologic subtypes, despite similarities in mutational status, suggests that lineage dictation, differentiation status and thus prognosis may be influenced by extracellular molecular cues (see *Chapter 1.3 Histologic Subtypes of Hepatoblastoma*, *Chapter 1.4 Molecular Profiling of Hepatoblastoma*) (24, 245, 320).

Chapter 1.8 Liver Tumorigenesis

Human liver cancer breaks down into several broad categories with the most frequently occurring including hepatocellular carcinoma (HCC), intrahepatic cholangiocarcinoma (ICC/CCA), and hepatoblastoma (HB). As reviewed briefly in the *Chapter 1.1 Liver Cancer Primer*, each of these liver cancers affects specific patient populations and is characterized by unique driver mutations with characteristic histology. Oncogenic cooperation between Wnt/ β -catenin and Hippo/YAP1 characterizes the majority of pediatric hepatoblastoma cases.

Tao et al, finds that oncogenic cooperation of YAP1 and β -catenin occurs in approximately 80% of children's hepatoblastoma (**Figure 1.14**) (31). The nuclear co-localization of YAP1 and β -catenin appears to be unique to hepatoblastoma. In HCC, while nuclear YAP1 was observed in upwards of >60% of samples, and nuclear β -catenin in >28% of cases, the presence of both YAP1 and β -catenin was found in <5% of adult HCC cases. In ICC, while nuclear YAP1 was found in >95% of cases, nuclear β -catenin was rare. Tao et al's observations in patient hepatoblastoma tissues suggests a meaningful role for cooperation between YAP1 and β -catenin, specific to hepatoblastoma (31).

Indeed, *in vivo* studies demonstrate that YAP1 cooperation with β -catenin is essential for hepatoblastoma tumor initiation in mice. Importantly, activation of either pathway independently does not lead to hepatoblastoma tumorigenesis *in vivo* (**Figure 1.15**) (31). Tao et al. established constitutive hepatoblastoma tumors

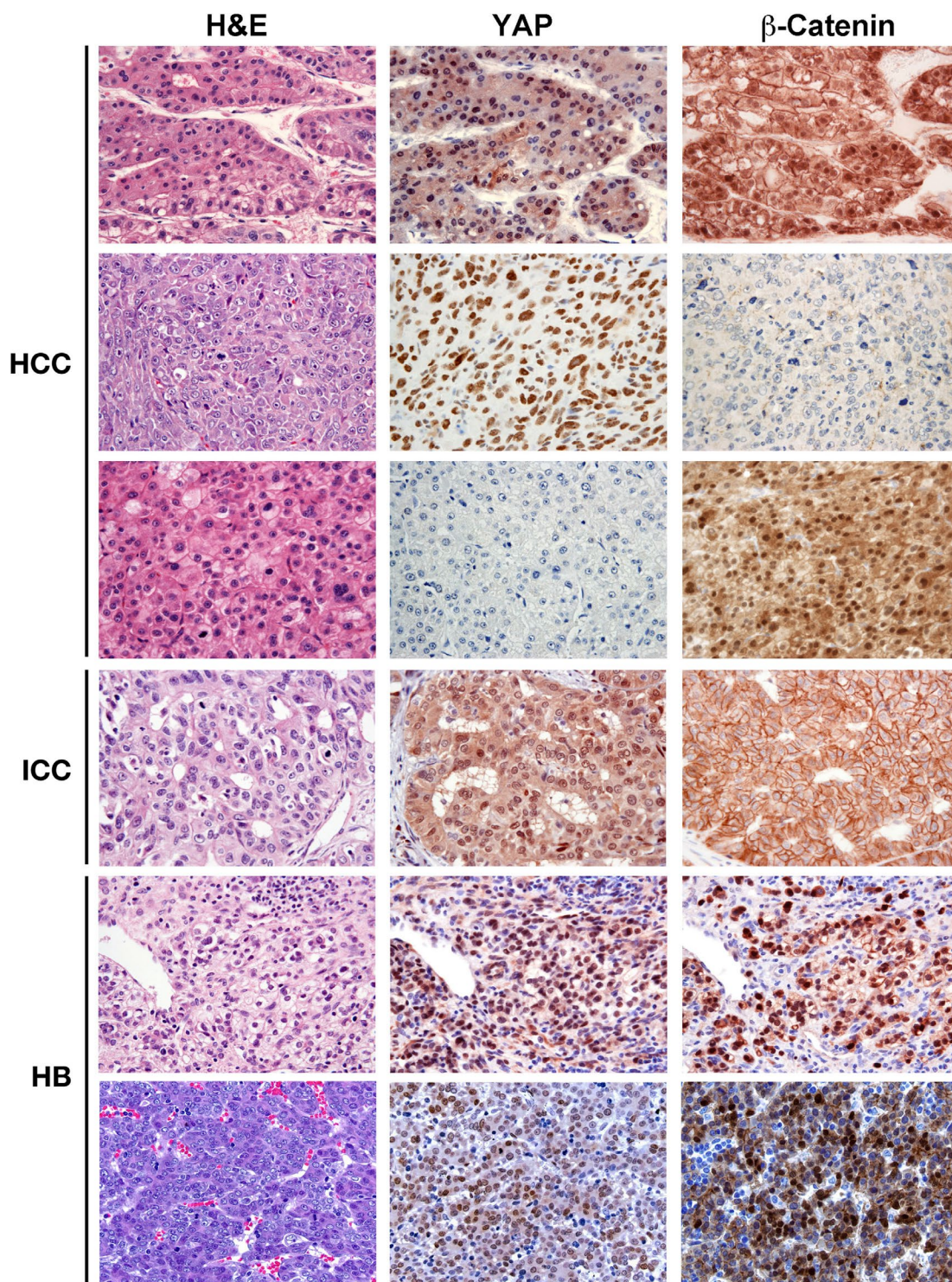


Figure 1.14 Immunohistochemical staining in patient liver tumor samples. Representative expression of YAP1 and β -catenin in patient tissues, with normal histology shown. *Reused with permission from Tao et al, 2014.*

by hydrodynamic injection (See *In Vivo Laboratory Models*, **Table 1.11**). Hydrodynamic injection of β -catenin and YAP1 typically resulted in a lethal burden of tumors by 11 weeks. The histology of tumors driven by this model is mixed, with the authors characterizing their tumors as primarily a crowded fetal mitotic subtype (See *Chapter 1.3 Histologic Subtypes of Hepatoblastoma*, **Figure 1.5**, **Table 1.4**)

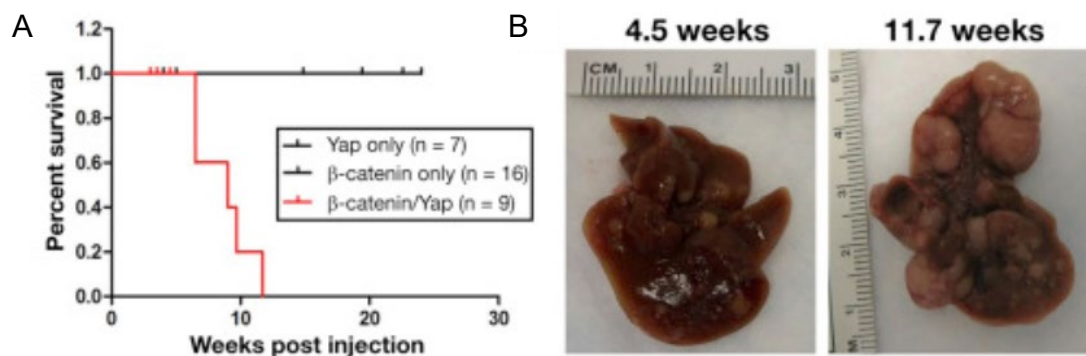


Figure 1.15 *In Vivo* generation of constitutive hepatoblastoma. (A) Survival Curve (B) β -catenin /YAP1 tumors. Adapted with permission from Tao et al, 2014.

(31).

Finally, using co-immunoprecipitation the authors found that β -catenin and YAP1 physically associate in hepatoblastoma, but not in hepatocellular carcinoma. These results are consistent with Fitamant et al's finding that YAP1 inhibition in adult HCC preferentially works in tumors without β -catenin mutations (23). Combined, these results are suggestive of oncogenic synergy that is exclusive to hepatoblastoma among liver neoplasms. In the following sections, I review the respective roles of β -catenin and YAP1 in liver tumorigenesis, and further how

these pathways cooperate and/or regulate one another to promote tumorigenesis in hepatoblastoma.

Wnt/ β -catenin Signaling in Liver Tumorigenesis

As discussed previously, the most common mutations in hepatoblastoma occur in *CTNNB1*/ β -catenin (See *Chapter 1.1 Liver Primer*, *Chapter 1.4 Genetic Alterations*) (**Table 1.2, Table 1.9, Figure 1.14**) (9-14, 321, 322). Most patients, pediatric and adult, with aberrant β -catenin have mutations in exon 3 of *CTNNB1*. Proteasomal targeting of β -catenin requires phosphorylation of multiple serine and threonine sites in exon 3 (See *Appendix III*) (323).

Typically, overexpression of oncogenic β -catenin alone does not induce liver cancer, hepatoblastoma or hepatocellular carcinoma (324). However, overexpression of oncogenic β -catenin does produce a phenotype. Specifically, Cadoret et al, found that β -catenin overexpression leads to hepatomegaly through increased proliferation without compensatory apoptosis (324). Similarly, Lemberger et al. found expression of oncogenic β -catenin in the liver was associated with increased liver size, and metabolic dysfunction in gluconeogenesis, and mitochondrial metabolism (325). Interestingly, transgenic expression of oncogenic β -catenin alone in liver progenitor Sox9⁺ cells, does lead to mixed liver lesions, HCC and hepatoblastoma, by 24 weeks (326). This work provides support for a fetal origin of hepatoblastoma, and some aggressive

subtypes of HCC.

In hepatoblastoma, β -catenin cooperates with YAP1 to initiate tumor formation. β -catenin can also act cooperatively with other known oncogenes to drive liver tumorigenesis. Specifically, β -catenin synergizes with the following oncogenes in murine models to drive HCC formation: HRAS Proto-Oncogene, GTPase/*HRAS* (327), v-AKT murine thymoma viral oncogene homolog 1/*AKT* (328), *MYC* (329), *MET* (185, 330), and KRAS Pro-Oncogene, GTPase/*KRAS* (331).

Under varied genetic contexts, oncogenic β -catenin promotes liver tumorigenesis with *different* transcription programs (1). Oncogenic β -catenin transcriptional programs can increase expression of proliferation, growth and stemness pathways through target gene expression including: Cyclin D1, Epidermal growth factor receptor (EGFR), Transforming growth factor β (TGF β) and TBX3, (31, 228, 319, 332-334).

While MYC is a target of β -catenin transcription in colorectal cancer (335, 336), in liver tumorigenesis Wnt/ β -catenin may not exert transcriptional control over MYC. Accordingly, following depletion of *Apc* (see *Appendix III*), only loss of β -catenin rescues proliferation in liver cells. Depleting Myc did not rescue Apc loss suggesting that, at least in the liver, Myc may be Wnt/ β -catenin independent (81). Supporting this observation, transcriptomic analysis in HCC patients revealed subgroups clustered by mutually exclusive Wnt and Myc signatures (337).

In hepatoblastoma, β -catenin's capacity to promote differential transcriptional programs is best captured by its differential activity in C1 and C2 tumors (**Figure 1.8, 1.9**) (See *Chapter 1.4 Cairo C1/C2 Classes*) (1, 217). C1 and C2 tumors have comparable rates of Wnt pathway mutations (~80%); however, C1 and C2 hepatoblastoma tumors have vastly different transcriptional programs downstream of activated β -catenin. In favorable prognosis C1 tumors, β -catenin promotes a transcriptional program similar to β -catenin's normal transcriptional function in Zone 3 of the liver, i.e. perivenous gene expression (**Figure 1.8, 1.9**) (see *Chapter 1.7 Liver Differentiation*) (1).

Conversely, in the poor prognosis C2 subtype, Wnt/ β -catenin target gene expression is comprised of pro-proliferative and anti-apoptotic target genes like Baculoviral inhibitor of apoptosis repeat-containing (BIRC5/Survivin), GPC3, DVL2/3, DKK1, and Axin (1). In HepG2 and Huh6 hepatoblastoma cell lines, si β -catenin partially reduced MYC protein expression. Notably, MYC and MYCN was also increased in the aggressive C2 tumors, but it was not directly resolved if its increased transcription was the result of Wnt/ β -Catenin in human tumors (See *Chapter 1.5 Laboratory Models*) (1).

Similarly, Tao et al. found that in hepatoblastoma-like HepG2 cells (see **Table 1.10**), small interfering RNAs (siRNAs) targeted against β -Catenin reduced MYC mRNA. MYC target levels were further reduced with the combination of si β -catenin and siYAP, highlighting the synergistic cooperation of YAP1 and β -catenin

in hepatoblastoma (31). Indeed, YAP1 also regulates MYC in the adult liver (See *Chapter 1.8 Crosstalk in Liver Tumorigenesis*). These results suggest that both Wnt and YAP1 control MYC expression in hepatoblastoma. *Chapter 1.8 Wnt and Hippo Crosstalk in Tumorigenesis* further reviews YAP1 and β -Catenin interactions in tumorigenesis.

Hippo/YAP1 Signaling in Liver Tumorigenesis

Activation of YAP1 (Hippo OFF) occurs in many epithelial tumor types (See *Appendix IV*) (2, 338). Dysregulated YAP1 has been linked to poor prognosis, increased rates of metastasis and invasion in multiple tumor types (i.e. colorectal, breast, lung, pancreatic, prostate, lung, etc.) (339-346). Indeed, nuclear YAP1 expression in HCC and ICC patients heralds poor prognosis (344, 347, 348). Further, amplification of the YAP1 locus occurs in approximately 10% of adult HCC patients (24). Despite the overwhelming YAP1 activation in upwards of 80% of children's tumors, no one has detected YAP1 amplifications or Hippo pathway mutations. (See *Chapter 1.4 Molecular Profiling of Hepatoblastoma*) (1, 14, 180).

Lee et al. recently reported that newly metastatic sentinel lymph nodes frequently activated YAP1. Lee et al. found that in lymph nodes YAP1 activity reprograms tumor metabolism to rely on fatty acid oxidation, potentially opening up a new therapeutic window to prevent metastatic spread (339). Likewise, in the adult liver, YAP1 activation preferentially promotes fatty acid oxidation in

periportal Zone 1 (See *Chapter 1.7 Liver Differentiation*).

Similarly to β -catenin, overexpression of hyperactivated YAP1 alone does not, at least in the short-term, produce liver tumors. YAP1 overexpression does produce liver hepatomegaly in the short-term (18, 349). Long-term overexpression of YAP1, or loss of upstream Hippo “ON” components like LATS1/2, Mps one binder 1a (MOB1A), and Macrophage stimulating 1 (MST1/2), promotes tumorigenesis by >15 months of age (22, 25, 350-352). These findings suggest that YAP1 is relevant for hepatocellular cancer tumor initiation. Further, for a subset of hepatocellular carcinomas without β -catenin mutations, YAP1 inhibition promotes tumor regression (23). This finding suggests that for a subset of HCC, tumor initiation and maintenance requires YAP1. In hepatoblastoma, YAP1 is required for tumor initiation *in vivo*, but the requirement of YAP1 for tumor maintenance remains unknown (31).

YAP1 promotes liver tumorigenesis primarily by upregulating genes necessary for liver growth and proliferation including Cellular communication network factor 2 (CTGF/CCN2), Cysteine rich angiogenic receptor-1 (CYR61), BIRC5/Survivin, Amphiregulin (AREG), Notch Receptor 1 (Notch1), and Notch ligand Jagged-1 (JAG1) (20, 26, 280, 353, 354). Specifically, Tschaharganeh et al, found that HCC human lines concomitantly upregulate YAP1, JAG1, and NOTCH pathway members (26). Similar to other reports, Tschaharganeh et al. also observed poor prognosis with YAP1 upregulation (26). They demonstrate that the

upregulation of NOTCH ligand JAG1, and subsequent upregulation of the NOTCH pathway relies on YAP1 binding to transcriptional co-activator TEAD4.

In liver tumorigenesis, the transcriptional oncogenic activity of YAP1 depends on its interaction with the family of co-transcription factors, Transcriptional enhancer factor TEF-1/ TEA domain family member (TEAD/TEFs) (See *Chapter 1.1 Liver Primer, Appendix IV*) (355, 356). YAP1 does not have a DNA binding domain; as such, YAP1 requires co-factors for initiating its transcriptional program (357). Liver tumorigenesis driven by YAP1 “*preferentially requires*” YAP1 partnering with TEAD family members (355). The predilection of YAP1 for TEAD as its oncogenic partner offers a therapeutic window; thus, multiple groups have sought to identify YAP1-TEAD disruptors. The first disruptor, Verteporfin, is not currently in clinical use, and has been demonstrated to have YAP1 independent effects (See *Chapter 5.7 YAP1 Targeted Therapies*) (358, 359). Accordingly, the clinical need for a selective YAP1 inhibitor has not been met.

More recently, Zhang et al. demonstrated that YAP1 oncogenic transcription in the liver requires an additional transcriptional co-factor, Transcription factor CP2 (*TCFP2*) (360). Zhang et al. found that without *TCFP2*, YAP1’s oncogenic potential in the liver was significantly impaired, including YAP1-TEAD interactions. Thus, disrupting YAP1-TCFP2 interactions may provide another strategy to dampen YAP1 oncogenic signaling. Whether YAP1 is reliant on TCFP2 interactions for hepatoblastoma tumorigenesis is unknown.

YAP1-TEAD also cooperates in a transcriptional network with MYC to drive liver tumorigenesis (361). Croci et al. found that both YAP1 and MYC target genes were prebound by TEAD co-factors and had active chromatin marks. The presence of YAP1 stabilized MYC binding to its target gene promoter sites, and together MYC-YAP1 promoted cell proliferation and cell cycle entry (361). Finally, a recent report found that in β -catenin/MYC induced murine HCC, YAP1 was required for oncogenicity, further supporting the cooperation between YAP1 and MYC in liver tumorigenesis (362).

In addition to cooperating with β -Catenin and MYC, YAP1 functions as a transcriptional regulator of liver tumorigenesis by controlling target gene expression from distal enhancers. In breast cancer cells, >90% of YAP1/TEAD bound regulatory regions overlap with enhancer elements. Specifically, activator-protein-1 (AP-1) complexes with YAP1/TEAD at the enhancer sites and augments activation of cell cycle and proliferation genes (363-365). Interestingly, YAP1's activity at distal enhancers requires TEAD (363). Galli et al. found that YAP1 likely exerts its transcriptional control at enhancers by recruiting the mediator complex to enhancers, allowing target promoters to come into range (364). It is unclear if YAP1 functions through AP-1 to act at distal enhancers in hepatoblastoma cancer cells.

Finally, a recent report suggests that the role of Hippo/YAP1 in liver tumorigenesis may be more complex than previously appreciated. While YAP1

activation within liver tumor cells promotes proliferation and cell cycle advance, YAP1 activation in peritumoral normal hepatocytes surrounding the tumor functions to limit tumorigenesis (366). Further investigation is needed to understand the differential transcriptional programs of YAP1 in normal hepatocytes, and in tumors.

Wnt and Hippo Crosstalk in Tumorigenesis

Hippo ON (i.e. YAP1 OFF) negatively regulates Wnt signaling (367, 368). (See *Appendix III/IV*). Conversely, Hippo OFF/YAP1 ON promotes nuclear accumulation of β -catenin, and target transcription of Wnt genes (31, 369). Hippo regulation of Wnt signaling occurs at multiple points in signal transduction: prevention of DVL recruitment to the membrane by cytoplasmic YAP1/Taz (367), cytoplasmic phosphorylated YAP1 preventing translocation of β -catenin to the nucleus (368, 369), and physical cooperation of nuclear YAP1 and nuclear β -catenin promoting target gene expression of canonical Wnt targets, MYC and Cyclin D1 (18, 21, 31).

Specifically, in kidney cells cytoplasmic “inactive” YAP1/TAZ, blocks phosphorylation and thus recruitment of DVL to the membrane. Transcriptional co-activator with PDZ-binding motif (TAZ) is a paralog of YAP1. Without DVL localizing to the membrane, the destruction complex remains active, and β -catenin cannot translocate to the nucleus (367). Similarly, in heart cells, nuclear YAP1

cooperates with β -catenin to promote β -catenin target gene expression (369).

Concordantly, knockout of Hippo ON components, thus increasing YAP1, also increase β -catenin nuclear translocation (369). Finally, in colorectal cancer cells, inactive cytoplasmic YAP1 was found to retain oncogenic β -catenin in the cytoplasm, preventing target gene transcription (368). Specifically, the TEAD binding domain of YAP1 interacts with the N-terminus of β -catenin (368, 369). This observation importantly shows that Hippo ON can suppress oncogenic Wnt signaling in tumorigenesis (368). The observations in kidney, heart, and colorectal cancer cells are consistent with observations in liver regeneration and tumorigenesis; in liver, YAP1 overexpression promotes further upregulation of Wnt targets, Cyclin D1 and MYC (18, 21, 31).

Curiously, Wnt signaling may also further stabilize YAP1, and downregulate differentiation signaling in liver tumorigenesis (370). Wang et al. finds that Tribbles Pseudokinase 2 (TRIB2) acts downstream of Wnt/TCF in liver cancer cells to regulate YAP1 and C/EBP α function (370). Specifically, TRIB2, a β -Catenin target gene, binds directly to β -Transducin Repeat containing E3 ubiquitin ligase (β -TrCP), preventing proteasomal degradation of YAP1. Thus, TRIB2 stabilizes YAP1. Curiously, at the same time, TRIB2 also leads to down regulation of the differentiation factor C/EBP α . In adult HCC, C/EBP α function as a tumor suppressor (371).

Finally, Wnt may also augment YAP1 expression via enhancers. In colorectal cancer cells, β -catenin/TCF4 binds to an enhancer in YAP1, promoting its expression. Concordantly, loss of β -catenin downregulates YAP1 expression (372). These results suggest that Wnt signaling may regulate and synergize with YAP1 (373). Further, in β -catenin mutant CRC cells, YAP1 is necessary for survival. Rosenbluh et al found that YAP1, T-box 5 (TBX5), and β -catenin form a complex necessary for survival of CRC cells. YES Proto-oncogene-1 (YES1) regulates the formation of the YAP1/TBX5/ β -catenin complex and directs the transcription of anti-apoptotic genes (373). These findings were recently recapitulated in adult liver tumorigenesis (362). Bisso et al, finds that cell survival downstream of β -catenin in HCC requires YAP1/TAZ (362).

In hepatoblastoma cells *in vitro*, siRNA knockdown of both β -catenin and YAP1 synergistically decreases cell survival (31). Further, knockdown of YAP1 significantly reduced β -catenin promoter activity, and target gene transcription in HepG2 cells (31). Finally, as discussed in earlier sections, β -catenin and YAP1 physically complex in hepatoblastoma cells, and not in hepatocellular carcinoma cells (31). Taken together, these findings suggest a synergistic role of Wnt/ β -Catenin and YAP1 in promoting hepatoblastoma tumor initiation.

Chapter 1.9 Hallmarks of Hepatoblastoma

Rationale

Hepatoblastoma is a stem-like embryonal tumor thought to arise from arrested embryonic liver stem cells (1, 152, 326). Typically, hepatoblastoma affects children under the age of five years old (60). Hepatoblastoma incidence is increasing, and risk factors include premature birth, low birth weight, parental smoking, and NICU exposures (34, 38, 60, 99, 114). Children may present with abdominal masses, nausea, and rarely paraneoplastic syndromes (125). The five-year overall survival is approximately 80%. For children with Stage IV tumors, prognosis is poor. Stage IV five-year OS is >27% (48, 49, 162). Currently, clinical treatment comprises surgical resection, chemotherapy, and liver transplantation (49, 151, 158).

Clinicians plan treatment largely based on disease extent. As many as 50-70% of children present with unresectable tumors and undergo pre-surgical chemotherapy in an attempt to render the tumor resectable (49). Pediatric chemotherapy has significant short-term and permanent toxicities, most notably nephrotoxicity, ototoxicity, secondary neoplasms and cardiomyopathies (48, 171). Alternative treatment strategies are desperately needed; thus, characterizing the molecular drivers and genetic vulnerabilities of hepatoblastoma is of utmost importance.

Chapter 1 introduced the principle of cancer “Hallmarks” - i.e. unifying

features characteristic of a class of neoplasms. Here I would like to propose that the current “Hallmarks of Hepatoblastoma” include: 1) *Essential oncogenic cooperation between YAP1 and β -catenin for tumor initiation* (31) 2) *Low mutational burden (>3/tumor) compared to adult liver cancer* (14) and 3) *Differentiation status informing prognosis* (1, 217) (**Figure 1.16**). Nearly 90% of

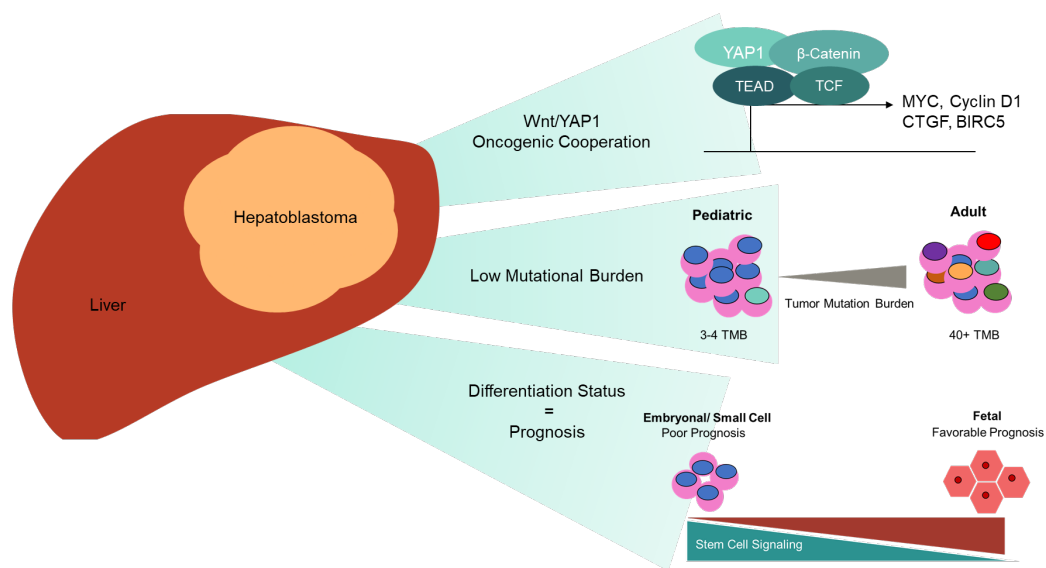


Figure 1.16 Hallmarks of hepatoblastoma. The “Hallmarks” of hepatoblastoma are oncogenic cooperation between YAP1 and β -catenin, genetic simplicity/low mutational burden, and differentiation status correlating with prognosis

children have Wnt pathway mutations, and approximately 80% have nuclear YAP1 and β -catenin (See *Chapter 1.4 Molecular Profiling of Hepatoblastoma*). Most children’s tumors have few mutations, and interestingly mutational status does not predict prognosis. For example, C1 well-differentiated favorable prognosis tumors have equivalent rates of Wnt pathway mutations to C2 poorly differentiated, poor prognosis tumors (See *Chapter 1.4 Cairo C1/C2 Classes*) (1).

While it is clear that oncogenic cooperation of β -catenin and YAP1 is necessary for hepatoblastoma tumor initiation *in vivo*; whether YAP1 hepatoblastoma tumor maintenance requires YAP1, and further if YAP1 represents a tractable therapeutic target, remains uninvestigated.

In this dissertation, I aim to explore the role of YAP1 in maintaining hepatoblastoma tumorigenesis using a new conditional mouse model driven by doxycycline-inducible hyperactive YAP1 (YAP1^{S127A}) and constitutively active β -catenin. Specifically, I show that YAP1 is essential for *in vivo* hepatoblastoma tumor maintenance. I find YAP1 withdrawal induces a cell fate switch in hepatoblastoma tumor cells promoting either apoptosis or a hepatocyte differentiation program. Remaining hepatoblastoma tumors cells are therapeutically differentiated towards “hepatocyte-like” cells that express mature hepatocyte markers and can partially rescue liver damage. YAP1 withdrawal reprograms hepatoblastoma tumor cells by modulating liver differentiation transcription factor (TF) occupancy.

Here I show that withdrawal of YAP1 overexpression alone is sufficient to significantly regress hepatoblastoma and reprogram a subset of tumor cells towards “hepatocyte-like” cells. These are the first *in vivo* findings to support YAP1 as a therapeutic target in hepatoblastoma.

CHAPTER II TUMOR MAINTENANCE REQUIRES YAP1

Chapter 2.1 Introduction

Hepatoblastoma Primer

Hepatoblastoma is the predominant primary pediatric liver cancer and most often diagnosed in children under five years of age. Advances in surgical resection and chemotherapy regimens have saved many young lives; however, the five-year survival rate remains at ~80% overall and ~27% for Stage IV tumors (41, 49, 56). For some children early surgical resection is curative, however, at the time of diagnosis an estimated 50% to 70% of children's tumors are too advanced for surgical resection (41).

A portion of these children's tumors may benefit from preoperative chemotherapy enabling tumor resection, but chemotherapy in young children has life-long adverse effects including ototoxicity, cardiomyopathy, nephrotoxicity, and secondary neoplasms (41, 49). Liver transplantation is another treatment strategy often employed, but is contraindicated in children with metastatic disease (42). (See *Chapter 1.3 Clinical Management of Hepatoblastoma*). To date, the clinical need for a HB targeted therapeutic remains unmet.

Tumor Initiation, Tumor Maintenance, and Oncogene Addiction

Nearly 80% of children's HB tumors have co-activation of β -catenin and YAP1 (31). In mice, hepatoblastoma initiation requires oncogenic cooperation between β -catenin and YAP1 (31). Further, the physical association of YAP1 and β -catenin is specific to hepatoblastoma, and not frequently observed in other types of liver cancer (See *Chapter 1.8, Liver Tumorigenesis*).

Tumor initiation refers to the process by which a normal cell transforms to a cancer cell. First proposed by Alfred Knudson, malignant transformation of a normal cell requires "two-hits". The "two-hit" hypothesis proposes that normal cells need 2+ genetic aberrations, whether loss of a tumor suppressor or oncogene activation, to progress to neoplasm (374). In hepatoblastoma, Tao et al, proposed the co-activation of β -catenin and YAP1 as the "two-hits" necessary for tumor initiation (31, 245). Notably, oncogenic protein expression that is necessary for tumor initiation, may not be necessary for the long-term proliferation and survival of a neoplasm, i.e. *tumor maintenance*.

Bernard Weinstein first introduced the term oncogene addiction in the early 2000s to describe the striking observation that despite other genetic abnormalities in a cancer cell, loss of *one oncogenic protein* sufficiently drives tumor regression (375). In other words, the expression of *only one* oncogenic protein is critical for tumor maintenance (376, 377).

A classic example of oncogenic proteins necessary for both tumor initiation and maintenance is the requirement of KRAS for pancreatic ductal adenocarcinoma (PDAC). In PDAC, mutation of KRAS initiates tumorigenesis, and KRAS oncogene expression remains key to mature tumor survival (378). Similarly, lung adenocarcinoma tumor initiation and maintenance require oncogenic KRAS expression (379).

Alternatively, in some tissue contexts, KRAS may be necessary for initiation but not for tumor maintenance. Specifically, Lim et al. finds that while transformation requires oncogenic RAS, tumor proliferation and survival needs activation of only one downstream RAS Effector, phosphatidylinositol 3-kinase/protein kinase B (PI3K/AKT) (380). Similarly, in prolactin-induced mammary cancer, tumor induction necessitates activation of oncogene Janus Kinase 2 (JAK2), but tumor progression and tumor survival does not rely on JAK2 expression (381).

Conversely, some proteins may be unnecessary or even counterproductive to tumor initiation but required for tumor maintenance. For example, in CRC the MAPK protein, p38 α , suppresses tumor induction, but proliferation of established CRC tumors demands p38 α expression (382). Likewise, in medulloblastoma, tumor initiation mandates repression of BRAC2 and CDKN1A Interacting Protein (BCCIP), but medulloblastoma tumor maintenance requires BCCIP (383).

Finally, if tumor initiation relies on 2+ cooperating oncogenes (i.e. YAP1 and β -Catenin in hepatoblastoma), which oncogenes if any, does tumor maintenance require? For example, Podsypanina et al, found that tumors initiated by both KRAS and MYC were *more sensitive* to loss of KRAS alone, then to MYC alone. Loss of both oncogenes was synergistic (384). These results suggest that oncogenic cooperation may function differently in tumor maintenance, then in tumor initiation.

Nevertheless, for hepatoblastoma it remains unclear if hepatoblastoma tumor survival necessitates expression of YAP1, and further if pediatric patients would benefit from YAP1 inhibitory therapies. To date, there are no conditional mouse models for hepatoblastoma facilitating genetic evaluation of oncogenic YAP1 (See *Chapter 1.5 Laboratory Models*). In *Chapter II*, I report generation of a new conditional mouse model of hepatoblastoma, and further, demonstrate that hepatoblastoma tumor maintenance requires YAP1 expression.

Chapter 2.2 Results

Attributions: Hydrodynamic injections to establish the mouse model were done in conjunction with former Xue lab postdoc, Dr. Haiwei Mou. Additionally, Dr. Haiwei Mou and Dr. Deniz Ozata assisted with RNA Sequencing library preparation. Dr. Xiao-Ou Zhang assisted with bioinformatic analysis.

Generation of conditional mouse model of hepatoblastoma

To engineer a conditional model of hepatoblastoma, I used hydrodynamic injection to co-deliver Sleeping Beauty transposon plasmids encoding *human* oncogenes including a TET-ON inducible YAP1^{S127A}, a constitutively expressed β -Catenin^{DeIN90} oncogene, and a luciferase reporter to the livers of mice expressing reverse tetracycline transactivator (Tg-rtTA) (**Figure 2.1A**) (185, 241, 385-387). The luciferase reporter and Sleeping Beauty transposase are encoded on the same plasmid (**Figure 2.1A**).

As an alternative approach for tumor initiation *in vivo*, I co-delivered a Sleeping Beauty rtTA (SB-rtTA) plasmid with my oncogenes and luciferase plasmids into wildtype FVB mice (**Figure 2.1A**). Previous work demonstrated co-expression of constitutive oncogenic YAP1^{S127A} and β -Catenin^{DeIN90} in mouse liver induces hepatoblastoma (See *Chapter 1.5 Laboratory Models*, *Chapter 1.8 Liver Tumorigenesis*)(31). YAP1^{S127A} and β -Catenin^{DeIN90} protein remain constitutively active by evading cytoplasmic retention and degradation (See *Chapter 1.5*

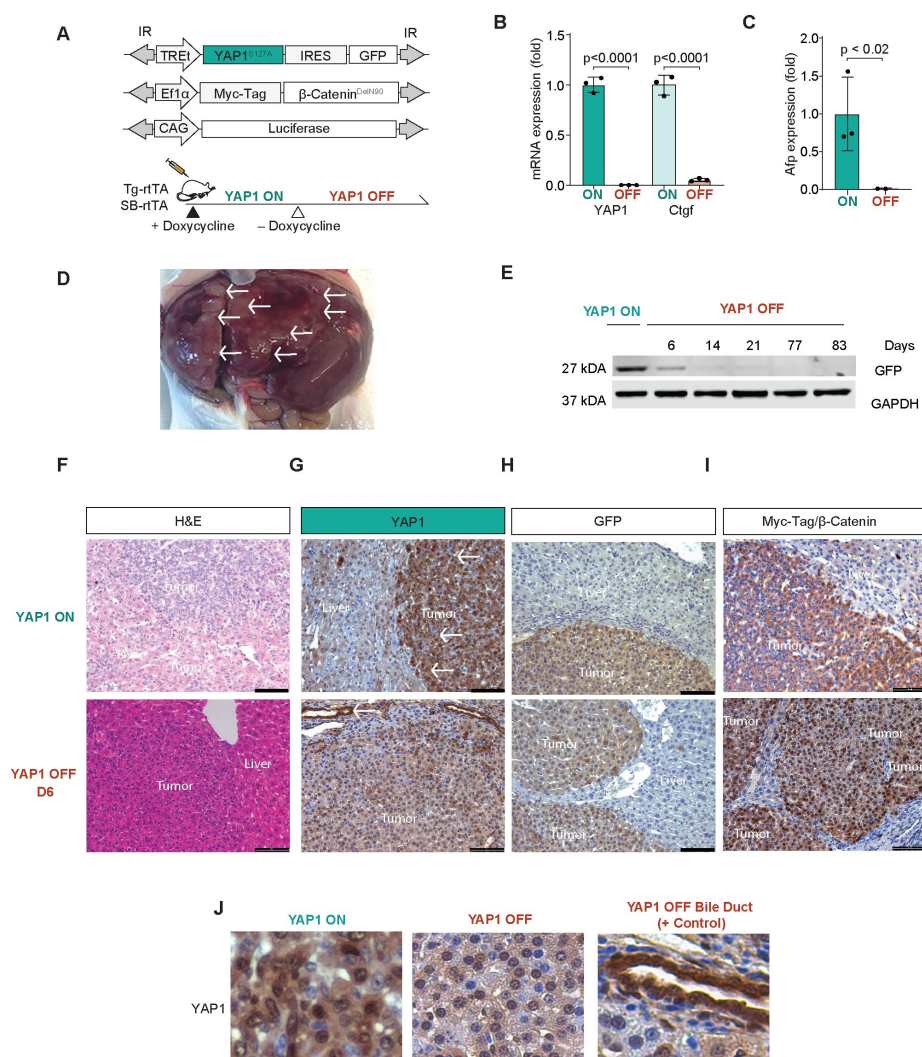


Figure 2.1 Conditional YAP1^{S127A} and constitutive β-catenin^{DelN90} drive hepatoblastoma in vivo (A) Sleeping Beauty transposon plasmids are hydrodynamically injected into the liver of transgenic rtTA mice (Tg-rTA). TREt encodes a TET-ON promoter, IR marks inverted repeats. Alternatively, rtTA was co-delivered with sleeping beauty plasmids to FVB mice by hydrodynamic injection (SB-rTA). (B-C) qPCR YAP1, Ctcf in YAP1 ON and YAP1 OFF D14-21, n=3 tumors per mouse, p < 0.0001 unpaired t-test, n=3 mice. qPCR of clinical HB marker Afp in YAP1 ON and YAP1 OFF D14-21, n=3 tumors per mouse, p < 0.02, unpaired t-test, n=3 mice. (D) Representative liver images, YAP1 ON SB-rTA mouse (E) Immunoblot of in vivo liver lysates (F-I) Representative H&E (20X lens) and IHC in YAP1 ON tumors, n=3 mice, YAP1 OFF D6 tumors, n=3, scale bars 100 μm (J) Enlarged sections from (G) YAP1 staining in YAP1 ON, YAP1 OFF D6, and positive control bile duct region in YAP1 OFF D6, Please note: 1A-C are a partial reprint of Figure 1, 1D is reprinted from Figure 3, and 1E-1I from Figure 1 and Supplemental Figure 1 as seen in Smith et al, Hepatology, 2020.

Laboratory Models, Chapter 1.8 Liver Tumorigenesis, Appendix III-IV (185, 386).

Using either transgenic Tg-rtTA or transposon SB-rtTA, human YAP1 overexpression can be reversibly regulated by feeding mice a diet with doxycycline (YAP1 ON) or without doxycycline (YAP1 OFF), so that I can study the relevance of modulating YAP1 expression *in vivo* in hepatoblastoma tumors (**Figure 2.1A**).

Consistent with previous work using constitutive YAP1, *in vivo* cooperation between inducible YAP1 and constitutive β -catenin drives the formation of large multi-focal liver tumors with hepatoblastoma features (**Figure 2.1D, F-I**). The TET-ON YAP1^{S127A} plasmid encodes a GFP reporter by an internal ribosomal entry site (IRES) (**Figure 2.1A**). By immunohistochemistry, YAP1 ON tumors were GFP-positive and express both nuclear β -catenin and nuclear YAP1 (**Figure 2.1F-I**). To functionally validate the conditional mouse model, I removed doxycycline to inhibit YAP1 (i.e. YAP1 OFF, **Figure 2.1A**). By Day 6, YAP1 nuclear expression was drastically reduced in hepatoblastoma tumors (**Figure 2.1G**). As an internal control, bile duct cells (marked with white arrow) remain positive for YAP1 adjacent to hepatoblastoma tumors (**Figure 2.1G**) (20).

The expression of YAP1 and its target gene, Ctgf, was significantly reduced in day 14 to 21 (D14-21) YAP1 OFF tumors (**Figure 2.1B**), demonstrating that the inducible YAP1 oncogene is rapidly inactivated (388). Additionally, I found that doxycycline withdrawal also silenced expression of GFP downstream of YAP1 (**Figure 2.1A, E**). Concordantly, α -fetoprotein (Afp), a clinical and prognostic

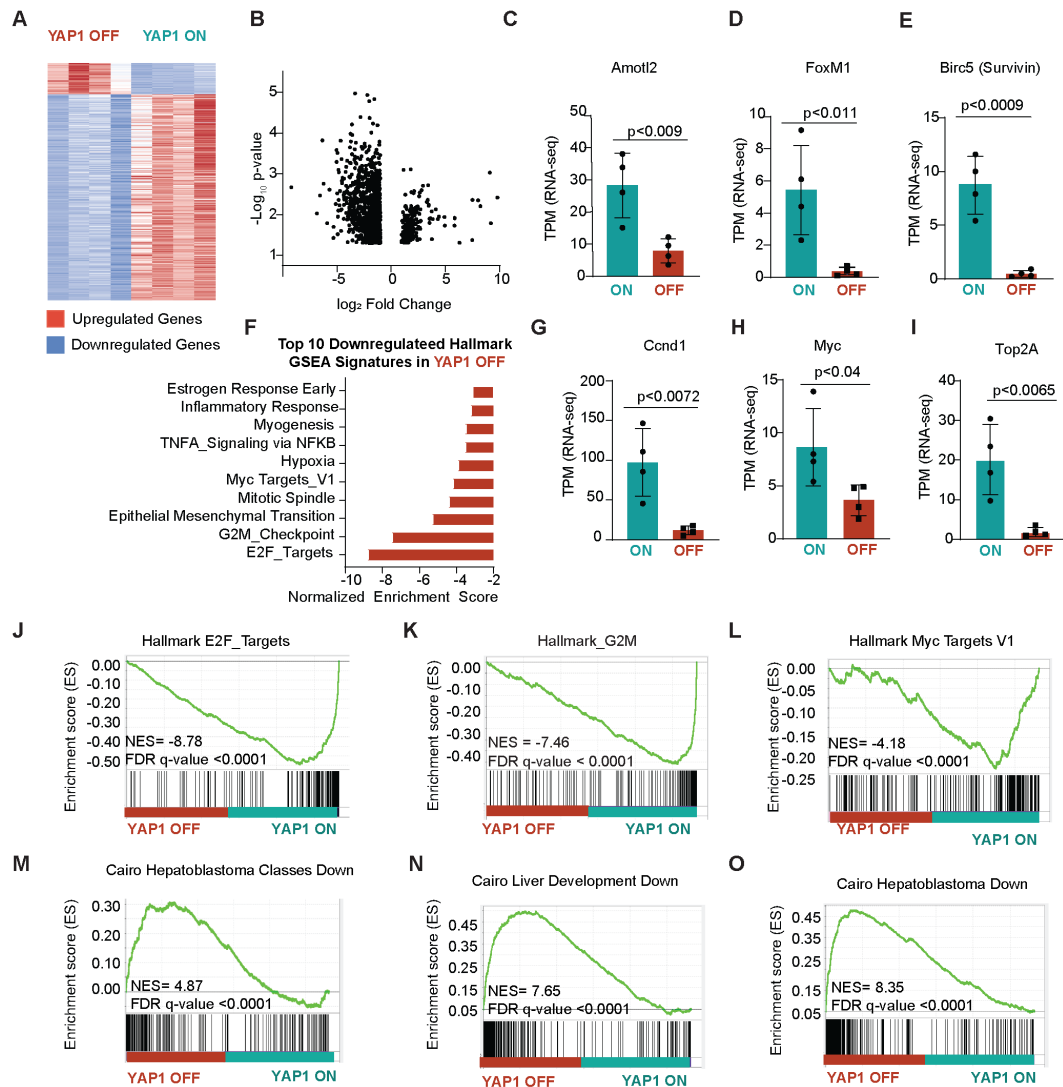


Figure 2.2 YAP1 withdrawal reprograms gene expression in murine hepatoblastoma.

(A) Heatmap of differentially expressed transcripts \log_2 fold change in YAP1 OFF D6 tumors compared to YAP1 ON tumors, $n=4$ tumors per group. (B) Volcano plot of differentially expressed genes in YAP1 OFF D6/YAP1 ON tumors. (C, D, E, G, H, I) TPM RNA-seq counts in YAP1 ON and YAP1 OFF D6 tumors, $n=4$ tumors per group, unpaired t-test. (F) Top 10 most downregulated Gene Set Enrichment Analysis (GSEA) Hallmark pathways in YAP1 OFF D6/ YAP1 ON tumors. (J-O) GSEA analysis in YAP1 OFF D6/ YAP1 ON tumors, FDR $q\text{-value} < 0.0001$. Please note: 2.2A-O is a partial reprint of Figure 2 from Smith et al, Hepatology, 2020.

(**Figure 2.1C**) (See *Chapter 1.3 Laboratory Findings and Imaging*) (135).

YAP1 withdrawal reprograms hepatoblastoma gene expression

To characterize the transcriptional landscape associated with YAP1 withdrawal, I compared the mRNA profiles of YAP1 ON and YAP1 OFF D6 early regressing tumors (**Figure 2.2A-B**). Consistent with the rapid inactivation of YAP1, many canonical YAP1 target genes were repressed in YAP1 OFF D6 murine tumors, including *Birc5*/Survivin, Angiomotin-like 2 (*Amotl2*), and Forkhead Box M1 (*FoxM1*) (See *Chapter 1.8 Hippo/YAP1 Signaling in Liver tumorigenesis*) (**Figure 2.2C-E**). In addition, six days of YAP1 inhibition suffices to downregulate many tumor-associated signatures, including proliferation signatures (*Hallmark G2M checkpoint, Mitotic Spindle, E2F targets*) (See *Chapter 1.4 Gene Expression Profiles*) (**Figure 2J-I**). *Appendix V* contains gene expression fold change of all coding genes with a p-value <0.05 for YAP1 OFF D6 tumors vs YAP1 ON.

Previous studies showed that YAP1 can co-regulate β -catenin target gene expression in vitro (4) (see *Chapter 1.8 Wnt and Hippo Crosstalk in Liver Tumorigenesis*). I observed that YAP1 inhibition alone, without modulation of oncogenic β -catenin, downregulates two canonical β -catenin target genes, *Myc* and *CyclinD1* (**Figure 2.2G-H**). Gene set enrichment analysis further suggests downregulation of *Myc* targets (*Hallmark_Myc_TargetsV1*) in YAP1 OFF D6 early regressing tumors (**Figure 2.2L**) (See *Section 1.8 Wnt and Hippo Crosstalk in*

Tumorigenesis). Thus, YAP1 inhibition in hepatoblastoma may partially abrogate the oncogenicity of β -catenin through downregulation of its target genes.

Conditional mouse model mimics aggressive human subtype

Children with well-differentiated HB tumors typically have higher five-year survival rates than children with tumors composed of undifferentiated cell types (1, 15, 180). Thus, differentiation status impacts HB prognosis (**Figure 1.16**) (See *Section 1.3 Clinical Treatment and Prognosis, Chapter 1.9 Hallmarks of Hepatoblastoma*). To this point, Cairo et al. first characterized children's hepatoblastoma tumors as either well-differentiated human pediatric hepatoblastoma Class 1 (C1) tumors with favorable outcomes or as undifferentiated highly proliferative Class 2 (C2) tumors with poor prognosis (**Figure 1.8, 1.9**) (See *Chapter 1.4 Cairo C1/C2 Classes*) (1).

Two recent publications have further stratified C1 and C2 classes proposing three sub-types of pediatric hepatoblastoma: characterized as favorable prognosis H1/C1, and two classes of intermediate to poor prognosis C2 tumors: H3/C2A and H2/C2B (**Figure 1.10**) (See *Chapter 1.4 Sumazin, Hooks Signatures*) (15, 180). All aforementioned studies point to underlying dysregulated Wnt signaling, regardless of tumor aggressiveness. Hooks et al. further suggests that the highly proliferative and aggressive C2-A subtype can be identified through

topoisomerase 2-alpha (Top2A) gene up-regulation and a simplified four-gene signature (180).

To characterize the subtype of hepatoblastoma recapitulated in my conditional model, I returned to my RNA-Sequencing of YAP1 ON tumors and YAP1 OFF D6. Using gene set enrichment analysis (GSEA), I found that six days of YAP1 withdrawal was sufficient to downregulate “C2” aggressive tumor signatures (**Figure 2M-O**). The *Cairo Hepatoblastoma Classes Down* gene signature discriminates between genes down regulated in invasive C2 tumors and favorable C1 tumors. Similarly, the *Cairo Hepatoblastoma* signature discriminates between tumor and normal liver (**Figure 2.2 M-O**). I find that YAP1 OFF upregulates GSEA signatures *Hepatoblastoma Classes Down*, *Cairo Hepatoblastoma Down*, and *Cairo Liver Development Down* (**Figure 2.2 M-O**).

To further characterize my conditional murine HB as congruent with a well-differentiated favorable C1 or a poor prognosis C2 subtype, I performed Ingenuity Pathway Analysis (IPA) comparing *YAP1 ON/YAP1 OFF D6* gene expression (**Figure 2.2A-B**) to *C2/C1 human hepatoblastoma microarray* from Cairo et al. (1). IPA Analysis revealed that top *Upstream Gene Pathways I*, *Canonical Pathways*, and *Disease/function IPA* signatures were congruent between YAP1 ON/OFF D6 mouse HB tumors and C2/C1 human HB tumors (**Figure 2.3A-C**) (389). These findings indicate that YAP1 ON tumors resemble aggressive C2 human HB tumors demonstrating the relevance of my model for evaluating therapeutic strategies.

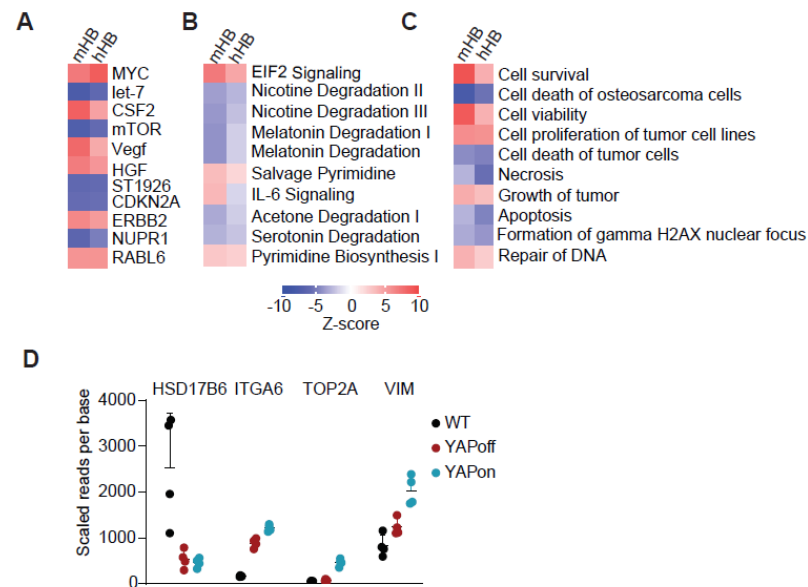


Figure 2.3 Conditional murine hepatoblastoma mimics the poor prognosis human subtype

(A-C) Mouse HB (mHB) gene signatures resemble human HB (hHB). IPA ingenuity analysis comparing YAP1 ON/OFF mouse HB to C2-poor/C1-favorable prognosis human HB microarray data from (1). Top 10 IPA Upstream Gene pathways I, Canonical Pathways, Disease/function signature pathways respectively (D) Hooks four gene signature in YAP1 ON, YAP1 OFF D6 tumors, and WT FVB RNA-seq for comparison. Figure 1.10 shows Hooks signature for comparison. YAP1 ON mirrors C2A, and YAP1 OFF mimics C1 tumors. *Please note: 2.3A-D is a partial reprint of Figure 1 and 2 from Smith et al, Hepatology, 2020.*

Finally, I used the Hooks 4-gene signature to further type my conditional murine tumors (**Figure 1.10**) (See Chapter 1.4 Hooks Four Gene Signature) (180).

To do so, I used RNA sequencing from WT FVB mice as a control sample to compare YAP1 ON, and YAP1 OFF D6 tumors. I find that my conditional murine tumor closely mimics the C2A proliferative subtype that expresses high levels of Top2A, and reduced levels of differentiation maker HSD17B6 (**Figure 2.2I, Figure 2.3D**) (180). Following withdrawal of YAP1, YAP1 OFF D6 tumors more closely

resemble C1 tumors using the four gene signature, suggesting that YAP1 status may mediate tumor aggressiveness (**Figure 2.3D**). Finally, consistent with Hooks et al (180), I find that my murine YAP1 ON tumors also upregulate GSEA Hallmark signatures *E2F targets*, *Miotic Spindle*, and *G2M* consistent with a C2A proliferative phenotype (**Figure 2.2 J-L**).

Taken together, these analyses suggest that YAP1 ON in conditional murine hepatoblastoma drives an aggressive phenotype consistent with the “C2” subgroup of pediatric tumors, and further, that withdrawal of YAP1 alone without , silencing of oncogenic of β -catenin, is enough to modulate the subtype of hepatoblastoma from a poor prognosis group, to a favorable group (**Figure 2.3**).

Genetic YAP1 inhibition results in >90% tumor regression

Using the luciferase reporter, I then serially monitored tumor progression over time in live mice using *in vivo* bioluminescent imaging. I found that YAP1 OFF tumors gradually regressed, and by 9 weeks luminescent signal was reduced 93% \pm 6% (n=3; **Figure 2.4A-F**).

Moreover, histological examination revealed ~10-fold fewer Ki67-positive proliferating cells in regressing YAP1 OFF D6-14 tumors than in YAP1 ON tumors (YAP1 ON, 242.5 ± 53.9 vs. YAP1 OFF, 26.8 ± 8.7 positive cells per 20 \times field; n=3) and a slight increase in cleaved caspase 3-positive apoptotic cells (YAP1 ON 0.416 ± 0.51 vs. YAP1 OFF 9.33 ± 8.75 positive cells per 20 \times field; n=3; **Figure**

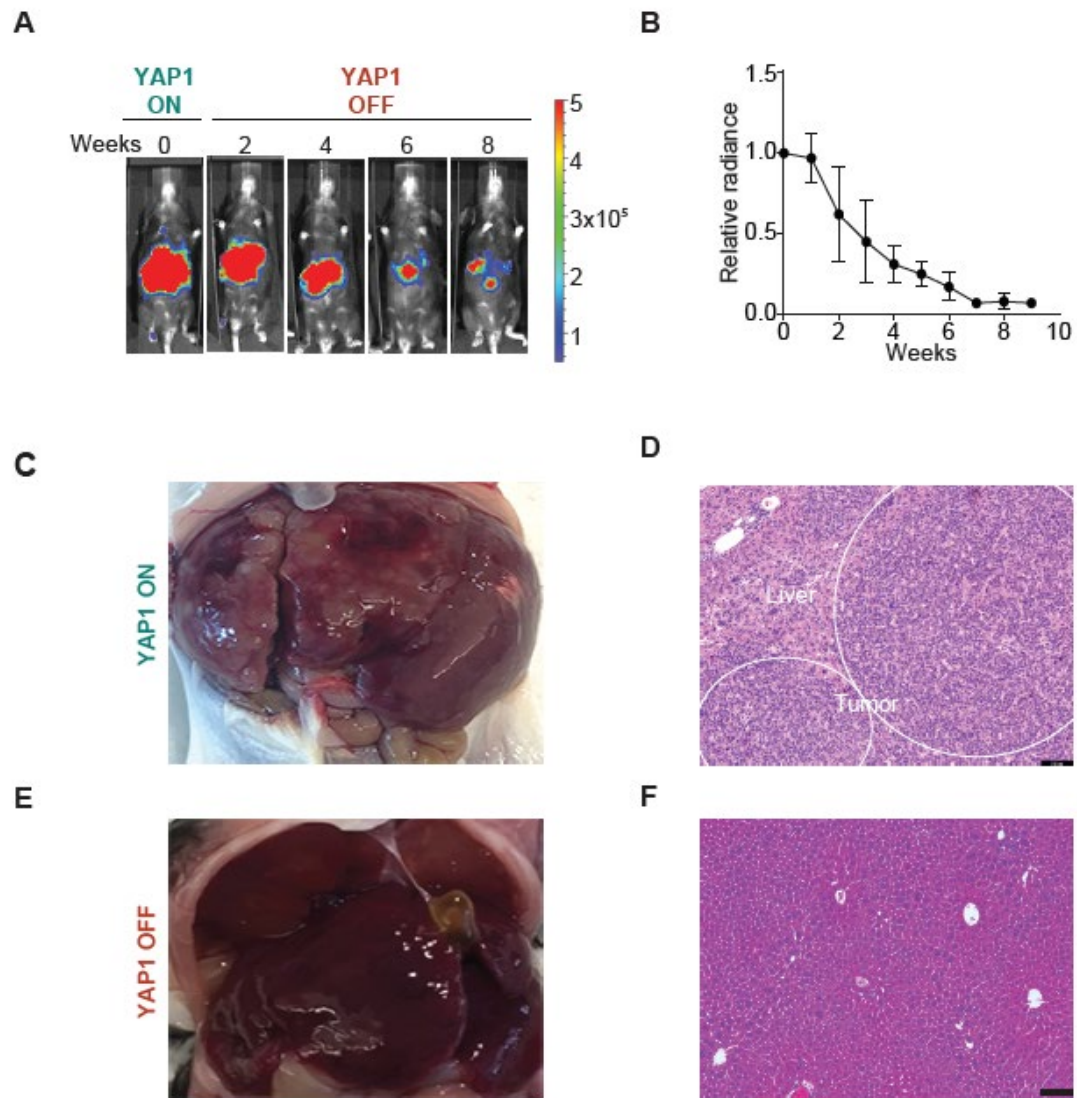


Figure 2.4 Genetic YAP1 inhibition results in >90% tumor regression in a conditional mouse model of hepatoblastoma. (A) Representative Luciferase imaging shows YAP1 OFF tumor regression, n=3 mice (B) Quantification of a. Mean relative luciferase; error bars are SEM, n=3 mice. (C-F) 10 weeks YAP1 OFF livers do not harbor macroscopic surface tumors compared to YAP1 ON. (C,E) Representative liver images, YAP1 ON SB-rtTA mouse and YAP1 OFF Tg-rtTA mice. (D,F) Paired histology from Panel C,E. YAP1 ON SB-rtTA mouse and YAP1 OFF Tg-rtTA mice are shown, scale bars 100 μ m. Note, Panel 2.2C is also shown in Figure 2.1C. Please note: 2.4A-F is a partial reprint of Figure 3 from Smith et al, *Hepatology*, 2020.

2.5A-D). These results indicate that genetic inhibition of YAP1 can regress hepatoblastoma driven by oncogenic YAP1 and β -catenin.

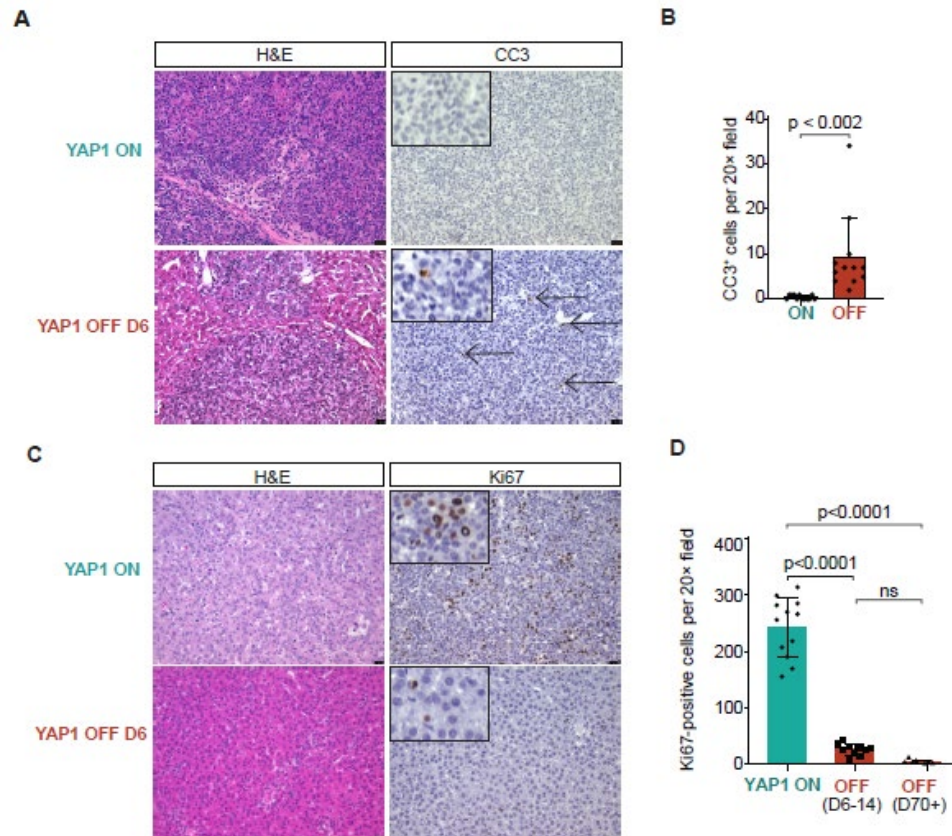


Figure 2.5 Genetic YAP1 inhibition promotes reduced proliferation and a mild increase in cleaved caspase-3 (CC3) *in vivo*. (A) Representative immunohistochemistry in YAP1 ON and YAP1 OFF D6 tumors, CC3, n=3, Scale bars 25 μ m. (B) Cleaved caspase 3 (CC3) positive cells in YAP1 ON and YAP1 OFF D3-14 tumors, n=4 20X sections per mouse, n=3 mice. (C) Representative immunohistochemistry in YAP1 ON and YAP1 OFF D6 tumors, Ki67, n=3, Scale bars 25 μ m. (D) Ki67+ cells per 20X field, n=4 20X sections per mouse, n=3 mice. One-Way Anova with Tukey multiple comparisons test. *Please note: 2.5A-D is a partial reprint of Figure 3, 4 and Supplemental Figure 2 from Smith et al, Hepatology, 2020.*

YAP1 withdrawal promotes long-term survival

I observed ~93% regression of HB tumors in YAP1 OFF livers by week 7, and no evidence of further regression or tumor relapse in weeks 8 or 9 (**Figure**

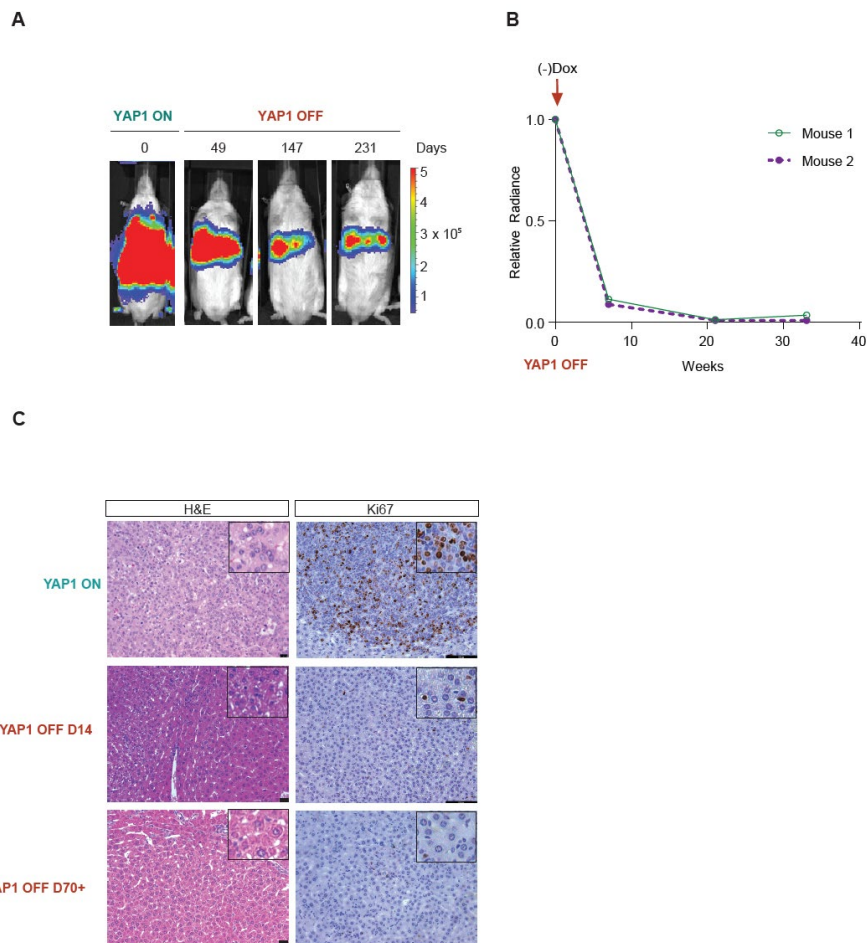


Figure 2.6. YAP1 withdrawal promotes long-term survival. (A) Long-term tumor regression in YAP1 OFF mice. Residual luminescent signal persists in YAP1 OFF mice (SB-rtTA plasmid) 231 days post-doxycycline withdrawal, n=2 mice. (B) Quantification of long term off relative luciferase signal, n=2, SB-rtTA mice (C) Representative histology and immunohistochemistry in YAP1 ON and YAP1 OFF tumors D14, D70, scale bars 100 μ m H&E, scale bars 25 μ m IHC. *Please note: 2.6A-C is a partial reprint of Figure 4, and Supplemental Figure 3 from Smith et al, Hepatology, 2020.*

2.4A-B), suggesting that tumor regression might be stable. After 10 weeks of YAP1 inhibition (Day 70) D70+, macroscopic examination of livers revealed no evidence of surface tumors (n=3; **Figure 2.4E**). Moreover, liver histology revealed a lack of obvious tumor nodules (**Figure 2.4F**), and proliferating Ki67-positive cells were virtually absent from YAP1 OFF D70+ livers (3.75 ± 2.83 positive cells per 20X field, n=3; **Figure 2.5C-D, 2.6C.**) compared to YAP1 ON tumors.

To evaluate long-term survival of YAP1 OFF mice, I allowed a cohort of mice to proceed with sustained YAP1 withdrawal (**Figure 2.6A**). Whereas YAP1 ON mice reached a lethal burden of tumors by 65.6 days on average post tumor initiation (n=8), YAP1 OFF mice were viable 230+ days after YAP1 OFF (n=2), and low levels of luciferase signal persisted in YAP1 OFF livers as mice aged (**Figure 2.6A-B**). Thus, sustained YAP1 withdrawal alone, without inactivation of oncogenic β -catenin, in this hepatoblastoma mouse model sufficiently drives durable tumor regression, providing long-term survival benefit.

Chapter 2.3 Discussion

In this chapter, I have shown that YAP1 inhibition represents a new targeted therapeutic strategy for the aggressive C2 subtype of pediatric hepatoblastoma resulting in >90% tumor regression. Thus, hepatoblastoma tumor maintenance requires YAP1.

Specifically, I have shown that hydrodynamic injection of mature hepatocytes with transposase plasmids encoding constitutive oncogenic β -catenin^{DeIN90} and doxycycline inducible YAP1^{S127A} drives hepatoblastoma-like tumors with features of embryonal, fetal, and mixed epithelial tumors (**Figure 2.1F-1**) (see *Chapter 1.3 Histologic subtypes of hepatoblastoma*). Inducible hepatoblastoma closely resembles other hydrodynamic models of hepatoblastoma first described by Tao et al (31) (See *Chapter 1.5 Laboratory Models*). Similar to the constitutive model, I observed induction of tumorigenesis around 4 weeks post-injection, and a lethal burden of tumors by approximately 11 weeks. Likewise, at 6+ weeks, YAP1 ON mice livers contained cream colored lesions that occupied the majority of visible liver (**Figure 2.1D**).

In my conditional TET-ON system, the YAP1 oncogene was rapidly inactivated once doxycycline was withdrawn. Nuclear YAP1 was substantially decreased in six-day YAP1 OFF livers (**Figure 2.1G**). This finding is consistent with the documented half-life of doxycycline in mice, approximately 6 hours (385, 390). Thus, full elimination of doxycycline from the plasma likely occurs ~50 hours.

Without doxycycline, YAP1^{S127A} expression is blunted, preventing nuclear translocation of YAP1 and its transcriptional program. The half-life of YAP1 protein *in vitro* is estimated to be approximately 20 hours in the nucleus, and 15 hours in the cytoplasm; thus complete degradation of nuclear YAP1^{S127A} could take upwards of four days following cessation of doxycycline treatment (391).

In the transposon inducible YAP1 plasmid (**Figure 2.1A**) GFP is encoded downstream of YAP1^{S127A} as an additional marker of *in vivo* transfected tumor cells. In my system, GFP expression remained detectable at six days by immunohistochemistry, and out until 14 days by western blot (**Figure 2.1E, H**). This is consistent with the longer half-life of GFP compared to YAP1, reported to be >26 hrs. *in vitro* (392).

Using transcriptomic profiling of YAP1 ON and YAP1 OFF D6 early regressing tumors, I observed that withdrawal of YAP1 alone, with continued oncogenic β -catenin signaling, is sufficient to downregulate GSEA pathways associated with the aggressive poor prognosis subtypes of human hepatoblastoma (**Figure 2.2-2.3**) (See *Chapter 1.4 Molecular Profiling of Hepatoblastoma*).

Further, YAP1 withdrawal, with continued β -Catenin signaling, induces apoptosis and tumor regression (**Figure 2.4-2.5**). In the adult liver, and similarly in hepatoblastoma, the crosstalk between Wnt and Hippo signaling remains complex, and poorly understood (See *Chapter 1.8 Liver Tumorigenesis*). For example, in

adult liver TRIB2, a β -catenin target gene, stabilizes YAP1 encouraging its nuclear translocation (371). Further, YAP1 promotes nuclear translocation of β -catenin, and promotes downstream expression of canonical β -catenin target genes, i.e. Myc and Cyclin D1 (18, 21, 31, 369). Indeed, in my conditional model, YAP1 withdrawal alone may be sufficient to induce tumor regression because it also dampens β -Catenin signaling (**Figure 2.2**) (4). I observe downregulation of Myc and Cyclin D1 with six days of YAP1 withdrawal (**Figure 2.2G-H**). Further, I find downregulation of the Myc Target V1 signature in YAP1 OFF tumors (**Figure 2.2**). Consistent with my findings, Tao et al. found that in hepatoblastoma-like HepG2 cells, YAP1 loss reduced β -catenin promoter activity, and target gene transcription (31). Further work will be needed to fully understand the crosstalk between β -Catenin and YAP1 *in vivo*.

These results provide preclinical evidence in favor of evaluating YAP1-targeted therapies, either alone or in combination, in the treatment of hepatoblastoma (See *Chapter 5.7 YAP1 Therapeutics*). Moreover, the >90% tumor regression suggests that YAP1 inhibition may benefit children as a neoadjuvant therapy to improve the resection of hepatoblastoma tumors, or as a post-resection adjuvant therapy to promote regression of residual disease.

The remarkable observation that YAP1 OFF mice retain stable reduced signal over the course of 200+ days, raised an interesting conundrum: If I cannot detect either grossly or histologically hepatoblastoma tumors, why do I observe

stable residual signal in YAP1 withdrawn mice? *Chapter III* will discuss the fate of hepatoblastoma cells after oncogene withdrawal and address the above conundrum.

Chapter 2.4 Tables

Table 2.1 Primer Sequences

Primer	Description	Sequence, 5' to 3'
P1	Human YAP1 qPCR_F	TAGCCCTGCGTAGCCAGTTA
P2	Human YAP1 qPCR_R	TCATGCTTAGTCCACTGTCTGT
P3	Mouse Gapdh qPCR_F	AGGTCGGTGTGAACGGATTTG
P4	Mouse Gapdh qPCR_R	TGTAGACCATGTAGTTGAGGTCA
P5	Mouse Afp qPCR_F	TGCTGCAAATTACCCATGAT
P6	Mouse Afp qPCR_R	CCAAAACTGGCTTGGATTT
P7	Mouse Ctgf_qPCR_F	GGGCCTCTTCTGCGATTTC
P8	Mouse Ctgf_qPCR_R	ATCCAGGCAAGTGCATTGGTA
P9	Human CYP3A5_qPCR_F	GGTGGTGATTCCAACCTTATGCT
P10	Human CYP3A5_qPCR_R	GCGTGTCTAATTTCAAGGGGA
P11	Human CES3_qPCR_F	CAACACCCGTCTTGACCAGTC
P12	Human CES3_qPCR_R	CTGGAACGCCTGGCATTG
P13	Human Sult2a1_qPCR_F	CGTGATGAGTTCGTGATAAGGG
P14	Human Sult2a1_qPCR_R	GGCAGAGAATCTCAGCCAACC
P15	Human OAT_qPCR_F	GTGGGGCTATACCGTGAAGG
P16	Human OAT_qPCR_R	TGGTCCAAAACCATCGTAACTG
P17	Human ApoA2_qPCR_F	CTGTGCTACTCCTCACCATCT
P18	Human ApoA2_qPCR_R	CTCTCCACACATGGCTCCTTT
P19	Human CYP2A6_qPCR_F	TCATGAAGATCAGTGAGCGCT
P21	Human CYP2A6_qPCR_R	TCATGTCCACACAGCACCA
P22	Human CYP2E1_qPCR_F	ATGTCTGCCCTCGGAGTCA
P23	Human CYP2E1_qPCR_R	CGATGATGGGAAGCGGGAAA
P24	Human CYP7A1_qPCR_F	GAGAAGGCAAACGGGTGAAC
P25	Human CYP7A1_qPCR_R	GGATTGGCACCAAATTGCAGA
P26	sgRNA_human_YAP1	TGCCCCAGACCGTGCCCATG

P27	sgRNA_Non_target	GCGAGGTATTCGGCTCCGCG
-----	------------------	----------------------

Table 2.1 IHC Antibodies

Antibody	Dilution	Secondary	Company	Catalog
YAP D8H1X	1:100	Rabbit	Cell Signaling Technology	14074
GFP D5.1	1:200	Rabbit	Cell Signaling Technology	2956
β -Catenin	1:200	Mouse	BD Bioscience	610154
FAH	1:400	Rabbit	Abcam	Ab83770
Cleaved Caspase 3	1:100	Rabbit	Cell Signaling Technology	9661
FoxA2/Hnf-3 β	1:200	Rabbit	Cell Signaling Technology	8186
Ki67 (SP6)	1:100	Rabbit	Thermo Fischer	MA5-14520
Myc-tag	1:100	Rabbit	Maine Medical	Vli01
RFP	1:400	Rabbit	Rockland	600-401-379
Hnf4 α	1:200	Goat	Santa Cruz	Sc-6556

Chapter 2.5 Materials and Methods

Plasmid Vectors

Addgene Plasmids:

H430, pT2/C-Luc//PGK-SB13, Addgene # 20207 (387)

H65, pT3-N90-Beta Catenin, Addgene #31785 (185)

Donated Plasmids:

H73, pT3-TREt- YAP1^{S127A}- IRES-GFP was a gift from the Scott Lowe lab (386).

H66, pT2-SB10 was a gift from the Hao Yin Lab.

Generated Plasmids

H592, pT2_PGK_rtTA

H592 was generated using the New England Biolabs Gibson protocol and master mix kit per the manufacturer's instructions (Cat # E5510S).

Animal Studies

All studies were performed with approval and in accordance with the University of Massachusetts Medical School Institutional Animal Care and Use Committee (IACUC). Mice were housed at University of Massachusetts Medical School Animal Facilities Core. Healthy male and female mice were used for studies and hydrodynamically injected at >8 weeks of age. Mouse strains purchased from Jax laboratories include: B6.Cg-Gt(ROSA)26Sortm1.1(CAG-rtTA3)Slowe/LdowJ

(Strain#029627), B6N.FVB(Cg)-Tg(CAG-rtTA3)4288Slowe/J (Strain #016532) and FVB/NJ (Strain #001800).

Hydrodynamic Injection

All plasmids used for *in vivo* injection were purified using the Qiagen Maxi-Prep Endotoxin-free Kit (Qiagen, 12362) according to the manufacturer's instructions. 4-15 ug per plasmid per mouse were mixed together in 0.9% sterile saline at room temperature. Mice were weighed prior to injection and dosed with 10% body weight of the saline mixture. Plasmids were then delivered to mice by hydrodynamic tail vein injection. Specifically, within 5-7 seconds plasmids were continuously and smoothly injected (239). Mice were then warmed by heat lamp or heat pad for a minimum of 30 min to recover from injection shock.

TET-ON Studies

To establish doxycycline-inducible tumors, mice were treated with doxycycline chow (625 mg/kg) (TD.01306, Envigo) for ~8 weeks following hydrodynamic injection. Doxycycline treated chow was refreshed weekly. Tumors were established in transgenic-rtTA (Tg-rtTA) mice and all downstream analyses were performed in Tg-rtTA mice unless otherwise noted in respective figure legends. The study endpoint for YAP1 ON tumor mice was 2+ signs of distress.

IVIS Bioluminescent imaging

At the indicated time post injection, mice were given 200 μ l luciferin (15 mg/ml) intraperitoneally. Signal was allowed to stabilize for 10 min, and mice were then anesthetized with 3-5 minutes of 1-3% isoflurane. Mice were loaded into the Perkin Elmer IVIS machine for capture of luminescent signal (1-minute standard exposure, scale 5e4 to 5e5 radiance).

Histology and Immunohistochemistry

Mouse liver tissue was fixed in 4% formalin overnight and then dehydrated in 70% ethanol for 24+ hrs. Tissues were embedded and cut as 4 μ m paraffin sections and stained for H&E by the UMassMed Morphology Core. Cut sections were prepared for immunohistochemistry staining by deparaffinization with xylene, and serial ethanol dilution for dehydration. Slides were then boiled 9m for antigen retrieval with 1 mM citrate buffer (pH6.0). Endogenous peroxide activities were inactivated with 3% hydrogen peroxide for 10 mins at room temperature. Mouse primary antibody samples were first treated with M.O.M. Mouse on Mouse Blocking Reagent (Vector Labs, MKB-2213) before tissue blocking. Next, samples were incubated with from ImmPRESS™ HRP Anti-Rabbit IgG (Peroxidase) Polymer Detection Kit (Vector labs, MP-7401-50) 5% normal horse serum for 1 hour at room temperature. Following blocking, tissues were incubated overnight with primary antibody at 4C (**Table 2.1**). Secondary antibody incubation was for one hour at

room temperature with secondary HRP antibody (Vector labs, MP-7401-50). Tissues were developed with diaminobenzidine (DAB) substrate/chromogen (Fisher Scientific, TA-125-QHDX). Next, hematoxylin was used to counterstain tissues followed by ethanol dehydration, and re-paraffinization with xylene. Slides were then sealed with a coverslip. H&E or IHC images were captured using a Leica DMI8 microscope. IHC slides were quantified by selection of four random fields per paraffin embedded section, and positive hepatocytes per 20X field counted.

Immunoblot

Whole cell extracts or mouse liver was lysed in RIPA buffer treated with 1:100 Halt phosphatase cocktail inhibitor (Thermo Fisher 78420) and 1:50 Roche Complete protease inhibitor (11836145001). Lysates were boiled for 5 minutes at 95C with Nupage 4X Sample buffer (Invitrogen NP0007). Protein concentration was measured using Pierce BCA Protein Assay Kit (Catalog #23225). Equal amounts of mouse liver protein were separated on a 4-12% Bis Tris gel and transferred to a nitrocellulose membrane and blocked with Odyssey Blocking buffer. Blots were probed with primary antibodies Gapdh 1:1000 (EMD MAB274), and GFP 1:2000 (CST 2956) overnight at 4C. Blots were then incubated with a fluorescent secondary antibody (LICOR) and imaged on the Odyssey Imaging Platform.

RNA Extraction, cDNA synthesis, Quantitative PCR

RNA was extracted from *in vitro* cell lines using the RNAeasy Qiagen RNA Isolation Kit (Catalog #74104) per the manufacturer's instructions. RNA was extracted from mouse liver tissue using TRIzol RNA Isolation Reagent (15596026) followed by a chloroform extraction. cDNA was synthesized using the High-Capacity cDNA Reverse Transcription Kit (4368814) and 1.5 ug RNA template. Quantitative PCR was performed using the SSoFast EvaGreen Supermix (1725200) and Real-Time PCR Detection System CFX96 by BioRad. Primers sequences are in **Table 2.1**.

RNA-Sequencing Library Preparation and Analysis

RNA-Sequencing (RNA-seq) libraries for YAP1 ON and YAP1 OFF D6 were prepared as previously described (15, 16). RNA sequencing was performed in YAP1 ON and YAP1 OFF D6 tumors without luciferase (n=4 tumors, n=1 mouse). Library quantification was performed using the KAPA Library Quantification Kit. Libraries were sequenced using the Illumina NextSeq 500 system. RNA-seq reads from each sample (n=4 tumors per group) were aligned to the reference genome using STAR (version 2.5.2b). RSEM (v1.2.31), GENCODE V19 gene annotation were used to quantify gene expression, and htSeq, DESeq2 (1.22.0) for identification of differentially expressed genes (17-20).

Ingenuity Analysis

Functional analyses were generated through the use of IPA (Qiagen, Inc) (389). Gene expression from RNA-sequencing of YAP1 ON and YAP1 OFF D6 tumors was compared to microarray expression for human C2 and C2 hepatoblastoma tumors. Microarray accession below.

Microarray Data Accession

Microarray data used in the IPA pathway analysis was accessed through ArrayExpress (<http://www.ebi.ac.uk/microarray-as/ae/>) under the accession numbers E-MEXP-1851 (HB transcriptome), E-MEXP-1852 (HB aCGH), and E-MEXP-1853 (mouse liver) (1).

Statistical Analysis

All statistical analyses were performed using GraphPad Prism 8 including One Way Anova with Tukey Test for analysis of 2+ samples, and Student's T-Test for comparison across 2-samples. All analyses are described in figure legends.

CHAPTER III YAP1 WITHDRAWAL INDUCES GENERATION OF “HB-HEPS”

Chapter 3.1 Introduction

In *Chapter II*, I demonstrated that YAP1 withdrawal promotes 90% regression in conditional murine hepatoblastoma tumors over the course of 9 weeks (**Figure 2.3**). I next sought to understand the fate of hepatoblastoma tumor cells following oncogene withdrawal. Historically, inactivation of a driver oncogene necessary for tumor maintenance was thought to result in one of two primary outcomes: tumor cells may 1) *undergo apoptosis/senescence and eventually be cleared*, or 2) *the tumor cells may regress slightly, and residual cells remain*

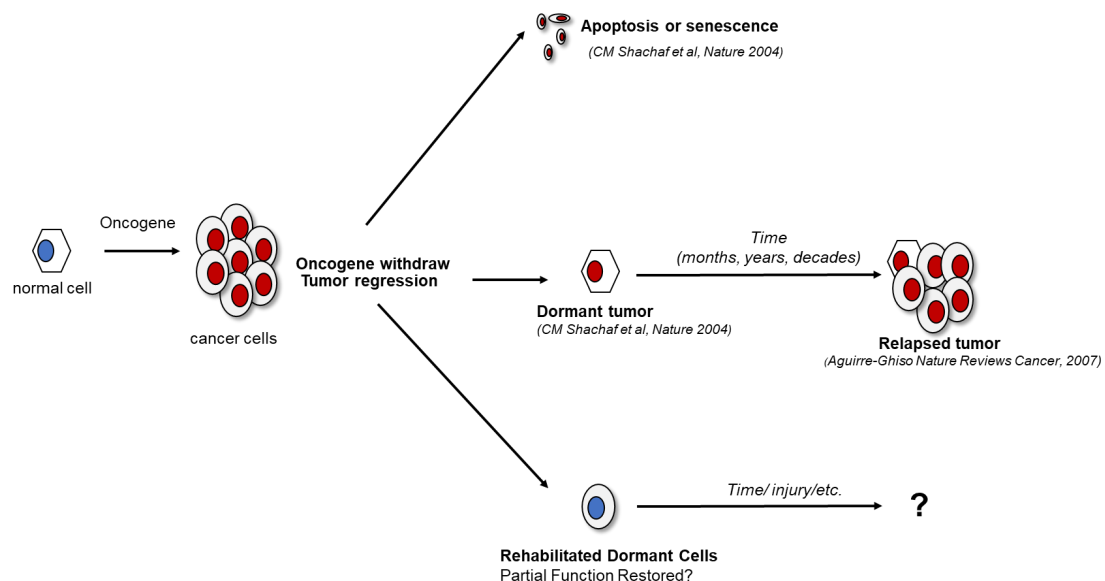


Figure 3.1 Outcomes of oncogene withdrawal. Following withdrawal of a necessary oncogene, tumors frequently undergo apoptosis, senescence or dormancy. I propose that in hepatoblastoma, YAP1 withdrawal promotes functional differentiation of tumor cells

dormant for a variable amount of time before relapse (Figure 3.1) (See Chapter 1.8 Liver Tumorigenesis). Importantly, withdrawal of an oncogene can have tissue-specific effects (233, 393-395). For example, MYC oncogene withdrawal results primarily in apoptosis in hematopoietic malignancies; whereas, in hepatocellular carcinoma MYC withdrawal promotes initial differentiation, dormancy and eventual relapse (233, 393-395).

In my model of hepatoblastoma, the lack of distinct tumor nodules at Day 70 (**Figure 2.4E**), the increase in apoptotic markers in early regressing tumors (**Figure 2.5A-B**), and the presence of residual luminescent signal (**Figure 2.6**) suggested that perhaps YAP1 withdrawal was promoting two alternative fates in hepatoblastoma cell: apoptosis or differentiation. I hypothesized that YAP1 withdrawal induced a cell fate switch promoting apoptosis in one subset of cells, and differentiation towards a hepatocyte-like state in another subset of tumor cells.

Hepatocytes are incredibly plastic. In liver development and regeneration, YAP1 signaling modulates liver cell fate, promoting a stem-like phenotype (See *Chapter 1.6 Liver Development, 1.7 Liver Differentiation*) (19, 20, 349). Specifically, YAP1 and differentiation signaling are often polarized (20). Specifically, YAP1 can control enhancer occupancy and downregulate expression of liver differentiation factors (See *Chapter 1.6 Liver Development, Chapter 1.7 Liver Development*) (20, 23, 283). Development of terminally differentiated hepatocytes requires expression of several HNF family members, including

HNF4 α . (259, 290, 301, 308, 311, 314). Extensively reviewed in *Chapter 1.7 Liver Differentiation*, proper liver zonation metabolic function of the liver including: fatty acid oxidation, xenobiotic metabolism and cholesterol synthesis requires coordinated expression of HNF family members (**Figure 1.12, Figure 1.13**). Importantly, and critical for the upcoming chapter, singular expression of any HNF family transcription factor is not sufficient to induce normal hepatocyte transcription (296-299).

The following chapter explores the fate of hepatoblastoma cells after YAP1 withdrawal, and further investigates what biological mechanisms promote differentiation in hepatoblastoma tumors. Using transcriptomic analysis, and ATAC-Seq, in *Chapter III* I show that YAP1 withdrawal globally reprograms the chromatin accessibility of a subset of tumor parentage cells. Specifically, loss of YAP1 promotes increased transcription factor binding at multiple HNF family member motifs promoting hepatocyte differentiation.

Chapter 3.2 Results

Attributions: Dr. Xiao-Ou Zhang assisted with bioinformatic analysis of RNA sequencing of YAP1 ON and YAP1 OFF D6 tumors. Bioinformatic analysis assistance was provided by Dr. Suet-Yan Kwan for TCGA analysis of human liver cancer microarray and RNA-sequencing. Dr. Suet-Yan Kwan and Qiang-Zhong Yin assisted with tissue culture and RT-qPCR for Huh6 cells treated with sgNT and sgYAP1. Tomas Rodriguez and Henry Pratt assisted with ATAC-seq library preparation, sequencing, and bioinformatic analysis of YAP1 ON, YAP1 OFF D6, hbHeps, and WT liver.

YAP1 Inhibited livers harbor tumor lineage cells

The persistent luminescence in YAP1 OFF D230+ livers suggested that, although tumors were significantly regressed, YAP1 OFF livers retain residual cells of tumor lineage. Indeed, staining YAP1 OFF D70+ livers for the Myc-tag fused to oncogenic β -catenin (**Figure 2.1A**) revealed regions of Myc-tag-positive cells with hepatocyte morphology (13 ± 9.9 residual nodules per liver section, $n=4$ mice; **Figure 3.2A-E**).

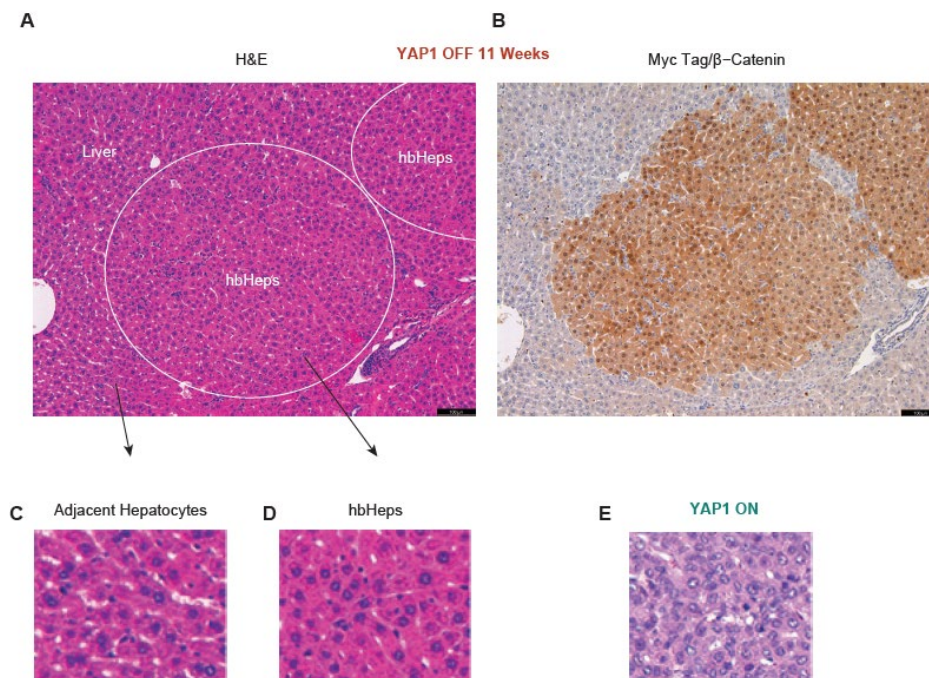


Figure 3.2 Sustained YAP1 withdrawal generates non-proliferative tumor lineage cells with hepatocyte morphology. (A-E) Myc-tag IHC detects residual cells of tumor lineage (circled area) with hepatocyte morphology in YAP1 OFF mice ($n=4$). I termed these cells hepatoblastoma-derived hepatocyte-like cells (hbHep). Scale bars are 100 μ m, YAP1 ON tumor H&E serves as a control. *Please note: 3.2A-E is a partial reprint of Figure 4 from Smith et al, Hepatology, 2020.*

Further, reintroducing doxycycline to the diet after tumor regression induced tumor growth (**Figure 3.3**). Nevertheless, with sustained YAP1 withdrawal, residual tumor lineage cells remain camouflaged within the liver (**Figure 3.2**). Because they are morphologically similar to normal hepatocytes, I have termed these residual tumor lineage cells “hepatoblastoma-derived hepatocyte-like cells” (hbHep cells).

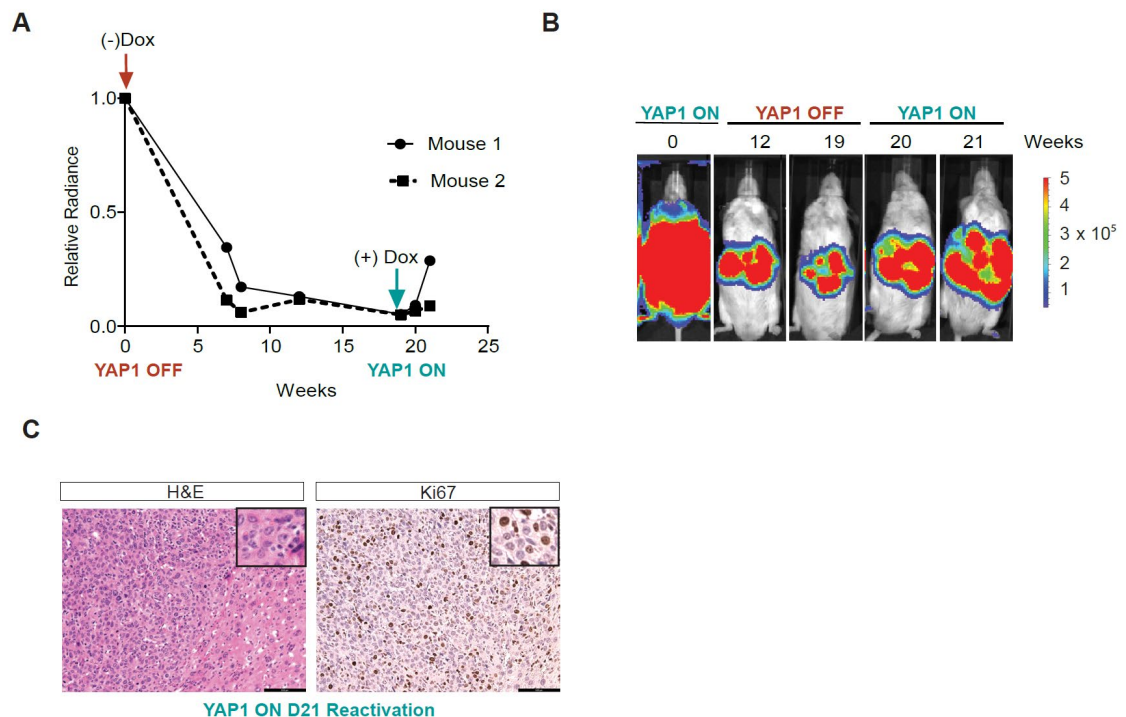


Figure 3.3 Reactivation of YAP1 promotes tumor proliferation. (A) Quantification of luminescent radiance, mice were treated with doxycycline for 8 weeks prior to withdrawal and monitored for 18+ weeks, n=2 SB-rtTA plasmid, n=3 Tg-rtTA not shown (B) Representative luminescent imaging in one SB-rtTA plasmid mouse. (C) Representative IHC Ki67 in SB-rtTA, (n=4 mice), Scale Bars 100 μ m. Please note: 3.3A-C is a reprint of Supplemental Figure 4 from Smith et al, Hepatology, 2020.

YAP1 inactivation promotes liver differentiation signaling

In my RNA-Seq analysis of early regressing YAP1 OFF tumors D6 (**Figure 2.2**), the top 10 upregulated GSEA hallmark pathways included multiple liver metabolic pathways associated with normal hepatocyte function, such as xenobiotic and fatty acid metabolism pathways. This finding suggests that YAP1

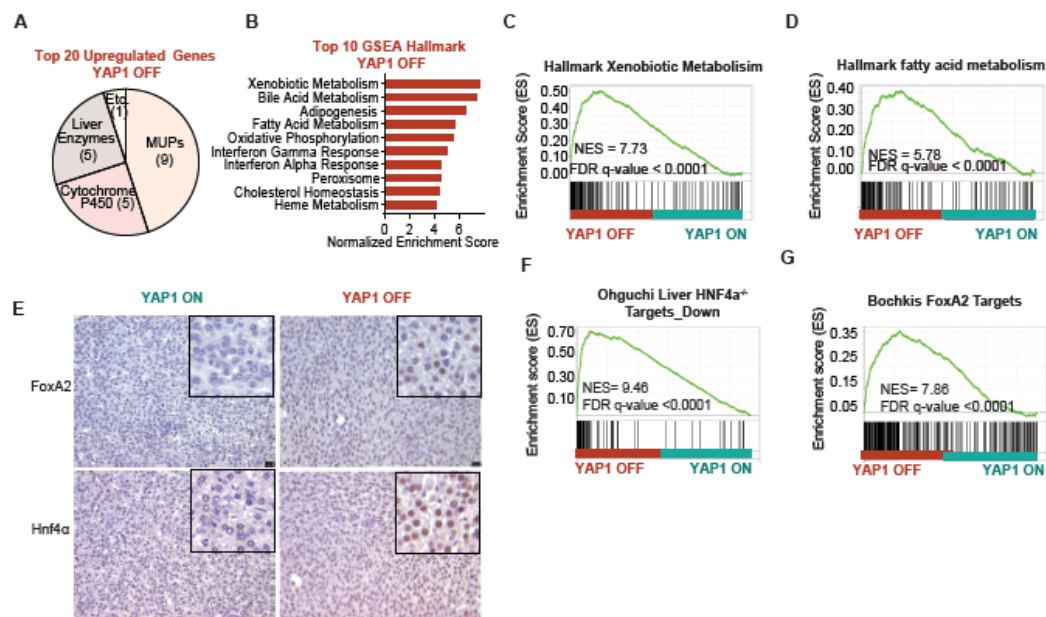


Figure 3.4 YAP1 withdrawal induces mature hepatocyte gene expression in hepatoblastoma tumors. (A) 20 most upregulated genes in YAP1 OFF tumor RNA-Seq include major urinary proteins (Mups), cytochrome p450 enzymes, and other metabolic liver enzymes. (B) Top GSEA signatures. (C-D) Representative GSEA Signatures. (E) YAP1 OFF induces hepatocyte differentiation factors Foxa2 and Hnf4a. Representative immunohistochemistry in YAP1 OFF D6 compared to YAP1 ON, scale bars 25 μ m. (F-G) Representative GSEA Signatures. *Please note: 3.4A-G is a partial reprint of Figure 5, and Supplemental Figure 5 from Smith et al, Hepatology, 2020.*

withdrawal induces mature hepatocyte gene expression in hepatoblastoma tumors (Figure 3.4A-D, Table 3.1). Tables can be found following the discussion section.

Consistent with the hepatocyte-like morphology of hbHeps, I hypothesized that

YAP1 inhibition activated a cell fate switch driving differentiation of HB tumor cells towards mature hepatocytes.

Discussed in *Chapter 3.1 Introduction*, YAP1 and differentiation signaling often work in opposition in the liver (See *Section 1.7 Liver Differentiation*) (21, 22, 25, 280, 283, 295). Indeed, GSEA analysis shows target genes of mouse Hnf4 α and FoxA2—transcription factors that promote hepatocyte differentiation were both upregulated in YAP1 OFF tumors (**Fig 3.4F-G**) (262, 295, 396). Further, immunohistochemistry revealed the presence of nuclear Hnf4 α and FoxA2 in

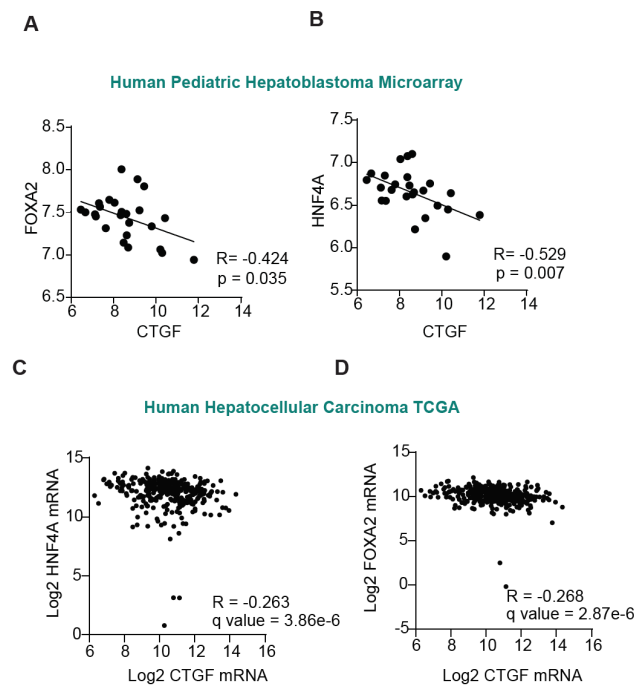


Figure 3.5 YAP1 target gene *CTGF* and *HNF4 α /FOXA2* are inversely correlated in human hepatoblastoma and hepatocellular carcinoma. (A-B) Inverse correlation between YAP1 target gene *CTGF* and differentiation markers in human hepatoblastoma microarray data (n=25)(1), Spearman's Correlation analysis. **(C-D)** Inverse correlation between YAP1 target gene *CTGF* and differentiation markers in human hepatocellular carcinoma TCGA data (n=348) (2), Spearman's Correlation analysis. *Please note: 3.5A-D is a partial reprint of Figure 5 from Smith et al, Hepatology, 2020.*

YAP1 OFF D6 tumors but not in YAP1 ON tumors (**Figure 3.4E**). Concordantly, in both human pediatric hepatoblastoma microarray (1) and human hepatocellular carcinoma TCGA datasets (2), the YAP1 target genes *CTGF* and *HNF4α/FOXA2* are inversely correlated, indicating the general role of YAP1 in suppressing differentiation in human liver cancer (**Figure 3.5A-D**).

I further explored this phenomenon in human hepatoblastoma cells. I used CRISPR/Cas9 to knock-out YAP1 in Huh6 hepatoblastoma cells. Huh6 cells are human hepatoblastoma cells from a 1 year old male patient heterozygous for CTNNB1 p.Gly34Val and known to express nuclear YAP1 (228). Following YAP1 knockout, I observed an increase in canonical liver markers indicative of a more

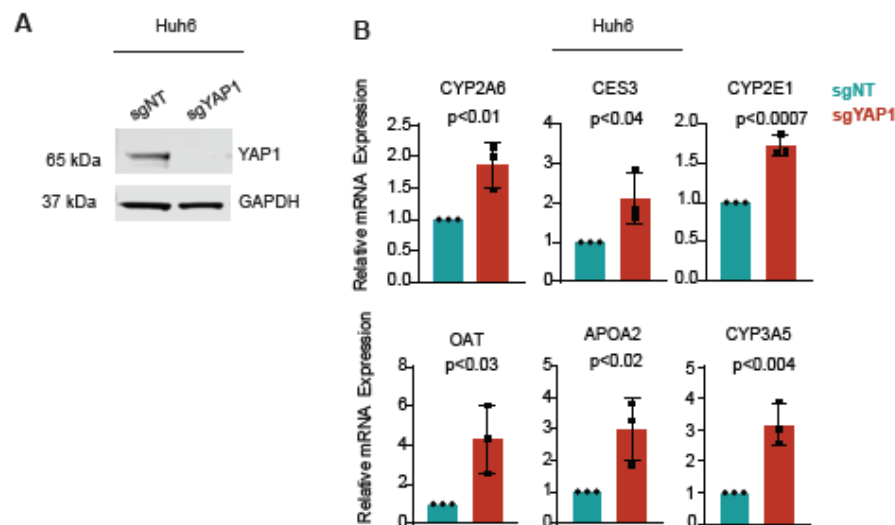


Figure 3.6 *In vitro* YAP1 knockdown in human hepatoblastoma cells upregulates markers of differentiation (A) Representative western blot, Huh6 cells, n=3 (B) qPCR relative quantification of hepatocyte differentiation genes in sgNT and sgYAP1 Huh6 cells, n=3. Please note: 3.6A-B is a partial reprint of Supplemental Figure 5 from Smith et al, *Hepatology*, 2020.

differentiated hepatocyte state including: Apolipoprotein A2 (ApoA2),

Carboxylesterase 3 (CES3), Cytochrome Cyp2A6, Cytochrome Cyp2e1, Cytochrome Cyp3A5, and Ornithine aminotransferase (OAT) (**Figure 3.6A-B**) (See *Chapter 1.7 Liver Differentiation*).

Further, the top 5 genes upregulated in YAP1 OFF D6 tumors belong to the family of major urinary proteins (Mups) (**Figure 3.7A-B, Table 3.1**). Mup proteins serve as a marker of mature hepatocytes (265, 266). Immunofluorescence detected virtually no Mup expression in YAP1 ON tumors, and partially restored levels of Mup in hbHep cells compared to adjacent normal hepatocytes in YAP1 OFF D70+ livers (**Figure 3.7A**). These findings further support YAP1 withdrawal

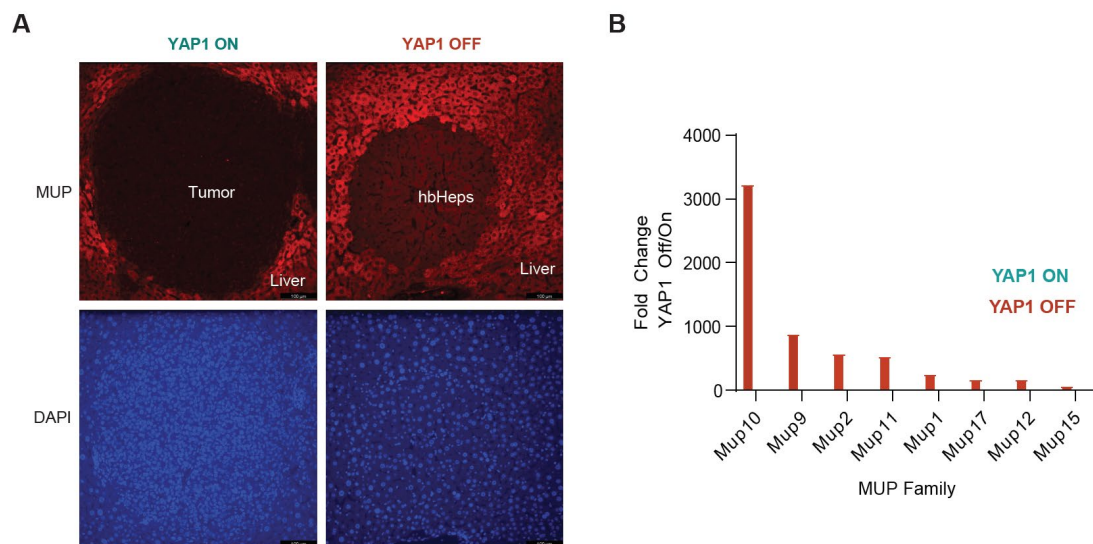


Figure 3.7 YAP1 withdrawal promotes upregulation of mature hepatocyte marker, Mup (A) Hepatocyte marker Mup is partially restored in long-term YAP1 OFF D70 hbHep cells compared to YAP1 ON tumors, scale bars 100 μ m. Representative immunofluorescence shown. (B) Fold change of gene expression in YAP1 ON vs. YAP1 OFF D6 tumors, n=4 tumors, p<0.05, Fold change>2. *Please note: 3.7A-B is a partial reprint of Figure 5, and Supplemental Figure 5 from Smith et al, Hepatology, 2020.*

promoting induction of mature hepatocyte gene expression in hepatoblastoma tumor cells.

Modulation of chromatin contributes to generation of hbHeps

I hypothesized that YAP1 withdrawal drives transcriptional reprogramming, upregulation of mature hepatocyte gene expression, and the subsequent

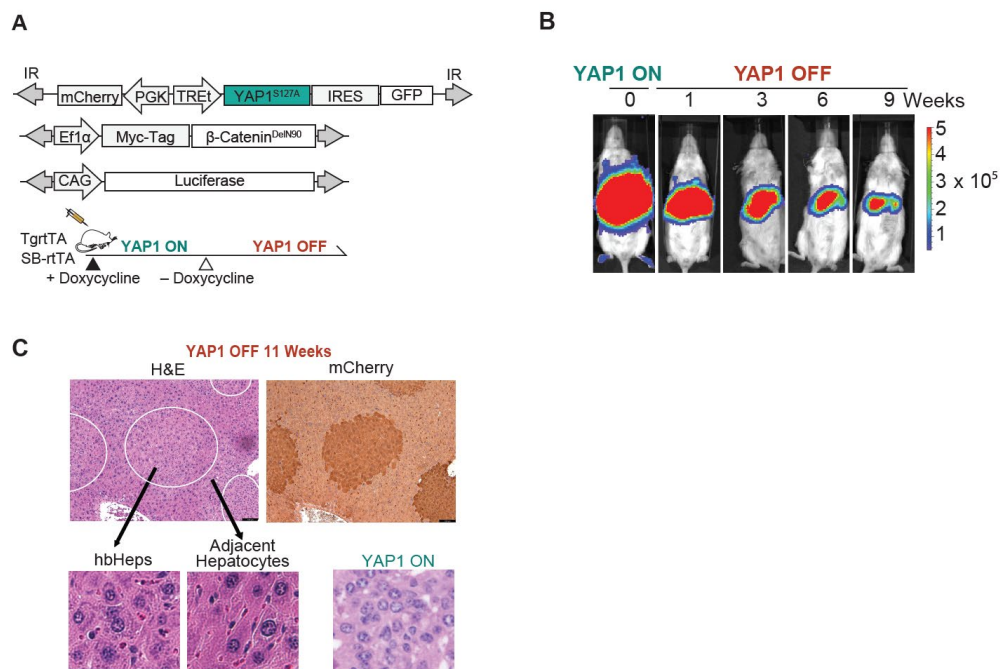


Figure 3.8 Generation of lineage tracing system to track “hbHep” cells (A) Lineage Tracing Schematic **(B)** Representative in vivo luminescent imaging in one SB-rTA plasmid mouse 8 weeks post-doxycycline withdrawal, validating lineage tracing model. The mouse was treated with doxycycline for 8 weeks prior to withdrawal. **(C)** H&E and immunohistochemistry from SB-rTA mouse in (B), validating lineage tracing construct, scale bars 100 μ m Please note: 3.8A-C is partial reprint of Supplemental Figure 6 from Smith et al, *Hepatology*, 2020.

generation of hbHep cells, in part through modulation of liver chromatin accessibility. YAP1 can exert transcriptional control through regulation of

chromatin structure, specifically enhancer regions (See *Chapter 1.8 Hippo/YAP1 in Liver Tumorigenesis*) (363, 365). To assess open chromatin structure, I

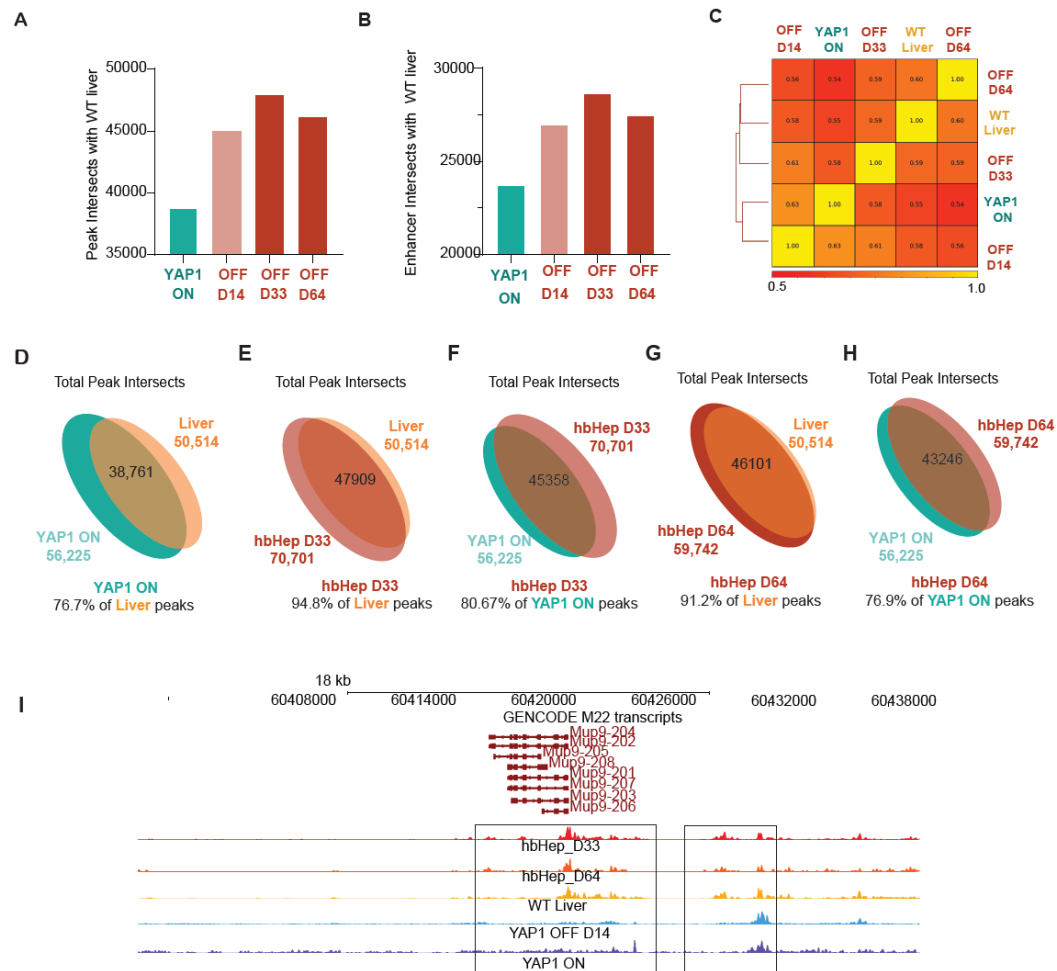


Figure 3.9 YAP1 withdrawal reprograms hepatoblastoma chromatin accessibility

(A) ATAC peak intersects shared with WT liver in YAP1 ON, YAP1 OFF D14 regressing tumor, and hbHeps YAP1 OFF D33 and D64 **(B)** Enhancer peak intersects shared with WT liver in YAP1 ON, YAP1 OFF D14 regressing tumor, and hbHeps YAP1 OFF D33 and D64. **(C)** Spearman correlation values with hierarchical clustering YAP1 ON, YAP1 OFF D14, hbHeps D33 and D64. **(D-H)** Total ATAC peak intersects between hbHeps D64 and WT liver, WT liver and YAP1 ON tumor. Not to scale. **(I)** Representative genome browser ATAC tracks for Mup9, gene found to be highly upregulated in RNA-seq YAP1 OFF D6/YAP1 ON. Please note: 3.9A-I is partial reprint of Figure 6, and Supplemental Figure 6 from Smith et al, *Hepatology*, 2020.

performed ATAC-seq in YAP1 ON, YAP1 OFF D14 tumors, hbHep cells (D33 and

D64) and normal liver (397). I isolated hbHep cells by fluorescently labeling them with mCherry upstream of TET- ON *YAP1*^{S127A} (**Figure 3.8A-C**). Using mCherry as a lineage tracing marker, I confirmed that the mCherry+ area in the YAP1 OFF livers were of the tumor lineage (**Figure 3.8A-C**).

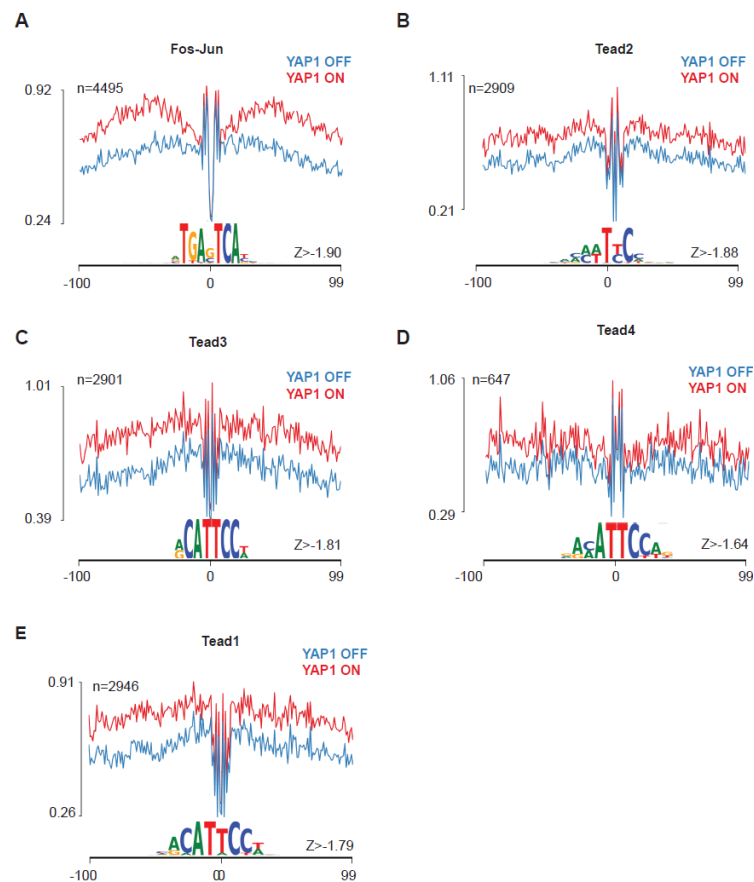


Figure 3.10 Decreased Tead and Fos-Jun occupancy in hbHeps D33 compared to YAP1 ON tumors (A-E) DNA Footprinting analysis of ATAC Seq. YAP1 OFF hbHeps D33 shows decreased occupancy at Tead1-4, and Fos-Jun motifs compared to YAP1 ON tumors. *Please note: 3.10A-E is a partial reprint of Figure 6, and Supplemental Figure 9 from Smith et al, Hepatology, 2020.*

By analyzing intersected ATAC-seq peaks between YAP1 ON, YAP1 OFF D14 regressing tumors, hbHep cells, and WT liver, I observed that hbHep cells share a higher percent of intersected ATAC peaks and enhancers with WT liver than with YAP1 ON (**Figure 3.9A-B, D-H**). Next, I performed hierarchical clustering for total peaks. Two hbHep samples and WT Liver clustered together whereas YAP1 ON and YAP1 OFF D14 regressing tumor formed another group (**Figure 3.9C**). Further, the YAP1 OFF D6 RNA-seq upregulated gene and mature hepatocyte marker, Mup9, has differential peaks in hbHeps and WT liver compared to YAP1 ON tumor (**Figure 3.9I**).

YAP1 Inhibition modulates liver transcription factor occupancy

Finally, to understand more clearly how YAP1 withdrawal promoted differentiation of hepatoblastoma tumor cells to hbHeps, I performed computational DNA Footprinting in regulatory regions in our ATAC-seq dataset. As expected, I observe decreased occupancy at Tead and Fos-Jun motifs in YAP1 OFF D33 hbHeps compared to YAP1 ON tumors (**Fig 3.10A-E, Table 3.2**). Further in YAP1 OFF D33 hbHeps, I observe increased occupancy at the motif of Retinoid X receptor alpha (Rxra), known to mediate xenobiotic CYP450 expression, and

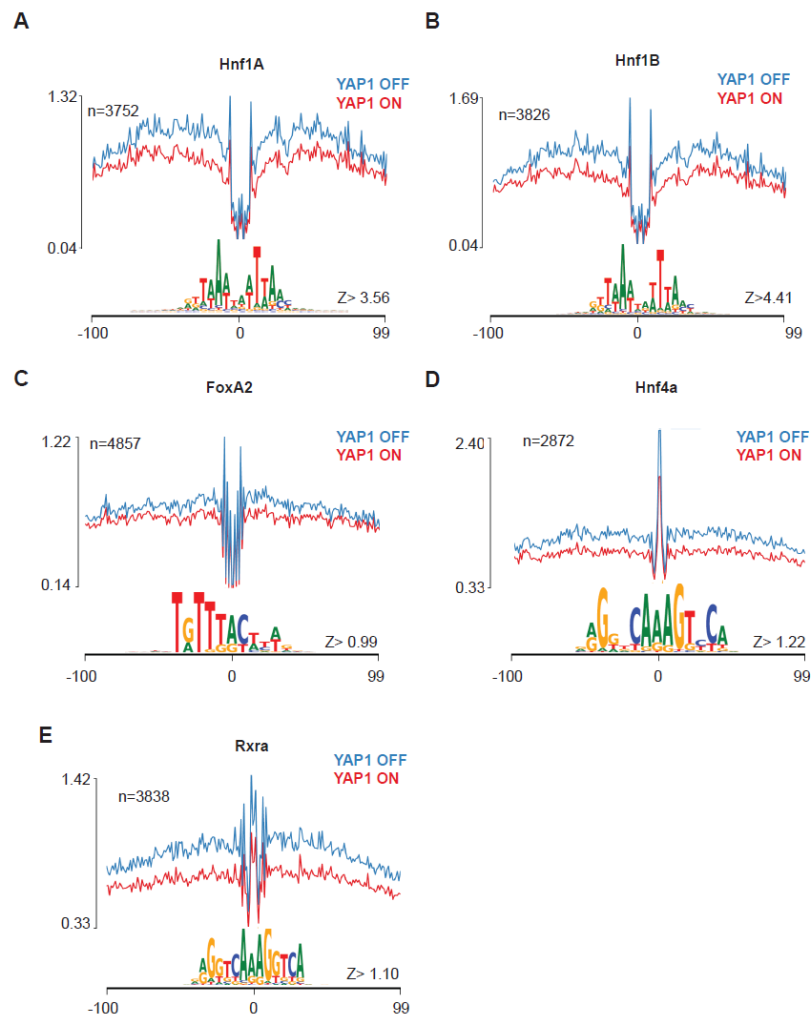


Figure 3.11 Increased occupancy at liver differentiation transcription factors in hbHeps D33 compared to YAP1 ON tumors. (A-E) DNA Footprinting analysis of ATAC Seq. YAP1 OFF hbHeps D33 shows increased occupancy at liver differentiation transcription factors compared to YAP1 ON tumors. *Please note: 3.10A-E is a partial reprint of Figure 6, and Supplemental Figure 9 from Smith et al, Hepatology, 2020.*

multiple canonical liver differentiation transcription factors belonging to the Hnf and FoxA families, including Hnf4 α , Hnf1 α , Hnf1B, Onecut1, Onecut3, FOXA1, and FOXA2 (**Figure 3.11A-E, Table 3.3**). These data indicate that YAP1 withdrawal drives transcriptional reprogramming and differentiation of hepatoblastoma tumor

cells into hbHeps by modulating occupancy of canonical liver differentiation transcription factors to promote mature hepatocyte gene expression.

Chapter 3.3 Discussion

Here I show that YAP1 withdrawal reprograms transcription in early and late regressing tumor cells, hbHeps, promoting mature hepatocyte gene expression. I propose that YAP1 withdrawal allows hepatoblastoma tumor cells to regain hepatocyte gene expression through modulation of transcription factor occupancy at critical HNF family member motifs (**Figure 3.11**). *Chapter 5.5* further examines what signals may be promoting apoptosis and differentiation driving the formation of hbHeps following YAP1 withdrawal.

Early regressing YAP1 OFF tumors (**Figure 2.2, Figure 3.4, 3.7**) express hepatocyte genes associated with multiple zones of the liver. As reviewed in *Chapter 1.7 Liver Differentiation*, the adult liver is subdivided into functional lobules comprised of three distinct zones with specific metabolic functions (**Figure 1.11**). Curiously, blunting YAP1 overexpression induces expression of multiple hepatocyte zones. I observed that YAP1 OFF D6 liver tumors compared to YAP1 ON tumors express increased levels of genes associated with periportal Zone 1, (GSEA signatures *Cholesterol Synthesis, Fatty Acid Metabolism*), and pericentral Zone 3 (GSEA signatures *Xenobiotic metabolism, Oxidative phosphorylation, and Adipogenesis*) (**Figure 3.4B**).

In the healthy adult liver, liver zonation is carefully preserved by Hippo/YAP1, Wnt, and HNF family signaling (See *Chapter 1.7 Liver Differentiation*) (19, 20, 22, 285, 289-291). Zone 1 hepatocytes are characterized by nuclear

YAP1, whereas Zone 3 hepatocytes have β -catenin nuclear expression (286). Thus, the current consensus is that YAP1 and β -catenin work in opposition in non-oncogenic liver tissue, driving independent zonal transcription patterns. This hypothesis is consistent with the synergistic capacity of cooperative YAP1 and β -Catenin to drive unchecked proliferation and promote tumorigenesis in hepatoblastoma.

Given the necessity of YAP1 for Zone 1 metabolism, it is reasonable to hypothesize that depletion of YAP1 overexpression would therefore drive a pericentral phenotype primarily characterized by β -catenin expression. Conversely, withdrawal of YAP1 expression may also promote reactivation of endogenous murine Yap1, driving a periportal phenotype. Finally, as discussed in *Chapter 1.7 Liver Differentiation*, HNF4 α and YAP1 function antagonistically to promote a Zone 1 periportal phenotype (20, 23, 283). YAP1 overexpression downregulates downregulate HNF4 α , promoting loss of Zone 1 identity (23, 293); therefore, in my model YAP1 withdrawal likely drives the increase in HNF4 α expression in our conditional model, promoting a Zone 1 phenotype.

Discussed above, I in fact observe evidence of both Zone 1 and Zone 3 metabolic capacities in YAP1 OFF livers (**Figure 3.4B**). Indeed, blunting YAP1 overexpression both upregulates HNF family members, including HNF4 α , that may be driving the observed increase in GSEA signatures associated with Zone 1 periportal hepatocytes. The increase in Zone 3 associated gene signatures is likely

mixed in etiology. My conditional model of hepatoblastoma primarily transfects Zone 3 pericentral hepatocytes by hydrodynamic injection (See *Chapter 1.5 Laboratory Models, Chapter 5.1 Mouse Models of Pediatric Liver Cancer*). Further, overexpressing oncogenic β -catenin that likely primarily drives a Zone 3 phenotype. Thus, there are likely multiple contributors to the Zone 3 phenotype observed in YAP1 OFF livers.

In my conditional system, sustained YAP1 withdrawal rehabilitates a subset of tumor cells into a hepatocyte-like state, hbHep cells. While oncogene inactivation can induce features of differentiation, if differentiated tumor cells regain functionality in a tissue context *in vivo* remains unclear (23, 233). *Chapter IV* seeks to characterize the functionality of the therapeutically differentiated hbHeps.

Chapter 3.4 Tables

Table 3.1 Top 20 Upregulated Coding Genes in YAP1 OFF. 20 most upregulated genes in YAP1 OFF D6/ YAP1 ON tumor RNA-Seq include major urinary proteins (Mups), cytochrome p450 enzymes, and other metabolic liver enzymes.

Gene	Gene Name	Fold Change	p-value
Mup22	major urinary protein 22	3755.29	0.00
Mup10	major urinary protein 10	3230.00	0.00
Mup9	major urinary protein 9	895.47	0.00
Mup2	major urinary protein 2	585.44	0.02
Mup11	major urinary protein 11	545.53	0.00
Sult3a1	sulfotransferase family 3A, member 1	299.86	0.01
Mup1	major urinary protein 1	259.14	0.00
Mup17	major urinary protein 17	179.48	0.00
Mup12	major urinary protein 12	177.24	0.04
Mup15	major urinary protein 15	78.69	0.05
A1bg	alpha-1-B glycoprotein	58.25	0.01
Sult2a8	sulfotransferase family	57.99	0.01
Cyp3a44	cytochrome P450, family 3, subfamily a, polypeptide 44	57.47	0.02
Ces3b	carboxylesterase 3B	30.89	0.02

Rfx4	regulatory factor X, 4	30.06	0.01
Cyp3a16	cytochrome P450, family 3, subfamily a, polypeptide 16	21.23	0.01
Cyp2b13	cytochrome P450, family 2, subfamily b, polypeptide 13	19.54	0.01
Cyp2c69	cytochrome P450, family 2, subfamily c, polypeptide 69	17.17	0.01
Ces3a	carboxylesterase 3A	14.19	0.01
Cyp2b9	cytochrome P450, family 2, subfamily b, polypeptide 9	13.58	0.04

Table 3.2. DNA Footprinting reveals increased occupancy of TEAD and FOS-JUN in YAP1 ON tumors compared to D33 hbHeps. Motifs with a z-score <-1 shown, Factor motif occupancy increased in YAP1 ON tumors compared to YAP1 OFF D33 hbHeps

Motif	Num	TC_YAPon	TC_YAPoff	Z_score
MA0080.4.SPI1	5007	0.778149	0.538991	-3.62052
MA0081.1.SPIB	6272	0.755879	0.600586	-3.03093
MA0645.1.ETV6	2693	0.924492	0.693585	-3.00384
MA0700.1.LHX2	25	0.683405	0.574311	-2.36181
MA1130.1.FOSL2::JUN	3888	0.750448	0.576744	-2.02294
MA1141.1.FOS::JUND	3339	0.752609	0.591832	-2.02104
MA0050.2.IRF1	11047	0.725148	0.63215	-2.00134
MA0635.1.BARHL2	529	0.679539	0.661234	-1.98751
MA0528.1.ZNF263	26793	0.961864	0.8601	-1.97823
MA0902.1.HOXB2	14	0.618762	0.457821	-1.96636
MA1134.1.FOS::JUNB	4283	0.733577	0.561284	-1.96465

MA0841.1.NFE2	3661	0.735318	0.578604	-1.92478
MA0099.3.FOS::JUN	4495	0.744406	0.578429	-1.90219
MA0640.1.ELF3	3248	0.967451	0.822858	-1.89177
MA1121.1.TEAD2	2909	0.792292	0.644182	-1.88482
MA1135.1.FOSB::JUNB	4721	0.731667	0.564872	-1.87261
MA0489.1.JUN(var.2)	4242	0.716737	0.568	-1.85442
MA0655.1.JDP2	4008	0.710884	0.548633	-1.84141
MA0808.1.TEAD3	2901	0.780134	0.618662	-1.81452
MA0149.1.EWSR1-FLI1	13626	0.898555	0.808222	-1.8074
MA0136.2.ELF5	4654	0.915554	0.757198	-1.80655
MA0090.2.TEAD1	2946	0.748555	0.600178	-1.79365
MA0471.1.E2F6	6216	1.001446	0.910616	-1.75167
MA0490.1.JUNB	4958	0.728213	0.577619	-1.74798
MA0486.2.HSF1	293	0.703584	0.634885	-1.686
MA0809.1.TEAD4	647	0.696452	0.571292	-1.64175
MA0687.1.SPIC	1986	0.70014	0.626577	-1.62383
MA1128.1.FOSL1::JUN	429	0.768187	0.666081	-1.53249
MA0827.1.OLIG3	44	0.51697	0.564302	-1.52551
MA1418.1.IRF3	2970	0.762067	0.678593	-1.51175
MA1137.1.FOSL1::JUNB	2233	0.723122	0.598112	-1.43477
MA0598.2.EHF	3268	1.00357	0.862099	-1.42871
MA0073.1.RREB1	16124	0.891048	0.796752	-1.41162
MA0818.1.BHLHE22	38	0.568836	0.474767	-1.40013
MA0057.1.MZF1(var.2)	4652	0.938087	0.854863	-1.36519
MA0778.1.NFKB2	2314	0.862555	0.74159	-1.34449
MA1138.1.FOSL2::JUNB	179	0.595233	0.484966	-1.33929

MA0517.1.STAT1::STAT2	6348	0.717002	0.626025	-1.3261
MA0694.1.ZBTB7B	385	1.058201	0.979285	-1.32292
MA0741.1.KLF16	6177	1.214019	1.132158	-1.29843
MA0491.1.JUND	689	0.682824	0.571315	-1.29697
MA1101.1.BACH2	4131	0.698715	0.612523	-1.29594
MA0062.2.Gabpa	3856	1.38778	1.277995	-1.26133
MA0641.1.ELF4	801	1.06468	0.957842	-1.25495
MA0076.2.ELK4	4828	1.178598	1.074044	-1.24491
MA0462.1.BATF::JUN	3723	0.690766	0.595798	-1.21229
MA0476.1.FOS	2537	0.691186	0.593478	-1.21043
MA0493.1.Klf1	8860	1.209899	1.127992	-1.1817
MA0098.3.ETS1	573	0.706173	0.584575	-1.17598
MA0163.1.PLAG1	5413	1.110323	1.027596	-1.15754
MA1153.1.Smad4	2638	0.730578	0.656664	-1.12025
MA0750.2.ZBTB7A	4768	1.217727	1.113749	-1.11617
MA0753.1.ZNF740	12500	1.027477	0.937335	-1.11131
MA0079.3.SP1	14445	1.338151	1.27327	-1.08826
MA0139.1.CTCF	8289	0.894397	0.831166	-1.08377
MA0516.1.SP2	19313	1.465544	1.402844	-1.08314
MA0525.2.TP63	341	0.957683	0.944956	-1.06602
MA0116.1.Znf423	2834	0.926574	0.851325	-1.0471
MA0865.1.E2F8	1633	0.875143	0.830128	-1.04313
MA0815.1.TFAP2C(var.3)	606	1.403677	1.282608	-1.03202
MA0150.2.Nfe2l2	2691	0.68869	0.631014	-1.02888
MA0657.1.KLF13	2124	1.24792	1.199901	-1.02637
MA0751.1.ZIC4	1009	1.184411	1.122232	-1.00912

MA1125.1.ZNF384	20604	0.674298	0.64212	-1.00197
MA0747.1.SP8	13194	1.284385	1.214146	-1.00064

Table 3.3 DNA Footprinting reveals increased occupancy in D33 hbHeps of canonical liver differentiation factors compared to YAP1 ON tumors. Motifs with a z-score>1 shown, Factor motif occupancy increased in YAP1 OFF D33 hbHeps compared to YAP1 ON

Motif	Num	TC_YAPon	TC_YAPoff	Z_score
MA0699.1.LBX2	12	0.32653967	0.52311015	5.924942502
MA0153.2.HNF1B	3826	0.80248743	1.0193863	4.415248951
MA0502.1.NFYB	1965	1.0852838	1.3233035	4.009027299
MA0060.3.NFYA	2274	0.997634	1.2149532	3.86143795
MA0046.2.HNF1A	3752	0.7699377	0.95962375	3.564307538
MA0755.1.CUX2	590	0.6183872	0.8066129	3.180869541
MA0679.1.ONECUT1	1000	0.6086101	0.7874461	3.121112524
MA0836.1.CEBPD	90	0.50474006	0.7128465	3.001319336
MA0754.1.CUX1	94	0.70393884	0.8852368	2.943199104
MA0611.1.Dux	2116	0.76220053	0.93064123	2.80685777
MA0837.1.CEBPE	332	0.6501896	0.8423744	2.62255491
MA0628.1.POU6F1	411	0.6863035	0.76014477	2.417984064
MA0910.1.Hoxd8	1949	0.610785	0.7277515	2.300017373

MA0897.1.Hmx2	145	0.6376049	0.82093495	2.298592894
MA0790.1.POU4F1	2261	0.6019612	0.7082293	2.209166145
MA0791.1.POU4F3	770	0.60553205	0.7336625	2.134941679
MA0757.1.ONECUT3	577	0.57527816	0.6667662	1.943141712
MA0780.1.PAX3	1268	0.52953994	0.6535507	1.909255033
MA0102.3.CEBPA	3341	0.61856204	0.7617427	1.907801839
MA0851.1.Foxj3	3709	0.5940336	0.69034183	1.782839857
MA0033.2.FOXL1	2503	0.7034454	0.7881816	1.780195203
MA0464.2.BHLHE40	86	0.70498097	0.85164917	1.73417386
MA0888.1.EVX2	72	0.5732519	0.65915495	1.69652474
MA0833.1.ATF4	1820	0.69059515	0.8065345	1.690420572
MA0602.1.Arid5a	1245	0.63892263	0.74046844	1.680034965
MA0115.1.NR1H2::RXRA	2978	0.61687076	0.79525775	1.664114558
MA0614.1.Foxj2	2968	0.63072777	0.71427464	1.61301998
MA0677.1.Nr2f6	1065	0.65457076	0.7937308	1.525219188
MA0846.1.FOXC2	5487	0.5905316	0.686183	1.518921543
MA0113.3.NR3C1	238	0.6162055	0.636031	1.516346913
MA1148.1.PPARA::RXRA	2981	0.6738655	0.8230723	1.511865996
MA0032.2.FOXC1	1404	0.5819075	0.6707976	1.479346836
MA0070.1.PBX1	1659	0.6675985	0.74833727	1.445946909
MA0043.2.HLF	311	0.62558126	0.7058281	1.429897282
MA0683.1.POU4F2	1771	0.675564	0.7543555	1.419908514

MA0148.3.FOXA1	4493	0.6352972	0.72453487	1.3642404
MA0831.2.TFE3	2401	0.8025362	0.8722045	1.361560911
MA0030.1.FOXF2	2474	0.65011775	0.7373259	1.309496832
MA0692.1.TFEB	2203	0.7947739	0.8445178	1.305278473
MA0713.1.PHOX2A	573	0.5099098	0.59086764	1.302812233
MA0604.1.Atf1	879	1.15482	1.2484417	1.29083315
MA0884.1.DUXA	1419	0.61196584	0.68826574	1.287731872
MA0723.1.VAX2	547	0.6083474	0.6636892	1.282320643
MA0707.1.MNX1	375	0.55833846	0.63539284	1.251303163
MA0838.1.CEBPG	1779	0.7832952	0.8846953	1.245730467
MA0603.1.Arntl	1927	0.92505246	1.0177896	1.235440893
MA1103.1.FOXB2	3425	0.65566	0.7317576	1.234158109
MA1112.1.NR4A1	1630	0.6442691	0.7784775	1.229674603
MA0114.3.Hnf4a	2872	0.6970709	0.9137632	1.224271023
MA0871.1.TFEC	768	0.7860029	0.8455651	1.213781852
MA0718.1.RAX	537	0.5957651	0.66168207	1.203849103
MA0847.1.FOXB2	2277	0.58222157	0.6544616	1.197576878
MA0135.1.Lhx3	2132	0.57173127	0.62766415	1.168965383
MA0466.2.CEBPB	11	0.75908935	0.89144915	1.150355013
MA0845.1.FOXB1	3573	0.586207	0.65885204	1.139548441
MA0468.1.DUX4	1519	0.62060034	0.6825238	1.126263037
MA1111.1.NR2F2	2646	0.6167436	0.7510032	1.125901033

MA0680.1.PAX7	169	0.5033955	0.5923587	1.116796798
MA0512.2.Rxra	3838	0.6730063	0.86270976	1.10981685
MA0675.1.NKX6-2	1272	0.5704339	0.6222491	1.102415025
MA0674.1.NKX6-1	244	0.5868199	0.66955346	1.090921281
MA0624.1.NFATC1	185	0.52410656	0.5987333	1.078537003
MA0706.1.MEOX2	134	0.5946885	0.6775434	1.063421218
MA0879.1.Dlx1	141	0.43387082	0.48311076	1.058160863
MA0093.2.USF1	3586	0.787873	0.8413811	1.04067287
MA0644.1.ESX1	42	0.47383732	0.5170309	1.039818465
MA0843.1.TEF	199	0.5475359	0.59046316	1.025762684
MA0065.2.Pparg::Rxra	6448	0.77363634	0.86374295	1.009155929
MA1099.1.Hes1	1890	1.2928712	1.3484945	1.00415519
MA0862.1.GMEB2	549	0.93862605	0.9989083	0.994277989
MA0047.2.Foxa2	4857	0.63744664	0.71984005	0.991057142

Chapter 3.5 Materials and Methods

Animal Studies

See Chapter II Methods

Generated Plasmids

H550, pT2_TreT_YAP^{S127A}_IRES_GFP_PGK_mcherry

H468_lentiV2_sgYAP1

Lentiv2_sgNon-target

H550 was generated using the New England Biolabs Gibson protocol and master mix kit per the manufacturer's instructions (Cat # E5510S). LentiCRISPR sgRNA cloning was performed according to Zhang Lab protocol as previously described (398).

Immunofluorescence

Immunofluorescence was performed on paraffin embedded slides of mouse liver prepared by the UMassMed Morphology Core as described above. Briefly, slides were deparaffinized in xylene, dehydrated in serial ethanol dilutions, boiled for 9 minutes with 1 mM citrate buffer (pH6.0) for antigen retrieval, blocked for one hour at room temperature in Perkin Elmer PNB Buffer 0.5% weight/volume (Catalog #FP1012), and incubated with primary antibody O/N at 4C. Secondary antibody was diluted in PNB block and slides were incubated for one hour at room

temperature and counterstained with DAPI (1 ug/ml) and mounted with Prolong Gold Antifade Mounting Media (Thermo Fisher, #P36934). Primary antibody used: MUP 1:200 Cedar Lane Labs, #GAM/MUP, Secondary AlexaFluor Goat 568, 1:200.

Microarray Data Accession

See Chapter II Methods

Statistical Analysis

See Chapter II Methods

TCGA and Microarray Analysis

For gene correlation analyses, correlation data from the TCGA HCC (n=348) data set was obtained from cBioPortal. E-MEXP-1851 (HB transcriptome) was obtained from ArrayExpress (n=25) (1). Briefly, gene expression data was analyzed using Spearman's correlation analysis (2).

Histology and Immunohistochemistry

See Chapter II Methods

IVIS Bioluminescent imaging

See Chapter II Methods

ATAC Sequencing Library Preparation and Analysis

Library Preparation

ATAC-seq was performed according to Corces et al. 2017 Supplementary Protocol 2 (397). Briefly, mCherry+ hbHep cell nodules were extracted from fresh liver under a Leica MZ FL II stereo-dissection fluorescent scope. Freshly extracted liver tissue was flash-frozen, transported and resuspended in homogenization buffer prior to douncing. 50,000 nuclei isolated by gradient centrifugation were used for 30min transposition reaction. Tagmented DNA was purified using Zymo Clean and Concentrator-5 (Zymo D4013) and amplified with custom oligonucleotides listed in Buenrostro et al. 2013 Supplementary Table 1 (399). Barcoded libraries were pooled for paired-end sequencing on two Illumina NextSeq High-Output 150-cycle cartridges.

ATAC-seq Pre-Analysis Processing

Demultiplexed FASTQs were trimmed by Cutadapt (400) and aligned to the mm10 reference genome with BWA-MEM (401). Alignments underwent PCR duplicate removal (<https://github.com/broadinstitute/picard>) and compression (402). Peaks/pileup-containing files (bigWig, bedGraph, bed) were generated by ZPeaks (<https://github.com/krews-community/zpeaks>).

ATAC-seq Analysis

To correct for differences in read-depth between samples, BAMs were normalized through random downsampling before analysis steps. Correlation matrices were generated by deepTools multiBigWigSummary and multiBamSummary with 1kb bin size discarding outliers (403). Pairwise comparison of open chromatin regions was conducted using Bedtools intersect (404). To minimize false-positive intersects, only peaks scoring >1.64 standard deviations above the corresponding sample mean ($Z > 1.64$) were retained. To visualize ATAC signal, BigWigs were internally normalized against background and plotted on the UMMS Genome Browser. (<http://genomebrowser.wenglab.org>).

Transcription Factor Footprinting

ATAC-seq output was further processed using a software and instructions from the Regulatory Genomics Toolbox (RGT) HMM-based footprinting pipeline, HINT, available at <http://regulatory-genomics.org/>. Preceding analysis, we dockerized RGT-HINT to overcome dependency conflicts. Transcription factor occupancy in regulatory regions was determined by matching motifs flanked by ATAC signal to known binding sequences in the JASPAR database. ([Khan et al. 2018](#)) Occupancy was scored and compared across samples in a pairwise manner. Line graphs for each motif are the default output of RGT-HINT. Z-score ranked scatterplots

($Z=1.64$ cutoff) were made by the R plot function. RGT motif “match” BED files were reformatted for use with bedtools intersect (steps available upon request) to isolate factor-specific binding sites. BED files were converted to BigBed format with bedToBigBed ([Kent et al. 2010](#)) and displayed on the UMMS Genome Browser.

CHAPTER IV HB-HEPS PARTIALLY RESCUE LIVER FUNCTION

Chapter 4.1 Introduction

I have shown that blunting YAP1 expression in hepatoblastoma without modulating β -catenin promotes tumor regression via apoptosis and differentiation, resulting in “hbHeps”. I am proposing that given the lack of short-term relapse, and the evidence of partially restored hepatocyte function from transcriptome and epigenetic profiling (*Chapter II and III*), that perhaps a third phenomenon is occurring. Following YAP1 silencing, I observe tumor regression; however, my dormant tumor cells, hbHeps, are “rehabilitated.” I propose that hbHeps have partial function restored and are passing as “normal” hepatocytes. Taken together, these observations suggest that YAP1 withdrawal in murine hepatoblastoma drives an intermediate phenotype not previously appreciated. In *Chapter IV*, I evaluate whether inactivation of oncogenic YAP1 drives hepatoblastoma towards a *functional* differentiated state.

My final aim is to investigate the functionality of hbHeps *in vivo*. Previous work showed that oncogene inactivation in adult cancer cells can induce markers of differentiation, but dormant tumor cells often persist and are prone to relapse (See *Chapter 3.1 Introduction*). It remains unknown whether oncogene inactivation can reprogram cancer cells *in vivo* into functional cells that contribute to normal tissue architecture and homeostasis.

To determine if hbHep cells have somatic hepatocyte function *in vivo*, I will examine the ability of hbHeps to rescue liver damage in a mouse model of Type I Tyrosinemia. Type I Tyrosinemia mice are deficient for the fumarylacetoacetate enzyme (Fah). *Fah*^{-/-} negative mice fail to fully metabolize tyrosine and accumulate toxic metabolites that cause liver damage, weight loss, and ultimately death.

FAH is the last enzyme in the synthesis of tyrosine and converts fumarylacetoacetate (FAA) to fumarate. FAA builds up in hepatocytes and is then converted into succinyl-acetoacetate and succinyl-acetone. Both succinyl-acetoacetate and succinyl-acetone are toxic metabolites in hepatocytes, interfere with the liver's ability to produce heme. Subsequently, the buildup of FAA, succinyl-acetoacetate, and succinyl-acetone promotes apoptosis of hepatocytes (272, 297, 405-409).

Loss of functional hepatocytes has a catastrophic effect for the mouse, and for human patients with Type I Tyrosinemia. Hepatocyte depletion disrupts all zonal functions of the liver lobule (See *Chapter 1.7 Liver Differentiation*). Specifically, hepatocyte loss prevents synthesis of cholesterol, glucose metabolism, xenobiotic metabolism, and heme production. As such, loss of normal hepatocytes leads to clinical liver failure in mice and patients. Patients and mice with Type I Tyrosinemia experience rapid weight loss with the onset of liver failure.

Most affected children who do not receive interventional care die within the first year of life (409). Similarly, without treatment, *Fah*^{-/-} negative mice rapidly

lose >15% of body weight between 2 and ~15 days (297, 405-407, 410, 411). FAH deficiency in humans and in mice can be treated with FDA approved 2-(2-nitro-4-trifluoro-methylbenzyl)-1,3 cyclohexanedione (Nitisone). Nitisone is also called NTBC. NTBC blocks the tyrosine degradation pathway at step two, preventing the toxic build-up of FAA, and its eventual conversion to succinyl-acetone. In children adherence to a low tyrosine diet and administration of NTBC is considered curative. Similarly, administration of NTBC in *Fah*^{-/-} negative mice blocks accumulation of FAA and preserves hepatocytes for normal liver function, and weight maintenance. *Fah*^{-/-} negative mice treated with NTBC are phenotypically normal.

Fah^{-/-} negative phenotypes can be fully rescued by repopulating the liver with *normal hepatocytes* following NTBC withdrawal (405, 406, 410-412). As *Fah*^{-/-} negative hepatocytes suffer from build-up of FAA and undergo apoptosis, *Fah*⁺ positive hepatocytes do not undergo apoptosis. The proliferation of *Fah*⁺ hepatocytes restores the functional/metabolic capacity of the liver rescuing the weight loss phenotype. If the cells used to repopulate the liver lack expression of critical liver metabolic enzymes, despite *Fah*⁺ overexpression, the weight loss phenotype will not be fully rescued. In my system, following loss of 10% body weight, mice are returned back onto NTBC to allow for recovery of expanded hepatocytes. The mice can subsequently be re-challenged with NTBC withdrawal for further hepatocyte expansion and liver repopulation (**Figure 4.1**).

To evaluate the functionality of hbHeps, I engineered a dual-function transposon plasmid that encodes a constitutively expressed mouse *Fah* gene and TET-ON inducible YAP1^{S127A} (YAP1-FAH). In *Chapter IV*, I will show establishment of hepatoblastoma in FAH^{-/-} mutant mice by delivering YAP1-FAH, β -catenin^{DelN90}, and SB-rtTA via hydrodynamic injection. I fed mice with doxycycline to induce YAP1 expression and HB tumor formation. Once tumors were established, I removed doxycycline and allowed tumors to regress. I then withdrew NTBC from

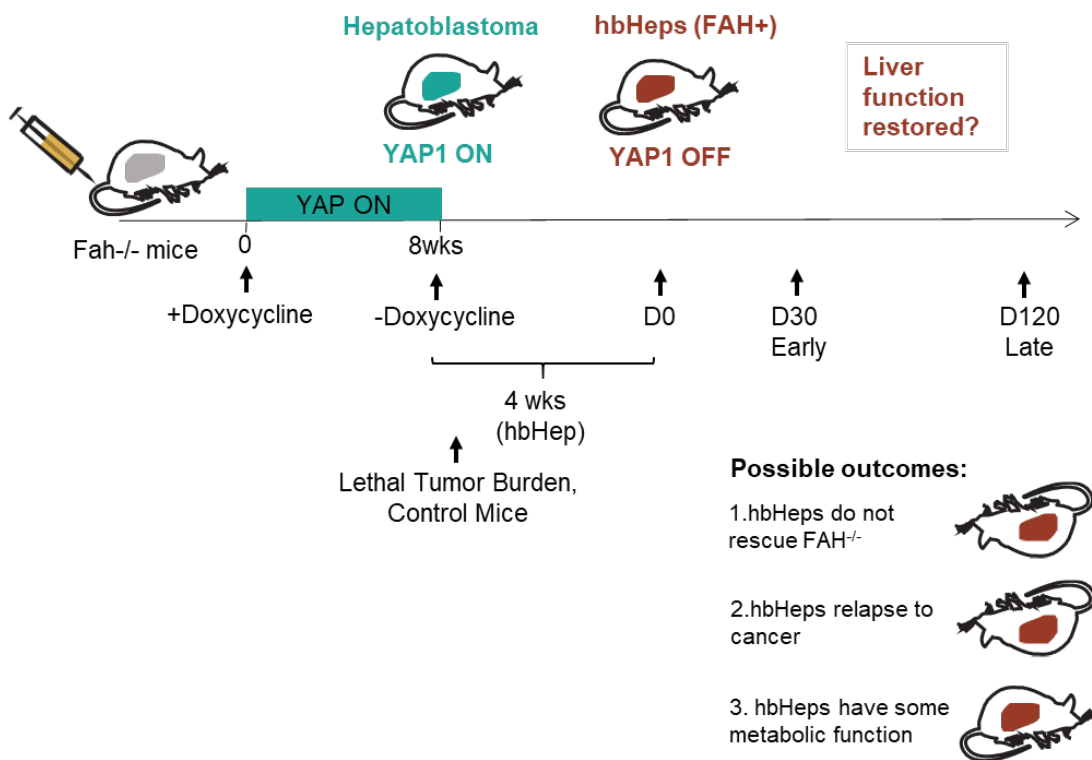


Figure 4.1 Schematic of experimental design. Conditional hepatoblastoma tumors are established in *Fah*^{-/-} mice. Following tumor establishment, doxycycline is withdrawn, YAP1 inhibited and hbHeps generated. After generation of hbHeps, mice are challenged with NTBC withdrawal. Possible outcomes include hbHeps do not rescue the weight loss phenotype, partial rescue, full rescue or rapid progression to malignancy.

the water supply to induce liver damage. As shown in **Figure 4.1**, I hypothesized that possible outcomes included 1) *rapid loss of body weight suggesting hbHeps do not rescue the phenotype* 2) *rapid progression to hepatoblastoma in the presence of liver damage* or 3) *rescue or partial rescue of the phenotype as evidenced by weight maintenance*.

Here I will show, untreated *Fah*^{-/-} control mice rapidly lost body weight (BW) and needed to be euthanized within 10 days, whereas *Fah*⁺-positive hbHeps partially rescued the phenotype in the short term and in the long-term (**Figure 4.1**).

Chapter 4.2 Results

Attributions: Dr. Max Hazeltine and Dr. SuetYan Kwan assisted with weighing Fah mice. Tomas Rodriguez assisted with bioinformatic analysis of RNA sequencing in hbHeps.

Generation of liver damage model system

Oncogene withdrawal in mouse models of adult liver cancer can induce features of hepatocyte differentiation, but it remains unknown if the differentiated tumor cells are functional and contribute to normal tissue architecture *in vivo* (23, 233). To determine if hbHep cells have somatic hepatocyte function *in vivo*, I assayed the ability of hbHeps to rescue liver damage in a mouse model of tyrosinemia. *Fah*^{-/-} negative mice (deficient for the fumarylacetoacetate enzyme) fail to fully metabolize tyrosine and accumulate toxic metabolites that cause liver damage, weight loss, and death. Fah deficiency can be rescued by NTBC (supplied in water), which blocks the buildup of toxic metabolites (296, 405, 411). For a more thorough review of Fah deficiency, please refer to *Chapter 4.1 Introduction*.

To interrogate the functional capacity of hbHeps, I engineered a dual-function transposon plasmid that encodes a constitutively expressed *Fah* gene and TET-ON inducible *YAP1*^{S127A} (YAP1-Fah; **Figure 4.2 A,B**). I delivered YAP1-Fah, β -catenin^{DelN90}, and SB-rtTA plasmids to *Fah*^{-/-} negative mice by

hydrodynamic injection and fed mice with doxycycline to induce YAP1 expression and hepatoblastoma tumor formation. Once tumors were established, I removed doxycycline and allowed tumors to regress (See *Chapter 2 Tumor Maintenance*

Requires YAP1, Chapter 1.5 Laboratory Models) (**Figure 4.2A**). I then withdraw NTBC from the water supply to induce liver damage and monitored mice for 10% total body weight loss.

hbHeps behave like functional hepatocytes in liver damage context

Untreated *Fah*^{-/-} negative control mice rapidly lost 10% of their total body weight and needed to be euthanized within 10 days, with a median of 2.5 days weight maintenance. Unlike *Fah*^{-/-} negative control mice, *Fah*⁺ positive hbHep mice maintained weight out to 23 days, with median weight maintenance of 13 days (**Figure 4.2C**). Immunohistochemistry in *Fah*⁺ hbHep mice revealed hbHep cells positive for both Myc-tagged/ β -catenin and the *Fah* enzyme (**Figure 4.2D-E**). Whereas *Fah*^{-/-} negative liver (in the control mice and in tissue adjacent to hbHep regions) showed abundant cell death, the *Fah*⁺ positive hbHep areas of the liver appeared healthy (**Figure 4.1E**). Thus, *Fah*⁺ positive hbHep cells can rescue liver function in *Fah*^{-/-} deficient mice, demonstrating that, in the short term, hbHeps, consistent with their reprogrammed transcriptional landscape, behave like functional hepatocytes in the context of liver damage.

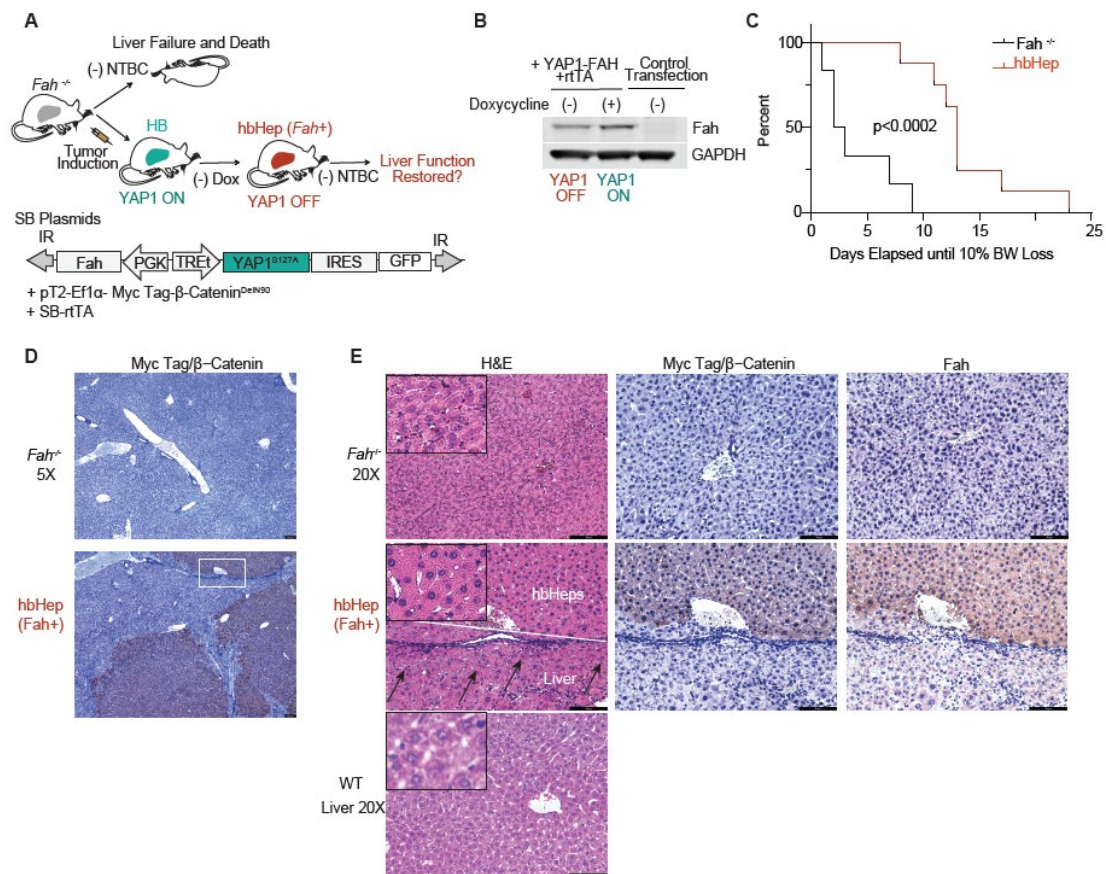


Figure 4.2 Hepatoblastoma-derived hepatocyte-like cells (hbHep cells) rescue liver damage in *Fah*^{-/-} mutant mice. (A) Experimental Design. A dual function transposon plasmid encodes a constitutive *Fah* gene and TET-ON inducible YAP1 (termed YAP1-Fah plasmid). The plasmid combination was injected in *Fah*^{-/-} mice to model HB tumor induction and regression. Only hbHep cells, but not host liver hepatocytes, express the *Fah* enzyme. (B) Validation of YAP1-Fah plasmid. Western blot in HCT116 cells transfected with indicated plasmids. (C) Kaplan Meier curve of hbHep expressing *Fah* (n=8) compared to untreated control *Fah*^{-/-} mice (n=6) following NTBC withdrawal. Number of days until 10% body weight loss is shown, p<0.002, Log-rank (Mantel-Cox) test. (D) hbHep mice post NTBC withdrawal harbor Myc-tag positive hbHep cells. Representative immunohistochemistry in control *Fah*^{-/-} mice and hbHep mice, n=3, scale bars 100 μm (5X lens). (E) The Myc tag positive hbHep cells are also positive for *Fah*. Representative immunohistochemistry (20X lens) in *Fah*^{-/-} mice and hbHep mice (n=3). WT liver H&E is for comparison, scale bars 100 μm. WT liver panel is also shown in Figure 4.3. The hbHep group shows serial liver sections of the white square region from panel d. White line denotes the border between hbHep area and host liver. Arrows denote dead hepatocytes in the *Fah*^{-/-} liver area. Please note: 4.2A-E is a partial reprint of Figure 7 from Smith et al, *Hepatology*, 2020.

To promote expansion and recovery of hbHep cells into the damaged *Fah*^{-/-} negative liver, I cycled my *Fah*⁺ positive hbHep mice onto NTBC cyclically following 10% body weight loss until weight restored (see *Chapter 4.1 Introduction*

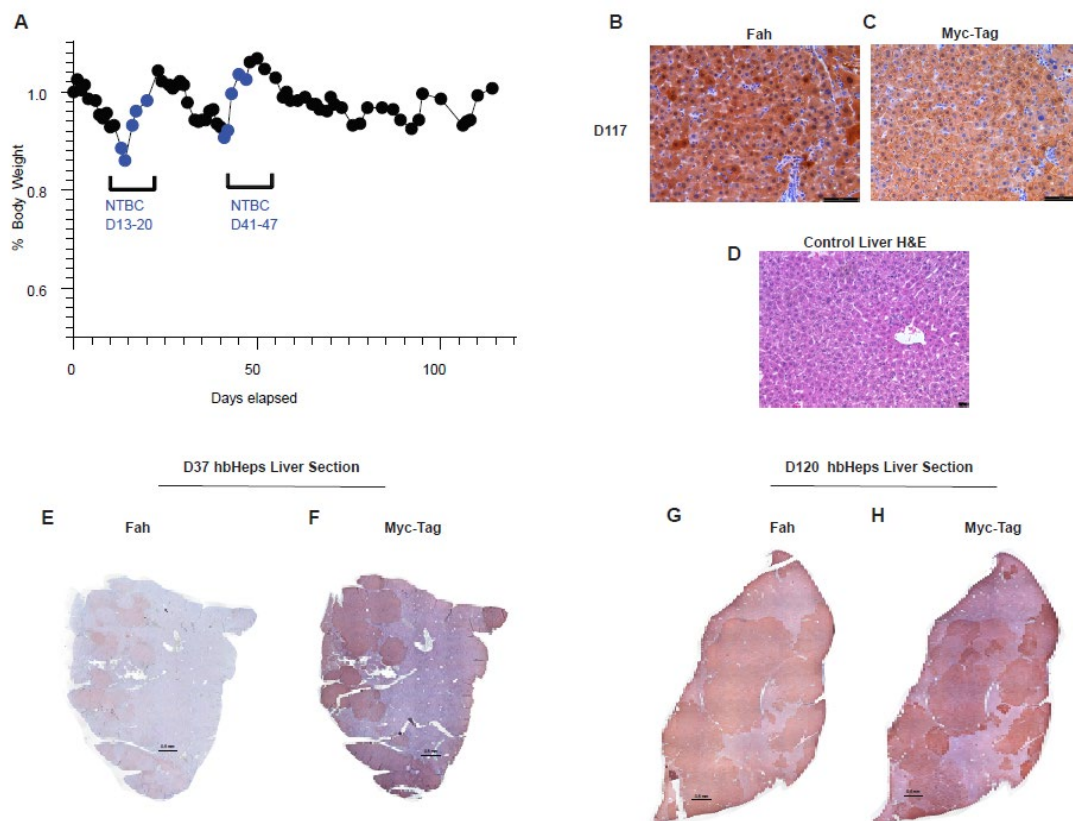


Figure 4.3 hbHeps repopulate the *Fah*^{-/-} liver and partially rescue long-term weight loss (A) Representative percent body weight for *Fah*^{-/-} mouse following initial NTBC withdrawal, Blue marks NTBC cycling following 10%body weight loss to promote hbHep recovery and expansion (see *Chapter 4.1 Introduction*), n=3, cycled mice maintained weight (>90%) for a maximum of 39.6 days on average \pm 23.7 days, range 24 to 67 days **(B-C)** Representative long-term hbHep immunohistochemistry, 20X, *Fah* and Myc Tag respectively in D114+ *Fah*^{-/-} mice, n=3 **(D)** Control liver, 20X, scale bar 25 μ m, *image also shown in Figure 4.1E* **(E-H)** Tile scanning of whole liver section, D37 and D121 respectively following NTBC challenge and cycling. Scale bar 0.5mm, *Fah* and Myc tag. *Please note: 4.3A-H is a partial reprint of Figure 7 from Smith et al, Hepatology, 2020.*

for a review of the *Fah*^{-/-} mouse model). Once weight restored (~100%), NTBC was removed from the water and weights continually monitored. Over the ~120 day period, mice were cycled 2-5X times on NTBC following 10% body weight loss to promote hbHep expansion (n=3) (**Figure 4.3**). Before needing to be returned to NTBC, cycled *Fah*⁺ positive hbHep mice-maintained weight (>90%) for a maximum of 39.6 days on average +/- 23.7 days SD (range 24 to 67 days, n=3) (**Figure 4.3A**). Comparably, untreated *Fah*^{-/-} negative control mice rapidly lost 10% of their total body weight required euthanasia between 2.5 and 10 days (**Figure 4.2C**).

On immunohistochemical examination, D114+ liver sections were grossly positive for *Fah* and Myc tag respectively (n=3 mice, D114+) (**Figure 4.3E-H**). Comparatively, early *Fah*⁺ positive hbHep mice (~D35) showed smaller regions of hbHeps by FAH and Myc tag staining (n=3) (**Figure 4.3E-F**). Myc and FAH nodular areas overlap in serial sections of liver, allowing for easy tracking of hbHep cells (**Figure 4.2A, Figure 4.3E-F**).

In the long-term hbHep mice D114+, gross examination of the liver under a dissection scope revealed 2-3 GFP+ lesions per mouse (*data not shown*). GFP+ tumors are presumed to be TET-ON escaper nodules. No other gross or histologic abnormalities were noted in the long-term hbHep mice. Please see *Chapter 5.1 Mouse Models of Pediatric Cancer* for a discussion of TET-ON promoter escape.

YAP1 withdrawal partially restores normal hepatocyte function in hbHeps

To further investigate the gene expression profile of hbHeps, I performed RNA-sequencing analysis in the three D114+ hbHep mice compared to *Fah*^{-/-} negative mice on NTBC. As reviewed in *Chapter 4.1 Introduction*, control *Fah*^{-/-} negative mice on NTBC do not experience accumulation of toxic metabolites and maintain healthy hepatocytes and normal hepatocyte gene expression.

Gene expression analyses comparing YAP1 ON, YAP1 OFF D6 regressing tumors, *Fah*⁺ hbHeps D114+, and WT *Fah*^{-/-} control mice revealed a gradual temporal progression towards normal hepatocyte function following YAP1 withdrawal in hepatoblastoma tumors (**Figure 4.4-B, D-E, Appendix VI hbHep Gene Expression Counts**).

To compare YAP1 ON, YAP1 regressing tumors, late hbHeps (D114+), and WT liver, I used Ingenuity Pathway Analysis (IPA) (389). Used previously in *Chapter II*, IPA analyses allows side-by-side comparison of multiple groups and identifies similarities and differences from catalogued signatures for *Upstream Regulators, Disease and Function pathways*, and *Canonical pathways*.

Using IPA analyses, I find loss of *Disease and Function* liver cancer signatures (*Liver Cancer, Liver Tumor, Liver Carcinoma*) in hbHeps compared to YAP1 ON tumor. Further, I find similarity in pathway scores between hbHeps and WT liver indicating that hbHeps more closely resemble WT liver than hepatoblastoma tumors (**Figure 4.4A-B, Table 4.1**). Further, I find that hbHep and

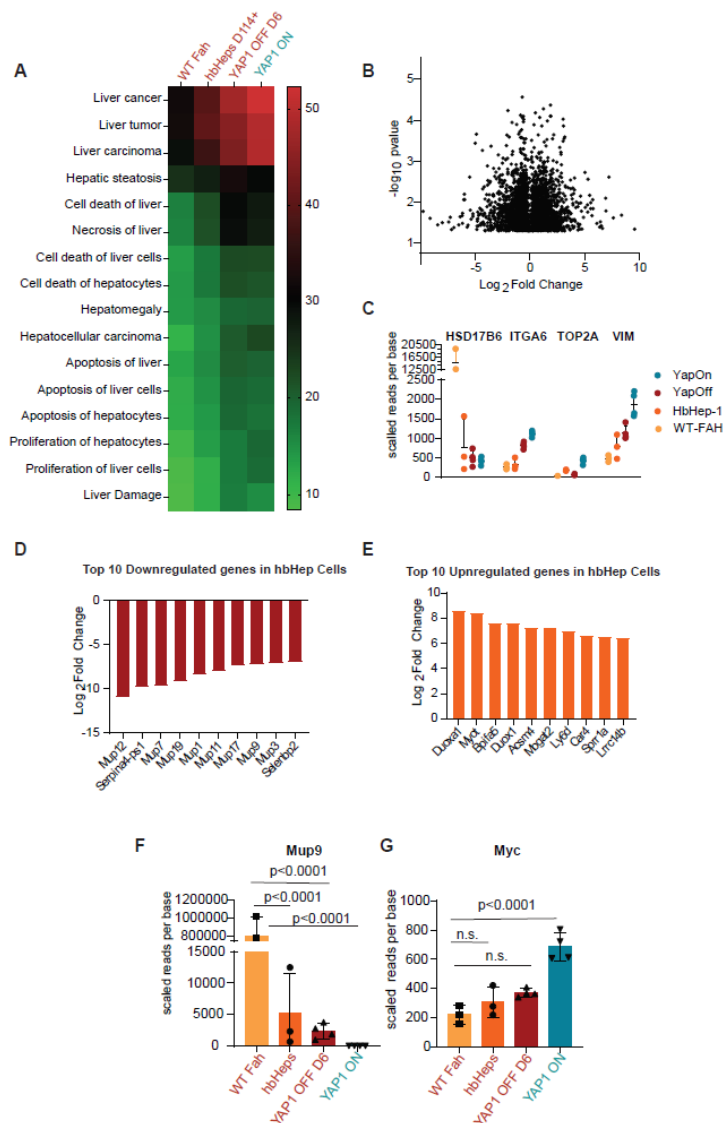


Figure 4.4 hbHeps show partially restored hepatocyte gene expression (A) IPA Ingenuity analysis *Disease and Function* signatures, curated, gene expression data from YAP1 ON , YAP1 OFF D6 tumors (n=4 tumors), hbHeps D114+ (n=3 mice), WT *Fah*^{-/-} mice +NTBC (n=3 mice), scale log(p-value) for pathway signature **(B)** volcano plot differentially expressed genes, hbHep D114+ *Fah*⁺ mice vs WT *Fah*^{-/-} mice +NTBC (n=3 mice) **(C)** Hooks 4-gene signature shown for gene expression data from YAP1 ON , YAP1 OFF D6 tumors (n=4 tumors), hbHeps D114+ (n=3 mice), WT *Fah*^{-/-} mice +NTBC (n=3 mice) **(D)** Top 10 downregulated genes in hbHep D114+ *Fah*⁺ mice vs WT *Fah*^{-/-} mice +NTBC (n=3 mice) **(E)** Top 10 upregulated genes in hbHep D114+ *Fah*⁺ mice vs WT *Fah*^{-/-} mice +NTBC (n=3 mice) **(F-G)** Normalized reads (scaled bases per read) for select genes in YAP1 ON , YAP1 OFF D6 tumors (n=4 tumors), hbHeps D114+ (n=3 mice), WT *Fah*^{-/-} mice +NTBC (n=3 mice). *Please note: 4.4 is a reprint of Supplemental Figure 11 from Smith et al, Hepatology, 2020.*

WT liver trend together on HNF4 α and MYC *Upstream Regulator* signatures (**Table 4.2**) (See *Chapter 1.7 Liver Differentiation*, *Chapter 1.8 Liver tumorigenesis*).

Similarly, in early YAP1 OFF D6 tumors, I observe upregulation of HNF4 α and its target genes; and, conversely, downregulation of Myc and its target genes (**Figure 2.2, Figure 3.4**). Indeed, examining scaled reads per base., i.e. normalized transcript count, I observe comparable levels of Myc expression between YAP1 OFF D6 tumors, hbHeps D114+, and WT liver (*Figure 4.5*). This finding suggests that YAP1 withdrawal sufficiently dampens the hepatoblastoma MYC signature observed in children's aggressive hepatoblastoma tumors (1, 217).

Besides loss of tumorigenic signaling in hbHeps, I also observe restoration of some hepatocyte metabolic function. Metabolic function of normal liver cells relies on maintenance of liver zonation (See *Chapter 1.7 Liver Differentiation*). I observe comparable scores for hbHeps and WT liver in both Zone 1 and Zone 3 liver specific IPA *Canonical* pathways including: *PXR/RXR Activation*, *Xenobiotic Metabolism*, *Oxidative Phosphorylation* and Zone 1 signature *Super-pathway of Cholesterol Biosynthesis* (**Table 4.3**) (see *Chapter 1.7 Liver Differentiation*).

Indeed, hbHeps do not fully recapitulate WT liver gene expression, but do partially recover expression of Mups, the mature hepatocyte marker (**Table 4.3**, *Appendix VI*). This finding is consistent with my immunofluorescence in hbHeps of Mup family proteins (See *Chapter III*). I observe increased levels of Mups in

hbHeps compared to tumor, but the level is not fully comparable to WT liver (**Figure 4.4F**, **Figure 3.7A-B**, *Appendix VI*).

Finally, I returned to the Hooks gene signature (See *Chapter 1.8*, *Chapter II*, **Figure 2.3**, **Figure 1.10**), and find that hbHeps do not recapitulate either poor prognosis C2 tumors that mimic YAP1 ON tumors, or favorable prognosis C1 tumors, as do YAP1 OFF D6 tumors. Instead, hbHeps more closely mimic WT liver function (**Figure 4.4C**). The Hooks gene signature from patient data can be found in **Figure 1.10** for comparison. Taken together, these findings suggest that hbHeps partially recapitulate gene expression associated with functional hepatocytes.

Chapter 4.3 Discussion

In *Chapter IV*, I show that Fah^+ positive hbHeps partially rescue weight in a model of liver damage. Specifically, I evaluated the functionality of hbHeps in a mouse model of Type I Tyrosinemia. Mice with tyrosinemia lack expression of functional *Fah*, leading to a buildup of toxic metabolites following digestion of tyrosine. Unprocessed tyrosine metabolites lead to hepatocyte apoptosis, loss of all liver zonation and normal hepatocyte metabolism (406, 407, 409-412). The $Fah^{-/-}$ negative phenotype can be rescued the chemical inhibitor, NTBC. Without NTBC, $Fah^{-/-}$ negative mice rapidly lose weight from liver failure due to loss of functional hepatocytes (See *Chapter 4.1 Introduction*).

I established tumors in $Fah^{-/-}$ negative mice on NTBC and withdrew NTBC to allow for establishment of hbHep cells. Following hbHep formation, I withdrew NTBC to evaluate if hbHeps could rescue the disease phenotype, i.e. maintain weight. Possible outcomes included: 1) *rapid weight loss without rescue suggesting hbHeps do not even partially resemble hepatocytes* 2) *recurrence of hepatoblastoma from hbHeps in the presence of liver damage* or 3) *partial or full rescue of weight loss with expansion of hbHeps into the $Fah^{-/-}$ liver* (**Figure 4.1**).

I find that, consistent with previous reports, untreated $Fah^{-/-}$ mice rapidly lost body weight (<10 days), and the liver rapidly underwent damage in the absence of NTBC (**Figure 4.2E**). Unlike untreated $Fah^{-/-}$ negative, Fah^+ positive hbHeps partially rescued the phenotype in the short term and in the long-term out

to 120+ days (**Figure 4.1-4.3**). Fah^+ positive hbHep mice maintained body weight following initial NTBC withdrawal out to 23 days (**Figure 4.2C**). Further, when Fah^+ positive hbHep mice were cycled back on to NTBC following 10% body weight loss, hbHeps repopulated the $Fah^{-/-}$ liver, and mice maintained weight (>90%) an average of 39 days maximally following NTBC withdrawal (**Figure 4.3**). Finally, I observed partial restoration of Mup gene expression levels, and similar signatures for Zone 1 and Zone 3 metabolism between HbHeps and WT liver (**Figure 4.4**). These results are consistent with a partial rescue of the phenotype (**Figure 4.1**).

Partial rescue of the $Fah^{-/-}$ deficient phenotype may result from the residual overexpression of oncogenic β -catenin. Indeed, while overexpression of β -catenin alone has not been found to promote tumorigenesis, oncogenic β -catenin alone can promote metabolic dysfunction and hepatomegaly (324, 325). Specifically, β -catenin overexpression in the liver leads to glycolytic dysfunction (325). Thus, while YAP1 withdrawal does downregulate some β -catenin target genes that promote tumorigenesis (**Figure 2.2, 4.2, Appendix V, VI**), overexpression of β -catenin in hbHeps may disrupt full restoration of mature hepatocyte gene expression. This is further discussed in *Chapter 5.6 Discussion*.

Another consideration is what factors may promote transformation of hbHeps into hepatoblastoma. At D114+ in Fah^+ positive hbHep mice, I did not observe evidence of YAP1 *independent* tumor proliferation; however, in adults, inflammation and liver damage promote development of HCC tumorigenesis (See

Chapter 1.1 Liver Cancer Primer). Indeed, Park et al. showed that obesity in adult mice promoted upregulation of interleukin-6 (IL-6), tumor necrosis factor (TNF), and signal transducer and activator of transcription 3 (STAT3) inflammatory signaling leading to increased rates of HCC (413). Further, inflammatory signaling from programmed death, including apoptosis and necroptosis, can promote liver tumorigenesis. This is consistent with the increased risk of HCC from fibrosis and cirrhosis in adult patients (5, 6). Indeed, multiple models of murine HCC rely on a chemically induced carcinogenesis to promote a pro-tumorigenic inflammatory environment (413, 414). As with other therapies that promote differentiation, consideration should be given to factors that may promote recurrence of tumorigenesis. The “permanence” of therapeutic differentiation is further discussed in *Chapter 5.6 Therapeutic Differentiation of Cancer Cells*.

In *Chapter IV*, I have shown that hbHeps regain partial hepatocyte functionality through a mouse model of liver damage and gene expression analyses. Specifically, I find that hbHeps rescue liver damage in a mouse model of tyrosinemia, and express increased levels of Mups and canonical liver enzymes. Finally, when compared with YAP1 ON tumor using the Hooks Hepatoblastoma signature, I find that hbHeps closely mimic WT liver.

Chapter 4.4 Tables

Table 4.1 Top 50 IPA Analysis *Upstream Regulator* Signatures in hbHeps

D114+, YAP1 OFF D6, and YAP1 ON tumors. Score is log(p-value) for specific IPA signature, generated from gene expression data for YAP1 ON tumors , YAP1 OFF D6 tumors, hbHeps D114+, and WT Fah^{-/-} liver.

Upstream Regulators	WT-FAH	HbHep	YAP1 Off	YAP1 On
HNF4A	151.4	126.5	129.4	108.0
1,2-dithiol-3-thione	75.1	73.3	68.0	57.9
methylprednisolone	58.1	56.1	74.1	68.0
RICTOR	55.5	57.9	62.2	59.4
TP53	37.6	50.4	55.9	62.7
pirinixic acid	44.5	51.6	51.2	52.4
NFE2L2	45.1	53.5	51.8	45.3
PPARA	36.0	38.4	46.6	47.3
metribolone	33.2	38.8	40.1	42.2
methapyrilene	28.6	40.1	38.9	37.8
MYC	22.4	33.9	38.9	52.5
ciprofibrate	28.9	37.2	41.1	34.3
ESR1	19.1	31.8	38.1	41.5
TO-901317	31.4	32.4	35.0	33.3
ACOX1	24.4	32.9	40.7	33.8
arsenic trioxide	25.2	31.1	30.8	33.2
MYCN	24.4	28.4	30.0	34.6
ST1926	27.3	29.1	29.7	28.5
uranyl nitrate	30.7	28.1	30.0	26.6
mono-(2-ethylhexyl)phthalate	28.0	27.5	28.1	31.8
CLPP	26.3	32.3	32.2	23.1
MAPT	22.2	27.2	29.4	34.2
nitrofurantoin	18.3	30.7	29.7	35.2
5-fluorouracil	21.0	28.5	26.6	37.0
CD 437	23.6	28.2	27.3	30.2
TLE3	27.9	29.2	30.3	21.6
HNF1A	27.5	24.8	27.6	26.4
POR	25.0	26.1	28.1	22.3
dexamethasone	14.2	18.6	35.0	40.2
gentamicin	22.6	26.4	25.6	22.6
APP	12.3	21.5	31.8	35.8
ONECUT1	24.9	22.7	24.1	21.6

imatinib	17.6	21.5	25.8	30.1
XBP1	22.7	22.8	22.1	23.0
PTEN	17.8	23.9	25.4	25.4
fenofibrate	16.4	23.9	23.7	21.6
NR1I2	20.5	22.7	22.6	21.5
Insulin	16.1	20.4	23.8	28.2
MAP4K4	22.4	24.7	18.9	17.3
LONP1	21.2	22.3	21.2	19.3
sirolimus	12.3	21.0	23.0	28.8
GnRH analog	17.3	20.3	22.0	20.5
dihydrotestosterone	15.3	17.2	21.8	27.5
lipopolysaccharide	6.7	13.7	32.8	32.3
torin1	18.4	21.3	16.2	17.4
valproic acid	14.4	18.4	19.3	21.3
INSR	14.5	17.7	21.6	21.6
beta-estradiol	9.7	15.7	22.6	30.0
tunicamycin	14.9	19.6	18.9	19.6
NR3C1	13.6	14.6	22.7	24.5
TGFB1	7.2	14.7	22.7	32.1

Table 4.2 Top 50 IPA Analysis *Disease and Function* signatures in hbHeps, YAP1 OFF D6, and YAP1 ON tumors. Score is log(p-value) for specific IPA signature, generated from gene expression data for YAP1 ON tumors , YAP1 OFF D6 tumors, hbHeps D114+, and WT Fah^{-/-} liver.

Disease and Function, Tox Functions	HbH ep	WT-FAH	YAP1 Off	YAP1 On
Liver cancer	39.5	31.9	47.6	52.3
Liver tumor	40.5	32.1	44.7	49.4
Liver carcinoma	36.7	29.3	43.7	49.2
Hepatic steatosis	27.3	25.1	32.4	29.9
Cell death of liver	22.2	16.6	29.9	28.0
Necrosis of liver	21.7	16.2	29.4	27.5
Cell death of kidney cells	20.2	16.1	23.1	25.6
Necrosis of liver parenchyma	17.6	14.6	22.6	22.0
Cell death of liver cells	17.5	13.6	22.4	22.3
Cell death of kidney cell lines	17.9	14.8	18.8	20.8
Cell death of hepatocytes	17.5	14.0	21.9	21.3
Hepatomegaly	15.6	13.9	19.3	19.7
Hepatocellular carcinoma	14.9	11.2	20.8	22.7
Apoptosis of liver	15.6	12.8	20.4	19.7

Apoptosis of liver cells	14.8	12.1	19.6	18.9
Apoptosis of hepatocytes	14.1	11.9	19.2	18.2
Hepatitis B virus-related hepatocellular carcinoma	16.3	12.4	16.2	15.8
Proliferation of hepatocytes	13.6	9.7	17.2	19.4
Proliferation of liver cells	11.9	8.8	17.2	18.9
Cell death of heart cells	11.8	10.1	13.6	16.6
Cell death of cardiomyocytes	11.7	10.0	13.5	16.6
Hepatitis B surface antigen-negative hepatitis C virus negative hepatocellular carcinoma	13.0	12.5	12.9	13.4
Liver Damage	11.8	8.4	16.9	15.3
Apoptosis of kidney cell lines	12.6	10.1	12.5	15.4
Cell death of heart	11.4	9.1	12.4	15.7
Apoptosis of heart	10.4	8.9	13.6	16.1
Apoptosis of cardiomyocytes	10.3	8.8	13.4	15.9
Apoptosis of heart cells	10.1	8.6	13.2	15.6
Intrahepatic cholestasis	11.4	12.1	12.0	10.6
Cell proliferation of kidney cell lines	10.5	7.2	12.4	15.7
Cholestasis	11.4	11.2	10.7	10.5
Nephrotoxicity	11.4	7.9	12.6	13.6
Nephromegaly	11.2	8.5	11.1	13.5
Proximal tubular toxicity	10.6	8.1	12.4	13.3
Progressive intrahepatic cholestasis	10.6	11.5	10.5	8.9
Progressive familial intrahepatic cholestasis type 1	10.1	11.1	10.1	8.6
Development of liver tumor	9.6	6.3	10.9	13.1
Enlargement of heart	9.0	6.4	10.9	12.3
Inflammation of liver	9.0	5.7	11.6	10.6
Hepatic injury	8.2	6.6	11.2	10.9
Microvesicular hepatic steatosis	8.6	8.2	8.5	10.1
Development of hepatocellular carcinoma	8.7	5.3	8.6	10.5
Hepatitis C virus-related hepatocellular carcinoma	8.0	7.6	7.9	7.3
Liver Regeneration	6.9	5.8	9.0	9.1
Liver Hypoplasia	7.4	4.5	8.1	8.6
Fibrosis of liver	6.9	4.6	7.9	8.5
Benign neoplasm of liver	7.6	5.1	6.1	6.5
Hepatic adenocarcinoma	6.7	3.9	7.2	9.0
Liver cholangiocarcinoma	6.7	4.3	7.2	8.4
Hepatocellular adenoma	6.7	4.9	5.9	6.3
Glomerulosclerosis	5.6	4.6	7.1	8.9

Table 4.3 Top 50 IPA Analysis *Canonical Pathways* signatures in hbHeps, YAP1 OFF D6, and YAP1 ON tumors. Score is log(p-value) for specific IPA

signature, generated from gene expression data for YAP1 ON tumors , YAP1 OFF D6 tumors, hbHeps D114+, and WT Fah^{-/-} liver.

Canonical Pathways	WT-FAH	HbHe	YAP1 Off	YAP1 On
Sirtuin Signaling Pathway	39.5	41.5	41.2	35.2
Mitochondrial Dysfunction	38.2	39.4	36.4	36.8
EIF2 Signaling	32.8	35.0	32.6	35.7
Oxidative Phosphorylation	29.2	30.6	27.4	25.1
Protein Ubiquitination Pathway	26.6	30.7	26.2	25.6
Regulation of eIF4 and p70S6K Signaling	24.9	25.7	25.5	25.0
NRF2-mediated Oxidative Stress Response	21.8	25.5	22.0	21.2
Acute Phase Response Signaling	18.9	19.2	25.5	24.6
mTOR Signaling	15.7	18.8	20.3	19.7
FXR/RXR Activation	15.8	13.8	18.2	17.4
PPAR α /RXR α Activation	13.7	14.5	19.9	15.2
PI3K/AKT Signaling	11.0	14.1	18.4	20.6
Iron homeostasis signaling pathway	14.1	15.2	14.5	13.3
Senescence Pathway	12.6	13.6	17.4	15.1
RAR Activation	12.2	13.4	16.9	11.7
Molecular Mechanisms of Cancer	7.2	11.6	16.7	18.1
Xenobiotic Metabolism Signaling	12.4	14.7	13.3	10.6
Hypoxia Signaling in the Cardiovascular System	11.4	12.1	14.4	12.8
LPS/IL-1 Mediated Inhibition of RXR Function	13.1	12.2	13.4	11.3
Unfolded protein response	11.0	12.5	11.6	12.3
PTEN Signaling	8.1	9.9	16.8	16.7
Integrin Signaling	8.7	11.8	12.5	16.9
Clathrin-mediated Endocytosis Signaling	10.0	12.0	12.3	14.1
LXR/RXR Activation	12.2	9.8	13.1	12.9
Prostate Cancer Signaling	11.0	9.9	11.7	13.9
Epithelial Adherens Junction Signaling	8.1	11.8	14.4	11.8
PXR/RXR Activation	11.5	11.4	13.0	8.5
IGF-1 Signaling	8.9	9.2	13.9	12.3
Insulin Receptor Signaling	9.9	9.4	11.8	11.2
HIPPO signaling	8.9	9.6	10.7	12.9
ERK/MAPK Signaling	8.0	9.0	10.5	13.1
Superpathway of Cholesterol Biosynthesis	10.2	10.6	10.6	8.8
B Cell Receptor Signaling	7.2	7.8	12.8	11.7
Mouse Embryonic Stem Cell Pluripotency	7.6	9.4	11.0	10.7
Phagosome Maturation	8.7	10.1	10.4	10.5
Ephrin Receptor Signaling	6.5	9.7	10.9	11.6
Breast Cancer Regulation by Stathmin1	4.6	9.6	11.6	12.9
Aryl Hydrocarbon Receptor Signaling	7.4	11.1	9.0	11.0

AMPK Signaling	9.9	8.7	10.1	10.1
p70S6K Signaling	7.1	8.8	11.2	10.1
NGF Signaling	8.9	9.2	9.1	8.9
Acute Myeloid Leukemia Signaling	7.4	8.6	10.9	10.5
Apoptosis Signaling	7.9	9.2	10.8	10.5
Chronic Myeloid Leukemia Signaling	8.1	8.3	10.4	10.7
Estrogen-Dependent Breast Cancer Signaling	7.0	8.7	10.6	10.6
VEGF Signaling	7.9	8.6	10.2	9.9
JAK/Stat Signaling	6.2	8.4	10.8	11.6
Production of Nitric Oxide and Reactive Oxygen Species in Macrophages	7.6	8.5	10.9	10.3
Germ Cell-Sertoli Cell Junction Signaling	6.2	9.4	10.2	10.8
Huntington's Disease Signaling	9.1	7.7	9.4	10.2
Remodeling of Epithelial Adherens Junctions	6.1	9.1	10.4	11.1

Chapter 4.5 Materials and Methods

Generated Plasmids

H549, pT2_TreT_YAP^{S127A}_IRES_GFP_PGK_Fah

H549 was generated using the New England Biolabs Gibson protocol and master mix kit per the manufacturer's instructions (Cat # E5510S). LentiCRISPR sgRNA cloning was performed according to Zhang Lab protocol as previously described (398).

Hydrodynamic Injection

See Chapter II Methods

TET-ON Studies

See Chapter II Methods

FAH Mouse Studies

See Chapter II Methods

Tumor was established in *Fah*^{-/-} DeltaExon5 mice as described above. Following tumor formation, doxycycline was withdrawn as previously described, and tumor regression monitored. During this time *Fah*^{-/-} mice were continuously treated with nitisone treated water NTBC (5 mg/ml) to prevent liver damage. Following tumor regression, NTBC was withdrawn and mouse weights monitored 2+ times weekly.

Mice were cycled back onto NTBC at 90% total body weight (TBW) and kept on NTBC until weight restored.

Histology and Immunohistochemistry

See Chapter II Methods

Tile scanning of liver sections was performed using the Leica DFC700 GT microscope at 5X magnification. LAS X Navigator and Leica linked imaging shading correction was used to merge the tiled images.

Cell culture

293fs and HCT116 were gifts from Dr. Tyler Jacks. Cells were cultured in Dulbecco's Modification of Eagle's Medium (DMEM) (Corning 10-013CV), 10% serum (vol/vol) and 1% penicillin/streptomycin (vol/vol) under standard conditions, 37C in 5% CO₂ tissue culture incubator.

Immunoblot

See Chapter II Methods

FAH 1:1000 (AbCam, Ab83770, Rb)

RNA Extraction, cDNA synthesis, Quantitative PCR

See Chapter II Methods

RNA-Sequencing Library Preparation and Analysis

RNA was extracted from hbHep FAH mice (n=3 mice), and control FAH^{-/-} treated with NTBC (n=3 mice) in duplicate. Extracted RNA was prepared into sequencing libraries, and sequenced by GENEWIZ, LLC. (South Plainfield, NJ, USA). Libraries were prepared using paired end-reads, and >15 million reads per sample. Samples were first quantified using the Qubit 2.0, and Agilent Tape Station. Libraries were sequenced using Illumina Hi-seq .

RNAseq Analysis

Transcript quantification was performed using kallisto according to Bray et al. (<https://doi.org/10.1038/nbt.3519>) Paired-end FASTQ files were pseudoaligned (100 bootstraps setting, -b 100) to an index built with an Ensembl FASTA (all cDNA; GRCm38.p6). Gene-level transcript aggregation and statistical comparison between genes (scaled-bases-per-read) were done using sleuth. (<https://doi.org/10.1038/nmeth.4324>) See code availability (JS_sleuth) for steps related to the generation of “sleuth objects” described by Pimentel et al.

code: https://www.dropbox.com/s/db2lxwyzo7znldi/JS_sleuth.txt?dl=0

Ingenuity Pathway Analysis

See Chapter II

CHAPTER V DISCUSSION

In the preceding four chapters, I establish the first conditional mouse model of pediatric hepatoblastoma. Using gene expression analyses, I find that my conditional model of hepatoblastoma more closely mimics the predominant poor prognosis C2 subtype of hepatoblastoma (See *Chapter 1.4*) (**Figure 2.1, 2.2, 2.3**). In mice with conditional hepatoblastoma, withdrawal of YAP1 alone is sufficient to induce >90% tumor regression (**Figure 2.4, Figure 2.6**).

Herein, I propose that YAP1 withdrawal induces a cell fate switch in hepatoblastoma tumor cells promoting either apoptosis or differentiation (**Figure 2.5, Figure 3.2-3.5**). Specifically, using ATAC-seq, I find that withdrawing YAP1 expression promotes differentiation of tumor cells to hepatocyte-like cells via increased binding at multiple canonical liver differentiation family member motifs (**Figure 3.4-3.11**). Thus, YAP1 withdrawal reprograms the epigenetic and transcriptional landscape of hepatoblastoma tumors (**Figure 3.8-3.11**).

Because of the resemblance of differentiated hepatoblastoma tumor cells to normal hepatocytes, I termed my tumor parentage cells, “hepatocyte-like hepatoblastoma cells” or hbHeps (**Figure 3.2**). Finally, I find that I can partially rescue a liver damage model through repopulation of the liver with hbHeps. This finding suggests that differentiated hepatoblastoma tumor cells are not dormant, but instead functional (**Figure 4.1-4.4**).

In *Chapter V Discussion*, I first consider generation of mouse models for modeling pediatric liver cancer. Next, I examine the role of YAP1 signaling in liver tumorigenesis and the requirement of YAP1 for tumor maintenance. Further, I discuss Wnt/ β -catenin signaling in the context of hepatoblastoma. I next consider how Wnt/ β -catenin and YAP1 may be interacting to maintain tumorigenesis in my model of hepatoblastoma. Specifically, I examine what cellular signals may promote apoptosis versus differentiation in YAP1 withdrawn tumors. Subsequently, I explore therapeutic differentiation as a treatment strategy, and potential shortcomings of YAP1 inhibition in hepatoblastoma tumors. Finally, I review the current suite of YAP1 therapeutics, and discuss their potential application in children with hepatoblastoma.

Chapter 5.1 Mouse Models of Hepatoblastoma

In *Chapter 5.1*, I discuss the generation of the first inducible mouse model of hepatoblastoma. Specifically, I examine hydrodynamic injection for liver tumorigenesis, inducible models, and Sleeping Beauty transposase systems. Finally, I recommend future directions for mouse modeling of hepatoblastoma. Herein, I propose that my hydrodynamic conditional model of hepatoblastoma addresses the need for a timely, inducible model that mimics the genetic landscape and histology of pediatric hepatoblastoma. My new conditional model allows for careful dissection of the epistatic relationship between YAP1 and β -catenin. Future modeling of hepatoblastoma should seek to address the need for a metastatic model.

In Vivo Modeling Primer

The rarity of orphan diseases, like hepatoblastoma, typically limits the availability of tractable *in vitro* and *in vivo* models (See *Chapter 1.5 Laboratory Models*). Transgenic mouse models are ideal for cancer modeling and therapeutic development. Transgenic models are preferred to xenograft models of human cell lines in immunocompromised mice, because immune-competent transgenic models more closely mirror the tumor-specific tissue microenvironment. Specifically, transgenic models better recapitulate the invading vasculature, immune components, and stromal cells, like fibroblasts, observed in human

tumors. To this point, xenograft models have failed to accurately predict efficacious human cancer drug targets.

Upwards of 95% of the time, murine drug targets discovered and investigated in xenograft models fail to translate to human tumors; thus, there is need for more stringent *in vivo* models that better recapitulate human cancer biology (415). Currently, there are human xenograft models of hepatoblastoma, but similarly to xenograft models used for other cancer types, hepatoblastoma xenografts have also failed to produce FDA approved targeted therapies to date for children with liver tumors (See *Chapter 1.4 Clinical Management of Hepatoblastoma*, *Chapter 1.5 Laboratory Models*) (**Table 1.10**) (227, 235-238).

Few genetic mutations frequently drive liver cancer transgenic mouse models. In mice, liver tumor establishment needs only loss of one tumor suppressor and overexpression of one oncogene. For example, liver specific overexpression of MYC and loss of the tumor suppressor, p53, sufficiently induces HCC tumorigenesis in mice (233). Alternatively, overexpression of two oncogenes can also drive rapid HCC formation *in vivo*. For example, as discussed in *Chapter 1.8 Liver Tumorigenesis*, synergistic cooperation between β -catenin and any of the following oncogenes *HRAS*, *AKT*, *MYC*, *MET*, and *KRAS*, generates HCC in mice (185, 327-331).

For most cancers, including adult liver cancer, a major caveat of transgenic models is their genetic simplicity. As discussed in *Chapter 1.1 Liver Primer*, most

adult liver tumors have >40 non-synonymous mutations(16); therefore, transgenic models typically do not capture the genetic diversity of adult tumors. However, the genetic simplicity of transgenic models more faithfully recapitulates pediatric tumor. For example, most children with hepatoblastoma have fewer than 4 non-synonymous mutations per tumors (14). While >80% of children have nuclear β -catenin and YAP1, typically children only have mutations in the Wnt pathway (See *Chapter 1.4 Molecular Profiling of Hepatoblastoma*). Thus, stable integration of constitutive YAP1 represents one major caveat of my conditional model (**Table 1.9, Figure 1.13**). *Chapter 5.2* examines sources of YAP1 activation in human hepatoblastoma.

For liver cancers, the use of transgenic mouse models allows for critical dissection of tumor biology. Mouse models allow interrogation of fundamental questions including but not limited to: 1) *what are the genetic dependencies in tumor initiation and tumor maintenance*, 2) *what factors promote invasion and metastasis* 3) *How do tumor cells interact with the microenvironment and other environmental cues* and 4) *what are viable therapeutic strategies?*

Answering the preceding critical questions in hepatoblastoma using traditional transgenic models has proven difficult. One of the challenges is that to date, there are no “pure” transgenic models of hepatoblastoma (See *Chapter 1.5 Laboratory Models*) (**Table 1.11**). Available transgenic models currently generate mixed liver lesions producing both hepatocellular carcinoma and hepatoblastoma

(227, 232-234). As discussed in *Chapter 1.1 Liver Primer*, while adult and pediatric cancer do share some similarities such as frequent mutations in the Wnt pathway, they have considerable differences in disease etiology, and response to chemotherapeutics (4-6, 45, 49, 162). Thus, mixed models may confound attempts to interrogate hepatoblastoma biology.

In contrast to traditional transgenic models, Tao et al's hydrodynamic model of hepatoblastoma in immune-competent mice produces pure hepatoblastoma resembling primarily the fetal mitotic and embryonal subtypes (See *Chapter 1.3 Histologic Subtypes of Hepatoblastoma*, *Chapter 5.1 Hydrodynamic Models*) (31). Accordingly, hydrodynamic injection suits *in vivo* modeling of hepatoblastoma. Hydrodynamic modeling of hepatoblastoma is further discussed in the upcoming section.

To date, there are no available hepatoblastoma models that allow for spatial and temporal control of oncogenesis; thus, *in vivo* probing of genetic interactions driving hepatoblastoma tumor progression remains limited. In *Chapter II*, I sought to address the lack of a somatic conditional model of hepatoblastoma. To generate a conditional model of hepatoblastoma, I employed hydrodynamic injection of transposon based doxycycline-inducible oncogenes (See *Chapter II Tumor Maintenance Requires YAP1*). In the upcoming sections, I further discuss the benefits and caveats of hydrodynamic injection, inducible systems, and transposons.

Hydrodynamic Models

While traditional transgenic models are the gold standard, they are significantly time-consuming, and often require the crossing of multiple strains to recapitulate the genetics of a tumor. Further, as discussed in the preceding section, traditional transgenic models have failed to recapitulate pure hepatoblastoma (See *Chapter 5.1 Generating Murine Models of Pediatric Cancer*).

For liver cancer research, the introduction of hydrodynamic injection (HDI) revolutionized the generation of “transgenic” and “knock-out/knock-in” mouse models. HDI allows for stable, somatic integration of plasmid DNA into the mouse liver genome; thus, HDI removes the need for generation of germline mutant strains, and breeding. Most hydrodynamic systems utilize a transposon-based system for stable integration into the genome (239, 240, 416). *Chapter 5.1 Sleeping Beauty Transposon Systems* extensively discusses transposons for liver cancer modeling. Hydrodynamic injection takes advantage of two key anatomic and physiologic features of the liver: 1) *the dual blood supply*, and 2) *the physical proximity of hepatocytes and vasculature*.

HDI involves delivery of a plasmid DNA/saline solution through the tail vein of the mouse. Unlike other tail vein injections, HDI requires the DNA/saline solution to be approximately equivalent to the mouse blood volume (~10% of the body weight). The entire solution must be delivered in under >9 seconds. Immediately after injection, the full volume travels up the tail vein into the inferior vena cava

(IVC). The IVC returns venous deoxygenated blood directly into the R atrium of the heart. The large volume DNA/saline solution overwhelms the R atrium, causing temporary heart congestion, and reversing the flow of the cardiac cycle (241).

The large DNA/saline bolus then moves backwards through the IVC following back into the hepatic veins. In the hepatic veins, backwards flowing DNA/saline solution comes into close proximity with Zone 3, pericentral hepatocytes (417, 418). Drainage into the portal vein, Zone 1 of the liver, is largely limited in mice, restricting transfection of these hepatocytes (See *Chapter 1.7 Liver Differentiation* for an explanation of liver zonation) (417). While liver is the primary target organ in HDI, the reversal of cardiac cycle leads to limited transfection of other organs. Less than >0.1% of total transfection in HDI is observed in kidney, heart, lung, and spleen (239, 240, 416, 417).

Following back-flow of the DNA/saline solution into the hepatic veins, surrounding Zone 3 hepatocytes are transfected. Because the endothelial cells and hepatocytes are physically associated, delivery of DNA solution into the vasculature satisfactorily transfects hepatocytes. High-pressure in the endothelial cells of the hepatic veins makes the membrane of both the endothelial cells and adjacent hepatocytes porous. The brief permeability of hepatocytes generated by the high-pressure volume allows for passage and trapping of the saline solution into the hepatocytes.

Introducing a high-speed, high-volume injection via the venous system, swells the liver to nearly 2.5X its size in the short-term (417). The large influx of volume into hepatocytes, and creation of membrane pores, promotes a proinflammatory environment in the liver. Several groups observed a transient increase in the liver function test, aspartate aminotransferase (AST), and evidence of liver damage (239, 240, 417, 418). While most liver damage resolves within seven days, the inflammatory state following hydrodynamic injection may contribute to early tumor initiation in currently unappreciated ways. While liver inflammation plays a clear role in the pathogenesis of HCC, liver inflammation has not been proposed to be a key etiologic factor in hepatoblastoma (See *Chapter 1.1 Liver Primer, Chapter 4 Discussion*). Additional studies are needed to understand if early inflammation modulates hepatoblastoma initiation in an appreciable way.

Hydrodynamic injection transfects mature adult hepatocytes; thus, the cell of origin in HDI liver cancer models is primarily Zone 3 *adult* hepatocytes. The cell of origin in hepatoblastoma is unknown; however, it is presumed that hepatoblastoma tumors originate from hepatoblasts or earlier stem-like progenitor cells (See *Chapter 1.6 Liver Development, Chapter 1.8 Liver Tumorigenesis*). Hepatoblastoma is frequently observed *in utero*, and in the early months of an infant's life before the liver matures; thus, many have theorized hepatoblastoma does not originate from mature hepatocytes (See *Chapter 1.2 Incidence and*

Associations) (47, 68, 69, 71, 109). Thus, cell of origin represents a key caveat in the use of hydrodynamic injection for the generation of hepatoblastoma.

Another consideration when using hydrodynamic injection for the generation of liver tumors is the heterogeneity of delivery to each hepatocyte. Each hepatocyte uptakes and integrates variable amounts of DNA solution leading to variable oncogene expression. However, the variable oncogene expression generated by hydrodynamic injection may be a benefit for therapeutic modeling as it likely more closely captures the unpredictability of expression seen in patient tumors, often missed by clonal xenograft models.

A final consideration with the use of HDI for generation of hepatoblastoma is the potential for off-target stable life-long expression of oncogenes in other tissue including the heart, lung, kidney, and spleen. When evaluating the phenotype of a mouse following hydrodynamic injection, researchers should consider the possibility of off-target genome integration and pathology.

In my conditional model of hepatoblastoma generated using hydrodynamic injection, I observe a stem-like proliferative signature in tumors with HDI co-expression of YAP1 and β -catenin. This observation suggests that while I am transfecting a mature hepatocyte as the cell of origin, I hypothesize the oncogenic cooperation drives reversion of the hepatocyte towards a more stem-like state to drive tumorigenesis. This is consistent with the constitutive hydrodynamic model of hepatoblastoma, and the previously appreciated plastic nature of hepatocytes.

Inducible Models

Conditional genetic systems allow researchers to evaluate the necessity or function of a gene in temporal and spatial context. In traditional transgenic models, overexpression or loss of a gene in the germline results in either embryonic lethality or competing phenotypes that may compromise evaluation of the target gene in the desired context. As such, conditional systems allow for controlled gene expression, and more careful dissection of epistatic relationships.

In my conditional model of hepatoblastoma, I employ a TET-ON system. Tetracycline-ON (TET-ON) systems, drive gene expression when reverse tetracycline controlled transactivator (rtTA) and doxycycline are both present (**Figure 2.1**) (See *Chapter 2*). The TET ON system is a synthetic technology where rtTA is modified to only recognize the TET promoter, in the presence of doxycycline (385, 419). In my model, the presence of doxycycline drives expression of YAP1^{S127A}, and withdrawal of doxycycline prevents transcription.

The use of inducible promoters, including TET-ON systems, for genetic studies is not without challenges. For example, TET-ON systems may suffer from “Leakiness”, i.e. induction of gene expression in the absence of substrate, doxycycline and rtTA. Leakiness can occur for a number of reasons including: 1) *insertion of a TET-ON promoter near an enhancer in the genome*, or 2) *mutations in the TET promoter enabling effector-independent transcription* (384, 420-422). For example, doxycycline inducible MYC and KRAS breast cancer models both

displayed somatic mutations in the rtTA transgene in recurrent tumors. Thus, *doxycycline independent, oncogene dependent* transcription promoted relapse in this model (384). Similarly, I also observed infrequent GFP+ recurrent lesions in late stage hbHep YAP1 OFF livers suggestive of *doxycycline independent, oncogene dependent* tumor growth (See *Chapter 4*).

Conversely, TET-ON inserted genetic systems may also be inadvertently silenced by proximity to insulators, or by methylation of chromosomal regions (422). Nevertheless, researchers should employ caution when evaluating phenotypes generated by TET-ON systems, and studies should be appropriately powered.

Sleeping Beauty Transposon Systems

The use of transposon-based systems in conjunction with hydrodynamic injection allows for the stable integration of plasmid DNA into the genome of hepatocytes; thus, researchers can generate transgenic livers for the study of cancer genes in a matter of weeks. Transposon based technologies are non-viral and can deliver varied genetic content including complementary DNA (cDNA), short-hairpin RNA (shRNA) or single-guide RNA (sgRNA) sequences for life-long somatic integration into chromosomes of mice, and human cells. Thus, transposon systems enable rapid knock-in, and knock-out genetic studies.

DNA Transposons, or movable “jumping genes”, facilitated by a DNA intermediate element, were first observed in fish (423). Since then, synthetic engineering of transposons has allowed for *in vitro* and *in vivo* “cutting and pasting” of desired sequences. Ivics et al. developed the first synthetic transposon system primarily used today for genetic modeling: *Sleeping Beauty* (SB) (424).

Specifically, Ivics et al. demonstrated that transposons can be used to insert a sequence of choice stably into the genome of human cells. They demonstrated the synthetic Sleeping Beauty transposase binds to inverted repeats, and facilitates a “precise cut-and-paste” transposition (424). The Sleeping Beauty system was then adapted for *in vivo* editing. Work from Takeda’s group showed that the transposase system could be modified to effectively generate mutant mice, and further used as a tool for genetic screens *in vivo* (425-427). A natural next step was to adapt the system for screening of cancer genes *in vivo* (428, 429).

In the context of liver cancer modeling, the use of Sleeping Beauty transposases, in conjunction with hydrodynamic injection, revolutionized the speed, and ease for genetic gain and loss of function studies. In 2008, Bell et al. described a new strategy in *Nature Protocols* to successfully modulate the Sleeping Beauty system for gene delivery into mouse hepatocytes by hydrodynamic delivery (430). As such, multiple groups have since demonstrated the reliability and versatility of using Sleeping Beauty transposases with HDI for generation of transgenic mouse livers (412, 431, 432).

The HDI SB system is comprised of two basic pieces: the transposon (i.e. the sequence to be inserted), and the transposase enzyme. The transposon is comprised of first a promoter of choice, and second the gene of interest. The promoter and desired sequence are flanked by inverted repeats, recognized by the transposase enzyme for “cut-and-paste.” In summary, the transposase enzyme recognizes inverted repeats in both the engineered transposon, and at various sites in chromosomes. Transposase then cuts and pastes the transposon sequence into the chromosome permanently. Transcription of inserted sequences can occur in as little as 72 hours (433).

Transposons and transposase can be delivered on separate plasmids. Indeed, in my conditional model of hepatoblastoma, the oncogenic transposons, β -catenin and YAP1, are delivered on separate plasmids, and a final plasmid encodes the SB Transposase enzyme (**Figure 2.1**) (See *Chapter 2*). Further, each transposon can be driven by a unique promoter, allowing for constitutive β -catenin expression while simultaneously facilitating inducible expression of YAP1 (**Figure 2.1**).

A major concern when using the Sleeping Beauty system for insertional mutagenesis, and generation of tumor models is the potential for disruption of normal gene function; consequently, the phenotype observed may be the result of an off-target effect. Luckily, normal gene disruption is uncommon in Sleeping Beauty systems due to intrinsic properties of the technology. Compared to viral

vectors, the Sleeping Beauty system is less likely to disrupt normal gene transcription because DNA transposition, i.e. “cut and paste”, occurs primarily in non-coding DNA regions (434, 435). Nevertheless, care must be taken in evaluating tumorigenic phenotypes established by Sleeping Beauty HDI.

Identically to its naturally occurring counterpart, synthetic Sleeping Beauty transposase enzyme recognizes thymine-adenine (TA) dinucleotide base pairs. TA base pairs are abundant in human and mouse genomes (424). Within the mouse genome, there are an estimated 200 million chromosomal sites for transposon integration (430). The transposase enzyme recognizes and binds the inverted repeats on the transposons containing gene of interests. Insertion of the transposon into the genome involves two Sleeping Beauty transposase enzymes binding to each end of the transposon, forming a circle bringing the ends of the transposon together. The Sleeping Beauty transposase enzyme complex then “cuts” the transposon/sequence of interest, and “pastes” into an unspecified TA-dinucleotide site on the chromosomal DNA (430).

The variable delivery of SB-plasmid DNA to hepatocytes by hydrodynamic injection likely influences the degree of DNA transposition on a cell-to-cell basis. Some cells may have only YAP1 or only β -catenin integration; however, as shown in Tao et al, in the short-term >12 weeks, expression of YAP1 or β -catenin alone does not lead to tumorigenesis (31). While β -catenin overexpression in adult hepatocytes has not been observed to produce liver tumors in the long-term (12+

weeks), YAP1 overexpression does promote HCC tumorigenesis. By 15 months of age, overexpression of YAP1 or loss of upstream Hippo proteins promotes tumorigenesis (see *Chapter 1.8 Liver Tumorigenesis*) (22, 25, 350-352). Hepatoblastoma tumorigenesis produces a lethal burden of tumors by >11 weeks. Further in my model, YAP1 is inactivated at approximately 8 weeks by withdrawal of doxycycline limiting the likelihood of HCC development erroneously (See *Chapter 2, Chapter 1.5 Laboratory Models*). As such, mice with hepatoblastoma should be evaluated in a time dependent manner.

In my model, it is reasonable to presume that each tumor cell generated by DNA transposition, has varying degrees of YAP1 and β -catenin somatic integration. Thus, each cell likely has variable overexpression of YAP1 and β -catenin oncogenes (See *Chapter 2*). As such, oncogene overexpression by transposition may have dosage dependent effects.

In my HDI SB model of hepatoblastoma, transcriptional output of YAP1 and β -catenin may be dependent on their levels of integration in the cell, and whether they are produced in the proper stoichiometric ratio to function as a transcriptional complex. Indeed, Li et al. found that protein members of a complex are made in an exact stoichiometry, and further that protein pathway members are translated by functional priority (436). Nevertheless, in my murine model I observe nuclear expression of both β -catenin and YAP1 across tumors and mice using the SB HDI system. This finding suggests that regardless of integration level, YAP1 and β -

catenin cooperate to initiate hepatoblastoma tumorigenesis. Further investigation is needed to understand how YAP1 and β -catenin interact in a dose-dependent manner.

Caveats of the Conditional Model of Mouse Hepatoblastoma

As discussed in prior sections of this chapter, generation of mouse models for the study of human tumorigenesis has allowed for more careful and thorough dissection of the major signaling pathways supporting and maintaining tumorigenesis. However, these models are not without caveats that should be considered when both designing experiments and interpreting data.

With consideration to my conditional model of hepatoblastoma, several key points should be highlighted, the first which apply to *all* mouse models. First, there are species specific variations between human and mouse physiology. While mice and humans share approximately 85% of their genomes, there are considerable differences in metabolic rate, xenobiotic metabolism, life span, and perhaps most notably for cancer research, in length of telomeres and presence of active telomerase (437).

Telomeres are the protective ends of chromosomes made up of tandem repeats (TTAGGG). Normally, telomeres shorten every time the cell divides (438). In humans, telomerase can lengthen telomeres by adding new tandem repeats; however, this function is typically only found in stem cells, or in cancer cells with

gain-of-function mutations in the catalytic subunit of telomerase, TERT (438). As such, critical telomere shortening without addition of new repeats by telomerase, typically results in apoptosis.

Introduced in *Chapter 1.1*, mutations in *TERT*, the enzymatic component of telomerase, are a defining feature of adult liver cancer and occur infrequently in hepatoblastoma (10, 14). The presence of active telomerase in mouse cells may accelerate tumorigenesis compared to human tumors and alter the tumors response to DNA Damaging agents. For modeling of adult tumors that frequently have telomerase mutations, this may be beneficial. In pediatric tumors, such as hepatoblastoma with infrequent *TERT* mutations, this may be a confounding issue.

Please refer to the preceding sections for caveats of hydrodynamic injection, inducible models, and transposase systems. Other major caveats primarily for the conditional model of hepatoblastoma include the cell of origin in the model, the lack of metastases, and the multifocal nature of the disease. Human hepatoblastoma tends to be unifocal (see *Chapter 1.5 Clinical Presentation*). Conversely, the hydrodynamic model transfects upwards of >20% of adult hepatocytes producing 30+ tumors per liver, which is rarely, if ever, recapitulated in human patients.

Future directions for mouse modeling of pediatric hepatoblastoma

My hydrodynamic conditional model of hepatoblastoma has many advantages including its genetic simplicity that mirrors human pediatric disease, reproducibility of human histology, and timeliness; however, mouse modeling of hepatoblastoma could be improved by further engineering the model to produce unifocal lesions and to generate representative metastatic disease. Hydrodynamic modeling of hepatoblastoma transfects >20% of hepatocytes, and SB insertional mutagenesis likely results in multiple copies of transposon(oncogene) per cell (See *Chapter 5.1 Sleeping Beauty Systems*). Thus, the combination of HDI and SB generates tumors covering the entire surface of the liver (**Figure 2.1**).

The HDI SB system generates a lethal burden of liver tumors by >11 weeks; thus, the current model does not facilitate the study of metastatic disease. Limiting the initial burden of liver tumors may allow sufficient time for progression to metastases. One strategy to limit the number of tumors formed, is to confine knock-in of oncogenes to certain genomic sites. To control insertion of oncogenes, oncogenes could be knocked-in in a site-specific manner using a CRISPR/Cas9 based system, i.e. CRISPR-SONIC (See *Appendix II*) (439). CRISPR-SONIC facilitates maximally two knock-ins per cell in an allele specific manner. To facilitate knock-in of oncogenic sequences, CRISPR-SONIC uses homology independent repair to integrate a sequence of choice into the endogenous mouse 3'-UTR of β -Actin. As such, oncogene expression is more tightly controlled and homogenous.

Further, the efficiency is slightly less than SB systems, which would likely decrease the liver disease burden, allowing more time for seeding of metastases.

Alternatively, more indolent unifocal lesions and potential metastases, could also be generated via transplantation of murine hepatoblastoma tumor cells by intrasplenic or intrahepatic injection (186). Previous groups have transplanted pediatric patient cells into the liver of immunocompromised mice generating an orthotopic model of hepatoblastoma (236, 238). Similarly, generation of a unifocal lesion in an immune-competent mouse could theoretically be generated by intrahepatic or intrasplenic transfer of syngeneic mouse hepatoblastoma cells into a single liver lobe. Caveats of this approach include: the potential immunogenicity of transplanted hepatoblastoma cells, and technical challenges in mechanically digesting and transplanting hepatoblastoma tumor cells due to their stem-like nature.

Unifocal hepatoblastoma lesions could also likely be generated by targeted electroporation of oncogenes to one lobe of the liver (288). As with injection of tumor cells into the liver, the presumed benefit of this model would be slower progression possibly facilitating the development of metastases more closely mimicking aggressive Stage 3-4 hepatoblastoma (See *Chapter 1.3 Clinical Presentation of Hepatoblastoma*). Continual improvement of mouse modeling of pediatric cancers will be crucial to better understand the signaling complexities of human tumorigenesis.

Chapter 5.2 Role of Hippo/YAP Signaling in Liver Cancer

Within *Chapter 5.2*, I first review the role of YAP1 broadly in liver tumorigenesis, and its downstream effectors. Next, given the lack of mutations in YAP1 in hepatoblastoma patients tumors, I consider mechanisms of YAP1 activation. Following the review of YAP1 activation, I explore the role of YAP1 in hepatoblastoma tumor maintenance, and its signaling partners. Finally, I examine liver differentiation triggered by YAP1 withdrawal. YAP1 and its interactions with Wnt/ β -Catenin, the role of YAP1 in cell fate, and finally the state of YAP1 therapeutics will be discussed in upcoming sections (See *Chapter 5.4, 5.5, 5.6, 5.7*).

Herein, I propose that YAP1 is essential for hepatoblastoma tumor maintenance without silencing oncogenic β -catenin. Further, I find that YAP1 promotes tumor maintenance through cooperation with its canonical co-transcription factors TEAD, and with oncogenic partners Fos-Jun in addition to β -catenin. Finally, I propose that YAP1 maintains stemness in hepatoblastoma tumors; thus, its withdrawal promotes differentiation by increasing binding at motifs of multiple differentiation transcription factors, consistent with the finding that no singular HNF family member is sufficient to maintain differentiation (See *Chapter 1.7 Liver Differentiation*).

YAP1 Signaling Primer

Summarized in *Chapter 1.8 Hippo Signaling in Liver Tumorigenesis*, constitutive YAP1 activity is a frequent characteristic of many tumor types including lung, pancreatic, breast, colorectal and all major subtypes of liver cancer (339-346). Nuclear YAP1 drives a pro-proliferation, anti-apoptotic transcriptional program (See *Appendix IV*). In both predominant subtypes of adult liver cancer, HCC and ICC, and pediatric hepatoblastoma, nuclear YAP1 signals poor prognosis (344, 347, 348).

While nuclear YAP1 expression is found across most major liver cancer subtypes; the nuclear co-localization of both YAP1 and β -Catenin is specific to hepatoblastoma (See *Chapter 1.8, Chapter 5.3*). Indeed, in my model of conditional model of hepatoblastoma, I observe nuclear expression of both YAP1 and β -Catenin in doxycycline induced tumors (**Figure 2.1**).

Introduced in *Chapter 1.8*, YAP1 alone is not sufficient in the short-term *in vivo* to induce tumorigenesis; however, 12+ weeks of constitutive activated YAP1 expression does promote development of HCC. Likewise, loss of Hippo pathway components, like MST1/2, also promotes tumorigenesis (22, 25, 350-352). In line with this, Nishimoto et al. found that in mouse embryonic stem cells overexpression of active YAP alone was sufficient for transformation to malignancy. Further, they find this effect is mediated through C-Myc (440). Previous reports suggest that Myc is downstream of Wnt signaling in hepatoblastoma; however, my observations

suggest that Myc and its target gene expression is regulated by YAP1. This will be further explored in *Chapter 5.4*.

Canonical/Non-Canonical YAP1 Signaling in Liver Tumorigenesis

YAP1 induces tumorigenesis by dysregulating cell cycle progression, conferring stemness, and upregulating anti-apoptotic programs. As such, YAP1 downstream transcriptional programs in tumors frequently include BIRC5, MYC, BCL2, NOTCH, JAG1, and FOXM1 (20, 26, 280, 353, 354, 373, 441). Similarly, I observe YAP1-induced transcription of BIRC5, and Myc in my murine tumors (Figure 2.2). Importantly, expression of MYC and BIRC5 is associated with the poor prognosis subtype of hepatoblastoma (See *Chapter 1.4*).

YAP1-TEAD

YAP1 does not have a DNA binding domain; as such, it requires co-factors to orchestrate its transcriptional program. Canonically, YAP1 exerts its oncogenic functions through the TEAD family of transcription factors; in agreement with this, DNA Footprinting in YAP1 ON tumors vs. YAP1 OFF tumors, reveals increased binding at the TEAD consensus motif 5'-CATTCCA/T-3' (See *Chapter III*) (**Figure 3.10**). This finding suggests that in murine hepatoblastoma, YAP1 exerts at least part of its oncogenic effects through TEAD1-4 family members. Indeed, Liu-Chittenden et al. demonstrated that YAP1 in the liver preferentially binds TEAD

family members to exert its oncogenic effects (358, 359). Consistent with previous reports from Dong et al, Chittenden et al. found that expressing a mutant form of TEAD disrupted expression of canonical YAP1 targets including CTGF, MYC, and BIRC5 (21, 355). Taken together, these results suggest that in my model, YAP1 likely upregulates expression of CTGF, MYC, and BIRC5 via TEAD binding partners (See *Chapter 2, Appendix IV*). Thus, YAP1-TEAD small molecule disruptors represent a potential class of YAP1 therapeutics for hepatoblastoma (See *Chapter 5.7* for further discussion).

Both Chittenden and Dong also find that loss of TEAD abrogates expression of liver stem markers AFP and GPC3 (1, 15, 258, 442(21, 355). Consistent with this observation, I find that YAP1 withdrawal significantly blunts expression of both Afp, and Gpc3 in murine tumors within six days (**Figure 2.2**, *Appendix V*). This finding is particularly relevant for hepatoblastoma and suggests that YAP1 downregulation of Afp and Gpc3 is TEAD dependent.

AFP and GPC3 are important biomarkers in hepatoblastoma; YAP1 control of these proteins, and more broadly stemness in hepatoblastoma remains under-investigated. Serum AFP levels track with disease progression in hepatoblastoma; therefore, decreasing levels of AFP with treatment confers good prognosis (See *Chapter 1.3 Laboratory Findings and Imaging*) (135, 136, 138). Further, Cui et al. found that a frequent event in hepatoblastoma is the hypomethylation/activation of AFP (199). Whether YAP1 participates in the epigenetic modulation of AFP is

unknown; however, YAP1 does exert part of its transcriptional function through activity at enhancers (See Chapter 1.8 Liver Tumorigenesis).

Comparatively, GPC3 has also been proposed as a marker of disease burden in hepatoblastoma, and is a known Wnt activator (98). GPC3 is mutated in the overgrowth syndrome Simpson Goblai Behmel. Children with Simpson Goblai Behmel have an increased risk of hepatoblastoma (**Table 1.2**) (See Chapter 1.2 *Incidence and Associations*). Finally, miRNAs that downregulate the expression of GPC3, are significantly lower in hepatoblastoma samples compared to normal liver. Higher levels of GPC3 may contribute to continued Wnt activation (220).

Thus, the rapid downregulation of two prognostic stem-like markers, Afp and Gpc3, in my murine tumors with YAP1 inhibition, suggests that YAP1 may be driving the aggressive stem-like phenotype of hepatoblastoma (See *Chapter 1.4, 5.7*). This will be further discussed in the upcoming section, *YAP1 and Hepatoblastoma Tumor Maintenance*.

YAP1 and Epigenetic Regulation

The YAP1/TEAD complex also regulates transcriptional output by actively binding to chromatin and regulating gene expression at the epigenetic level. First summarized in *Chapter 1.8*, Croci et al. elegantly showed that YAP1 promoted MYC target gene expression in liver tumors. Specifically, MYC target gene chromatin was actively designated by prebound TEAD co-factors. The subsequent binding of YAP1 at these sites in turn stabilized MYC binding and promoted target

gene expression. Thus, together YAP1 and MYC promoted cell cycle entry (361). Consistent with Croci et al's findings, in my mouse model of hepatoblastoma, I observe downregulation of the GSEA signature *MYC Targets V1* following YAP1 withdrawal (**Figure 2.2**) (*Appendix V*).

In breast cancer cells, Zanconato et al. demonstrated that YAP1/TEAD, together with Fos-Jun dimer activator protein 1 (AP-1), controls target expression through distant enhancers. Similarly, to Myc target gene regulation, TEAD is necessary for YAP1 binding and activity at enhancers (363-365). Indeed, in my DNA-Footprinting of YAP1 ON Tumors, I observe increased binding at Fos-Jun motifs consistent with Zanconato's observations in breast cancer tumors (**Figure 3.10**).

TEAD Independent Transcription

YAP1 can have TEAD independent transcriptional activity by complexing with other transcriptional co-factors to drive alternative gene expression programs (*Appendix IV*). YAP1 has been described to complex with a number of transcriptional co-factors including: TCFP2, Paired box 3 (PAX3), RUNX Family Transcription Factor (RUNX), Tumor protein p73, TBX5, and SMAD Family member4 (SMAD4) (198, 360, 373, 442-448). Interestingly, Zhang et al. proposed that in adult liver tumorigenesis, TFCP2 functions as a non-canonical YAP1 co-factor, and is required for YAP1-TEAD dependent transcription (See *Chapter 1.8*)

(360). Zhang et al finds that in HCC, YAP1's oncogenic activity is reduced without TFCP2.

Notably, in my DNA foot-printing of YAP1 ON Tumor compared to hbHeps, I did not observe differential signal at the TFCP2 motif (**Table 3.1, 3.2**). Whether YAP1 tumorigenesis relies on TFCP2 and is sensitive to TFCP2 loss requires further investigation. YAP1 has also been described to bind p73 (198, 443, 444), and TBX5 (373, 445); however, similarly to TFCP2, I do not observe increased signal at their motifs in YAP1 ON tumors compared to hbHeps (**Table 3.1, 3.2**). Indeed, additional functional studies are needed to understand the role of non-canonical transcription co-factors in hepatoblastoma YAP1 tumorigenesis.

YAP1 Activation in Hepatoblastoma

The most common mutation observed in hepatoblastoma is in *CTNNB1* / β -Catenin (~80%). Further, an estimated 90% of children have Wnt pathway mutations (APC, Axin, etc.) (**Table 1.9**) (See *Chapter 1.4*) (1, 14). Despite nuclear accumulation of YAP1 in upwards of 80% of children's hepatoblastoma tumors, YAP1 has not been found to be mutated in hepatoblastoma (**Figure 1.13**) (31). Further, while loss of upstream Hippo pathway members (LATS1/2, MST1/2, etc) causes YAP1 hyperactivation in mouse models of liver cancer, this phenomenon has not been observed in children's tumors (22, 25, 30). Finally, amplification of

the YAP1 locus, seen in ~10% of adult HCC patients, has also not been observed in children's tumors (24).

The second most common observed mutation in hepatoblastoma is in the proto-oncogene NFE2I2/NRF2 (10% of cases) (**Table 1.9**) (See *Chapter 1.4*) (14). Recently, NFE2I2/NRF2 was found to complex with Taz, a paralog of YAP1, and promote tumorigenesis in glioblastoma (See *Appendix IV*). Previous results suggest that NRF2 associates with β -catenin in hepatoblastoma, and that loss of NRF2 blunts tumor proliferation (186). If NRF2 mutations lead to YAP1 activation in hepatoblastoma remains unknown.

The lack of detected amplifications and mutations in YAP1 suggests that epigenetic modifications of Hippo pathway members may be responsible for YAP1 hyperactivation in children's tumors. Indeed, hypermethylation of *RASSF1A*, a known Hippo regulatory component, is a frequent event in children's tumors. Sakamoto et al. found that in a sample of 20 children's tumors, >80% had hypermethylation/silencing of *RASSF1A* (193). Further, *RASSF1A* hypermethylation is associated with poor prognosis (193). In ES cells, *RASSF1A* blocks self-renewal by dysregulating cooperative signaling between YAP1 and β -catenin (198). Thus, a reasonable assumption is that hypermethylation of *RASSF1A* may promote the cooperative oncogenic binding of β -catenin and YAP1 in hepatoblastoma (See *Chapter 1.9 Wnt and Hippo Crosstalk in Tumorigenesis*).

Whether YAP1 downstream of *RASSF1A* hypermethylation promotes self-renewal of hepatoblastoma tumor cells requires further investigation.

The Hippo pathway can be activated or inactivated by G coupled proteins in a context dependent manner (See *Appendix IV*). Current findings suggest that primarily GPCR/Gs-coupled receptors activate Hippo signaling (202, 449). Indeed, Honda et al. found that in 74 cases of hepatoblastoma, 25% had hypermethylation/inactivation of a suspected tumor suppressor, G coupled protein receptor 180 (*GPR180*). Similarly, to *RASSF1A*, *GPR180* hypermethylation also portends poor prognosis (201) (See *Chapter 1.4*). Thus, loss of *GPR180* expression may contribute to YAP1 activation in hepatoblastoma tumorigenesis. An important caveat is that YAP1 activation was not checked in samples downstream of *RASSF1A* or *GPR180* hypermethylation. *In vivo* functional exploration of upstream YAP1 activation is needed.

Given the lack of clear etiologies for YAP1 activation, mouse modeling of hepatoblastoma, including my conditional model, utilizes overexpression of constitutively active YAP1 (**Figure 2.1**). Understanding the cause of YAP1 activation will therefore improve *in vivo* modeling.

YAP1 and Hepatoblastoma Tumor Maintenance

Summarized in *Chapter II Introduction*, tumor initiation and tumor maintenance are distinct processes. Tumor initiation typically requires at least two genetic

lesions for sustained malignant transformation (374). For hepatoblastoma, the concurrent hyperactivation of both of β -catenin and YAP1 is sufficient to induce tumorigenesis *in vivo* (See *Chapter 1.5 Laboratory Models*, *Chapter 1.8 Liver Tumorigenesis*) (31, 245).

Defining Tumor Initiation and Tumor Maintenance

The role of oncogenes in other cancer types has demonstrated that while expression of an oncogenic protein may be required for tumor initiation, the tumor may not be reliant on expression of said oncogene for long-term survival, i.e. maintenance. (376-381). Further, when two oncogenes are necessary for initiation, the tumor may be more sensitive to loss of only one of the two oncogenes. For example, Varmus's group demonstrated that breast cancer initiated by MYC and KRAS, was intrinsically more reliant on KRAS than MYC expression for tumor proliferation and survival (384). Given that oncogenic cooperation may have functionally distinct roles in tumor initiation and tumor maintenance, I sought to evaluate whether hepatoblastoma initiated by both YAP1 and β -catenin was sensitive to loss of YAP1 alone.

YAP1 promotes proliferation, survival and stemness in hepatoblastoma

In *Chapter II*, I demonstrate using a new conditional mouse model of hepatoblastoma, that both hepatoblastoma tumor initiation and maintenance require YAP1. I propose that YAP1 maintains tumor survival in hepatoblastoma

through 1) *promoting proliferation and cell cycle progression through upregulation of Myc and its target genes*, 2) *suppressing apoptosis through expression of anti-death proteins* 3) *maintaining liver stemness by blunting canonical differentiation signaling*.

In my model, following 8+ weeks of doxycycline for tumor establishment (**Figure 2.1**), doxycycline is removed from the food to block YAP1 overexpression (**Figure 2.4**). Within six days of YAP1 withdrawal, I observe a reduction in Ki67 staining, demonstrating halted proliferation in the absence of YAP1 (**Figure 2.5**). Indeed, expression of pro-proliferation genes (i.e. Ctgf, Myc, Cyclin D1), was drastically reduced following loss of YAP1 overexpression (**Figure 2.2, Appendix V**) Further using gene expression analyses, I observed that YAP1 loss was sufficient to downregulate cell cycle progression signatures including *Hallmark G2M checkpoint, Mitotic Spindle, and E2F targets* (**Figure 2.2-2.3**)(See *Chapter 1.4 Molecular Profiling of Hepatoblastoma*).

Loss of proliferative capacity in YAP1 OFF tumors is further supported by the durable regression and loss of Ki67 staining observed at later time points D70+, and in hbHeps (*Chapter II, Chapter IV*). Finally, as discussed in *Chapter 5.1 Canonical YAP1 Signaling*, YAP1 withdrawal downregulates Myc target gene signatures in YAP1 OFF tumors (**Figure 2.2**). Consistent with my observation, YAP1 has previously been found to bind to and regulate MYC target gene promoters (361).

In addition to promoting cessation of proliferation, YAP1 withdrawal promotes upregulated CC3+ in YAP1 OFF tumors. In line with this, when I compared gene expression from YAP1 ON tumors to YAP1 OFF tumors, and microarray from human C2 poor prognosis tumors to C1 favorable, I see downregulation of IPA signatures *Cell death of tumor*, *Necrosis*, *Apoptosis* in both YAP1 ON tumors and human C2 tumors (**Figure 2.3**). Finally, with loss of YAP1, I observe downregulation of canonical anti-apoptotic protein, Birc5 (Survivin) (**Figure 2.2**, *Appendix V*). BIRC5 is differentially expressed between C2 poor prognosis and C1 favorable prognosis tumors. In my conditional system, modulating YAP1 alone sufficiently downregulates many of the proliferative and apoptotic genes associated with poor prognosis (**Figure 2.3**, *Chapter 1.3, 1.4, 1.8*).

Like other classic proto-oncogenes, in my murine model of hepatoblastoma, YAP1 maintains tumor survival in large part through supporting a proliferative and anti-apoptotic transcription program. I would like to propose that YAP1 further supports hepatoblastoma tumor maintenance through maintenance of stemness. Supporting my hypothesis, Yimlamai et al. beautifully demonstrated in the liver that YAP1 alone first maintains a pool of hepatocyte progenitor cells, and second that overexpression of YAP1 can stably dedifferentiate mature liver cells *in vivo* into stem-like progenitors (20). YAP1, and its paralog TAZ, have also been found to maintain stem-like populations, often called cancer stem cells (CSCs), in other tumor types including lung and breast cancer (341, 450-452).

The cancer stem cell population in hepatoblastoma remains unknown; however, AFP and GPC3 are frequently used as markers for stem-like populations in hepatoblastoma and HCC (See *Chapter 1.2, 1.3*). Indeed, high AFP expression and GPC3 expression are associated with chemo-resistant, poor prognosis subtypes of hepatoblastoma (1, 15, 98, 258, 453). As discussed in *Chapter 5.2 Canonical YAP1 Signaling*, loss of YAP1 is sufficient to downregulate AFP and GPC3 expression.

In my murine model, I have observed that YAP1 withdrawal without blunting of oncogenic β -Catenin, halts proliferation, increases apoptosis, and promotes stable differentiation of residual tumor cells to partially functional, hbHeps. The lack of immediate relapse following YAP1 withdrawal, and reliance of YAP1 for proliferation potential suggests that YAP1 may be modulating the self-renewal capacity of hepatoblastoma tumors. To this point, I observe downregulation of proteins associated with chemoresistance following YAP1 withdrawal (**Figure 2.2 ,2.3**) (See *Chapter 5.7* for further discussion). Nevertheless, identifying hepatoblastoma's stem cell population and interrogating what maintains said population requires further investigation.

YAP1 and Differentiation

In the adult liver, YAP1, Wnt, and HNF family differentiation signaling are carefully titrated and largely work in opposition to maintain normal liver lobule

function (19, 20, 22, 285, 289-291). The spatial separation of Wnt and YAP1 signaling under normal contexts in hepatocytes is consistent with the oncogenic potential of cooperative signaling between these two pathways. In the preceding section, I detailed how YAP1 overexpression supports expression of stem-like properties; in agreement with this, I find that YAP1 withdrawal rapidly commutes the proliferative and stem-like nature of hepatoblastoma.

Further, following YAP1 withdrawal, I observe rapid upregulation of gene signatures associated with mature hepatocyte gene expression (**Figure 3.4-3.6**). In fact, the top 20 upregulated genes in YAP1 OFF D6 tumors are liver enzymes expressed across all zones of the adult liver lobule (See *Chapter 1.7 Liver Differentiation*). Specifically, I observe increased expression of periportal gene signatures (*i.e. Fatty Acid Metabolism*), and pericentral signatures like *Xenobiotic metabolism* (**Figure 3.4B**).

In the normal liver, Zone 1 periportal region is balanced by expression of endogenous YAP1 and HNF4 α . Conversely, Zone 3 pericentral hepatocytes are characterized by Wnt signaling. Of note, in my conditional model I am primarily generating tumor cells from Zone 3 pericentral hepatocytes (See *Chapter 5.1 Hydrodynamic Models*). Further, I am not changing β -catenin overexpression in the hepatoblastoma tumor cells. Taken together, a reasonable hypothesis is that loss of YAP1 overexpression in hepatoblastoma tumors would drive expression of primarily a pericentral phenotype characterized by Zone 3 signatures. However,

following YAP1 withdrawal, in addition to a Zone 3 phenotype, I also observe induction of Zone 1 characteristics as evidenced by induction of HNF4 α nuclear expression, and upregulation of GSEA signature *HNF4 α Target genes* (See *Chapter 1.7*). In the adult liver, suppression of YAP1 overexpression increases HNF4 α expression (20, 23, 283, 293).

In *Chapter III and IV*, I find that YAP1 withdrawal promotes the re-differentiation of regressing tumor parentage cells into hbHeps. I propose that YAP1 withdrawal reprograms tumor transcription in part through modulating transcription factor occupancy at critical HNF family member motifs (**Figure 3.11**). Specifically, I find evidence of increase occupancy at the motifs for Hnf4 α , Hnf1 α /B, Onecut1/3, and FOXA1/2 (**Figure 3.11A-E**).

Consistent with my observations, Alder et al. finds that in liver development, nuclear YAP1 influences the enhancer site choice of HNF family members, HNF4 α and FoxA2 (See *Chapter 1.6 Liver Development*) (20, 283). Interestingly, Fitamant et al. also finds upregulation of HNF4 α following YAP1 loss in adult HCC, but this effect is confined to hepatocytes *without* β -catenin mutations (23). In the normal liver, Wnt and Hippo signaling are zonally distributed. As such, differential sensitivity to YAP1 in HCC compared to hepatoblastoma may reflect the differentiation status of the tumor. Fitamant et al. also describes “residual nodules” filling in tumor spaces following YAP1 inhibition, I hypothesize that Fitamant et al. are likely observing generation of “hbHeps”.

Critically, multiple groups have demonstrated that no single HNF family member can fully rescue normal liver function (296-299) (**Figure 1.12**). To this point, in my partially functional, histologically “normal” hbHeps I observe the upregulation of nearly all HNF family members. Further investigation is required to fully appreciate how YAP1 modulates HNF Family expression in hepatoblastoma.

Chapter 5.3 Wnt signaling in Liver Cancer

In *Chapter 5.3*, I review the role of Wnt/ β -Catenin signaling in hepatoblastoma tumorigenesis. First, I discuss the role of Wnt activation in liver cancer generally. Then I review the predominant Wnt pathway mutations in hepatoblastoma, followed by a discussion on differential Wnt signaling in hepatoblastoma subtypes. Herein, I will propose that my conditional model of hepatoblastoma recapitulates Wnt signaling observed in the aggressive C2 subtype of hepatoblastoma. Further, I will suggest that Myc, a classic β -catenin, target is under the transcriptional control of both Wnt and YAP1 control in this model.

Wnt/ β -Catenin Signaling in Liver Tumorigenesis

Wnt signaling is frequently activated in liver tumorigenesis, and similarly to YAP1 is thought to promote a proliferative, stem-like program. Particularly, β -catenin promotes proliferation through downstream expression of Cyclin D1, Myc, TGF β and TBX3 (31, 228, 319, 332-334). The timing of Wnt signaling in both the developing liver and in the adult liver is critical for normal liver function (See *Chapter 1.6 Liver Development*, *Chapter 1.7 Liver Differentiation*). Alone, β -catenin expression is not sufficient to promote liver tumorigenesis, hepatoblastoma or hepatocellular carcinoma (See *Chapter 1.8 Liver Tumorigenesis*) (324). As such, in adult liver tumorigenesis β -catenin cooperates with other oncogenes (i.e.

HRAS, KRAS, AKT, MET, MYC) to drive HCC (185, 327-331). The cooperation between β -catenin and YAP1 to initiate tumor formation appears to be specific to hepatoblastoma (*Chapter 1.8 Liver Tumorigenesis*) (31).

Wnt Pathway Activation in Hepatoblastoma

In contrast to the lack of YAP1 activating mutations in liver cancer (See *Chapter 5.2*), nearly 30% of adult HCC patients, and upwards of 80% hepatoblastoma cases have *CTNNB1* mutations (See *Chapter 1.1, 1.4*) (**Figure 1.2, Table 1.9**). Upwards of >90% of children with hepatoblastoma have Wnt pathway activations including mutations in *APC* and *AXIN1/2* (See *Chapter 1.2, 1.4*) (1, 14, 15, 87, 88, 182). For unknown reasons, *CTNNB1* mutations are infrequent in the other predominant adult subtype of liver cancer, ICC (**Table 1.2, Table 1.9, Figure 1.13**) (9-14, 321, 322).

Most *CTNNB1* mutations in hepatoblastoma occur in exon 3. When the Wnt pathway is inactive, β -catenin is phosphorylated by GSK3 β on specific serine residue/ threonine residues. Phosphorylation of β -catenin marks it for degradation by β -Transducin repeat containing protein (β -TRCP), an E3 ubiquitin ligase. Mutations and deletions in exon 3 shield β -Catenin from phosphorylation and subsequent degradation by the destruction complex; therefore, β -catenin with exon 3 anomalies can continually translocate to the nucleus to act as a transcriptional co-factor (See *Appendix III*) (323).

My model mimics the loss of serine and threonine mutations critical for β -Catenin destruction. Specifically, I am employing a constitutively active human β -Catenin with loss of the first 90 amino acids. Critical serine and threonine residues occur between amino acid 30-70 (**Figure 2, Appendix III**). In Wnt OFF contexts, β -catenin is found at the adherens junctions. With overexpression of constitutive β -Catenin I observe primarily nuclear β -Catenin in my model (**Figure 2.2**). Hypermethylation of Wnt inhibitors and downregulation of *inhibitory* Wnt microRNA's have also been observed in hepatoblastoma (See Chapter 1.4) (193, 194, 219, 220).

Differential Wnt Signaling in Hepatoblastoma

Nearly all children with hepatoblastoma have Wnt pathway activation. Further, C1 favorable prognosis and C2 poor prognosis have comparable rates of *CTNNB1* mutations. Interestingly, in C1 and C2 tumors, Cairo et al, finds that β -catenin directs vastly different transcription. For example, Cairo et al. finds that in favorable well-differentiated C1 tumors, β -catenin target expression mirrors pericentral Zone 3 signatures. Reviewed in *Chapter 1.7*, in the adult liver Wnt signaling maintains normal function of the Zone 3 liver lobule (1). In my model, I observe induction of Zone 3 perivenous genes as soon as six days after withdrawing YAP1 (**Figure 2.2, Appendix V**). These findings suggest that in hepatoblastoma, the Wnt/ β -catenin program is influenced by YAP1 status and is

context dependent; thus, YAP1 withdrawal allows β -Catenin to default towards its canonical transcription pattern.

In the C2 aggressive subtype, Cairo et al. describes Wnt/ β -catenin transcription as driving expression of proliferative, stem and anti-apoptotic proteins like BIRC5 (Survivin), GPC3, and MYC (1). Indeed, in my murine model I find that loss of YAP1, with continued expression of oncogenic β -catenin, reduces expression of Birc5, GPC3, and Myc (**Figure 2.2**, *Appendix V*). These findings are consistent with the hypothesis that YAP1 is essential for β -catenin-dependent transcription of pro-proliferation and anti-apoptotic genes. Cooperative signaling between β -catenin and YAP1 will be further discussed in the following section.

Chapter 5.4 Crosstalk between Wnt and Hippo Signaling

In the previous section, I demonstrated that YAP1 modulates β -catenin transcription in hepatoblastoma tumors. Specifically, for expression of β -catenin C2 aggressive targets in hepatoblastoma (Myc, Birc5, and GPC3), YAP1 is required. Here I discuss YAP1 regulation of Wnt/ β -catenin signaling broadly in liver tumorigenesis, and vice versa. In my model, understanding how YAP1 and β -catenin cooperate to maintain tumorigenesis requires further investigation; however, preliminary findings suggest that YAP1 withdrawal modulates Wnt signaling by downregulating expression of canonical β -catenin oncogenic targets, and upregulating differentiation targets like C/EBP α , previously thought to be under the control of β -catenin.

YAP1 Regulation of Wnt/ β -Catenin

Previously in hepatoblastoma-like HepG2 cells, Tao et al. demonstrated that loss of YAP1 suppressed β -Catenin promoter activity, and target gene expression (31). This finding is consistent with my observation *in vivo* that conditional loss of YAP1 with doxycycline withdrawal reduces expression of Cyclin D1, Myc, Birc5, and GPC3 (**Figure 2.2**). Further, long-term YAP1 withdrawal in hbHeps results in sustained downregulation of Myc (**Figure 4.4**). Thus, in hepatoblastoma tumors *in vivo*, YAP1 regulates some canonical β -catenin targets. To this point the remarkable regression of hepatoblastoma tumor cells

with YAP1 loss alone, may be due in part to YAP1's control over β -Catenin oncogenic targets.

Consistent with my finding that Myc is primarily under the transcriptional control of YAP1 in the mouse liver, Reed et al. found that in mouse liver loss of the Wnt tumor suppressor *Apc* (See Appendix III), could not be rescued by loss of Myc alone (81). Conversely, in colorectal cancer cells, Myc is a direct target of β -catenin transcription (335, 336). Therefore β -catenin target transcription may be tissue specific. Indeed, in heart cells YAP1 signaling has also been shown to promote nuclear translocation of β -catenin, and target gene expression (31, 369).

Conversely, Hippo ON signaling downregulates Wnt signaling (See *Chapter 1.8*) (367, 368). Specifically, cytoplasmic YAP1 and its paralog Taz increase activity of the destruction complex (See *Chapter 1.8 Liver Tumorigenesis*) (367-369). Specifically, the TEAD binding domain of cytoplasmic YAP1 prevents nuclear translocation and activity of oncogenic β -catenin by binding to its N-terminus domain and keeping β -catenin in the cytoplasm.

Finally, in hepatoblastoma YAP1 withdrawal may modulate β -catenin signaling through upregulation of HNF4 α . In developing and adult liver, YAP1 controls enhancer binding of HNF family members including, HNF4 α (283). Further, in adult HCC, YAP1 inhibition promotes upregulation of HNF4 α (23). Congruently, in my system I observe both increase of HNF4 α expression in YAP1 OFF tumors (*Chapter II*), and increased occupancy at HNF4 α motifs in hbHeps

(*Chapter III*). In the adult liver, HNF4 α and β -Catenin both contend for binding with TCF to promote differential transcriptional programs (292) (See *Chapter 1.7 Liver Differentiation*). I hypothesize that the increase in HNF4 α outcompetes β -catenin for TCF binding, promoting further downregulation of oncogenic β -catenin targets, promoting differentiation. In summary, my findings support the observation that YAP1 ON promotes upregulation of Wnt targets, and conversely that Hippo ON/ YAP1 OFF leads to downregulation of oncogenic Wnt signaling in hepatoblastoma tumors (368) (18, 21, 31).

Wnt Regulation of YAP1 in Liver Cancer

In hepatoblastoma cells *in vitro*, cell survival is synergistically decreased by siRNA knockdown of both β -catenin and YAP1. Further Tao et al. also observes synergistic decrease in mRNA expression for Birc5, Cyr61, Myc and Cyclin D1 with siRNA knockdown of both si β -catenin and siYAP1(31). Finally, Tao et al. also finds that β -catenin knockdown in hepatoblastoma cells decreases YAP1 mRNA (31). Tao et al. suggests that these findings reflect a “cooperative role” for Wnt and Hippo signaling in hepatoblastoma transcription; and, further that β -catenin may regulate YAP1 in this context.

Conversely, I find evidence that YAP1 may regulate β -catenin transcription *in vivo* (see proceeding section). *In vivo* regulation of YAP1 by β -catenin in my

conditional model requires further investigation. Indeed, I have generated an inducible β -catenin for future *in vivo* studies (*data not shown*).

Consistent with Tao et al's observations *in vitro*, β -catenin regulation of YAP1 has also been observed in adult HCC and in colorectal cancer. Specifically, in adult HCC, β -catenin expression upregulates TRIB2 and downregulates the differentiation factor C/EBP α (370). Wang et al. finds that TRIB2 binds β -TrCP and protects YAP1 from being degraded (See *Chapter 1.8 Liver Tumorigenesis, Appendix IV*) (371). Interestingly, using ATAC-seq, in D33 and D64 hbHep cells, I observe increased binding at the C/EBP α motif, despite continual expression of oncogenic β -catenin (*Chapter III, Table 3.3*). In gene expression analyses of hbHeps, I do observe upregulation of TRIB2 relative to WT FAH liver consistent with remaining oncogenic β -catenin expression (*Appendix VI*).

In colorectal cancer, Wnt signaling has also been shown to promote YAP1 expression through β -catenin/TCF4 binding to a YAP1 enhancer (372). Finally, in both CRC cells and in adult liver cancer, YAP1 is necessary for survival downstream of β -catenin (362, 373). The regulation of YAP1 by β -catenin remains to be tested in my *in vivo* model; however, given the cooperative signaling observed *in vitro* in hepatoblastoma cell lines by Tao et al, I hypothesize that β -catenin likely does regulate and indeed augment YAP1 signaling *in vivo*. Generating a conditional model of hepatoblastoma with inducible β -catenin will allow for further exploration of Wnt, Hippo crosstalk.

Chapter 5.5 Cell Fate Switch: Apoptosis or hbHeps?

In the preceding chapters, I have shown that YAP1 withdrawal promotes tumor regression through induction of apoptosis and differentiation. Following YAP1 inhibition, how do tumor cells make the choice between apoptosis and differentiation? In *Chapter 5.5*, I turn to cell fate choices in developing embryonic stem cells for clues. Hepatoblastoma is a stem-like tumor believed to arise from a progenitor liver cell; additionally, its global genome methylation mimics embryonal liver. Indeed, as discussed in *Chapter 1.6 Liver Development*, embryonic tissues and cancers share remarkable parallels in gene expression, and tissue architecture (1, 14, 15, 17, 242-244).

In developing embryonic stem cells, apoptosis and differentiation are temporally coordinated to promote maturation. Therefore, I will examine how following YAP1 withdrawal, apoptosis and differentiation may work in concert in hepatoblastoma to promote tumor regression. Specifically, I review how in embryonic stem cells, p53 and Hippo/YAP1 cooperate to promote differentiation first, followed by selective apoptosis in cells that retain unneeded pluripotency. Reviewed in *Chapter 1.4*, most hepatoblastomas retain normal p53 expression, increasing my interest in the potential role of p53 in cell fate acquisition following YAP1 withdrawal.

Herein, I consider the possibility that in my murine model, differentiation occurs first following YAP1 withdrawal, and is accompanied by regular apoptosis

in a subset of cells, promoting sustained tumor regression and mature hepatocyte gene expression.

Cancer and Development

Following withdrawal of YAP1 overexpression in murine hepatoblastoma tumors, I observe evidence of at least two cell fates promoted by loss of YAP1 alone. Specifically, I observe evidence of apoptosis and differentiation. First introduced in *Chapter 1.6 Liver Development*, hepatoblastoma is theorized to derive from early bipotent liver progenitor cells from embryonic D9-D11(245). Histologically, human and murine hepatoblastoma mimic early liver progenitor, embryonal, and fetal hepatocytes. Further, molecular characterization of aggressive subtypes of hepatoblastoma shows a stem-like signature (*See Chapter 1.4 Molecular Profiling of Hepatoblastoma*) (1, 14, 217). To this point, methylation patterns in hepatoblastoma closely mimic embryonic and fetal patterns (200).

Taken together, these findings highlight the connection between development and tumorigenesis. Indeed, multiple groups have found striking similarities between gene expression in developing organs and tumorigenesis in the corresponding tissues (242-244). As such, I turned to the biology of liver development and embryonic stem cells for clues as to what factors promote apoptosis or differentiation following YAP1 withdrawal in hepatoblastoma.

In embryonic stem (ES) cells, apoptosis and differentiation work in concert to promote normal tissue development. ES cells that fail to exit self-renewal, maintaining unchecked proliferative capacity, are selected to undergo apoptosis, preserving the newly differentiating tissue (454, 455). In the context of developing tissues, apoptosis works to promote and maintain a differentiated state by “culling” rogue pluripotent stem cells. Here I propose that in the stem-like embryonic tumor, hepatoblastoma, apoptosis and differentiation cooperate to maintain tumor regression.

Differentiation or Apoptosis?

In embryonic stem cells, overexpression of YAP1 promotes stemness, expression of pro-survival proteins like BIRC5, and suppression of anti-apoptotic proteins like B-cell Lymphoma 2 (BCL-2), B-cell Lymphoma extra-large (BCL-XL), and MCL Apoptosis Regulator, BCL2 Family Member (MCL-1) (456). Accordingly, a defining feature of YAP1 driven malignancies is frequently the upregulation of antiapoptotic proteins, with simultaneous pro-proliferation signaling (373). Similarly, in my murine model of hepatoblastoma I observe both upregulation of proliferation associated signatures in YAP1 ON tumors, and expression of anti-apoptotic proteins like BIRC5 (**Figure 2.2F**).

In my bulk RNA-sequencing expression analysis of YAP1 OFF D6 regressing tumors compared to YAP1 ON tumors, the top 20 upregulated genes

were associated with differentiation- including the Mup family mature hepatocyte markers, cytochrome p450 enzymes, and metabolism markers (**Figure 3.4A**). Similarly, the top ten upregulated GSEA Hallmark signatures were related to mature hepatocyte gene expression (**Figure 3.4B**). These results suggest that the predominant expression pattern “de-repressed” following YAP1 inhibition, in this model, is differentiation.

However, I do observe evidence of apoptosis in YAP1 withdrawn tumors, and slow tumor regression over time (**Figure 2.4-2.5**). The bulk RNA-seq data in YAP1 OFF D6 tumors, in conjunction with the sparse CC3+ IHC staining, suggest that the population of YAP1 OFF cells immediately undergoing apoptosis is small. As a result, I may not detect the gene signature associated with pre-apoptotic YAP1 OFF cells. Indeed, loss of YAP1 in both tumors and stem cells induces apoptosis (23, 31, 456). Specifically, embryonic stem cell survival just after exiting self-renewal requires YAP1 (456). Consistent with my observations of increased CC3+ staining and downregulation of BIRC5 *in vivo* with YAP1 withdrawal, Tao et al. found that knockdown of YAP1 in hepatoblastoma-like cells *in vitro* induced apoptosis, and decreased cell proliferation (31).

The choice between apoptosis and differentiation may be an early cell decision rapidly following reduction in YAP1 transcription. As discussed in *Chapter 5.1 Murine Models*, my model of hepatoblastoma was generated using the sleeping beauty transposase system. As such, each tumor cell hydrodynamically

transfected likely has varying level of YAP1 oncogene expression. Further, chromosomal integration of the TET-ON system varies cell-cell promoting variable doxycycline responsiveness (See *Chapter 5.1 Inducible Models, Transposase Systems*). Withdrawal of doxycycline may result in variable reductions of YAP1 expression in a time-dependent manner. Indeed, dose dependent cell fate determination has been observed after withdrawal of Ras in multiple tumor types (457-459).

Thus, at YAP1 OFF D6, as evidenced by the IHC (Figure 2.1), some YAP1 expression remains. I hypothesize that residual YAP1 expression may render hepatoblastoma tumor cells apoptosis-deficient through upregulation of anti-apoptotic proteins. Indeed, in embryonic stem cells and liver tumors, YAP1 overexpression represses apoptosis (454).

Cell Fate and p53

Alternatively, cell fate choice may be influenced by temporal activation of p53 in hepatoblastoma cells. Unlike adult liver tumors where loss or mutation of tumor suppressor p53 (TP53) is a common event (>30%), most hepatoblastomas retain WT p53, perhaps accounting for the observed efficacy of chemotherapy compared to adult liver malignancies (**Figure 1.2, Table 1.9**). The role of WT p53 in hepatoblastoma remains under investigated.

Interestingly, in embryonic stem cells (ESCs) p53 activation promotes *first* differentiation, followed by apoptosis in select cells. Lin et al, shows that after activation, p53 binds to the promoter of and suppresses transcription of Homeobox Nanog (Nanog), a known stem gene required for self-renewal. Nanog is frequently transcribed downstream of active Hedgehog signaling. Indeed, hedgehog signaling has also been implicated in hepatoblastoma (See *Chapter 1.4 Molecular Characteristics of Hepatoblastoma*) (195, 196, 206-208, 460). How and if YAP1 and Hedgehog signaling interact to maintain hepatoblastoma stemness requires further investigation; however, ATAC-seq DNA Footprinting of YAP1 ON tumor cells compared to hbHeps does not show increased binding at the primary Hedgehog transcription factor, Glioma-associated oncogene homolog 1 (Gli1) (**Table 3.1, 3.2**).

Nevertheless, p53 promotes differentiation in ESCs. Following loss of stemness, p53 then induces apoptosis in select ESCs (461). In my murine model, perhaps differentiation occurs first as evidenced by the upregulation of differentiation signatures. But, similarly to its role in ESC cells, does activated p53 promote eventual apoptosis in a subset of poorly differentiated hepatoblastoma cells that retain self-renewal capacity leading to the slow regression I observe? (**Figure 2.4**).

Hippo/YAP1 and p53

The relationship between Hippo/YAP1 and p53 as described in the literature is varied and complex. Similar to the interactions between Hippo and Wnt signaling, Hippo and p53 signaling are regulated in a development and tissue-specific manner. Previous reports suggest that de-repression or activation of the Hippo pathway stabilizes and activates p53, by inhibiting the MDM2 proto-oncogene (MDM2). MDM2 is a E3 ubiquitin ligase that targets p53 for degradation (462). Alyon et al. shows that during tissue development and differentiation Hippo kinase LATS1/2 and p53 cooperate to ensure terminal differentiation (462-464). In the adult heart and liver, Hippo and p53 similarly cooperate to maintain differentiation by restricting proliferation and promoting apoptosis to control organ size (19, 369).

The relationship between YAP1 and p53 in hepatoblastoma in adult liver cancer remains poorly characterized. In pancreatic cancers, a role for WT p53 in the suppression of YAP1 was recently described (465). In breast cancer cells, it appears that YAP1 and mutant p53 cooperate to drive G2/M progression (466). Nevertheless, whether WT activated p53 influences tumor cell fate by promoting apoptosis and/or differentiation in YAP1 OFF D6 tumors requires further investigation.

Chapter 5.6 Therapeutic Differentiation of Cancer Cells

YAP1 inhibition promotes long-term survival and stable regression in hepatoblastoma tumors; specifically, I find that YAP1 inhibition terminally rehabilitates a subset of tumor cells into hepatocyte-like cells with mature hepatocyte gene expression. In *Chapter 5.6*, I consider YAP1 as a candidate for differentiation therapy. I first review the principles of differentiation therapy; namely, that successful differentiation therapies simultaneously promote sustained tissue maturation, and halt self-renewal. Here I propose that YAP1 inhibition represents a tractable differentiation therapy because it promotes mature hepatocyte gene expression in YAP1 OFF tumors promoting the formation of hbHeps. Further, YAP1 withdrawal in murine tumors downregulates stem markers suggesting that YAP1 inhibition may be sufficient to block self-renewal of tumor cells.

Differentiation Therapy Primer

Classic anti-cancer therapies are predicated on the idea that all cancer cells must be fully eliminated for clinical benefit. Therapies must either promote cell death, immune clearance, or a combination of both. However, emerging evidence over the last twenty years suggests that tumor cells may be rewired epigenetically or transcriptionally to downregulate oncogenic signaling and reactivate mature differentiated cellular programs. Multiple groups have observed

therapeutic differentiation of tumor cells *in vivo* with removal of oncogenes or with tumor suppressor restoration (23, 233, 393-395, 467-469). Thus, by modulating master oncogenic regulators, researchers may be able to titrate expression profiles for cells to differentiate and participate in normal tissue architecture, without further malignant progression.

Indeed, modulation of the master transcriptional repressor fusion gene, Promyelocytic Leukemia Protein-Retinoic Acid Receptor α (PML-RAR α), with differentiation therapy in acute promyelocytic leukemia (APL) results in a >95% cure rate. Specifically, treating APL patients with retinoic acid (RA) and arsenic works to dissociate the PML-RAR α repressor, allowing for epigenetic and transcriptional rewiring of myeloid cells. Thus, administration of RA and arsenic in APL sustainably upregulates differentiation signaling with therapeutic benefit (470-472). In his opinion on differentiation therapy, de Thé posits that the success of differentiation therapy in APL is due to the ability of RA and arsenic to potentiate terminal differentiation of myeloid cells, and to blunt the self-renewing capacity of a subset of APL CSCs (473).

To date, there are limited approved differentiation therapies for solid tumors with the clinical benefit observed in APL. However, with better understanding of the genetic wiring of tumor cells, and further what factors maintain differentiation and stemness respectively, design and approval of rational successful therapeutic strategies is likely.

Stemness and Differentiation in Hepatoblastoma

In hepatoblastoma, the CSC population responsible for tumor self-renewal remains unknown. Cancer stem cells (CSCs) are theorized to be a small subset of cancer cells within a larger malignancy that possess a unique capacity for proliferation, self-renewal, and plasticity. To that end, CSCs mediate refractory and therapy resistant disease (474). While the stem cell population in hepatoblastoma remains elusive, several groups have carefully documented YAP1's role in promoting a stem signature in ES cells, hepatoblastoma and adult liver (31, 281, 373, 456). In the adult liver YAP1 expression promotes both proliferation and a pluripotent cell lineage; as such, targeting YAP1 in hepatoblastoma may hit both requirements of successful differentiation therapy 1) *promotion of terminal maturation* and 2) *abrogation of stemness*.

In my murine model of hepatoblastoma, I observe evidence of sustained maturation of hepatoblastoma tumor cells with survival of YAP1 withdrawn mice for 230+ days (**Figure 2.6**). Further, in the long-term D120+ hbHep *Fah*^{-/-} mice, I observe evidence of terminally differentiated cells through histology and gene expression analyses (**Figure 4.1-4.4**). Compared to hepatoblastoma tumors that do not express Mup mature hepatocyte protein marker, hbHeps partially restore Mup levels (Figure 3.4, Figure 4.4). Further, I observe congruency between hbHeps and WT mice Zone 3 and Zone 1 *IPA* gene signatures for *PAR/RXR*,

oxidative phosphorylation, cholesterol synthesis, and xenobiotic metabolism (Appendix VI).

Caveats to Differentiation Therapy

Caveats to YAP1 differentiation therapy in both my model of hepatoblastoma, and potentially in treated children include: remaining oncogenic β -catenin expression in residual tumor cells, burden of “rehabilitated cells”, therapeutic toxicities, and treatment resistance (20, 23, 283). In my model and presumably in patients, hepatoblastoma is driven by oncogenic cooperation of both β -catenin and YAP1 (See *Chapter 1.4 Molecular Profiling of Hepatoblastoma, Chapter 1.5 Laboratory Models*). I observe greater than 90% tumor regression driven by apoptosis and differentiation with withdrawal of YAP1 alone. As such, mutant β -catenin remains activated in differentiated hbHeps (**Figure 2.1, Figure 3.2, Figure 4.2-4.3**).

In my *Fah*^{-/-} model, I forced upwards of >70% damaged total liver mass reconstituted by hbHeps. Indeed, I observed body weight maintenance for an average of 38.67 days following NTBC cycling in *Fah*⁺ hbHep mice (**Figure 4.3**) (See *Chapter 4.1 Introduction* for a review of the *Fah* model). While my mice did maintain weight longer than *Fah*^{-/-} mice, I still observe weight fluctuations (**Figure 4.3A**). I hypothesize continued overexpression of β -catenin contributes to incomplete metabolic restoration of hbHeps. To this point, a previous report from

Lemberger et al, describes lethal metabolic dysfunction from constitutive β -catenin overexpression in healthy hepatocytes (325). Specifically, Lemberger et al. found that hepatocytes were deficient in glucose and mitochondrial metabolism, and mice were characterized by hepatomegaly and low body weight (325).

I propose that Lemberger's results and my own observations may be explained, by improper liver zonation due to continued overexpression of β -catenin. Continued overexpression of β -catenin alone drives primarily a pericentral phenotype and promotes loss of crucial metabolic functions performed by perivenous hepatocytes like gluconeogenesis, cholesterol and urea synthesis (325). As discussed in *Chapter 1.7 Liver Differentiation*, maintenance of liver zonation is temporally and spatially controlled by Wnt and Hippo signaling. Thus, modulating Wnt and Hippo signaling can disrupt normal liver zonation with catastrophic metabolic effects (See *Chapter 4.1 Introduction*) (20, 23, 283, 292). Nevertheless, in hbHeps, I observe evidence of both Zone 1 perivenous and Zone 3 pericentral phenotypes, suggesting that YAP1 withdrawal modulates β -catenin's transcriptional output (See *Chapter 5.4 Crosstalk between Wnt and Hippo*).

Thus, a child's tumor burden compared to normal liver may determine the appropriateness of YAP1 differentiation therapy. If there is limited healthy liver tissue, liver function may be compromised if hbHeps are the primary workhorse of the liver. Conversely, if YAP1 differentiation therapy is used adjuvantly to differentiate residual disease, metabolic dysfunction is likely to be mild as normal

hepatocytes will compensate. *Chapter 5.7* further discusses the use of YAP1 targeted therapies.

Challenges to Permanent Therapeutic Differentiation

As alluded to in the prior sub-section, successful YAP1 differentiation therapy may require combination with a secondary agent, i.e. chemotherapeutic, Wnt inhibitor, Hedgehog Inhibitor, Notch Inhibitor (See *Chapter 1.4 Molecular Characterization of Hepatoblastoma*, *Chapter 5.5 Cell Fate Switches*). Similarly, as discussed in the beginning of this section, successful differentiation therapy of the hematologic malignancy APL requires both RA and arsenic for stable disease regression. Identification of the CSC population in hepatoblastoma will better guide the ideal combinatorial strategy. Ideally a secondary agent will support terminal maturation, and augment inhibition of self-renewal if YAP1 inhibition alone proves clinically insufficient.

The permanence of therapeutic differentiation in hepatoblastoma rests on 1) *eradication of self-renewal capacity of tumor cells* 2) *the stability of the differentiated state with YAP1 inhibition*, and 3) *the likelihood of acquiring secondary mutations in hbHeps*. Whether YAP1 inhibition promotes loss of CSCs the self-renewing capacity of hepatoblastoma tumor cells remains to be tested.

Further, my model suggests that long term YAP1 inhibition may be necessary for sustained differentiation (*Chapter II, Chapter III*). As such, similar to

other targeted therapies, resistance is possible. I hypothesize that sustained YAP1 inhibition may lead to classic gatekeeper mutations as seen in other oncogenes (i.e. T709M in EGFR) (475). Besides oncogene reactivation, hepatoblastoma tumor progression may be promoted by upregulation of other oncogenic pathways as observed with KRAS inhibition and YAP1 rescue of tumorigenic potential in lung and pancreatic cancer (342, 451, 476).

Finally, the stability of the differentiated state in my model hinges on the likelihood of hbHeps acquiring secondary activating mutations. While there is evidence in my model that YAP1 withdrawal also dampens oncogenic β -catenin signaling through downregulation of its canonical target genes Myc and Cyclin D1, β -catenin remains overexpressed and may still exert some of its oncogenic effects despite YAP1 withdrawal (**Figure 2.2**). To this point, the two-hit hypothesis suggests that acquisition of additional mutations or epigenetic injury in the presence of oncogenic β -catenin may be sufficient for disease recurrence (See *Chapter 2.1 Introduction*). Thus, determining what environmental and genetic factors promote tumorigenesis in hbHeps requires further investigation.

Chapter 5.7 YAP1 Targeted Therapies for Hepatoblastoma

I have shown that YAP1 inhibition is critical for hepatoblastoma tumor maintenance *in vivo*, suggesting that YAP1 is a therapeutic target in hepatoblastoma. In *Chapter 5.7*, I first briefly outline the state of anti-cancer therapies for hepatoblastoma. Next, I review the current arsenal of YAP1 targeted therapeutics. Finally, I will consider how YAP1 therapies may be applied for therapeutic benefit in hepatoblastoma. Here I propose that, YAP1 therapeutics may prove clinically effective as a presurgical debulking or post-surgical agent. Further, given preliminary evidence in other tumor types that YAP1 confers chemoresistance, I propose that YAP1 inhibition could sensitize children's tumors to chemotherapy.

YAP1 Therapeutics, Primer

The current standard of care for medical management of hepatoblastoma utilizes a mixture of alkylating and DNA-damage agents: cisplatin, doxorubicin, vincristine and 5-fluorouracil (48, 49) (See *Chapter 1.3 Clinical Management of Hepatoblastoma*). Currently, several clinical trials are testing multiple kinase inhibitors targeting tyrosine kinases, and the MAPK pathway for use in hepatoblastoma (See *Chapter 1.3 Clinical Treatment and Prognosis*) (**Table 1.8**).

Historically, kinases were presumed to be the most tractable drug targets (477). Indeed the majority of targeted anti-cancer drugs on the market to date,

inhibit oncogenic kinases including tyrosine kinase inhibitors (TKIs), and MAPK inhibitors (i.e. EGFR-Gefitinib/Erlotinib, BRAF-Vemurafenib, MEK-Trametinib etc.) (475, 478-480). There are currently 35+ FDA approved kinase inhibitors for treatment of various malignancies (481). However, a number of oncogenes driving both tumor initiation and tumor maintenance in many malignancies are not kinases, but are actually transcription factors, most notably MYC and YAP1 (233, 362, 394, 482, 483).

Indeed, YAP1 underlies tumorigenesis of many neoplasms including breast cancer, lung cancer, uveal melanoma, and subtypes of liver cancer (24, 340, 342, 451, 476); however, development of a specific and clinically usable YAP1 targeted small molecule has lagged, in part, due to the difficulty of generating compounds against transcription factors. Targeting of transcription factors requires disrupting either DNA-protein or protein-protein interactions. The difficulty in targeting protein-protein interactions lies in the lack of clear binding pockets, easily found in in most kinases. Protein-protein interactions often have flat surfaces, challenging rational small molecule design (477, 484)

Because YAP1 is a co-transcription factor without a DNA binding domain, YAP1-specific inhibitors would need to target the YAP1-TEAD interaction. Alternatively, a small molecule disrupting TEAD-DNA binding may also have some YAP1 specificity. Indeed, some progress has been made towards development of a YAP1 small molecule; however, to date these compounds lack specificity (358,

359, 485). The next section reviews current strategies to inactivate YAP1 or conversely, derepress Hippo signaling.

YAP1 Small Molecules

The arsenal of YAP1-targeted agents evaluated in cell culture and mouse models includes small molecules, synthetic peptides, antagomirs (antimirs), and nanoparticles containing anti-sense oligonucleotides (ASOs) or small interfering RNAs (siRNAs)

YAP1-TEAD Disruptors

Introduced in the preceding section, most small molecules with specificity for YAP1, target the YAP1-TEAD interaction. A commonly used YAP1 inhibitor *in vitro* and *in vivo*, Verteporfin, was first described by Liu-Chittenden et al. to disrupt YAP1's binding to its co-transcriptional activator, TEAD, thus abrogating YAP1's proliferation program (355)(460, 461). In uveal melanoma cells, Verteporfin was shown to downregulate canonical YAP1 targets CTGF, and CYR61 (486). Calling into question verteporfin's specificity, multiple groups have demonstrated YAP1-independent anti-oncogenic effects of Verteporfin in multiple cancer types, (358, 359).

Monoclonal Antibodies

Other strategies to inhibit YAP1 in sensitive tumor types include regulating YAP1 through upstream signaling nodes, or by downregulating YAP1 target genes. YAP exerts its oncogenic effects through upregulation of pro-proliferation genes such as CTGF and CYR61. In breast cancer and hematologic malignancies, monoclonal antibodies against CTGF and/or CYR61 have shown some efficacy *in vitro* and *in vivo* (485, 487-489). However, these biologics have not been tested in models of liver cancer.

Further, targeting single downstream genes of YAP1 may have limited clinical benefit. YAP1 exerts its oncogenic effect through multiple signaling nodes; thus, inhibition of one protein is unlikely to fully blunt YAP1's oncogenic activity. Accordingly, in my model of murine hepatoblastoma, YAP1 loss has multiple effects including induction of apoptosis, de-repression of differentiation signaling, and reprogramming the chromatin accessibility of tumor-lineage cells (**Figure 2.2, Figure 2.5, Figure 3.9, Figure 4.4**). Thus, given the paucity of evidence for silencing singular downstream YAP1 targets in liver cancer, hepatoblastoma patients will likely experience greater clinical benefit from molecules that disrupt the YAP1-TEAD interaction or directly target YAP1 for degradation.

Therapeutic Peptides

Another recently published strategy for targeting YAP1 utilizes a peptide mimic of Vestigial Like Family Member 4 (VGLL4) (490). VGLL4, like YAP1, also

lacks a DNA binding domain and primarily functions as a transcriptional co-activator. In lung cancer, and multiple gastrointestinal (GI) cancers including gastric cancer, pancreatic cancer, colorectal and HCC, VGLL4 functions as a tumor suppressor, antagonizing YAP1 activity (490-493). Jiao et al, shows that a peptide mimicking VGLL4 binds TEAD, outcompeting YAP1 for its preferred oncogenic transcriptional co-activator and silencing downstream transcription in gastric cancer (490).

Therapeutic peptides are small chains of 50 or fewer amino acids designed to bind to a protein of interest. Therapeutic peptides can either promote or inhibit target activity (494). As reviewed by Marqus et al., peptides have a number of inherent benefits, the most important being the low toxicity and high target specificity. However, delivery of peptides for treatment of malignancies is challenging due to the low oral bioavailability and rapid clearance. Further, the hydrophobic structure of peptides makes delivery through the cellular membrane challenging(494). Nevertheless, investigating the role of VGLL4 in hepatoblastoma may provide an additional avenue to disrupt YAP1 signaling in children's tumors.

Small RNAs

Below I cover the use of RNA therapeutics including antagomirs (anti-mirs), antisense oligonucleotides (ASOs) and small interfering RNAs (siRNAs) for therapeutic targeting of YAP1 in hepatoblastoma. Hippo signaling acts to

sequester YAP1 in the cytoplasm, targeting YAP1 for degradation (See *Appendix IV*). Thus, re-activating or conversely “de-repressing” the Hippo pathway may present another strategy to modulate YAP1 activity for therapeutic benefit in hepatoblastoma. microRNAs (miRNAs) are small RNAs that modulate gene expression post-transcriptionally (See *Chapter 1.4 MicroRNA Regulation*). In other tissue contexts, two miRNAs have been described to repress Hippo signaling, mir302 and mir135b (495, 496). Specifically, Lin et al, found that using both a microRNA sponge and an antimir against mir-135b in lung cancer slows tumor progression, in part by relieving suppression of Hippo kinase LATS2 (See *Appendix IV*) (496).

As suggested by the name, antagomirs are small RNAs designed complementary to a desired miRNA. Consequently, antagomirs silence the miRNAs effects. Similarly, miRNA sponges sequester miRNAs; however, miRNA sponges tend to be less specific than antimirs. Antimirs as anti-cancer agents have several challenges for liver cancer including delivery, and target identification.

In hepatoblastoma specifically, the regulation of Hippo/YAP1 by miRNAs is poorly understood, with few reports investigating miRNAs in hepatoblastoma (See *Chapter 1.4 microRNA Regulation*). Thus, target identification precludes antagomir therapy in hepatoblastoma. Additionally, YAP1’s global downregulation of miRNAs in malignancies could further complicate antagomir therapy. Mori et al, shows that in YAP1 liver tumors, YAP1 complexes with p72 to drive upregulation of MYC

target transcription, and downregulation of *all miRNAs* by repressing transcription of miRNA machinery (497). Thus, target abundance may also present a challenge in antagomir therapy for hepatoblastoma, and other YAP1-driven neoplasms.

The RNA therapeutic class also includes siRNAs and ASOs in the toolkit to silence gene expression. ASOs refer to RNA therapeutics delivered as single strands; thus, ASO's do not require processing by the cell's miRNA machinery to bind to and modulate their target sequence. Unlike ASOs, siRNAs are delivered as dsRNAs, and need RISC complex processing for the guide strand to reach the target sequence and suppress gene expression (498). I am not going to belabor the differences between ASOs and siRNAs, but currently the choice of ASO or siRNA for therapeutic development remains debated. Nevertheless, delivery of both ASOs and siRNAs to liver tumors remains challenging.

The addition of a N-acetylgalactosamine (GalNAc) chemical modification to an ASO or siRNA facilitates high efficiency RNA therapeutic delivery to normal hepatocytes. GalNAc is a ligand for the Asialoglycoprotein receptor (ASGR) protein. Normal hepatocytes selectively express high levels of ASGR (499-501). However, in adult HCC liver tumors ASGR expression is minimal, limiting the efficacy of GalNAc-conjugate RNA therapeutics. Expression of ASGR in human hepatoblastoma tumors has not been systemically evaluated; however, preliminary evidence from my RNA-sequencing analysis of YAP1 ON mouse tumors suggests that hepatoblastoma tumors do retain ASGR expression. It is

unknown if ASGR expression in tumors is sufficient for therapeutic uptake (*Appendix IV*).

Alternatively, siRNAs/ASOs can be delivered using lipid nanoparticles as shown by Fitamant et al (23). Fitamant et al, delivered siYAP by lipid nanoparticle (LNP) *in vivo* and showed therapeutic benefit in an aggressive subset of HCC. Packaging RNA therapeutics as lipid nanoparticles does have some disadvantages including expense, and limited tissue accumulation. Despite these challenges, delivery of RNA therapeutics by LNP may be a viable strategy for hepatoblastoma.

Clinical Applications

YAP1 targeted therapies may provide clinical benefit in children with hepatoblastoma as both neoadjuvant and adjuvant therapies. For example, children with unifocal surgically resectable Class 2 tumors may benefit from YAP1 targeted therapy following surgical resection in conjunction with chemotherapy or alone (See *Chapter 1.3 Clinical Management, Chapter 1.4 Molecular Profiling*). I hypothesize that YAP1 inhibition in residual tumor cells following resection will promote a mixture of apoptosis and differentiation, preventing tumor recurrence and progression.

Alternatively, in the 50-70% of children with tumors that are not surgically resectable at time of diagnosis, a YAP1 targeted therapy could be employed to

promote tumor regression in conjunction with or independently of chemotherapy. With both adjuvant and neoadjuvant YAP1 therapeutic strategies, continued treatment to maintain terminal differentiation of residual tumor cells may be necessary. Long-term effects of systemic YAP1 inhibition are unknown; however, liver-specific targeted therapy may reduce some toxicity.

Chemotherapy serves as standard medical management for hepatoblastoma (see *Chapter 1.3 Clinical Management of Hepatoblastoma*); however, children with aggressive subtypes of hepatoblastoma, *Cairo Class II*, *Hooks C2A* etc., are frequently insensitive to alkylating and DNA-damaging chemotherapeutics (1, 14, 15, 180). Hooks et al. found that aggressive C2 tumors characterized by increased expression of MYC, YAP1 targets, and stem-related genes, also upregulate family members of the FANCD2/BRACA pathway (**Figure 1.10, Figure 2.2, Appendix V**) (180). Hooks et al. proposes that upregulation of DNA damage repair enzymes may be responsible for the limited efficacy of DNA damaging chemotherapeutics (i.e doxorubicin) in children with C2 tumors. Interestingly, in my RNA-sequencing analysis of YAP1 OFF D6 tumors, I observe downregulation of FANCD2, FANCI, and Top2A with YAP1 withdrawal (**Figure 2.2, Appendix IV**). These findings suggest that YAP1 inhibition may sensitize children's tumors to chemotherapy. Future work will determine how and if YAP1 modulates chemoresistance in hepatoblastoma tumors.

CONCLUDING REMARKS AND FUTURE DIRECTIONS

Summary of Findings and Model

Pediatric hepatoblastoma is the predominant pediatric liver cancer; however, the relative rarity of hepatoblastoma has severely limited the availability of technical resources to explore therapeutic options. As such, despite rapid improvements in chemotherapeutic and surgical resection strategies, the five year survival rate for Stage IV hepatoblastomas remains poor, >27%. To date, there are no approved targeted therapies for hepatoblastoma.

Hepatoblastoma tumor initiation *in vivo* requires co-expression of β -catenin and YAP1. Indeed, upwards of 80% of children with hepatoblastoma were found to have nuclear co-localization of both β -catenin and YAP1. The cooperation of Wnt and Hippo/YAP1 signaling for tumorigenesis appears to be specific to hepatoblastoma, and is not commonly found in other liver tumors.

While YAP1 and β -catenin are necessary for tumor initiation *in vivo*, hepatoblastoma tumor maintenance *in vivo* remains under investigated. In colorectal cancer, YAP1 has been demonstrated to be critical for β -catenin mutant tumor survival. As such, I hypothesized that YAP1 primarily maintains hepatoblastoma tumorigenesis, and is critical for tumor survival and proliferation.

To address the requirement of YAP1 for hepatoblastoma tumorigenesis, I generated the first conditional model of pediatric hepatoblastoma. Doxycycline inducible YAP1 and constitute β -catenin drive hydrodynamic conditional model

promoting development of hepatoblastoma tumors that resemble the poor prognosis subtype of hepatoblastoma. Further, my conditional model recapitulates the genetic simplicity of pediatric cancers, like hepatoblastoma. Finally, it offers many technical advantages including timeliness, reproducible histology that mirrors human disease, and conditional gene expression for dissection of tumorigenesis with and without YAP1.

Herein, I find that YAP1 is necessary for hepatoblastoma tumor maintenance. Loss of YAP1 halts proliferation, leads to a loss of stemness markers, promotes an increase in apoptosis, downregulates canonical β -catenin target genes like Myc and Cyclin D1, and promotes upregulation of differentiation signaling (**Figure 5.1**). Further, YAP1 loss alone without withdrawing oncogenic β -catenin converts the gene expression of murine hepatoblastoma from a poor prognosis C2 group, to a favorable C1 group.

YAP1 loss activates a cell fate switch promoting both apoptosis and differentiation of tumor cells into functional hepatocyte-like cells. I propose that in hepatoblastoma tumors, similar to embryonic stem cells, apoptosis and differentiation are coordinated to promote sustained tumor regression (**Figure 5.1**). I hypothesize that YAP1 withdrawal mediates long-term therapeutic regression through downregulation of stemness and proliferation markers, and promotion of functional differentiation in tumor cells. Thus, in children with hepatoblastoma YAP1 inhibition presents a tractable differentiation therapy because it both

reprograms transcription promoting hepatocyte maturation and downregulates markers of stemness.

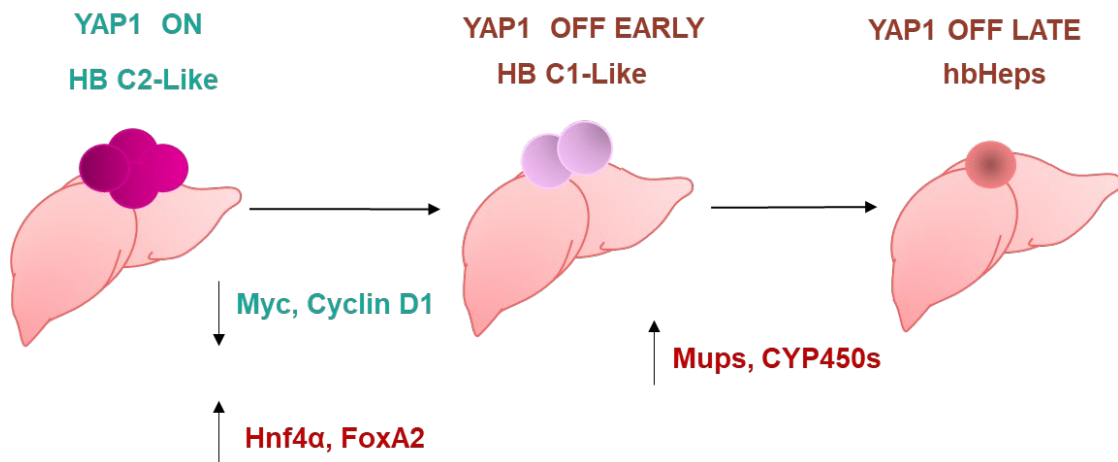


Figure 5.1 Experimental Model. Loss of YAP1 overexpression alone in murine hepatoblastoma downregulates pro-proliferative and survival signaling promoting long-term survival in mice. Six days of YAP1 withdrawal alters the gene expression of hepatoblastoma from poor prognosis Cairo C2 subtype to a favorable prognosis C1 subtype. Specifically, YAP1 withdrawal activates a cell fate switch promoting apoptosis and terminal differentiation in a subset of tumor lineage cells, hbHeps. hbHep cells regain normal hepatocyte histology and partial gene expression. YAP1 withdrawal promotes generation of hbHeps through modification of differentiation transcription factor (TF) occupancy.

Future Directions

Future directions for inquiry include first investigation of β -catenin in tumor maintenance, and its regulation of YAP1 *in vivo*. In hepatoblastoma, does β -catenin bind YAP1 enhancers *in vivo*, augmenting YAP1 expression? Further, is loss of both β -catenin and YAP1 synergistic in hepatoblastoma tumors; or, is YAP1 the primary oncogenic factor necessary for hepatoblastoma maintenance? Herein, I show long-term survival and stable regression with loss of YAP1 alone suggesting

that YAP1 inhibition alone is sufficient. Nevertheless, *in vivo* exploration is needed to investigate β -catenin's regulation of YAP1 and its role in hepatoblastoma tumor maintenance.

Recurrence of disease is frequently associated with residual cancer stem cells that maintain the ability to proliferate and evade chemotherapeutics. The cancer stem cell population in hepatoblastoma also remains unknown. What markers identify the cancer stem cell population in hepatoblastoma, and is YAP1 critical for maintenance of this population? In line with this, does YAP1 loss directly eradicate the self-renewal capacity of hepatoblastoma tumor cells?

To this point, YAP1 expression has been historically associated with chemoresistance in adult tumors. Cancer stem cells often confer chemoresistance; indeed, in my model I see that YAP1 inhibition downregulates genes previously associated with chemoresistance in hepatoblastoma tumors. Loss of stemness markers with YAP1 withdrawal supports a role for YAP1 in cancer stem cell maintenance in hepatoblastoma; however, further investigation is needed to understand if and how YAP1 makes hepatoblastoma tumors more susceptible to chemotherapeutics, and further if the increased sensitivity is due to ablation of a cancer stem cell population.

Finally, what factors mediate cell fate choice between apoptosis and differentiation downstream of YAP1 loss? Given the predominance of WT p53 in hepatoblastoma tumors and the observed role of p53 in embryonic stem cells for

titrating apoptosis and differentiation, does p53 modulate cell fate choice in hepatoblastoma?

Looking forward, successful treatment of hepatoblastoma and other rare cancers will require continued curation of technical resources including generation of *in vitro* patient cell lines, and mouse models that faithfully recapitulate human disease. Engineering conditional genetic models provides the critical opportunity to investigate gene regulation *in vivo*, and to interrogate tumor biology within the whole organism. In this dissertation, I have generated a new conditional model to better understand hepatoblastoma tumorigenesis with the goal of therapeutic development. Finally, I have demonstrated that YAP1 therapies may represent a new strategy for the treatment of childhood liver cancer.

APPENDIX I CRISPR-CAS9 INDUCES EXON SKIPPING

This work was published in *Genome Biology*, and is reproduced with permission from *Springer Nature*, through the Creative Commons license (502). Components of the main text and main figures are reproduced here *Appendix I*. The entire manuscript, and supplemental material are accessible at [Genome Biology](#). This work was completed in conjunction with former Xue lab postdoctoral fellow, Dr. Haiwei Mou. Dr. Mou and I are co-first authors on this publication. Additional assistance was provided by co-authors: Lingtao Peng, Hao Yin, Jill Moore, Xiao-Ou Zhang, Chun-Qing Song, Ankur Sheel, Qiongqiong Wu, Deniz M. Ozata, Yingxiang Li, Daniel G. Anderson, Charles P. Emerson, Erik J. Sontheimer, Melissa J. Moore, and Zhiping Weng. The work was performed in the lab of Dr. Wen Xue.

Introduction

CRISPR/Cas9 genome editing has transformed the study of gene function in many organisms (503-507). Guide RNAs direct the Cas9 nuclease to create double-strand DNA breaks at complementary target sites in the genome. Repair of these double-strand DNA breaks by non-homologous end-joining (NHEJ) often introduces small insertions or deletions (indels) that shift the open reading frame, thereby inactivating the target gene. CRISPR therefore provides a simple way to generate loss-of-function (LOF) mutations in virtually any gene in the mammalian

genome (503). Nonetheless CRISPR can also induce off-target editing at genomic positions that imperfectly match the sgRNA sequence, which calls for the implementation of strategies to reduce off-target effects (508, 509). Besides off-target editing, it remains unknown whether CRISPR-mediated editing has unintended consequence at the post-transcriptional level of the target gene.

We have previously used *in vivo* delivery of CRISPR to inactivate tumor suppressor genes in mice (510-512). We also showed that CRISPR can edit oncogenes or disease genes through homolog-directed-repair (406, 408, 510). Here we show that CRISPR-mediated editing of mammalian exons can induce exon skipping. Exon skipping can result from alternative splicing or from genomic deletions that remove exons. Moreover, exon skipping can produce mRNAs with intact reading frames that encode functional proteins.

Methods

CRISPR vectors

sgRNAs (Additional file 1: Table S1) were cloned into the lentiV2 (Addgene 52961) or pX330 (Addgene 42230) vectors using standard protocols (513).

Cell culture and infection

Cell culture conditions were as described (514). 293fs cells were used to package lentiviruses encoding individual sgRNA and Cas9. KP cells or C2C12 cells were

infected with lentiV2 lentiviruses and selected with puromycin. For Fig. 3a, cells were transduced with sgCtnnb1.2 cloned into lentiGuide-Puro vector (Addgene 52963). lenti Cas9-Blast (Addgene 52962), dCas9-BFP (Addgene 46910), or dCas9-KRAB-BFP (Addgene 46911). Cells were selected with puromycin, blasticidin, or FACS sorted for BFP.

Isolation of single-cell clones

KP or NIH-3T3 cells transduced with lentiviruses Cas9 and sgRNAs targeting *Kras*, *Ctnnb1*, or *p65*, and were selected with puromycin for 4 days. For each transduction, 500 puromycin-resistant cells were seeded into a 100-mm dish and cultured until cell colonies were observed under microscope. Individual colonies were transferred to 12-well plates—one colony per well—and grown to confluence. Genomic DNA and total RNA was isolated, and PCR or RT-PCR was used to identify clones with indels, deletions, or insertions and exon skipping. Genomic PCR products were cloned into a TOPO vector to sequence alleles with indels or deletions.

CRISPR-induced insertion/deletion detection

Genomic DNA from cells was harvested by quick extraction buffer (Epibio), sgRNA target sites were amplified by PCR, and the products were sequenced on an Illumina NextSeq 500 (514). We mapped the reads to the reference sequence

using BWA (version 0.7.5) and SAMtools (version 0.1.19). VarScan2 (version 2.3) was used to identify insertions and deletions with the 'pileup2indel' mode and parameters '--min-var-freq', '--min-avg-qual', and '--p-value'

RNA-sequencing and bioinformatics analysis

RNA-seq libraries were generated using Illumina TruSeq kit, as described (451). Paired-end 75-nt sequencing was performed using NextSeq. Reads were trimmed and primer sequences were removed using Trimmomatic (v 0.30). Reads were aligned to the mm10 genome using STAR (version 2.3.0e) with default parameters, and uniquely mapping reads were selected. Redundant read pairs were removed using Samtools (version 0.0.19). For each gene annotated in GENCODE M7, the number of reads per gene was calculated using HTSeq. Percent exon 2 inclusion (Percentage Splicing Index, PSI or Ψ) for *Kras* was calculated as: (exon 1-2 + exon 2-3)/(exon 1-2 + exon 2-3 + exon 1-3). For global alternative splicing analysis, alternatively spliced exons were called using MISO 0.5.3 with default settings (515) and filtered with stringent cutoffs ($\Delta\Psi \geq 0.2$, total reads ≥ 10 , and Bayes factor ≥ 10).

Western blot analysis

Protein lysates from cultured cells were prepared in RIPA buffer with proteinase and phosphatase inhibitors. Proteins were separated on 4-12% NuPage Bis-Tris

gels (Life Technologies, NP0321), transferred to nitrocellulose membrane, and probed with 1:1,000 anti- β -Catenin antibody (BD 610154) or 1:5,000 anti-Actin antibody (CST 8457).

RT-PCR and TOPO cloning

RNA was purified using RNeasy Mini Kit (Qiagen). First strand cDNA was synthesized using Superscript (ABI), and target sequences were amplified using LA-Taq (Clontech) or Herculase II (Agilent). Primers were listed in Additional file 1: Table S2. Gel bands were quantified using the ImageQuant TL software. Exon skipping products were gel purified, re-amplified using the same PCR protocol to increase yield, and cloned into a TOPO vector. TOPO clones were submitted to Genewiz for sequencing. Representative results from two lentiviral infections are shown.

Availability of Data and Materials

Deep sequencing data are available under BioProject ID: PRJNA375870.

Significant Results and Discussion

Results

We recently used CRISPR to disrupt the *Kras* oncogene in two independent lung adenocarcinoma cell lines (516), which were derived from *Kras*^{G12D}; *p53*^{fl/fl}

(KP) mice (517, 518). We isolated two single-cell clones each carrying frameshifting deletions in exon 2 (**Figure A1.1 A**): KP1 carries a 2-nt “-CG” deletion in the G12D allele and a 1-nt “-C” deletion in the otherwise wild-type *Kras* allele;

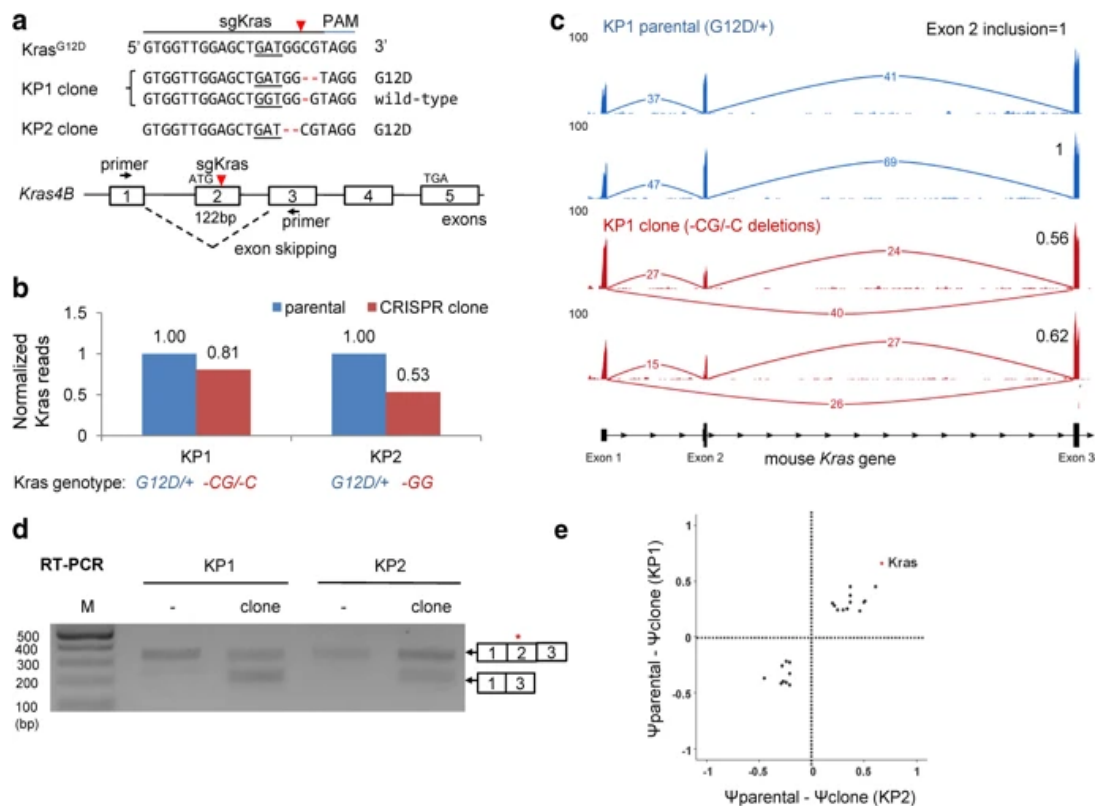


Figure A1.1 sgRNA targeting *Kras* induces exon skipping in single cell clones.

(a) Schematic of an sgRNA targeting exon 2 of the mouse *Kras* gene (sgKras). The red arrowhead denotes the Cas9 cleavage site. KP1 and KP2 cell lines were transduced with lentivirus that encodes Cas9 and sgKras. Two single-cell clones (KP1 clone and KP2 clone) harbor frameshift deletions. Black arrows indicate the positions of RT-PCR primers. The G12D codon is underlined. (b) Normalized *Kras* read counts from RNA-Seq analysis of KP parental cells (blue) and KP clones (red). RNA-Seq was done twice for KP2 clone and three times for the other groups. “+” denotes wild-type allele. (c) RNA-Seq showing partial exon 2 skipping in KP1 clones. RNA-Seq numbers indicate reads spanning the indicated exon junctions. Two representative biological replicates are shown. (d) RT-PCR analysis of *Kras* mRNA detects an exon 2 skipped band. The expected band sizes are 331 bp and 209 bp. M, molecular marker. “*” denotes indels in PCR products from clones. (e) Scatter plot showing 22 exon events that change in both KP1 and KP2 clones. Exclusion of *Kras* exon 2 is the most frequent event. Ψ , Percentage Splicing Index.

and KP2 carries a 2-nt “-GG” deletion. Neither clone produces full length *Kras* protein (516), indicating that all three deletions disrupt the *Kras* reading frame.

Frameshift mutations in early exons are known to trigger nonsense-mediated decay (NMD) (519), which eliminates mRNAs with premature termination codons. When we analyzed mRNA sequencing (RNA-Seq) data, however, we found that apparent *Kras* mRNA levels (i.e., total normalized mRNA reads) were only reduced by 19% in KP1 cells and 47% in KP2 cells, compared to parental KP cells (**Figure A1.1B**). Both clones produced fewer exon 2 reads, but normal levels of exon 1 and 3 reads (**Figure A1.1C**), suggesting that exon 2 might be skipped in the KP1 and KP2 clones. Indeed, we detected exon 1-3 junction reads, indicating that exon 2 was skipped (**Figure A1.1C**, *supplemental data not shown*). Calculating the ratio between exon 2 reads and total reads, we found that exon 2 is included in only 64.0 ± 9.1 % of *Kras* reads from KP1-clone (**Figure A1.1C**, *supplemental data not shown*). Similar exon 2 skipping was observed in KP2-clones (*data not shown*). Concordantly, reverse transcription of *Kras* mRNA followed by PCR (RT-PCR) yielded two products: one corresponded to intact *Kras* cDNA, and the other corresponded to the exon 1-3 isoform (**Figure A1.1D**). The exon 1-3 isoform retains a partial *Kras* open reading frame that could initiate translation from an ATG codon in exon 3 (*data not shown*) and produce a severely truncated *Kras* protein.

Editing of *Kras* did not induce alternative splicing genome-wide. We identified 97 alternatively spliced exons in KP1 cells, and 177 events in KP2 cells. KP1 and

KP2 clones shared 22 cassette inclusion or exclusion events, with the exclusion of *Kras* exon 2 being the greatest change in both clones (**Figure A1.1E**,

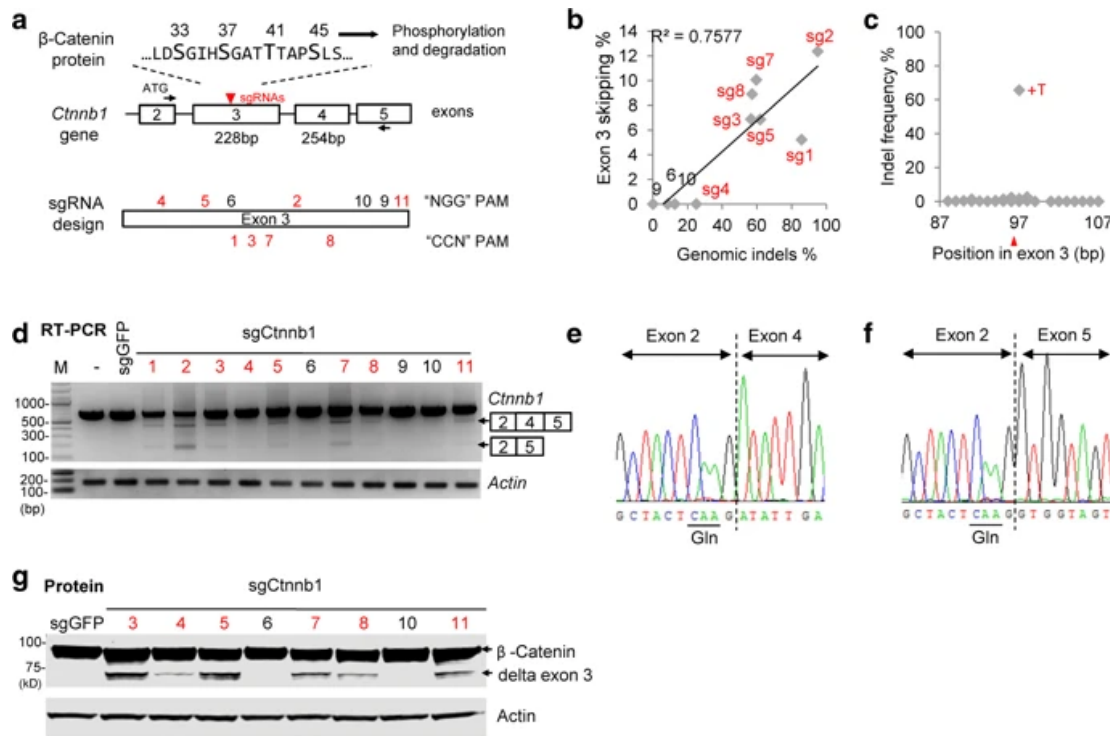


Figure A1.2 *Ctnnb1* sgRNAs targeting exon 3 induces exon skipping. (a) Schematic of the *Ctnnb1* gene. The in-frame exon 3 encodes an inhibitory domain: phosphorylation amino acids 33, 37, 41, and 45 promotes degradation of the β -Catenin protein. Loss of exon 3 stabilizes β -Catenin. Eleven sgRNAs were designed to target exon 3: strong sgRNAs in red, and weak sgRNAs in black, respectively. sgRNAs that use "NGG" PAM are shown above exon 3, and those that use "CCN" PAM are shown below exon 3. (b) Correlation between exon 3 skipping and sgRNA efficiency. Genomic indels were measured by deep sequencing. KP cells were infected with lentivirus. Exon 3 skipping efficiencies are from (d). Indels of sg11 were not determined. sgRNAs that induce >20% indels are marked in red. (c) Distribution of sg1 indels shows that a T insertion (+T) at the Cas9 cleavage site nucleotide 97 of exon 3 (red arrowhead) was the most frequent. PAM sequence is in blue. (d) RT-PCR using primers spanning exons 2 and 5 shows partial exon skipping. M, molecular marker. sgGFP is a control sgRNA. Exon 3 skipping bands were quantified using ImageQuant TL software and normalized to full length cDNA bands. sg4 showed visible weak bands that could not be quantified. (e-f) TOPO cloning and Sanger sequencing confirmed that the two major lower RT-PCR bands in (c) are alternative splicing of exon 2-4 and exon 2-5, respectively. (g) Western blot analysis of β -Catenin. Full length β -Catenin is ~86 kD. β -Catenin without exon 3 (delta exon 3) is ~77 kDa. Actin served as a loading control.

supplemental data not shown).

Thus, editing of *Kras* exon 2 specifically induced skipping of *Kras* exon 2. Notably, whereas mouse *Kras*^{G12D} (GGU to GAU) transcripts do not skip exon 2 in parental KP cells, we found that ~15% of human *KRAS*^{G12S} (codon 12 GGU to AGU) transcripts skip exon 2 in the A549 human lung cancer cell line (*data not shown*). We were unable to predict the gain or loss of exon splice enhancers or silencers (520), but our data suggest that sequences near *Kras* codon 12 promote exon 2 inclusion in mouse and human *Kras*. Exon skipping induced by CRISPR editing was not limited to *Kras* or to mouse KP cells. A recent study showed that CRISPR editing of *FLOT1* exon 3 in HeLa cells can cause skipping of exon 3, exon 4, or exons 3, 4, and 5 (521). We also detected infrequent exon skipping when we targeted exon 11 of *LMNA* in human HCT116 cells (*data not shown*). Skipping *LMNA* exon 11 produces an in-frame transcript that could be translated into a neomorphic protein.

To further explore the idea that exon skipping could produce a functional in-frame transcript, we asked whether CRISPR-mediated editing of *Ctnnb1* exon 3 might induce exon skipping and cause a gain-of-function phenotype. Exon 3 of *Ctnnb1* encodes phosphoacceptor residues that promote degradation of the β -Catenin transcription factor (522); genetic excision of *Ctnnb1* exon 3—which is in frame with exon 4—stabilizes a constitutively active β -Catenin that accumulates in the nucleus (523, 524).

We designed 11 sgRNAs that target regions along *Ctnnb1* exon 3 (*Ctnnb1*-sg1 to -sg11), transduced individual sgRNAs into KP cells, and used high-throughput sequencing to analyze the extent of editing at the sgRNA target site in each line (**Figure A1.2B**, *supplemental data not shown*). Three sgRNAs (sg6, sg9, and sg10) inefficiently targeted *Ctnnb1*. Eight of the *Ctnnb1* sgRNAs (sg1 to sg5, sg7, sg8, and sg11), however, induced indels at their target sites with frequencies that exceeded 20%. For example, *Ctnnb1*-sg1 generated +T insertions in about 65% of reads (**Figure A1.2C**). In each population targeted by a strong *Ctnnb1* sgRNA, we detected three RT-PCR products that span exons 2 to 5 (**Figure A1.2D**). The major product corresponds to the normally spliced transcript that includes exon 3. The other two products correspond to alternatively spliced transcripts: one that skips exon 3 (i.e., exon 2-4 splicing, **Figure A1.2E**) and one that skips both exons 3 and 4 (i.e., exon 2-5 splicing, **Figure A1.2F**). *Ctnnb1* sgRNAs targeting either DNA strand induced exon skipping, and Cas9 nuclease activity was essential for exon skipping (**Figure A1.3A**).

Western blot analysis revealed that cell populations transduced with the strong sgRNAs produce a smaller ~74kD β -Catenin protein that corresponds in size to that expected from the exon 2-4 splice product (**Figure A1.2G**). The full length β -Catenin protein was not significantly depleted 4 days after transduction.

To test whether the alternative splicing is dependent on the continuous expression of Cas9 or sgRNA in the lentiviral vectors, we co-transfected Cas9 and

Ctnnb1-sg1 or a non-targeting sgRNA control. Seven days after transfection, when transfected Cas9 and guide RNAs should be depleted, we examined β -Catenin localization by immunofluorescence. In mouse fibroblast cells transfected with a non-targeting control sgRNA, β -Catenin localized to cell junctions (*data not shown*).

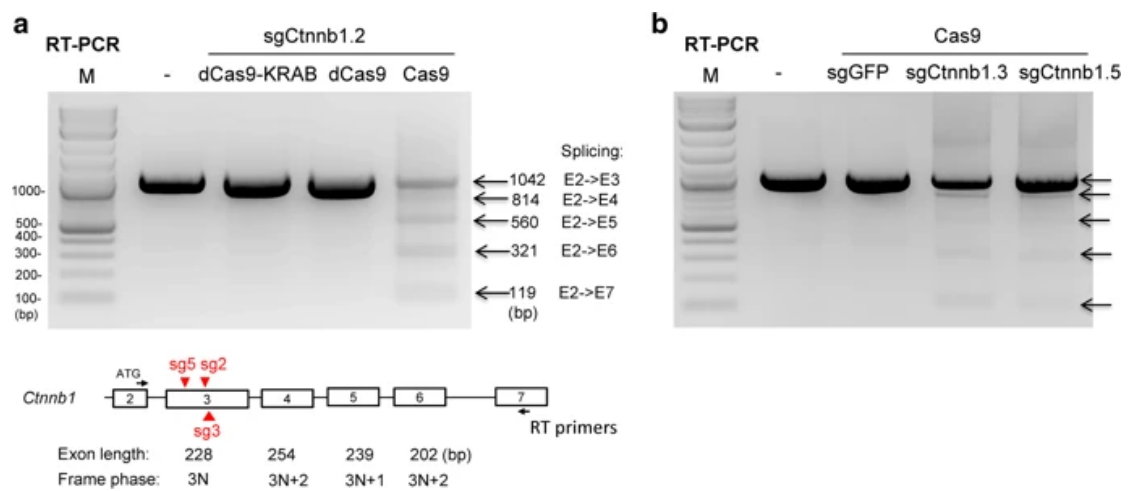


Figure A1.3 Cas9 nuclease activity required for skipping of one or more exons.

(a) RT-PCR analysis of *Ctnnb1* mRNA in KP cells transduced with lentiviruses that encode sgCtnnb1.2 and nuclease-defective Cas9 (dCas9), dCas9-KRAB fusion, or wild-type Cas9. RT-PCR was performed using primers in exons 2 and 7 on transduced KP cell populations after puromycin selection and FACS sorting. The exon length and reading frame phase are shown. Only the exon 2-4 splice product retains an in-frame β -Catenin coding sequence. (b) RT-PCR analysis of *Ctnnb1* mRNA in KP cells transduced with lentiviruses that encode Cas9 and sgGFP, sg3, or sg5. “–”, untreated.

By contrast, in many cells transfected with *Ctnnb1*-sg1, we detected β -Catenin in the nucleus (*data not shown*). These results suggest that continuous editing is not required for exon skipping and that exon 3 skipping induced by CRISPR-mediated editing of *Ctnnb1* exon 3 produces a gain-of-function β -Catenin isoform.

We further analyzed transcripts spanning exons 2 to 7 in cell populations treated with *Ctnnb1*-sg2, -sg3, and -sg5. In addition to the full-length isoform, we detected four transcripts with exon 2 apparently spliced to each downstream exon (i.e., exon 2-4, exon 2-5, exon 2-6, and exon 2-7; **Figure A1.3A-B**). We don't understand the mechanism of this apparently promiscuous exon skipping induced by *Ctnnb1* exon 3 editing, nor have we been able to correlate promiscuous exon skipping with specific target sites or indel mutations in exon 3. Nevertheless, we isolated a *Ctnnb1*-sg3 edited clone that suggests a potential mechanism (*data not shown*). This biallelic clone contains a 3-bp in-frame deletion on one allele and a large 832-bp deletion on the other; the 832-bp deletion fuses the 5' end of intron 2 to the 3' end of exon 4 (*data not shown*). We detected two transcripts in these cells: the properly spliced transcript that includes the 3-bp deletion, and a transcript that includes intron 2 fused to exon 4 (*data not shown*). These results suggest that apparent exon skipping detected in populations of edited cells could reflect genome rearrangements that remove exons.

Two experiments support the idea that a single sgRNA can induce large genomic deletions that remove exons. For example, we isolated 15 clones from mouse 3T3 cells transiently transfected with Cas9 and *Ctnnb1*-sg1, and found that 4 clones (i.e., clones 4, 5, 13, and 15) showed apparent exon skipping by RT-PCR. Genomic PCR revealed genome rearrangements in three of these clones: large deletions (>500 bp) and smaller deletions (~100 bp) in clones 4 and 15, and large

insertions in clones 13 and 15 (*data not shown*). Moreover, after targeting exon 6 of *p65/RelA*, we isolated a biallelic *p65* clone (#15): one allele harbors a 1-nt “+A” insertion, and the other harbors a 2,268-bp deletion that removes exons 5, 6, and 7 (*data not shown*). In *p65* clone #15, we detected the fully spliced transcript and an exon 4-8 splice product (*data not shown*). Both alleles encode frameshifted transcripts, and both *p65* transcripts are present at lower levels than wild type (*data not shown*). We also isolated an edited *p65* clone (#31) homozygous for the same

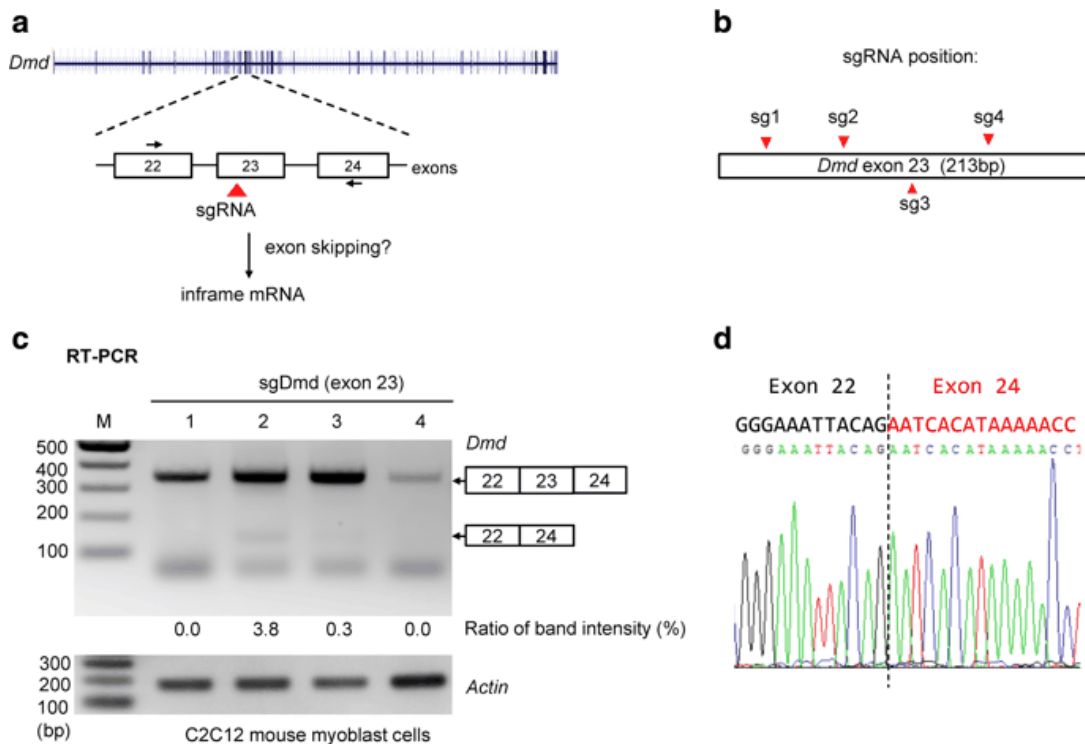


Figure A1.4 An sgRNA targeting exon 23 of *Dmd* can partially restore in-frame dystrophin mRNA. (a) Schematic of sgRNA targeting and skipping of mouse *Dmd* exon 23, and location of primers for RT-PCR analysis. Skipping of exon 23 will generate in-frame mRNA. (b) sgRNA target sites in *Dmd* exon 23. (c) RT-PCR analysis of C2C12 mouse myoblast cells transduced with lentiviruses that encode Cas9 and sgDmd1, 2, 3, or 4. The expected band sizes are 353 bp and 140 bp. M, molecular marker. (d) Sequence analysis of the 140-bp cDNA band from sgDmd2-treated cells confirmed splicing of exon 22 to exon 24.

+A insertion as in clone #15, but clone #31 does not produce alternatively spliced transcripts. Thus, the exon 4-8 spliced transcript in clone #15 results from the deletion of exons 5, 6, and 7. These large exon deletion events were unexpected and would be missed using typical PCR-based screening assays.

The ability to cause a gain-of-function activity by inducing exon skipping or exon excision suggested that CRISPR-mediated editing using a single sgRNA might be a useful way to partially rescue function to a disease gene that requires low-level rescue. CRISPR-mediated homologous DNA repair has been used to correct premature stop codon mutations in the *Dmd* gene in a mouse model of DMD (525), and several groups have used CRISPR to delete *Dmd* exons and partially restore *Dmd* expression (526-529). We designed four sgRNA/Cas9 lentiviruses that target different sites in exon 23 of the *Dmd* gene (**Figure A1.4A-B**), and transduced mouse C2C12 myoblasts, a cell line widely used as a model for Duchenne muscular dystrophy (DMD) (530). In C2C12 cells transduced with *Dmd* sgRNAs, we detected an RT-PCR product that corresponds to the normal splice product containing exon 23. Sequencing these RT-PCR products revealed that only *Dmd*-sg2 efficiently edited *Dmd* exon 23, as evidenced by mixed sequence peaks beyond the sgRNA target site (*data not shown*). In cells transduced with *Dmd*-sg2, we also detected an RT-PCR product corresponding to exon 22 spliced to exon 24 (**Figure A1.4C-D**). Thus, targeting exon 23 with one sgRNA might be sufficient to induce partial exon skipping and produce an intact dystrophin open reading frame.

DMD is a classic example of a disease in which a small amount of functional restoration can provide substantial clinical benefit (531).

Discussion

Whereas gene inactivation is most often the goal of CRISPR-mediated editing, our findings identify exon skipping as an unintended consequence of genome editing. We also show that exon skipping can result from indels that cause alternative splicing or from larger deletions that remove exons. Novel splice isoforms could encode proteins that retain partial function and should be carefully considered when interpreting phenotypes that result from CRISPR-induced mutations.

The frequency with which CRISPR-induced indels cause exon skipping is difficult to predict. Nevertheless, exon skipping caused by point mutations—including nonsense, missense, and translationally silent mutations—is well documented (532-535), and our results complement a recent study, which showed that CRISPR-mediated editing of the human *FLOT1* gene can cause exon skipping by alternative splicing (521). Roles for nonsense-mediated decay or cis-acting regulatory elements have been proposed, but mechanisms remain elusive. DNA damage has also been shown to regulate exon skipping (536). Our data do not resolve whether the DNA damage, the indel, or the premature stop codon induces exon skipping, but they are consistent with the model that some indel mutations

disrupt cis-acting sequences that promote splicing (532). Future studies are needed to determine how CRISPR-induced indels cause alternative splicing and identify rules for predicting when exon skipping will occur.

We detected an unexpectedly high frequency of large deletions induced by CRISPR using a single sgRNA. We and others previously showed that two sgRNAs can generate large genomic deletion or inversion (514, 537). However, large deletions induced by a single sgRNA have not been systematically analyzed in the literature. We initially missed these large deletions with the short-range PCR assays typically used to genotype CRISPR clones. We therefore recommend that, whenever possible, long-range PCR be used to genotype CRISPR clones. In many cases, large deletions will disrupt gene function and accomplish the goal of a CRISPR-mediated genome editing experiment. But our findings warrant careful analysis of editing events, because the aberrant juxtaposition and splicing of exons could result in neomorphic alleles.

Although exon skipping is an unintended consequence of CRISPR-mediated editing, we have shown that exon skipping can produce mRNAs that encode gain-of-function or partially functional proteins. Thus exon skipping induced by CRISPR-mediated editing might be harnessed as a way to restore partial function to disease genes, in much the way that exon skipping induced by antisense oligonucleotides is being explored as a therapeutic to treat genetic diseases that result from splicing mutations (538)

APPENDIX II CRISPR-SONIC CANCER MODELING

This work was published in *Genome Medicine*, and is adapted here with permission from *Springer Nature*, through the Creative Commons license (439). Components of the main text are reproduced here *Appendix II*. The entire manuscript can be reviewed at [Genome Medicine](#). This work was completed in conjunction with postdoctoral fellows Dr. Haiwei Mou, and Dr. Deniz Ozata. Dr. Mou, Dr. Ozata and I are co-first authors on this publication. Additional assistance was provided by co-authors: Dr. Ankur Sheel, Dr. Suet-Yan Kwan, Dr. Alper Kuckural, Dr. Zachary Kennedy, Soren Hough and Yueying Cao. The work was performed in the laboratory of Dr. Wen Xue.

Introduction

Genome editing has been revolutionized by the CRISPR/Cas9 system (503). CRISPR/Cas9 introduces double-strand breaks (DSBs) at a target genomic locus through an easily programmable single guide RNA and the Cas9 enzyme. CRISPR/Cas9-mediated DSBs typically trigger one of two major pathways for DNA repair: 1) *homology-independent repair*, such as non-homologous end recombination (NHEJ), or 2) *homology-directed repair (HDR)* with an endogenous or exogenous homologous DNA template (503, 539). Homology-independent pathways, i.e. NHEJ, have been widely used for disruption of genes by inducing

either frame-shifts or premature stop codons, while HDR is frequently used to precisely edit genes or insert large sequences. However, the utility of HDR for *in vivo* gene knock-in has been limited by the relatively low editing efficiency of HDR compared to that of the NHEJ pathway (540).

Previously, we and others showed CRISPR/Cas9 could be employed to generate loss-of-function mutations in tumor suppressor genes, making *in vivo* cancer studies more efficient (510, 541-547). Gain-of-function alleles can also be made by CRISPR/Cas9 and HDR donor (510, 548, 549). However, the low efficiency of HDR-based gene knock-in presents a significant hurdle for researchers aiming to model *in vivo* gain-of-function mutations in oncogenes.

While the overall cancer death rate continues to decline, cancer is still the number two cause of death nationally; in part, due to our limited understanding of the underlying biology of many cancer types. New methods of rapid *in vivo* modeling are needed to understand cancer biology. Liver cancer is a major cancer type with poor prognosis (550, 551). Specifically, liver cancer incidence in the United States has tripled in the last forty years, and liver cancer deaths have been increasing since 2000 (4). Transposon mediated integration utilizing sleeping beauty system is an established way to study multiple gain-of-function of oncogenes in the liver (239-241). Although transposons are powerful genetic tools, it is difficult to control the integration site and copy number. Thus, a rapid and

precise method allowing a greater degree of targeted somatic oncogene knock-in is needed for liver cancer

Recent studies have demonstrated that homology-independent pathways can be utilized to insert large sequences *in vivo* (552-554). Two guide RNAs make knock-in feasible: one guide RNA targets the genomic insertion locus, and the other linearizes the non-homologous plasmid template containing the desired sequence for integration. A similar strategy using 28bp microhomology arms has also been reported (410).

Here we developed CRISPR-based Somatic Oncogene kNock In for Cancer Modeling (CRISPR-SONIC), a method for rapid *in vivo* cancer modeling. To first validate our approach, we started with the *in vitro* integration of a GFP reporter sequence into the 3' UTR of β -actin. We confirmed this integration by analyzing and sequencing genomic PCR amplicons and by assessing GFP expression driven by the endogenous mouse β -actin promoter through flow cytometry. Next, we used hydrodynamic injection to deliver the CRISPR-SONIC system to somatic hepatocytes and found targeted genomic integration of both GFP reporter and oncogenes such as *HRAS*^{G12V} or *Kras*^{G12D}. Both integrated *HRAS*^{G12V} and *Kras*^{G12D} are functional *in vivo*, demonstrated by rapid induction of intrahepatic cholangiocarcinoma (ICC) in mice (555). Moreover, we further showed our strategy could be used to generate bioluminescent *in vivo* cancer models.

Methods

CRISPR vectors

Guide RNAs targeting *Actb* and *p53* were cloned into the pX330 (Addgene 42230) vectors using standard protocols and primers (**Additional file 1: Table S1-2**) (504). The sgA guide targeting the donor plasmid (Addgene, 83807) and IRES-GFP donor were purchased from Addgene (Addgene, 83575). IRES-HRAS^{G12V} was cloned into Addgene 83575. IRES-Kras^{G12D}-IRES-GFP and IRES-Kras^{G12D}-IRES-luciferase were Gibson cloned into Addgene 83575.

Cell culture

Neuro2a cell line is from the University of Massachusetts Medical School Cell line Freezer program. 293fs, GreenGo and KP cells are from Dr. Tyler Jacks. Cells were cultured in Dulbecco's Modification of Eagle's Medium (DMEM) (Corning 10-013CV) with 10% serum (vol/vol) and 1% penicillin/streptomycin (vol/vol) under standard cell culture conditions, 37C in 5% CO₂ tissue culture incubator.

Transfection

Neuro2A and GreenGo cells were cultured in 6-well plate at 30% confluency for transfection. Lipofectamine 3000 (Invitrogen, L3000015) was used for GreenGo cell transfection, and Lipofectamine 2000 (Invitrogen, 11668027) was used for Neuro2A cell transfection according to the manufacturer's instructions. A total of 2 ug DNA was transfected per well (i.e. 0.66 ug sgA, 0.66 ug SgActin-Cas9, 0.66 ug

Donor). Cells were collected for either flow cytometry or genomic DNA isolation five days post-transfection.

Transduction and Infection

293fs cells were plated at 40% confluency in 6-well plates one day prior to transduction. 293fs cells were transfected for lentiviral production with 600 ng sgActin-3'UTR_1, sgActin3'UTR_2, sgNon-targeting, or sgSf3b3 with packaging plasmids (556). KP cells, Kras^{G12D};p53^{-/-} mouse lung cancer cells(556), were infected with lentivirus (+ 2.5 ug/ml polybrene) and selected with 1.5 ug/ml puromycin.

Cell Viability Assay

2000 cells post-selection were seeded in black-wall clear bottom 96-well plates in twelve wells per sample. 72 hours after plating, cell viability was assessed using Promega Cell Titer Glo Luminescent Viability Assay (G7570) per the manufacturer's instructions. Luminescence at an integration time of 1 s was measure on plate reader.

Colony Formation

2000 cells post-selection were seeded in 6-well plates and incubated for ten days. After ten days, cells were first fixed with 4% formalin, and then stained with 0.5% crystal violet solution. Plates were imaged with a Nikon scanner.

Immunoblot

Whole cell extracts were lysed in RIPA buffer treated with 1:100 Halt phosphatase cocktail inhibitor (Thermo Fisher 78420) and 1:50 Roche Complete protease inhibitor (11836145001). Lysates were boiled for 5 minutes at 95C with Nupage 4X Sample buffer (Invitrogen NP0007). Equal amounts of protein from whole cell extracts were separated on a 4-12% Bis Tris gel and transferred to a nitrocellulose membrane and blocked with Odyssey Blocking buffer. Blots were probed with primary antibodies B-actin 1:1000 (CST 4970), Gapdh 1:1000 (EMD MAB274), Hras 1:500 (Millipore OP23), and GFP 1:2000 (CST 2956) overnight at 4C. Blots were then incubated with a fluorescent secondary antibody (LICOR) and imaged on the Odyssey Imaging Platform.

Genomic DNA purification and PCR

Genomic DNA was purified from cells using the Roche Genomic DNA purification kit (Cat no. 11796828001) at least five days post-transfection. 100 ng genomic DNA were used as template for sgActin integration PCR, and 300 ng genomic DNA

was used as a template for sgp53 integration. LA-Taq (Clontech) or Herculase II (Agilent) were used for PCR.

TOPO Cloning

PCR amplicons were first gel extracted using Qiagen QIAquick Gel Extraction kit (28704) per the manufacturer's instructions. Gel purified PCR fragments were then TOPO cloned using the Zero Blunt TOPO PCR cloning kit (K2835) for sequencing. TOPO clones were miniprepmed using the Qiagen Spin Miniprep kit (272014), and sanger sequencing was performed by Genewiz.

Flow cytometry

Cells were transfected with lipofectamine 3000 as described above. Five days after transfection, cells were trypsinized, washed, and re-suspended in 500 uL PBS and loaded to flow cytometry (BD, Accuri™ C6) for detection of GFP positive cells. 20,000 events were collected for each sample. Samples were analyzed and gated for dead cells and singlets using Flow Jo Software.

Hydrodynamic tail vein injection

All plasmids used for the *in vivo* study were purified by Qiagen Maxi-Prep Endotoxin-free Kit (Qiagen, 12362) according to the manufacturer's instructions. 15 µg per plasmid per mouse were mixed together in 2 ml 0.9% sterile saline at

room temperature. Plasmids were then delivered to mice by hydrodynamic tail vein injection. Specifically, within 5-7 seconds, all 2 ml mixed plasmids were continuously and smoothly injected (239). Mice were then warmed by heat lamp for 30 min to recover from injection shock.

Histology and Immunohistochemistry

Mouse liver tissue was collected from sacrificed mice, fixed with 4% formalin overnight followed by dehydration for 24+ hours in 70% ethanol. Tissues were then embedded in paraffin by the UMassMed Morphology Core. H&E staining was performed by the Morphology Core according to common methods on 4 μ m paraffin sections. Immunohistochemistry staining was performed following standard protocols. Briefly, tumor sections were deparaffinized with xylene, and dehydrated with serial ethanol dilutions. Slides were then boiled for 9 minutes with 1 mM citrate buffer (pH6.0) for antigen retrieval. Next, 3% hydrogen peroxide was used to inactivate endogenous peroxidase activities for 10 mins at room temperature. Tissues were then blocked with 5% normal horse serum from ImmPRESS™ HRP Anti-Rabbit IgG (Peroxidase) Polymer Detection Kit (Vector labs, MP-7401-50) for 1 hour at room temperature. Slides were then incubated with primary antibody against Ck19 1:200 (Abcam, 133496) or GFP 1:200 (CST, 2956) overnight at 4 degrees Celsius. Secondary HRP anti-rabbit antibody (Vector labs, MP-7401-50) was incubated with sections for 1 hour at room temperature,

followed by incubation with substrate/chromogen (Fisher Scientific, TA-125-QHDX). Slides were then counterstained with hematoxylin, dehydrated in ethanol, followed by a xylene wash and sealed with a coverslip for long-term storage. H&E or IHC images were captured using a Leica DMI8 microscope. IHC slides were quantified by selection of five random fields per paraffin embedded section, and positive hepatocytes per 20X field counted.

IVIS imaging

At the indicated time post injection, mice were given 200 μ l luciferin (15 mg/ml) intraperitoneally. Signal was allowed to stabilize for 10 min, and then loaded into the Perkin Elmer IVIS machine for capture of luminescent signal (1minute exposure).

Significant Results and Discussion

CRISPR-SONIC mediated homology-independent IRES-GFP integration in mouse cells

Although CRISPR/Cas9 can facilitate the integration of large DNA sequences into a target locus and is applicable for human cells (552-554), a flexible *in vivo* gene knock-in method has not been established for cancer mouse models. To knock-in desired sequences, we chose the β -actin locus because it is

robustly expressed in most mouse cell types and organs (557). We designed a guide RNA targeting the 3' UTR of β -actin locus. We also adopted a published donor plasmid containing IRES (Internal Ribosome Entry Site) sequence to express gene of interest (GOI) and an sgRNA (named sgA) to linearize the circular plasmid donor (553). We then designed a strategy to flexibly clone any GOI

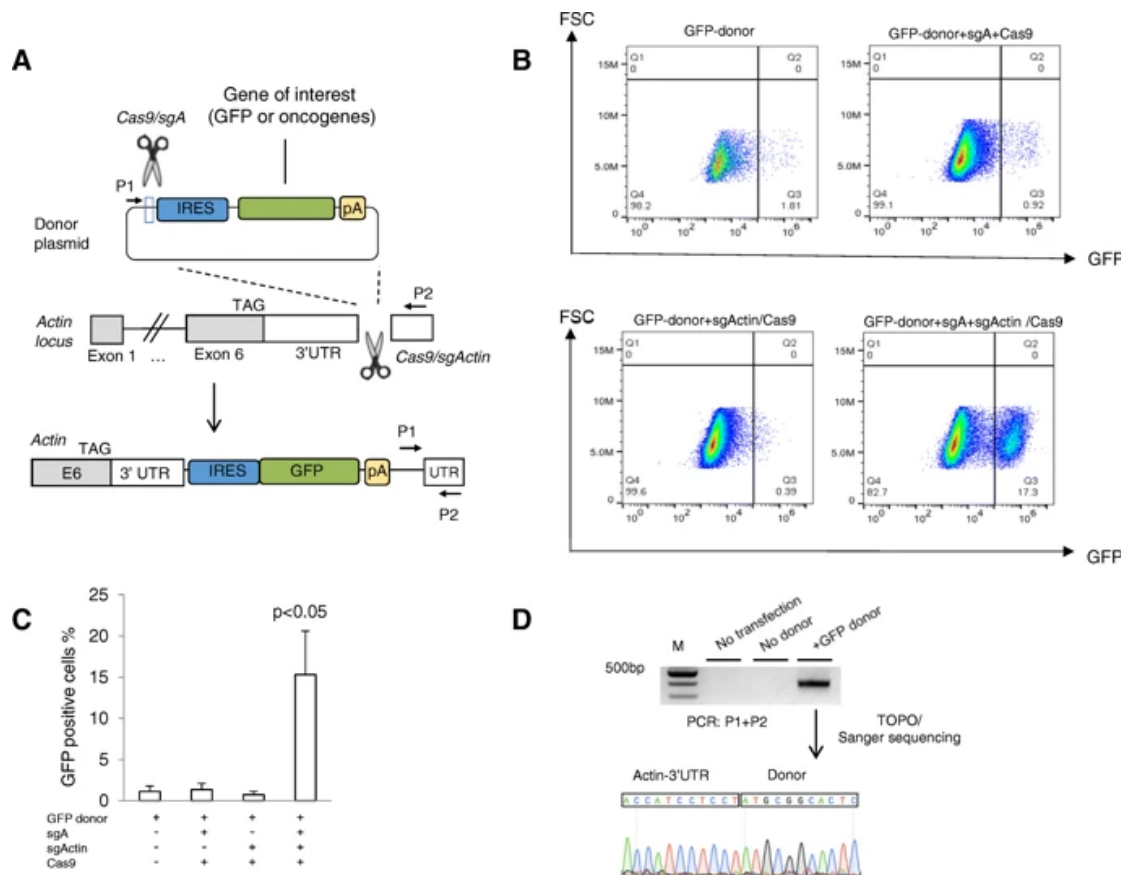


Figure A2.1 CRISPR-SONIC enables homology-independent IRES-GFP integration in mouse cells. (A) Schematic showing the target genomic locus, guide RNAs and donor plasmid. **(B)** Neuro2A cells were transfected with indicated plasmids. Five days post-transfection, cells were trypsinized, washed with PBS, re-suspended in PBS and analyzed by flow cytometry for detection of GFP positive cells. **(C)** Statistical analysis of percentage of GFP positive cells. Reported as mean percentage. Error bars are s.d. (n=3). **(D)** PCR detecting genomic integration and representative sanger sequencing. M, molecular weight DNA ladder.

sequence into the donor plasmid. In this CRISPR-SONIC system, knock-in occurs in three steps: (1) Cas9 and sgActin cuts the 3' UTR of β -actin; (2) Cas9 and sgA linearizes the donor plasmid; (3) linearized donor is inserted in the 3' UTR of β -actin through NHEJ. If insertion occurs in the correct orientation, expression of the GOI will be driven by the endogenous β -actin promoter and the IRES signal respectively (**Figure A2.1 A**). Finally, the poly A signal ensures transcription termination after the GOI.

We transfected combinations of two guide RNAs/Cas9 and the plasmid GFP donor into Neuro2A mouse neuroblastoma cell line and days post-transfection (Fig. 1B). FACS analysis detected $15.3 \pm 5.3\%$ GFP positive cells post-transfection (Fig. 1C). Control transfections, GFP donor alone, GFP donor + sgActin/Cas9, and GFP donor + sgA + Cas9, all produced a low percentage level of GFP by flow cytometry five days after transfection (**Figure A2.1 B-C**). We confirmed successful GFP donor integration in the Neuro2a genome by PCR amplifying the fused GFP donor/ β -actin DNA sequence and sanger sequencing the amplicon (**Figure A2.1 D**).

To evaluate CRISPR-SONIC efficiency in other cell lines, we performed the same transfection in GreenGo cells and observed low integration efficiency ($\sim 1\%$) likely due to a single nucleotide polymorphism (SNP) two nucleotides adjacent to the SgActin PAM sequence reducing CRISPR cutting (*Data not shown*).

As described above, CRISPR-SONIC occurs in three steps with sgA linearizing the circular donor plasmid prior to its insertion in the 3' UTR of β -actin. Next, we tested whether a linear DNA donor could alternatively be used for CRISPR-SONIC. To generate a linear donor, we PCR amplified and gel purified the IRES-GFP donor sequence. We then tested whether our IRES-GFP amplicon could be transacted with sgActin/Cas9 for efficient integration into the 3' UTR of β -actin. Using Neuro2a cells, we found that approximately 6% of cells were GFP

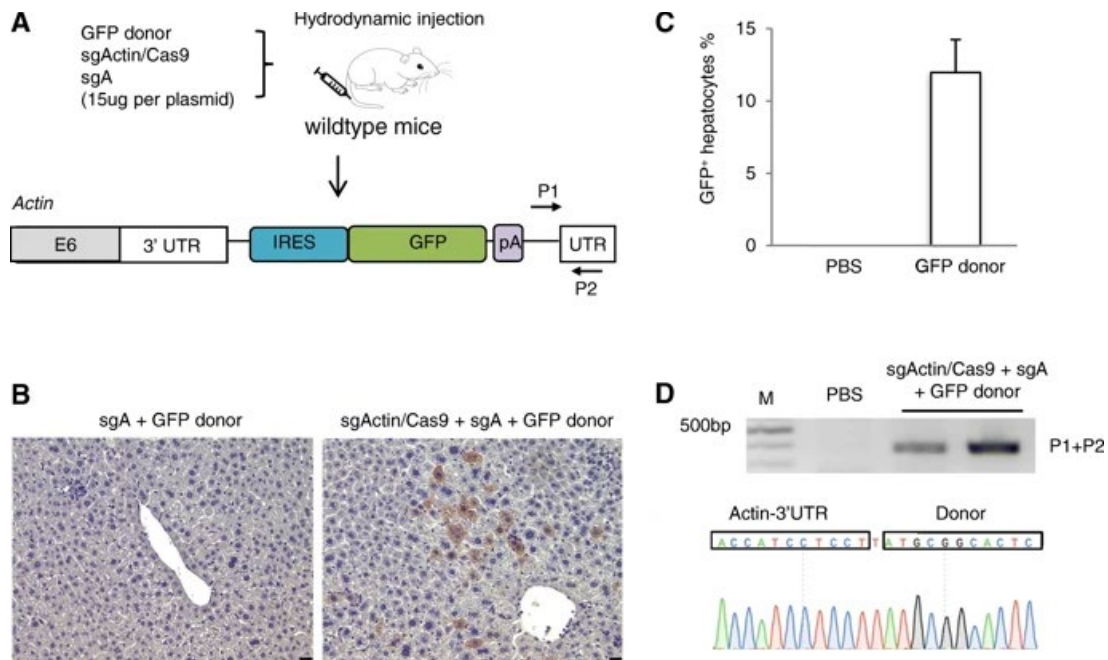


Figure A2.2 CRISPR-SONIC enables efficient IRES-GFP integration *in vivo*. (A) Schematic showing the target genomic locus, guide RNAs and donor plasmid for *in vivo* integration. Hydrodynamic tail vein injection was performed to deliver the plasmids to FVB mice. 7 days later, mouse livers were collected for histological analysis or genomic DNA purification. (B) IHC was performed to examine the GFP positive cells from liver slides. Scale bars are 25 μ m. (C) Statistical analysis of IHC GFP-positive cells from three mice. Error bars are s.d. (n=1 for PBS and n=3 mice for GFP donor). (D) Genomic PCR detected integration bands. The last two lanes are biological replicate samples.

positive five days post-transfection with linear donor, compared to approximately 19% of cells transfected with circular GFP donor, sgA, and Sg-Actin/Cas9 (*Data not shown*).

Interestingly, co-injection of PCR donor plus sgActin/Cas9 by hydrodynamic injection did not generate GFP+ cell in mouse liver (data not shown). It is possible that the linear PCR product is not stable *in vivo* or unable to efficiently translocate into the nucleus. More investigation will be required to understand variances in integration efficiency between circular and linear donor plasmids.

Efficient and targeted homology-independent integration of IRES GFP in mouse liver

Following *in vitro* validation of our editing strategy, we then tested our strategy *in vivo*. We used hydrodynamic tail-vein injection to deliver CRISPR-SONIC to mouse hepatocytes (239-241). We again used sgActin/Cas9, sgA and the GFP donor plasmids for targeted integration (**Figure A2.2 A**). Seven days after hydrodynamic injection, mice (n = 3) were sacrificed for liver tissue collection. By immunohistochemistry (IHC) staining, we detected $12.0 \pm 2.3\%$ GFP-positive hepatocytes *in vivo* ($p < 0.05$ compared to control group) (**Figure A2.2 B and C**). Next, we confirmed IRES-GFP sequence integration at the target locus through PCR detection of the expected band and subsequent sanger sequencing of the amplicon (**Figure A2 D**).

Development of intrahepatic cholangiocarcinoma following CRISPR-SONIC of oncogenic *HRAS*^{G12V}

ICC is an aggressive cancer type lacking effective therapy (558). TP53 (26-44% of cases) and KRAS (16-18%) are top driver mutations in ICC (559, 560). Previous studies showed that oncogenic HRAS or KRAS can cooperate with p53 loss to drive ICC in mouse models using Cre-LoxP or transposons (555, 561). To determine whether we could apply CRISPR-SONIC to knock-in oncogenic Ras such as *HRAS*^{G12V} to model ICC *in vivo*, we cloned a *HRAS*^{G12V} donor plasmid with human HRAS sequence (**Figure A2.3 A**) (562). First, we validated the HRAS donor plasmid *in vitro*. Five days post transfection of the CRISPR-SONIC plasmids in Neuro2A cells, we detected HRAS over-expression by western blot using GFP donor as a control (**Figure A2.3 B**). Next hydrodynamic injection was used to deliver the CRISPR-SONIC components to a mouse strain with p53 liver knockout (p53fl/fl;Alb-cre/+) (**Figure A2.3 A**) (563, 564).

One-month post injection, we observed gross tumor formation in the livers, 8.0±4.0 tumors per mouse (**Figure A2.3 3C and D**). As a control, mice injected with sgActin/Cas9, sgA and GFP donor did not develop liver tumors (**Figure A2.3 D**, p<0.05). To confirm that *HRAS*^{G12V} was integrated into the β -actin locus, we detected the expected PCR bands and sanger-sequenced the bands (**Figure A2.3 E**). Finally, to better characterize the tumors, we collected tumor tissue for

histologic analyses. Using IHC, we observed that tumors are positive for the primary ICC marker, cytokeratin 19 (Ck19) (**Figure A2.3 F**) (288, 565-567).

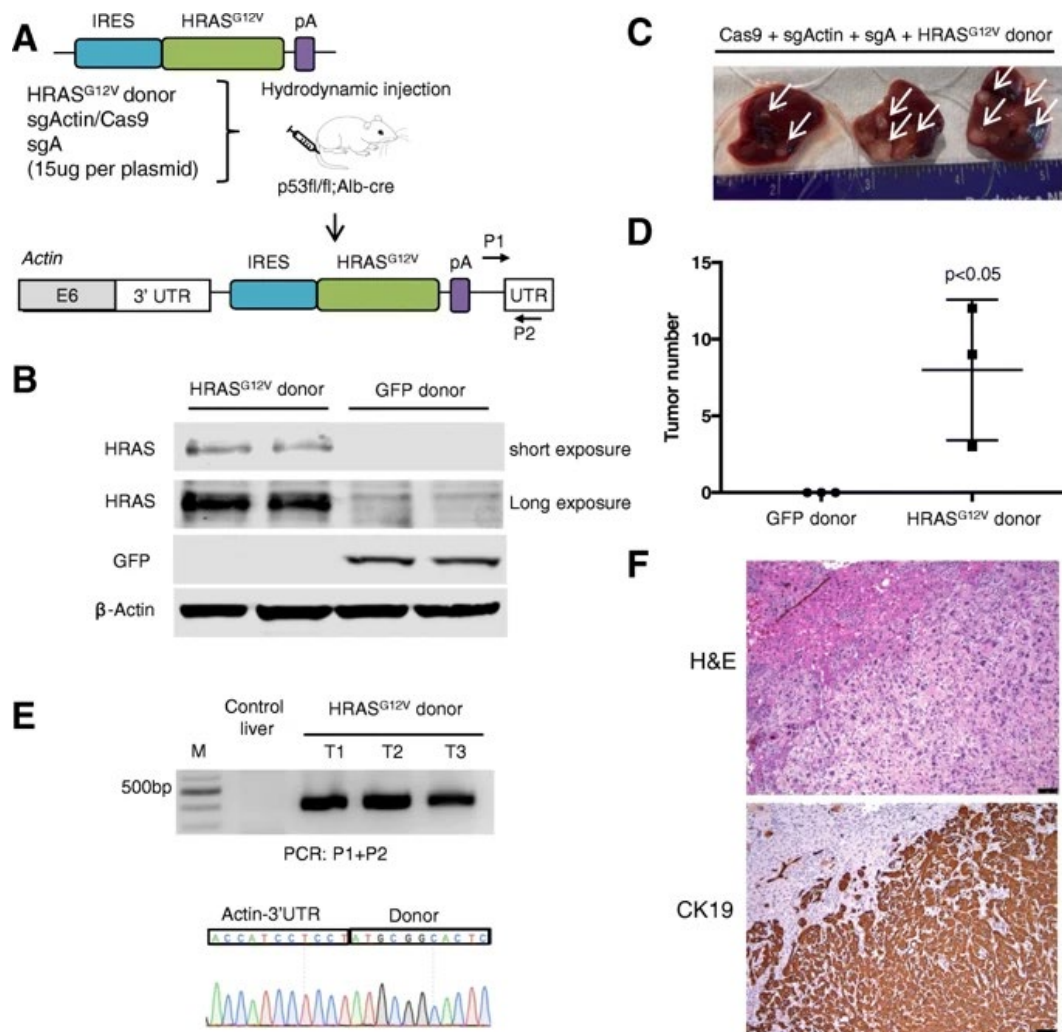


Figure A2.3 CRISPR-Sonic enables IRES-HRAS^{G12V} integration *in vivo* for tumor modeling. (A) Schematic showing the target genomic locus, guide RNAs and donor plasmid for *in vivo* integration (B) Western blot confirms HRAS overexpression resulting from targeted integration of Neuro2A cells 5 days post transfection. (C) Liver tumors images from injected mice harvested at one month. (D) Number of surface liver tumors. Error bars are s.d. (n=3 mice). (E) PCR detected integration band in liver tumor genomic DNA. T1-T3 are tumors from three mice (n=3) (F) Liver tumors are positive for the ICC marker Ck19. Scale bars are 25 μ m.

CRISPR-SONIC enables combinatorial *Kras*^{G12D} knock-in and p53 knockout in immunocompetent mice

To test whether the use of CRISPR-SONIC could be broadly used to model cancer driven by different oncogenes, we cloned another oncogenic Ras, *Kras*^{G12D}, into our donor plasmid. ICC driven by *Kras*^{G12D} also requires loss of function in p53 (555). To track *Kras*^{G12D} integration and expression, we included an IRES-GFP cassette after *Kras* that would make the resulting tumors GFP positive (**Figure A2.4 A**)

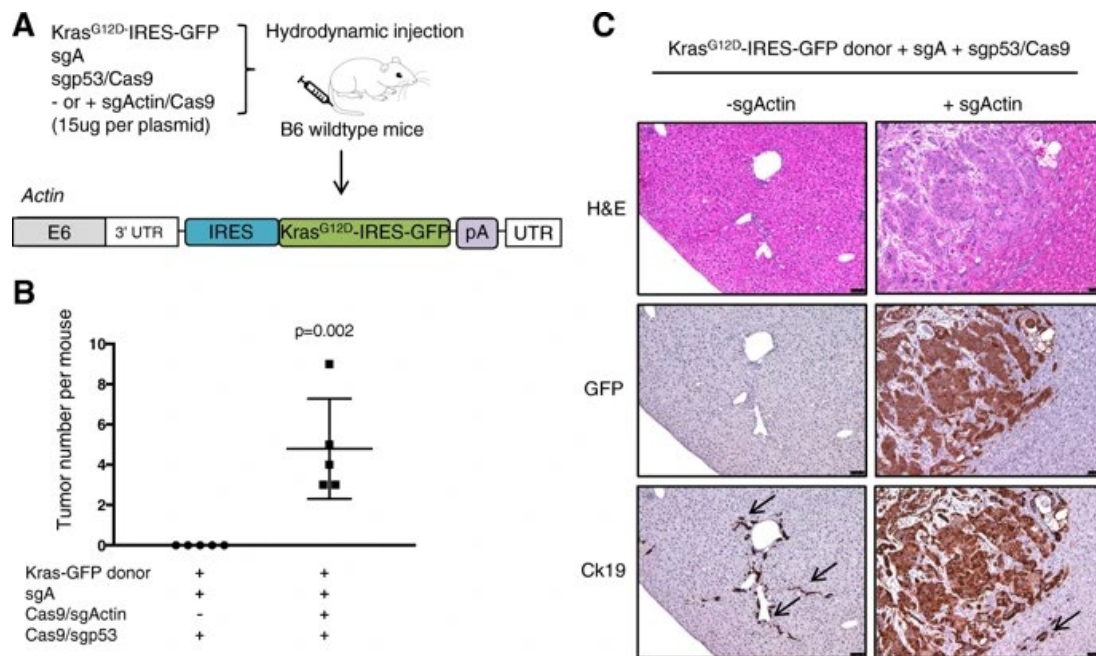


Figure A2.4 CRISPR-SONIC enables combinatorial *Kras* knockin and p53 knockout in B6 wildtype mice. (A) Schematic showing the target genomic locus, guide RNAs and donor plasmid for *in vivo* integration. (B) Quantification of liver tumor per mouse. **Error bars are s.d.** (n=5 mice). (C) Representative H&E and IHC staining detected GFP positive and Ck19 positive tumor cells in +sgActin mice. Arrows denote internal control Ck19 staining in bile ducts. Scale bars are 75 μ m.

Next, we co-injected CRISPR-SONIC plasmids (Kras-donor, sgActin/Cas9 and sgA) with a guide RNA targeting *p53* (sgp53) (542) to knockout p53 in hepatocytes of wildtype B6 mice (termed “+sgActin group” in **Figure A2.4 A**). One-month post hydrodynamic injection, we sacrificed this cohort of mice (n = 5) and observed liver tumor formation (Fig. 4B). IHC staining revealed GFP and Ck19 positive tumor cells with abundant stroma, a known feature of ICC (288) (**Figure A2.4 C**).

Generation of bioluminescent tumors using CRISPR-SONIC

Bioluminescent labeling of tumors enables researchers to monitor tumor initiation and progression in live animals over time. Real-time analysis in live animals provides clear advantages for understanding dynamics of tumor growth. We engineered a donor plasmid containing an IRES-luciferase sequence after oncogenic *Kras*^{G12D} and injected mice using the same *in vivo* integration strategy (**Figure A2.5 A**). Five weeks following hydrodynamic injection, we used *in vivo* bioluminescent imaging to quantify tumor formation over time and observed positive signal indicative of tumorigenesis (**Figure A2.5 B**). Weekly imaging allowed for measurement and tracking of tumor growth over time (**Figure A2.5 C**). Following live imaging, downstream H&E and IHC staining of Ck19 confirmed ICC

formation (**Figure A2.5 D**). These data suggest that our method facilitates one-step oncogene and reporter knock-in to facilitate live tumor imaging.

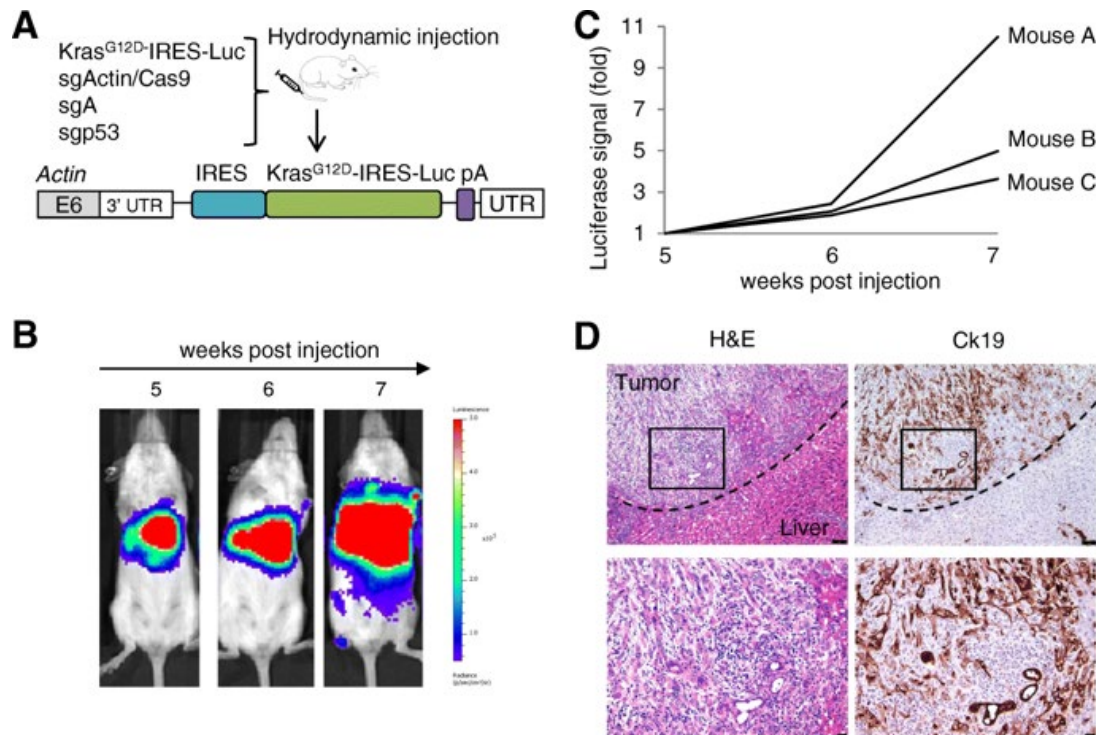


Figure A2.5 CRISPR/Cas9 enables generation of bioluminescent liver tumors.

(**A**) Schematic showing the target genomic locus, guide RNAs and donor plasmid. Hydrodynamic tail vein injection was performed to deliver the CRISPR/Cas9 system to FVB mice. (**B-C**) IVIS imaging was performed weekly. (**D**) H&E and Ck19 IHC staining of liver tumors. Dashed lines denote tumor/liver border. Scale bars are 25 μ m.

Discussion

Herein we reported a flexible system for targeted somatic oncogene knock-in to facilitate *in vivo* cancer modeling. This method enables rapid knock-in of gain-of-function oncogenes and reporter genes in mice.

CRISPR-SONIC enables efficient homology-independent DNA integration *in vivo*. Previous somatic integration strategies for cancer modeling, i.e. point mutations or gene knock-in, relied on low-efficiency HDR, limiting the ease of its application both *in vitro* and *in vivo* (406, 548). To satisfy the need for rapid and efficient modeling of cancer *in vivo*, we turned to CRISPR/Cas9 homology independent targeted integration. While homology-independent pathways, i.e. NHEJ, are typically more efficient, they are also more error-prone and therefore more frequently utilized for gene disruption rather than DNA integration. To combat this limitation, we adopted a donor with an IRES sequence before the coding region of our gene of interest (553). Compared to a microhomology-mediated end-joining (MMEJ) strategy to knockin 2A-GFP at Actin (410), small indel mutations before IRES do not affect translation of the gene of interest in our system.

We used the same strategy *in vivo* and found similarly high efficiency of GFP integration at the target locus. Our IHC staining indicated approximately ~10% of the hepatocytes were GFP positive (Fig. 2). This is a significant improvement compared to a 0.5% HDR knock-in efficiency we previously reported using hydrodynamic injection of an HDR donor (510).

CRISPR-SONIC enables in vivo modeling of ICC

We tested our strategy using Ras isoforms, but presumably any desired oncogenic DNA sequence could be used and tailored to the cancer type of interest.

We first chose the well-characterized oncogenic HRAS^{G12V} mutant as a donor and used p53^{fl/fl};Alb-cre/+ mice which harbor p53 knockout mutations in the liver. As expected, we observed tumor formation after CRISPR-SONIC mediated *HRAS*^{G12V} integration (Fig. 3). We then used an oncogenic *Kras*^{G12D} as a donor and delivered this to wildtype B6 or FVB mice along with a guide RNA targeting *p53*. As expected, CRISPR-SONIC delivery of mutant Kras cooperated with sgp53 to induce ICC *in vivo* (Fig. 4).

Next, we expanded our CRISPR-SONIC system to include knock-in of a bioluminescent marker to enable researchers to follow tumor initiation and maintenance in real time. Integrating this luciferase donor allowed us to dynamically quantify tumor size in our model of ICC (Fig. 5).

Caveats and Solutions

CRISPR-SONIC provides a targeted and higher efficiency knock-in for cancer modeling, however, several caveats need to be considered when applying the technology. First, while CRISPR-SONIC offers a higher degree of genomic targeting than the random genetic insertions associated with transposon delivery, the CRISPR-SONIC system can result in off-target insertions. The donor may insert at off-target sites of the associated sgRNAs or the DSBs that naturally occur in cells (568). To mitigate the off-target effects of the CRISPR-SONIC system, screening sgRNAs with minimal off-target effects may help to reduce integration

at CRISPR off-target sites; although, the donor may still integrate at the DSBs that naturally occur in cells.

When the CRISPR-SONIC system (SgA, sgActin, Donor) is co-delivered with a sgRNA targeting a tumor suppressor (i.e. p53) for generation of tumor, CRISPR-SONIC can integrate at both sgRNA sites- sgActin and sgp53. Notably delivery of SgA, sgp53 and donor did not produce either GFP positive expression *in vitro* or result in tumor formation *in vivo*. However, by genomic PCR we did detect *in vivo* integration of the donor plasmid at the sgp53 site despite the lack of tumor formation. Future studies are required to determine the degree of off-target donor insertion.

The second major caveat is that the donor vector can be integrated in both orientations (554). As expected, we also detected inverted integration in the total liver DNA. Users should note that CRISPR-SONIC cassettes inserted antisense to the promoter will not be detected by GFP flow cytometry. Further, cassettes inserted distal to a promoter will also go undetected by flow cytometry. During our development of CRISPR-SONIC, we focused on the phenotype driven by the forward orientation of our donor. Future work will determine whether the reverse orientation of the inserted plasmid sequence has adverse effects *in vivo*. A recently published HITI method used inverted sgRNA sites flanking the GOI to reduce reverse insertion. Reverse insertion without indels will create an intact sgRNA

target sequence and will be subjected to additional Cas9 cutting until forward insertion or indels occur to eliminate sgRNA binding sites (554).

Third, the level of expression of the GOI must also be considered when designing sgRNAs and donor plasmids for CRISPR-SONIC. We chose to target the 3' UTR of the β -actin locus as the preferred target site for integration due to the strong promoter activity of mouse actin. As such, it is possible that the RAS expression level in our system is different from that of transposon RAS (569). When lower expression is desired, integration can be engineered at the endogenous gene locus (548, 554).

An additional consideration when using the CRISPR-SONIC system is that the Actin 3' UTR may have a role in regulating β -Actin expression or function. Recent studies showed that Cas9 targeting can induce long deletions which may affect beta-actin function and subsequently cell viability (502, 554). Of note, infecting KP cells ($Kras^{G12D}$ $p53^{-/-}$ mouse lung cancer cells) with two guides against the actin UTR does not result in reduced expression of β -Actin or notably change cell morphology; however, it does moderately reduce cell proliferation by viability and colony formation assays. The effect is modest compared to an sgRNA targeting an essential gene, *Sf3b3*. One possible explanation is that the off-target effects of sgActinUTR contributed to the effects on cell viability. Users should exercise caution when selecting the on-target locus for integration, and further it is advisable to test multiple guides against the on-target locus before proceeding.

Finally, unlike transposon-based delivery the CRISPR-SONIC system does not allow for unlimited multiplexing of gain-of-function alleles. Multiple transposons expressing different transgenes can insert in the genome of one hepatocyte (241, 570). Thus, the transposon delivery system better accommodates users wishing to multiplex 2+ gain of function alleles. However; it should be noted that CRISPR-SONIC could be employed for multiplexing up to two insertions per diploid cell (i.e. two alleles of Actin 3' UTRs per cell).

Conclusions

In conclusion, our method facilitates flexible oncogene knock-in to rapidly model cancer *in vivo*. Further, while we show CRISPR-SONIC delivery via hydrodynamic delivery in the liver, CRISPR-SONIC cancer modeling may also potentially be applied to other tissues with delivery by lentivirus or adeno-associated virus respectively. Finally, CRISPR-SONIC may also be applied to study other genetic disease including loss-of-function diseases, by knocking-in of a rescue gene at a safe harbor gene.

APPENDIX III REVIEW OF CANONICAL WNT SIGNALING

Wnt Signaling ON/ β -catenin ON

As reviewed in Russel et al (248), Wnt/ β -catenin is a signal transduction pathway that promotes cell fate, and cell proliferation in a context and tissue dependent manner (**Figure A3.1**). Wnt signaling is first activated by secreted glycoproteins, Wnt ligands. Wnt ligands are only active following post-translational glycosylation and palmitoylation modifications in the endoplasmic reticulum by the enzyme, porcupine (PORCN). Following modification, Wnt ligands are trafficked to the cell membrane by G-protein Coupled Receptor HPR177 (Wntless) and secreted into the extracellular space. Secreted Wnt ligands bind to a trimeric receptor made up of Frizzled, LRP5, and LRP6.

Wnt ligand binding to both Frizzled and LRP5/6, triggers phosphorylation of LRP5/6. Phosphorylation of LRP5/6 recruits DVL and Axin, a scaffold member of the β -catenin destruction complex to the membrane. Recruitment of Axin to the membrane critically disrupts the destruction complex, inhibiting phosphorylation and proteasomal degradation of β -catenin. DVL complexing to Frizzled, LRP5/6 is essential for recruitment of Axin to the membrane, and disruption of the destruction complex. The destruction complex is comprised of Axin, APC, casein kinase 1 α (CK1 α), and glycogen synthase kinase 3 β (GSK3 β).

Non-phosphorylated β -catenin can freely translocate to the nucleus, where it complexes with TCF transcription factors for expression of target genes. β -

catenin does not have its own DNA binding domain; thus, it acts as a transcriptional co-activator and must complex with other transcription factors to promote gene expression.

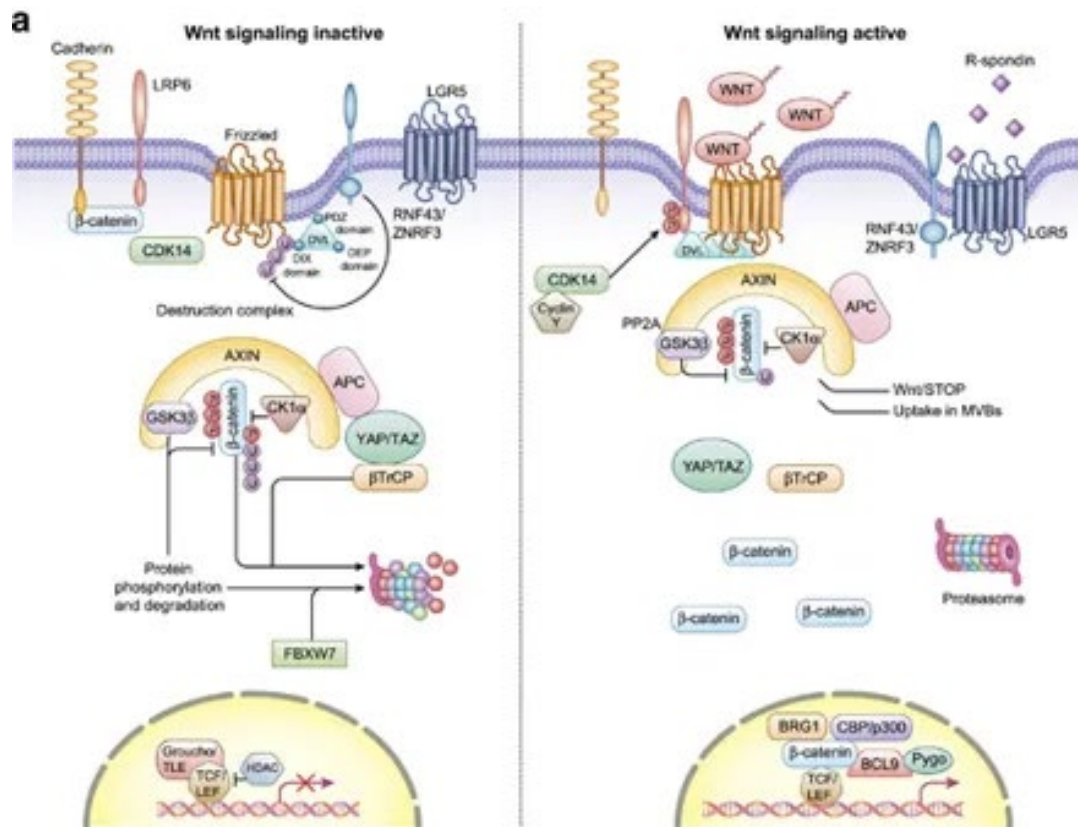


Figure A3.1 Canonical Wnt Signaling. Adapted with permission from Zhan et al, 2017.

Wnt Signaling OFF/ β -catenin OFF

In the absence of secreted, modified Wnt ligands, the Wnt pathway is OFF, and cellular levels of β -catenin are routinely low due to unchecked activity of the destruction complex. β -catenin once synthesized is typically retained at the cellular membrane adherens junctions by E-Cadherin (CDH1). If β -catenin is

released from the adherens junctions, it is immediately targeted to the destruction complex.

The complex is formed first by the Axin serving as a scaffold protein, and joined by APC, CK1 α , and GS3K β . Following formation of the complex, β -catenin is then phosphorylated by GS3K β on serine residues 33,37 and threonine residue 41. It is additionally phosphorylated by CK1 α , on serine residue 45. Following phosphorylation, β -catenin is seen by a member of the E3 ubiquitin ligase complex, β -Transducin repeat containing protein (β -TRCP). Phosphorylated β -catenin is then ubiquitinated and degraded (**Figure A3.1**)(571).

APPENDIX IV REVIEW OF CANONICAL HIPPO SIGNALING

Hippo Signaling ON/ YAP1 OFF

Hippo/YAP1 signaling is dysregulated in many cancer types, including adult and pediatric cancer. In non-transformed liver cells, Hippo/YAP1 functions to control organ size, cell proliferation and differentiation (19-22, 283, 350, 572). When the Hippo pathway is ON, YAP1 is phosphorylated downstream of a series of kinases, retained in the cytoplasm and prevented from nuclear translocation, and transcription activation (22, 350).

Upstream activation of the Hippo pathway remains debated; but several reports demonstrate that specific G-protein coupled receptor (GPCR) activate Hippo signaling, while others inactivate Hippo, activating YAP1. Hippo activation is presumed to occur primarily by GPCR receptors coupling with Gs upon binding of glucagon or epinephrine(202) (449). Following upstream activation, MST1/2 kinase is phosphorylated in a complex with its adaptor protein, Salvador Family WW Domain Containing Protein 1 (SAV1). In turn MST1/2, phosphorylates the downstream LATS1/2 kinase. LATS1/1 kinase then complex together with scaffold protein MOB Kinase Activator 1 (MOB1). LATS1/2 phosphorylates YAP1 at 1+ serine residues. The kinase cascade responsible for phosphorylation of YAP1 seems to be tissue-dependent; indeed, in liver one report shows that MST1/2 can phosphorylate YAP1 without LATS1/2 (25). AKT has also been reported to phosphorylate YAP1 on the S127 residue (443). Following phosphorylation, YAP1

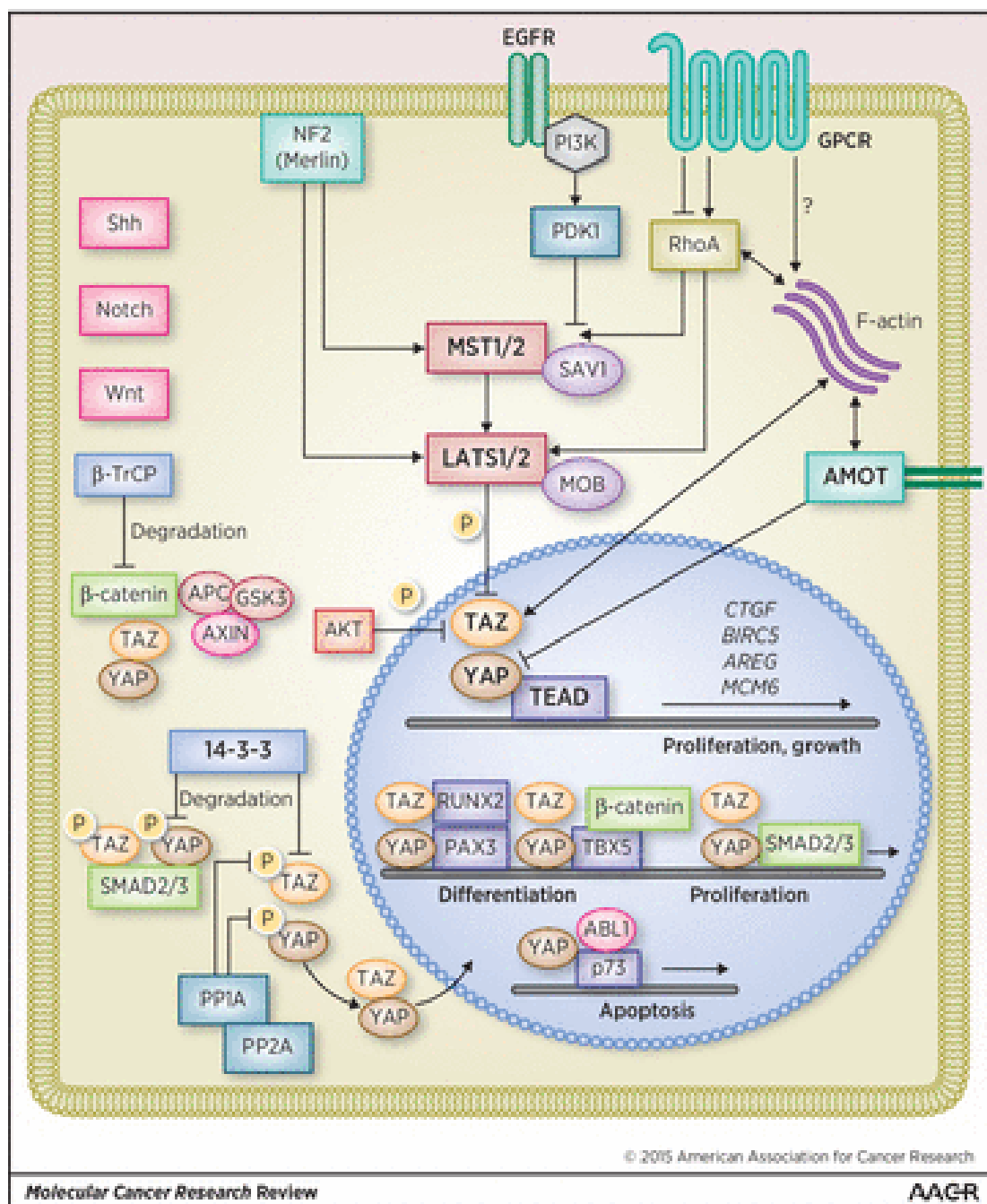


Figure A4.1 Hippo Pathway and Transcription Regulation. Reused with permission from Ehmer et al, 2016.

is maintained in the cytoplasm. YAP1 plasmid is then marked for degradation by 14-3-3 proteins and degraded by ubiquitin proteasomal degradation (**Figure A4.1**) (573). Phosphorylated residue serine127 serves as the anchoring site for 14-3-3 protein degradation (574).

Alternatively, YAP1 was also found to targeted for degradation by phosphorylation from LATS1/2 kinases at residue S381, additional phosphorylation from CK1 Δ/ϵ , and then degradation by the E3 ubiquitin ligase, SCF- β -TRCP. These degradation components are part also part of the Wnt destruction complex (575).

Hippo signaling also inactivates a paralogue of YAP1, known as transcriptional co-activator with PDZ-binding motif (TAZ). While YAP1 and TAZ appear functionally similar, they do have divergent roles in a tissue-based context in proliferation, stemness, and cancer (573).

Hippo Signaling OFF/ YAP1 ON

Hippo OFF signaling allows YAP1 to remain hypo-phosphorylated where it translocates to the nucleus and functions as a transcriptional co-activator. YAP1 does not have a DNA binding site, so it complexes with other factors to work as a transcription factor. Canonically, YAP1 works with the TEAD family of transcription factors to drive pro-proliferation and anti-apoptotic gene programs (280, 576). A number of upstream signaling nodes have been described to inactivate Hippo and

contribute to YAP1 activation including: EGFR (577, 578), Wnt/ β -catenin (579), Notch (20), AKT/PI3K (580), Hedgehog signaling (460), GPCRS (581-583) and Protease Activated Receptors (PARS) (583) (**Figure A4.1**).

APPENDIX V MURINE HEPATOBLASTOMA GENE EXPRESSION

**Table A5.1 RNA-Sequencing Fold Change TPM Fold Change, YAP1 OFF D6/
YAP1 ON Murine Tumors, n=4 tumors, coding genes with a p-value>0.05 shown**

Gene	Name	YAP1 OFF/ YAP1 ON (TPM FC)	p-value
Gm21320	#N/A	3755.29	0.00
Mup10	major urinary protein 10	3230.00	0.00
Mup9	major urinary protein 9	895.47	0.00
Mup2	major urinary protein 2	585.44	0.02
Mup11	major urinary protein 11	545.53	0.00
Sult3a1	sulfotransferase family 3A, member 1	299.86	0.01
Mup1	major urinary protein 1	259.14	0.00
Mup17	major urinary protein 17	179.48	0.00
Mup12	major urinary protein 12	177.24	0.04
Mup15	major urinary protein 15	78.69	0.05
A1bg	alpha-1-B glycoprotein	58.25	0.01
Sult2a8	#N/A	57.99	0.01
Cyp3a44	cytochrome P450, family 3, subfamily a, polypeptide 44	57.47	0.02
Ces3b	carboxylesterase 3B	30.89	0.02
Rfx4	regulatory factor X, 4 (influences HLA class II expression)	30.06	0.01
Cyp3a16	cytochrome P450, family 3, subfamily a, polypeptide 16	21.23	0.01
Cyp2b13	cytochrome P450, family 2, subfamily b, polypeptide 13	19.54	0.01
Cyp2c69	cytochrome P450, family 2, subfamily c, polypeptide 69	17.17	0.01
Ces3a	carboxylesterase 3A	14.19	0.01
Cyp2b9	cytochrome P450, family 2, subfamily b, polypeptide 9	13.58	0.04
Cpsf4l	cleavage and polyadenylation specific factor 4-like	13.27	0.01
Cyp3a41b	cytochrome P450, family 3, subfamily a, polypeptide 41B	12.42	0.01
Cyp3a41a	cytochrome P450, family 3, subfamily a, polypeptide 41A	11.65	0.01
Mup3	major urinary protein 3	11.64	0.02

Cyp2c40	cytochrome P450, family 2, subfamily c, polypeptide 40	11.06	0.01
Cyp17a1	cytochrome P450, family 17, subfamily a, polypeptide 1	10.94	0.01
Sult2a1	sulfotransferase family 2A, dehydroepiandrosterone (DHEA)-preferring, member 1	10.60	0.00
Car3	carbonic anhydrase 3	10.33	0.00
Cyp2g1	cytochrome P450, family 2, subfamily g, polypeptide 1	9.80	0.00
Sult2a2	sulfotransferase family 2A, dehydroepiandrosterone (DHEA)-preferring, member 2	7.61	0.00
Cyp26b1	cytochrome P450, family 26, subfamily b, polypeptide 1	6.95	0.00
Oat	ornithine aminotransferase	6.64	0.01
Cyp26a1	cytochrome P450, family 26, subfamily a, polypeptide 1	6.56	0.01
Cyp2c54	cytochrome P450, family 2, subfamily c, polypeptide 54	6.41	0.01
Cyp2c37	cytochrome P450, family 2, subfamily c, polypeptide 37	6.40	0.01
Ido2	indoleamine 2,3-dioxygenase 2	6.38	0.02
Gm21748	NA	6.25	0.00
Slc10a1	solute carrier family 10 (sodium/bile acid cotransporter family), member 1	6.20	0.02
Lrit2	leucine-rich repeat, immunoglobulin-like and transmembrane domains 2	6.17	0.04
Gm4756	#N/A	6.10	0.01
Gm21860	NA	5.97	0.00
Lrit1	leucine-rich repeat, immunoglobulin-like and transmembrane domains 1	5.82	0.02
Sult2a5	sulfotransferase family 2A, dehydroepiandrosterone (DHEA)-preferring, member 5	5.55	0.02
Dio1	deiodinase, iodothyronine, type I	5.44	0.01
Orm3	orosomucoid 3	5.29	0.02
Serpina3k	serine (or cysteine) peptidase inhibitor, clade A, member 3K	5.27	0.04
Aox3	aldehyde oxidase 3	5.16	0.01
Ugt3a1	UDP glycosyltransferases 3 family, polypeptide A1	5.14	0.01
Lin7a	lin-7 homolog A (C. elegans)	5.09	0.01
Nat8f2	#N/A	5.07	0.01
P2ry4	pyrimidinergic receptor P2Y, G-protein coupled, 4	5.01	0.03
Acacb	acetyl-Coenzyme A carboxylase beta	4.97	0.03

Ces1b	carboxylesterase 1B	4.92	0.01
Slc22a26	solute carrier family 22 (organic cation transporter), member 26	4.82	0.02
Rtp3	receptor transporter protein 3	4.64	0.01
Upp2	uridine phosphorylase 2	4.63	0.02
Sc5d	sterol-C5-desaturase (fungal ERG3, delta-5-desaturase) homolog (S. cerevisiae)	4.56	0.01
Ces1f	carboxylesterase 1F	4.55	0.03
Sult2a4	sulfotransferase family 2A, dehydroepiandrosterone (DHEA)-preferring, member 4	4.50	0.01
Car5a	#N/A	4.46	0.01
Ugt2b37	UDP glucuronosyltransferase 2 family, polypeptide B37	4.42	0.01
Rdh9	retinol dehydrogenase 9	4.36	0.03
Cyp2d40	cytochrome P450, family 2, subfamily d, polypeptide 40	4.35	0.00
Stx1b	syntaxin 1B	4.33	0.01
Cyp2c29	cytochrome P450, family 2, subfamily c, polypeptide 29	4.33	0.01
Acss2	acyl-CoA synthetase short-chain family member 2	4.28	0.02
F11	coagulation factor XI	4.23	0.03
Slc47a1	solute carrier family 47, member 1	4.21	0.02
Apoa2	apolipoprotein A-II	4.20	0.00
Hsd3b7	hydroxy-delta-5-steroid dehydrogenase, 3 beta- and steroid delta-isomerase 7	4.14	0.01
Slc27a5	solute carrier family 27 (fatty acid transporter), member 5	4.06	0.02
Slco1a1	solute carrier organic anion transporter family, member 1a1	4.06	0.01
Sucnr1	succinate receptor 1	4.02	0.04
Haao	3-hydroxyanthranilate 3,4-dioxygenase	4.02	0.01
Ces1d	carboxylesterase 1D	4.01	0.01
Pbld2	#N/A	4.00	0.03
Cyp8b1	cytochrome P450, family 8, subfamily b, polypeptide 1	3.93	0.02
Mbl2	mannose-binding lectin (protein C) 2	3.93	0.02
Ces1e	carboxylesterase 1E	3.86	0.02
Ccl4	chemokine (C-C motif) ligand 4	3.86	0.01
Agxt	alanine-glyoxylate aminotransferase	3.84	0.03
Serpina6	serine (or cysteine) peptidase inhibitor, clade A, member 6	3.83	0.02

Rdh16f2	#N/A	3.83	0.04
Lhpp	phospholysine phosphohistidine inorganic pyrophosphate phosphatase	3.76	0.01
Urad	ureidoimidazoline (2-oxo-4-hydroxy-4- carboxy-5) decarboxylase	3.76	0.03
Adh4	alcohol dehydrogenase 4 (class II), pi polypeptide	3.75	0.02
Ugt2a3	UDP glucuronosyltransferase 2 family, polypeptide A3	3.72	0.02
Ccl3	chemokine (C-C motif) ligand 3	3.71	0.02
Prlr	prolactin receptor	3.70	0.02
Klkb1	kallikrein B, plasma 1	3.66	0.02
Sdr9c7	4short chain dehydrogenase/reductase family 9C, member 7	3.64	0.01
Sult1d1	sulfotransferase family 1D, member 1	3.62	0.00
Ang	angiogenin, ribonuclease, RNase A family, 5	3.62	0.01
Neb	nebulin	3.60	0.04
Lipc	lipase, hepatic	3.59	0.01
Cyp2c70	cytochrome P450, family 2, subfamily c, polypeptide 70	3.58	0.01
Aspdh	aspartate dehydrogenase domain containing	3.55	0.01
Sult1c2	sulfotransferase family, cytosolic, 1C, member 2	3.53	0.02
Nat8f1	#N/A	3.53	0.01
Phlda1	pleckstrin homology-like domain, family A, member 1	3.52	0.02
Abca8a	ATP-binding cassette, sub-family A (ABC1), member 8a	3.51	0.04
Fabp1	fatty acid binding protein 1, liver	3.50	0.03
Csrp3	cysteine and glycine-rich protein 3	3.49	0.00
Gm4952	predicted gene 4952	3.42	0.02
Ces2c	carboxylesterase 2C	3.42	0.01
Scd1	stearoyl-Coenzyme A desaturase 1	3.36	0.03
Gnmt	glycine N-methyltransferase	3.32	0.01
Cyp1a2	cytochrome P450, family 1, subfamily a, polypeptide 2	3.30	0.03
Gbp10	#N/A	3.30	0.02
Gpcpd1	glycerophosphocholine phosphodiesterase GDE1 homolog (S. cerevisiae)	3.26	0.02
Rhbg	Rhesus blood group-associated B glycoprotein	3.25	0.04
Psen2	presenilin 2	3.23	0.01

Slc16a10	solute carrier family 16 (monocarboxylic acid transporters), member 10	3.18	0.02
Abcb11	ATP-binding cassette, sub-family B (MDR/TAP), member 11	3.17	0.03
Slc2a5	solute carrier family 2 (facilitated glucose transporter), member 5	3.14	0.02
Slco1b2	solute carrier organic anion transporter family, member 1b2	3.12	0.01
Cxcl10	chemokine (C-X-C motif) ligand 10	3.11	0.02
Cyp2c39	cytochrome P450, family 2, subfamily c, polypeptide 39	3.06	0.03
Cyp7b1	cytochrome P450, family 7, subfamily b, polypeptide 1	3.06	0.02
Saa4	serum amyloid A 4	3.02	0.04
Gstt3	glutathione S-transferase, theta 3	3.02	0.04
Pde9a	phosphodiesterase 9A	3.02	0.05
Nr0b2	nuclear receptor subfamily 0, group B, member 2	3.00	0.02
Ppm1k	protein phosphatase 1K (PP2C domain containing)	3.00	0.05
Hrg	histidine-rich glycoprotein	2.99	0.03
Hgd	homogentisate 1, 2-dioxygenase	2.98	0.02
Bco2	beta-carotene oxygenase 2	2.98	0.02
Cyp2c68	cytochrome P450, family 2, subfamily c, polypeptide 68	2.97	0.01
Calr3	calreticulin 3	2.95	0.03
Ass1	argininosuccinate synthetase 1	2.95	0.03
Slc17a3	solute carrier family 17 (sodium phosphate), member 3	2.95	0.02
Apon	apolipoprotein N	2.95	0.03
F7	coagulation factor VII	2.93	0.03
Cyp2c67	cytochrome P450, family 2, subfamily c, polypeptide 67	2.89	0.02
Fn3k	fructosamine 3 kinase	2.88	0.05
Igfals	insulin-like growth factor binding protein, acid labile subunit	2.86	0.04
Hpd	4-hydroxyphenylpyruvic acid dioxygenase	2.84	0.03
Adh7	alcohol dehydrogenase 7 (class IV), mu or sigma polypeptide	2.83	0.01
Hmgcs1	3-hydroxy-3-methylglutaryl-Coenzyme A synthase 1	2.81	0.04
D130043K22Rik	RIKEN cDNA D130043K22 gene	2.81	0.02
Rnf125	ring finger protein 125	2.79	0.04
Keg1	kidney expressed gene 1	2.79	0.04

Slc6a12	solute carrier family 6 (neurotransmitter transporter, betaine/GABA), member 12	2.77	0.05
Kyat1	#N/A	2.77	0.04
Phospho1	phosphatase, orphan 1	2.77	0.04
AcsM1	acyl-CoA synthetase medium-chain family member 1	2.76	0.04
Idi1	isopentenyl-diphosphate delta isomerase	2.74	0.02
Otc	ornithine transcarbamylase	2.72	0.03
Tmem254c	transmembrane protein 254c	2.71	0.01
Paox	polyamine oxidase (exo-N4-amino)	2.70	0.02
Slc22a27	solute carrier family 22, member 27	2.70	0.05
Tmem254b	transmembrane protein 254b	2.69	0.01
Cdo1	cysteine dioxygenase 1, cytosolic	2.68	0.02
Hopx	HOP homeobox	2.68	0.01
Prodh2	proline dehydrogenase (oxidase) 2	2.67	0.01
C8g	complement component 8, gamma polypeptide	2.66	0.01
Dpyd	dihydropyrimidine dehydrogenase	2.66	0.05
Gulo	gulonolactone (L-) oxidase	2.64	0.04
Ube2u	ubiquitin-conjugating enzyme E2U (putative)	2.64	0.04
Aldh8a1	aldehyde dehydrogenase 8 family, member A1	2.64	0.03
Lrrc14b	leucine rich repeat containing 14B	2.63	0.02
Ghr	growth hormone receptor	2.63	0.02
Slc22a1	solute carrier family 22 (organic cation transporter), member 1	2.62	0.02
Tmem254a	transmembrane protein 254a	2.58	0.01
Mapk15	mitogen-activated protein kinase 15	2.58	0.03
Pglyrp2	peptidoglycan recognition protein 2	2.55	0.04
Sult1b1	sulfotransferase family 1B, member 1	2.54	0.01
Pcp4l1	Purkinje cell protein 4-like 1	2.54	0.04
Tymp	thymidine phosphorylase	2.52	0.05
Gm9992	predicted gene 9992	2.51	0.04
Cxcl9	chemokine (C-X-C motif) ligand 9	2.51	0.04
Insc	inscuteable homolog (Drosophila)	2.51	0.04
Cyp51	cytochrome P450, family 51	2.51	0.04
Gm36028	#N/A	2.49	0.02
Cyp3a25	cytochrome P450, family 3, subfamily a, polypeptide 25	2.49	0.02
Nnmt	nicotinamide N-methyltransferase	2.49	0.01

Gcgr	glucagon receptor	2.49	0.02
Apoc3	apolipoprotein C-III	2.48	0.00
Fdps	farnesyl diphosphate synthetase	2.48	0.03
Ugt1a2	UDP glucuronosyltransferase 1 family, polypeptide A2	2.46	0.01
BC024139	cDNA sequence BC024139	2.45	0.04
Pecr	peroxisomal trans-2-enoyl-CoA reductase	2.45	0.05
Ces2a	carboxylesterase 2A	2.45	0.04
Inca1	inhibitor of CDK, cyclin A1 interacting protein 1	2.43	0.01
Pon1	paraoxonase 1	2.42	0.01
Ndrp2	N-myc downstream regulated gene 2	2.40	0.05
Nudt7	nudix (nucleoside diphosphate linked moiety X)-type motif 7	2.39	0.01
Rdh16f1	#N/A	2.39	0.03
Tm7sf2	transmembrane 7 superfamily member 2	2.39	0.04
Rdh16	retinol dehydrogenase 16	2.37	0.03
Cmb1	carboxymethylenebutenolidase-like (Pseudomonas)	2.36	0.01
Eif4ebp3	eukaryotic translation initiation factor 4E binding protein 3	2.35	0.05
Spp2	secreted phosphoprotein 2	2.35	0.01
Cyp2j5	cytochrome P450, family 2, subfamily j, polypeptide 5	2.33	0.04
Ugt3a2	UDP glycosyltransferases 3 family, polypeptide A2	2.33	0.03
Ugt2b5	UDP glucuronosyltransferase 2 family, polypeptide B5	2.32	0.03
Gas1	growth arrest specific 1	2.32	0.05
Mup21	major urinary protein 21	2.32	0.03
Asic5	acid-sensing (proton-gated) ion channel family member 5	2.30	0.03
A2ml1	#N/A	2.29	0.04
Gcat	glycine C-acetyltransferase (2-amino-3-ketobutyrate-coenzyme A ligase)	2.29	0.04
Igf1	insulin-like growth factor 1	2.27	0.05
Ptgds	prostaglandin D2 synthase (brain)	2.26	0.03
Mreg	melanoregulin	2.25	0.03
Acmsd	amino carboxymuconate semialdehyde decarboxylase	2.25	0.02
Adh1	alcohol dehydrogenase 1 (class I)	2.25	0.05
Tlcd2	TLC domain containing 2	2.24	0.05
Iigp1	interferon inducible GTPase 1	2.24	0.05

Clec2d	C-type lectin domain family 2, member d	2.22	0.00
Car1	carbonic anhydrase 1	2.21	0.03
Msmo1	methylsterol monooxygenase 1	2.21	0.03
Chchd10	coiled-coil-helix-coiled-coil-helix domain containing 10	2.18	0.04
Trim12a	tripartite motif-containing 12A	2.17	0.03
Asgr1	asialoglycoprotein receptor 1	2.16	0.03
Slc22a29	solute carrier family 22, member 29	2.15	0.01
MLXipl	MLX interacting protein-like	2.13	0.04
Serpina7	serine (or cysteine) peptidase inhibitor, clade A (alpha-1 antiproteinase, antitrypsin), member 7	2.13	0.03
Car8	carbonic anhydrase 8	2.13	0.02
Zfand4	zinc finger, AN1-type domain 4	2.13	0.02
Mfsd4b3	#N/A	2.11	0.04
Mvd	#N/A	2.10	0.05
Sgk2	serum/glucocorticoid regulated kinase 2	2.10	0.04
Dcxr	dicarbonyl L-xylulose reductase	2.08	0.04
Rarres2	retinoic acid receptor responder (tazarotene induced) 2	2.02	0.01
Bcl6b	B cell CLL/lymphoma 6, member B	1.94	0.03
Ccl5	chemokine (C-C motif) ligand 5	1.94	0.04
Tstd3	thiosulfate sulfurtransferase (rhodanese)-like domain containing 3	1.94	0.05
Arrdc1	arrestin domain containing 1	0.50	0.05
Mybl1	myeloblastosis oncogene-like 1	0.50	0.01
Igsf6	immunoglobulin superfamily, member 6	0.50	0.01
Lat2	linker for activation of T cells family, member 2	0.50	0.04
Cdca4	cell division cycle associated 4	0.50	0.02
Lsm3	LSM3 homolog, U6 small nuclear RNA associated (<i>S. cerevisiae</i>)	0.50	0.01
Kitl	kit ligand	0.50	0.05
Pik3c2a	phosphatidylinositol 3-kinase, C2 domain containing, alpha polypeptide	0.50	0.04
Fam118a	family with sequence similarity 118, member A	0.50	0.01
Dck	deoxycytidine kinase	0.50	0.03
Rpl14	ribosomal protein L14	0.50	0.00
Nlrp3	NLR family, pyrin domain containing 3	0.50	0.05
C1qb	complement component 1, q subcomponent, beta polypeptide	0.50	0.04
Rps16	ribosomal protein S16	0.49	0.00

Rbl1	retinoblastoma-like 1 (p107)	0.49	0.03
Tmem237	transmembrane protein 237	0.49	0.03
Lins1	#N/A	0.49	0.03
Sass6	spindle assembly 6 homolog (C. elegans)	0.49	0.05
Bst1	bone marrow stromal cell antigen 1	0.49	0.03
Cenpc1	centromere protein C1	0.49	0.04
I830077J02Rik	RIKEN cDNA I830077J02 gene	0.49	0.03
Pcna	proliferating cell nuclear antigen	0.49	0.01
Prdx5	peroxiredoxin 5	0.49	0.01
Qpct	glutaminy-peptide cyclotransferase (glutaminy cyclase)	0.49	0.04
Lsm4	LSM4 homolog, U6 small nuclear RNA associated (S. cerevisiae)	0.49	0.01
Gemin7	gem (nuclear organelle) associated protein 7	0.49	0.01
Rab2b	RAB2B, member RAS oncogene family	0.49	0.02
Npm1	nucleophosmin 1	0.49	0.01
Apex2	apurinic/aprimidinic endonuclease 2	0.49	0.04
Lyz1	lysozyme 1	0.49	0.01
Tdrp	testis development related protein	0.49	0.04
Exoc6	exocyst complex component 6	0.49	0.03
Tipin	timeless interacting protein	0.49	0.03
Rps27a	ribosomal protein S27A	0.49	0.00
Cd207	CD207 antigen	0.49	0.01
Pcna-ps2	proliferating cell nuclear antigen pseudogene 2	0.49	0.01
Tmem17	transmembrane protein 17	0.49	0.00
Mnat1	menage a trois 1	0.49	0.02
Tctex1d2	Tctex1 domain containing 2	0.49	0.03
Rps15a	ribosomal protein S15A	0.49	0.00
Fam105a	family with sequence similarity 105, member A	0.48	0.01
Rps18	ribosomal protein S18	0.48	0.00
Oxct1	3-oxoacid CoA transferase 1	0.48	0.04
Tsc22d3	TSC22 domain family, member 3	0.48	0.03
Mllt11	myeloid/lymphoid or mixed-lineage leukemia (trithorax homolog, Drosophila); translocated to, 11	0.48	0.05
Zfp322a	zinc finger protein 322A	0.48	0.01
Hist3h2a	histone cluster 3, H2a	0.48	0.01
Rdm1	RAD52 motif 1	0.48	0.01

Eri2	exoribonuclease 2	0.48	0.02
BC147527	cDNA sequence BC147527	0.48	0.01
Eef1b2	eukaryotic translation elongation factor 1 beta 2	0.48	0.00
Gmnn	geminin	0.48	0.00
Nt5c3b	5'-nucleotidase, cytosolic IIIB	0.48	0.01
Sgcb	sarcoglycan, beta (dystrophin-associated glycoprotein)	0.48	0.04
Ggh	gamma-glutamyl hydrolase	0.48	0.00
Zfp449	zinc finger protein 449	0.48	0.03
Topbp1	topoisomerase (DNA) II binding protein 1	0.48	0.04
Rhobtb3	Rho-related BTB domain containing 3	0.48	0.05
Derl3	Der1-like domain family, member 3	0.48	0.03
Zfp40	zinc finger protein 40	0.48	0.01
Snrpe	small nuclear ribonucleoprotein E	0.48	0.00
Lyz2	lysozyme 2	0.48	0.01
Rpl9	ribosomal protein L9	0.48	0.00
1810032O08Rik	RIKEN cDNA 1810032O08 gene	0.48	0.00
Rpl31	ribosomal protein L31	0.48	0.00
Dynlt1a	dynein light chain Tctex-type 1A	0.48	0.00
1-Mar	#N/A	0.48	0.04
Ctss	cathepsin S	0.48	0.03
Ubtd2	ubiquitin domain containing 2	0.48	0.04
Klhl6	kelch-like 6	0.48	0.04
Gpx8	glutathione peroxidase 8 (putative)	0.48	0.00
Tk1	thymidine kinase 1	0.48	0.03
Crip1	cysteine-rich protein 1 (intestinal)	0.47	0.01
Miip	migration and invasion inhibitory protein	0.47	0.04
Zfp808	zinc finger protein 80	0.47	0.02
Hyls1	hydroletharus syndrome 1	0.47	0.01
Plek2	pleckstrin 2	0.47	0.03
Acot1	acyl-CoA thioesterase 1	0.47	0.03
Tusc3	tumor suppressor candidate 3	0.47	0.02
Clec4n	C-type lectin domain family 4, member n	0.47	0.02
Rpl15	ribosomal protein L15	0.47	0.00
Bag2	BCL2-associated athanogene 2	0.47	0.02
Bzw2	basic leucine zipper and W2 domains 2	0.47	0.03
Zfp934	zinc finger protein 934	0.47	0.01

Arl6	ADP-ribosylation factor-like 6	0.47	0.04
Gm9493	predicted gene 9493	0.47	0.00
Apold1	apolipoprotein L domain containing 1	0.47	0.04
Tyrobp	TYRO protein tyrosine kinase binding protein	0.47	0.00
Haus1	HAUS augmin-like complex, subunit 1	0.47	0.00
Bcl2a1d	B cell leukemia/lymphoma 2 related protein A1d	0.47	0.01
Nme4	NME/NM23 nucleoside diphosphate kinase 4	0.47	0.01
Gm33543	#N/A	0.47	0.03
Wsb1	WD repeat and SOCS box-containing 1	0.47	0.02
Rpl3	ribosomal protein L3	0.47	0.00
Rpl9-ps6	ribosomal protein L9, pseudogene 6	0.47	0.00
Tax1bp3	Tax1 (human T cell leukemia virus type I) binding protein 3	0.47	0.02
Nenf	neuron derived neurotrophic factor	0.47	0.00
Hgf	hepatocyte growth factor	0.47	0.05
Mis18a	MIS18 kinetochore protein homolog A (S. pombe)	0.47	0.02
Rpl35	ribosomal protein L35	0.47	0.00
Rbbp8	retinoblastoma binding protein 8	0.47	0.03
Ankrd49	ankyrin repeat domain 49	0.47	0.01
Tuba1a	tubulin, alpha 1A	0.47	0.04
Rps24	ribosomal protein S24	0.47	0.00
Gnb1l	guanine nucleotide binding protein (G protein), beta polypeptide 1-like	0.47	0.04
Platr25	#N/A	0.47	0.01
Rps7	ribosomal protein S7	0.46	0.00
Npl	N-acetylneuraminate pyruvate lyase	0.46	0.03
Siva1	SIVA1, apoptosis-inducing factor	0.46	0.01
Rpl39	ribosomal protein L39	0.46	0.00
Ndc1	NDC1 transmembrane nucleoporin	0.46	0.05
Hddc2	HD domain containing 2	0.46	0.01
Bambi	BMP and activin membrane-bound inhibitor	0.46	0.02
Aoc2	amine oxidase, copper containing 2 (retina-specific)	0.46	0.04
Ifngr1	interferon gamma receptor 1	0.46	0.04
Gdpd3	glycerophosphodiester phosphodiesterase domain containing 3	0.46	0.03
Fam171b	family with sequence similarity 171, member B	0.46	0.03

Taf1d	TATA box binding protein (Tbp)-associated factor, RNA polymerase I, D	0.46	0.00
Hspbap1	Hspb associated protein 1	0.46	0.03
Gm2000	predicted gene 2000	0.46	0.00
Aph1c	anterior pharynx defective 1c homolog (C. elegans)	0.46	0.02
Hat1	histone aminotransferase 1	0.46	0.01
Ncf2	neutrophil cytosolic factor 2	0.46	0.04
Naip5	NLR family, apoptosis inhibitory protein 5	0.46	0.03
Tuba1b	tubulin, alpha 1B	0.46	0.04
Sgce	sarcoglycan, epsilon	0.46	0.03
Arhgap15	Rho GTPase activating protein 15	0.46	0.01
Ncoa7	nuclear receptor coactivator 7	0.46	0.03
Gins1	GIN5 complex subunit 1 (Psf1 homolog)	0.46	0.02
Rfc3	replication factor C (activator 1) 3	0.46	0.00
Atad5	ATPase family, AAA domain containing 5	0.46	0.04
Cd300c2	#N/A	0.46	0.01
Rps8	ribosomal protein S8	0.46	0.00
Unc119	unc-119 homolog (C. elegans)	0.46	0.04
Gen1	Gen homolog 1, endonuclease (Drosophila)	0.46	0.02
Spire1	spire homolog 1 (Drosophila)	0.46	0.05
Naip6	NLR family, apoptosis inhibitory protein 7	0.45	0.03
Rpl32	ribosomal protein L32	0.45	0.00
Hamp	hepcidin antimicrobial peptide	0.45	0.03
P2ry12	purinergic receptor P2Y, G-protein coupled 12	0.45	0.01
Ell3	elongation factor RNA polymerase II-like 3	0.45	0.01
Gm11007	predicted gene 11007	0.45	0.02
Rpp38	ribonuclease P/MRP 38 subunit	0.45	0.00
1500011B03Rik	RIKEN cDNA 1500011B03 gene	0.45	0.00
AB124611	cDNA sequence AB124611	0.45	0.01
Psph	phosphoserine phosphatase	0.45	0.01
Tnfaip8	tumor necrosis factor, alpha-induced protein 8	0.45	0.01
Ear2	eosinophil-associated, ribonuclease A family, member 2	0.45	0.02
Gmfg	glia maturation factor, gamma	0.45	0.00

Rgs2	regulator of G-protein signaling 2	0.45	0.01
Vsig10l	ZV-set and immunoglobulin domain containing 10 like	0.45	0.04
Zfp90	zinc finger protein 90	0.45	0.03
Cd300lf	CD300 antigen like family member F	0.45	0.05
Zfp821	zinc finger protein 821	0.45	0.04
Gm10269	predicted gene 10269	0.45	0.00
Ngf	nerve growth factor	0.45	0.03
Fam216a	family with sequence similarity 216, member A	0.45	0.01
Tlr8	toll-like receptor 8	0.45	0.04
Rnaseh2b	ribonuclease H2, subunit B	0.45	0.01
Cytip	cytohesin 1 interacting protein	0.45	0.01
Tyms	thymidylate synthase	0.45	0.02
Ccdc77	coiled-coil domain containing 77	0.45	0.02
Gm5141	predicted gene 5141	0.45	0.05
Odc1	ornithine decarboxylase, structural 1	0.44	0.01
Lair1	leukocyte-associated Ig-like receptor 1	0.44	0.01
Acot9	acyl-CoA thioesterase 9	0.44	0.00
Ptpn18	protein tyrosine phosphatase, non-receptor type 18	0.44	0.01
Rcan1	regulator of calcineurin 1	0.44	0.03
E2f2	E2F transcription factor 2	0.44	0.05
Fpr1	formyl peptide receptor 1	0.44	0.02
Jazf1	JAZF zinc finger 1	0.44	0.04
Ltc4s	leukotriene C4 synthase	0.44	0.02
Brip1	BRCA1 interacting protein C-terminal helicase 1	0.44	0.05
Mrps6	mitochondrial ribosomal protein S6	0.44	0.00
Nemp2	#N/A	0.44	0.05
Msh5	mutS homolog 5 (E. coli)	0.44	0.01
Sectm1a	secreted and transmembrane 1A	0.44	0.03
Adgb	androglobin	0.44	0.03
Ulbp1	UL16 binding protein 1	0.44	0.05
Micu3	mitochondrial calcium uptake family, member 3	0.44	0.02
My12b	myosin, light chain 12B, regulatory	0.44	0.04
Dok3	docking protein 3	0.44	0.03
H3f3a	H3 histone, family 3A	0.44	0.02
Skp2	S-phase kinase-associated protein 2 (p45)	0.44	0.02

Sparc	secreted acidic cysteine rich glycoprotein	0.44	0.05
Ppic	peptidylprolyl isomerase C	0.44	0.00
Adgrl3	#N/A	0.44	0.05
Ccdc102a	coiled-coil domain containing 102A	0.44	0.05
Sh3bgrl3	SH3 domain binding glutamic acid-rich protein-like 3	0.44	0.05
Eci2	enoyl-Coenzyme A delta isomerase 2	0.44	0.01
Fam72a	family with sequence similarity 72, member A	0.44	0.01
Htra2	HtrA serine peptidase 2	0.44	0.04
Cklf	chemokine-like factor	0.44	0.00
Tceal9	#N/A	0.44	0.00
Ctnnbip1	catenin beta interacting protein 1	0.44	0.04
Cpt1c	carnitine palmitoyltransferase 1c	0.44	0.04
Stx1a	syntaxin 1A (brain)	0.44	0.05
BC028528	cDNA sequence BC028528	0.44	0.00
Trpc1	transient receptor potential cation channel, subfamily C, member 1	0.43	0.03
Ift43	intraflagellar transport 43	0.43	0.04
Smim6	small integral membrane protein 6	0.43	0.01
Dok2	docking protein 2	0.43	0.02
Tmem191c	transmembrane protein 191C	0.43	0.05
H2-Q1	histocompatibility 2, Q region locus 1	0.43	0.04
Gm28285	NA	0.43	0.00
Rnaseh2a	ribonuclease H2, large subunit	0.43	0.02
Mindy4	#N/A	0.43	0.04
Rps19	ribosomal protein S19	0.43	0.00
Rhebl1	Ras homolog enriched in brain like 1	0.43	0.04
Tmsb15l	thymosin beta 15b like	0.43	0.00
Abcc5	ATP-binding cassette, sub-family C (CFTR/MRP), member 5	0.43	0.04
Sccpdh	saccharopine dehydrogenase (putative)	0.43	0.01
Clec10a	C-type lectin domain family 10, member A	0.43	0.01
Serpina3i	serine (or cysteine) peptidase inhibitor, clade A, member 3I	0.43	0.04
Dynll1	dynein light chain LC8-type 1	0.43	0.02
Pla2g12a	phospholipase A2, group XIIA	0.43	0.03
Dse	dermatan sulfate epimerase	0.43	0.02
Dynlt1f	dynein light chain Tctex-type 1F	0.42	0.00

Il18rap	interleukin 18 receptor accessory protein	0.42	0.03
Ms4a6d	membrane-spanning 4-domains, subfamily A, member 6D	0.42	0.00
Nrep	neuronal regeneration related protein	0.42	0.01
Myc	myelocytomatosis oncogene	0.42	0.04
Ctsk	cathepsin K	0.42	0.02
Flywch2	FLYWCH family member 2	0.42	0.00
Slc25a43	solute carrier family 25, member 43	0.42	0.05
C1qtnf12	#N/A	0.42	0.00
B9d1	B9 protein domain 1	0.42	0.01
Ube2s	ubiquitin-conjugating enzyme E2S	0.42	0.01
Zfp697	zinc finger protein 697	0.42	0.02
Ly6d	lymphocyte antigen 6 complex, locus D	0.42	0.02
Prim1	DNA primase, p49 subunit	0.42	0.00
Tm4sf4	transmembrane 4 superfamily member 4	0.42	0.01
Ntpcr	nucleoside-triphosphatase, cancer-related	0.42	0.01
Mtbp	Mdm2, transformed 3T3 cell double minute p53 binding protein	0.42	0.01
Klhd8b	kelch domain containing 8B	0.42	0.05
Pdgfc	platelet-derived growth factor, C polypeptide	0.42	0.05
Sertad1	SERTA domain containing 1	0.42	0.01
Fam102b	family with sequence similarity 102, member B	0.42	0.04
Fabp7	fatty acid binding protein 7, brain	0.41	0.01
Ccdc68	coiled-coil domain containing 68	0.41	0.01
Mcm7	minichromosome maintenance deficient 7 (<i>S. cerevisiae</i>)	0.41	0.03
Tagap	T cell activation Rho GTPase activating protein	0.41	0.03
Dusp4	dual specificity phosphatase 4	0.41	0.05
Hist1h4m	histone cluster 1, H4m	0.41	0.00
Tspan17	tetraspanin 17	0.41	0.05
Cysl1r1	cysteinyl leukotriene receptor 1	0.41	0.01
Rack1	#N/A	0.41	0.00
Nmb	neuromedin B	0.41	0.02
Rnf180	ring finger protein 180	0.41	0.04
Cr2	complement receptor 2	0.41	0.02
Ly86	lymphocyte antigen 86	0.41	0.01
Maged2	melanoma antigen, family D, 2	0.41	0.02

Klf10	Kruppel-like factor 10	0.41	0.02
Rgs10	regulator of G-protein signalling 10	0.41	0.00
Trem2	triggering receptor expressed on myeloid cells 2	0.41	0.01
Il33	interleukin 33	0.41	0.03
Mycn	v-myc myelocytomatosis viral related oncogene, neuroblastoma derived (avian)	0.41	0.03
Mcm8	minichromosome maintenance deficient 8 (<i>S. cerevisiae</i>)	0.41	0.01
Sfxn1	sideroflexin 1	0.41	0.03
Cebpd	CCAAT/enhancer binding protein (C/EBP), delta	0.41	0.01
Ap1s2	adaptor-related protein complex 1, sigma 2 subunit	0.41	0.01
Pth1	peptidyl-tRNA hydrolase 1 homolog (<i>S. cerevisiae</i>)	0.41	0.02
Fcgr1	Fc receptor, IgG, high affinity I	0.41	0.03
Fam60a	family with sequence similarity 60, member A	0.40	0.01
Rps25	ribosomal protein S25	0.40	0.05
1810062G17Rik	RIKEN cDNA 1810062G17 gene	0.40	0.00
Cdkn2d	cyclin-dependent kinase inhibitor 2D (p19, inhibits CDK4)	0.40	0.01
Cpeb1	cytoplasmic polyadenylation element binding protein 1	0.40	0.04
Ccdc14	coiled-coil domain containing 14	0.40	0.05
Lrrc75a	leucine rich repeat containing 75A	0.40	0.03
Orc6	origin recognition complex, subunit 6	0.40	0.00
Rgs1	regulator of G-protein signaling 1	0.40	0.01
Cav2	caveolin 2	0.40	0.00
Card9	caspase recruitment domain family, member 9	0.40	0.04
Rapgef1	Rap guanine nucleotide exchange factor (GEF)-like 1	0.40	0.03
Raet1e	retinoic acid early transcript 1E	0.40	0.03
Pcolce2	procollagen C-endopeptidase enhancer 2	0.40	0.04
Tmsb4x	thymosin, beta 4, X chromosome	0.40	0.00
Tef	thyrotroph embryonic factor	0.40	0.03
Rras2	related RAS viral (r-ras) oncogene homolog 2	0.40	0.03
Ptpro	protein tyrosine phosphatase, receptor type, O	0.40	0.03
Vrk1	vaccinia related kinase 1	0.40	0.02

Smc4	structural maintenance of chromosomes 4	0.40	0.02
Prim2	DNA primase, p58 subunit	0.40	0.02
Sla	src-like adaptor	0.40	0.01
Zdhhc2	zinc finger, DHHC domain containing 2	0.40	0.02
Rpl12	ribosomal protein L12	0.39	0.00
Sirpb1b	signal-regulatory protein beta 1B	0.39	0.00
Moap1	modulator of apoptosis 1	0.39	0.02
Fhl2	four and a half LIM domains 2	0.39	0.05
Rps12-ps3	ribosomal protein S12, pseudogene 3	0.39	0.00
Cd63	CD63 antigen	0.39	0.02
B3glct	beta-3-glucosyltransferase	0.39	0.04
Fgd2	FYVE, RhoGEF and PH domain containing 2	0.39	0.02
Rfc4	replication factor C (activator 1) 4	0.39	0.00
Slc22a17	solute carrier family 22 (organic cation transporter), member 17	0.39	0.02
Cep72	centrosomal protein 72	0.39	0.04
Sgk1	serum/glucocorticoid regulated kinase 1	0.39	0.01
Rrp1b	ribosomal RNA processing 1 homolog B (<i>S. cerevisiae</i>)	0.39	0.03
Lpcat2	lysophosphatidylcholine acyltransferase 2	0.39	0.02
Edn1	endothelin 1	0.39	0.04
Arl11	ADP-ribosylation factor-like 11	0.39	0.02
Rps12	ribosomal protein S12	0.39	0.00
Il1r1	interleukin 1 receptor, type I	0.39	0.02
Nrip2	nuclear receptor interacting protein 2	0.38	0.03
Dab1	disabled 1	0.38	0.04
Rab34	RAB34, member RAS oncogene family	0.38	0.02
Xlr	X-linked lymphocyte-regulated	0.38	0.00
Rem1	rad and gem related GTP binding protein 1	0.38	0.04
Cavin2	#N/A	0.38	0.03
Abca9	ATP-binding cassette, sub-family A (ABC1), member 9	0.38	0.04
Adamts12	a disintegrin-like and metalloproteinase (reprolysin type) with thrombospondin type 1 motif, 12	0.38	0.04
Tube1	epsilon-tubulin 1	0.38	0.03
Ncf1	neutrophil cytosolic factor 1	0.38	0.05
Gpx7	glutathione peroxidase 7	0.38	0.01

Nradd	neurotrophin receptor associated death domain	0.38	0.04
D130040H23Rik	RIKEN cDNA D130040H23 gene	0.38	0.01
Atad2	ATPase family, AAA domain containing 2	0.38	0.02
P2rx5	purinergic receptor P2X, ligand-gated ion channel, 5	0.38	0.03
Galk1	galactokinase 1	0.38	0.01
Camk2b	calcium/calmodulin-dependent protein kinase II, beta	0.38	0.05
Lum	lumican	0.38	0.05
Hmgn2	high mobility group nucleosomal binding domain 2	0.38	0.01
Bcl2a1a	B cell leukemia/lymphoma 2 related protein A1a	0.38	0.00
Fkbp10	FK506 binding protein 10	0.38	0.04
Ms4a6b	membrane-spanning 4-domains, subfamily A, member 6B	0.38	0.00
Tnfrsf12a	tumor necrosis factor receptor superfamily, member 12a	0.38	0.00
Spry1	sprouty homolog 1 (Drosophila)	0.38	0.04
Hist2h4	histone cluster 2, H4	0.37	0.00
Myo7a	myosin VIIA	0.37	0.04
Lhx6	LIM homeobox protein 6	0.37	0.05
Ccl2	chemokine (C-C motif) ligand 2	0.37	0.04
Mcf2l	mcf.2 transforming sequence-like	0.37	0.04
Clec4a2	C-type lectin domain family 4, member a2	0.37	0.00
Rundc3b	RUN domain containing 3B	0.37	0.01
Zfr2	zinc finger RNA binding protein 2	0.37	0.04
Per3	period circadian clock 3	0.37	0.03
BC016579	cDNA sequence, BC016579	0.37	0.01
Pkn3	protein kinase N3	0.37	0.04
Ms4a4c	membrane-spanning 4-domains, subfamily A, member 4C	0.37	0.01
Rrm1	ribonucleotide reductase M1	0.37	0.04
Clca3a1	#N/A	0.37	0.01
Txnip	thioredoxin interacting protein	0.37	0.03
Serpinb6b	serine (or cysteine) peptidase inhibitor, clade B, member 6b	0.37	0.02
Prelid2	PRELI domain containing 2	0.37	0.00
Nrg1	neuregulin 1	0.37	0.04
H2afz	H2A histone family, member Z	0.37	0.00

6-Sep	#N/A	0.37	0.04
Tmem41a	transmembrane protein 41a	0.37	0.02
Klra2	killer cell lectin-like receptor, subfamily A, member 2	0.37	0.00
Gfra2	glial cell line derived neurotrophic factor family receptor alpha 2	0.37	0.03
Cdc25b	cell division cycle 25B	0.37	0.05
Pdk3	pyruvate dehydrogenase kinase, isoenzyme 3	0.37	0.02
Rab31	RAB31, member RAS oncogene family	0.37	0.02
Rpl22l1	ribosomal protein L22 like 1	0.37	0.00
Pck2	phosphoenolpyruvate carboxykinase 2 (mitochondrial)	0.37	0.04
Wdhd1	WD repeat and HMG-box DNA binding protein 1	0.37	0.01
Ctla2b	cytotoxic T lymphocyte-associated protein 2 beta	0.36	0.00
Papss1	3'-phosphoadenosine 5'-phosphosulfate synthase 1	0.36	0.04
Hist3h2ba	histone cluster 3, H2ba	0.36	0.03
Gpsm1	G-protein signalling modulator 1 (AGS3-like, <i>C. elegans</i>)	0.36	0.03
Mcub	#N/A	0.36	0.04
Pdlim2	PDZ and LIM domain 2	0.36	0.01
Peg3	paternally expressed 3	0.36	0.03
Tmsb10	thymosin, beta 10	0.36	0.00
Bcl2	B cell leukemia/lymphoma 2	0.36	0.03
Pole2	polymerase (DNA directed), epsilon 2 (p59 subunit)	0.36	0.00
Dbf4	DBF4 homolog (<i>S. cerevisiae</i>)	0.36	0.01
Gcnt1	glucosaminyl (N-acetyl) transferase 1, core 2	0.36	0.02
Nlrc4	NLR family, CARD domain containing 4	0.35	0.01
Vps37d	vacuolar protein sorting 37D (yeast)	0.35	0.04
Mms22l	MMS22-like, DNA repair protein	0.35	0.01
Impa2	inositol (myo)-1(or 4)-monophosphatase 2	0.35	0.02
Serpinb6a	serine (or cysteine) peptidase inhibitor, clade B, member 6a	0.35	0.00
Csf2rb	colony stimulating factor 2 receptor, beta, low-affinity (granulocyte-macrophage)	0.35	0.04
Angptl4	angiopoietin-like 4	0.35	0.02
Kdelr3	KDEL (Lys-Asp-Glu-Leu) endoplasmic reticulum protein retention receptor 3	0.35	0.02

Itgae	integrin alpha E, epithelial-associated	0.35	0.02
Fstl1	folliculin-like 1	0.35	0.04
Atp6v0e2	ATPase, H ⁺ transporting, lysosomal V0 subunit E2	0.35	0.02
Mcm4	minichromosome maintenance deficient 4 homolog (S. cerevisiae)	0.35	0.05
Zc2hc1a	zinc finger, C2HC-type containing 1A	0.35	0.01
Tm6sf1	transmembrane 6 superfamily member 1	0.35	0.03
Gm9780	predicted gene 9780	0.35	0.00
Pla2g7	phospholipase A2, group VII (platelet-activating factor acetylhydrolase, plasma)	0.35	0.00
Gm5148	predicted gene 5148	0.35	0.02
Hist2h2ab	histone cluster 2, H2ab	0.35	0.00
Gm5150	predicted gene 5150	0.34	0.00
Corin	corin	0.34	0.04
Tmem136	transmembrane protein 136	0.34	0.04
Plac9b	placenta specific 9b	0.34	0.01
Myzap	myocardial zonula adherens protein	0.34	0.02
F3	coagulation factor III	0.34	0.04
Xrcc2	X-ray repair complementing defective repair in Chinese hamster cells 2	0.34	0.01
Sirpb1c	NA	0.34	0.02
Phlda3	pleckstrin homology-like domain, family A, member 3	0.34	0.04
Tstd1	thiosulfate sulfurtransferase (rhodanese)-like domain containing 1	0.34	0.00
Prmt2	protein arginine N-methyltransferase 2	0.34	0.03
Fen1	flap structure specific endonuclease 1	0.34	0.03
Pafah1b3	platelet-activating factor acetylhydrolase, isoform 1b, subunit 3	0.34	0.00
Plscr2	phospholipid scramblase 2	0.34	0.00
Gm10282	predicted pseudogene 10282	0.34	0.00
Ms4a6c	membrane-spanning 4-domains, subfamily A, member 6C	0.34	0.00
Mpped2	metallophosphoesterase domain containing 2	0.34	0.02
Grhl2	grainyhead-like 2 (Drosophila)	0.34	0.02
Sdsl	serine dehydratase-like	0.34	0.04
Specc1	sperm antigen with calponin homology and coiled-coil domains 1	0.34	0.04
Arhgap22	Rho GTPase activating protein 22	0.34	0.04
Gm20503	NA	0.34	0.03

Palb2	partner and localizer of BRCA2	0.34	0.01
Pdlim4	PDZ and LIM domain 4	0.34	0.02
Cenpq	centromere protein Q	0.33	0.00
Veph1	ventricular zone expressed PH domain-containing 1	0.33	0.04
Lrrc1	leucine rich repeat containing 1	0.33	0.01
Mbd4	methyl-CpG binding domain protein 4	0.33	0.01
Lmnb1	lamin B1	0.33	0.04
Cd33	CD33 antigen	0.33	0.01
Rin1	Ras and Rab interactor 1	0.33	0.01
Bhlhb9	basic helix-loop-helix domain containing, class B9	0.33	0.03
Tnfaip8l2	tumor necrosis factor, alpha-induced protein 8-like 2	0.33	0.00
Cenpw	centromere protein W	0.33	0.00
Dync2li1	dynein cytoplasmic 2 light intermediate chain 1	0.33	0.03
Bmp4	bone morphogenetic protein 4	0.33	0.03
Lgals4	lectin, galactose binding, soluble 4	0.33	0.00
Cd209a	CD209a antigen	0.33	0.01
Hist2h2ac	histone cluster 2, H2ac	0.33	0.00
Kcne3	potassium voltage-gated channel, Isk-related subfamily, gene 3	0.33	0.00
Slfn9	schlafen 9	0.33	0.03
Dbp	D site albumin promoter binding protein	0.33	0.03
Fancb	Fanconi anemia, complementation group B	0.33	0.01
Hist1h4j	histone cluster 1, H4j	0.33	0.00
B4galt6	UDP-Gal:betaGlcNAc beta 1,4-galactosyltransferase, polypeptide 6	0.33	0.04
Gm609	predicted gene 609	0.33	0.05
P3h4	#N/A	0.33	0.01
Eps8	epidermal growth factor receptor pathway substrate 8	0.33	0.02
Mturn	maturin, neural progenitor differentiation regulator homolog (Xenopus)	0.33	0.02
Mcm2	modifier of chinchilla-mottled 2	0.33	0.04
Kif24	kinesin family member 24	0.33	0.01
Alox5ap	arachidonate 5-lipoxygenase activating protein	0.32	0.01
Acot2	acyl-CoA thioesterase 2	0.32	0.02
Ms4a4a	membrane-spanning 4-domains, subfamily A, member 4A	0.32	0.02

Poc1a	POC1 centriolar protein homolog A (Chlamydomonas)	0.32	0.01
Wdr62	WD repeat domain 62	0.32	0.02
Plat	plasminogen activator, tissue	0.32	0.02
Smim3	small integral membrane protein 3	0.32	0.00
Chek2	checkpoint kinase 2	0.32	0.00
Schip1	predicted gene, 21949	0.32	0.03
Arhgap19	Rho GTPase activating protein 19	0.32	0.01
Hells	helicase, lymphoid specific	0.32	0.01
Slc25a24	solute carrier family 25 (mitochondrial carrier, phosphate carrier), member 24	0.32	0.05
Lgals1	lectin, galactose binding, soluble 1	0.32	0.00
Slc25a4	solute carrier family 25 (mitochondrial carrier, adenine nucleotide translocator), member 4	0.32	0.01
Hist1h4k	histone cluster 1, H4k	0.32	0.01
Pkmyt1	protein kinase, membrane associated tyrosine/threonine 1	0.31	0.02
Wfdc2	WAP four-disulfide core domain 2	0.31	0.01
Gm9844	predicted pseudogene 9844	0.31	0.00
Hilpda	hypoxia inducible lipid droplet associated	0.31	0.00
Sh2d1b1	SH2 domain containing 1B1	0.31	0.01
Ifnlr1	interferon lambda receptor 1	0.31	0.05
Cfap43	cilia and flagella associated protein 43	0.31	0.04
Enah	enabled homolog (Drosophila)	0.31	0.03
Dzip1l	DAZ interacting protein 1-like	0.31	0.04
Gm9922	predicted gene 9922	0.31	0.01
Tagln	transgelin	0.31	0.00
Ccdc158	coiled-coil domain containing 158	0.31	0.00
Cdc45	cell division cycle 45	0.31	0.01
Tamm41	TAM41, mitochondrial translocator assembly and maintenance protein, homolog (S. cerevisiae)	0.31	0.01
Hsd17b13	hydroxysteroid (17-beta) dehydrogenase 13	0.31	0.01
Plac9a	placenta specific 9a	0.31	0.00
Susd3	sushi domain containing 3	0.31	0.01
Rcan3	regulator of calcineurin 3	0.31	0.02
Ccl6	chemokine (C-C motif) ligand 6	0.31	0.00
Fkbp1b	FK506 binding protein 1b	0.31	0.02
Nrtn	neurturin	0.31	0.00

Selenoh	#N/A	0.31	0.00
Phldb1	pleckstrin homology-like domain, family B, member 1	0.30	0.04
Pmp22	peripheral myelin protein 22	0.30	0.03
Plid6	phospholipase D family, member 6	0.30	0.02
Kazn	kazrin, periplakin interacting protein	0.30	0.01
Tspan6	tetraspanin 6	0.30	0.00
Selenbp2	selenium binding protein 2	0.30	0.03
Fam174b	family with sequence similarity 174, member B	0.30	0.03
Slc7a6	solute carrier family 7 (cationic amino acid transporter, γ^+ system), member 6	0.30	0.02
Pkhd1	polycystic kidney and hepatic disease 1	0.30	0.05
Rnf32	ring finger protein 32	0.30	0.01
Hacd4	#N/A	0.30	0.00
9530077C05Rik	RIKEN cDNA 9530077C05 gene	0.30	0.04
Gm2007	predicted gene 2007	0.30	0.01
Slc30a3	solute carrier family 30 (zinc transporter), member 3	0.30	0.02
Nucb2	nucleobindin 2	0.30	0.04
Epdr1	ependymin related protein 1 (zebrafish)	0.29	0.01
My12a	myosin, light chain 12A, regulatory, non-sarcomeric	0.29	0.01
Mapk13	mitogen-activated protein kinase 13	0.29	0.01
Tmem119	transmembrane protein 119	0.29	0.05
Anxa3	annexin A3	0.29	0.00
8-Sep	#N/A	0.29	0.05
Agpat4	1-acylglycerol-3-phosphate O-acyltransferase 4 (lysophosphatidic acid acyltransferase, delta)	0.29	0.02
Ccdc18	coiled-coil domain containing 18	0.29	0.01
P4ha2	procollagen-proline, 2-oxoglutarate 4-dioxygenase (proline 4-hydroxylase), alpha II polypeptide	0.29	0.03
Fry	furry homolog (Drosophila)	0.29	0.04
Fcgr3	Fc receptor, IgG, low affinity III	0.29	0.00
Yap1	yes-associated protein 1	0.29	0.05
Cenpk	centromere protein K	0.29	0.00
Ms4a8a	membrane-spanning 4-domains, subfamily A, member 8A	0.29	0.00
BC034090	cDNA sequence BC034090	0.29	0.04
Eps8l1	EPS8-like 1	0.29	0.01

H2afx	H2A histone family, member X	0.29	0.01
Mcm6	minichromosome maintenance deficient 6 (MIS5 homolog, <i>S. pombe</i>) (<i>S. cerevisiae</i>)	0.29	0.02
Anxa2	annexin A2	0.29	0.02
Wfdc3	WAP four-disulfide core domain 3	0.29	0.00
Nrg4	neuregulin 4	0.29	0.02
Zgrf1	zinc finger, GRF-type containing 1	0.29	0.01
Fbxo5	F-box protein 5	0.29	0.00
Tmsb15b1	thymosin beta 15b1	0.29	0.00
Krt23	keratin 23	0.29	0.02
Pdzk1ip1	PDZK1 interacting protein 1	0.29	0.01
Dapp1	dual adaptor for phosphotyrosine and 3-phosphoinositides 1	0.28	0.01
S100a4	S100 calcium binding protein A4	0.28	0.00
Kcnh7	potassium voltage-gated channel, subfamily H (eag-related), member 7	0.28	0.03
Tmem150b	transmembrane protein 150B	0.28	0.02
Vldlr	very low density lipoprotein receptor	0.28	0.02
Asns	asparagine synthetase	0.28	0.01
Gnai1	guanine nucleotide binding protein (G protein), alpha inhibiting 1	0.28	0.02
Rad18	RAD18 E3 ubiquitin protein ligase	0.28	0.00
Ssbp2	single-stranded DNA binding protein 2	0.28	0.00
Ccr2	chemokine (C-C motif) receptor 2	0.28	0.00
Lmcd1	LIM and cysteine-rich domains 1	0.28	0.03
6720489N17Rik	RIKEN cDNA 6720489N17 gene	0.28	0.00
Gm6169	predicted gene 6169	0.28	0.03
Tcte2	t-complex-associated testis expressed 2	0.28	0.02
Syng1	synaptogyrin 1	0.28	0.00
Amotl2	angiomin-like 2	0.28	0.01
Tgfb2	transforming growth factor, beta 2	0.28	0.04
Hist1h3e	histone cluster 1, H3e	0.28	0.00
Hist1h4b	histone cluster 1, H4b	0.27	0.00
Hist1h4n	histone cluster 1, H4n	0.27	0.00
Chaf1b	chromatin assembly factor 1, subunit B (p60)	0.27	0.02
Fam81a	family with sequence similarity 81, member A	0.27	0.03
Ncapg2	non-SMC condensin II complex, subunit G2	0.27	0.01

Relt	RELt tumor necrosis factor receptor	0.27	0.03
Pdgfrl	platelet-derived growth factor receptor-like	0.27	0.04
Fkbp11	FK506 binding protein 11	0.27	0.00
Ihh	Indian hedgehog	0.27	0.02
Prrg4	proline rich Gla (G-carboxyglutamic acid) 4 (transmembrane)	0.27	0.04
Tmem221	transmembrane protein 221	0.27	0.03
Them6	thioesterase superfamily member 6	0.27	0.01
Wisp2	WNT1 inducible signaling pathway protein 2	0.27	0.04
Tmem246	transmembrane protein 246	0.27	0.02
Haspin	#N/A	0.27	0.02
Cep112	centrosomal protein 112	0.27	0.00
Dab2	disabled 2, mitogen-responsive phosphoprotein	0.27	0.03
Plp2	proteolipid protein 2	0.27	0.03
Trpv4	transient receptor potential cation channel, subfamily V, member 4	0.27	0.05
Cdca7l	cell division cycle associated 7 like	0.27	0.02
Zfp57	zinc finger protein 57	0.27	0.01
Stk17b	serine/threonine kinase 17b (apoptosis-inducing)	0.27	0.00
Cep295nl	#N/A	0.26	0.01
Ddit4	DNA-damage-inducible transcript 4	0.26	0.02
Hist1h2ba	histone cluster 1, H2ba	0.26	0.00
Tcf19	transcription factor 19	0.26	0.03
Tuft1	tuftelin 1	0.26	0.02
Htra3	HtrA serine peptidase 3	0.26	0.02
Zfp850	zinc finger protein 850	0.26	0.04
Trim34b	tripartite motif-containing 34B	0.26	0.00
Il1rl2	interleukin 1 receptor-like 2	0.26	0.01
Enc1	ectodermal-neural cortex 1	0.26	0.04
Vill	villin-like	0.26	0.03
Rasd1	RAS, dexamethasone-induced 1	0.26	0.01
Adcy1	adenylate cyclase 1	0.26	0.03
Ajuba	ajuba LIM protein	0.25	0.02
Milr1	mast cell immunoglobulin like receptor 1	0.25	0.00
S100a6	S100 calcium binding protein A6 (calcyclin)	0.25	0.00
Cox6b2	cytochrome c oxidase subunit VIb polypeptide 2	0.25	0.00

Lig1	ligase I, DNA, ATP-dependent	0.25	0.04
E2f7	E2F transcription factor 7	0.25	0.04
2610524H06Rik	RIKEN cDNA 2610524H06 gene	0.25	0.00
Pycr1	pyrroline-5-carboxylate reductase 1	0.25	0.02
Hmgb2	high mobility group box 2	0.25	0.00
Ccnf	cyclin F	0.25	0.02
Ptgr1	prostaglandin reductase 1	0.25	0.01
Tesmin	#N/A	0.25	0.02
Eda2r	ectodysplasin A2 receptor	0.25	0.05
Id1	inhibitor of DNA binding 1	0.25	0.01
Syce2	synaptonemal complex central element protein 2	0.25	0.00
Nrm	nurim (nuclear envelope membrane protein)	0.25	0.02
Ccdc34	coiled-coil domain containing 34	0.25	0.01
Tgif2	TGFB-induced factor homeobox 2	0.25	0.00
Plk4	polo-like kinase 4	0.25	0.00
Col23a1	collagen, type XXIII, alpha 1	0.25	0.03
Afp	alpha fetoprotein	0.25	0.01
Spint1	serine protease inhibitor, Kunitz type 1	0.25	0.03
Mthfd1l	methylenetetrahydrofolate dehydrogenase (NADP+ dependent) 1-like	0.24	0.00
Hist1h2br	histone cluster 1 H2br	0.24	0.03
Crym	crystallin, mu	0.24	0.02
Smc2	structural maintenance of chromosomes 2	0.24	0.01
Jdp2	Jun dimerization protein 2	0.24	0.01
Hist1h2ac	histone cluster 1, H2ac	0.24	0.00
Rbm3	RNA binding motif protein 3	0.24	0.00
Ccne1	cyclin E1	0.24	0.01
Ikzf4	IKAROS family zinc finger 4	0.24	0.03
Cks1b	CDC28 protein kinase 1b	0.24	0.00
L3mbtl1	l(3)mbt-like (Drosophila)	0.24	0.01
Zfp651	zinc finger protein 651	0.23	0.03
4930579G24Rik	RIKEN cDNA 4930579G24 gene	0.23	0.00
Usp2	ubiquitin specific peptidase 2	0.23	0.02
Ypel1	yippee-like 1 (Drosophila)	0.23	0.01
Gadd45b	growth arrest and DNA-damage-inducible 45 beta	0.23	0.01

Pkia	protein kinase inhibitor, alpha	0.23	0.00
Ranbp17	RAN binding protein 17	0.23	0.03
Hist1h2bg	histone cluster 1, H2bg	0.23	0.00
Ddah2	dimethylarginine dimethylaminohydrolase 2	0.23	0.02
Ncapd2	non-SMC condensin I complex, subunit D2	0.23	0.01
Syt9	synaptotagmin IX	0.23	0.03
Tet1	tet methylcytosine dioxygenase 1	0.23	0.00
Igdcc4	immunoglobulin superfamily, DCC subclass, member 4	0.23	0.04
Cenpa	centromere protein A	0.23	0.00
Pole	polymerase (DNA directed), epsilon	0.23	0.03
Chn1	chimerin 1	0.23	0.04
Hspb2	heat shock protein 2	0.23	0.00
Klc3	kinesin light chain 3	0.23	0.03
Mapk8ip1	mitogen-activated protein kinase 8 interacting protein 1	0.23	0.02
Eif3j2	eukaryotic translation initiation factor 3, subunit J2	0.23	0.03
Vcan	versican	0.23	0.04
Ranbp3l	RAN binding protein 3-like	0.22	0.00
Prune2	prune homolog 2 (Drosophila)	0.22	0.02
Tead4	TEA domain family member 4	0.22	0.03
Hspa12a	heat shock protein 12A	0.22	0.03
Acta2	actin, alpha 2, smooth muscle, aorta	0.22	0.03
Bicc1	bicaudal C homolog 1 (Drosophila)	0.22	0.04
P4htm	prolyl 4-hydroxylase, transmembrane (endoplasmic reticulum)	0.22	0.03
Olfm2	olfactomedin 2	0.22	0.03
Chaf1a	chromatin assembly factor 1, subunit A (p150)	0.22	0.04
Trip13	thyroid hormone receptor interactor 13	0.22	0.00
Glpr2	GLI pathogenesis-related 2	0.22	0.01
Sgpp2	sphingosine-1-phosphate phosphatase 2	0.22	0.04
Incenp	inner centromere protein	0.22	0.02
Cenpn	centromere protein N	0.22	0.01
Per1	period circadian clock 1	0.22	0.02
BC055324	cDNA sequence BC055324	0.22	0.01
Fxyd3	FXDY domain-containing ion transport regulator 3	0.22	0.00
Arhgap11a	Rho GTPase activating protein 11A	0.22	0.01

Dsn1	DSN1, MIND kinetochore complex component, homolog (<i>S. cerevisiae</i>)	0.22	0.01
Bdh2	NA	0.22	0.00
Ctps	cytidine 5'-triphosphate synthase	0.22	0.01
Timp2	tissue inhibitor of metalloproteinase 2	0.21	0.04
Ogn	osteoglycin	0.21	0.02
Tnfaip6	tumor necrosis factor alpha induced protein 6	0.21	0.00
Ctxn1	cortexin 1	0.21	0.03
Mybl2	myeloblastosis oncogene-like 2	0.21	0.04
Hist1h4a	histone cluster 1, H4a	0.21	0.00
Hist1h1d	histone cluster 1, H1d	0.21	0.00
Timp1	tissue inhibitor of metalloproteinase 1	0.21	0.01
C1qtnf6	C1q and tumor necrosis factor related protein 6	0.21	0.02
Ror1	receptor tyrosine kinase-like orphan receptor 1	0.21	0.02
Ska2	spindle and kinetochore associated complex subunit 2	0.21	0.00
Ltk	leukocyte tyrosine kinase	0.20	0.05
Arhgap33	Rho GTPase activating protein 33	0.20	0.01
Slc15a2	solute carrier family 15 (H ⁺ /peptide transporter), member 2	0.20	0.01
Ankrd29	ankyrin repeat domain 29	0.20	0.00
Ccne2	cyclin E2	0.20	0.00
Ager	advanced glycosylation end product-specific receptor	0.20	0.03
Cd163	CD163 antigen	0.20	0.04
Ddias	DNA damage-induced apoptosis suppressor	0.20	0.00
Fcrls	Fc receptor-like S, scavenger receptor	0.20	0.00
Gstm5	glutathione S-transferase, mu 5	0.20	0.00
Ankrd37	ankyrin repeat domain 37	0.20	0.00
Hist1h4f	histone cluster 1, H4f	0.20	0.00
Ppp1r3g	protein phosphatase 1, regulatory (inhibitor) subunit 3G	0.20	0.01
Dio3	deiodinase, iodothyronine type III	0.20	0.02
AA986860	expressed sequence AA986860	0.20	0.02
Hist1h3f	histone cluster 1, H3f	0.20	0.00
Efna4	ephrin A4	0.19	0.03
Ube2t	ubiquitin-conjugating enzyme E2T (putative)	0.19	0.00
Bora	bora, aurora kinase A activator	0.19	0.01

Rims2	regulating synaptic membrane exocytosis 2	0.19	0.04
Depdc1b	DEP domain containing 1B	0.19	0.00
Krt7	keratin 7	0.19	0.05
Asf1b	anti-silencing function 1B histone chaperone	0.19	0.01
Gtse1	G two S phase expressed protein 1	0.19	0.01
Trim59	tripartite motif-containing 59	0.19	0.00
Fcgbp	Fc fragment of IgG binding protein	0.19	0.02
Mad2l1	MAD2 mitotic arrest deficient-like 1	0.19	0.00
Hist2h3c2	histone cluster 2, H3c2	0.19	0.01
Tppp3	tubulin polymerization-promoting protein family member 3	0.19	0.01
Kif18a	kinesin family member 18A	0.18	0.00
Nsl1	NSL1, MIND kinetochore complex component, homolog (<i>S. cerevisiae</i>)	0.18	0.01
Fgd3	FYVE, RhoGEF and PH domain containing 3	0.18	0.03
Sema3c	sema domain, immunoglobulin domain (Ig), short basic domain, secreted, (semaphorin) 3C	0.18	0.01
S100a11	S100 calcium binding protein A11	0.18	0.01
Cnksr1	connector enhancer of kinase suppressor of Ras 1	0.18	0.02
Hist1h2ak	histone cluster 1, H2ak	0.18	0.00
Cyp4f18	cytochrome P450, family 4, subfamily f, polypeptide 18	0.18	0.01
Rasl10a	RAS-like, family 10, member A	0.18	0.01
Spc25	SPC25, NDC80 kinetochore complex component, homolog (<i>S. cerevisiae</i>)	0.18	0.01
Nmnat2	nicotinamide nucleotide adenylyltransferase 2	0.18	0.04
Mgl2	macrophage galactose N-acetyl-galactosamine specific lectin 2	0.18	0.01
Chek1	checkpoint kinase 1	0.18	0.00
Ticrr	TOPBP1-interacting checkpoint and replication regulator	0.18	0.01
Tmem151a	transmembrane protein 151A	0.18	0.02
Kif20b	kinesin family member 20B	0.18	0.00
Hebp2	heme binding protein 2	0.17	0.00
Olfml2b	olfactomedin-like 2B	0.17	0.03
Chtf18	CTF18, chromosome transmission fidelity factor 18	0.17	0.01
Hist1h3i	histone cluster 1, H3i	0.17	0.00
Calml4	calmodulin-like 4	0.17	0.00

Rab3b	RAB3B, member RAS oncogene family	0.17	0.01
Fbp2	fructose biphosphatase 2	0.17	0.00
Prph	peripherin	0.17	0.02
Chrnbl	cholinergic receptor, nicotinic, beta polypeptide 1 (muscle)	0.17	0.02
Bard1	BRCA1 associated RING domain 1	0.17	0.01
Hist2h3b	histone cluster 2, H3b	0.17	0.00
Spdl1	spindle apparatus coiled-coil protein 1	0.17	0.01
Hist1h2bf	histone cluster 1, H2bf	0.17	0.00
1810010D01Rik	#N/A	0.17	0.02
A430105119Rik	RIKEN cDNA A430105119 gene	0.17	0.01
Spr1a	small proline-rich protein 1A	0.17	0.01
Slc35f2	solute carrier family 35, member F2	0.17	0.02
Gpr141	G protein-coupled receptor 141	0.17	0.00
Hist1h3h	histone cluster 1, H3h	0.17	0.00
Tedc1	#N/A	0.17	0.01
Rgs11	regulator of G-protein signaling 11	0.17	0.01
Scube3	signal peptide, CUB domain, EGF-like 3	0.16	0.04
Adamdec1	ADAM-like, decysin 1	0.16	0.00
Cgref1	cell growth regulator with EF hand domain 1	0.16	0.00
Ptgfr	prostaglandin F receptor	0.16	0.01
Klf5	Kruppel-like factor 5	0.16	0.05
Rrm2	ribonucleotide reductase M2	0.16	0.01
Cbr3	carbonyl reductase 3	0.16	0.00
Pde6c	phosphodiesterase 6C, cGMP specific, cone, alpha prime	0.16	0.00
Polq	polymerase (DNA directed), theta	0.16	0.04
Dtna	dystrobrevin alpha	0.16	0.01
Hist1h3d	histone cluster 1, H3d	0.16	0.00
Fads3	fatty acid desaturase 3	0.16	0.02
Gins2	#N/A	0.16	0.00
Tacc3	transforming, acidic coiled-coil containing protein 3	0.16	0.00
C330027C09Rik	RIKEN cDNA C330027C09 gene	0.16	0.00
1810010H24Rik	RIKEN cDNA 1810010H24 gene	0.16	0.03
Mis18bp1	MIS18 binding protein 1	0.15	0.00
Klhc7a	kelch domain containing 7A	0.15	0.02

Mcm5	minichromosome maintenance deficient 5, cell division cycle 46 (<i>S. cerevisiae</i>)	0.15	0.01
Ncaph	non-SMC condensin I complex, subunit H	0.15	0.01
Apoa4	apolipoprotein A-IV	0.15	0.01
Adam33	a disintegrin and metallopeptidase domain 33	0.15	0.02
2310007B03Rik	RIKEN cDNA 2310007B03 gene	0.15	0.02
Cdca8	cell division cycle associated 8	0.15	0.01
Ccr1	chemokine (C-C motif) receptor 1	0.15	0.00
Hist1h3g	histone cluster 1, H3g	0.15	0.00
Mgat4c	MGAT4 family, member C	0.15	0.00
Hist4h4	histone cluster 4, H4	0.15	0.00
Rad51	RAD51 homolog	0.15	0.00
Omd	osteomodulin	0.15	0.00
Clspn	claspin	0.15	0.00
Ankrd1	ankyrin repeat domain 1 (cardiac muscle)	0.15	0.03
Ercc6l	excision repair cross-complementing rodent repair deficiency complementation group 6 like	0.14	0.00
Ctgf	connective tissue growth factor	0.14	0.01
Chrdl1	chordin-like 1	0.14	0.04
Hist1h2bh	histone cluster 1, H2bh	0.14	0.00
B4galt2	UDP-Gal:betaGlcNAc beta 1,4-galactosyltransferase, polypeptide 2	0.14	0.00
Pclaf	#N/A	0.14	0.00
Stmn1	stathmin 1	0.14	0.00
Uhrf1	ubiquitin-like, containing PHD and RING finger domains, 1	0.14	0.02
Fignl1	fidgetin-like 1	0.14	0.00
Rad54l	RAD54 like (<i>S. cerevisiae</i>)	0.14	0.01
Fstl3	follicle-stimulating-like 3	0.14	0.03
Zwilch	zwilch kinetochore protein	0.14	0.00
Kifc5b	kinesin family member C5B	0.14	0.01
Cbr2	carbonyl reductase 2	0.14	0.02
Kif14	kinesin family member 14	0.14	0.01
Hist1h3b	histone cluster 1, H3b	0.13	0.00
Sult2b1	sulfotransferase family, cytosolic, 2B, member 1	0.13	0.01
Hist1h2ab	histone cluster 1, H2ab	0.13	0.00
Hist1h2bn	histone cluster 1, H2bn	0.13	0.00

Cenpe	centromere protein E	0.13	0.02
Traip	TRAF-interacting protein	0.13	0.00
Bub1b	budding uninhibited by benzimidazoles 1 homolog, beta (<i>S. cerevisiae</i>)	0.13	0.01
Aurka	aurora kinase A	0.13	0.00
Efemp1	epidermal growth factor-containing fibulin-like extracellular matrix protein 1	0.13	0.02
Glis2	GLIS family zinc finger 2	0.13	0.02
Espl1	extra spindle pole bodies 1, separase	0.13	0.01
Nkain1	Na ⁺ /K ⁺ transporting ATPase interacting 1	0.13	0.01
Kif23	kinesin family member 23	0.13	0.01
Fam83b	family with sequence similarity 83, member B	0.13	0.01
Hist1h2bl	histone cluster 1, H2bl	0.13	0.00
Rad54b	RAD54 homolog B (<i>S. cerevisiae</i>)	0.13	0.00
Dtl	denticleless homolog (<i>Drosophila</i>)	0.13	0.00
Hist1h3a	histone cluster 1, H3a	0.13	0.00
Hist1h2ae	histone cluster 1, H2ae	0.13	0.00
Slc4a3	solute carrier family 4 (anion exchanger), member 3	0.13	0.02
Rad51ap1	RAD51 associated protein 1	0.13	0.00
Hist1h2bp	histone cluster 1, H2bp	0.13	0.00
Cidec	cell death-inducing DFFA-like effector c	0.13	0.01
Gprc5a	G protein-coupled receptor, family C, group 5, member A	0.13	0.04
Tinag	tubulointerstitial nephritis antigen	0.13	0.00
Hist1h2bk	histone cluster 1, H2bk	0.12	0.00
Oip5	Opa interacting protein 5	0.12	0.00
Hist1h2ag	histone cluster 1, H2ag	0.12	0.00
Lamc2	laminin, gamma 2	0.12	0.03
Lce6a	late cornified envelope 6A	0.12	0.00
Hist1h2ai	histone cluster 1, H2ai	0.12	0.00
Cenps	#N/A	0.12	0.00
Ccnd1	cyclin D1	0.12	0.01
Hist1h2ad	histone cluster 1, H2ad	0.12	0.00
Hist1h2ao	histone cluster 1, H2ao	0.12	0.00
Hist1h2ap	histone cluster 1, H2ap	0.12	0.00
Arhgef39	Rho guanine nucleotide exchange factor (GEF) 39	0.12	0.00
2810408A11Rik	RIKEN cDNA 2810408A11 gene	0.12	0.00

Hist1h2bj	histone cluster 1, H2bj	0.12	0.00
Hist1h2ah	histone cluster 1, H2ah	0.12	0.00
Ttll10	tubulin tyrosine ligase-like family, member 10	0.12	0.01
Fam13c	family with sequence similarity 13, member C	0.12	0.01
Hist1h2bb	histone cluster 1, H2bb	0.12	0.00
Neurl1b	neuralized E3 ubiquitin protein ligase 1B	0.12	0.02
Ect2	ect2 oncogene	0.12	0.00
Fancd2	Fanconi anemia, complementation group D2	0.11	0.00
Pcolce	procollagen C-endopeptidase enhancer protein	0.11	0.02
Phgdh	3-phosphoglycerate dehydrogenase	0.11	0.01
Stil	Scf/Tal1 interrupting locus	0.11	0.00
Fam46b	family with sequence similarity 46, member B	0.11	0.02
Ttc22	tetratricopeptide repeat domain 22	0.11	0.01
Prc1	protein regulator of cytokinesis 1	0.11	0.01
Actr3b	ARP3 actin-related protein 3B	0.11	0.00
Cdca5	cell division cycle associated 5	0.11	0.00
Ppp2r2b	protein phosphatase 2, regulatory subunit B, beta	0.11	0.03
Arnt2	aryl hydrocarbon receptor nuclear translocator 2	0.11	0.05
1700011H14Rik	RIKEN cDNA 1700011H14 gene	0.11	0.00
Kif15	kinesin family member 15	0.11	0.00
Cryab	crystallin, alpha B	0.11	0.01
Hist1h2af	histone cluster 1, H2af	0.11	0.00
Hist2h2bb	histone cluster 2, H2bb	0.10	0.00
Hist1h2an	histone cluster 1, H2an	0.10	0.00
Spag5	sperm associated antigen 5	0.10	0.00
Slit2	slit homolog 2 (Drosophila)	0.10	0.02
Hist1h3c	histone cluster 1, H3c	0.10	0.00
Racgap1	Rac GTPase-activating protein 1	0.10	0.00
Sftpd	surfactant associated protein D	0.10	0.01
Hist1h1a	histone cluster 1, H1a	0.10	0.00
Cdca2	cell division cycle associated 2	0.10	0.00
Sgo2a	#N/A	0.10	0.00
Adamts17	a disintegrin-like and metallopeptidase (reprolysin type) with thrombospondin type 1 motif, 17	0.10	0.00

Pak3	p21 protein (Cdc42/Rac)-activated kinase 3	0.10	0.01
Ankle1	ankyrin repeat and LEM domain containing 1	0.10	0.00
Hist1h2bm	histone cluster 1, H2bm	0.10	0.00
Psat1	phosphoserine aminotransferase 1	0.10	0.00
Kif22	kinesin family member 22	0.10	0.00
Hist1h1b	histone cluster 1, H1b	0.10	0.00
Kn1	#N/A	0.10	0.00
Epn3	epsin 3	0.10	0.02
Exo1	exonuclease 1	0.10	0.02
Arxes2	adipocyte-related X-chromosome expressed sequence 2	0.10	0.01
Cfap44	cilia and flagella associated protein 44	0.10	0.00
Fa2h	fatty acid 2-hydroxylase	0.10	0.01
Kif4	kinesin family member 4	0.10	0.00
Spp1	secreted phosphoprotein 1	0.10	0.01
Nusap1	nucleolar and spindle associated protein 1	0.09	0.00
Diaph3	#N/A	0.09	0.01
Mki67	antigen identified by monoclonal antibody Ki 67	0.09	0.02
Top2a	topoisomerase (DNA) II alpha	0.09	0.01
Ncapg	non-SMC condensin I complex, subunit G	0.09	0.00
Aurkb	aurora kinase B	0.09	0.00
Cdk1	cyclin-dependent kinase 1	0.09	0.00
Kntc1	kinetochore associated 1	0.09	0.01
Neil3	nei like 3 (E. coli)	0.09	0.00
Parm1	prostate androgen-regulated mucin-like protein 1	0.09	0.03
Gsta1	glutathione S-transferase, alpha 1 (Ya)	0.09	0.01
Cep55	centrosomal protein 55	0.09	0.00
H1fx	H1 histone family, member X	0.08	0.04
Klrg2	killer cell lectin-like receptor subfamily G, member 2	0.08	0.02
Prr11	proline rich 11	0.08	0.01
Klra17	killer cell lectin-like receptor, subfamily A, member 17	0.08	0.00
Kifc1	kinesin family member C1	0.08	0.01
Sgo1	#N/A	0.08	0.00
Cenpp	centromere protein P	0.08	0.00

Esco2	establishment of cohesion 1 homolog 2 (<i>S. cerevisiae</i>)	0.08	0.00
Apela	#N/A	0.08	0.01
Anln	anillin, actin binding protein	0.08	0.00
Bub1	budding uninhibited by benzimidazoles 1 homolog (<i>S. cerevisiae</i>)	0.08	0.00
Scn7a	sodium channel, voltage-gated, type VII, alpha	0.08	0.01
Stc2	stanniocalcin 2	0.08	0.01
Ube2c	ubiquitin-conjugating enzyme E2C	0.08	0.00
Ccl17	chemokine (C-C motif) ligand 17	0.08	0.00
Aspm	asp (abnormal spindle)-like, microcephaly associated (<i>Drosophila</i>)	0.08	0.01
Wnt6	wingless-type MMTV integration site family, member 6	0.08	0.02
Fanca	#N/A	0.08	0.01
Cenpu	centromere protein U	0.08	0.00
Zfp185	zinc finger protein 185	0.08	0.01
Mxd3	Max dimerization protein 3	0.08	0.00
Bex1	brain expressed gene 1	0.07	0.00
Cdkn3	cyclin-dependent kinase inhibitor 3	0.07	0.00
Csrnp3	cysteine-serine-rich nuclear protein 3	0.07	0.00
Pimreg	#N/A	0.07	0.00
Tpx2	TPX2, microtubule-associated protein homolog (<i>Xenopus laevis</i>)	0.07	0.01
Parbbp	PARP1 binding protein	0.07	0.00
Ccnb1	cyclin B1	0.07	0.00
Dlgap5	discs, large (<i>Drosophila</i>) homolog-associated protein 5	0.07	0.00
Capn11	calpain 11	0.07	0.02
Mastl	microtubule associated serine/threonine kinase-like	0.07	0.01
Gpc3	glypican 3	0.07	0.02
Pla2g5	phospholipase A2, group V	0.07	0.01
Knstrn	kinetochore-localized astrin/SPAG5 binding	0.07	0.00
Ndc80	NDC80 homolog, kinetochore complex component (<i>S. cerevisiae</i>)	0.07	0.00
Kif18b	kinesin family member 18B	0.07	0.01
Ccna2	cyclin A2	0.07	0.00
Tmem130	transmembrane protein 130	0.07	0.03
Foxm1	forkhead box M1	0.07	0.01
Fam83d	family with sequence similarity 83, member D	0.07	0.00

Plk1	polo-like kinase 1	0.06	0.01
Psrc1	proline/serine-rich coiled-coil 1	0.06	0.00
Hist1h2be	histone cluster 1, H2be	0.06	0.05
Nuf2	NUF2, NDC80 kinetochore complex component, homolog (<i>S. cerevisiae</i>)	0.06	0.00
Cdca3	cell division cycle associated 3	0.06	0.00
Gm3776	#N/A	0.06	0.01
Pif1	PIF1 5'-to-3' DNA helicase homolog (<i>S. cerevisiae</i>)	0.06	0.00
Kif20a	kinesin family member 20A	0.06	0.00
Ckap2l	cytoskeleton associated protein 2-like	0.06	0.01
Iqgap3	IQ motif containing GTPase activating protein 3	0.06	0.01
Cenph	centromere protein H	0.06	0.00
Mrgprb3	MAS-related GPR, member B3	0.06	0.00
Birc5	baculoviral IAP repeat-containing 5	0.05	0.00
Chst9	carbohydrate (N-acetylgalactosamine 4-O) sulfotransferase 9	0.05	0.00
Cdc20	cell division cycle 20	0.05	0.00
Fanci	Fanconi anemia, complementation group I	0.05	0.00
Cenpf	centromere protein F	0.05	0.01
Kif2c	predicted pseudogene 4961	0.05	0.00
Shcbp1	Shc SH2-domain binding protein 1	0.05	0.00
2900011O08Rik	RIKEN cDNA 2900011O08 gene	0.05	0.01
Fgfbp1	fibroblast growth factor binding protein 1	0.05	0.00
Ifitm7	interferon induced transmembrane protein 7	0.04	0.00
Ckap2	cytoskeleton associated protein 2	0.04	0.00
Pbk	PDZ binding kinase	0.04	0.00
Paqr6	progesterone and adiponectin receptor family member VI	0.04	0.01
Ska1	spindle and kinetochore associated complex subunit 1	0.04	0.00
Tceal5	transcription elongation factor A (SII)-like 5	0.04	0.02
Fam107a	family with sequence similarity 107, member A	0.04	0.01
Mrgprb2	MAS-related GPR, member B2	0.04	0.00
Hmmr	hyaluronan mediated motility receptor (RHAMM)	0.04	0.00
Cdc25c	cell division cycle 25C	0.04	0.01
Ccnb2	cyclin B2	0.04	0.00

Melk	maternal embryonic leucine zipper kinase	0.03	0.00
Klk1b22	kallikrein 1-related peptidase b22	0.03	0.00
Hs3st2	heparan sulfate (glucosamine) 3-O-sulfotransferase 2	0.03	0.01
Troap	trophinin associated protein	0.03	0.01
Krt4	keratin 4	0.03	0.03
Ska3	spindle and kinetochore associated complex subunit 3	0.03	0.00
Ttk	Ttk protein kinase	0.03	0.00
Cenpi	centromere protein I	0.03	0.00
Depdc1a	DEP domain containing 1a	0.03	0.00
Muc13	mucin 13, epithelial transmembrane	0.03	0.01
Asb15	ankyrin repeat and SOCS box-containing 15	0.03	0.02
Gli2	GLI-Kruppel family member GLI2	0.03	0.04
Rbp7	retinol binding protein 7, cellular	0.02	0.00
Dlk2	delta-like 2 homolog (Drosophila)	0.02	0.02
Meig1	meiosis expressed gene 1	0.01	0.00
Spink1	#N/A	0.01	0.00
Gal3st2	galactose-3-O-sulfotransferase 2	0.01	0.00
Igf2bp1	insulin-like growth factor 2 mRNA binding protein 1	0.01	0.01
Psca	prostate stem cell antigen	0.00	0.00

APPENDIX VI HBHEP CELL GENE EXPRESSION

Table A6.1. Top genes downregulated in hbHep cells compared to WT Fah mice. Fold change >2, p<0.05.

GENE	log ₂ FC (hbHep/WT FAH)	p-value
Mup12	-10.9341	0.014889
Serpina4-ps1	-9.76974	0.001569
Mup7	-9.71292	0.04988
Mup19	-9.13001	0.003227
Mup1	-8.43892	0.006537
Mup11	-8.0165	0.005159
Mup17	-7.432	0.004695
Mup9	-7.28374	0.002753
Mup3	-7.16747	0.010285
Selenbp2	-6.94493	0.008428
Mup21	-6.87233	0.044361
Obp2a	-6.74178	0.023833
Gm21320	-6.50443	0.006204
Gm8893	-6.37885	0.00236
Mup16	-6.19085	0.002144
Mup14	-6.1701	0.005054
Capn8	-6.15655	0.002429
Cyp2b10	-6.05286	0.000376
Obox4-ps3	-5.99797	0.000389
Htr1d	-5.97285	0.00044
Mup20	-5.75433	0.012994
Mup13	-5.74294	0.008958
Mup2	-5.66416	0.007254
Mup-ps28	-5.50328	0.000178
Slc13a2	-5.44457	0.002057
Sult5a1	-5.43206	0.011464
Cnmd	-5.36754	0.003489
Mup10	-5.20677	0.001722
Wfdc21	-5.20463	0.002437
1810046K07Rik	-5.16102	0.000176
Gm10319	-4.99041	2.72E-07
Cyp2f2	-4.8854	1.58E-05
Obox4-ps1	-4.84706	0.00632

Lmod2	-4.82225	0.008566
Sult2a8	-4.80735	0.003726
Gm11340	-4.80571	0.00705
Scgb1c1	-4.78827	0.01958
Serpina1c	-4.7762	0.001111
Gm13559	-4.76064	0.008024
Gm20523	-4.6977	0.026389
Enho	-4.68796	0.006739
Mup-ps19	-4.6861	0.00194
Mup18	-4.68247	0.0179
Gm8941	-4.62931	0.00211
Cyp8b1	-4.57399	0.000603
Gm11341	-4.55664	0.025523
Gm7656	-4.52531	0.010738
Gtpbp4-ps1	-4.50647	0.021309
C9	-4.4866	0.004496
Bdh2	-4.47672	0.000922
Wisp3	-4.4693	0.004343
Olfm3	-4.46061	0.001519
AL772386.1	-4.37207	0.011281
Tdrd1	-4.36295	0.058786
Ces3b	-4.36278	0.001532
Erp27	-4.35521	0.005287
Hal	-4.34271	1.48E-06
Sds	-4.32079	0.000219
Arg1	-4.27852	0.001727
Hsd17b6	-4.27195	0.003347
Elovl3	-4.23001	0.02592
Serpina9	-4.19407	0.006415
Htra4	-4.18365	0.004898
Dclk3	-4.17995	8.71E-05
Gm5766	-4.17705	0.005999
Tekt1	-4.16161	0.002605
Kcnk1	-4.14183	0.023926
Mup-ps8	-4.13202	0.002298
Cyp7b1	-4.11936	0.01077
Mup-ps17	-4.11665	0.01546
Aspg	-4.10992	0.000206
Serpina12	-4.10583	0.021618

Slc22a28	-4.08799	0.013259
Serpina1d	-4.01748	0.002224
Mup5	-3.99921	0.003023
Efna3	-3.97576	0.014433
Egfem1	-3.95877	0.017283
Sult2a7	-3.95534	0.000163
Syde2	-3.91787	0.001187
Stpg2	-3.91525	0.024714
Calcr	-3.91102	0.014749
Mup8	-3.88261	5.91E-05
Gls2	-3.86942	2.86E-05
Tdrd9	-3.86297	0.013313
Cyp2c53-ps	-3.84229	0.028981
Gm4956	-3.84039	0.000407
Stpg3	-3.83618	0.005099
Sfxn1	-3.83471	2.23E-05
Gm7808	-3.81155	0.011486
Grm8	-3.78381	0.016368
AC113593.4	-3.77339	0.048863
Dio1	-3.76402	0.002839
Ptgds	-3.75721	0.045649
Ppp1r42	-3.74687	0.000395
Icam4	-3.73075	0.000975
Inmt	-3.70533	0.000453
Ak4	-3.67894	3.4E-05
Cyp2c54	-3.67698	0.001412
Irx3	-3.67018	0.004849
Gpr12	-3.66463	0.026556
Serpina1b	-3.65187	0.001244
Cryl1	-3.64068	0.00257
C8a	-3.63315	0.002449
Uroc1	-3.62185	8.54E-05
Gm18499	-3.6171	0.058804
Serpina3k	-3.61312	0.003613
Ces1e	-3.61211	0.000706
Adh6-ps1	-3.61155	0.010799
Vsx1	-3.58792	0.034485
Asic5	-3.58358	0.004077
Slco1a1	-3.57249	0.014162

Myl7	-3.55519	6.75E-05
Akap3	-3.54499	0.006589
Serpina3c	-3.51975	0.007622
Olfir52	-3.50758	0.034753
Serpina1a	-3.506	0.000859
Hsd3b2	-3.49251	0.005321
Gm5640	-3.49243	0.000285
Sox10	-3.46239	0.05271
Mup6	-3.45558	0.029316
Gm21064	-3.42694	0.009626
Gm16399	-3.40823	0.044788
Serpina3m	-3.40726	0.001735
Serpina3l-ps	-3.40601	0.015316
Gm48407	-3.40285	0.023901
Mug4-ps	-3.40112	0.038718
Pnmal1	-3.39656	0.009528
Gm47250	-3.38736	0.00659
Slc44a4	-3.37152	0.003252
Sdr9c7	-3.35451	0.000952
Otc	-3.34881	0.002322
Cyp2u1	-3.34537	0.000325
Serpina1e	-3.34288	8.08E-05
Nlrp5-ps	-3.32431	0.02042
Slc22a7	-3.31978	2.04E-05
Tstd1	-3.31814	0.000354
Wdr63	-3.31489	0.037403
Gm7298	-3.30837	0.027206
Cpne6	-3.30022	0.013956
Lama3	-3.29267	0.000274
Amdhd1	-3.29252	0.000921
Mup-ps4	-3.26777	0.004243
AC113593.3	-3.25947	0.043687
Cyp2j5	-3.2486	0.001556
Gm8971	-3.24761	0.00289
Cym	-3.24484	0.022048
Sdsl	-3.23423	0.000675
Acsm2	-3.22811	0.004505
Fmo3	-3.22539	0.010104
Tbc1d30	-3.21248	7.83E-05

Cyp2a12	-3.2083	0.002507
Aldh1b1	-3.20216	0.000686
Gm11185	-3.16469	0.001507
Cadm4	-3.15138	0.014083
Gm44578	-3.1448	0.001771
Ush2a	-3.13708	0.017973
Mcm10	-3.11782	0.003184
Dpy19l3	-3.09067	8.3E-05
Ttc30a2	-3.08668	0.010522
Gm6580	-3.07323	0.035323
Blm	-3.06438	1.64E-05
Gm9157	-3.05866	0.058368
Grem2	-3.04376	0.01279
Gm18313	-3.02013	0.025142
Jph1	-3.00353	0.005406
Ugt2b1	-2.98913	0.006731
Orm3	-2.96541	0.002473
Slc10a1	-2.96056	0.000568
Aqp8	-2.9584	0.000226
Tex45	-2.94976	0.003769
Gcnt4	-2.94693	0.000275
B4galnt3	-2.94533	0.000802
Smim22	-2.93851	0.00489
Upk3b	-2.93386	0.056141
Etnppl	-2.93314	0.002921
Cfhr3	-2.93221	0.003872
Calhm1	-2.90087	0.023291
Gm11926	-2.90087	0.023291
Tcf24	-2.89967	0.003569
Hao1	-2.88396	0.001806
Gbx1	-2.88187	0.008404
Prom2	-2.88005	0.017505
Pde6h	-2.87682	0.008606
Gldc	-2.87576	0.0008
Cfap100	-2.86085	0.023532
Gm5638	-2.85869	0.016959
Meig1	-2.85459	0.021782
Serpinb1a	-2.84712	1.37E-05
Serpina3a	-2.84391	0.006134

Rida	-2.84123	0.003988
Keg1	-2.83769	0.003057
Tpi-rs4	-2.83515	0.040504
Brinp1	-2.8344	0.03009
Dhrs2	-2.83197	0.009062
Myom2	-2.81817	4.12E-05
Ftcd	-2.81791	8.39E-05
H2-BI	-2.81731	0.000382
Hsd17b13	-2.81654	0.000796
Foxq1	-2.81358	0.039067
Cadps2	-2.80966	0.000996
Ces1d	-2.80671	0.001358
Olfr541	-2.8061	0.004081
Gm14409	-2.80088	0.059891
Trhde	-2.78947	0.000349
Ces4a	-2.78377	0.027172
Ugt3a1	-2.76052	0.00089
Dnaic1	-2.75566	0.010385
Gas1	-2.75269	0.0054
Retsat	-2.75145	0.000637
Cps1	-2.73833	3.3E-05
Slc6a16	-2.7339	0.00418
Odf3b	-2.73004	0.001378
Spag4	-2.72432	0.00173
Slc3a1	-2.72185	0.003309
Catsper3	-2.72158	0.002888
Sema3e	-2.70994	0.002448
Gypc	-2.70543	6.65E-05
Olfr733	-2.6978	0.012091
Gm13607	-2.68276	0.058321
Ctnnbip1	-2.66951	8.89E-05
Upp2	-2.66754	0.005722
Gm5936	-2.6639	0.002958
AC168062.1	-2.64636	0.053244
Serpina11	-2.63666	0.007213
Chrne	-2.62182	0.000435
Prap1	-2.62055	0.002939
Gm4952	-2.61753	0.008394
CT009550.4	-2.61285	0.057334

Ccdc151	-2.6103	0.000238
Nat8f1	-2.59356	0.002454
Ces1c	-2.59229	0.007104
Gm6257	-2.58779	0.058136
Gm11453	-2.58034	0.051203
Caln1	-2.57828	0.001584
Cyp2d34	-2.57714	0.000225
Zfp-ps	-2.56638	0.003283
Hsd11b1	-2.56327	0.003048
Vwc2	-2.54211	0.046953
Ppp1r3b	-2.53452	0.000378
Sgcd	-2.5307	0.02063
Osbpl5	-2.52887	0.000624
Cspg5	-2.52867	0.004567
Nrep	-2.52312	0.002564
Spsb4	-2.52132	0.015655
Nkx3-1	-2.52118	0.023707
Csta1	-2.51941	0.0054
Scnn1a	-2.51174	0.002499
Efh1	-2.5109	0.004132
Mug1	-2.504	1.35E-05
Car3	-2.50277	0.000925
Gm7208	-2.5015	0.007526
Gm5901	-2.50145	0.03412
Car1	-2.49283	0.003533
S1pr5	-2.49179	0.000135
Slc2a5	-2.49021	3.62E-05
Gm6520	-2.47345	0.017174
Prok1	-2.47012	0.028995
Hhip1	-2.4689	0.006222
AC114008.1	-2.45869	0.001375
Gm6863	-2.45228	0.020646
C8b	-2.45012	0.014909
Mug-ps1	-2.44614	0.000116
Hectd2	-2.44045	0.004398
Sfrp1	-2.4384	0.002502
Olfr1135	-2.43421	0.051148
Col27a1	-2.4334	0.005027
Gm6981	-2.43137	0.040218

Hpd1	-2.43021	0.007644
Slc25a31	-2.42367	0.035984
	-2.42367	0.035984
Ttc34	-2.41942	0.015685
Olfr542-ps1	-2.41886	0.030921
Pigr	-2.39912	0.001031
Eif4ebp3	-2.39741	0.00056
A530016L24Rik	-2.39106	0.005455
Amer2	-2.38371	0.010798
Gm266	-2.37627	0.050059
AC154598.1	-2.36995	0.039073
Rd3	-2.36859	0.000114
Fn3k	-2.36789	0.00111
Apol8	-2.36733	0.016918
Bik	-2.36394	4.37E-05
Fmod	-2.35996	0.032237
Afmid	-2.35774	0.000533
Gm15264	-2.35703	0.000688
Nudt11	-2.3552	0.013117
AC122858.2	-2.35154	0.044241
AC113593.1	-2.34401	0.006373
Rnf26	-2.33733	0.035557
Ttll8	-2.33303	0.016014
Tmigd1	-2.32866	0.02701
Kyat1	-2.32088	0.00018
Gjb6	-2.3107	0.021834
A630076J17Rik	-2.30579	0.012733
Crhr2	-2.29903	0.044311
Fam47e	-2.27925	0.000269
Olfr1087	-2.27341	0.009178
Gm35570	-2.27004	2.97E-05
Cyp2a4	-2.26502	0.002761
Tymp	-2.26154	0.001289
Cpsf4l	-2.25265	0.00499
Serpinf1	-2.25175	0.000915
P2ry4	-2.24711	0.00926
Gm11437	-2.23322	0.002619
Clic5	-2.23222	0.000842
Gm13363	-2.23146	0.022612

Gm7652	-2.21777	0.002465
Xirp1	-2.21759	0.029596
Urad	-2.21755	0.000151
Rufy4	-2.20904	0.003383
Igf1	-2.20731	0.00162
Igfals	-2.20477	0.002462
Pdlim3	-2.20083	0.031733
Fahd1	-2.19985	0.001472
Slc25a47	-2.19193	0.000316
Nxph1	-2.19185	0.059538
Ces1b	-2.19154	0.000704
Plk5	-2.19053	0.002183
Hgfac	-2.1899	0.000484
Gm7658	-2.1888	0.024526
Wnt7b	-2.18785	0.032662
Dusp1	-2.18191	0.01602
Ahcy	-2.18005	0.001589
Lor	-2.17829	0.017937
Hamp2	-2.17252	0.009924
Tedc2	-2.17244	0.003408
Cyp2j9	-2.17168	0.003271
Il1rap	-2.16764	0.002241
Gm1141	-2.16688	0.025754
St8sia1	-2.16681	0.029241
Gm44216	-2.16453	0.025898
Vmn2r-ps91	-2.16453	0.025898
Gm43225	-2.16331	0.055389
Gm47968	-2.16011	0.00455
Fndc5	-2.16007	0.000945
Gm37515	-2.15565	0.010358
Gm21049	-2.15429	0.000611
Tnnc1	-2.15313	0.011548
Spatc1l	-2.14848	0.003073
Uox	-2.14535	0.001078
Stag3	-2.14418	0.02376
Nrg4	-2.14258	0.00014
Ngb	-2.1414	0.033904
Slc10a2	-2.13665	0.006387
Olfr69	-2.13236	0.008167

Thrsp	-2.13052	0.001378
Ppp1r14a	-2.12987	0.005221
Gm7646	-2.11691	0.027345
BC021767	-2.11485	0.004843
Cyp2c50	-2.11289	0.004106
Mapk15	-2.10684	0.002654
Gm12935	-2.10559	0.030487
Gm45834	-2.09726	0.007813
Clec2h	-2.09167	0.026546
Spry4	-2.0903	0.00829
Pbld2	-2.08783	0.001151
Gstp2	-2.08762	0.011958
Olfr805	-2.08355	0.029469
Mgmt	-2.0787	0.006353
Rasl2-9	-2.07807	0.032642
Serinc4	-2.07655	0.004897
Slc17a2	-2.07619	0.00377
Aadat	-2.07428	0.003994
Chchd7	-2.07053	0.003798
Aspdh	-2.06686	0.003217
Epp13	-2.06532	0.007177
Map2k6	-2.06014	0.000217
Ces2a	-2.057	0.007148
Slc15a5	-2.05586	0.004007
Gm15502	-2.05089	0.010812
AC166574.2	-2.05053	0.05374
Apom	-2.04975	0.008811
Car14	-2.04001	0.004733
Slc35e3	-2.03028	0.001231
Sox12	-2.0265	0.006343
Akr1c21	-2.02261	0.018056
Nrtn	-2.01499	0.004001
Apon	-2.01334	0.006131
Abcc6	-2.01128	0.000303
Sema4f	-2.00901	0.000665
Gm20695	-2.00888	0.013406
Ido2	-2.00874	4.55E-05
Colgalt2	-2.00743	0.00246
Slc15a2	-2.00563	0.027394

Table A6.2 Top genes upregulated in hbHeps compared to WT Fah mice, fold change >2, p<0.05

GENE	log ₂ FC (hbHep/WT FAH)	p-value
Olfr1315-ps1	12.82356	0.020586
Gm13502	9.58998	0.010507
Duoxa1	8.607451	0.019046
Myot	8.404986	0.002327
Bpifa5	7.654454	0.002918
Duox1	7.6394	0.032044
Acsn4	7.285949	0.029969
Mogat2	7.251751	3.32E-05
Ly6d	6.97036	0.001555
Gm42517	6.946244	0.000457
Car4	6.649517	0.008673
Gm43302	6.600846	0.01638
Sprr1a	6.548212	0.008269
Lrrc14b	6.466565	0.003962
Nptx1	6.401229	0.027025
Lcn2	6.397081	0.008625
Ubd	6.235434	0.057535
Gm38392	6.134869	0.006878
H2-Q1	6.009321	0.022861
H2-Q2	5.792648	0.001253
Sema3b	5.760989	0.000503
Spire2	5.693927	0.002426
Gm11843	5.608904	0.022159
Rasl10b	5.579147	0.000739
Mmp24	5.567492	0.001135
Kif26b	5.532683	0.042844
Akr1b7	5.491944	0.023709
Gm379	5.485735	0.000243
Scn4b	5.450283	0.059781
Mcpt4	5.426534	0.046766
Olfr980	5.331508	5.89E-05
Apcdd1	5.30468	0.001527
Tuba8	5.286562	0.0008
Col8a1	5.214484	0.03635
Mmp7	5.152281	0.022639

Tbx1	5.085062	0.001593
Slc22a3	5.05002	2.06E-05
A930009A15Rik	5.028944	0.024326
Pkp1	4.91924	0.002341
Gabrb3	4.894803	0.024597
Elovl7	4.868598	0.016162
Crybb1	4.868183	0.026611
Gbp10	4.838644	0.043162
Sbspon	4.786229	0.028551
Oat	4.784846	0.011391
Plat	4.780168	0.037709
Wnt11	4.772975	0.015281
Fgfbp1	4.725774	0.003561
Cln6	4.67187	0.000745
Asb11	4.653602	0.000289
6030419C18Rik	4.64774	0.001405
Cyp3a41b	4.633619	0.04694
Rhbg	4.578917	0.011199
Fermt1	4.578194	0.006361
A4gnt	4.55546	0.028752
4933400A11Rik	4.51362	0.059473
Adcy8	4.505906	0.006089
Ren1	4.466836	0.000766
Hmgcll1	4.456871	0.006464
Lhpp	4.404327	0.001088
Usp18	4.403793	0.011722
Fgl2	4.397988	0.006255
Prkg2	4.3685	0.044903
Cdkn2a	4.304313	0.04499
Cd63	4.266666	0.000663
Cpe	4.234346	0.035615
Guca2a	4.231957	0.021315
Ccnd1	4.221289	0.00113
Bex1	4.175853	0.041368
Igdcc4	4.172031	0.020042
Fam83b	4.161423	0.004264
Glms-ps1	4.160726	0.027733
AC157515.1	4.130342	0.032201
Cyp2c55	4.092232	0.00448

Wnk4	4.091228	0.030716
Vldlr	4.091095	1.97E-05
Ctla4	4.089711	0.01352
Fosl1	4.083193	0.000298
Trim16	4.075525	0.005018
Atp10a	4.07273	0.004109
Inpp5j	4.040837	0.058363
Rragd	4.021469	0.000212
Sp5	3.987304	0.008346
Scd2	3.978985	0.040476
Tmprss11f	3.966592	0.002904
Mmp13	3.959869	0.041559
Mybl1	3.954882	0.001099
Ppbp	3.944569	0.000235
Olig1	3.913109	0.058203
Slc1a2	3.90929	0.003973
Bmp8b	3.90586	0.050031
Ifi27l2b	3.902079	0.013611
Ckap2l	3.891609	0.010023
Fndc10	3.888078	0.000344
Nkx1-2	3.852325	0.019162
Slc1a4	3.850037	0.043763
Muc13	3.824216	0.043957
Tmem40	3.817848	0.01445
Nrg1	3.807239	0.000203
Gnai1	3.807018	0.006049
Pdk4	3.800061	0.0454
Endod1	3.796257	0.007389
Gm10645	3.78236	0.035464
Mpped2	3.779045	0.022615
Oas1a	3.778996	0.043084
Rdh9	3.775241	0.004529
Rtn4rl2	3.770764	0.035426
Lef1	3.765196	0.001495
Blnk	3.75669	0.019713
Tmem71	3.745044	0.0141
Axin2	3.737575	0.000149
Aqp7	3.733388	0.001618
Hcar2	3.723118	7.15E-05

Cystm1	3.718576	0.004255
Glul	3.712042	0.016832
Syt14	3.705167	0.031301
Wnt16	3.701608	0.048884
D630003M21Rik	3.684193	0.009742
Gm16574	3.683147	0.02146
AC168977.2	3.677012	0.02013
AC124709.2	3.663212	0.004408
Ccl8	3.652774	0.028966
Ptpn14	3.640753	0.012382
Oas2	3.634479	0.007388
Tnfsf8	3.627406	0.054143
Gbp6	3.619987	0.024658
2310007B03Rik	3.609806	0.002032
Oas1g	3.59417	0.018158
Ms4a14	3.591485	0.000879
Prom1	3.590778	0.005475
Igkv9-120	3.576004	0.032327
Robo1	3.569561	0.001635
Ckap2	3.564066	0.004379
Lrmda	3.553971	0.001324
Mki67	3.539513	0.007088
Sdcbp2	3.527391	0.021098
Opn1sw	3.512269	0.035079
Tox	3.508025	0.000149
Oasl1	3.507693	0.015442
Rpl31-ps8	3.493978	0.003219
4933406M09Rik	3.471694	0.038503
Cd44	3.463565	0.001343
Slfn4	3.4619	0.025061
Cyp3a41a	3.459505	0.044993
Themis	3.457105	0.0038
Cxcl10	3.45003	0.058161
Uap1l1	3.431631	0.001121
Rcan2	3.427422	0.007561
Mt4	3.425978	0.028782
Tbx4	3.425179	0.020602
Corin	3.423008	0.032078
Rab33a	3.413077	0.020663

Rec114	3.409871	0.00664
Esm1	3.399529	0.009707
Phospho1	3.386003	0.031351
Cdkn3	3.378835	0.015522
Gm7162	3.371593	0.00424
Lgals3	3.370285	0.00504
Flywch2	3.366622	0.027311
Eif4e3	3.333232	0.000392
Anxa2	3.330069	0.001302
Gm7666	3.328255	0.058267
Nupr1	3.312887	0.034859
Slco1a4	3.309966	0.000689
Rpl7a-ps9	3.309722	0.049382
Ccl2	3.308731	0.007123
Trim59	3.299504	0.047305
Lgr5	3.267193	9.18E-05
Tlr9	3.265467	0.044687
Pgm5	3.248852	0.000148
Msantd3	3.247693	0.003244
Myzap	3.24677	0.029213
Hapln4	3.228129	0.027265
Calml4	3.223935	0.040313
Tnfrsf19	3.222605	0.028437
Ascl4	3.215522	0.041252
Ifi207	3.21549	0.020401
Casp12	3.213515	0.019155
Wfdc3	3.211174	0.000518
Depdc1a	3.203833	0.01291
Treh	3.201026	1.37E-06
Gm17743	3.189908	0.056503
Gm18852	3.189468	0.005266
Orm2	3.182187	0.00612
Gm6746	3.181546	0.001888
Slc13a3	3.175179	0.001264
Gm4322	3.165073	0.036713
Oas3	3.160013	0.021698
Zfp296	3.156547	0.010081
Gm8145	3.149003	0.017741
Scn2a	3.140349	0.001405

L3mbtl1	3.137741	0.030565
Gm5626	3.133538	1.99E-05
Gipc2	3.105801	0.000343
Rab44	3.10385	0.008925
Nhs	3.091429	0.043841
Lrtm2	3.086523	0.00014
Duox2	3.08228	0.052366
1810062G17Rik	3.077587	0.03902
Il1rn	3.067271	0.048997
Gramd1b	3.066299	0.00386
Serpib6a	3.060343	0.014422
1700003F12Rik	3.057012	0.023391
Gtse1	3.054042	4.03E-07
Fndc9	3.050126	0.000608
Tmem252	3.048336	0.000221
Gm15916	3.043275	0.019307
Tmem178	3.039859	0.011397
Mab21l3	3.034574	0.011532
Cds1	3.030151	0.05396
Tff3	3.028204	0.035843
Hmgcs1	3.020929	0.019537
Epdr1	3.01584	0.001934
AC132444.2	3.015178	0.00595
AC132444.4	3.015178	0.00595
AC133103.6	3.015178	0.00595
Rsad2	3.014805	0.049815
Il7	3.009948	0.006488
Dab2ip	3.00808	0.027165
Gm9353	2.99051	0.01858
Ifi44l	2.988191	0.01724
Sectm1a	2.986039	0.054069
Ikzf2	2.983865	0.001364
Avpr1a	2.982357	0.003187
Gm3712	2.975644	0.008062
Ddr1	2.97231	0.031575
Atp6v0d2	2.968344	0.018551
Fam126a	2.967349	0.000175
BC023105	2.958592	0.015236
Gm44922	2.957398	0.013324

Slc1a5	2.953994	0.001515
Sema3g	2.942514	0.009727
Ch25h	2.938855	0.042735
Hspb1	2.929251	0.002249
Gm5340	2.927865	0.05683
Nr4a1	2.91918	0.008259
Ldhb	2.91136	0.024878
Cacna2d4	2.904392	0.005348
Npdc1	2.904021	0.001235
Phlda3	2.903971	0.000633
Mal	2.902876	0.000142
Syt15	2.899971	3.3E-06
Osbpl3	2.897527	0.00527
Syt12	2.896163	0.004461
Ucp2	2.890546	1.43E-05
Psd4	2.890162	0.000421
Tas2r126	2.888783	0.007877
Gm16011	2.888783	0.007877
Phlda2	2.874201	0.026491
Plk1	2.871847	0.016985
Atf3	2.870621	0.001049
Sgol2a	2.8648	0.00549
Ppp1r3g	2.864493	0.050839
Tcf7	2.864467	0.007778
Mas1	2.863642	0.000232
Pak1	2.855547	8.73E-05
Fbln1	2.848786	0.042112
Ifi27	2.846606	0.024954
Olfr1459	2.842642	0.001904
Sqle	2.841871	0.002256
Il22ra1	2.831167	0.004811
Teddm2	2.830282	0.006899
Fxyd4	2.819957	0.057757
3110035E14Rik	2.819749	0.00843
Gpr141	2.816668	0.028106
Gm9553	2.814078	0.04564
Dusp8	2.809726	0.009427
2010003K11Rik	2.807604	0.000207
Siglec1	2.797464	0.021699

Traip	2.790414	0.008766
Arhgef16	2.785842	0.007048
Gm16016	2.776652	0.023593
Dlgap5	2.775701	0.018005
Prokr2	2.774919	0.003881
Lipg	2.774716	0.045636
H2-T-ps	2.774218	0.029485
Dmpk	2.765311	0.001127
Tpx2	2.758247	6.45E-05
Ttk	2.757734	0.00542
Gm9922	2.755469	0.020911
Mpeg1	2.753614	0.043319
Scamp5	2.749406	0.005162
Slpi	2.747676	0.030077
Myo1f	2.745771	0.044679
Adgrg2	2.743802	0.043702
Gm15823	2.740324	0.006378
Cryba4	2.737605	0.012838
Eid2	2.736127	0.005136
Oas1h	2.736095	0.000907
Ikzf3	2.734793	0.030814
Cdkn2b	2.733862	0.000295
BC029722	2.732947	0.009372
Ackr3	2.732826	0.056772
Wfdc18	2.725519	0.007255
Bub1	2.722883	0.00173
Atp6v0e2	2.721448	0.000364
Nuf2	2.72027	0.02174
Ypel4	2.717146	0.015244
Serpinb10	2.698468	0.000341
Car2	2.6961	0.000572
Ccnb1	2.69445	0.006755
Gm2619	2.694129	0.007109
Camp	2.692486	0.05553
Runx1	2.691162	0.003127
Myo7b	2.686988	0.017142
Cdhr2	2.685327	0.025103
Teddm1b	2.675903	0.056029
Gulo	2.675308	0.01372

Gm12024	2.673686	0.04644
Foxc1	2.67254	0.026848
Adrb2	2.67058	0.038956
Wdfy4	2.667867	0.016389
Cdc20	2.667428	0.017923
Ccnb2	2.663527	0.02284
A730049H05Rik	2.656584	0.038555
Myo15b	2.656578	0.056673
Ccr1	2.655604	0.028508
Aldh18a1	2.655316	0.003741
Gm14886	2.654996	0.003674
Cdc6	2.653679	0.003
Slc25a24	2.642566	0.041132
Gm17230	2.640462	0.002878
Itgax	2.634743	0.036281
Gm13786	2.63139	0.040318
Olfr755-ps1	2.62939	0.019516
Cd3e	2.626672	0.00016
Gm12340	2.619264	0.006924
Gm14828	2.619031	0.006932
Egr1	2.617918	0.00518
Bub1b	2.614948	0.012371
Ndrp1	2.614726	0.036457
Trib2	2.602461	0.016005
Amelx	2.600207	0.005597
Nfe2	2.596258	0.01652
9430097D07Rik	2.59382	0.028449
Rsph1	2.591199	0.017894
Sptb	2.588947	0.013988
Tlr7	2.588103	0.059463
Abcb1a	2.586819	0.004757
Gm4263	2.57973	0.016011
Gm44917	2.573033	0.009323
Dusp14	2.565411	0.005644
Dlx4	2.563061	0.057072
Fcer1a	2.554789	0.036561
Gm18867	2.552509	0.042837
Src	2.539372	0.000538
Clec4d	2.538925	0.003282

Melff	2.538732	0.005089
Gm30708	2.538123	0.032504
Unc13b	2.532423	0.044315
Traf1	2.529951	0.013106
Lgals1	2.523324	0.002095
Racgap1	2.521488	0.008864
Ankrd1	2.515266	0.002162
Mgat3	2.514919	0.004502
Acot2	2.512907	0.005523
Gas7	2.512351	0.000551
Stil	2.507852	0.004266
Dapp1	2.505712	0.005756
Popdc2	2.503734	0.000764
Gm47496	2.502317	0.041977
Scube1	2.501884	0.008438
Ar	2.501131	0.010024
Dyrk3	2.497832	0.00506
Klf6	2.494066	0.000988
Fchsd1	2.492743	0.000324
Cysltr2	2.490957	0.028047
Acod1	2.490693	0.007662
Vopp1	2.481034	0.012615
Gm48670	2.479441	0.010387
Tbx3	2.478863	0.001114
Ska1	2.476798	0.001294
Chst11	2.475139	0.0132
Gm6545	2.473212	0.045838
Lilr4b	2.472783	0.031924
Gm7030	2.469077	0.01228
Gm48592	2.468819	0.012701
Klhl23	2.464329	0.001557
Ifi205	2.463666	0.023304
Galnt15	2.463611	0.002126
Gm21860	2.463611	0.01878
Gm21748	2.463611	0.01878
Gzmk	2.459404	0.037032
Cx3cr1	2.4558	0.00809
Dnah1	2.453097	0.013553
Itpr3	2.447614	0.022444

Gm43738	2.443201	0.048154
Ifit1	2.43998	0.033764
Lynx1	2.438272	0.001511
Panx1	2.43737	0.006168
Gm7334	2.431177	0.000482
Sema5a	2.430595	0.041201
H2afy3	2.427668	0.042315
Gm11892	2.424333	0.028887
Olfm1	2.419369	0.014543
Tspan32	2.416945	0.027305
Lect2	2.415141	0.010625
Ghrhr	2.413453	0.032008
Glpr1	2.412056	0.046394
H2-Oa	2.412049	0.046197
Ccdc146	2.40447	0.02266
Tspan5	2.403322	8.99E-05
Zfp503	2.402318	0.004185
Hist1h2ak	2.398762	0.028315
Pbk	2.396743	0.006464
Mtmr11	2.396286	2.47E-05
Cdkn2c	2.393297	0.018301
Ifit2	2.39124	0.033071
Fdps	2.387855	0.031201
Gstm2	2.385587	0.000607
Gm45234	2.384379	0.011691
Sox4	2.38286	0.002129
Arhgef2	2.379832	0.01238
Gbp8	2.379695	0.034684
Gstm3	2.374772	0.00012
Gm5294	2.371301	0.006451
Nol3	2.370281	0.005419
Olf17	2.368629	0.049095
Ly6e	2.368378	0.059392
AA986860	2.368104	8.09E-06
Mme	2.366542	0.008369
Gm20056	2.362209	0.022978
Gm48318	2.361082	0.032888
Ddx60	2.353987	0.020998
1700027J19Rik	2.353399	0.057428

Kifc1	2.352721	0.001233
Eya2	2.348783	0.023809
Kif20a	2.348752	0.010011
Samd9l	2.348737	0.050806
Lrrc19	2.338417	0.049961
B4galt6	2.334153	0.009848
Pdgfc	2.332115	0.001437
Gm48739	2.330883	0.019423
5430437J10Rik	2.327766	0.013843
Cfap99	2.324149	0.050373
Nipal1	2.320272	0.012947
Hist1h1b	2.319377	0.00172
Hist1h3g	2.319122	0.011517
Serinc2	2.310072	0.059861
Synpo	2.308991	0.021632
Csprs	2.298918	0.000479
Nek2	2.297655	0.00093
Slc41a2	2.297629	0.02013
Flt3	2.296084	0.037467
Cd9	2.293969	0.008299
Gm7909	2.293105	0.012306
Psrc1	2.290644	0.006374
Sowahb	2.289475	0.012823
Gm16072	2.28781	0.039572
Ttll10	2.284394	0.003674
Gm11969	2.283999	0.028278
Timp1	2.283882	0.000476
Rasl11b	2.282211	0.000524
Tnfsf13	2.282209	0.038715
Fam83d	2.282182	0.000789
Anxa5	2.281557	0.005503
Rpl26-ps4	2.279635	0.051024
Gm14007	2.279635	0.051024
Ccdc85b	2.273505	0.049966
Osm	2.273381	0.005322
Gm6793	2.271819	0.049725
Zfp13	2.270189	0.006745
Plet1	2.26892	0.002248
Ccna2	2.267175	0.005497

Olfr16	2.266159	0.024158
Gm18955	2.263844	0.024912
Lilrb4a	2.262766	0.01458
Slfn1	2.26133	0.0433
Gm19684	2.260613	0.003044
Rspo2	2.260165	0.055507
Cdca2	2.259794	7.95E-05
Rasgrf2	2.253239	0.015652
Fam196b	2.251164	0.004306
Rhpn1	2.250548	0.017822
Art2a-ps	2.250064	0.004801
Klc3	2.249798	0.015512
Vcan	2.248954	0.003461
Cyp2c39	2.24866	0.009587
Flvcr2	2.24796	0.015368
Gm11865	2.247765	0.025502
Myo5a	2.245875	0.006201
Wisp1	2.240448	0.006589
Nkg7	2.239224	0.036504
Isyna1	2.233873	0.003753
Sirpa	2.23159	0.052554
Hsf2bp	2.227021	0.037326
Lacc1	2.226106	0.000636
S100a11	2.22303	0.001017
Rbp1	2.222322	0.034513
Prtn3	2.219522	0.046563
Gm7473	2.21889	0.002795
H2al3	2.216584	0.056199
Lrrc8b	2.21329	0.005177
Apobr	2.213249	0.000814
Spire1	2.210307	0.004654
Plek	2.207971	0.021718
Scn1b	2.207717	0.020247
Gm12230	2.206589	0.047942
Ccdc3	2.199975	0.019978
Mdfic	2.19757	0.005323
Ptpn7	2.197444	0.02406
Troap	2.191309	0.037364
Gm8189	2.191044	8.34E-05

Adap1	2.190855	0.011664
Gbp9	2.190603	0.007436
Top2a	2.190221	0.000176
Evl	2.183299	0.034978
Rhoq	2.178287	0.000227
Tlr6	2.17704	0.018068
Dusp9	2.169035	0.057416
Xaf1	2.166636	0.048151
Naip6	2.165849	0.0239
Rgs2	2.165295	0.025958
Fancd2	2.164737	0.008694
Gm45930	2.16177	0.014256
Hmmr	2.161312	0.000735
Gpx2	2.159264	0.049219
Prnd	2.158953	0.014329
Olfm2	2.157117	0.031193
H60b	2.156437	0.024138
Cpeb1	2.154599	0.002794
Cybb	2.153684	0.056913
Bicc1	2.152324	0.002613
Ydjc	2.148682	0.014051
Lcp2	2.147838	0.00427
Jun	2.145739	0.016118
Sla	2.142923	0.030905
Rpl30-ps2	2.142075	0.031387
H2-Q5	2.14016	0.003485
Skap1	2.140038	0.027809
Mlkl	2.139195	4.09E-05
Hpca	2.138896	0.031825
Arhgap11a	2.138582	0.000139
Mvd	2.138481	0.035252
Gm19345	2.137752	0.041066
Tlr1	2.136286	0.038754
Thsd4	2.135168	0.059551
Elf4	2.133213	0.009403
Ect2	2.133011	0.001743
Gdf3	2.132922	0.023578
Spink1	2.131752	0.029513
Apbb1ip	2.130865	0.00384

Kcnj8	2.129517	0.012311
Akna	2.128002	0.009984
Tinag	2.125892	0.033946
Slc6a8	2.124998	0.000354
Fmnl1	2.124683	0.02979
Gm44503	2.123959	0.041915
Gm17956	2.117801	0.05961
Gm10693	2.117357	0.054947
Gm15367	2.117144	0.05669
Pcdhgc4	2.117124	0.047715
Gm4759	2.11441	0.011637
Ccl4	2.112623	0.027824
Gm15739	2.112158	0.005765
Gm21973	2.105249	0.002468
Gm13623	2.10091	0.05322
Col4a5	2.096024	0.005323
Rasa4	2.092356	0.024142
Gm6034	2.088813	0.056207
Hpgds	2.088168	0.013558
Dnah5	2.088004	0.000614
Dock2	2.081475	0.02628
Wipf1	2.078822	0.017089
Cenpf	2.077479	3.72E-05
Arhgap22	2.076993	0.002184
Apol9a	2.074033	0.004123
Ttyh1	2.073223	0.021184
Hist1h3c	2.072917	0.009146
Lilrb4	2.069853	0.0256
Kn11	2.066381	0.008821
Cd72	2.06224	0.025145
Batf3	2.062055	0.030607
2310034G01Rik	2.061444	0.013525
Dusp2	2.059463	0.036437
Gpr18	2.059425	0.004896
Gm14984	2.059419	0.001585
Cdca3	2.059084	0.055826
Gm15737	2.05778	0.025218
Hepacam	2.056648	0.014182
Gstm6	2.053691	0.020868

Cd24a	2.051973	0.00029
Znrf3	2.04933	0.001816
Cd14	2.048406	0.006442
Dnaja4	2.043288	0.018249
Dtx4	2.036586	9.5E-05
Fut7	2.035204	0.051597
4930578G10Rik	2.034274	0.001309
Mrv1	2.03371	0.018334
Slc7a8	2.033373	0.017235
Gucy2c	2.032352	0.008612
Elmo1	2.028476	0.007757
Meis3	2.026453	0.006886
Depdc1b	2.025349	0.027305
Aspm	2.020536	0.003452
Bcam	2.020003	0.006752
Igsf11	2.019865	2.18E-05
Myof	2.017046	0.001797
Gm7592	2.011409	0.05037
Gapdh-ps15	2.008539	0.023375
Nt5e	2.006007	0.002833
Iqgap3	2.002867	0.000703

REFERENCES

1. Cairo S, Armengol C, De Reynies A, Wei Y, Thomas E, Renard CA, Goga A, Balakrishnan A, Semeraro M, Gresh L, Pontoglio M, Strick-Marchand H, Levillayer F, Nouet Y, Rickman D, Gauthier F, Branchereau S, Brugieres L, Laithier V, Bouvier R, Boman F, Basso G, Michiels JF, Hofman P, Arbez-Gindre F, Jouan H, Rousselet-Chapeau MC, Berrebi D, Marcellin L, Plenat F, Zachar D, Joubert M, Selves J, Pasquier D, Bioulac-Sage P, Grotzer M, Childs M, Fabre M, Buendia MA. Hepatic stem-like phenotype and interplay of Wnt/beta-catenin and Myc signaling in aggressive childhood liver cancer. *Cancer Cell*. 2008;14(6):471-84. Epub 2008/12/09. doi: 10.1016/j.ccr.2008.11.002. PubMed PMID: 19061838.
2. Uhlen M, Zhang C, Lee S, Sjostedt E, Fagerberg L, Bidkhorji G, Benfeitas R, Arif M, Liu Z, Edfors F, Sanli K, von Feilitzen K, Oksvold P, Lundberg E, Hober S, Nilsson P, Mattsson J, Schwenk JM, Brunnstrom H, Glimelius B, Sjoblom T, Edqvist PH, Djureinovic D, Micke P, Lindskog C, Mardinoglu A, Ponten F. A pathology atlas of the human cancer transcriptome. *Science*. 2017;357(6352). Epub 2017/08/19. doi: 10.1126/science.aan2507. PubMed PMID: 28818916.
3. Hanahan D, Weinberg RA. The hallmarks of cancer. *Cell*. 2000;100(1):57-70. Epub 2000/01/27. PubMed PMID: 10647931.
4. Howlader N NA, Krapcho M, et al (eds). SEER Cancer Statistics Review, 1975-2015, National Cancer Institute [web]. SEER Website: National Cancer Institute 2017 [January 2019]; April 2018:[Available from: https://seer.cancer.gov/csr/1975_2015/].
5. Forner A, Reig M, Bruix J. Hepatocellular carcinoma. *Lancet*. 2018;391(10127):1301-14. Epub 2018/01/09. doi: 10.1016/S0140-6736(18)30010-2. PubMed PMID: 29307467.
6. El-Serag HB. Epidemiology of viral hepatitis and hepatocellular carcinoma. *Gastroenterology*. 2012;142(6):1264-73.e1. Epub 2012/04/28. doi: 10.1053/j.gastro.2011.12.061. PubMed PMID: 22537432; PMCID: PMC3338949.
7. Welzel TM, Graubard BI, Quraishi S, Zeuzem S, Davila JA, El-Serag HB, McGlynn KA. Population-attributable fractions of risk factors for hepatocellular carcinoma in the United States. *The American journal of gastroenterology*. 2013;108(8):1314-21. Epub 2013/06/12. doi: 10.1038/ajg.2013.160. PubMed PMID: 23752878; PMCID: PMC4105976.
8. Schlesinger S, Aleksandrova K, Pischon T, Jenab M, Fedirko V, Trepo E, Overvad K, Roswall N, Tjonneland A, Boutron-Ruault MC, Fagherazzi G, Racine A, Kaaks R, Grote VA, Boeing H, Trichopoulou A, Pantzalis M, Kritikou M, Mattiello A, Sieri S, Sacerdote C, Palli D, Tumino R, Peeters PH, Bueno-de-Mesquita HB, Weiderpass E, Quiros JR, Zamora-Ros R, Sanchez MJ, Arriola L, Ardanaz E, Tormo MJ, Nilsson P, Lindkvist B, Sund M, Rolandsson O, Khaw KT, Wareham N, Travis RC, Riboli E, Nothlings U. Diabetes mellitus, insulin

treatment, diabetes duration, and risk of biliary tract cancer and hepatocellular carcinoma in a European cohort. *Annals of oncology : official journal of the European Society for Medical Oncology*. 2013;24(9):2449-55. Epub 2013/05/31. doi: 10.1093/annonc/mdt204. PubMed PMID: 23720454; PMCID: PMC3755330.

9. Schulze K, Nault JC, Villanueva A. Genetic profiling of hepatocellular carcinoma using next-generation sequencing. *J Hepatol*. 2016;65(5):1031-42. Epub 2016/10/19. doi: 10.1016/j.jhep.2016.05.035. PubMed PMID: 27262756.

10. Schulze K, Imbeaud S, Letouzé E, Alexandrov LB, Calderaro J, Rebouissou S, Couchy G, Meiller C, Shinde J, Soysouvanh F, Calatayud A-L, Pinyol R, Pelletier L, Balabaud C, Laurent A, Blanc J-F, Mazzaferro V, Calvo F, Villanueva A, Nault J-C, Bioulac-Sage P, Stratton MR, Llovet JM, Zucman-Rossi J. Exome sequencing of hepatocellular carcinomas identifies new mutational signatures and potential therapeutic targets. *Nature Genetics*. 2015;47(5):505-11. doi: 10.1038/ng.3252.

11. Totoki Y, Tatsuno K, Covington KR, Ueda H, Creighton CJ, Kato M, Tsuji S, Donehower LA, Slagle BL, Nakamura H, Yamamoto S, Shinbrot E, Hama N, Lehmkuhl M, Hosoda F, Arai Y, Walker K, Dahdouli M, Gotoh K, Nagae G, Gingras M-C, Muzny DM, Ojima H, Shimada K, Midorikawa Y, Goss JA, Cotton R, Hayashi A, Shibahara J, Ishikawa S, Guiteau J, Tanaka M, Urushidate T, Ohashi S, Okada N, Doddapaneni H, Wang M, Zhu Y, Dinh H, Okusaka T, Kokudo N, Kosuge T, Takayama T, Fukayama M, Gibbs RA, Wheeler DA, Aburatani H, Shibata T. Trans-ancestry mutational landscape of hepatocellular carcinoma genomes. *Nature Genetics*. 2014;46(12):1267-73. doi: 10.1038/ng.3126.

12. Cleary SP, Jeck WR, Zhao X, Chen K, Selitsky SR, Savich GL, Tan T-X, Wu MC, Getz G, Lawrence MS, Parker JS, Li J, Powers S, Kim H, Fischer S, Guindi M, Ghanekar A, Chiang DY. Identification of driver genes in hepatocellular carcinoma by exome sequencing. *Hepatology*. 2013;58(5):1693-702. doi: 10.1002/hep.26540.

13. Guichard C, Amaddeo G, Imbeaud S, Ladeiro Y, Pelletier L, Maad IB, Calderaro J, Bioulac-Sage P, Letexier M, Degos F, Clément B, Balabaud C, Chevet E, Laurent A, Couchy G, Letouzé E, Calvo F, Zucman-Rossi J. Integrated analysis of somatic mutations and focal copy-number changes identifies key genes and pathways in hepatocellular carcinoma. *Nature Genetics*. 2012;44(6):694-8. doi: 10.1038/ng.2256.

14. Eichenmüller M, Trippel F, Kreuder M, Beck A, Schwarzmayer T, Haberle B, Cairo S, Leuschner I, von Schweinitz D, Strom TM, Kappler R. The genomic landscape of hepatoblastoma and their progenies with HCC-like features. *J Hepatol*. 2014;61(6):1312-20. Epub 2014/08/20. doi: 10.1016/j.jhep.2014.08.009. PubMed PMID: 25135868.

15. Sumazin P, Chen Y, Trevino LR, Sarabia SF, Hampton OA, Patel K, Mistretta TA, Zorman B, Thompson P, Heczey A, Comerford S, Wheeler DA,

- Chintagumpala M, Meyers R, Rakheja D, Finegold MJ, Tomlinson G, Parsons DW, Lopez-Terrada D. Genomic analysis of hepatoblastoma identifies distinct molecular and prognostic subgroups. *Hepatology*. 2017;65(1):104-21. Epub 2016/10/25. doi: 10.1002/hep.28888. PubMed PMID: 27775819.
16. Vogelstein B, Papadopoulos N, Velculescu VE, Zhou S, Diaz LA, Kinzler KW. Cancer Genome Landscapes. *Science*. 2013;339(6127):1546-58. doi: 10.1126/science.1235122.
 17. Armengol C, Cairo S, Fabre M, Buendia MA. Wnt signaling and hepatocarcinogenesis: the hepatoblastoma model. *Int J Biochem Cell Biol*. 2011;43(2):265-70. Epub 2009/08/04. doi: 10.1016/j.biocel.2009.07.012. PubMed PMID: 19646548.
 18. Camargo FD, Gokhale S, Johnnidis JB, Fu D, Bell GW, Jaenisch R, Brummelkamp TR. YAP1 increases organ size and expands undifferentiated progenitor cells. *Current biology : CB*. 2007;17(23):2054-60. Epub 2007/11/06. doi: 10.1016/j.cub.2007.10.039. PubMed PMID: 17980593.
 19. Patel SH, Camargo FD, Yimlamai D. Hippo Signaling in the Liver Regulates Organ Size, Cell Fate, and Carcinogenesis. *Gastroenterology*. 2017;152(3):533-45. Epub 2016/12/23. doi: 10.1053/j.gastro.2016.10.047. PubMed PMID: 28003097; PMCID: PMC5285449.
 20. Yimlamai D, Christodoulou C, Galli GG, Yanger K, Pepe-Mooney B, Gurung B, Shrestha K, Cahan P, Stanger BZ, Camargo FD. Hippo pathway activity influences liver cell fate. *Cell*. 2014;157(6):1324-38. Epub 2014/06/07. doi: 10.1016/j.cell.2014.03.060. PubMed PMID: 24906150; PMCID: PMC4136468.
 21. Dong J, Feldmann G, Huang J, Wu S, Zhang N, Comerford SA, Gayyed MF, Anders RA, Maitra A, Pan D. Elucidation of a universal size-control mechanism in *Drosophila* and mammals. *Cell*. 2007;130(6):1120-33. Epub 2007/09/25. doi: 10.1016/j.cell.2007.07.019. PubMed PMID: 17889654; PMCID: PMC2666353.
 22. Lu L, Li Y, Kim SM, Bossuyt W, Liu P, Qiu Q, Wang Y, Halder G, Finegold MJ, Lee JS, Johnson RL. Hippo signaling is a potent in vivo growth and tumor suppressor pathway in the mammalian liver. *Proc Natl Acad Sci U S A*. 2010;107(4):1437-42. Epub 2010/01/19. doi: 10.1073/pnas.0911427107. PubMed PMID: 20080689; PMCID: PMC2824398.
 23. Fitamant J, Kottakis F, Benhamouche S, Tian HS, Chuvin N, Parachoniak CA, Nagle JM, Perera RM, Lapouge M, Deshpande V, Zhu AX, Lai A, Min B, Hoshida Y, Avruch J, Sia D, Camprecios G, McClatchey AI, Llovet JM, Morrissey D, Raj L, Bardeesy N. YAP Inhibition Restores Hepatocyte Differentiation in Advanced HCC, Leading to Tumor Regression. *Cell reports*. 2015. Epub 2015/03/17. doi: 10.1016/j.celrep.2015.02.027. PubMed PMID: 25772357; PMCID: PMC4565791.

24. Zender L, Spector MS, Xue W, Flemming P, Cordon-Cardo C, Silke J, Fan ST, Luk JM, Wigler M, Hannon GJ, Mu D, Lucito R, Powers S, Lowe SW. Identification and validation of oncogenes in liver cancer using an integrative oncogenomic approach. *Cell*. 2006;125(7):1253-67. Epub 2006/07/04. doi: 10.1016/j.cell.2006.05.030. PubMed PMID: 16814713; PMCID: PMC3026384.
25. Zhou D, Conrad C, Xia F, Park JS, Payer B, Yin Y, Lauwers GY, Thasler W, Lee JT, Avruch J, Bardeesy N. Mst1 and Mst2 maintain hepatocyte quiescence and suppress hepatocellular carcinoma development through inactivation of the Yap1 oncogene. *Cancer Cell*. 2009;16(5):425-38. Epub 2009/11/03. doi: 10.1016/j.ccr.2009.09.026. PubMed PMID: 19878874; PMCID: PMC3023165.
26. Tschaharganeh DF, Chen X, Latzko P, Malz M, Gaida MM, Felix K, Ladu S, Singer S, Pinna F, Gretz N, Sticht C, Tomasi ML, Delogu S, Evert M, Fan B, Ribback S, Jiang L, Brozzetti S, Bergmann F, Dombrowski F, Schirmacher P, Calvisi DF, Breuhahn K. Yes-associated protein up-regulates Jagged-1 and activates the Notch pathway in human hepatocellular carcinoma. *Gastroenterology*. 2013;144(7):1530-42.e12. Epub 2013/02/20. doi: 10.1053/j.gastro.2013.02.009. PubMed PMID: 23419361; PMCID: PMC3665638.
27. Sun Z, Xu R, Li X, Ren W, Ou C, Wang Q, Zhang H, Zhang X, Ma J, Wang H, Li G. Prognostic Value of Yes-Associated Protein 1 (YAP1) in Various Cancers: A Meta-Analysis. *PloS one*. 2015;10(8):e0135119. Epub 2015/08/12. doi: 10.1371/journal.pone.0135119. PubMed PMID: 26263504; PMCID: PMC4532485.
28. Xu MZ, Yao T-J, Lee NPY, Ng IOL, Chan Y-T, Zender L, Lowe SW, Poon RTP, Luk JM. Yes-associated protein is an independent prognostic marker in hepatocellular carcinoma. *Cancer*. 2009;115(19):4576-85. doi: 10.1002/cncr.24495.
29. Lee K-P, Lee J-H, Kim T-S, Kim T-H, Park H-D, Byun J-S, Kim M-C, Jeong W-I, Calvisi DF, Kim J-M, Lim D-S. The Hippo-Salvador pathway restrains hepatic oval cell proliferation, liver size, and liver tumorigenesis. *Proceedings of the National Academy of Sciences of the United States of America*. 2010;107(18):8248-53. Epub 2010/04/19. doi: 10.1073/pnas.0912203107. PubMed PMID: 20404163.
30. Song H, Mak KK, Topol L, Yun K, Hu J, Garrett L, Chen Y, Park O, Chang J, Simpson RM, Wang C-Y, Gao B, Jiang J, Yang Y. Mammalian Mst1 and Mst2 kinases play essential roles in organ size control and tumor suppression. *Proceedings of the National Academy of Sciences of the United States of America*. 2010;107(4):1431-6. Epub 2010/01/08. doi: 10.1073/pnas.0911409107. PubMed PMID: 20080598.
31. Tao J, Calvisi DF, Ranganathan S, Cigliano A, Zhou L, Singh S, Jiang L, Fan B, Terracciano L, Armeanu-Ebinger S, Ribback S, Dombrowski F, Evert M, Chen X, Monga SPS. Activation of beta-catenin and Yap1 in human

- hepatoblastoma and induction of hepatocarcinogenesis in mice. *Gastroenterology*. 2014;147(3):690-701. Epub 2014/05/20. doi: 10.1053/j.gastro.2014.05.004. PubMed PMID: 24837480; PMCID: PMC4143445.
32. Bruix J, Sherman M, American Association for the Study of Liver D. Management of hepatocellular carcinoma: an update. *Hepatology*. 2011;53(3):1020-2. Epub 2011/03/05. doi: 10.1002/hep.24199. PubMed PMID: 21374666; PMCID: PMC3084991.
33. Feng J, Polychronidis G, Heger U, Frongia G, Mehrabi A, Hoffmann K. Incidence trends and survival prediction of hepatoblastoma in children: a population-based study. *Cancer Commun (Lond)*. 2019;39(1):62. Epub 2019/10/28. doi: 10.1186/s40880-019-0411-7. PubMed PMID: 31651371; PMCID: PMC6813130.
34. Feng T-C, Zai H-Y, Jiang W, Zhu Q, Jiang B, Yao L, Li X-Y, Wang Z-M. Survival and analysis of prognostic factors for hepatoblastoma: based on SEER database. *Ann Transl Med*. 2019;7(20):555-. doi: 10.21037/atm.2019.09.76. PubMed PMID: 31807536.
35. Bismuth H, Chiche L, Adam R, Castaing D, Diamond T, Dennison A. Liver resection versus transplantation for hepatocellular carcinoma in cirrhotic patients. *Ann Surg*. 1993;218(2):145-51. Epub 1993/08/01. doi: 10.1097/00000658-199308000-00005. PubMed PMID: 8393649; PMCID: PMC1242923.
36. Malogolowkin MH, Katzenstein HM, Meyers RL, Krailo MD, Rowland JM, Haas J, Finegold MJ. Complete surgical resection is curative for children with hepatoblastoma with pure fetal histology: a report from the Children's Oncology Group. *Journal of clinical oncology : official journal of the American Society of Clinical Oncology*. 2011;29(24):3301-6. Epub 2011/07/18. doi: 10.1200/JCO.2010.29.3837. PubMed PMID: 21768450.
37. Tiao GM, Bobey N, Allen S, Nieves N, Alonso M, Bucuvalas J, Wells R, Ryckman F. The current management of hepatoblastoma: A combination of chemotherapy, conventional resection, and liver transplantation. *The Journal of Pediatrics*. 2005;146(2):204-11. doi: 10.1016/j.jpeds.2004.09.011.
38. Feng J, He Y, Wei L, Chen D, Yang H, Tan R, Chen Z. Assessment of Survival of Pediatric Patients With Hepatoblastoma Who Received Chemotherapy Following Liver Transplant or Liver Resection. *JAMA Network Open*. 2019;2(10):e1912676-e. doi: 10.1001/jamanetworkopen.2019.12676.
39. Villanueva A. Hepatocellular Carcinoma. *N Engl J Med*. 2019;380(15):1450-62. Epub 2019/04/11. doi: 10.1056/NEJMra1713263. PubMed PMID: 30970190.
40. Czauderna P, Garnier H. Hepatoblastoma: current understanding, recent advances, and controversies. *F1000Res*. 2018;7:53. Epub 2018/01/30. doi: 10.12688/f1000research.12239.1. PubMed PMID: 29375822; PMCID: PMC5770992.

41. Trobaugh-Lotrario AD, Meyers RL, O'Neill AF, Feusner JH. Unresectable hepatoblastoma: current perspectives. *Hepat Med.* 2017;9:1-6. Epub 2017/02/17. doi: 10.2147/HMER.S89997. PubMed PMID: 28203111; PMCID: PMC5293365.
42. Trobaugh-Lotrario AD, Meyers RL, Tiao GM, Feusner JH. Pediatric liver transplantation for hepatoblastoma. *Transl Gastroenterol Hepatol.* 2016;1:44. Epub 2017/02/01. doi: 10.21037/tgh.2016.04.01. PubMed PMID: 28138611; PMCID: PMC5244811.
43. Qin S, Bai Y, Lim HY, Thongprasert S, Chao Y, Fan J, Yang TS, Bhudhisawasdi V, Kang WK, Zhou Y, Lee JH, Sun Y. Randomized, multicenter, open-label study of oxaliplatin plus fluorouracil/leucovorin versus doxorubicin as palliative chemotherapy in patients with advanced hepatocellular carcinoma from Asia. *J Clin Oncol.* 2013;31(28):3501-8. Epub 2013/08/28. doi: 10.1200/jco.2012.44.5643. PubMed PMID: 23980077.
44. Yeo W, Mok TS, Zee B, Leung TW, Lai PB, Lau WY, Koh J, Mo FK, Yu SC, Chan AT, Hui P, Ma B, Lam KC, Ho WM, Wong HT, Tang A, Johnson PJ. A randomized phase III study of doxorubicin versus cisplatin/interferon alpha-2b/doxorubicin/fluorouracil (PIAF) combination chemotherapy for unresectable hepatocellular carcinoma. *Journal of the National Cancer Institute.* 2005;97(20):1532-8. Epub 2005/10/20. doi: 10.1093/jnci/dji315. PubMed PMID: 16234567.
45. Zaanen A, Williet N, Hebban M, Dabakuyo TS, Fartoux L, Mansourbakht T, Dubreuil O, Rosmorduc O, Cattani S, Bonnetain F, Boige V, Taieb J. Gemcitabine plus oxaliplatin in advanced hepatocellular carcinoma: a large multicenter AGO study. *J Hepatol.* 2013;58(1):81-8. Epub 2012/09/20. doi: 10.1016/j.jhep.2012.09.006. PubMed PMID: 22989572.
46. Llovet JM, Ricci S, Mazzaferro V, Hilgard P, Gane E, Blanc JF, de Oliveira AC, Santoro A, Raoul JL, Forner A, Schwartz M, Porta C, Zeuzem S, Bolondi L, Greten TF, Galle PR, Seitz JF, Borbath I, Haussinger D, Giannaris T, Shan M, Moscovici M, Voliotis D, Bruix J, Group SIS. Sorafenib in advanced hepatocellular carcinoma. *N Engl J Med.* 2008;359(4):378-90. Epub 2008/07/25. doi: 10.1056/NEJMoa0708857. PubMed PMID: 18650514.
47. Meyers RL, Rowland JR, Krailo M, Chen Z, Katzenstein HM, Malogolowkin MH. Predictive power of pretreatment prognostic factors in children with hepatoblastoma: a report from the Children's Oncology Group. *Pediatr Blood Cancer.* 2009;53(6):1016-22. Epub 2009/07/10. doi: 10.1002/pbc.22088. PubMed PMID: 19588519; PMCID: PMC4408767.
48. Perilongo G, Shafford E, Plaschkes J, Liver Tumour Study Group of the International Society of Paediatric O. SIOPEL trials using preoperative chemotherapy in hepatoblastoma. *Lancet Oncol.* 2000;1:94-100. Epub 2002/03/22. PubMed PMID: 11905674.
49. Ortega JA, Douglass EC, Feusner JH, Reynolds M, Quinn JJ, Finegold MJ, Haas JE, King DR, Liu-Mares W, Sensel MG, Krailo MD. Randomized

comparison of cisplatin/vincristine/fluorouracil and cisplatin/continuous infusion doxorubicin for treatment of pediatric hepatoblastoma: A report from the Children's Cancer Group and the Pediatric Oncology Group. *J Clin Oncol*. 2000;18(14):2665-75. Epub 2000/07/15. doi: 10.1200/JCO.2000.18.14.2665. PubMed PMID: 10894865.

50. Society AC. Cancer Facts & Figures 2020, Key Statistics for Childhood Cancers 2020.

51. Emre S, McKenna GJ. Liver tumors in children. *Pediatr Transplant*. 2004;8(6):632-8. Epub 2004/12/16. doi: 10.1111/j.1399-3046.2004.00268.x. PubMed PMID: 15598339.

52. Linabery AM, Ross JA. Trends in childhood cancer incidence in the U.S. (1992-2004). *Cancer*. 2008;112(2):416-32. Epub 2007/12/13. doi: 10.1002/cncr.23169. PubMed PMID: 18074355.

53. FAQs About Rare Diseases. Genetic and Rare Disease Information Center, National Center for Advancing and Translating Science 2017. Epub 11/30/2017.

54. Schieppati A, Henter JL, Daina E, Aperia A. Why rare diseases are an important medical and social issue. *Lancet*. 2008;371(9629):2039-41. Epub 2008/06/17. doi: 10.1016/S0140-6736(08)60872-7. PubMed PMID: 18555915.

55. United States cancer statistics: 1999–2009 incidence, WONDER Online Database. United States Department of Health and Human Services, Centers for Disease Control and Prevention and National Cancer Institute. 2011.

56. Lopez-Terrada D, Alaggio R, de Davila MT, Czauderna P, Hiyama E, Katzenstein H, Leuschner I, Malogolowkin M, Meyers R, Ranganathan S, Tanaka Y, Tomlinson G, Fabre M, Zimmermann A, Finegold MJ, Children's Oncology Group Liver Tumor C. Towards an international pediatric liver tumor consensus classification: proceedings of the Los Angeles COG liver tumors symposium. *Mod Pathol*. 2014;27(3):472-91. Epub 2013/09/07. doi: 10.1038/modpathol.2013.80. PubMed PMID: 24008558.

57. Weinberg AG, Finegold MJ. Primary hepatic tumors of childhood. *Hum Pathol*. 1983;14(6):512-37. Epub 1983/06/01. doi: 10.1016/s0046-8177(83)80005-7. PubMed PMID: 6303939.

58. Dehner LP. Hepatic tumors in the pediatric age group: a distinctive clinicopathologic spectrum. *Perspect Pediatr Pathol*. 1978;4:217-68. Epub 1978/01/01. PubMed PMID: 215962.

59. Finegold MJ, Egler RA, Goss JA, Guillerman RP, Karpen SJ, Krishnamurthy R, O'Mahony CA. Liver tumors: pediatric population. Liver transplantation : official publication of the American Association for the Study of Liver Diseases and the International Liver Transplantation Society. 2008;14(11):1545-56. Epub 2008/11/01. doi: 10.1002/lt.21654. PubMed PMID: 18975283.

60. Darbari A, Sabin KM, Shapiro CN, Schwarz KB. Epidemiology of primary hepatic malignancies in U.S. children. *Hepatology*. 2003;38(3):560-6. Epub 2003/08/27. doi: 10.1053/jhep.2003.50375. PubMed PMID: 12939582.
61. Spector LG, Birch J. The epidemiology of hepatoblastoma. *Pediatr Blood Cancer*. 2012;59(5):776-9. Epub 2012/06/14. doi: 10.1002/pbc.24215. PubMed PMID: 22692949.
62. Ikeda H, Matsuyama S, Tanimura M. Association between hepatoblastoma and very low birth weight: A trend or a chance? *The Journal of Pediatrics*. 1997;130(4):557-60. doi: [https://doi.org/10.1016/S0022-3476\(97\)70239-7](https://doi.org/10.1016/S0022-3476(97)70239-7).
63. Ribons LA, Slovis TL. Hepatoblastoma and birth weight. *J Pediatr*. 1998;132(4):750. Epub 1998/05/15. doi: 10.1016/s0022-3476(98)70380-4. PubMed PMID: 9580786.
64. Tanimura M, Matsui I, Abe J, Ikeda H, Kobayashi N, Ohira M, Yokoyama M, Kaneko M. Increased risk of hepatoblastoma among immature children with a lower birth weight. *Cancer Res*. 1998;58(14):3032-5. Epub 1998/07/29. PubMed PMID: 9679968.
65. Riley HK, Freyer DR. #631 Frequent occurrence of prematurity among children with hepatoblastoma: a preliminary study. *Journal of Pediatric Hematology/Oncology*. 1996;18(4):446. PubMed PMID: 00043426-199611000-00070.
66. Feusner J, Plaschkes J. Hepatoblastoma and low birth weight: a trend or chance observation? *Med Pediatr Oncol*. 2002;39(5):508-9. Epub 2002/09/14. doi: 10.1002/mpo.10176. PubMed PMID: 12228908.
67. Bulterys M GM, Smith MA et al. . Hepatic tumors. In: Reis LAG SM, Gurney JG et a, editor. *Cancer Incidence and Survival Among Children and Adolescents: United States SEER Program*. Bethesda, MD National Institutes of Health; 1999. p. 91-7.
68. Huang L-C, Ho M, Chang W-C, Chen H-Y, Hung Y-C, Chiu T-H. Prenatal Diagnosis of Fetal Hepatoblastoma with a Good Neonatal Outcome: Case Report and Narrative Literature Review. *Pediatric Hematology and Oncology*. 2011;28(2):150-4. doi: 10.3109/08880018.2010.536299.
69. Catanzarite V, Hilfiker M, Daneshmand S, Willert J. Prenatal diagnosis of fetal hepatoblastoma: case report and review of the literature. *J Ultrasound Med*. 2008;27(7):1095-8. doi: 10.7863/jum.2008.27.7.1095. PubMed PMID: 18577676.
70. Ergin H, Yildirim B, Dagdeviren E, Yagci B, Ozen F, Şen N, Duzcan E. A Prenatally Detected Case of Congenital Hepatoblastoma. *Pathology & Oncology Research*. 2008;14(1):97-100. doi: 10.1007/s12253-008-9001-8.
71. Shih J-C, Tsao P-N, Huang S-F, Yen BL-J, Lin J-H, Lee C-N, Hsieh F-J. Antenatal diagnosis of congenital hepatoblastoma in utero. *Ultrasound in Obstetrics & Gynecology*. 2000;16(1):94-7. doi: 10.1046/j.1469-0705.2000.00168.x.

72. Lai M, Burjonrappa S. Perinatal hemorrhage complicating neonatal hepatoblastoma: case report. *Journal of Pediatric Surgery*. 2012;47(10):e29-e32. doi: <https://doi.org/10.1016/j.jpedsurg.2012.05.030>.
73. Tomlinson GE, Kappler R. Genetics and epigenetics of hepatoblastoma. *Pediatr Blood Cancer*. 2012;59(5):785-92. Epub 2012/07/19. doi: 10.1002/pbc.24213. PubMed PMID: 22807084.
74. Kitanovski L, Ovcak Z, Jazbec J. Multifocal hepatoblastoma in a 6-month-old girl with trisomy 18: a case report. *Journal of Medical Case Reports*. 2009;3(1):8319. doi: 10.4076/1752-1947-3-8319.
75. Ahmad N, Wheeler K, Stewart H, Campbell C. Hepatoblastoma in a mosaic trisomy 18 child with hemihypertrophy. *BMJ Case Rep*. 2016;2016:bcr2015211380. doi: 10.1136/bcr-2015-211380. PubMed PMID: 26795740.
76. Farmakis SG, Barnes AM, Carey JC, Braddock SR. Solid tumor screening recommendations in trisomy 18. *American Journal of Medical Genetics Part A*. 2019;179(3):455-66. doi: 10.1002/ajmg.a.61029.
77. Rubinfeld B, Souza B, Albert I, Muller O, Chamberlain S, Masiarz F, Munemitsu S, Polakis P. Association of the APC gene product with beta-catenin. *Science*. 1993;262(5140):1731-4. doi: 10.1126/science.8259518.
78. Munemitsu S, Albert I, Souza B, Rubinfeld B, Polakis P. Regulation of intracellular beta-catenin levels by the adenomatous polyposis coli (APC) tumor-suppressor protein. *Proceedings of the National Academy of Sciences*. 1995;92(7):3046-50. doi: 10.1073/pnas.92.7.3046.
79. Rubinfeld B, Albert I, Porfiri E, Fiol C, Munemitsu S, Polakis P. Binding of GSK3 β to the APC- β -Catenin Complex and Regulation of Complex Assembly. *Science*. 1996;272(5264):1023-6. doi: 10.1126/science.272.5264.1023.
80. Morin PJ, Vogelstein B, Kinzler KW. Apoptosis and APC in colorectal tumorigenesis. *Proceedings of the National Academy of Sciences*. 1996;93(15):7950-4. doi: 10.1073/pnas.93.15.7950.
81. Reed KR, Athineos D, Meniel VS, Wilkins JA, Ridgway RA, Burke ZD, Muncan V, Clarke AR, Sansom OJ. B-catenin deficiency, but not Myc deletion, suppresses the immediate phenotypes of APC loss in the liver. *Proceedings of the National Academy of Sciences*. 2008;105(48):18919-23. doi: 10.1073/pnas.0805778105.
82. Dow LE, O'Rourke KP, Simon J, Tschaharganeh DF, van Es JH, Clevers H, Lowe SW. Apc Restoration Promotes Cellular Differentiation and Reestablishes Crypt Homeostasis in Colorectal Cancer. *Cell*. 2015;161(7):1539-52. Epub 2015/06/20. doi: 10.1016/j.cell.2015.05.033. PubMed PMID: 26091037; PMCID: PMC4475279.
83. Hughes LJ, Michels VV. Risk of hepatoblastoma in familial adenomatous polyposis. *American Journal of Medical Genetics*. 1992;43(6):1023-5. doi: 10.1002/ajmg.1320430621.

84. Triana Junco P, Cano EM, Dore M, Jimenez Gomez J, Sanchez Galan A, Vilanova-Sanchez A, Andres A, Encinas JL, Martinez L, Hernandez F, Lopez Santamaria M. Prognostic Factors for Liver Transplantation in Unresectable Hepatoblastoma. *European journal of pediatric surgery : official journal of Austrian Association of Pediatric Surgery [et al] = Zeitschrift fur Kinderchirurgie*. 2019;29(1):28-32. Epub 2018/08/08. doi: 10.1055/s-0038-1668148. PubMed PMID: 30086577.
85. Trobaugh-Lotrario AD, López-Terrada D, Li P, Feusner JH. Hepatoblastoma in patients with molecularly proven familial adenomatous polyposis: Clinical characteristics and rationale for surveillance screening. *Pediatric Blood & Cancer*. 2018;65(8):e27103. doi: 10.1002/pbc.27103.
86. Garber JE, Li FP, Kingston JE, Krush AJ, Strong LC, Finegold MJ, Bertario L, Bulow S, Filippone A, Jr., Gedde-Dahl T, Jr., et al. Hepatoblastoma and familial adenomatous polyposis. *Journal of the National Cancer Institute*. 1988;80(20):1626-8. Epub 1988/12/21. doi: 10.1093/jnci/80.20.1626. PubMed PMID: 2848134.
87. Hirschman BA, Pollock BH, Tomlinson GE. The Spectrum of APC Mutations in Children with Hepatoblastoma from Familial Adenomatous Polyposis Kindreds. *The Journal of Pediatrics*. 2005;147(2):263-6. doi: <https://doi.org/10.1016/j.jpeds.2005.04.019>.
88. Yang A, Sisson R, Gupta A, Tiao G, Geller JL. Germline APC mutations in hepatoblastoma. *Pediatr Blood Cancer*. 2018;65(4). Epub 2017/12/19. doi: 10.1002/pbc.26892. PubMed PMID: 29251405.
89. Soejima H, Higashimoto K. Epigenetic and genetic alterations of the imprinting disorder Beckwith–Wiedemann syndrome and related disorders. *Journal of Human Genetics*. 2013;58(7):402-9. doi: 10.1038/jhg.2013.51.
90. Davies SM. Maintenance of Genomic Imprinting at the IGF2 Locus in Hepatoblastoma. *Cancer Research*. 1993;53(20):4781-3.
91. Ross JA, Radloff GA, Davies SM. H19 and IGF-2 allele-specific expression in hepatoblastoma. *British Journal of Cancer*. 2000;82(4):753-6. doi: 10.1054/bjoc.1999.0992.
92. Rainier S, Dobry CJ, Feinberg AP. Loss of Imprinting in Hepatoblastoma. *Cancer Research*. 1995;55(9):1836-8.
93. Li X, Adam G, Cui H, Sandstedt B, Ohlsson R, Ekstrom TJ. Expression, promoter usage and parental imprinting status of insulin-like growth factor II (IGF2) in human hepatoblastoma: uncoupling of IGF2 and H19 imprinting. *Oncogene*. 1995;11(2):221-9. Epub 1995/07/20. PubMed PMID: 7624139.
94. Fukuzawa R, Umezawa A, Ochi K, Urano F, Ikeda H, Hata J. High frequency of inactivation of the imprinted H19 gene in "sporadic" hepatoblastoma. *Int J Cancer*. 1999;82(4):490-7. Epub 1999/07/15. doi: 10.1002/(sici)1097-0215(19990812)82:4<490::aid-ijc4>3.0.co;2-i. PubMed PMID: 10404060.

95. Scelfo RAM, Schwienbacher C, Veronese A, Gramantieri L, Bolondi L, Querzoli P, Nenci I, Calin GA, Angioni A, Barbanti-Brodano G, Negrini M. Loss of methylation at chromosome 11p15.5 is common in human adult tumors. *Oncogene*. 2002;21(16):2564-72. doi: 10.1038/sj.onc.1205336.
96. Honda S, Arai Y, Haruta M, Sasaki F, Ohira M, Yamaoka H, Horie H, Nakagawara A, Hiyama E, Todo S, Kaneko Y. Loss of imprinting of IGF2 correlates with hypermethylation of the H19 differentially methylated region in hepatoblastoma. *British Journal of Cancer*. 2008;99(11):1891-9. doi: 10.1038/sj.bjc.6604754.
97. Kalish JM, Doros L, Helman LJ, Hennekam RC, Kuiper RP, Maas SM, Maher ER, Nichols KE, Plon SE, Porter CC, Rednam S, Schultz KAP, States LJ, Tomlinson GE, Zelle K, Druley TE. Surveillance Recommendations for Children with Overgrowth Syndromes and Predisposition to Wilms Tumors and Hepatoblastoma. *Clinical Cancer Research*. 2017;23(13):e115-e22. doi: 10.1158/1078-0432.Ccr-17-0710.
98. Zynger DL, Gupta A, Luan C, Chou PM, Yang GY, Yang XJ. Expression of glypican 3 in hepatoblastoma: an immunohistochemical study of 65 cases. *Hum Pathol*. 2008;39(2):224-30. Epub 2007/10/24. doi: 10.1016/j.humpath.2007.06.006. PubMed PMID: 17949790.
99. Ikeda H, Hachitanda Y, Tanimura M, Maruyama K, Koizumi T, Tsuchida Y. Development of unfavorable hepatoblastoma in children of very low birth weight. *Cancer*. 1998;82(9):1789-96. doi: 10.1002/(sici)1097-0142(19980501)82:9<1797::Aid-cncr28>3.0.Co;2-z.
100. Oue T, Kubota A, Okuyama H, Kawahara H, Nara K, Kawa K, Kitajima H. Hepatoblastoma in children of extremely low birth weight: A report from a single perinatal center. *Journal of Pediatric Surgery*. 2003;38(1):134-7. doi: 10.1053/jpsu.2003.50027.
101. Reynolds P, Urayama KY, Von Behren J, Feusner J. Birth characteristics and hepatoblastoma risk in young children. *Cancer*. 2004;100(5):1070-6. doi: 10.1002/cncr.20061.
102. McLaughlin CC, Baptiste MS, Schymura MJ, Nasca PC, Zdeb MS. Maternal and Infant Birth Characteristics and Hepatoblastoma. *American Journal of Epidemiology*. 2006;163(9):818-28. doi: 10.1093/aje/kwj104.
103. Spector LG, Johnson KJ, Soler JT, Puumala SE. Perinatal risk factors for hepatoblastoma. *British Journal of Cancer*. 2008;98(9):1570-3. doi: 10.1038/sj.bjc.6604335.
104. Maruyama K, Ikeda H, Tsuchida TK, Yoshiaki. Prenatal and postnatal histories of very low birthweight infants who developed hepatoblastoma*. *Pediatrics International*. 1999;41(1):82-9. doi: 10.1046/j.1442-200x.1999.01022.x.
105. Turcotte LM, Georgieff MK, Ross JA, Feusner JH, Tomlinson GE, Malogolowkin MH, Krailo MD, Miller N, Fonstad R, Spector LG. Neonatal medical

- exposures and characteristics of low birth weight hepatoblastoma cases: a report from the Children's Oncology Group. *Pediatric blood & cancer*. 2014;61(11):2018-23. Epub 2014/07/15. doi: 10.1002/pbc.25128. PubMed PMID: 25044669.
106. Ansell P, Mitchell CD, Roman E, Simpson J, Birch JM, Eden TOB. Relationships between perinatal and maternal characteristics and hepatoblastoma: a report from the UKCCS. *European Journal of Cancer*. 2005;41(5):741-8. doi: 10.1016/j.ejca.2004.10.024.
 107. Latini G, Gallo F, De Felice C. Birth characteristics and hepatoblastoma risk in young children. *Cancer*. 2004;101(1):210-. doi: 10.1002/cncr.20357.
 108. Maloney EK, Waxman DJ. trans-Activation of PPARAlpha and PPARgamma by structurally diverse environmental chemicals. *Toxicology and applied pharmacology*. 1999;161(2):209-18. Epub 1999/12/03. doi: 10.1006/taap.1999.8809. PubMed PMID: 10581215.
 109. Heck JE, Meyers TJ, Lombardi C, Park AS, Cockburn M, Reynolds P, Ritz B. Case-control study of birth characteristics and the risk of hepatoblastoma. *Cancer Epidemiology*. 2013;37(4):390-5. doi: <https://doi.org/10.1016/j.canep.2013.03.004>.
 110. Donohoe CL, Doyle SL, Reynolds JV. Visceral adiposity, insulin resistance and cancer risk. *Diabetology & Metabolic Syndrome*. 2011;3(1):12. doi: 10.1186/1758-5996-3-12.
 111. Renehan AG, Zwahlen M, Egger M. Adiposity and cancer risk: new mechanistic insights from epidemiology. *Nature Reviews Cancer*. 2015;15(8):484-98. doi: 10.1038/nrc3967.
 112. Kyrgiou M, Kalliala I, Markozannes G, Gunter MJ, Paraskeva E, Gabra H, Martin-Hirsch P, Tsilidis KK. Adiposity and cancer at major anatomical sites: umbrella review of the literature. *BMJ*. 2017;356:j477. doi: 10.1136/bmj.j477.
 113. Contreras ZA, Ritz B, Virk J, Cockburn M, Heck JE. Maternal pre-pregnancy and gestational diabetes, obesity, gestational weight gain, and risk of cancer in young children: a population-based study in California. *Cancer Causes & Control*. 2016;27(10):1273-85. doi: 10.1007/s10552-016-0807-5.
 114. Johnson KJ, Williams KS, Ross JA, Krailo MD, Tomlinson GE, Malogolowkin MH, Feusner JH, Spector LG. Parental Tobacco and Alcohol Use and Risk of Hepatoblastoma in Offspring: A Report from the Children's Oncology Group. *Cancer Epidemiology Biomarkers & Prevention*. 2013;22(10):1837-43. doi: 10.1158/1055-9965.Epi-13-0432.
 115. de Fine Licht S, Schmidt LS, Rod NH, Schmiegelow K, Lähteenmäki PM, Kogner P, Träger C, Stokland T, Schüz J. Hepatoblastoma in the Nordic countries. *International Journal of Cancer*. 2012;131(4):E555-E61. doi: 10.1002/ijc.27351.

116. Sorahan T, Lancashire RJ. Parental cigarette smoking and childhood risks of hepatoblastoma: OSCC data. *British Journal of Cancer*. 2004;90(5):1016-8. doi: 10.1038/sj.bjc.6601651.
117. Fraga CG, Motchnik PA, Wyrobek AJ, Rempel DM, Ames BN. Smoking and low antioxidant levels increase oxidative damage to sperm DNA. *Mutation Research/Fundamental and Molecular Mechanisms of Mutagenesis*. 1996;351(2):199-203. doi: [https://doi.org/10.1016/0027-5107\(95\)00251-0](https://doi.org/10.1016/0027-5107(95)00251-0).
118. Hargreave M, Jensen A, Toender A, Andersen KK, Kjaer SK. Fertility treatment and childhood cancer risk: a systematic meta-analysis. *Fertility and sterility*. 2013;100(1):150-61. doi: <https://doi.org/10.1016/j.fertnstert.2013.03.017>.
119. Puumala SE, Ross JA, Feusner JH, Tomlinson GE, Malogolowkin MH, Krailo MD, Spector LG. Parental infertility, infertility treatment and hepatoblastoma: a report from the Children's Oncology Group. *Human Reproduction*. 2012;27(6):1649-56. doi: 10.1093/humrep/des109.
120. Olshan AF, Smith J, Cook MN, Grufferman S, Pollock BH, Stram DO, Seeger RC, Look AT, Cohn SL, Castleberry RP, Bondy ML. Hormone and fertility drug use and the risk of neuroblastoma: a report from the Children's Cancer Group and the Pediatric Oncology Group. *Am J Epidemiol*. 1999;150(9):930-8. Epub 1999/11/05. doi: 10.1093/oxfordjournals.aje.a010101. PubMed PMID: 10547138.
121. Brinton LA, Kruger Kjaer S, Thomsen BL, Sharif HF, Graubard BI, Olsen JH, Bock JE. Childhood tumor risk after treatment with ovulation-stimulating drugs. *Fertility and sterility*. 2004;81(4):1083-91. Epub 2004/04/07. doi: 10.1016/j.fertnstert.2003.08.042. PubMed PMID: 15066468.
122. Doyle P, Bunch KJ, Beral V, Draper GJ. Cancer incidence in children conceived with assisted reproduction technology. *Lancet*. 1998;352(9126):452-3. Epub 1998/08/26. doi: 10.1016/s0140-6736(05)79186-8. PubMed PMID: 9708757.
123. Bruinsma F, Venn A, Lancaster P, Speirs A, Healy D. Incidence of cancer in children born after in-vitro fertilization. *Human reproduction (Oxford, England)*. 2000;15(3):604-7. Epub 2000/02/25. doi: 10.1093/humrep/15.3.604. PubMed PMID: 10686204.
124. Mallol-Mesnard N, Menegaux F, Lacour B, Hartmann O, Frappaz D, Doz F, Bertozzi AI, Chastagner P, Hemon D, Clavel J. Birth characteristics and childhood malignant central nervous system tumors: the ESCALE study (French Society for Childhood Cancer). *Cancer detection and prevention*. 2008;32(1):79-86. Epub 2008/04/09. doi: 10.1016/j.cdp.2008.02.003. PubMed PMID: 18396378.
125. Hiyama E. Pediatric hepatoblastoma: diagnosis and treatment. *Transl Pediatr*. 2014;3(4):293-9. doi: 10.3978/j.issn.2224-4336.2014.09.01. PubMed PMID: 26835349.

126. Hadzic N, Finegold MJ. Liver neoplasia in children. *Clin Liver Dis*. 2011;15(2):443-62, vii-x. Epub 2011/06/22. doi: 10.1016/j.cld.2011.03.011. PubMed PMID: 21689623.
127. Towbin AJ, Braojos Braga FDC, Zhang B, Geller JI, Tiao GM, Podberesky DJ. Fractures in children with newly diagnosed hepatoblastoma. *Pediatr Radiol*. 2018;48(4):581-5. Epub 2017/12/10. doi: 10.1007/s00247-017-4050-3. PubMed PMID: 29222581.
128. Archer D, Babyn P, Gilday D, Greenberg MA. Potentially misleading bone scan findings in patients with hepatoblastoma. *Clin Nucl Med*. 1993;18(12):1026-31. doi: 10.1097/00003072-199312000-00004. PubMed PMID: 8293620.
129. Tavasoli A, Mehrasma M, Hooman N, Afshar Khas L. Severe hypertension and encephalopathy due to Renin-producing hepatoblastoma. *Iran J Cancer Prev*. 2013;6(4):227-30. PubMed PMID: 25250139.
130. Grunewald TGP, Luettichau Iv, Welsch U, Dörr H-G, Höpner F, Kovacs K, Burdach S, Rabl W. First report of ectopic ACTH syndrome and PTHrP-induced hypercalcemia due to a hepatoblastoma in a child 2010;162(4):813. doi: 10.1530/eje-09-0961.
131. Wendt S, Shelso J, Wright K, Furman W. Neoplastic causes of abnormal puberty. *Pediatric blood & cancer*. 2014;61(4):664-71. Epub 2013/10/24. doi: 10.1002/pbc.24825. PubMed PMID: 24155044.
132. Sahani DV, Kalva SP. Imaging the Liver. *The Oncologist*. 2004;9(4):385-97. doi: 10.1634/theoncologist.9-4-385.
133. McCarville MB, Roebuck DJ. Diagnosis and staging of hepatoblastoma: Imaging aspects. *Pediatric Blood & Cancer*. 2012;59(5):793-9. doi: 10.1002/pbc.24221.
134. Schnater JM, Aronson DC, Plaschkes J, Perilongo G, Brown J, Otte JB, Brugieres L, Czauderna P, MacKinlay G, Vos A. Surgical view of the treatment of patients with hepatoblastoma: results from the first prospective trial of the International Society of Pediatric Oncology Liver Tumor Study Group. *Cancer*. 2002;94(4):1111-20. Epub 2002/03/29. PubMed PMID: 11920482.
135. Koh KN, Park M, Kim BE, Bae KW, Kim KM, Im HJ, Seo JJ. Prognostic implications of serum alpha-fetoprotein response during treatment of hepatoblastoma. *Pediatr Blood Cancer*. 2011;57(4):554-60. Epub 2011/03/04. doi: 10.1002/pbc.23069. PubMed PMID: 21370433.
136. Rojas Y, Guillerman RP, Zhang W, Vasudevan SA, Nuchtern JG, Thompson PA. Relapse surveillance in AFP-positive hepatoblastoma: re-evaluating the role of imaging. *Pediatric Radiology*. 2014;44(10):1275-80. doi: 10.1007/s00247-014-3000-6.
137. Sandoval JA, Malkas LH, Hickey RJ. Clinical significance of serum biomarkers in pediatric solid mediastinal and abdominal tumors. *Int J Mol Sci*. 2012;13(1):1126-53. Epub 2012/02/09. doi: 10.3390/ijms13011126. PubMed PMID: 22312308; PMCID: PMC3269742.

138. Lovvorn HN, Ayers D, Zhao Z, Hilmes M, Prasad P, Shinall MC, Berch B, Neblett WW, O'Neill JA. Defining hepatoblastoma responsiveness to induction therapy as measured by tumor volume and serum α -fetoprotein kinetics. *Journal of Pediatric Surgery*. 2010;45(1):121-9. doi: <https://doi.org/10.1016/j.jpedsurg.2009.10.023>.
139. Meyers RL, Maibach R, Hiyama E, Häberle B, Krailo M, Rangaswami A, Aronson DC, Malogolowkin MH, Perilongo G, von Schweinitz D, Ansari M, Lopez-Terrada D, Tanaka Y, Alaggio R, Leuschner I, Hishiki T, Schmid I, Watanabe K, Yoshimura K, Feng Y, Rinaldi E, Saraceno D, Derosa M, Czauderna P. Risk-stratified staging in paediatric hepatoblastoma: a unified analysis from the Children's Hepatic tumors International Collaboration. *The Lancet Oncology*. 2017;18(1):122-31. Epub 2016/11/22. doi: 10.1016/S1470-2045(16)30598-8. PubMed PMID: 27884679.
140. Cruz RJ, Jr., Ranganathan S, Mazariegos G, Soltys K, Nayyar N, Sun Q, Bond G, Shaw PH, Haberman K, Krishnamurti L, Marsh JW, Humar A, Sindhi R. Analysis of national and single-center incidence and survival after liver transplantation for hepatoblastoma: new trends and future opportunities. *Surgery*. 2013;153(2):150-9. Epub 2013/01/22. doi: 10.1016/j.surg.2012.11.006. PubMed PMID: 23331862.
141. De Ioris M, Brugieres L, Zimmermann A, Keeling J, Brock P, Maibach R, Pritchard J, Shafford L, Zsiros J, Czauderna P, Perilongo G. Hepatoblastoma with a low serum alpha-fetoprotein level at diagnosis: the SIOPEL group experience. *European journal of cancer (Oxford, England : 1990)*. 2008;44(4):545-50. Epub 2008/01/02. doi: 10.1016/j.ejca.2007.11.022. PubMed PMID: 18166449.
142. Haas JE, Feusner JH, Finegold MJ. Small cell undifferentiated histology in hepatoblastoma may be unfavorable. *Cancer*. 2001;92(12):3130-4. Epub 2001/12/26. doi: 10.1002/1097-0142(20011215)92:12<3130::aid-cnrcr10115>3.0.co;2-#. PubMed PMID: 11753992.
143. Trobaugh-Lotrario AD, Tomlinson GE, Finegold MJ, Gore L, Feusner JH. Small cell undifferentiated variant of hepatoblastoma: adverse clinical and molecular features similar to rhabdoid tumors. *Pediatric blood & cancer*. 2009;52(3):328-34. doi: 10.1002/pbc.21834. PubMed PMID: 18985717.
144. Tornout JMV, Buckley JD, Quinn JJ, Feusner JH, Krailo MD, King DR, Hammond GD, Ortega JA. Timing and magnitude of decline in alpha-fetoprotein levels in treated children with unresectable or metastatic hepatoblastoma are predictors of outcome: a report from the Children's Cancer Group. *Journal of Clinical Oncology*. 1997;15(3):1190-7. doi: 10.1200/jco.1997.15.3.1190. PubMed PMID: 9060563.
145. Haas JE, Muczynski KA, Krailo M, Ablin A, Land V, Vietti TJ, Hammond GD. Histopathology and prognosis in childhood hepatoblastoma and hepatocarcinoma. *Cancer*. 1989;64(5):1082-95. Epub 1989/09/01. doi:

10.1002/1097-0142(19890901)64:5<1082::aid-cnrcr2820640520>3.0.co;2-g.
PubMed PMID: 2547506.

146. Brown J, Perilongo G, Shafford E, Keeling J, Pritchard J, Brock P, Dicks-Mireaux C, Phillips A, Vos A, Plaschkes J. Pretreatment prognostic factors for children with hepatoblastoma-- results from the International Society of Paediatric Oncology (SIOP) study SIOPEL 1. *European journal of cancer (Oxford, England : 1990)*. 2000;36(11):1418-25. Epub 2000/07/19. doi: 10.1016/s0959-8049(00)00074-5. PubMed PMID: 10899656.

147. Roebuck DJ, Aronson D, Clapuyt P, Czauderna P, de Ville de Goyet J, Gauthier F, Mackinlay G, Maibach R, McHugh K, Olsen ØE, Otte J-B, Pariente D, Plaschkes J, Childs M, Perilongo G. 2005 PRETEXT: a revised staging system for primary malignant liver tumours of childhood developed by the SIOPEL group. *Pediatric Radiology*. 2007;37(2):123-32. doi: 10.1007/s00247-006-0361-5.

148. Towbin AJ, Meyers RL, Woodley H, Miyazaki O, Weldon CB, Morland B, Hiyama E, Czauderna P, Roebuck DJ, Tiao GM. 2017 PRETEXT: radiologic staging system for primary hepatic malignancies of childhood revised for the Paediatric Hepatic International Tumour Trial (PHITT). *Pediatr Radiol*. 2018;48(4):536-54. Epub 2018/02/11. doi: 10.1007/s00247-018-4078-z. PubMed PMID: 29427028.

149. Roebuck DJ, Aronson D, Clapuyt P, Czauderna P, de Ville de Goyet J, Gauthier F, Mackinlay G, Maibach R, McHugh K, Olsen OE, Otte JB, Pariente D, Plaschkes J, Childs M, Perilongo G. 2005 PRETEXT: a revised staging system for primary malignant liver tumours of childhood developed by the SIOPEL group. *Pediatr Radiol*. 2007;37(2):123-32; quiz 249-50. Epub 2006/12/23. doi: 10.1007/s00247-006-0361-5. PubMed PMID: 17186233; PMCID: PMC1805044.

150. Meyers AB, Towbin AJ, Geller JI, Podberesky DJ. Hepatoblastoma imaging with gadoxetate disodium-enhanced MRI—typical, atypical, pre- and post-treatment evaluation. *Pediatric Radiology*. 2012;42(7):859-66. doi: 10.1007/s00247-012-2366-6.

151. Otte JB, Pritchard J, Aronson DC, Brown J, Czauderna P, Maibach R, Perilongo G, Shafford E, Plaschkes J. Liver transplantation for hepatoblastoma: results from the International Society of Pediatric Oncology (SIOP) study SIOPEL-1 and review of the world experience. *Pediatr Blood Cancer*. 2004;42(1):74-83. Epub 2004/01/31. doi: 10.1002/pbc.10376. PubMed PMID: 14752798.

152. Czauderna P, Haeberle B, Hiyama E, Rangaswami A, Krailo M, Maibach R, Rinaldi E, Feng Y, Aronson D, Malogolowkin M, Yoshimura K, Leuschner I, Lopez-Terrada D, Hishiki T, Perilongo G, von Schweinitz D, Schmid I, Watanabe K, Derosa M, Meyers R. The Children's Hepatic tumors International Collaboration (CHIC): Novel global rare tumor database yields new prognostic factors in hepatoblastoma and becomes a research model. *European journal of*

- cancer (Oxford, England : 1990). 2016;52:92-101. Epub 2015/12/15. doi: 10.1016/j.ejca.2015.09.023. PubMed PMID: 26655560; PMCID: PMC5141607.
153. Meyers RL, Tiao G, de Ville de Goyet J, Superina R, Aronson DC. Hepatoblastoma state of the art: pre-treatment extent of disease, surgical resection guidelines and the role of liver transplantation. *Curr Opin Pediatr*. 2014;26(1):29-36. Epub 2013/12/24. doi: 10.1097/MOP.0000000000000042. PubMed PMID: 24362406.
154. Board PDQPTE. Childhood Liver Cancer Treatment (PDQ(R)): Health Professional Version. PDQ Cancer Information Summaries. Bethesda (MD): National Cancer Institute (US); 2002.
155. Tagge EP, Tagge DU, Reyes J, Tzakis A, Iwatsuki S, Starzl TE, Wiener ES. Resection, including transplantation, for hepatoblastoma and hepatocellular carcinoma: impact on survival. *J Pediatr Surg*. 1992;27(3):292-6; discussion 7. Epub 1992/03/01. doi: 10.1016/0022-3468(92)90849-3. PubMed PMID: 1323649; PMCID: PMC2977957.
156. Giacomantonio M, Ein SH, Mancier K, Stephens CA. Thirty years of experience with pediatric primary malignant liver tumors. *J Pediatr Surg*. 1984;19(5):523-6. Epub 1984/10/01. doi: 10.1016/s0022-3468(84)80095-0. PubMed PMID: 6094781.
157. Tiao GM, Bobey N, Allen S, Nieves N, Alonso M, Bucuvalas J, Wells R, Ryckman F. The current management of hepatoblastoma: a combination of chemotherapy, conventional resection, and liver transplantation. *J Pediatr*. 2005;146(2):204-11. Epub 2005/02/04. doi: 10.1016/j.jpeds.2004.09.011. PubMed PMID: 15689909.
158. Czauderna P, Otte JB, Aronson DC, Gauthier F, Mackinlay G, Roebuck D, Plaschkes J, Perilongo G. Guidelines for surgical treatment of hepatoblastoma in the modern era--recommendations from the Childhood Liver Tumour Strategy Group of the International Society of Paediatric Oncology (SIOPEL). *European journal of cancer (Oxford, England : 1990)*. 2005;41(7):1031-6. Epub 2005/05/03. doi: 10.1016/j.ejca.2005.02.004. PubMed PMID: 15862752.
159. Meyers RL, Katzenstein HM, Krailo M, McGahren ED, 3rd, Malogolowkin MH. Surgical resection of pulmonary metastatic lesions in children with hepatoblastoma. *J Pediatr Surg*. 2007;42(12):2050-6. Epub 2007/12/18. doi: 10.1016/j.jpedsurg.2007.08.030. PubMed PMID: 18082706.
160. Perilongo G, Brown J, Shafford E, Brock P, De Camargo B, Keeling JW, Vos A, Philips A, Pritchard J, Plaschkes J. Hepatoblastoma presenting with lung metastases: treatment results of the first cooperative, prospective study of the International Society of Paediatric Oncology on childhood liver tumors. *Cancer*. 2000;89(8):1845-53. Epub 2000/10/24. doi: 10.1002/1097-0142(20001015)89:8<1845::aid-cnrcr27>3.0.co;2-d. PubMed PMID: 11042582.
161. Becker K, Furch C, Schmid I, von Schweinitz D, Haberle B. Impact of postoperative complications on overall survival of patients with hepatoblastoma.

- Pediatr Blood Cancer. 2015;62(1):24-8. Epub 2014/09/25. doi: 10.1002/pbc.25240. PubMed PMID: 25251521.
162. Ortega JA, Krailo MD, Haas JE, King DR, Ablin AR, Quinn JJ, Feusner J, Campbell JR, Lloyd DA, Cherlow J, et al. Effective treatment of unresectable or metastatic hepatoblastoma with cisplatin and continuous infusion doxorubicin chemotherapy: a report from the Childrens Cancer Study Group. *J Clin Oncol*. 1991;9(12):2167-76. Epub 1991/12/01. doi: 10.1200/jco.1991.9.12.2167. PubMed PMID: 1720452.
163. Douglass EC, Reynolds M, Finegold M, Cantor AB, Glicksman A. Cisplatin, vincristine, and fluorouracil therapy for hepatoblastoma: a Pediatric Oncology Group study. *J Clin Oncol*. 1993;11(1):96-9. Epub 1993/01/01. doi: 10.1200/jco.1993.11.1.96. PubMed PMID: 8380296.
164. Pritchard J, Brown J, Shafford E, Perilongo G, Brock P, Dicks-Mireaux C, Keeling J, Phillips A, Vos A, Plaschkes J. Cisplatin, doxorubicin, and delayed surgery for childhood hepatoblastoma: a successful approach--results of the first prospective study of the International Society of Pediatric Oncology. *J Clin Oncol*. 2000;18(22):3819-28. Epub 2000/11/15. doi: 10.1200/jco.2000.18.22.3819. PubMed PMID: 11078495.
165. Aronson DC, Meyers RL. Malignant tumors of the liver in children. *Seminars in pediatric surgery*. 2016;25(5):265-75. Epub 2016/12/14. doi: 10.1053/j.sempedsurg.2016.09.002. PubMed PMID: 27955729.
166. Xianliang H, Jianhong L, Xuewu J, Zhongxian C. Cure of hepatoblastoma with transcatheter arterial chemoembolization. *J Pediatr Hematol Oncol*. 2004;26(1):60-3. Epub 2004/01/07. doi: 10.1097/00043426-200401000-00018. PubMed PMID: 14707717.
167. Malogolowkin MH, Stanley P, Steele DA, Ortega JA. Feasibility and toxicity of chemoembolization for children with liver tumors. *J Clin Oncol*. 2000;18(6):1279-84. Epub 2000/03/15. doi: 10.1200/jco.2000.18.6.1279. PubMed PMID: 10715298.
168. Yang T, Yang J, Tan T, Pan J, Hu C, Li J, Zou Y. Cure of Hepatoblastoma Through Transcatheter Arterial Chemoembolization. *Global pediatric health*. 2017;4:2333794x17742750. Epub 2017/12/12. doi: 10.1177/2333794x17742750. PubMed PMID: 29226184; PMCID: PMC5714075 conflicts of interest with respect to the research, authorship, and/or publication of this article.
169. Chen B, Chen J, Luo Q, Guo C. Effective Strategy of the Combination of High-Intensity Focused Ultrasound and Transarterial Chemoembolization for Improving Outcome of Unresectable and Metastatic Hepatoblastoma: a Retrospective Cohort Study. *Translational Oncology*. 2014;7(6):788-94. doi: <https://doi.org/10.1016/j.tranon.2014.09.006>.
170. Zsiros J, Maibach R, Shafford E, Brugieres L, Brock P, Czauderna P, Roebuck D, Childs M, Zimmermann A, Laithier V, Otte JB, de Camargo B, MacKinlay G, Scopinaro M, Aronson D, Plaschkes J, Perilongo G. Successful

treatment of childhood high-risk hepatoblastoma with dose-intensive multiagent chemotherapy and surgery: final results of the SIOPEL-3HR study. *J Clin Oncol*. 2010;28(15):2584-90. Epub 2010/04/22. doi: 10.1200/jco.2009.22.4857. PubMed PMID: 20406943.

171. Zsiros J, Brugieres L, Brock P, Roebuck D, Maibach R, Zimmermann A, Childs M, Pariente D, Laithier V, Otte JB, Branchereau S, Aronson D, Rangaswami A, Ronghe M, Casanova M, Sullivan M, Morland B, Czauderna P, Perilongo G. Dose-dense cisplatin-based chemotherapy and surgery for children with high-risk hepatoblastoma (SIOPEL-4): a prospective, single-arm, feasibility study. *Lancet Oncol*. 2013;14(9):834-42. Epub 2013/07/09. doi: 10.1016/s1470-2045(13)70272-9. PubMed PMID: 23831416; PMCID: PMC3730732.

172. Ninane J, Perilongo G, Stalens J-P, Guglielmi M, Otte J-B, Mancini A. Effectiveness and toxicity of cisplatin and doxorubicin (PLADO) in childhood hepatoblastoma and hepatocellular carcinoma: A siop pilot study. *Medical and Pediatric Oncology*. 1991;19(3):199-203. doi: 10.1002/mpo.2950190310.

173. D'Antiga L, Vallortigara F, Cillo U, Talenti E, Rugge M, Zancan L, Dall'Igna P, De Salvo GL, Perilongo G. Features predicting unresectability in hepatoblastoma. *Cancer*. 2007;110(5):1050-8. Epub 2007/07/31. doi: 10.1002/cncr.22876. PubMed PMID: 17661341.

174. Molmenti EP, Wilkinson K, Molmenti H, Roden JS, Squires RH, Fasola CG, Tomlinson G, Nagata DE, D'Amico L, Lopez MJ, Savino LM, Marubashi S, Sanchez EQ, Goldstein RM, Levy MF, Andrews W, Andersen JA, Klintmalm GB. Treatment of unresectable hepatoblastoma with liver transplantation in the pediatric population. *American journal of transplantation : official journal of the American Society of Transplantation and the American Society of Transplant Surgeons*. 2002;2(6):535-8. Epub 2002/07/18. doi: 10.1034/j.1600-6143.2002.20607.x. PubMed PMID: 12118897.

175. Pham TA, Gallo AM, Concepcion W, Esquivel CO, Bonham CA. Effect of Liver Transplant on Long-term Disease-Free Survival in Children With Hepatoblastoma and Hepatocellular Cancer. *JAMA surgery*. 2015;150(12):1150-8. Epub 2015/08/27. doi: 10.1001/jamasurg.2015.1847. PubMed PMID: 26308249.

176. Reyes JD, Carr B, Dvorchik I, Kocoshis S, Jaffe R, Gerber D, Mazariegos GV, Bueno J, Selby R. Liver transplantation and chemotherapy for hepatoblastoma and hepatocellular cancer in childhood and adolescence. *J Pediatr*. 2000;136(6):795-804. Epub 2000/06/06. PubMed PMID: 10839879.

177. Austin MT, Leys CM, Feurer ID, Lovvorn HN, 3rd, O'Neill JA, Jr., Pinson CW, Pietsch JB. Liver transplantation for childhood hepatic malignancy: a review of the United Network for Organ Sharing (UNOS) database. *J Pediatr Surg*. 2006;41(1):182-6. Epub 2006/01/18. doi: 10.1016/j.jpedsurg.2005.10.091. PubMed PMID: 16410130.

178. Trobaugh-Lotrario AD, Meyers RL, Tiao GM, Feusner JH. Pediatric liver transplantation for hepatoblastoma. *Transl Gastroenterol Hepatol*. 2016;1:44-. doi: 10.21037/tgh.2016.04.01. PubMed PMID: 28138611.
179. Ringe B, Wittekind C, Bechstein WO, Bunzendahl H, Pichlmayr R. The role of liver transplantation in hepatobiliary malignancy. A retrospective analysis of 95 patients with particular regard to tumor stage and recurrence. *Annals of surgery*. 1989;209(1):88-98. Epub 1989/01/01. doi: 10.1097/00000658-198901000-00013. PubMed PMID: 2535924; PMCID: PMC1493890.
180. Hooks KB, Audoux J, Fazli H, Lesjean S, Ernault T, Dugot-Senant N, Leste-Lasserre T, Hagedorn M, Rousseau B, Danet C, Branchereau S, Brugieres L, Taque S, Guettier C, Fabre M, Rullier A, Buendia MA, Commes T, Grosset CF, Raymond AA. New insights into diagnosis and therapeutic options for proliferative hepatoblastoma. *Hepatology*. 2018;68(1):89-102. Epub 2017/11/21. doi: 10.1002/hep.29672. PubMed PMID: 29152775.
181. Jia D, Dong R, Jing Y, Xu D, Wang Q, Chen L, Li Q, Huang Y, Zhang Y, Zhang Z, Liu L, Zheng S, Xia Q, Wang H, Dong K, He X. Exome sequencing of hepatoblastoma reveals novel mutations and cancer genes in the Wnt pathway and ubiquitin ligase complex. *Hepatology*. 2014;60(5):1686-96. Epub 2014/06/11. doi: 10.1002/hep.27243. PubMed PMID: 24912477.
182. Koch A, Denkhaus D, Albrecht S, Leuschner I, von Schweinitz D, Pietsch T. Childhood Hepatoblastomas Frequently Carry a Mutated Degradation Targeting Box of the β -Catenin Gene. *Cancer Research*. 1999;59(2):269-73.
183. Lopez-Terrada D, Gunaratne PH, Adesina AM, Pulliam J, Hoang DM, Nguyen Y, Mistretta TA, Margolin J, Finegold MJ. Histologic subtypes of hepatoblastoma are characterized by differential canonical Wnt and Notch pathway activation in DLK+ precursors. *Hum Pathol*. 2009;40(6):783-94. Epub 2009/02/10. doi: 10.1016/j.humpath.2008.07.022. PubMed PMID: 19200579.
184. Koch A, Waha A, Hartmann W, Hrychuk A, Schuller U, Waha A, Wharton KA, Jr., Fuchs SY, von Schweinitz D, Pietsch T. Elevated expression of Wnt antagonists is a common event in hepatoblastomas. *Clin Cancer Res*. 2005;11(12):4295-304. Epub 2005/06/17. doi: 10.1158/1078-0432.CCR-04-1162. PubMed PMID: 15958610.
185. Tward AD, Jones KD, Yant S, Cheung ST, Fan ST, Chen X, Kay MA, Wang R, Bishop JM. Distinct pathways of genomic progression to benign and malignant tumors of the liver. *Proc Natl Acad Sci U S A*. 2007;104(37):14771-6. Epub 2007/09/06. doi: 10.1073/pnas.0706578104. PubMed PMID: 17785413; PMCID: PMC1964540.
186. Comerford SA, Hinnant EA, Chen Y, Bansal H, Klapproth S, Rakheja D, Finegold MJ, Lopez-Terrada D, O'Donnell KA, Tomlinson GE, Hammer RE. Hepatoblastoma modeling in mice places Nrf2 within a cancer field established by mutant β -catenin. *JCI Insight*. 2016;1(16):e88549-e. doi: 10.1172/jci.insight.88549. PubMed PMID: 27734029.

187. Dawson MA, Kouzarides T. Cancer epigenetics: from mechanism to therapy. *Cell*. 2012;150(1):12-27. Epub 2012/07/10. doi: 10.1016/j.cell.2012.06.013. PubMed PMID: 22770212.
188. Greger V, Passarge E, Hopping W, Messmer E, Horsthemke B. Epigenetic changes may contribute to the formation and spontaneous regression of retinoblastoma. *Human genetics*. 1989;83(2):155-8. Epub 1989/09/01. doi: 10.1007/bf00286709. PubMed PMID: 2550354.
189. Merlo A, Herman JG, Mao L, Lee DJ, Gabrielson E, Burger PC, Baylin SB, Sidransky D. 5' CpG island methylation is associated with transcriptional silencing of the tumour suppressor p16/CDKN2/MTS1 in human cancers. *Nat Med*. 1995;1(7):686-92. Epub 1995/07/01. doi: 10.1038/nm0795-686. PubMed PMID: 7585152.
190. Baylin SB, Jones PA. A decade of exploring the cancer epigenome — biological and translational implications. *Nature Reviews Cancer*. 2011;11(10):726-34. doi: 10.1038/nrc3130.
191. Shim Y-H, Park H-J, Choi MS, Kim JS, Kim H, Kim JJ, Jang J-J, Yu E. Hypermethylation of the p16 Gene and Lack of p16 Expression in Hepatoblastoma. *Modern Pathology*. 2003;16(5):430-6. doi: 10.1097/01.MP.0000066799.99032.A7.
192. Honda S, Miyagi H, Suzuki H, Minato M, Haruta M, Kaneko Y, Hatanaka KC, Hiyama E, Kamijo T, Okada T, Taketomi A. RASSF1A methylation indicates a poor prognosis in hepatoblastoma patients. *Pediatric surgery international*. 2013;29(11):1147-52. Epub 2013/08/31. doi: 10.1007/s00383-013-3371-z. PubMed PMID: 23989600.
193. Sakamoto LHT, De Camargo B, Cajaiba M, Soares FA, Vettore AL. MT1G Hypermethylation: A Potential Prognostic Marker for Hepatoblastoma. *Pediatric Research*. 2010;67(4):387-93. doi: 10.1203/PDR.0b013e3181d01863.
194. Shih YL, Hsieh CB, Lai HC, Yan MD, Hsieh TY, Chao YC, Lin YW. SFRP1 suppressed hepatoma cells growth through Wnt canonical signaling pathway. *Int J Cancer*. 2007;121(5):1028-35. Epub 2007/04/20. doi: 10.1002/ijc.22750. PubMed PMID: 17443492.
195. Eichenmuller M, Gruner I, Hagl B, Haberle B, Muller-Hocker J, von Schweinitz D, Kappler R. Blocking the hedgehog pathway inhibits hepatoblastoma growth. *Hepatology*. 2009;49(2):482-90. Epub 2009/01/30. doi: 10.1002/hep.22649. PubMed PMID: 19177589.
196. Tada M, Kanai F, Tanaka Y, Tateishi K, Ohta M, Asaoka Y, Seto M, Muroyama R, Fukai K, Imazeki F, Kawabe T, Yokosuka O, Omata M. Down-Regulation of Hedgehog-Interacting Protein through Genetic and Epigenetic Alterations in Human Hepatocellular Carcinoma. *Clinical Cancer Research*. 2008;14(12):3768-76. doi: 10.1158/1078-0432.Ccr-07-1181.
197. Nagai H, Naka T, Terada Y, Komazaki T, Yabe A, Jin E, Kawanami O, Kishimoto T, Konishi N, Nakamura M, Kobayashi Y, Emi M. Hypermethylation

- associated with inactivation of the SOCS-1 gene, a JAK/STAT inhibitor, in human hepatoblastomas. *J Hum Genet.* 2003;48(2):65-9. Epub 2003/02/26. doi: 10.1007/s100380300008. PubMed PMID: 12601549.
198. Papaspyropoulos A, Bradley L, Thapa A, Leung CY, Toskas K, Koennig D, Pefani D-E, Raso C, Grou C, Hamilton G, Vlahov N, Grawenda A, Haider S, Chauhan J, Buti L, Kanapin A, Lu X, Buffa F, Dianov G, von Kriegsheim A, Matallanas D, Samsonova A, Zernicka-Goetz M, O'Neill E. RASSF1A uncouples Wnt from Hippo signalling and promotes YAP mediated differentiation via p73. *Nature communications.* 2018;9(1):424-. doi: 10.1038/s41467-017-02786-5. PubMed PMID: 29382819.
199. Cui X, Liu B, Zheng S, Dong K, Dong R. Genome-wide analysis of DNA methylation in hepatoblastoma tissues. *Oncol Lett.* 2016;12(2):1529-34. Epub 2016/06/28. doi: 10.3892/ol.2016.4789. PubMed PMID: 27446465.
200. Maschietto M, Rodrigues TC, Kashiwabara AY, de Araujo ÉSS, Marques Aguiar TF, da Costa CML, da Cunha IW, Dos Reis Vasques L, Cypriano M, Brentani H, de Toledo SRC, Pearson PL, Carraro DM, Rosenberg C, Krepischi ACV. DNA methylation landscape of hepatoblastomas reveals arrest at early stages of liver differentiation and cancer-related alterations. *Oncotarget.* 2016;8(58):97871-89. doi: 10.18632/oncotarget.14208. PubMed PMID: 29228658.
201. Honda S, Minato M, Suzuki H, Fujiyoshi M, Miyagi H, Haruta M, Kaneko Y, Hatanaka KC, Hiyama E, Kamijo T, Okada T, Taketomi A. Clinical prognostic value of DNA methylation in hepatoblastoma: Four novel tumor suppressor candidates. *Cancer science.* 2016;107(6):812-9. Epub 2016/03/19. doi: 10.1111/cas.12928. PubMed PMID: 26991471; PMCID: PMC4968605.
202. Yu F-X, Zhao B, Panupinthu N, Jewell Jenna L, Lian I, Wang Lloyd H, Zhao J, Yuan H, Tumaneng K, Li H, Fu X-D, Mills Gordon B, Guan K-L. Regulation of the Hippo-YAP Pathway by G-Protein-Coupled Receptor Signaling. *Cell.* 2012;150(4):780-91. doi: 10.1016/j.cell.2012.06.037.
203. Tomlinson GE, Douglass EC, Pollock BH, Finegold MJ, Schneider NR. Cytogenetic evaluation of a large series of hepatoblastomas: numerical abnormalities with recurring aberrations involving 1q12-q21. *Genes, chromosomes & cancer.* 2005;44(2):177-84. Epub 2005/06/28. doi: 10.1002/gcc.20227. PubMed PMID: 15981236.
204. Gray SG, Eriksson T, Ekström C, Holm S, Schweinitz Dv, Kogner P, Sandstedt B, Pietsch T, Ekstöm TJ. Altered expression of members of the IGF-axis in hepatoblastomas. *British Journal of Cancer.* 2000;82(9):1561-7. doi: 10.1054/bjoc.1999.1179.
205. Hartmann W, Waha A, Koch A, Goodyer CG, Albrecht S, von Schweinitz D, Pietsch T. p57(KIP2) is not mutated in hepatoblastoma but shows increased transcriptional activity in a comparative analysis of the three imprinted genes p57(KIP2), IGF2, and H19. *The American journal of pathology.*

- 2000;157(4):1393-403. Epub 2000/10/06. doi: 10.1016/s0002-9440(10)64652-4. PubMed PMID: 11021841; PMCID: PMC1850179.
206. Oue T, Yoneda A, Uehara S, Yamanaka H, Fukuzawa M. Increased expression of the hedgehog signaling pathway in pediatric solid malignancies. *J Pediatr Surg.* 2010;45(2):387-92. Epub 2010/02/16. doi: 10.1016/j.jpedsurg.2009.10.081. PubMed PMID: 20152358.
207. Li Y-C, Deng Y-H, Guo Z-H, Zhang M-M, Zhu J, Pu C-L, Xiang C-P, Guo C-B. Prognostic value of hedgehog signal component expressions in hepatoblastoma patients. *Eur J Med Res.* 2010;15(11):468-74. doi: 10.1186/2047-783x-15-11-468. PubMed PMID: 21159571.
208. Yamanaka H, Oue T, Uehara S, Fukuzawa M. Forskolin, a Hedgehog signal inhibitor, inhibits cell proliferation and induces apoptosis in pediatric tumor cell lines. *Molecular medicine reports.* 2010;3(1):133-9. Epub 2010/01/01. doi: 10.3892/mmr_00000230. PubMed PMID: 21472212.
209. Ebert MS, Sharp PA. Roles for microRNAs in conferring robustness to biological processes. *Cell.* 2012;149(3):515-24. Epub 2012/05/01. doi: 10.1016/j.cell.2012.04.005. PubMed PMID: 22541426; PMCID: PMC3351105.
210. Zhang B, Pan X, Cobb GP, Anderson TA. microRNAs as oncogenes and tumor suppressors. *Developmental biology.* 2007;302(1):1-12.
211. Dews M, Homayouni A, Yu D, Murphy D, Sevignani C, Wentzel E, Furth EE, Lee WM, Enders GH, Mendell JT, Thomas-Tikhonenko A. Augmentation of tumor angiogenesis by a Myc-activated microRNA cluster. *Nat Genet.* 2006;38(9):1060-5. Epub 2006/08/01. doi: 10.1038/ng1855. PubMed PMID: 16878133; PMCID: PMC2669546.
212. Calin GA, Croce CM. Chronic lymphocytic leukemia: interplay between noncoding RNAs and protein-coding genes. *Blood.* 2009;114(23):4761-70. Epub 2009/09/12. doi: 10.1182/blood-2009-07-192740. PubMed PMID: 19745066; PMCID: PMC2786287.
213. Xiong Y, Fang JH, Yun JP, Yang J, Zhang Y, Jia WH, Zhuang SM. Effects of MicroRNA-29 on apoptosis, tumorigenicity, and prognosis of hepatocellular carcinoma. *Hepatology.* 2010;51(3):836-45.
214. He L, He X, Lim LP, de Stanchina E, Xuan Z, Liang Y, Xue W, Zender L, Magnus J, Ridzon D, Jackson AL, Linsley PS, Chen C, Lowe SW, Cleary MA, Hannon GJ. A microRNA component of the p53 tumour suppressor network. *Nature.* 2007;447(7148):1130-4. Epub 2007/06/08. doi: 10.1038/nature05939. PubMed PMID: 17554337; PMCID: PMC4590999.
215. Hayes J, Peruzzi PP, Lawler S. MicroRNAs in cancer: biomarkers, functions and therapy. *Trends in Molecular Medicine.* 2014;20(8):460-9. doi: 10.1016/j.molmed.2014.06.005.
216. Lee RC, Feinbaum RL, Ambros V. The *C. elegans* heterochronic gene *lin-4* encodes small RNAs with antisense complementarity to *lin-14*. *Cell.*

- 1993;75(5):843-54. Epub 1993/12/03. doi: 10.1016/0092-8674(93)90529-y. PubMed PMID: 8252621.
217. Cairo S, Wang Y, de Reynies A, Duroure K, Dahan J, Redon MJ, Fabre M, McClelland M, Wang XW, Croce CM, Buendia MA. Stem cell-like micro-RNA signature driven by Myc in aggressive liver cancer. *Proc Natl Acad Sci U S A*. 2010;107(47):20471-6. Epub 2010/11/10. doi: 10.1073/pnas.1009009107. PubMed PMID: 21059911; PMCID: PMC2996672.
218. von Frowein J, Pagel P, Kappler R, von Schweinitz D, Roscher A, Schmid I. MicroRNA-492 is processed from the keratin 19 gene and up-regulated in metastatic hepatoblastoma. *Hepatology*. 2011;53(3):833-42. doi: 10.1002/hep.24125.
219. Indersie E, Lesjean S, Hooks KB, Sagliocco F, Ernault T, Cairo S, Merched-Sauvage M, Rullier A, Le Bail B, Taque S, Grotzer M, Branchereau S, Guettier C, Fabre M, Brugieres L, Hagedorn M, Buendia MA, Grosset CF. MicroRNA therapy inhibits hepatoblastoma growth in vivo by targeting beta-catenin and Wnt signaling. *Hepatology communications*. 2017;1(2):168-83. Epub 2018/02/07. doi: 10.1002/hep4.1029. PubMed PMID: 29404451; PMCID: PMC5721429.
220. Cartier F, Indersie E, Lesjean S, Charpentier J, Hooks KB, Ghousein A, Desplat A, Dugot-Senant N, Trézéguet V, Sagliocco F, Hagedorn M, Grosset CF. New tumor suppressor microRNAs target glypican-3 in human liver cancer. *Oncotarget*. 2017;8(25):41211-26. doi: 10.18632/oncotarget.17162. PubMed PMID: 28476031.
221. Yang Y, Del Re DP, Nakano N, Sciarretta S, Zhai P, Park J, Sayed D, Shirakabe A, Matsushima S, Park Y, Tian B, Abdellatif M, Sadoshima J. miR-206 Mediates YAP-Induced Cardiac Hypertrophy and Survival. *Circulation research*. 2015;117(10):891-904. Epub 2015/09/04. doi: 10.1161/circresaha.115.306624. PubMed PMID: 26333362; PMCID: PMC4747867.
222. Zheng Y, Zhao C, Zhang N, Kang W, Lu R, Wu H, Geng Y, Zhao Y, Xu X. Serum microRNA miR-206 is decreased in hyperthyroidism and mediates thyroid hormone regulation of lipid metabolism in HepG2 human hepatoblastoma cells. *Molecular medicine reports*. 2018;17(4):5635-41. Epub 2018/02/26. doi: 10.3892/mmr.2018.8633. PubMed PMID: 29484422.
223. Ruan T, He X, Yu J, Hang Z. MicroRNA-186 targets Yes-associated protein 1 to inhibit Hippo signaling and tumorigenesis in hepatocellular carcinoma. *Oncol Lett*. 2016;11(4):2941-5. Epub 2016/04/14. doi: 10.3892/ol.2016.4312. PubMed PMID: 27073580; PMCID: PMC4812570.
224. Chen M, Wu L, Tu J, Zhao Z, Fan X, Mao J, Weng Q, Wu X, Huang L, Xu M, Ji J. miR-590-5p suppresses hepatocellular carcinoma chemoresistance by targeting YAP1 expression. *EBioMedicine*. 2018;35:142-54. Epub 2018/08/13. doi: 10.1016/j.ebiom.2018.08.010. PubMed PMID: 30111512.

225. Hu Y, Yang C, Yang S, Cheng F, Rao J, Wang X. miR-665 promotes hepatocellular carcinoma cell migration, invasion, and proliferation by decreasing Hippo signaling through targeting PTPRB. *Cell Death & Disease*. 2018;9(10):954. doi: 10.1038/s41419-018-0978-y.
226. Liu AM, Poon RT, Luk JM. MicroRNA-375 targets Hippo-signaling effector YAP in liver cancer and inhibits tumor properties. *Biochemical and biophysical research communications*. 2010;394(3):623-7. Epub 2010/03/17. doi: 10.1016/j.bbrc.2010.03.036. PubMed PMID: 20226166.
227. Rikhi RR, Spady KK, Hoffman RI, Bateman MS, Bateman M, Howard LE. Hepatoblastoma: A Need for Cell Lines and Tissue Banks to Develop Targeted Drug Therapies. *Front Pediatr*. 2016;4:22-. doi: 10.3389/fped.2016.00022. PubMed PMID: 27047905.
228. Matsumoto S, Yamamichi T, Shinzawa K, Kasahara Y, Nojima S, Kodama T, Obika S, Takehara T, Morii E, Okuyama H, Kikuchi A. GREB1 induced by Wnt signaling promotes development of hepatoblastoma by suppressing TGFbeta signaling. *Nat Commun*. 2019;10(1):3882. Epub 2019/08/30. doi: 10.1038/s41467-019-11533-x. PubMed PMID: 31462641; PMCID: PMC6713762.
229. Liu P, Calvisi DF, Kiss A, Cigliano A, Schaff Z, Che L, Ribback S, Dombrowski F, Zhao D, Chen X. Central role of mTORC1 downstream of YAP/TAZ in hepatoblastoma development. *Oncotarget*. 2017;8(43):73433-47. doi: 10.18632/oncotarget.20622. PubMed PMID: 29088718.
230. Lopez-Terrada D, Cheung SW, Finegold MJ, Knowles BB. Hep G2 is a hepatoblastoma-derived cell line. *Hum Pathol*. 2009;40(10):1512-5. Epub 2009/09/16. doi: 10.1016/j.humpath.2009.07.003. PubMed PMID: 19751877.
231. Van Dyke T, Jacks T. Cancer modeling in the modern era: progress and challenges. *Cell*. 2002;108(2):135-44. Epub 2002/02/08. PubMed PMID: 11832204.
232. Day CP, Merlino G, Van Dyke T. Preclinical mouse cancer models: a maze of opportunities and challenges. *Cell*. 2015;163(1):39-53. Epub 2015/09/26. doi: 10.1016/j.cell.2015.08.068. PubMed PMID: 26406370; PMCID: PMC4583714.
233. Shachaf CM, Kopelman AM, Arvanitis C, Karlsson A, Beer S, Mandl S, Bachmann MH, Borowsky AD, Ruebner B, Cardiff RD, Yang Q, Bishop JM, Contag CH, Felsher DW. MYC inactivation uncovers pluripotent differentiation and tumour dormancy in hepatocellular cancer. *Nature*. 2004;431(7012):1112-7. Epub 2004/10/12. doi: 10.1038/nature03043. PubMed PMID: 15475948.
234. Nguyen LH, Robinton DA, Seligson MT, Wu L, Li L, Rakheja D, Comerford SA, Ramezani S, Sun X, Parikh MS, Yang EH, Powers JT, Shinoda G, Shah SP, Hammer RE, Daley GQ, Zhu H. Lin28b is sufficient to drive liver cancer and necessary for its maintenance in murine models. *Cancer Cell*. 2014;26(2):248-61. Epub 2014/08/15. doi: 10.1016/j.ccr.2014.06.018. PubMed PMID: 25117712; PMCID: PMC4145706.

235. Berger M, Neth O, Ilmer M, Garnier A, Salinas-Martín MV, de Agustín Asencio JC, von Schweinitz D, Kappler R, Muñoz M. Hepatoblastoma cells express truncated neurokinin-1 receptor and can be growth inhibited by aprepitant in vitro and in vivo. *Journal of Hepatology*. 2014;60(5):985-94. doi: <https://doi.org/10.1016/j.jhep.2013.12.024>.
236. Woodfield SE, Shi Y, Patel RH, Jin J, Major A, Sarabia SF, Starosolski Z, Zorman B, Gupta SS, Chen Z, Ibarra AM, Bissig KD, Ghaghada KB, Sumazin P, Lopez-Terrada D, Vasudevan SA. A Novel Cell Line Based Orthotopic Xenograft Mouse Model That Recapitulates Human Hepatoblastoma. *Sci Rep*. 2017;7(1):17751. Epub 2017/12/21. doi: 10.1038/s41598-017-17665-8. PubMed PMID: 29259231; PMCID: PMC5736579.
237. Eicher C, Dewerth A, Thomale J, Ellerkamp V, Hildenbrand S, Warmann SW, Fuchs J, Armeanu-Ebinger S. Effect of sorafenib combined with cytostatic agents on hepatoblastoma cell lines and xenografts. *Br J Cancer*. 2013;108(2):334-41. Epub 2012/12/22. doi: 10.1038/bjc.2012.539. PubMed PMID: 23257893; PMCID: PMC3566826.
238. Bissig-Choisat B, Kettlun-Leyton C, Legras XD, Zorman B, Barzi M, Chen LL, Amin MD, Huang YH, Pautler RG, Hampton OA, Prakash MM, Yang D, Borowiak M, Muzny D, Doddapaneni HV, Hu J, Shi Y, Gaber MW, Hicks MJ, Thompson PA, Lu Y, Mills GB, Finegold M, Goss JA, Parsons DW, Vasudevan SA, Sumazin P, Lopez-Terrada D, Bissig KD. Novel patient-derived xenograft and cell line models for therapeutic testing of pediatric liver cancer. *J Hepatol*. 2016;65(2):325-33. Epub 2016/04/28. doi: 10.1016/j.jhep.2016.04.009. PubMed PMID: 27117591; PMCID: PMC5668139.
239. Liu F, Song Y, Liu D. Hydrodynamics-based transfection in animals by systemic administration of plasmid DNA. *Gene Ther*. 1999;6(7):1258-66. Epub 1999/08/24. doi: 10.1038/sj.gt.3300947. PubMed PMID: 10455434.
240. Li J, Yao Q, Liu D. Hydrodynamic cell delivery for simultaneous establishment of tumor growth in mouse lung, liver and kidney. *Cancer Biology & Therapy*. 2011;12(8):737-41. doi: 10.4161/cbt.12.8.16442. PubMed PMID: PMC3218527.
241. Chen X, Calvisi DF. Hydrodynamic transfection for generation of novel mouse models for liver cancer research. *The American journal of pathology*. 2014;184(4):912-23. Epub 2014/02/01. doi: 10.1016/j.ajpath.2013.12.002. PubMed PMID: 24480331; PMCID: PMC3969989.
242. Wong DJ, Liu H, Ridky TW, Cassarino D, Segal E, Chang HY. Module map of stem cell genes guides creation of epithelial cancer stem cells. *Cell Stem Cell*. 2008;2(4):333-44. Epub 2008/04/10. doi: 10.1016/j.stem.2008.02.009. PubMed PMID: 18397753; PMCID: PMC2628721.
243. Ben-Porath I, Thomson MW, Carey VJ, Ge R, Bell GW, Regev A, Weinberg RA. An embryonic stem cell-like gene expression signature in poorly differentiated aggressive human tumors. *Nat Genet*. 2008;40(5):499-507. Epub

2008/04/30. doi: 10.1038/ng.127. PubMed PMID: 18443585; PMCID: PMC2912221.

244. Naxerova K, Bult CJ, Peaston A, Fancher K, Knowles BB, Kasif S, Kohane IS. Analysis of gene expression in a developmental context emphasizes distinct biological leitmotifs in human cancers. *Genome biology*. 2008;9(7):R108-R. Epub 2008/07/08. doi: 10.1186/gb-2008-9-7-r108. PubMed PMID: 18611264.

245. Bell D, Ranganathan S, Tao J, Monga SP. Novel Advances in Understanding of Molecular Pathogenesis of Hepatoblastoma: A Wnt/beta-Catenin Perspective. *Gene expression*. 2017;17(2):141-54. Epub 2016/12/13. doi: 10.3727/105221616x693639. PubMed PMID: 27938502; PMCID: PMC5311458.

246. Walthall K, Cappon GD, Hurtt ME, Zoetis T. Postnatal development of the gastrointestinal system: A species comparison. *Birth Defects Research Part B: Developmental and Reproductive Toxicology*. 2005;74(2):132-56. doi: 10.1002/bdrb.20040.

247. Haegel H, Larue L, Ohsugi M, Fedorov L, Herrenknecht K, Kemler R. Lack of beta-catenin affects mouse development at gastrulation. *Development (Cambridge, England)*. 1995;121(11):3529-37. Epub 1995/11/01. PubMed PMID: 8582267.

248. Russell JO, Monga SP. Wnt/beta-Catenin Signaling in Liver Development, Homeostasis, and Pathobiology. *Annu Rev Pathol*. 2018;13:351-78. Epub 2017/11/11. doi: 10.1146/annurev-pathol-020117-044010. PubMed PMID: 29125798; PMCID: PMC5927358.

249. Goessling W, North TE, Lord AM, Ceol C, Lee S, Weidinger G, Bourque C, Strijbosch R, Haramis AP, Puder M, Clevers H, Moon RT, Zon LI. APC mutant zebrafish uncover a changing temporal requirement for wnt signaling in liver development. *Developmental biology*. 2008;320(1):161-74. Epub 2008/07/01. doi: 10.1016/j.ydbio.2008.05.526. PubMed PMID: 18585699.

250. Tan X, Yuan Y, Zeng G, Apte U, Thompson MD, Cieply B, Stolz DB, Michalopoulos GK, Kaestner KH, Monga SP. Beta-catenin deletion in hepatoblasts disrupts hepatic morphogenesis and survival during mouse development. *Hepatology*. 2008;47(5):1667-79. Epub 2008/04/09. doi: 10.1002/hep.22225. PubMed PMID: 18393386; PMCID: PMC4449338.

251. Decaens T, Godard C, de Reynies A, Rickman DS, Tronche F, Couty JP, Perret C, Colnot S. Stabilization of beta-catenin affects mouse embryonic liver growth and hepatoblast fate. *Hepatology*. 2008;47(1):247-58. Epub 2007/11/27. doi: 10.1002/hep.21952. PubMed PMID: 18038450.

252. vTan X, Apte U, Micsenyi A, Kotsagrellos E, Luo J-H, Ranganathan S, Monga DK, Bell A, Michalopoulos GK, Monga SPS. Epidermal growth factor receptor: a novel target of the Wnt/beta-catenin pathway in liver. *Gastroenterology*. 2005;129(1):285-302. doi: 10.1053/j.gastro.2005.04.013. PubMed PMID: 16012954.

253. Si-Tayeb K, Lemaigre FP, Duncan SA. Organogenesis and development of the liver. *Dev Cell*. 2010;18(2):175-89. Epub 2010/02/18. doi: 10.1016/j.devcel.2010.01.011. PubMed PMID: 20159590.
254. Miyajima A, Tanaka M, Itoh T. Stem/Progenitor Cells in Liver Development, Homeostasis, Regeneration, and Reprogramming. *Cell Stem Cell*. 2014;14(5):561-74. doi: 10.1016/j.stem.2014.04.010.
255. Zhang W, Yatskievych TA, Baker RK, Antin PB. Regulation of Hex gene expression and initial stages of avian hepatogenesis by Bmp and Fgf signaling. *Developmental biology*. 2004;268(2):312-26. Epub 2004/04/06. doi: 10.1016/j.ydbio.2004.01.019. PubMed PMID: 15063170.
256. Shin D, Shin CH, Tucker J, Ober EA, Rentzsch F, Poss KD, Hammerschmidt M, Mullins MC, Stainier DY. Bmp and Fgf signaling are essential for liver specification in zebrafish. *Development (Cambridge, England)*. 2007;134(11):2041-50. Epub 2007/05/18. doi: 10.1242/dev.000281. PubMed PMID: 17507405.
257. Wandzioch E, Zaret KS. Dynamic signaling network for the specification of embryonic pancreas and liver progenitors. *Science*. 2009;324(5935):1707-10. Epub 2009/06/27. doi: 10.1126/science.1174497. PubMed PMID: 19556507; PMCID: PMC2771431.
258. Yang L, Wang WH, Qiu WL, Guo Z, Bi E, Xu CR. A single-cell transcriptomic analysis reveals precise pathways and regulatory mechanisms underlying hepatoblast differentiation. *Hepatology*. 2017;66(5):1387-401. Epub 2017/07/07. doi: 10.1002/hep.29353. PubMed PMID: 28681484; PMCID: PMC5650503.
259. Battle MA, Konopka G, Parviz F, Gagli AL, Yang C, Sladek FM, Duncan SA. Hepatocyte nuclear factor 4 α orchestrates expression of cell adhesion proteins during the epithelial transformation of the developing liver. *Proceedings of the National Academy of Sciences*. 2006;103(22):8419-24. doi: 10.1073/pnas.0600246103.
260. Heo J, Factor VM, Uren T, Takahama Y, Lee JS, Major M, Feinstone SM, Thorgeirsson SS. Hepatic precursors derived from murine embryonic stem cells contribute to regeneration of injured liver. *Hepatology*. 2006;44(6):1478-86. Epub 2006/11/30. doi: 10.1002/hep.21441. PubMed PMID: 17133486.
261. Lüdtke TH-W, Christoffels VM, Petry M, Kispert A. Tbx3 promotes liver bud expansion during mouse development by suppression of cholangiocyte differentiation. *Hepatology*. 2009;49(3):969-78. doi: 10.1002/hep.22700.
262. Li J, Ning G, Duncan SA. Mammalian hepatocyte differentiation requires the transcription factor HNF-4 α . *Genes Dev*. 2000;14(4):464-74. Epub 2000/02/26. PubMed PMID: 10691738; PMCID: PMC316377.
263. Sackett SD, Li Z, Hurtt R, Gao Y, Wells RG, Brondell K, Kaestner KH, Greenbaum LE. Foxl1 is a marker of bipotential hepatic progenitor cells in mice.

- Hepatology. 2009;49(3):920-9. Epub 2008/12/24. doi: 10.1002/hep.22705. PubMed PMID: 19105206; PMCID: PMC2931830.
264. Dorrell C, Erker L, Schug J, Kopp JL, Canaday PS, Fox AJ, Smirnova O, Duncan AW, Finegold MJ, Sander M, Kaestner KH, Grompe M. Prospective isolation of a bipotential clonogenic liver progenitor cell in adult mice. *Genes Dev.* 2011;25(11):1193-203. Epub 2011/06/03. doi: 10.1101/gad.2029411. PubMed PMID: 21632826; PMCID: PMC3110957.
265. Malato Y, Naqvi S, Schurmann N, Ng R, Wang B, Zape J, Kay MA, Grimm D, Willenbring H. Fate tracing of mature hepatocytes in mouse liver homeostasis and regeneration. *J Clin Invest.* 2011;121(12):4850-60. Epub 2011/11/23. doi: 10.1172/JCI59261. PubMed PMID: 22105172; PMCID: PMC3226005.
266. Fan B, Malato Y, Calvisi DF, Naqvi S, Razumilava N, Ribback S, Gores GJ, Dombrowski F, Evert M, Chen X, Willenbring H. Cholangiocarcinomas can originate from hepatocytes in mice. *J Clin Invest.* 2012;122(8):2911-5. Epub 2012/07/17. doi: 10.1172/JCI63212. PubMed PMID: 22797301; PMCID: PMC3408746.
267. Kennedy S, Rettinger S, Wayne Flye M, Ponder KP. Experiments in transgenic mice show that hepatocytes are the source for postnatal liver growth and do not stream. *Hepatology.* 1995;22(1):160-8. doi: 10.1002/hep.1840220126.
268. Furuyama K, Kawaguchi Y, Akiyama H, Horiguchi M, Kodama S, Kuhara T, Hosokawa S, Elbahrawy A, Soeda T, Koizumi M, Masui T, Kawaguchi M, Takaori K, Doi R, Nishi E, Kakinoki R, Deng JM, Behringer RR, Nakamura T, Uemoto S. Continuous cell supply from a Sox9-expressing progenitor zone in adult liver, exocrine pancreas and intestine. *Nat Genet.* 2011;43(1):34-41. Epub 2010/11/30. doi: 10.1038/ng.722. PubMed PMID: 21113154.
269. Ober EA, Lemaigre FP. Development of the liver: Insights into organ and tissue morphogenesis. *J Hepatol.* 2018;68(5):1049-62. Epub 2018/01/18. doi: 10.1016/j.jhep.2018.01.005. PubMed PMID: 29339113.
270. Suzuki A, Sekiya S, Onishi M, Oshima N, Kiyonari H, Nakauchi H, Taniguchi H. Flow cytometric isolation and clonal identification of self-renewing bipotent hepatic progenitor cells in adult mouse liver. *Hepatology.* 2008;48(6):1964-78. Epub 2008/10/07. doi: 10.1002/hep.22558. PubMed PMID: 18837044.
271. Shin S, Walton G, Aoki R, Brondell K, Schug J, Fox A, Smirnova O, Dorrell C, Erker L, Chu AS, Wells RG, Grompe M, Greenbaum LE, Kaestner KH. Foxl1-Cre-marked adult hepatic progenitors have clonogenic and bilineage differentiation potential. *Genes Dev.* 2011;25(11):1185-92. Epub 2011/06/03. doi: 10.1101/gad.2027811. PubMed PMID: 21632825; PMCID: PMC3110956.
272. Overturf K, al-Dhalimy M, Ou CN, Finegold M, Grompe M. Serial transplantation reveals the stem-cell-like regenerative potential of adult mouse

- hepatocytes. *The American journal of pathology*. 1997;151(5):1273-80. PubMed PMID: 9358753.
273. Micsenyi A, Tan X, Sneddon T, Luo J-H, Michalopoulos GK, Monga SPS. β -Catenin is temporally regulated during normal liver development. *Gastroenterology*. 2004;126(4):1134-46. doi: 10.1053/j.gastro.2003.12.047.
274. Touboul T, Chen S, To CC, Mora-Castilla S, Sabatini K, Tukey RH, Laurent LC. Stage-specific regulation of the WNT/ β -catenin pathway enhances differentiation of hESCs into hepatocytes. *Journal of hepatology*. 2016;64(6):1315-26. Epub 2016/02/26. doi: 10.1016/j.jhep.2016.02.028. PubMed PMID: 26921690.
275. Li Y, Rankin SA, Sinner D, Kenny AP, Krieg PA, Zorn AM. Sfrp5 coordinates foregut specification and morphogenesis by antagonizing both canonical and noncanonical Wnt11 signaling. *Genes & development*. 2008;22(21):3050-63. doi: 10.1101/gad.1687308. PubMed PMID: 18981481.
276. McLin VA, Rankin SA, Zorn AM. Repression of Wnt/beta-catenin signaling in the anterior endoderm is essential for liver and pancreas development. *Development (Cambridge, England)*. 2007;134(12):2207-17. Epub 2007/05/18. doi: 10.1242/dev.001230. PubMed PMID: 17507400.
277. Gualdi R, Bossard P, Zheng M, Hamada Y, Coleman JR, Zaret KS. Hepatic specification of the gut endoderm in vitro: cell signaling and transcriptional control. *Genes Dev*. 1996;10(13):1670-82. Epub 1996/07/01. doi: 10.1101/gad.10.13.1670. PubMed PMID: 8682297.
278. Bossard P, Zaret KS. GATA transcription factors as potentiators of gut endoderm differentiation. *Development (Cambridge, England)*. 1998;125(24):4909-17. Epub 1998/11/13. PubMed PMID: 9811575.
279. Septer S, Edwards G, Gunewardena S, Wolfe A, Li H, Daniel J, Apte U. Yes-associated protein is involved in proliferation and differentiation during postnatal liver development. *American journal of physiology Gastrointestinal and liver physiology*. 2012;302(5):G493-503. Epub 2011/12/24. doi: 10.1152/ajpgi.00056.2011. PubMed PMID: 22194415; PMCID: PMC3311431.
280. Zhao B, Ye X, Yu J, Li L, Li W, Li S, Yu J, Lin JD, Wang CY, Chinnaiyan AM, Lai ZC, Guan KL. TEAD mediates YAP-dependent gene induction and growth control. *Genes Dev*. 2008;22(14):1962-71. Epub 2008/06/27. doi: 10.1101/gad.1664408. PubMed PMID: 18579750; PMCID: PMC2492741.
281. Miyamura N, Hata S, Itoh T, Tanaka M, Nishio M, Itoh M, Ogawa Y, Terai S, Sakaida I, Suzuki A, Miyajima A, Nishina H. YAP determines the cell fate of injured mouse hepatocytes in vivo. *Nat Commun*. 2017;8:16017. Epub 2017/07/07. doi: 10.1038/ncomms16017. PubMed PMID: 28681838; PMCID: PMC5504293.
282. Su T, Bondar T, Zhou X, Zhang C, He H, Medzhitov R. Two-signal requirement for growth-promoting function of Yap in hepatocytes. *eLife*. 2015;4:e02948. doi: 10.7554/eLife.02948.

283. Alder O, Cullum R, Lee S, Kan AC, Wei W, Yi Y, Garside VC, Bilenky M, Griffith M, Morrissy AS, Robertson GA, Thiessen N, Zhao Y, Chen Q, Pan D, Jones SJM, Marra MA, Hoodless PA. Hippo signaling influences HNF4A and FOXA2 enhancer switching during hepatocyte differentiation. *Cell reports*. 2014;9(1):261-71. Epub 2014/09/30. doi: 10.1016/j.celrep.2014.08.046. PubMed PMID: 25263553; PMCID: PMC4612615.
284. Felmlee DJ, Grün D, Baumert TF. Zooming in on liver zonation. *Hepatology*. 2018;67(2):784-7. doi: 10.1002/hep.29554.
285. Burke ZD, Reed KR, Pheasant TJ, Sansom OJ, Clarke AR, Tosh D. Liver zonation occurs through a beta-catenin-dependent, c-Myc-independent mechanism. *Gastroenterology*. 2009;136(7):2316-24.e1-3. Epub 2009/03/10. doi: 10.1053/j.gastro.2009.02.063. PubMed PMID: 19268669.
286. Brosch M, Kattler K, Herrmann A, von Schönfels W, Nordström K, Seehofer D, Damm G, Becker T, Zeissig S, Nehring S, Reichel F, Moser V, Thangapandi RV, Stickel F, Baretton G, Röcken C, Muders M, Matz-Soja M, Krawczak M, Gasparoni G, Hartmann H, Dahl A, Schafmayer C, Walter J, Hampe J. Epigenomic map of human liver reveals principles of zoned morphogenic and metabolic control. *Nature Communications*. 2018;9(1):4150. doi: 10.1038/s41467-018-06611-5.
287. Halpern KB, Shenhav R, Matcovitch-Natan O, Tóth B, Lemze D, Golan M, Massasa EE, Baydatch S, Landen S, Moor AE, Brandis A, Giladi A, Stokar-Avihail A, David E, Amit I, Itzkovitz S. Single-cell spatial reconstruction reveals global division of labour in the mammalian liver. *Nature*. 2017;542(7641):352-6. doi: 10.1038/nature21065.
288. Seehawer M, Heinzmann F, D'Artista L, Harbig J, Roux PF, Hoenicke L, Dang H, Klotz S, Robinson L, Dore G, Rozenblum N, Kang TW, Chawla R, Buch T, Vucur M, Roth M, Zuber J, Luedde T, Sipos B, Longerich T, Heikenwalder M, Wang XW, Bischof O, Zender L. Necroptosis microenvironment directs lineage commitment in liver cancer. *Nature*. 2018;562(7725):69-75. Epub 2018/09/14. doi: 10.1038/s41586-018-0519-y. PubMed PMID: 30209397.
289. Colletti M, Cicchini C, Conigliaro A, Santangelo L, Alonzi T, Pasquini E, Tripodi M, Amicone L. Convergence of Wnt signaling on the HNF4alpha-driven transcription in controlling liver zonation. *Gastroenterology*. 2009;137(2):660-72. Epub 2009/05/21. doi: 10.1053/j.gastro.2009.05.038. PubMed PMID: 19454287.
290. Parviz F, Matullo C, Garrison WD, Savatski L, Adamson JW, Ning G, Kaestner KH, Rossi JM, Zaret KS, Duncan SA. Hepatocyte nuclear factor 4alpha controls the development of a hepatic epithelium and liver morphogenesis. *Nat Genet*. 2003;34(3):292-6. Epub 2003/06/17. doi: 10.1038/ng1175. PubMed PMID: 12808453.
291. Benhamouche S, Decaens T, Godard C, Chambrey R, Rickman DS, Moinard C, Vasseur-Cognet M, Kuo CJ, Kahn A, Perret C, Colnot S. Apc tumor suppressor gene is the "zonation-keeper" of mouse liver. *Dev Cell*.

- 2006;10(6):759-70. Epub 2006/06/03. doi: 10.1016/j.devcel.2006.03.015. PubMed PMID: 16740478.
292. Gougelet A, Torre C, Veber P, Sartor C, Bachelot L, Denechaud PD, Godard C, Moldes M, Burnol AF, Dubuquoy C, Terris B, Guillonnet F, Ye T, Schwarz M, Braeuning A, Perret C, Colnot S. T-cell factor 4 and beta-catenin chromatin occupancies pattern zonal liver metabolism in mice. *Hepatology*. 2014;59(6):2344-57. Epub 2013/11/12. doi: 10.1002/hep.26924. PubMed PMID: 24214913.
293. Stanulovic VS, Kymizi I, Kruithof-de Julio M, Hoogenkamp M, Vermeulen JL, Ruijter JM, Talianidis I, Hakvoort TB, Lamers WH. Hepatic HNF4alpha deficiency induces periportal expression of glutamine synthetase and other pericentral enzymes. *Hepatology*. 2007;45(2):433-44. Epub 2007/01/30. doi: 10.1002/hep.21456. PubMed PMID: 17256722.
294. Lau HH, Ng NHJ, Loo LSW, Jasmen JB, Teo AKK. The molecular functions of hepatocyte nuclear factors – In and beyond the liver. *Journal of Hepatology*. 2018;68(5):1033-48. doi: 10.1016/j.jhep.2017.11.026.
295. Costa RH, Kalinichenko VV, Holterman AX, Wang X. Transcription factors in liver development, differentiation, and regeneration. *Hepatology*. 2003;38(6):1331-47. Epub 2003/12/04. doi: 10.1016/j.jhep.2003.09.034. PubMed PMID: 14647040.
296. Huang P, He Z, Ji S, Sun H, Xiang D, Liu C, Hu Y, Wang X, Hui L. Induction of functional hepatocyte-like cells from mouse fibroblasts by defined factors. *Nature*. 2011;475(7356):386-9. Epub 2011/05/13. doi: 10.1038/nature10116. PubMed PMID: 21562492.
297. Huang P, Zhang L, Gao Y, He Z, Yao D, Wu Z, Cen J, Chen X, Liu C, Hu Y, Lai D, Hu Z, Chen L, Zhang Y, Cheng X, Ma X, Pan G, Wang X, Hui L. Direct reprogramming of human fibroblasts to functional and expandable hepatocytes. *Cell Stem Cell*. 2014;14(3):370-84. Epub 2014/03/04. doi: 10.1016/j.stem.2014.01.003. PubMed PMID: 24582927.
298. Sekiya S, Suzuki A. Direct conversion of mouse fibroblasts to hepatocyte-like cells by defined factors. *Nature*. 2011;475(7356):390-3. doi: 10.1038/nature10263.
299. Xiang C, Du Y, Meng G, Soon Yi L, Sun S, Song N, Zhang X, Xiao Y, Wang J, Yi Z, Liu Y, Xie B, Wu M, Shu J, Sun D, Jia J, Liang Z, Sun D, Huang Y, Shi Y, Xu J, Lu F, Li C, Xiang K, Yuan Z, Lu S, Deng H. Long-term functional maintenance of primary human hepatocytes in vitro. *Science*. 2019;364(6438):399-402. doi: 10.1126/science.aau7307.
300. Hayhurst GP, Lee YH, Lambert G, Ward JM, Gonzalez FJ. Hepatocyte nuclear factor 4alpha (nuclear receptor 2A1) is essential for maintenance of hepatic gene expression and lipid homeostasis. *Molecular and cellular biology*. 2001;21(4):1393-403. Epub 2001/02/07. doi: 10.1128/mcb.21.4.1393-1403.2001. PubMed PMID: 11158324; PMCID: PMC99591.

301. Kuo CJ, Conley PB, Chen L, Sladek FM, Darnell JE, Crabtree GR. A transcriptional hierarchy involved in mammalian cell-type specification. *Nature*. 1992;355(6359):457-61. doi: 10.1038/355457a0.
302. Santangelo L, Marchetti A, Cicchini C, Conigliaro A, Conti B, Mancone C, Bonzo JA, Gonzalez FJ, Alonzi T, Amicone L, Tripodi M. The stable repression of mesenchymal program is required for hepatocyte identity: a novel role for hepatocyte nuclear factor 4alpha. *Hepatology*. 2011;53(6):2063-74. Epub 2011/03/09. doi: 10.1002/hep.24280. PubMed PMID: 21384409; PMCID: PMC6624426.
303. Lee YH, Sauer B, Gonzalez FJ. Laron dwarfism and non-insulin-dependent diabetes mellitus in the Hnf-1alpha knockout mouse. *Molecular and cellular biology*. 1998;18(5):3059-68. Epub 1998/05/05. doi: 10.1128/mcb.18.5.3059. PubMed PMID: 9566924; PMCID: PMC110684.
304. Pontoglio M, Sreenan S, Roe M, Pugh W, Ostrega D, Doyen A, Pick AJ, Baldwin A, Velho G, Froguel P, Levisetti M, Bonner-Weir S, Bell GI, Yaniv M, Polonsky KS. Defective insulin secretion in hepatocyte nuclear factor 1alpha-deficient mice. *J Clin Invest*. 1998;101(10):2215-22. Epub 1998/05/29. doi: 10.1172/jci2548. PubMed PMID: 9593777; PMCID: PMC508809.
305. Chen WS, Manova K, Weinstein DC, Duncan SA, Plump AS, Prezioso VR, Bachvarova RF, Darnell JE, Jr. Disruption of the HNF-4 gene, expressed in visceral endoderm, leads to cell death in embryonic ectoderm and impaired gastrulation of mouse embryos. *Genes Dev*. 1994;8(20):2466-77. Epub 1994/10/15. doi: 10.1101/gad.8.20.2466. PubMed PMID: 7958910.
306. Duncan SA, Nagy A, Chan W. Murine gastrulation requires HNF-4 regulated gene expression in the visceral endoderm: tetraploid rescue of Hnf-4(-/-) embryos. *Development (Cambridge, England)*. 1997;124(2):279-87. Epub 1997/01/01. PubMed PMID: 9053305.
307. Lee CS, Friedman JR, Fulmer JT, Kaestner KH. The initiation of liver development is dependent on Foxa transcription factors. *Nature*. 2005;435(7044):944-7. Epub 2005/06/17. doi: 10.1038/nature03649. PubMed PMID: 15959514.
308. Samadani U, Costa RH. The transcriptional activator hepatocyte nuclear factor 6 regulates liver gene expression. *Molecular and cellular biology*. 1996;16(11):6273-84. Epub 1996/11/01. doi: 10.1128/mcb.16.11.6273. PubMed PMID: 8887657; PMCID: PMC231630.
309. Cereghini S. Liver-enriched transcription factors and hepatocyte differentiation. *FASEB journal : official publication of the Federation of American Societies for Experimental Biology*. 1996;10(2):267-82. Epub 1996/02/01. PubMed PMID: 8641560.
310. Kyrmizi I, Hatzis P, Katrakili N, Tronche F, Gonzalez FJ, Talianidis I. Plasticity and expanding complexity of the hepatic transcription factor network

- during liver development. *Genes Dev.* 2006;20(16):2293-305. Epub 2006/08/17. doi: 10.1101/gad.390906. PubMed PMID: 16912278; PMCID: PMC1553211.
311. Duncan SA, Navas MA, Dufort D, Rossant J, Stoffel M. Regulation of a Transcription Factor Network Required for Differentiation and Metabolism. *Science.* 1998;281(5377):692-5. doi: 10.1126/science.281.5377.692.
312. Hatzis P, Talianidis I. Regulatory mechanisms controlling human hepatocyte nuclear factor 4alpha gene expression. *Molecular and cellular biology.* 2001;21(21):7320-30. doi: 10.1128/MCB.21.21.7320-7330.2001. PubMed PMID: 11585914.
313. Strazzabosco M. Foxa1 and Foxa2 regulate bile duct development in mice. *Journal of hepatology.* 2010;52(5):765-7. Epub 2010/02/18. doi: 10.1016/j.jhep.2009.12.022. PubMed PMID: 20347503.
314. Odom DT, Zizlsperger N, Gordon DB, Bell GW, Rinaldi NJ, Murray HL, Volkert TL, Schreiber J, Rolfe PA, Gifford DK, Fraenkel E, Bell GI, Young RA. Control of pancreas and liver gene expression by HNF transcription factors. *Science.* 2004;303(5662):1378-81. Epub 2004/02/28. doi: 10.1126/science.1089769. PubMed PMID: 14988562; PMCID: PMC3012624.
315. Ning BF, Ding J, Yin C, Zhong W, Wu K, Zeng X, Yang W, Chen YX, Zhang JP, Zhang X, Wang HY, Xie WF. Hepatocyte nuclear factor 4 alpha suppresses the development of hepatocellular carcinoma. *Cancer Res.* 2010;70(19):7640-51. Epub 2010/09/30. doi: 10.1158/0008-5472.Can-10-0824. PubMed PMID: 20876809.
316. Walesky C, Edwards G, Borude P, Gunewardena S, O'Neil M, Yoo B, Apte U. Hepatocyte nuclear factor 4 alpha deletion promotes diethylnitrosamine-induced hepatocellular carcinoma in rodents. *Hepatology.* 2013;57(6):2480-90. Epub 2013/01/15. doi: 10.1002/hep.26251. PubMed PMID: 23315968; PMCID: PMC3669646.
317. Lazarevich NL, Cheremnova OA, Varga EV, Ovchinnikov DA, Kudrjavitseva EI, Morozova OV, Fleishman DI, Engelhardt NV, Duncan SA. Progression of HCC in mice is associated with a downregulation in the expression of hepatocyte nuclear factors. *Hepatology.* 2004;39(4):1038-47. doi: 10.1002/hep.20155.
318. Bonzo JA, Ferry CH, Matsubara T, Kim JH, Gonzalez FJ. Suppression of hepatocyte proliferation by hepatocyte nuclear factor 4alpha in adult mice. *The Journal of biological chemistry.* 2012;287(10):7345-56. Epub 2012/01/14. doi: 10.1074/jbc.M111.334599. PubMed PMID: 22241473; PMCID: PMC3293558.
319. Renard C-A, Labalette C, Armengol C, Cougot D, Wei Y, Cairo S, Pineau P, Neuveut C, de Reyniès A, Dejean A, Perret C, Buendia M-A. Tbx3 Is a Downstream Target of the Wnt/ β -Catenin Pathway and a Critical Mediator of β -Catenin Survival Functions in Liver Cancer. *Cancer Research.* 2007;67(3):901-10. doi: 10.1158/0008-5472.Can-06-2344.

320. Dan YY, Riehle KJ, Lazaro C, Teoh N, Haque J, Campbell JS, Fausto N. Isolation of multipotent progenitor cells from human fetal liver capable of differentiating into liver and mesenchymal lineages. *Proc Natl Acad Sci U S A*. 2006;103(26):9912-7. Epub 2006/06/20. doi: 10.1073/pnas.0603824103. PubMed PMID: 16782807; PMCID: PMC1502553.
321. Zou S, Li J, Zhou H, Frech C, Jiang X, Chu JSC, Zhao X, Li Y, Li Q, Wang H, Hu J, Kong G, Wu M, Ding C, Chen N, Hu H. Mutational landscape of intrahepatic cholangiocarcinoma. *Nature Communications*. 2014;5(1):5696. doi: 10.1038/ncomms6696.
322. Taniguchi K, Roberts LR, Aderca IN, Dong X, Qian C, Murphy LM, Nagorney DM, Burgart LJ, Roche PC, Smith DI, Ross JA, Liu W. Mutational spectrum of beta-catenin, AXIN1, and AXIN2 in hepatocellular carcinomas and hepatoblastomas. *Oncogene*. 2002;21(31):4863-71. Epub 2002/07/09. doi: 10.1038/sj.onc.1205591. PubMed PMID: 12101426.
323. Liu C, Li Y, Semenov M, Han C, Baeg GH, Tan Y, Zhang Z, Lin X, He X. Control of beta-catenin phosphorylation/degradation by a dual-kinase mechanism. *Cell*. 2002;108(6):837-47. Epub 2002/04/17. doi: 10.1016/s0092-8674(02)00685-2. PubMed PMID: 11955436.
324. Cadoret A, Ovejero C, Saadi-Kheddouci S, Souil E, Fabre M, Romagnolo B, Kahn A, Perret C. Hepatomegaly in transgenic mice expressing an oncogenic form of beta-catenin. *Cancer Res*. 2001;61(8):3245-9. Epub 2001/04/20. PubMed PMID: 11309273.
325. Lemberger UJ, Fuchs CD, Schöfer C, Bileck A, Gerner C, Stojakovic T, Taketo MM, Trauner M, Egger G, Österreicher CH. Hepatocyte specific expression of an oncogenic variant of β -catenin results in lethal metabolic dysfunction in mice. *Oncotarget*. 2018;9(13):11243-57. doi: 10.18632/oncotarget.24346. PubMed PMID: 29541410.
326. Mokkapati S, Niopek K, Huang L, Cunliffe KJ, Ruteshouser EC, deCaestecker M, Finegold MJ, Huff V. beta-catenin activation in a novel liver progenitor cell type is sufficient to cause hepatocellular carcinoma and hepatoblastoma. *Cancer Res*. 2014;74(16):4515-25. Epub 2014/05/23. doi: 10.1158/0008-5472.CAN-13-3275. PubMed PMID: 24848510; PMCID: PMC4134699.
327. Harada N, Oshima H, Katoh M, Tamai Y, Oshima M, Taketo MM. Hepatocarcinogenesis in mice with beta-catenin and Ha-ras gene mutations. *Cancer Res*. 2004;64(1):48-54. Epub 2004/01/20. doi: 10.1158/0008-5472.can-03-2123. PubMed PMID: 14729607.
328. Stauffer JK, Scarzello AJ, Andersen JB, De Kluyver RL, Back TC, Weiss JM, Thorgeirsson SS, Wiltrott RH. Coactivation of AKT and β -catenin in mice rapidly induces formation of lipogenic liver tumors. *Cancer research*. 2011;71(7):2718-27. Epub 2011/02/15. doi: 10.1158/0008-5472.CAN-10-2705. PubMed PMID: 21324921.

329. Calvisi DF, Conner EA, Ladu S, Lemmer ER, Factor VM, Thorgeirsson SS. Activation of the canonical Wnt/ β -catenin pathway confers growth advantages in c-Myc/E2F1 transgenic mouse model of liver cancer. *Journal of Hepatology*. 2005;42(6):842-9. doi: 10.1016/j.jhep.2005.01.029.
330. Tao J, Xu E, Zhao Y, Singh S, Li X, Couchy G, Chen X, Zucman-Rossi J, Chikina M, Monga SPS. Modeling a human hepatocellular carcinoma subset in mice through coexpression of met and point-mutant β -catenin. *Hepatology* (Baltimore, Md). 2016;64(5):1587-605. Epub 2016/05/28. doi: 10.1002/hep.28601. PubMed PMID: 27097116.
331. Tao J, Zhang R, Singh S, Poddar M, Xu E, Oertel M, Chen X, Ganesh S, Abrams M, Monga SP. Targeting beta-catenin in hepatocellular cancers induced by coexpression of mutant beta-catenin and K-Ras in mice. *Hepatology*. 2017;65(5):1581-99. Epub 2016/12/17. doi: 10.1002/hep.28975. PubMed PMID: 27981621; PMCID: PMC5397318.
332. Patil MA, Lee SA, Macias E, Lam ET, Xu C, Jones KD, Ho C, Rodriguez-Puebla M, Chen X. Role of cyclin D1 as a mediator of c-Met- and beta-catenin-induced hepatocarcinogenesis. *Cancer research*. 2009;69(1):253-61. doi: 10.1158/0008-5472.CAN-08-2514. PubMed PMID: 19118010.
333. Kim E, Lisby A, Ma C, Lo N, Ehmer U, Hayer KE, Furth EE, Viatour P. Promotion of growth factor signaling as a critical function of beta-catenin during HCC progression. *Nat Commun*. 2019;10(1):1909. Epub 2019/04/25. doi: 10.1038/s41467-019-09780-z. PubMed PMID: 31015417; PMCID: PMC6478918.
334. Tan X, Apte U, Micsenyi A, Kotsagrellos E, Luo J-H, Ranganathan S, Monga DK, Bell A, Michalopoulos GK, Monga SPS. Epidermal growth factor receptor: a novel target of the Wnt/beta-catenin pathway in liver. *Gastroenterology*. 2005;129(1):285-302. doi: 10.1053/j.gastro.2005.04.013. PubMed PMID: 16012954.
335. He TC, Sparks AB, Rago C, Hermeking H, Zawel L, da Costa LT, Morin PJ, Vogelstein B, Kinzler KW. Identification of c-MYC as a target of the APC pathway. *Science*. 1998;281(5382):1509-12. Epub 1998/09/04. doi: 10.1126/science.281.5382.1509. PubMed PMID: 9727977.
336. Yochum GS, Sherrick CM, Macpartlin M, Goodman RH. A beta-catenin/TCF-coordinated chromatin loop at MYC integrates 5' and 3' Wnt responsive enhancers. *Proc Natl Acad Sci U S A*. 2010;107(1):145-50. Epub 2009/12/08. doi: 10.1073/pnas.0912294107. PubMed PMID: 19966299; PMCID: PMC2806753.
337. Hoshida Y, Nijman SM, Kobayashi M, Chan JA, Brunet JP, Chiang DY, Villanueva A, Newell P, Ikeda K, Hashimoto M, Watanabe G, Gabriel S, Friedman SL, Kumada H, Llovet JM, Golub TR. Integrative transcriptome analysis reveals common molecular subclasses of human hepatocellular carcinoma. *Cancer Res*. 2009;69(18):7385-92. Epub 2009/09/03. doi:

- 10.1158/0008-5472.Can-09-1089. PubMed PMID: 19723656; PMCID: PMC3549578.
338. Steinhardt AA, Gayyed MF, Klein AP, Dong J, Maitra A, Pan D, Montgomery EA, Anders RA. Expression of Yes-associated protein in common solid tumors. *Hum Pathol.* 2008;39(11):1582-9. Epub 2008/08/16. doi: 10.1016/j.humpath.2008.04.012. PubMed PMID: 18703216; PMCID: PMC2720436.
339. Lee CK, Jeong SH, Jang C, Bae H, Kim YH, Park I, Kim SK, Koh GY. Tumor metastasis to lymph nodes requires YAP-dependent metabolic adaptation. *Science.* 2019;363(6427):644-9. Epub 2019/02/09. doi: 10.1126/science.aav0173. PubMed PMID: 30733421.
340. Cheng H, Zhang Z, Rodriguez-Barrueco R, Borczuk A, Liu H, Yu J, Silva JM, Cheng SK, Perez-Soler R, Halmos B. Functional genomics screen identifies YAP1 as a key determinant to enhance treatment sensitivity in lung cancer cells. *Oncotarget.* 2016;7(20):28976-88. Epub 2015/12/31. doi: 10.18632/oncotarget.6721. PubMed PMID: 26716514; PMCID: PMC5045371.
341. Kim T, Yang SJ, Hwang D, Song J, Kim M, Kyum Kim S, Kang K, Ahn J, Lee D, Kim MY, Kim S, Seung Koo J, Seok Koh S, Kim SY, Lim DS. A basal-like breast cancer-specific role for SRF-IL6 in YAP-induced cancer stemness. *Nat Commun.* 2015;6:10186. Epub 2015/12/17. doi: 10.1038/ncomms10186. PubMed PMID: 26671411; PMCID: PMC4703869.
342. Lee KW, Lee SS, Kim SB, Sohn BH, Lee HS, Jang HJ, Park YY, Kopetz S, Kim SS, Oh SC, Lee JS. Significant association of oncogene YAP1 with poor prognosis and cetuximab resistance in colorectal cancer patients. *Clin Cancer Res.* 2015;21(2):357-64. Epub 2014/11/13. doi: 10.1158/1078-0432.Ccr-14-1374. PubMed PMID: 25388162; PMCID: PMC4513664.
343. Wang L, Shi S, Guo Z, Zhang X, Han S, Yang A, Wen W, Zhu Q. Overexpression of YAP and TAZ is an independent predictor of prognosis in colorectal cancer and related to the proliferation and metastasis of colon cancer cells. *PloS one.* 2013;8(6):e65539. Epub 2013/06/14. doi: 10.1371/journal.pone.0065539. PubMed PMID: 23762387; PMCID: PMC3677905.
344. Xu MZ, Yao TJ, Lee NP, Ng IO, Chan YT, Zender L, Lowe SW, Poon RT, Luk JM. Yes-associated protein is an independent prognostic marker in hepatocellular carcinoma. *Cancer.* 2009;115(19):4576-85. Epub 2009/06/25. doi: 10.1002/cncr.24495. PubMed PMID: 19551889; PMCID: PMC2811690.
345. Kang W, Tong JH, Chan AW, Lee TL, Lung RW, Leung PP, So KK, Wu K, Fan D, Yu J, Sung JJ, To KF. Yes-associated protein 1 exhibits oncogenic property in gastric cancer and its nuclear accumulation associates with poor prognosis. *Clin Cancer Res.* 2011;17(8):2130-9. Epub 2011/02/25. doi: 10.1158/1078-0432.Ccr-10-2467. PubMed PMID: 21346147.

346. Diep CH, Zucker KM, Hostetter G, Watanabe A, Hu C, Munoz RM, Von Hoff DD, Han H. Down-regulation of Yes Associated Protein 1 expression reduces cell proliferation and clonogenicity of pancreatic cancer cells. *PloS one*. 2012;7(3):e32783. Epub 2012/03/08. doi: 10.1371/journal.pone.0032783. PubMed PMID: 22396793; PMCID: PMC3291657.
347. Reis H, Bertram S, Pott L, Canbay A, Gallinat A, Baba HA. Markers of Hippo-Pathway Activity in Tumor Forming Liver Lesions. *Pathology & Oncology Research*. 2017;23(1):33-9. doi: 10.1007/s12253-016-0079-0.
348. Sohn BH, Shim J-J, Kim S-B, Jang KY, Kim SM, Kim JH, Hwang JE, Jang H-J, Lee H-S, Kim S-C, Jeong W, Kim SS, Park ES, Heo J, Kim YJ, Kim D-G, Leem S-H, Kaseb A, Hassan MM, Cha M, Chu I-S, Johnson RL, Park Y-Y, Lee J-S. Inactivation of Hippo Pathway Is Significantly Associated with Poor Prognosis in Hepatocellular Carcinoma. *Clinical Cancer Research*. 2016;22(5):1256-64. doi: 10.1158/1078-0432.Ccr-15-1447.
349. Chen Q, Zhang N, Xie R, Wang W, Cai J, Choi KS, David KK, Huang B, Yabuta N, Nojima H, Anders RA, Pan D. Homeostatic control of Hippo signaling activity revealed by an endogenous activating mutation in YAP. *Genes Dev*. 2015;29(12):1285-97. Epub 2015/06/26. doi: 10.1101/gad.264234.115. PubMed PMID: 26109051; PMCID: PMC4495399.
350. Lee KP, Lee JH, Kim TS, Kim TH, Park HD, Byun JS, Kim MC, Jeong WI, Calvisi DF, Kim JM, Lim DS. The Hippo-Salvador pathway restrains hepatic oval cell proliferation, liver size, and liver tumorigenesis. *Proc Natl Acad Sci U S A*. 2010;107(18):8248-53. Epub 2010/04/21. doi: 10.1073/pnas.0912203107. PubMed PMID: 20404163; PMCID: PMC2889558.
351. Nishio M, Hamada K, Kawahara K, Sasaki M, Noguchi F, Chiba S, Mizuno K, Suzuki SO, Dong Y, Tokuda M, Morikawa T, Hikasa H, Eggenschwiler J, Yabuta N, Nojima H, Nakagawa K, Hata Y, Nishina H, Mimori K, Mori M, Sasaki T, Mak TW, Nakano T, Itami S, Suzuki A. Cancer susceptibility and embryonic lethality in Mob1a/1b double-mutant mice. *J Clin Invest*. 2012;122(12):4505-18. Epub 2012/11/13. doi: 10.1172/jci63735. PubMed PMID: 23143302; PMCID: PMC3533542.
352. Nishio M, Sugimachi K, Goto H, Wang J, Morikawa T, Miyachi Y, Takano Y, Hikasa H, Itoh T, Suzuki SO, Kurihara H, Aishima S, Leask A, Sasaki T, Nakano T, Nishina H, Nishikawa Y, Sekido Y, Nakao K, Shin-Ya K, Mimori K, Suzuki A. Dysregulated YAP1/TAZ and TGF-beta signaling mediate hepatocarcinogenesis in Mob1a/1b-deficient mice. *Proc Natl Acad Sci U S A*. 2016;113(1):E71-80. Epub 2015/12/25. doi: 10.1073/pnas.1517188113. PubMed PMID: 26699479; PMCID: PMC4711826.
353. Ahn EY, Kim JS, Kim GJ, Park YN. RASSF1A-Mediated Regulation of AREG via the Hippo Pathway in Hepatocellular Carcinoma. *Molecular Cancer Research*. 2013;11(7):748-58. doi: 10.1158/1541-7786.Mcr-12-0665.

354. Mooring M, Fowl BH, Lum SZC, Liu Y, Yao K, Softic S, Kirchner R, Bernstein A, Singhi AD, Jay DG, Kahn CR, Camargo FD, Yimlamai D. Hepatocyte Stress Increases Expression of Yes-Associated Protein and Transcriptional Coactivator With PDZ-Binding Motif in Hepatocytes to Promote Parenchymal Inflammation and Fibrosis. *Hepatology*.n/a(n/a). doi: 10.1002/hep.30928.
355. Liu-Chittenden Y, Huang B, Shim JS, Chen Q, Lee SJ, Anders RA, Liu JO, Pan D. Genetic and pharmacological disruption of the TEAD-YAP complex suppresses the oncogenic activity of YAP. *Genes Dev.* 2012;26(12):1300-5. Epub 2012/06/09. doi: 10.1101/gad.192856.112. PubMed PMID: 22677547; PMCID: PMC3387657.
356. Lamar JM, Stern P, Liu H, Schindler JW, Jiang ZG, Hynes RO. The Hippo pathway target, YAP, promotes metastasis through its TEAD-interaction domain. *Proc Natl Acad Sci U S A.* 2012;109(37):E2441-50. Epub 2012/08/15. doi: 10.1073/pnas.1212021109. PubMed PMID: 22891335; PMCID: PMC3443162.
357. Low BC, Pan CQ, Shivashankar GV, Bershadsky A, Sudol M, Sheetz M. YAP/TAZ as mechanosensors and mechanotransducers in regulating organ size and tumor growth. *FEBS letters.* 2014;588(16):2663-70. Epub 2014/04/22. doi: 10.1016/j.febslet.2014.04.012. PubMed PMID: 24747426.
358. Dasari VR, Mazack V, Feng W, Nash J, Carey DJ, Gogoi R. Verteporfin exhibits YAP-independent anti-proliferative and cytotoxic effects in endometrial cancer cells. *Oncotarget.* 2017;8(17):28628-40. doi: 10.18632/oncotarget.15614. PubMed PMID: 28404908.
359. Zhang H, Ramakrishnan SK, Triner D, Centofanti B, Maitra D, Györfy B, Sebolt-Leopold JS, Dame MK, Varani J, Brenner DE, Fearon ER, Omary MB, Shah YM. Tumor-selective proteotoxicity of verteporfin inhibits colon cancer progression independently of YAP1. *Science Signaling.* 2015;8(397):ra98-ra. doi: 10.1126/scisignal.aac5418.
360. Zhang X, Sun F, Qiao Y, Zheng W, Liu Y, Chen Y, Wu Q, Liu X, Zhu G, Chen Y, Yu Y, Pan Q, Wang J. TFCP2 Is Required for YAP-Dependent Transcription to Stimulate Liver Malignancy. *Cell reports.* 2017;21(5):1227-39. doi: 10.1016/j.celrep.2017.10.017.
361. Croci O, De Fazio S, Biagioni F, Donato E, Caganova M, Curti L, Doni M, Sberna S, Aldeghi D, Biancotto C, Verrecchia A, Olivero D, Amati B, Campaner S. Transcriptional integration of mitogenic and mechanical signals by Myc and YAP. *Genes Dev.* 2017;31(20):2017-22. Epub 2017/11/17. doi: 10.1101/gad.301184.117. PubMed PMID: 29141911; PMCID: PMC5733494.
362. Bisso A, Filipuzzi M, Gamarra Figueroa GP, Brumana G, Biagioni F, Doni M, Ceccotti G, Tanaskovic N, Morelli MJ, Pendino V, Chiacchiera F, Pasini D, Olivero D, Campaner S, Sabò A, Amati B. Cooperation between MYC and β -catenin in liver tumorigenesis requires Yap/Taz. *Hepatology*.n/a(n/a). doi: 10.1002/hep.31120.

363. Stein C, Bardet AF, Roma G, Bergling S, Clay I, Ruchti A, Agarinis C, Schmelzle T, Bouwmeester T, Schubeler D, Bauer A. YAP1 Exerts Its Transcriptional Control via TEAD-Mediated Activation of Enhancers. *PLoS Genet.* 2015;11(8):e1005465. Epub 2015/08/22. doi: 10.1371/journal.pgen.1005465. PubMed PMID: 26295846; PMCID: PMC4546604.
364. Galli GG, Carrara M, Yuan WC, Valdes-Quezada C, Gurung B, Pepe-Mooney B, Zhang T, Geeven G, Gray NS, de Laat W, Calogero RA, Camargo FD. YAP Drives Growth by Controlling Transcriptional Pause Release from Dynamic Enhancers. *Mol Cell.* 2015;60(2):328-37. Epub 2015/10/07. doi: 10.1016/j.molcel.2015.09.001. PubMed PMID: 26439301; PMCID: PMC4624327.
365. Zanconato F, Forcato M, Battilana G, Azzolin L, Quaranta E, Bodega B, Rosato A, Bicciato S, Cordenonsi M, Piccolo S. Genome-wide association between YAP/TAZ/TEAD and AP-1 at enhancers drives oncogenic growth. *Nat Cell Biol.* 2015;17(9):1218-27. Epub 2015/08/11. doi: 10.1038/ncb3216. PubMed PMID: 26258633; PMCID: PMC6186417.
366. Moya IM, Castaldo SA, Van den Mooter L, Soheily S, Sansores-Garcia L, Jacobs J, Mannaerts I, Xie J, Verboven E, Hillen H, Algueró-Nadal A, Karaman R, Van Haele M, Kowalczyk W, De Waegeneer M, Verhulst S, Karras P, van Huffel L, Zender L, Marine J-C, Roskams T, Johnson R, Aerts S, van Grunsven LA, Halder G. Peritumoral activation of the Hippo pathway effectors YAP and TAZ suppresses liver cancer in mice. *Science.* 2019;366(6468):1029-34. doi: 10.1126/science.aaw9886.
367. Varelas X, Miller BW, Sopko R, Song S, Gregorieff A, Fellouse FA, Sakuma R, Pawson T, Hunziker W, McNeill H, Wrana JL, Attisano L. The Hippo pathway regulates Wnt/beta-catenin signaling. *Dev Cell.* 2010;18(4):579-91. Epub 2010/04/24. doi: 10.1016/j.devcel.2010.03.007. PubMed PMID: 20412773.
368. Imajo M, Miyatake K, Imura A, Miyamoto A, Nishida E. A molecular mechanism that links Hippo signalling to the inhibition of Wnt/beta-catenin signalling. *The EMBO journal.* 2012;31(5):1109-22. Epub 2012/01/12. doi: 10.1038/emboj.2011.487. PubMed PMID: 22234184; PMCID: PMC3297994.
369. Heallen T, Zhang M, Wang J, Bonilla-Claudio M, Klysik E, Johnson RL, Martin JF. Hippo Pathway Inhibits Wnt Signaling to Restrain Cardiomyocyte Proliferation and Heart Size. *Science.* 2011;332(6028):458-61. doi: 10.1126/science.1199010.
370. Wang J, Park JS, Wei Y, Rajurkar M, Cotton JL, Fan Q, Lewis BC, Ji H, Mao J. TRIB2 acts downstream of Wnt/TCF in liver cancer cells to regulate YAP and C/EBPalpha function. *Mol Cell.* 2013;51(2):211-25. Epub 2013/06/19. doi: 10.1016/j.molcel.2013.05.013. PubMed PMID: 23769673; PMCID: PMC4007693.
371. Iakova P, Awad SS, Timchenko NA. Aging reduces proliferative capacities of liver by switching pathways of C/EBPalpha growth arrest. *Cell.*

2003;113(4):495-506. Epub 2003/05/22. doi: 10.1016/s0092-8674(03)00318-0. PubMed PMID: 12757710.

372. Konsavage WM, Jr., Kyler SL, Rennoll SA, Jin G, Yochum GS. Wnt/beta-catenin signaling regulates Yes-associated protein (YAP) gene expression in colorectal carcinoma cells. *The Journal of biological chemistry*. 2012;287(15):11730-9. Epub 2012/02/18. doi: 10.1074/jbc.M111.327767. PubMed PMID: 22337891; PMCID: PMC3320921.

373. Rosenbluh J, Nijhawan D, Cox AG, Li X, Neal JT, Schafer EJ, Zack TI, Wang X, Tsherniak A, Schinzel AC, Shao DD, Schumacher SE, Weir BA, Vazquez F, Cowley GS, Root DE, Mesirov JP, Beroukhi R, Kuo CJ, Goessling W, Hahn WC. beta-Catenin-driven cancers require a YAP1 transcriptional complex for survival and tumorigenesis. *Cell*. 2012;151(7):1457-73. Epub 2012/12/19. doi: 10.1016/j.cell.2012.11.026. PubMed PMID: 23245941; PMCID: PMC3530160.

374. Knudson AG. Two genetic hits (more or less) to cancer. *Nature Reviews Cancer*. 2001;1(2):157-62. doi: 10.1038/35101031.

375. Weinstein IB. Cancer. Addiction to oncogenes--the Achilles heel of cancer. *Science*. 2002;297(5578):63-4. Epub 2002/07/06. doi: 10.1126/science.1073096. PubMed PMID: 12098689.

376. Sharma SV, Settleman J. Oncogene addiction: setting the stage for molecularly targeted cancer therapy. *Genes Dev*. 2007;21(24):3214-31. Epub 2007/12/15. doi: 10.1101/gad.1609907. PubMed PMID: 18079171.

377. Luo J, Solimini NL, Elledge SJ. Principles of cancer therapy: oncogene and non-oncogene addiction. *Cell*. 2009;136(5):823-37. Epub 2009/03/10. doi: 10.1016/j.cell.2009.02.024. PubMed PMID: 19269363; PMCID: PMC2894612.

378. Collins MA, Bednar F, Zhang Y, Brisset J-C, Galbán S, Galbán CJ, Rakshit S, Flannagan KS, Adsay NV, Pasca di Magliano M. Oncogenic Kras is required for both the initiation and maintenance of pancreatic cancer in mice. *The Journal of Clinical Investigation*. 2012;122(2):639-53. doi: 10.1172/JCI59227.

379. Fisher GH, Wellen SL, Klimstra D, Lenczowski JM, Tichelaar JW, Lizak MJ, Whitsett JA, Koretsky A, Varmus HE. Induction and apoptotic regression of lung adenocarcinomas by regulation of a K-Ras transgene in the presence and absence of tumor suppressor genes. *Genes Dev*. 2001;15(24):3249-62. Epub 2001/12/26. doi: 10.1101/gad.947701. PubMed PMID: 11751631; PMCID: PMC312852.

380. Lim K-H, Counter CM. Reduction in the requirement of oncogenic Ras signaling to activation of PI3K/AKT pathway during tumor maintenance. *Cancer Cell*. 2005;8(5):381-92. doi: <https://doi.org/10.1016/j.ccr.2005.10.014>.

381. Sakamoto K, Triplett AA, Schuler LA, Wagner KU. Janus kinase 2 is required for the initiation but not maintenance of prolactin-induced mammary cancer. *Oncogene*. 2010;29(39):5359-69. doi: 10.1038/onc.2010.274.

382. Gupta J, del Barco Barrantes I, Igea A, Sakellariou S, Pateras Ioannis S, Gorgoulis Vassilis G, Nebreda Angel R. Dual Function of p38 α MAPK in Colon Cancer: Suppression of Colitis-Associated Tumor Initiation but Requirement for Cancer Cell Survival. *Cancer Cell*. 2014;25(4):484-500. doi: <https://doi.org/10.1016/j.ccr.2014.02.019>.
383. Huang Y-Y, Dai L, Gaines D, Droz-Rosario R, Lu H, Liu J, Shen Z. *BCCIP* Suppresses Tumor Initiation but Is Required for Tumor Progression. *Cancer Research*. 2013;73(23):7122-33. doi: 10.1158/0008-5472.Can-13-1766.
384. Podsypanina K, Politi K, Beverly LJ, Varmus HE. Oncogene cooperation in tumor maintenance and tumor recurrence in mouse mammary tumors induced by *Myc* and mutant *Kras*. *Proceedings of the National Academy of Sciences*. 2008;105(13):5242-7. doi: 10.1073/pnas.0801197105.
385. Kistner A, Gossen M, Zimmermann F, Jerecic J, Ullmer C, Lubbert H, Bujard H. Doxycycline-mediated quantitative and tissue-specific control of gene expression in transgenic mice. *Proc Natl Acad Sci U S A*. 1996;93(20):10933-8. Epub 1996/10/01. PubMed PMID: 8855286; PMCID: PMC38261.
386. Tschaharganeh DF, Xue W, Calvisi DF, Evert M, Michurina TV, Dow LE, Banito A, Katz SF, Kastenhuber ER, Weissmueller S, Huang CH, Lechel A, Andersen JB, Capper D, Zender L, Longerich T, Enikolopov G, Lowe SW. p53-dependent Nestin regulation links tumor suppression to cellular plasticity in liver cancer. *Cell*. 2014;158(3):579-92. Epub 2014/08/02. doi: 10.1016/j.cell.2014.05.051. PubMed PMID: 25083869; PMCID: PMC4221237.
387. Wiesner SM, Decker SA, Larson JD, Ericson K, Forster C, Gallardo JL, Long C, Demorest ZL, Zamora EA, Low WC, SantaCruz K, Largaespada DA, Ohlfest JR. De novo induction of genetically engineered brain tumors in mice using plasmid DNA. *Cancer Res*. 2009;69(2):431-9. Epub 2009/01/17. doi: 10.1158/0008-5472.CAN-08-1800. PubMed PMID: 19147555; PMCID: PMC2701484.
388. Urtasun R, Latasa MU, Demartis MI, Balzani S, Goñi S, Garcia-Irigoyen O, Elizalde M, Azcona M, Pascale RM, Feo F, Bioulac-Sage P, Balabaud C, Muntané J, Prieto J, Berasain C, Avila MA. Connective tissue growth factor autocriny in human hepatocellular carcinoma: Oncogenic role and regulation by epidermal growth factor receptor/yes-associated protein-mediated activation. *Hepatology*. 2011;54(6):2149-58. doi: 10.1002/hep.24587.
389. Kramer A, Green J, Pollard J, Jr., Tugendreich S. Causal analysis approaches in Ingenuity Pathway Analysis. *Bioinformatics*. 2014;30(4):523-30. Epub 2013/12/18. doi: 10.1093/bioinformatics/btt703. PubMed PMID: 24336805; PMCID: PMC3928520.
390. Lucchetti J, Fracasso C, Balducci C, Passoni A, Forloni G, Salmona M, Gobbi M. Plasma and Brain Concentrations of Doxycycline after Single and Repeated Doses in Wild-Type and APP23 Mice. *J Pharmacol Exp Ther*.

- 2019;368(1):32-40. Epub 2018/11/07. doi: 10.1124/jpet.118.252064. PubMed PMID: 30396916.
391. Hein AL, Brandquist ND, Ouellette CY, Seshacharyulu P, Enke CA, Ouellette MM, Batra SK, Yan Y. PR55 α regulatory subunit of PP2A inhibits the MOB1/LATS cascade and activates YAP in pancreatic cancer cells. *Oncogenesis*. 2019;8(11):63. doi: 10.1038/s41389-019-0172-9.
392. Corish P, Tyler-Smith C. Attenuation of green fluorescent protein half-life in mammalian cells. *Protein Engineering, Design and Selection*. 1999;12(12):1035-40. doi: 10.1093/protein/12.12.1035.
393. Wu CH, van Riggelen J, Yetil A, Fan AC, Bachireddy P, Felsher DW. Cellular senescence is an important mechanism of tumor regression upon c-Myc inactivation. *Proc Natl Acad Sci U S A*. 2007;104(32):13028-33. Epub 2007/08/01. doi: 10.1073/pnas.0701953104. PubMed PMID: 17664422; PMCID: PMC1941831.
394. Felsher DW, Bishop JM. Reversible tumorigenesis by MYC in hematopoietic lineages. *Mol Cell*. 1999;4(2):199-207. Epub 1999/09/17. PubMed PMID: 10488335.
395. Jain M, Arvanitis C, Chu K, Dewey W, Leonhardt E, Trinh M, Sundberg CD, Bishop JM, Felsher DW. Sustained loss of a neoplastic phenotype by brief inactivation of MYC. *Science*. 2002;297(5578):102-4. Epub 2002/07/06. doi: 10.1126/science.1071489. PubMed PMID: 12098700.
396. Spath GF, Weiss MC. Hepatocyte nuclear factor 4 provokes expression of epithelial marker genes, acting as a morphogen in dedifferentiated hepatoma cells. *J Cell Biol*. 1998;140(4):935-46. Epub 1998/03/21. doi: 10.1083/jcb.140.4.935. PubMed PMID: 9472044; PMCID: PMC2141753.
397. Corces MR, Trevino AE, Hamilton EG, Greenside PG, Sinnott-Armstrong NA, Vesuna S, Satpathy AT, Rubin AJ, Montine KS, Wu B, Kathiria A, Cho SW, Mumbach MR, Carter AC, Kasowski M, Orloff LA, Risca VI, Kundaje A, Khavari PA, Montine TJ, Greenleaf WJ, Chang HY. An improved ATAC-seq protocol reduces background and enables interrogation of frozen tissues. *Nat Methods*. 2017;14(10):959-62. Epub 2017/08/29. doi: 10.1038/nmeth.4396. PubMed PMID: 28846090; PMCID: PMC5623106.
398. Shalem O, Sanjana NE, Hartenian E, Shi X, Scott DA, Mikkelsen T, Heckl D, Ebert BL, Root DE, Doench JG, Zhang F. Genome-scale CRISPR-Cas9 knockout screening in human cells. *Science*. 2014;343(6166):84-7. Epub 2013/12/18. doi: 10.1126/science.1247005. PubMed PMID: 24336571; PMCID: PMC4089965.
399. Buenrostro JD, Giresi PG, Zaba LC, Chang HY, Greenleaf WJ. Transposition of native chromatin for fast and sensitive epigenomic profiling of open chromatin, DNA-binding proteins and nucleosome position. *Nat Methods*. 2013;10(12):1213-8. Epub 2013/10/08. doi: 10.1038/nmeth.2688. PubMed PMID: 24097267; PMCID: PMC3959825.

400. Martin M. Cutadapt removes adapter sequences from high-throughput sequencing reads. *EMBnetjournal*. 2011;17:10-2. doi: <https://doi.org/10.14806/ej.17.1.200>.
401. Li H. Aligning Sequence Reads, Clone Sequences and Assembly Contigs with BWA-MEM. arXiv 2013. PubMed PMID: <http://arxiv.org/abs/1303.3997>.
402. Li H, Handsaker B, Wysoker A, Fennell T, Ruan J, Homer N, Marth G, Abecasis G, Durbin R, Genome Project Data Processing S. The Sequence Alignment/Map format and SAMtools. *Bioinformatics*. 2009;25(16):2078-9. Epub 2009/06/10. doi: 10.1093/bioinformatics/btp352. PubMed PMID: 19505943; PMCID: PMC2723002.
403. Ramírez F, Ryan DP, Grüning B, Bhardwaj V, Kilpert F, Richter AS, Heyne S, Dündar F, Manke T. deepTools2: a next generation web server for deep-sequencing data analysis. *Nucleic Acids Res*. 2016;44(W1):W160-W5. Epub 2016/04/13. doi: 10.1093/nar/gkw257. PubMed PMID: 27079975.
404. Quinlan AR, Hall IM. BEDTools: a flexible suite of utilities for comparing genomic features. *Bioinformatics*. 2010;26(6):841-2. Epub 2010/01/30. doi: 10.1093/bioinformatics/btq033. PubMed PMID: 20110278; PMCID: PMC2832824.
405. Grompe M, al-Dhalimy M, Finegold M, Ou CN, Burlingame T, Kennaway NG, Soriano P. Loss of fumarylacetoacetate hydrolase is responsible for the neonatal hepatic dysfunction phenotype of lethal albino mice. *Genes Dev*. 1993;7(12A):2298-307. Epub 1993/12/01. doi: 10.1101/gad.7.12a.2298. PubMed PMID: 8253378.
406. Yin H, Song CQ, Dorkin JR, Zhu LJ, Li Y, Wu Q, Park A, Yang J, Suresh S, Bizhanova A, Gupta A, Bolukbasi MF, Walsh S, Bogorad RL, Gao G, Weng Z, Dong Y, Koteliensky V, Wolfe SA, Langer R, Xue W, Anderson DG. Therapeutic genome editing by combined viral and non-viral delivery of CRISPR system components in vivo. *Nat Biotechnol*. 2016;34(3):328-33. Epub 2016/02/02. doi: 10.1038/nbt.3471. PubMed PMID: 26829318; PMCID: PMC5423356.
407. Endo F, Sun MS. Tyrosinaemia type I and apoptosis of hepatocytes and renal tubular cells. *J Inherit Metab Dis*. 2002;25(3):227-34. doi: 10.1023/a:1015646400182. PubMed PMID: 12137232.
408. Yin H, Xue W, Chen S, Bogorad RL, Benedetti E, Grompe M, Koteliensky V, Sharp PA, Jacks T, Anderson DG. Genome editing with Cas9 in adult mice corrects a disease mutation and phenotype. *Nat Biotechnol*. 2014;32:551-3. Epub 2014/04/01. doi: nbt.2884 [pii] 10.1038/nbt.2884 [doi]. PubMed PMID: 24681508.
409. Grompe M, al-Dhalimy M, Finegold M, Ou CN, Burlingame T, Kennaway NG, Soriano P. Loss of fumarylacetoacetate hydrolase is responsible for the neonatal hepatic dysfunction phenotype of lethal albino mice. *Genes & development*. 1993;7(12A):2298-307. doi: 10.1101/gad.7.12a.2298. PubMed PMID: 8253378.

410. Yao X, Wang X, Liu J, Hu X, Shi L, Shen X, Ying W, Sun X, Wang X, Huang P, Yang H. CRISPR/Cas9 - Mediated Precise Targeted Integration In Vivo Using a Double Cut Donor with Short Homology Arms. *EBioMedicine*. 2017;20:19-26. Epub 2017/05/22. doi: 10.1016/j.ebiom.2017.05.015. PubMed PMID: 28527830; PMCID: PMC5478232.
411. Huch M, Dorrell C, Boj SF, van Es JH, Li VS, van de Wetering M, Sato T, Hamer K, Sasaki N, Finegold MJ, Haft A, Vries RG, Grompe M, Clevers H. In vitro expansion of single Lgr5+ liver stem cells induced by Wnt-driven regeneration. *Nature*. 2013;494(7436):247-50. Epub 2013/01/29. doi: 10.1038/nature11826. PubMed PMID: 23354049; PMCID: PMC3634804.
412. Wangensteen KJ, Wilber A, Keng VW, He Z, Matise I, Wangensteen L, Carson CM, Chen Y, Steer CJ, Mclvor RS, Largaespada DA, Wang X, Ekker SC. A facile method for somatic, lifelong manipulation of multiple genes in the mouse liver. *Hepatology*. 2008;47(5):1714-24. doi: 10.1002/hep.22195.
413. Park EJ, Lee JH, Yu G-Y, He G, Ali SR, Holzer RG, Osterreicher CH, Takahashi H, Karin M. Dietary and genetic obesity promote liver inflammation and tumorigenesis by enhancing IL-6 and TNF expression. *Cell*. 2010;140(2):197-208. doi: 10.1016/j.cell.2009.12.052. PubMed PMID: 20141834.
414. Pok S, Wen V, Shackel N, Alsop A, Pyakurel P, Fahrner A, Farrell GC, Teoh NC. Cyclin E facilitates dysplastic hepatocytes to bypass G1/S checkpoint in hepatocarcinogenesis. *J Gastroenterol Hepatol*. 2013;28(9):1545-54. doi: 10.1111/jgh.12216. PubMed PMID: 23574010.
415. Sharpless NE, DePinho RA. The mighty mouse: genetically engineered mouse models in cancer drug development. *Nature Reviews Drug Discovery*. 2006;5(9):741-54. doi: 10.1038/nrd2110.
416. Chen X, Calvisi DF. Hydrodynamic transfection for generation of novel mouse models for liver cancer research. *The American journal of pathology*. 2014;184(4):912-23. Epub 2014/01/28. doi: 10.1016/j.ajpath.2013.12.002. PubMed PMID: 24480331.
417. Kanefuji T, Yokoo T, Suda T, Abe H, Kamimura K, Liu D. Hemodynamics of a hydrodynamic injection. *Mol Ther Methods Clin Dev*. 2014;1:14029-. doi: 10.1038/mtm.2014.29. PubMed PMID: 26015971.
418. Zhang G, Gao X, Song YK, Vollmer R, Stolz DB, Gasiorowski JZ, Dean DA, Liu D. Hydroporation as the mechanism of hydrodynamic delivery. *Gene Ther*. 2004;11(8):675-82. doi: 10.1038/sj.gt.3302210. PubMed PMID: 14724673.
419. Furth PA, St Onge L, Böger H, Gruss P, Gossen M, Kistner A, Bujard H, Hennighausen L. Temporal control of gene expression in transgenic mice by a tetracycline-responsive promoter. *Proceedings of the National Academy of Sciences of the United States of America*. 1994;91(20):9302-6. doi: 10.1073/pnas.91.20.9302. PubMed PMID: 7937760.
420. Weidenfeld I, Gossen M, Löw R, Kentner D, Berger S, Görlich D, Bartsch D, Bujard H, Schöning K. Inducible expression of coding and inhibitory RNAs from

- retargetable genomic loci. *Nucleic Acids Res.* 2009;37(7):e50-e. doi: 10.1093/nar/gkp108.
421. Qu Z, Thottassery JV, Van Ginkel S, Manuvakhova M, Westbrook L, Roland-Lazenby C, Hays S, Kern FG. Homogeneity and long-term stability of tetracycline-regulated gene expression with low basal activity by using the rtTA2S-M2 transactivator and insulator-flanked reporter vectors. *Gene.* 2004;327(1):61-73. doi: <https://doi.org/10.1016/j.gene.2003.10.029>.
422. Loew R, Heinz N, Hampf M, Bujard H, Gossen M. Improved Tet-responsive promoters with minimized background expression. *BMC Biotechnology.* 2010;10(1):81. doi: 10.1186/1472-6750-10-81.
423. Radice AD, Bugaj B, Fitch DH, Emmons SW. Widespread occurrence of the Tc1 transposon family: Tc1-like transposons from teleost fish. *Molecular & general genetics : MGG.* 1994;244(6):606-12. Epub 1994/09/28. doi: 10.1007/bf00282750. PubMed PMID: 7969029.
424. Ivics Z, Hackett PB, Plasterk RH, Izsvák Z. Molecular Reconstruction of *Sleeping Beauty*, a Tc1-like Transposon from Fish, and Its Transposition in Human Cells. *Cell.* 1997;91(4):501-10. doi: 10.1016/S0092-8674(00)80436-5.
425. Horie K, Yusa K, Yae K, Odajima J, Fischer SEJ, Keng VW, Hayakawa T, Mizuno S, Kondoh G, Ijiri T, Matsuda Y, Plasterk RHA, Takeda J. Characterization of *Sleeping Beauty* Transposition and Its Application to Genetic Screening in Mice. *Molecular and cellular biology.* 2003;23(24):9189-207. doi: 10.1128/mcb.23.24.9189-9207.2003.
426. Horie K, Kuroiwa A, Ikawa M, Okabe M, Kondoh G, Matsuda Y, Takeda J. Efficient chromosomal transposition of a Tc1-mariner-like transposon *Sleeping Beauty* in mice. *Proceedings of the National Academy of Sciences.* 2001;98(16):9191-6. doi: 10.1073/pnas.161071798.
427. Keng VW, Yae K, Hayakawa T, Mizuno S, Uno Y, Yusa K, Kokubu C, Kinoshita T, Akagi K, Jenkins NA, Copeland NG, Horie K, Takeda J. Region-specific saturation germline mutagenesis in mice using the *Sleeping Beauty* transposon system. *Nat Methods.* 2005;2(10):763-9. Epub 2005/09/24. doi: 10.1038/nmeth795. PubMed PMID: 16179923.
428. Collier LS, Carlson CM, Ravimohan S, Dupuy AJ, Largaespada DA. Cancer gene discovery in solid tumours using transposon-based somatic mutagenesis in the mouse. *Nature.* 2005;436(7048):272-6. Epub 2005/07/15. doi: 10.1038/nature03681. PubMed PMID: 16015333.
429. Dupuy AJ, Akagi K, Largaespada DA, Copeland NG, Jenkins NA. Mammalian mutagenesis using a highly mobile somatic *Sleeping Beauty* transposon system. *Nature.* 2005;436(7048):221-6. Epub 2005/07/15. doi: 10.1038/nature03691. PubMed PMID: 16015321.
430. Bell JB, Podetz-Pedersen KM, Aronovich EL, Belur LR, McIvor RS, Hackett PB. Preferential delivery of the *Sleeping Beauty* transposon system to

- livers of mice by hydrodynamic injection. *Nat Protoc.* 2007;2(12):3153-65. doi: 10.1038/nprot.2007.471. PubMed PMID: 18079715.
431. Mikkelsen JG, Yant SR, Meuse L, Huang Z, Xu H, Kay MA. Helper-Independent Sleeping Beauty transposon-transposase vectors for efficient nonviral gene delivery and persistent gene expression in vivo. *Mol Ther.* 2003;8(4):654-65. doi: 10.1016/s1525-0016(03)00216-8. PubMed PMID: 14529839.
432. Yant SR, Meuse L, Chiu W, Ivics Z, Izsvak Z, Kay MA. Somatic integration and long-term transgene expression in normal and haemophilic mice using a DNA transposon system. *Nature genetics.* 2000;25(1):35-41. doi: 10.1038/75568. PubMed PMID: 10802653.
433. Aronovich EL, Bell JB, Belur LR, Gunther R, Koniar B, Erickson DCC, Schachern PA, Matise I, McIvor RS, Whitley CB, Hackett PB. Prolonged expression of a lysosomal enzyme in mouse liver after Sleeping Beauty transposon-mediated gene delivery: implications for non-viral gene therapy of mucopolysaccharidoses. *J Gene Med.* 2007;9(5):403-15. doi: 10.1002/jgm.1028. PubMed PMID: 17407189.
434. Berry C, Hannenhalli S, Leipzig J, Bushman FD. Selection of target sites for mobile DNA integration in the human genome. *PLoS Comput Biol.* 2006;2(11):e157-e. doi: 10.1371/journal.pcbi.0020157. PubMed PMID: 17166054.
435. Yant SR, Wu X, Huang Y, Garrison B, Burgess SM, Kay MA. High-resolution genome-wide mapping of transposon integration in mammals. *Molecular and cellular biology.* 2005;25(6):2085-94. doi: 10.1128/MCB.25.6.2085-2094.2005. PubMed PMID: 15743807.
436. Li G-W, Burkhardt D, Gross C, Weissman Jonathan S. Quantifying Absolute Protein Synthesis Rates Reveals Principles Underlying Allocation of Cellular Resources. *Cell.* 2014;157(3):624-35. doi: <https://doi.org/10.1016/j.cell.2014.02.033>.
437. Prowse KR, Greider CW. Developmental and tissue-specific regulation of mouse telomerase and telomere length. *Proceedings of the National Academy of Sciences of the United States of America.* 1995;92(11):4818-22. doi: 10.1073/pnas.92.11.4818. PubMed PMID: 7761406.
438. Blackburn EH. Structure and function of telomeres. *Nature.* 1991;350(6319):569-73. doi: 10.1038/350569a0.
439. Mou H, Ozata DM, Smith JL, Sheel A, Kwan SY, Hough S, Kucukural A, Kennedy Z, Cao Y, Xue W. CRISPR-SONIC: targeted somatic oncogene knock-in enables rapid in vivo cancer modeling. *Genome Med.* 2019;11(1):21. Epub 2019/04/17. doi: 10.1186/s13073-019-0627-9. PubMed PMID: 30987660.
440. Nishimoto M, Uranishi K, Asaka MN, Suzuki A, Mizuno Y, Hirasaki M, Okuda A. Transformation of normal cells by aberrant activation of YAP via cMyc

with TEAD. *Scientific Reports*. 2019;9(1):10933. doi: 10.1038/s41598-019-47301-6.

441. Eisinger-Mathason TSK, Mucaj V, Biju KM, Nakazawa MS, Gohil M, Cash TP, Yoon SS, Skuli N, Park KM, Gerecht S, Simon MC. Deregulation of the Hippo pathway in soft-tissue sarcoma promotes FOXM1 expression and tumorigenesis. *Proceedings of the National Academy of Sciences*. 2015;112(26):E3402-E11. doi: 10.1073/pnas.1420005112.

442. Zaidi SK, Sullivan AJ, Medina R, Ito Y, van Wijnen AJ, Stein JL, Lian JB, Stein GS. Tyrosine phosphorylation controls Runx2-mediated subnuclear targeting of YAP to repress transcription. *The EMBO journal*. 2004;23(4):790-9. doi: 10.1038/sj.emboj.7600073.

443. Basu S, Totty NF, Irwin MS, Sudol M, Downward J. Akt phosphorylates the Yes-associated protein, YAP, to induce interaction with 14-3-3 and attenuation of p73-mediated apoptosis. *Molecular cell*. 2003;11(1):11-23. doi: 10.1016/s1097-2765(02)00776-1. PubMed PMID: 12535517.

444. Strano S, Munarriz E, Rossi M, Castagnoli L, Shaul Y, Sacchi A, Oren M, Sudol M, Cesareni G, Blandino G. Physical interaction with Yes-associated protein enhances p73 transcriptional activity. *The Journal of biological chemistry*. 2001;276(18):15164-73. Epub 2001/01/24. doi: 10.1074/jbc.M010484200. PubMed PMID: 11278685.

445. Murakami M, Nakagawa M, Olson EN, Nakagawa O. A WW domain protein TAZ is a critical coactivator for TBX5, a transcription factor implicated in Holt-Oram syndrome. *Proceedings of the National Academy of Sciences of the United States of America*. 2005;102(50):18034-9. Epub 2005/12/06. doi: 10.1073/pnas.0509109102. PubMed PMID: 16332960.

446. Alarcón C, Zaromytidou A-I, Xi Q, Gao S, Yu J, Fujisawa S, Barlas A, Miller AN, Manova-Todorova K, Macias MJ, Sapkota G, Pan D, Massagué J. Nuclear CDKs drive Smad transcriptional activation and turnover in BMP and TGF-beta pathways. *Cell*. 2009;139(4):757-69. doi: 10.1016/j.cell.2009.09.035. PubMed PMID: 19914168.

447. Varelas X, Sakuma R, Samavarchi-Tehrani P, Peerani R, Rao BM, Dembowy J, Yaffe MB, Zandstra PW, Wrana JL. TAZ controls Smad nucleocytoplasmic shuttling and regulates human embryonic stem-cell self-renewal. *Nature cell biology*. 2008;10(7):837-48. Epub 2008/06/22. doi: 10.1038/ncb1748. PubMed PMID: 18568018.

448. Manderfield LJ, Engleka KA, Aghajanian H, Gupta M, Yang S, Li L, Baggs JE, Hogenesch JB, Olson EN, Epstein JA. Pax3 and hippo signaling coordinate melanocyte gene expression in neural crest. *Cell reports*. 2014;9(5):1885-95. Epub 2014/11/26. doi: 10.1016/j.celrep.2014.10.061. PubMed PMID: 25466249.

449. Yu F-X, Luo J, Mo J-S, Liu G, Kim Young C, Meng Z, Zhao L, Peyman G, Ouyang H, Jiang W, Zhao J, Chen X, Zhang L, Wang C-Y, Bastian Boris C,

- Zhang K, Guan K-L. Mutant Gq/11 Promote Uveal Melanoma Tumorigenesis by Activating YAP. *Cancer Cell*. 2014;25(6):822-30. doi: 10.1016/j.ccr.2014.04.017.
450. Cordenonsi M, Zanconato F, Azzolin L, Forcato M, Rosato A, Frasson C, Inui M, Montagner M, Parenti AR, Poletti A, Daidone MG, Dupont S, Basso G, Bicciato S, Piccolo S. The Hippo transducer TAZ confers cancer stem cell-related traits on breast cancer cells. *Cell*. 2011;147(4):759-72. doi: 10.1016/j.cell.2011.09.048. PubMed PMID: 22078877.
451. Shao DD, Xue W, Krall EB, Bhutkar A, Piccioni F, Wang X, Schinzel AC, Sood S, Rosenbluh J, Kim JW, Zwang Y, Roberts TM, Root DE, Jacks T, Hahn WC. KRAS and YAP1 converge to regulate EMT and tumor survival. *Cell*. 2014;158(1):171-84. Epub 2014/06/24. doi: 10.1016/j.cell.2014.06.004. PubMed PMID: 24954536; PMCID: PMC4110062.
452. Basu-Roy U, Bayin NS, Rattanakorn K, Han E, Placantonakis DG, Mansukhani A, Basilico C. Sox2 antagonizes the Hippo pathway to maintain stemness in cancer cells. *Nature communications*. 2015;6:6411-. doi: 10.1038/ncomms7411. PubMed PMID: 25832504.
453. Zender L, Xue W, Cordón-Cardo C, Hannon GJ, Lucito R, Powers S, Flemming P, Spector MS, Lowe SW. Generation and analysis of genetically defined liver carcinomas derived from bipotential liver progenitors. *Cold Spring Harb Symp Quant Biol*. 2005;70:251-61. doi: 10.1101/sqb.2005.70.059. PubMed PMID: 16869761.
454. Fujita J, Crane AM, Souza MK, Dejosez M, Kyba M, Flavell RA, Thomson JA, Zwaka TP. Caspase Activity Mediates the Differentiation of Embryonic Stem Cells. *Cell Stem Cell*. 2008;2(6):595-601. doi: 10.1016/j.stem.2008.04.001.
455. Wang Eric S, Reyes Nichole A, Melton C, Huskey Noelle E, Momcilovic O, Goga A, Billelloch R, Oakes Scott A. Fas-Activated Mitochondrial Apoptosis Culls Stalled Embryonic Stem Cells to Promote Differentiation. *Current Biology*. 2015;25(23):3110-8. doi: 10.1016/j.cub.2015.10.020.
456. LeBlanc L, Lee B-K, Yu AC, Kim M, Kambhampati AV, Dupont SM, Seruggia D, Ryu BU, Orkin SH, Kim J. Yap1 safeguards mouse embryonic stem cells from excessive apoptosis during differentiation. *eLife*. 2018;7:e40167. doi: 10.7554/eLife.40167.
457. Sarkisian CJ, Keister BA, Stairs DB, Boxer RB, Moody SE, Chodosh LA. Dose-dependent oncogene-induced senescence in vivo and its evasion during mammary tumorigenesis. *Nature cell biology*. 2007;9(5):493-505. Epub 2007/04/22. doi: 10.1038/ncb1567. PubMed PMID: 17450133.
458. Burgess MR, Hwang E, Mroue R, Bielski CM, Wandler AM, Huang BJ, Firestone AJ, Young A, Lacap JA, Crocker L, Asthana S, Davis EM, Xu J, Akagi K, Le Beau MM, Li Q, Haley B, Stokoe D, Sampath D, Taylor BS, Evangelista M, Shannon K. KRAS Allelic Imbalance Enhances Fitness and Modulates MAP Kinase Dependence in Cancer. *Cell*. 2017;168(5):817-29.e15. doi: <https://doi.org/10.1016/j.cell.2017.01.020>.

459. Wang J, Liu Y, Li Z, Wang Z, Tan LX, Ryu M-J, Meline B, Du J, Young KH, Ranheim E, Chang Q, Zhang J. Endogenous oncogenic Nras mutation initiates hematopoietic malignancies in a dose- and cell type-dependent manner. *Blood*. 2011;118(2):368-79. Epub 2011/05/17. doi: 10.1182/blood-2010-12-326058. PubMed PMID: 21586752.
460. Fernandez-L A, Northcott PA, Dalton J, Fraga C, Ellison D, Angers S, Taylor MD, Kenney AM. YAP1 is amplified and up-regulated in hedgehog-associated medulloblastomas and mediates Sonic hedgehog-driven neural precursor proliferation. *Genes & Development*. 2009;23(23):2729-41. doi: 10.1101/gad.1824509.
461. Lin T, Chao C, Saito Si, Mazur SJ, Murphy ME, Appella E, Xu Y. p53 induces differentiation of mouse embryonic stem cells by suppressing Nanog expression. *Nature cell biology*. 2005;7(2):165-71. Epub 2004/12/26. doi: 10.1038/ncb1211. PubMed PMID: 15619621.
462. Aylon Y, Michael D, Shmueli A, Yabuta N, Nojima H, Oren M. A positive feedback loop between the p53 and Lats2 tumor suppressors prevents tetraploidization. *Genes & Development*. 2006;20(19):2687-700. doi: 10.1101/gad.1447006.
463. Aylon Y, Sarver A, Tovy A, Ainbinder E, Oren M. Lats2 is critical for the pluripotency and proper differentiation of stem cells. *Cell Death Differ*. 2014;21(4):624-33. Epub 2014/01/10. doi: 10.1038/cdd.2013.188. PubMed PMID: 24413153.
464. Aylon Y, Ofir-Rosenfeld Y, Yabuta N, Lapi E, Nojima H, Lu X, Oren M. The Lats2 tumor suppressor augments p53-mediated apoptosis by promoting the nuclear proapoptotic function of ASPP1. *Genes & development*. 2010;24(21):2420-9. doi: 10.1101/gad.1954410. PubMed PMID: 21041410.
465. Mello SS, Valente LJ, Raj N, Seoane JA, Flowers BM, McClendon J, Biegging-Rolett KT, Lee J, Ivanochko D, Kozak MM, Chang DT, Longacre TA, Koong AC, Arrowsmith CH, Kim SK, Vogel H, Wood LD, Hruban RH, Curtis C, Attardi LD. A p53 Super-tumor Suppressor Reveals a Tumor Suppressive p53-Ptpn14-Yap Axis in Pancreatic Cancer. *Cancer Cell*. 2017;32(4):460-73.e6. doi: <https://doi.org/10.1016/j.ccell.2017.09.007>.
466. Di Agostino S, Sorrentino G, Ingallina E, Valenti F, Ferraiuolo M, Bicciato S, Piazza S, Strano S, Del Sal G, Blandino G. YAP enhances the pro-proliferative transcriptional activity of mutant p53 proteins. *EMBO Rep*. 2016;17(2):188-201. Epub 2015/12/21. doi: 10.15252/embr.201540488. PubMed PMID: 26691213.
467. Morris JPt, Yashinskie JJ, Koche R, Chandwani R, Tian S, Chen C-C, Baslan T, Marinkovic ZS, Sánchez-Rivera FJ, Leach SD, Carmona-Fontaine C, Thompson CB, Finley LWS, Lowe SW. α -Ketoglutarate links p53 to cell fate during tumour suppression. *Nature*. 2019;573(7775):595-9. Epub 2019/09/18. doi: 10.1038/s41586-019-1577-5. PubMed PMID: 31534224.

468. Chin L, Tam A, Pomerantz J, Wong M, Holash J, Bardeesy N, Shen Q, O'Hagan R, Pantginis J, Zhou H, Horner JW, 2nd, Cordon-Cardo C, Yancopoulos GD, DePinho RA. Essential role for oncogenic Ras in tumour maintenance. *Nature*. 1999;400(6743):468-72. Epub 1999/08/10. doi: 10.1038/22788. PubMed PMID: 10440378.
469. Wendel HG, de Stanchina E, Cepero E, Ray S, Emig M, Fridman JS, Veach DR, Bornmann WG, Clarkson B, McCombie WR, Kogan SC, Hochhaus A, Lowe SW. Loss of p53 impedes the antileukemic response to BCR-ABL inhibition. *Proc Natl Acad Sci U S A*. 2006;103(19):7444-9. Epub 2006/05/03. doi: 10.1073/pnas.0602402103. PubMed PMID: 16651519; PMCID: PMC1455409.
470. Martens JH, Brinkman AB, Simmer F, Francoijs KJ, Nebbioso A, Ferrara F, Altucci L, Stunnenberg HG. PML-RARalpha/RXR Alters the Epigenetic Landscape in Acute Promyelocytic Leukemia. *Cancer Cell*. 2010;17(2):173-85. Epub 2010/02/18. doi: 10.1016/j.ccr.2009.12.042. PubMed PMID: 20159609.
471. Cicconi L, Divona M, Ciardi C, Ottone T, Ferrantini A, Lavorgna S, Alfonso V, Paoloni F, Piciocchi A, Avvisati G, Ferrara F, Di Bona E, Albano F, Breccia M, Cerqui E, Sborgia M, Kropp MG, Santoro A, Levis A, Sica S, Amadori S, Voso MT, Mandelli F, Lo-Coco F. PML-RARalpha kinetics and impact of FLT3-ITD mutations in newly diagnosed acute promyelocytic leukaemia treated with ATRA and ATO or ATRA and chemotherapy. *Leukemia*. 2016;30(10):1987-92. Epub 2016/05/03. doi: 10.1038/leu.2016.122. PubMed PMID: 27133819.
472. Burnett AK, Russell NH, Hills RK, Bowen D, Kell J, Knapper S, Morgan YG, Lok J, Grech A, Jones G, Khwaja A, Friis L, McMullin MF, Hunter A, Clark RE, Grimwade D. Arsenic trioxide and all-trans retinoic acid treatment for acute promyelocytic leukaemia in all risk groups (AML17): results of a randomised, controlled, phase 3 trial. *Lancet Oncol*. 2015;16(13):1295-305. Epub 2015/09/19. doi: 10.1016/s1470-2045(15)00193-x. PubMed PMID: 26384238.
473. de Thé H. Differentiation therapy revisited. *Nature Reviews Cancer*. 2018;18(2):117-27. doi: 10.1038/nrc.2017.103.
474. Beck B, Blanpain C. Unravelling cancer stem cell potential. *Nature Reviews Cancer*. 2013;13(10):727-38. doi: 10.1038/nrc3597.
475. Lynch TJ, Bell DW, Sordella R, Gurubhagavatula S, Okimoto RA, Brannigan BW, Harris PL, Haserlat SM, Supko JG, Haluska FG, Louis DN, Christiani DC, Settleman J, Haber DA. Activating mutations in the epidermal growth factor receptor underlying responsiveness of non-small-cell lung cancer to gefitinib. *N Engl J Med*. 2004;350(21):2129-39. Epub 2004/05/01. doi: 10.1056/NEJMoa040938. PubMed PMID: 15118073.
476. Kapoor A, Yao W, Ying H, Hua S, Liewen A, Wang Q, Zhong Y, Wu CJ, Sadanandam A, Hu B, Chang Q, Chu GC, Al-Khalil R, Jiang S, Xia H, Fletcher-Sanankone E, Lim C, Horwitz GI, Viale A, Pettazzoni P, Sanchez N, Wang H, Protopopov A, Zhang J, Heffernan T, Johnson RL, Chin L, Wang YA, Draetta G, DePinho RA. Yap1 activation enables bypass of oncogenic Kras addiction in

- pancreatic cancer. *Cell*. 2014;158(1):185-97. Epub 2014/06/24. doi: 10.1016/j.cell.2014.06.003. PubMed PMID: 24954535; PMCID: PMC4109295.
477. Bushweller JH. Targeting transcription factors in cancer — from undruggable to reality. *Nature Reviews Cancer*. 2019;19(11):611-24. doi: 10.1038/s41568-019-0196-7.
478. Chapman PB, Hauschild A, Robert C, Haanen JB, Ascierto P, Larkin J, Dummer R, Garbe C, Testori A, Maio M, Hogg D, Lorigan P, Lebbe C, Jouary T, Schadendorf D, Ribas A, O'Day SJ, Sosman JA, Kirkwood JM, Eggermont AM, Dreno B, Nolop K, Li J, Nelson B, Hou J, Lee RJ, Flaherty KT, McArthur GA, Group B-S. Improved survival with vemurafenib in melanoma with BRAF V600E mutation. *N Engl J Med*. 2011;364(26):2507-16. Epub 2011/06/07. doi: 10.1056/NEJMoa1103782. PubMed PMID: 21639808; PMCID: PMC3549296.
479. Flaherty KT, Puzanov I, Kim KB, Ribas A, McArthur GA, Sosman JA, O'Dwyer PJ, Lee RJ, Grippo JF, Nolop K, Chapman PB. Inhibition of mutated, activated BRAF in metastatic melanoma. *N Engl J Med*. 2010;363(9):809-19. Epub 2010/09/08. doi: 10.1056/NEJMoa1002011. PubMed PMID: 20818844; PMCID: PMC3724529.
480. Infante JR, Fecher LA, Falchook GS, Nallapareddy S, Gordon MS, Becerra C, DeMarini DJ, Cox DS, Xu Y, Morris SR, Peddareddigari VGR, Le NT, Hart L, Bendell JC, Eckhardt G, Kurzrock R, Flaherty K, Burris HA, Messersmith WA. Safety, pharmacokinetic, pharmacodynamic, and efficacy data for the oral MEK inhibitor trametinib: a phase 1 dose-escalation trial. *The Lancet Oncology*. 2012;13(8):773-81. doi: [https://doi.org/10.1016/S1470-2045\(12\)70270-X](https://doi.org/10.1016/S1470-2045(12)70270-X).
481. Bhullar KS, Lagarón NO, McGowan EM, Parmar I, Jha A, Hubbard BP, Rupasinghe HPV. Kinase-targeted cancer therapies: progress, challenges and future directions. *Mol Cancer*. 2018;17(1):48-. doi: 10.1186/s12943-018-0804-2. PubMed PMID: 29455673.
482. Xu Y, Poggio M, Jin HY, Shi Z, Forester CM, Wang Y, Stumpf CR, Xue L, Devericks E, So L, Nguyen HG, Griselin A, Gordan JD, Umetsu SE, Reich SH, Worland ST, Asthana S, Barna M, Webster KR, Cunningham JT, Ruggero D. Translation control of the immune checkpoint in cancer and its therapeutic targeting. *Nature medicine*. 2019;25(2):301-11. Epub 2019/01/14. doi: 10.1038/s41591-018-0321-2. PubMed PMID: 30643286.
483. Kortlever RM, Sodir NM, Wilson CH, Burkhart DL, Pellegrinet L, Brown Swigart L, Littlewood TD, Evan GI. Myc Cooperates with Ras by Programming Inflammation and Immune Suppression. *Cell*. 2017;171(6):1301-15.e14. Epub 2017/12/02. doi: 10.1016/j.cell.2017.11.013. PubMed PMID: 29195074.
484. Arkin MR, Tang Y, Wells JA. Small-molecule inhibitors of protein-protein interactions: progressing toward the reality. *Chem Biol*. 2014;21(9):1102-14. doi: 10.1016/j.chembiol.2014.09.001. PubMed PMID: 25237857.
485. Ziemssen F, Heimann H. Evaluation of verteporfin pharmacokinetics--redefining the need of photosensitizers in ophthalmology. *Expert Opin Drug*

- Metab Toxicol. 2012;8(8):1023-41. Epub 2012/07/05. doi: 10.1517/17425255.2012.701617. PubMed PMID: 22762303.
486. Ma Y-W, Liu Y-Z, Pan J-X. Verteporfin induces apoptosis and eliminates cancer stem-like cells in uveal melanoma in the absence of light activation. *Am J Cancer Res.* 2016;6(12):2816-30. PubMed PMID: 28042502.
487. Pobbati AV, Han X, Hung AW, Weiguang S, Huda N, Chen G-Y, Kang C, Chia CSB, Luo X, Hong W, Poulsen A. Targeting the Central Pocket in Human Transcription Factor TEAD as a Potential Cancer Therapeutic Strategy. *Structure.* 2015;23(11):2076-86. Epub 2015/10/22. doi: 10.1016/j.str.2015.09.009. PubMed PMID: 26592798.
488. Neesse A, Frese KK, Bapiro TE, Nakagawa T, Sternlicht MD, Seeley TW, Pilarsky C, Jodrell DI, Spong SM, Tuveson DA. CTGF antagonism with mAb FG-3019 enhances chemotherapy response without increasing drug delivery in murine ductal pancreas cancer. *Proceedings of the National Academy of Sciences of the United States of America.* 2013;110(30):12325-30. Epub 2013/07/08. doi: 10.1073/pnas.1300415110. PubMed PMID: 23836645.
489. Lin J, Huo R, Wang L, Zhou Z, Sun Y, Shen B, Wang R, Li N. A novel anti-Cyr61 antibody inhibits breast cancer growth and metastasis in vivo. *Cancer Immunol Immunother.* 2012;61(5):677-87. Epub 2011/11/03. doi: 10.1007/s00262-011-1135-y. PubMed PMID: 22048717.
490. Jiao S, Wang H, Shi Z, Dong A, Zhang W, Song X, He F, Wang Y, Zhang Z, Wang W, Wang X, Guo T, Li P, Zhao Y, Ji H, Zhang L, Zhou Z. A peptide mimicking VGLL4 function acts as a YAP antagonist therapy against gastric cancer. *Cancer cell.* 2014;25(2):166-80. doi: 10.1016/j.ccr.2014.01.010. PubMed PMID: 24525233.
491. Feng X, Lu T, Li J, Yang R, Hu L, Ye Y, Mao F, He L, Xu J, Wang Z, Liu Y, Zhang Y, Ji H, Zhao Y, Cheng S, Tian W, Zhang L. The novel tumor suppressor IRF2BP2 regulates Hippo pathway in liver cancer via a feedback loop. *Hepatology.* n/a(n/a). doi: 10.1002/hep.30961.
492. Mann KM, Ward JM, Yew CCK, Kovochich A, Dawson DW, Black MA, Brett BT, Sheetz TE, Dupuy AJ, Australian Pancreatic Cancer Genome I, Chang DK, Biankin AV, Waddell N, Kassahn KS, Grimmond SM, Rust AG, Adams DJ, Jenkins NA, Copeland NG. Sleeping Beauty mutagenesis reveals cooperating mutations and pathways in pancreatic adenocarcinoma. *Proceedings of the National Academy of Sciences of the United States of America.* 2012;109(16):5934-41. Epub 2012/03/15. doi: 10.1073/pnas.1202490109. PubMed PMID: 22421440.
493. Jiao S, Li C, Hao Q, Miao H, Zhang L, Li L, Zhou Z. VGLL4 targets a TCF4–TEAD4 complex to coregulate Wnt and Hippo signalling in colorectal cancer. *Nature Communications.* 2017;8(1):14058. doi: 10.1038/ncomms14058.

494. Marqus S, Pirogova E, Piva TJ. Evaluation of the use of therapeutic peptides for cancer treatment. *Journal of Biomedical Science*. 2017;24(1):21. doi: 10.1186/s12929-017-0328-x.
495. Tian Y, Liu Y, Wang T, Zhou N, Kong J, Chen L, Snitow M, Morley M, Li D, Petrenko N, Zhou S, Lu M, Gao E, Koch WJ, Stewart KM, Morrissey EE. A microRNA-Hippo pathway that promotes cardiomyocyte proliferation and cardiac regeneration in mice. *Sci Transl Med*. 2015;7(279):279ra38-ra38. doi: 10.1126/scitranslmed.3010841. PubMed PMID: 25787764.
496. Lin C-W, Chang Y-L, Chang Y-C, Lin J-C, Chen C-C, Pan S-H, Wu C-T, Chen H-Y, Yang S-C, Hong T-M, Yang P-C. MicroRNA-135b promotes lung cancer metastasis by regulating multiple targets in the Hippo pathway and LZTS1. *Nature Communications*. 2013;4(1):1877. doi: 10.1038/ncomms2876.
497. Mori M, Triboulet R, Mohseni M, Schlegelmilch K, Shrestha K, Camargo Fernando D, Gregory Richard I. Hippo Signaling Regulates Microprocessor and Links Cell-Density-Dependent miRNA Biogenesis to Cancer. *Cell*. 2014;156(5):893-906. doi: 10.1016/j.cell.2013.12.043.
498. Watts JK, Corey DR. Silencing disease genes in the laboratory and the clinic. *J Pathol*. 2012;226(2):365-79. Epub 2011/11/09. doi: 10.1002/path.2993. PubMed PMID: 22069063.
499. Witzigmann D, Quagliata L, Schenk SH, Quintavalle C, Terracciano LM, Huwyler J. Variable asialoglycoprotein receptor 1 expression in liver disease: Implications for therapeutic intervention. *Hepatology Research*. 2016;46(7):686-96. doi: 10.1111/hepr.12599.
500. Prakash TP, Graham MJ, Yu J, Carty R, Low A, Chappell A, Schmidt K, Zhao C, Aghajan M, Murray HF, Riney S, Booten SL, Murray SF, Gaus H, Crosby J, Lima WF, Guo S, Monia BP, Swayze EE, Seth PP. Targeted delivery of antisense oligonucleotides to hepatocytes using triantennary N-acetyl galactosamine improves potency 10-fold in mice. *Nucleic Acids Res*. 2014;42(13):8796-807. doi: 10.1093/nar/gku531.
501. Kim Y, Jo M, Schmidt J, Luo X, Prakash TP, Zhou T, Klein S, Xiao X, Post N, Yin Z, MacLeod AR. Enhanced Potency of GalNAc-Conjugated Antisense Oligonucleotides in Hepatocellular Cancer Models. *Molecular Therapy*. 2019;27(9):1547-57. doi: 10.1016/j.ymthe.2019.06.009.
502. Mou H, Smith JL, Peng L, Yin H, Moore J, Zhang XO, Song CQ, Sheel A, Wu Q, Ozata DM, Li Y, Anderson DG, Emerson CP, Sontheimer EJ, Moore MJ, Weng Z, Xue W. CRISPR/Cas9-mediated genome editing induces exon skipping by alternative splicing or exon deletion. *Genome Biol*. 2017;18(1):108. Epub 2017/06/16. doi: 10.1186/s13059-017-1237-8. PubMed PMID: 28615073; PMCID: PMC5470253.
503. Doudna JA, Charpentier E. Genome editing. The new frontier of genome engineering with CRISPR-Cas9. *Science*. 2014;346(6213):1258096. Epub 2014/11/29. doi: 10.1126/science.1258096. PubMed PMID: 25430774.

504. Cong L, Ran FA, Cox D, Lin S, Barretto R, Habib N, Hsu PD, Wu X, Jiang W, Marraffini LA, Zhang F. Multiplex genome engineering using CRISPR/Cas systems. *Science*. 2013;339(6121):819-23. Epub 2013/01/05. doi: 10.1126/science.1231143. PubMed PMID: 23287718; PMCID: PMC3795411.
505. Mali P, Yang L, Esvelt KM, Aach J, Guell M, DiCarlo JE, Norville JE, Church GM. RNA-guided human genome engineering via Cas9. *Science*. 2013;339(6121):823-6. Epub 2013/01/05. doi: science.1232033 [pii] 10.1126/science.1232033 [doi]. PubMed PMID: 23287722.
506. Mali P, Esvelt KM, Church GM. Cas9 as a versatile tool for engineering biology. *Nat Methods*. 2013;10(10):957-63. Epub 2013/10/01. doi: nmeth.2649 [pii] 10.1038/nmeth.2649 [doi]. PubMed PMID: 24076990.
507. Sander JD, Joung JK. CRISPR-Cas systems for editing, regulating and targeting genomes. *Nat Biotechnol*. 2014;32(4):347-55. Epub 2014/03/04. doi: nbt.2842 [pii] 10.1038/nbt.2842 [doi]. PubMed PMID: 24584096.
508. Fu Y, Foden JA, Khayter C, Maeder ML, Reyon D, Joung JK, Sander JD. High-frequency off-target mutagenesis induced by CRISPR-Cas nucleases in human cells. *Nat Biotechnol*. 2013;31(9):822-6. Epub 2013/06/25. doi: nbt.2623 [pii] 10.1038/nbt.2623 [doi]. PubMed PMID: 23792628.
509. Hsu PD, Scott DA, Weinstein JA, Ran FA, Konermann S, Agarwala V, Li Y, Fine EJ, Wu X, Shalem O, Cradick TJ, Marraffini LA, Bao G, Zhang F. DNA targeting specificity of RNA-guided Cas9 nucleases. *Nat Biotechnol*. 2013;31(9):827-32. Epub 2013/07/23. doi: nbt.2647 [pii] 10.1038/nbt.2647 [doi]. PubMed PMID: 23873081.
510. Xue W, Chen S, Yin H, Tammela T, Papagiannakopoulos T, Joshi NS, Cai W, Yang G, Bronson R, Crowley DG, Zhang F, Anderson DG, Sharp PA, Jacks T. CRISPR-mediated direct mutation of cancer genes in the mouse liver. *Nature*. 2014;514(7522):380-4. Epub 2014/08/15. doi: 10.1038/nature13589. PubMed PMID: 25119044; PMCID: PMC4199937.
511. Wang D, Mou H, Li S, Li Y, Hough S, Tran K, Li J, Yin H, Anderson DG, Sontheimer E, Weng Z, Gao G, Xue W. Adenovirus-mediated somatic genome editing of Pten by CRISPR/Cas9 in mouse liver in spite of Cas9-specific immune responses. *Hum Gene Ther*. 2015. Epub 2015/06/19. doi: 10.1089/hum.2015.087 [doi]. PubMed PMID: 26086867.
512. Song CQ, Li Y, Mou H, Moore J, Park A, Pomyen Y, Hough S, Kennedy Z, Fischer A, Yin H, Anderson DG, Conte D, Jr., Zender L, Wang XW, Thorgeirsson S, Weng Z, Xue W. Genome-Wide CRISPR Screen Identifies Regulators of Mitogen-Activated Protein Kinase as Suppressors of Liver Tumors in Mice. *Gastroenterology*. 2016;152(5):1161–73.e1. Epub 2016/12/14. doi: 10.1053/j.gastro.2016.12.002. PubMed PMID: 27956228.

513. Sanjana NE, Shalem O, Zhang F. Improved vectors and genome-wide libraries for CRISPR screening. *Nat Methods*. 2014;11(8):783-4. Epub 2014/07/31. doi: nmeth.3047 [pii] 10.1038/nmeth.3047 [doi]. PubMed PMID: 25075903.
514. Li Y, Park A, Mou H, Anderson DG, Jacks T, Weng ZP, Xue W. A versatile reporter system for CRISPR-mediated chromosomal rearrangements. *Genome Biology*. 2015;16(1):111. Epub 2015/04/08. doi: nbt.3199 [pii] 10.1038/nbt.3199 [doi]. PubMed PMID: 25849900.
515. Katz Y, Wang ET, Airoidi EM, Burge CB. Analysis and design of RNA sequencing experiments for identifying isoform regulation. *Nat Methods*. 2010;7(12):1009-15. Epub 2010/11/09. doi: 10.1038/nmeth.1528. PubMed PMID: 21057496; PMCID: PMC3037023.
516. Mou H, Moore J, Malonia SK, Li Y, Ozata DM, Hough S, Song CQ, Smith JL, Fischer A, Weng Z, Green MR, Xue W. Genetic disruption of oncogenic Kras sensitizes lung cancer cells to Fas receptor-mediated apoptosis. *Proc Natl Acad Sci U S A*. 2017. Epub 2017/03/23. doi: 10.1073/pnas.1620861114. PubMed PMID: 28320962.
517. Tuveson DA, Shaw AT, Willis NA, Silver DP, Jackson EL, Chang S, Mercer KL, Grochow R, Hock H, Crowley D, Hingorani SR, Zaks T, King C, Jacobetz MA, Wang L, Bronson RT, Orkin SH, DePinho RA, Jacks T. Endogenous oncogenic K-ras(G12D) stimulates proliferation and widespread neoplastic and developmental defects. *Cancer Cell*. 2004;5(4):375-87. PubMed PMID: 15.
518. Xue W, Meylan E, Oliver TG, Feldser DM, Winslow MM, Bronson R, Jacks T. Response and Resistance to NF-kappaB Inhibitors in Mouse Models of Lung Adenocarcinoma. *Cancer Discov*. 2011;1(3):236-47. PubMed PMID: 105.
519. Popp MW, Maquat LE. Leveraging Rules of Nonsense-Mediated mRNA Decay for Genome Engineering and Personalized Medicine. *Cell*. 2016;165(6):1319-22. Epub 2016/06/04. doi: 10.1016/j.cell.2016.05.053. PubMed PMID: 27259145; PMCID: PMC4924582.
520. Cartegni L, Wang J, Zhu Z, Zhang MQ, Krainer AR. ESEfinder: A web resource to identify exonic splicing enhancers. *Nucleic Acids Res*. 2003;31(13):3568-71. Epub 2003/06/26. PubMed PMID: 12824367; PMCID: PMC169022.
521. Kapahnke M, Banning A, Tikkanen R. Random Splicing of Several Exons Caused by a Single Base Change in the Target Exon of CRISPR/Cas9 Mediated Gene Knockout. *Cells*. 2016;5(4). Epub 2016/12/17. doi: 10.3390/cells5040045. PubMed PMID: 27983621; PMCID: PMC5187529.
522. Moon RT, Kohn AD, De Ferrari GV, Kaykas A. WNT and beta-catenin signalling: diseases and therapies. *Nat Rev Genet*. 2004;5(9):691-701. Epub 2004/09/17. doi: 10.1038/nrg1427 [doi] nrg1427 [pii]. PubMed PMID: 15372092.

523. Iwao K, Nakamori S, Kameyama M, Imaoka S, Kinoshita M, Fukui T, Ishiguro S, Nakamura Y, Miyoshi Y. Activation of the beta-catenin gene by interstitial deletions involving exon 3 in primary colorectal carcinomas without adenomatous polyposis coli mutations. *Cancer Res.* 1998;58(5):1021-6. Epub 1998/03/21. PubMed PMID: 9500465.
524. Harada N, Tamai Y, Ishikawa T, Sauer B, Takaku K, Oshima M, Taketo MM. Intestinal polyposis in mice with a dominant stable mutation of the beta-catenin gene. *Embo j.* 1999;18(21):5931-42. Epub 1999/11/02. doi: 10.1093/emboj/18.21.5931. PubMed PMID: 10545105; PMCID: PMC1171659.
525. Long C, McAnally JR, Shelton JM, Mireault Aa, Bassel-Duby R, Olson EN. Prevention of muscular dystrophy in mice by CRISPR/Cas9-mediated editing of germline DNA. *Science.* 2014;345(August):1184-8. doi: 10.1126/science.1254445.
526. Long C, Amoasii L, Mireault AA, McAnally JR, Li H, Sanchez-Ortiz E, Bhattacharyya S, Shelton JM, Bassel-Duby R, Olson EN. Postnatal genome editing partially restores dystrophin expression in a mouse model of muscular dystrophy. *Science.* 2016;351(6271):400-3. Epub 2016/01/02. doi: 10.1126/science.aad5725. PubMed PMID: 26721683; PMCID: PMC4760628.
527. Nelson CE, Hakim CH, Ousterout DG, Thakore PI, Moreb EA, Castellanos Rivera RM, Madhavan S, Pan X, Ran FA, Yan WX, Asokan A, Zhang F, Duan D, Gersbach CA. In vivo genome editing improves muscle function in a mouse model of Duchenne muscular dystrophy. *Science.* 2016;351(6271):403-7. Epub 2016/01/02. doi: 10.1126/science.aad5143. PubMed PMID: 26721684; PMCID: PMC4883596.
528. Tabebordbar M, Zhu K, Cheng JK, Chew WL, Widrick JJ, Yan WX, Maesner C, Wu EY, Xiao R, Ran FA, Cong L, Zhang F, Vandenberghe LH, Church GM, Wagers AJ. In vivo gene editing in dystrophic mouse muscle and muscle stem cells. *Science.* 2016;351(6271):407-11. Epub 2016/01/02. doi: 10.1126/science.aad5177. PubMed PMID: 26721686; PMCID: PMC4924477.
529. Bengtsson NE, Hall JK, Odom GL, Phelps MP, Andrus CR, Hawkins RD, Hauschka SD, Chamberlain JR, Chamberlain JS. Muscle-specific CRISPR/Cas9 dystrophin gene editing ameliorates pathophysiology in a mouse model for Duchenne muscular dystrophy. *Nat Commun.* 2017;8:14454. Epub 2017/02/15. doi: 10.1038/ncomms14454. PubMed PMID: 28195574; PMCID: PMC5316861.
530. Yaffe D, Saxel O. Serial passaging and differentiation of myogenic cells isolated from dystrophic mouse muscle. *Nature.* 1977;270(5639):725-7. Epub 1977/12/22. PubMed PMID: 563524.
531. Robinson-Hamm JN, Gersbach CA. Gene therapies that restore dystrophin expression for the treatment of Duchenne muscular dystrophy. *Human genetics.* 2016;135(9):1029-40. Epub 2016/08/21. doi: 10.1007/s00439-016-1725-z. PubMed PMID: 27542949; PMCID: PMC5006996.

532. Liu HX, Cartegni L, Zhang MQ, Krainer AR. A mechanism for exon skipping caused by nonsense or missense mutations in BRCA1 and other genes. *Nat Genet.* 2001;27(1):55-8. Epub 2001/01/04. doi: 10.1038/83762. PubMed PMID: 11137998.
533. Cartegni L, Chew SL, Krainer AR. Listening to silence and understanding nonsense: exonic mutations that affect splicing. *Nat Rev Genet.* 2002;3(4):285-98. Epub 2002/04/23. doi: 10.1038/nrg775. PubMed PMID: 11967553.
534. Wang Z, Rolish ME, Yeo G, Tung V, Mawson M, Burge CB. Systematic identification and analysis of exonic splicing silencers. *Cell.* 2004;119(6):831-45. Epub 2004/12/21. doi: 10.1016/j.cell.2004.11.010. PubMed PMID: 15607979.
535. Singh G, Pratt G, Yeo GW, Moore MJ. The Clothes Make the mRNA: Past and Present Trends in mRNP Fashion. *Annu Rev Biochem.* 2015;84:325-54. Epub 2015/03/19. doi: 10.1146/annurev-biochem-080111-092106. PubMed PMID: 25784054; PMCID: PMC4804868.
536. Kalantari R, Chiang CM, Corey DR. Regulation of mammalian transcription and splicing by Nuclear RNAi. *Nucleic Acids Res.* 2016;44(2):524-37. Epub 2015/11/28. doi: 10.1093/nar/gkv1305. PubMed PMID: 26612865; PMCID: PMC4737150.
537. Canver MC, Bauer DE, Dass A, Yien YY, Chung J, Masuda T, Maeda T, Paw BH, Orkin SH. Characterization of genomic deletion efficiency mediated by clustered regularly interspaced palindromic repeats (CRISPR)/Cas9 nuclease system in mammalian cells. *J Biol Chem.* 2014;289(31):21312-24. Epub 2014/06/08. doi: M114.564625 [pii] 10.1074/jbc.M114.564625 [doi]. PubMed PMID: 24907273.
538. Burghes AH, McGovern VL. Antisense oligonucleotides and spinal muscular atrophy: skipping along. *Genes Dev.* 2010;24(15):1574-9. Epub 2010/08/04. doi: 10.1101/gad.1961710. PubMed PMID: 20679391; PMCID: PMC2912553.
539. Richardson CD, Kazane KR, Feng SJ, Zelin E, Bray NL, Schafer AJ, Floor SN, Corn JE. CRISPR-Cas9 genome editing in human cells occurs via the Fanconi anemia pathway. *Nat Genet.* 2018;50(8):1132-9. Epub 2018/07/29. doi: 10.1038/s41588-018-0174-0. PubMed PMID: 30054595.
540. Chu VT, Weber T, Wefers B, Wurst W, Sander S, Rajewsky K, Kuhn R. Increasing the efficiency of homology-directed repair for CRISPR-Cas9-induced precise gene editing in mammalian cells. *Nat Biotechnol.* 2015;33(5):543-8. Epub 2015/03/25. doi: 10.1038/nbt.3198. PubMed PMID: 25803306.
541. Sanchez-Rivera FJ, Papagiannakopoulos T, Romero R, Tammela T, Bauer MR, Bhutkar A, Joshi NS, Subbaraj L, Bronson RT, Xue W, Jacks T. Rapid modelling of cooperating genetic events in cancer through somatic genome editing. *Nature.* 2014;516(7531):428-31. Epub 2014/10/23. doi: 10.1038/nature13906. PubMed PMID: 25337879; PMCID: PMC4292871.

542. Dow LE, Fisher J, O'Rourke KP, Muley A, Kastenhuber ER, Livshits G, Tschaharganeh DF, Socci ND, Lowe SW. Inducible in vivo genome editing with CRISPR-Cas9. *Nat Biotechnol.* 2015;33:390-4. Epub 2015/02/19. doi: nbt.3155 [pii]
10.1038/nbt.3155 [doi]. PubMed PMID: 25690852.
543. Mou H, Kennedy Z, Anderson DG, Yin H, Xue W. Precision cancer mouse models through genome editing with CRISPR-Cas9. *Genome Med.* 2015;7(1):53. Epub 2015/06/11. doi: 10.1186/s13073-015-0178-7 [doi]
178 [pii]. PubMed PMID: 26060510.
544. Winters IP, Murray CW, Winslow MM. Towards quantitative and multiplexed in vivo functional cancer genomics. *Nat Rev Genet.* 2018. Epub 2018/09/30. doi: 10.1038/s41576-018-0053-7. PubMed PMID: 30267031.
545. Sanchez-Rivera FJ, Jacks T. Applications of the CRISPR-Cas9 system in cancer biology. *Nat Rev Cancer.* 2015;15:387-95. Epub 2015/06/05. doi: nrc3950 [pii]
10.1038/nrc3950 [doi]. PubMed PMID: 26040603.
546. Song CQ, Xue W. CRISPR-Cas-related technologies in basic and translational liver research. *Nat Rev Gastroenterol Hepatol.* 2018;15:251–2. Epub 2018/02/15. doi: 10.1038/nrgastro.2018.11. PubMed PMID: 29443117.
547. Yin H, Xue W, Anderson DG. CRISPR–Cas: a tool for cancer research and therapeutics. *Nature Reviews Clinical Oncology.* 2019. doi: 10.1038/s41571-019-0166-8.
548. Winters IP, Chiou SH, Paulk NK, McFarland CD, Lalgudi PV, Ma RK, Lisowski L, Connolly AJ, Petrov DA, Kay MA, Winslow MM. Multiplexed in vivo homology-directed repair and tumor barcoding enables parallel quantification of Kras variant oncogenicity. *Nat Commun.* 2017;8(1):2053. Epub 2017/12/14. doi: 10.1038/s41467-017-01519-y. PubMed PMID: 29233960; PMCID: PMC5727199.
549. Ge DT, Tipping C, Brodsky MH, Zamore PD. Rapid Screening for CRISPR-Directed Editing of the Drosophila Genome Using white Coconversion. *G3 (Bethesda, Md).* 2016;6(10):3197-206. Epub 2016/08/21. doi: 10.1534/g3.116.032557. PubMed PMID: 27543296; PMCID: PMC5068941.
550. Xue W, Wang XW. The search for precision models clinically relevant to human liver cancer. *Hepatic Oncology.* 2015;2(4):315-9. doi: 10.2217/hep.15.24.
551. Zucman-Rossi J, Villanueva A, Nault JC, Llovet JM. Genetic landscape and biomarkers of hepatocellular carcinoma. *Gastroenterology.* 2015;149:1226-39. Epub 2015/06/24. doi: S0016-5085(15)00869-0 [pii]
10.1053/j.gastro.2015.05.061 [doi]. PubMed PMID: 26099527.
552. Auer TO, Duroure K, De Cian A, Concordet JP, Del Bene F. Highly efficient CRISPR/Cas9-mediated knock-in in zebrafish by homology-independent DNA repair. *Genome Res.* 2014;24(1):142-53. Epub 2013/11/02. doi: 10.1101/gr.161638.113. PubMed PMID: 24179142; PMCID: PMC3875856.

553. He X, Tan C, Wang F, Wang Y, Zhou R, Cui D, You W, Zhao H, Ren J, Feng B. Knock-in of large reporter genes in human cells via CRISPR/Cas9-induced homology-dependent and independent DNA repair. *Nucleic Acids Res.* 2016;44(9):e85. Epub 2016/02/07. doi: 10.1093/nar/gkw064. PubMed PMID: 26850641; PMCID: PMC4872082.
554. Suzuki K, Tsunekawa Y, Hernandez-Benitez R, Wu J, Zhu J, Kim EJ, Hatanaka F, Yamamoto M, Araoka T, Li Z, Kurita M, Hishida T, Li M, Aizawa E, Guo S, Chen S, Goebel A, Soligalla RD, Qu J, Jiang T, Fu X, Jafari M, Esteban CR, Berggren WT, Lajara J, Nunez-Delicado E, Guillen P, Campistol JM, Matsuzaki F, Liu GH, Magistretti P, Zhang K, Callaway EM, Zhang K, Belmonte JC. In vivo genome editing via CRISPR/Cas9 mediated homology-independent targeted integration. *Nature.* 2016;540(7631):144-9. Epub 2016/11/17. doi: 10.1038/nature20565. PubMed PMID: 27851729; PMCID: PMC5331785.
555. O'Dell MR, Huang JL, Whitney-Miller CL, Deshpande V, Rothberg P, Grose V, Rossi RM, Zhu AX, Land H, Bardeesy N, Hezel AF. Kras(G12D) and p53 mutation cause primary intrahepatic cholangiocarcinoma. *Cancer Res.* 2012;72(6):1557-67. Epub 2012/01/24. doi: 10.1158/0008-5472.CAN-11-3596. PubMed PMID: 22266220; PMCID: PMC3306549.
556. Mou H, Moore J, Malonia SK, Li Y, Ozata DM, Hough S, Song CQ, Smith JL, Fischer A, Weng Z, Green MR, Xue W. Genetic disruption of oncogenic Kras sensitizes lung cancer cells to Fas receptor-mediated apoptosis. *Proc Natl Acad Sci U S A.* 2017;114(14):3648-53. Epub 2017/03/23. doi: 10.1073/pnas.1620861114. PubMed PMID: 28320962.
557. Bunnell TM, Burbach BJ, Shimizu Y, Ervasti JM. beta-Actin specifically controls cell growth, migration, and the G-actin pool. *Mol Biol Cell.* 2011;22(21):4047-58. Epub 2011/09/09. doi: 10.1091/mbc.E11-06-0582. PubMed PMID: 21900491; PMCID: PMC3204067.
558. Marquardt JU, Andersen JB, Thorgeirsson SS. Functional and genetic deconstruction of the cellular origin in liver cancer. *Nat Rev Cancer.* 2015;15(11):653-67. Epub 2015/10/24. doi: nrc4017 [pii] 10.1038/nrc4017 [doi]. PubMed PMID: 26493646.
559. Nakamura H, Arai Y, Totoki Y, Shiota T, Elzawahry A, Kato M, Hama N, Hosoda F, Urushidate T, Ohashi S, Hiraoka N, Ojima H, Shimada K, Okusaka T, Kosuge T, Miyagawa S, Shibata T. Genomic spectra of biliary tract cancer. *Nat Genet.* 2015;47(9):1003-10. Epub 2015/08/11. doi: 10.1038/ng.3375. PubMed PMID: 26258846.
560. Ong CK, Subimerb C, Pairojkul C, Wongkham S, Cutcutache I, Yu W, McPherson JR, Allen GE, Ng CC, Wong BH, Myint SS, Rajasegaran V, Heng HL, Gan A, Zang ZJ, Wu Y, Wu J, Lee MH, Huang D, Ong P, Chan-on W, Cao Y, Qian CN, Lim KH, Ooi A, Dykema K, Furge K, Kukongviriyapan V, Sripa B, Wongkham C, Yongvanit P, Futreal PA, Bhudhisawasdi V, Rozen S, Tan P, Teh

- BT. Exome sequencing of liver fluke-associated cholangiocarcinoma. *Nat Genet.* 2012;44(6):690-3. Epub 2012/05/09. doi: ng.2273 [pii] 10.1038/ng.2273 [doi]. PubMed PMID: 22561520.
561. Ju HL, Ahn SH, Kim DY, Baek S, Chung SI, Seong J, Han KH, Ro SW. Investigation of oncogenic cooperation in simple liver-specific transgenic mouse models using noninvasive in vivo imaging. *PLoS One.* 2013;8(3):e59869. Epub 2013/04/05. doi: 10.1371/journal.pone.0059869. PubMed PMID: 23555816; PMCID: PMC3610734.
562. Xue W, Zender L, Miething C, Dickins RA, Hernando E, Krizhanovsky V, Cordon-Cardo C, Lowe SW. Senescence and tumour clearance is triggered by p53 restoration in murine liver carcinomas. *Nature.* 2007;445(7128):656-60. PubMed PMID: 67.
563. Katz SF, Lechel A, Obenaus AC, Begus-Nahrman Y, Kraus JM, Hoffmann EM, Duda J, Eshraghi P, Hartmann D, Liss B, Schirmacher P, Kestler HA, Speicher MR, Rudolph KL. Disruption of Trp53 in livers of mice induces formation of carcinomas with bilineal differentiation. *Gastroenterology.* 2012;142(5):1229-39. Epub 2012/02/22. doi: S0016-5085(12)00204-1 [pii] 10.1053/j.gastro.2012.02.009 [doi]. PubMed PMID: 22342966.
564. Song CQ, Li Y, Mou H, Moore J, Park A, Pomyen Y, Hough S, Kennedy Z, Fischer A, Yin H, Anderson DG, Conte D, Jr., Zender L, Wang XW, Thorgeirsson S, Weng Z, Xue W. Genome-Wide CRISPR Screen Identifies Regulators of Mitogen-Activated Protein Kinase as Suppressors of Liver Tumors in Mice. *Gastroenterology.* 2017;152(5):1161–73.e1. Epub 2016/12/14. doi: 10.1053/j.gastro.2016.12.002. PubMed PMID: 27956228.
565. Rullier A, Le Bail B, Fawaz R, Blanc JF, Saric J, Bioulac-Sage P. Cytokeratin 7 and 20 expression in cholangiocarcinomas varies along the biliary tract but still differs from that in colorectal carcinoma metastasis. *Am J Surg Pathol.* 2000;24(6):870-6. Epub 2000/06/08. PubMed PMID: 10843291.
566. Maeda T, Kajiyama K, Adachi E, Takenaka K, Sugimachi K, Tsuneyoshi M. The expression of cytokeratins 7, 19, and 20 in primary and metastatic carcinomas of the liver. *Mod Pathol.* 1996;9(9):901-9. Epub 1996/09/01. PubMed PMID: 8878022.
567. Tsuji M, Kashiwara T, Terada N, Mori H. An immunohistochemical study of hepatic atypical adenomatous hyperplasia, hepatocellular carcinoma, and cholangiocarcinoma with alpha-fetoprotein, carcinoembryonic antigen, CA19-9, epithelial membrane antigen, and cytokeratins 18 and 19. *Pathol Int.* 1999;49(4):310-7. Epub 1999/06/12. PubMed PMID: 10365850.
568. Tsai SQ, Joung JK. Defining and improving the genome-wide specificities of CRISPR-Cas9 nucleases. *Nat Rev Genet.* 2016;17(5):300-12. Epub 2016/04/19. doi: nrg.2016.28 [pii] 10.1038/nrg.2016.28 [doi]. PubMed PMID: 27087594.

569. Dauch D, Rudalska R, Cossa G, Nault JC, Kang TW, Wuestefeld T, Hohmeyer A, Imbeaud S, Yevsa T, Hoenicke L, Patsar T, Bozko P, Malek NP, Longerich T, Laufer S, Poso A, Zucman-Rossi J, Eilers M, Zender L. A MYC-aurora kinase A protein complex represents an actionable drug target in p53-altered liver cancer. *Nat Med*. 2016;22(7):744-53. Epub 2016/05/24. doi: 10.1038/nm.4107. PubMed PMID: 27213815.
570. Weber J, Ollinger R, Friedrich M, Ehmer U, Barenboim M, Steiger K, Heid I, Mueller S, Maresch R, Engleitner T, Gross N, Geumann U, Fu B, Segler A, Yuan D, Lange S, Strong A, de la Rosa J, Esposito I, Liu P, Cadinanos J, Vassiliou GS, Schmid RM, Schneider G, Unger K, Yang F, Braren R, Heikenwalder M, Varela I, Saur D, Bradley A, Rad R. CRISPR/Cas9 somatic multiplex-mutagenesis for high-throughput functional cancer genomics in mice. *Proc Natl Acad Sci U S A*. 2015;112(45):13982-7. Epub 2015/10/29. doi: 1512392112 [pii] 10.1073/pnas.1512392112 [doi]. PubMed PMID: 26508638.
571. Zhan T, Rindtorff N, Boutros M. Wnt signaling in cancer. *Oncogene*. 2017;36(11):1461-73. doi: 10.1038/onc.2016.304.
572. Lu L, Li Y, Kim SM, Bossuyt W, Liu P, Qiu Q, Wang Y, Halder G, Finegold MJ, Lee J-S, Johnson RL. Hippo signaling is a potent in vivo growth and tumor suppressor pathway in the mammalian liver. *Proceedings of the National Academy of Sciences of the United States of America*. 2010;107(4):1437-42. Epub 2010/01/04. doi: 10.1073/pnas.0911427107. PubMed PMID: 20080689.
573. Ehmer U, Sage J. Control of Proliferation and Cancer Growth by the Hippo Signaling Pathway. *Molecular Cancer Research*. 2016;14(2):127-40. doi: 10.1158/1541-7786.Mcr-15-0305.
574. Zhao B, Wei X, Li W, Udan RS, Yang Q, Kim J, Xie J, Ikenoue T, Yu J, Li L, Zheng P, Ye K, Chinnaiyan A, Halder G, Lai Z-C, Guan K-L. Inactivation of YAP oncoprotein by the Hippo pathway is involved in cell contact inhibition and tissue growth control. *Genes & development*. 2007;21(21):2747-61. doi: 10.1101/gad.1602907. PubMed PMID: 17974916.
575. Zhao B, Li L, Tumaneng K, Wang CY, Guan KL. A coordinated phosphorylation by Lats and CK1 regulates YAP stability through SCF(beta-TRCP). *Genes Dev*. 2010;24(1):72-85. Epub 2010/01/06. doi: 10.1101/gad.1843810. PubMed PMID: 20048001; PMCID: PMC2802193.
576. Vassilev A, Kaneko KJ, Shu H, Zhao Y, DePamphilis ML. TEAD/TEF transcription factors utilize the activation domain of YAP65, a Src/Yes-associated protein localized in the cytoplasm. *Genes & Development*. 2001;15(10):1229-41. doi: 10.1101/gad.888601.
577. Xia H, Dai X, Yu H, Zhou S, Fan Z, Wei G, Tang Q, Gong Q, Bi F. EGFR-PI3K-PDK1 pathway regulates YAP signaling in hepatocellular carcinoma: the mechanism and its implications in targeted therapy. *Cell Death & Disease*. 2018;9(3):269. doi: 10.1038/s41419-018-0302-x.

578. Reddy BVVG, Irvine KD. Regulation of Hippo signaling by EGFR-MAPK signaling through Ajuba family proteins. *Developmental cell*. 2013;24(5):459-71. doi: 10.1016/j.devcel.2013.01.020. PubMed PMID: 23484853.
579. Azzolin L, Panciera T, Soligo S, Enzo E, Bicciato S, Dupont S, Bresolin S, Frasson C, Basso G, Guzzardo V, Fassina A, Cordenonsi M, Piccolo S. YAP/TAZ incorporation in the β -catenin destruction complex orchestrates the Wnt response. *Cell*. 2014;158(1):157-70. Epub 2014/06/26. doi: 10.1016/j.cell.2014.06.013. PubMed PMID: 24976009.
580. Fan R, Kim N-G, Gumbiner BM. Regulation of Hippo pathway by mitogenic growth factors via phosphoinositide 3-kinase and phosphoinositide-dependent kinase-1. *Proceedings of the National Academy of Sciences*. 2013;110(7):2569-74. doi: 10.1073/pnas.1216462110.
581. Zhang Y, Xia H, Ge X, Chen Q, Yuan D, Chen Q, Leng W, Chen L, Tang Q, Bi F. CD44 acts through RhoA to regulate YAP signaling. *Cellular Signalling*. 2014;26(11):2504-13. doi: <https://doi.org/10.1016/j.cellsig.2014.07.031>.
582. Dupont S, Morsut L, Aragona M, Enzo E, Giulitti S, Cordenonsi M, Zanconato F, Le Digabel J, Forcato M, Bicciato S, Elvassore N, Piccolo S. Role of YAP/TAZ in mechanotransduction. *Nature*. 2011;474(7350):179-83. doi: 10.1038/nature10137.
583. Mo J-S, Yu F-X, Gong R, Brown JH, Guan K-L. Regulation of the Hippo-YAP pathway by protease-activated receptors (PARs). *Genes & Development*. 2012;26(19):2138-43. doi: 10.1101/gad.197582.112.